

**The mechanism of racemisation of 5-substituted
hydantoins in aqueous solution**

Stefania Narduolo

A thesis submitted for Degree of Doctor of Philosophy
School of Chemistry
Cardiff University

December 2011

UMI Number: U585521

All rights reserved

INFORMATION TO ALL USERS

The quality of this reproduction is dependent upon the quality of the copy submitted.

In the unlikely event that the author did not send a complete manuscript and there are missing pages, these will be noted. Also, if material had to be removed, a note will indicate the deletion.



UMI U585521

Published by ProQuest LLC 2013. Copyright in the Dissertation held by the Author.
Microform Edition © ProQuest LLC.

All rights reserved. This work is protected against
unauthorized copying under Title 17, United States Code.



ProQuest LLC
789 East Eisenhower Parkway
P.O. Box 1346
Ann Arbor, MI 48106-1346

100896



DECLARATION

This work has not been submitted in substance for any other degree or award at this or any other university or place of learning, nor is being submitted concurrently in candidature for any degree or other award.

Signed Storhaug (candidate) Date 28/05/2012

STATEMENT 1

This thesis is being submitted in partial fulfillment of the requirements for the degree PhD.

Signed Storhaug (candidate) Date 28/05/2012

STATEMENT 2

This thesis is the result of my own independent work/investigation, except where otherwise stated.

Other sources are acknowledged by explicit references.

Signed Storhaug (candidate) Date 28/05/2012

STATEMENT 3

I hereby give consent for my thesis, if accepted, to be available for photocopying and for inter-library loan, and for the title and summary to be made available to outside organisations.

Signed Storhaug (candidate) Date 28/05/2012

To my parents

Summary

This thesis describes our studies of the racemisation of substituted hydantoins and is divided in six chapters.

Chapter 1 presents the concepts of chirality and racemisation and its implications in drug development. The literature on the stereolability of 5-substituted hydantoins is summarised. Chapter 2 describes detailed kinetic and mechanistic studies of the racemisation of (*S*)-5-benzylhydantoin and (*S*)-3-*N*-methyl-5-benzylhydantoin, aimed at establishing the mechanistic aspects of racemisation of these molecules. Kinetics of H/D exchange and racemisation, kinetic isotope effects, and solvent kinetic isotope effects all favour the S_E1 mechanism of racemisation as opposed to the S_E2 process proposed by others.

Chapter 3 discusses the effects of structural modifications on the stereolability of a series of model 5-substituted hydantoins with improved water solubility as compared to (*S*)-5-benzylhydantoin and (*S*)-3-*N*-methyl-5-benzylhydantoin. Hydantoins containing a protonated amino or an ammonium group showed increased stereolability. This finding was attributed to intramolecular facilitation of racemisation by the positive charge. The primary and solvent kinetic isotope effects on the racemisation of two model 5-substituted hydantoins were determined and again supported an S_E1 mechanism of racemisation.

Chapter 4 deals with solvent effects on racemisation and H/D exchange of a series of 5-benzylhydantoins. DMSO added to phosphate buffers showed a marked rate-increasing effect for all of the substrates under study. Co-added 2-propanol and dioxane showed a rate-decreasing effect on neutral hydantoins and a rate-increasing effect on a cationic hydantoin. Solvent effects on the basicity of anionic catalysts and phenomena of preferential solvation were proposed as important factors affecting the rate constants in mixed media.

Chapter 5 reports the preliminary results of exploratory experiments aimed at assessing potentials and limitations of VCD and IR spectroscopy for kinetic and mechanistic studies of racemisation.

Finally, Chapter 6 summarises our findings and presents recommendation for future work.

Acknowledgments

First and foremost I thank my supervisor, Dr Niek Buurma, to whom I am especially grateful for giving me the opportunity to work on this project, for his expertise and invaluable and enthusiastic guidance and support throughout this PhD. Thanks for the time patiently spent in very useful conversation, which helped overcome the difficulties encountered in this research and writing-up.

I thank Prof. Barry Carpenter and Dr Anne Marie O'Donoghue for accepting to read this thesis. Prof. Carpenter and Dr O'Donoghue, as well as Prof. Lloyd-Jones, are also gratefully acknowledged for very helpful comments and suggestions during group-meetings and/or during the "UK POC group meetings".

I would like to thank my mentor Dr Nick Tomkinson and examiners Prof. Keith Smith and Dr Ian Fallis for contributing to this research with useful questions and comments during the *viva-voce* examinations.

I thank Dr Andrew Leach, Dr Simone Tomasi and Dr Nabil Asaad from AstraZeneca, for help and suggestions and for hospitality at AstraZeneca.

I gratefully thank Dr Robert Richardson for invaluable help in the lab, discussions and support, Dr Lavinia Onel for her kind help with data analyses, friendship, and very appreciated practical help, Dr G. S. M. Sundaram and, last in chronological time of joining the POC group, but not at all least, Dr Julia Rehbein.

Thanks to my past, present and "temporary" colleagues in the POC Centre: Larry, Mihaela, Mazin, Ismail, Andy, Alicja, Zuzka, Josie, Jamie, Azzedine, Ed and Daniela, for being a fantastic lab-company, always ready to help...and laugh and to Dr Eric Tipmann.

Thank you to the library and technical staff of Cardiff University for very kind helpfulness.

I am grateful to Linda and Malcolm for warm hospitality, help, encouragement and patience in particular in the last period of my stay in Cardiff and for fantastic dinners and pleasant chats.

Finally I would like to thank all those not mentioned but remembered people who, in many different ways, helped me during these years of PhD.

I thank Cardiff University and AstraZeneca for hospitality and support.

Very special thanks are for my family, for their constant helpful presence, extensive and invaluable support, encouragement and patience.

A note on stereochemical representations

In this thesis solid and broken wedges have been used to represent absolute configuration at chiral centres. Plain bonds have been used to depict mixtures of enantiomers or diastereoisomers or when the stereochemistry was unknown or not defined. Wavy bonds have been used in some schemes to place special emphasis on the racemic nature of chiral molecules, especially as a consequence of phenomena of racemisation.

List of abbreviations

v	Volume
ml	Millilitre
t	Time
min	Minutes
s	Seconds
rt	Room temperature
°C	Degree Celsius
K	Kelvin
g	Gram
mg	Milligram
nm	Nanometre
mm	Millimetre
cm	Centimetre

mmole	Millimole
M	Molar
mM	Millimolar
kcal	Kilocalorie
cal	Calorie
<i>I</i>	ionic strength
S_E	Electrophilic substitution
S_N	Nucleophilic substitution
pH	$-\log [H^+]$
pD	$-\log [D^+]$
$pH^{25^\circ C}$	Uncorrected reading of a pH-meter for an H ₂ O-based sample at room temperature, when the sample is not used at room temperature.
pH^{**}	Uncorrected reading of the pH-meter for a D ₂ O-based sample at room temperature, when the sample is not used at room temperature.
pH^*	Uncorrected reading of the pH meter for a D ₂ O-based sample at room temperature, when the sample is used at room temperature.
HB	H ₂ O phosphate buffer
DB	D ₂ O phosphate buffer
k_{obs}	Observed rate constant
k_{rac}	Rate constant of racemisation
$k_{H/D}$	Rate constant of H/D exchange
HHyd	Protonated hydantoin
BHyd	Deprotonated hydantoin
Hyd _{tot}	Total hydantoin
[phosphate _{tot}]	Total concentration of phosphate buffer

k_0	Rate constant for non-catalysed processes
k_{OD^-}	Rate constant for deuterioxide-catalysed processes
$k_{\text{phosphate tot}}$	Rate constant for phosphate-catalysed processes
$k_{\text{buffer, basic component}}$	Rate constant for racemisation catalysed by the basic component of the buffer
$k_{0BH_{yd}}$ and $k_{0HH_{yd}}$	Rate constants for the uncatalysed racemisation of deprotonated (<i>Bhyd</i>) and protonated (<i>Hhyd</i>) (<i>S</i>)-5-benzylhydantoin
$k_{OD^-BH_{yd}}$ and $k_{OD^-HH_{yd}}$	Catalytic rate constants for the deuterioxide-catalysed racemisation of deprotonated (<i>Bhyd</i>) and protonated (<i>Hhyd</i>) (<i>S</i>)-5-benzylhydantoin
$k_{D_2PO_4^-BH_{yd}}$ and $k_{D_2PO_4^-HH_{yd}}$	Rate constants for racemisation with the monobasic form of the buffer acting as a catalyst on deprotonated (<i>Bhyd</i>) and protonated (<i>Hhyd</i>) (<i>S</i>)-5-benzylhydantoin
$k_{DPO_4^{2-}BH_{yd}}$ and $k_{DPO_4^{2-}HH_{yd}}$	Rate constants of racemisation with the dibasic form of the buffer acting as a catalyst on deprotonated (<i>Bhyd</i>) and protonated (<i>Hhyd</i>) (<i>S</i>)-5-benzylhydantoin
H/D exchange	Proton deuterium exchange
K_a	Acid dissociation constant
pK_a	$-\log K_a$
pK_a^{**}	pK_a determined based on pH ^{**} readings
θ	Circular Dichroism or Ellipticity
Hz	Hertz
MHz	Megahertz
ppm	Part per million
k_{ROH}	Rate constant in non-deuterated alcohol
k_{ROD}	Rate constant in deuterated alcohol
k_{H_2O}	Rate constant in H ₂ O or H ₂ O mixed media
k_{D_2O}	Rate constant in D ₂ O or D ₂ O mixed media

k_H	Rate constant of reaction of a non-deuterium-labelled substrate
k_D	Rate constant of reaction of a deuterium-labelled substrate
HRMS	High resolution mass spectrum
GC-MS	Gas chromatography–mass spectrometry
EI	Electron impact (ionization)
APCI	Atmospheric pressure chemical ionization
ESI	Electrospray ionization
λ	Wavelength
ν	Wave number
M.p.	Melting point
CDI	Carbonyldiimidazole
Pd/C	Palladium on carbon
THF	Tetrahydrofuran
TFE	Trifluoroethanol
DIOX	Dioxane
IP	2-propanol
DMSO	Dimethyl sulfoxide
TRIS	tris(hydroxymethyl)aminomethane
PPTS	pyridinium p-toluenesulfonate
THP	Tetrahydropyranyl
Me	Methyl
Et	Ethyl
Ph	Phenyl
Ar	Aromatic
NMR	Nuclear magnetic resonance

J	Coupling constant
δ	Chemical shift
ppm	Parts per million
ΔH^\ddagger	Enthalpy of activation
ΔS^\ddagger	Entropy of activation
e.u.	Entropic units ($\text{cal}\cdot\text{K}^{-1}\cdot\text{mol}^{-1}$)
HPLC	High-performance (pressure) liquid chromatography
FT-IR	Fourier Transform Infra Red
UV-Vis	Ultra Violet -Visible
VCD	Vibrational Circular Dichroism
CD or ECD	Electronic Circular Dichroism
ϵ	Dielectric constant or extinction coefficient
μ	Dipole moment
$E_T(30)$	Transition energy at 25°C for the long-wavelength absorption band of Reichardt's pyridinium- <i>N</i> -phenoxide betaine dye ¹
π^*	Kamlet and Taft's solvatochromic parameter of solvent dipolarity / polarizability ²
α	Kamlet and Taft's solvatochromic parameter of solvent hydrogen-bond-donor acidity ²
β	Kamlet and Taft's solvatochromic parameter of solvent hydrogen-bond-acceptor basicity ² or Brønsted parameter ³
$[\alpha]_D^c$	Specific rotation, given with temperature, expressed in °C and wavelength (D). D refers to the D line of the emission spectrum of sodium ($\lambda=589\text{ nm}$). ⁴
DFT	Density Functional Theory
MM	Molecular Mechanics
FF	Force Field

MMFF94	Merck Molecular Force Field ⁵
B3PW91	Becke three-parameter and Perdew-Wang functionals ⁶
B3LYP	Becke three-parameter and Lee-Yang-Parr functionals ⁶

List of contents

Chapter 1

Enantiomers and racemisation

1.1. Chirality: some definitions and historical background.....	1
1.2. The problem of racemisation in drug development.....	5
1.2.1. Some studies on the racemisation of drugs under various conditions.....	6
1.3. Structure and stereolability.....	15
1.3.1. Chiral centres potentially liable to racemise.....	15
1.3.2. Stereolability and carbon acid acidity.....	16
1.3.3. Quantitative studies on carbon acid acidity.....	19
1.4. The hydantoins ring in drug development.....	27
1.5. The racemisation of hydantoins.....	28
1.6. Solvent effects on reactions of racemisation and H/D exchange.....	39
1.6.1. Solvents and solvent properties.....	39
1.6.2. The effect of the medium on racemisation and H/D exchange: examples reported in the published literature.....	39
1.6.3. The effect of the medium on equilibria.....	45

1.7. Aim of the thesis.....	46
References.....	47

Chapter 2

The kinetics and mechanism of racemisation of (*S*)-5-benzylhydantoin and (*S*)-3-*N*-methyl-5-benzylhydantoin.

2.1. Introduction.....	56
2.2. Syntheses.....	58
2.3. Kinetic studies.....	61
2.3.1. Racemisation of (<i>S</i>) 5-benzylhydantoin in phosphate buffers.....	61
2.3.2. The effect of pH** on the rate constants of racemisation.....	63
2.3.3. Racemisation of (<i>S</i>)-3- <i>N</i> -methyl-5-benzylhydantoin in phosphate buffers	67
2.3.4. H/D exchange of (<i>S</i>)-5-benzylhydantoin.....	73
2.4. Mechanistic aspects.....	76
2.4.1. The comparison of the rate constants of racemisation and H/D exchange of (<i>S</i>)-5-benzylhydantoin in phosphate buffers.....	76
2.4.2. The H/D exchange of deuterium-labelled 5-benzylhydantoins 2.1a and 2.2a	77
2.4.3. Brønsted correlation for base-catalysed racemisation of 5-benzylhydantoins.....	79
2.4.4. Kinetic isotope effects for racemisation of 2.1 and 2.2	81
2.4.4.1. The solvent kinetic isotope effect.....	81

2.4.4.2. The primary kinetic isotope effect.....	83
2.4.5. Kinetic consequences of racemisation of (S)-5-benzylhydantoins 2.1 and 2.2 by the S _E 1 and S _E 2 mechanisms.....	84
2.5. Conclusions.....	88
2.6. Experimental Part 1.....	89
2.7. Experimental Part 2.....	101
Acknowledgments	104
References.....	105

Chapter 3

The effect of structural modifications on the kinetics and mechanism of racemisation of 5-substituted hydantoins.

3.1. Introduction.....	111
3.2. Structural modifications in position 3.....	112
3.2.1. Syntheses.....	112
3.2.2. Kinetic studies.....	115
3.2.3. Activation parameters for racemisation of 3.2 , 3.3 and 3.5	122
3.2.4. Mechanistic considerations.....	125
3.2.4.1. The possible mechanisms of intramolecular participation of the cationic groups in the racemisation of 3.4 and 3.5	125
3.2.4.2. The slight rate depressing effect of alkyl groups.....	132
3.3. Structural modifications in position 5.....	134

3.3.1. Syntheses.....	135
3.3.2. Kinetic studies.....	137
3.4. Conclusions.....	142
3.5. Experimental Part 1.....	144
3.6. Experimental Part 2.....	162
Acknowledgments.....	165
References.....	165

Chapter 4

The effect of cosolvents on the racemisation of substituted hydantoins in aqueous solutions

4.1. Introduction.....	171
4.2. DMSO, 2-propanol, trifluoroethanol, and dioxane as co-solvents: a few characteristics.....	172
4.3. Kinetic studies.....	174
4.3.1. The effect of d ₆ -DMSO and d ₈ -2-propanol on the kinetics of H/D exchange and racemisation of (<i>S</i>)-5-benzylhydantoins.....	174
4.3.1.1. Kinetic studies in the presence of 33% added co-solvent	174
4.3.1.2. Kinetic studies in the presence of 25% added co-solvent.....	179
4.3.2. Solvent kinetic isotope effects in mixed media.....	182
4.3.3. The effect of added co-solvents on p <i>K</i> _a	183

4.3.4. Medium effects and the stereochemical course of H/D exchange of (<i>S</i>)-5-benzylhydantoin 4.1.....	184
4.4. Discussion.....	186
4.4.1. The effect of co-solvents on the rate constants of racemisation and H/D exchange of neutral benzylhydantoins.....	187
4.4.2. The effect of co-solvents on the rate constants of racemisation and H/D exchange of the cationic hydantoin 4.4.....	189
4.4.3. The solvent kinetic isotope effect for racemisation and the comparison of the rate constants of racemisation and H/D exchange in mixed media: mechanistic implications.....	189
4.5. Conclusions.....	190
4.6. Experimental.....	191
References.....	195

Chapter 5

Exploring the use of IR and VCD spectroscopy for the study of reaction mechanisms involving stereogenic centres.

5.1. The potentials of Vibrational Circular Dichroism (VCD) spectroscopy...	199
5.1.1. The VCD technique.....	199
5.1.2. Calculated VCD spectra.....	200
5.1.2.1. Prediction of VCD spectra of model chiral molecules.....	200
5.1.2.2. Testing the performance of the method for the prediction of VCD spectra.....	208

5.1.2.3. Calculation of VCD spectra - Conclusions.....	210
5.1.3. The use of VCD spectroscopy for kinetic and mechanistic studies of racemisation of 5-substituted hydantoins.....	212
5.1.3.1. Kinetic considerations regarding expected signals.....	212
5.1.3.2. Calculated IR and VCD spectra for 5-benzylhydantoin.....	214
5.1.3.3. Experimental IR spectra for 5-benzylhydantoin and 3- <i>N</i> -methyl-5- benzylhydantoin.....	217
5.1.3.4. Recording VCD spectra: the VCD spectrum of the standard compound (+)-camphor.....	219
5.1.3.5. Conclusions for section 5.1.3.....	222
5.2. Structure-acidity correlations by IR Spectroscopy.....	223
5.2.1. Literature correlation analyses using infrared spectral data.....	223
5.2.2. Correlation analysis for 5-benzylhydantoins	226
5.3. Conclusion.....	230
5.4. Experimental	230
Acknowledgments.....	233
References.....	233

Chapter 6

Epilogue

6.1. Conclusions	236
6.2. Future work.....	237

References.....	238
Appendix 1.....	240
Appendix 2.....	269
Appendix 3.....	287
Appendix 4.....	311

References

1. Reichardt, C., *Solvents and Solvent Effects in Organic Chemistry*. Third ed.; WILEY VCH: Weinheim, 2003; p 416.
2. Reichardt, C., *Solvents and Solvent Effects in Organic Chemistry*. Third ed.; WILEY VCH: Weinheim, 2003; p 431.
3. Maskill, H., *The Physical Basis of Organic Chemistry*. Oxford University Press: Oxford New York, 1985; p 420.
4. Vollhardt, P., *Chimica Organica*. Zanichelli Editore S.p.A.: Bologna, 1998; p 153.
5. Halgren, T. A., *Journal of Computational Chemistry* **1996**, *17* (5-6), 490-519.
6. Jensen, F., *Introduction to Computational Chemistry*. John Wiley & Sons: Chichester New York Weinheim Brisbane Singapore Toronto, 1999; p 177-194.

Chapter 1

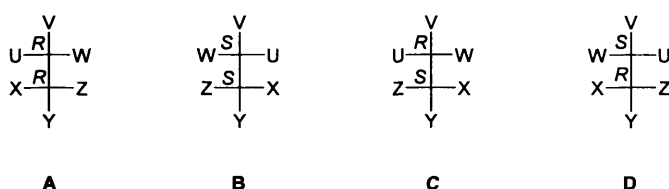
Enantiomers and racemisation

1.1. Chirality: some definitions and historical background

“It’s the same thing....only different!” is the title of an interesting review by Silas Smith¹ on the links between toxicity and chirality in different common chemical compounds. A pair of *enantiomers* are, in a way, “the same thing” since they share the same molecular and structural formula but they are “different” with respect to their spatial arrangement.

In particular, *enantiomers* are two mirror image molecules which are not superimposable. Objects of which the mirror images are not superimposable are also called *chiral*, from the Greek term “χειρ”² which means “hand”. The differences between enantiomers become apparent when they interact with polarized light; all chiral compounds exhibit optical activity.³ The observation that chiral molecules interact with polarised light led, in the 19th century, to the first intuitions about molecular asymmetry. In 1832 Biot observed that solutions of (2*R*, 3*R*) tartaric acid (**Scheme 1.1**), naturally occurring in acidulous fruit juices, were able to rotate the plane of the polarised light. By contrast, solutions of racemic tartaric acid, initially called “racemic acid”, were optically inactive. “*Racemic acid*”⁴ had been accidentally prepared by Kestner during the preparation of tartaric acid, “with which it is associated in the juice of the grape”.⁵ Later, in 1848, Pasteur was able to rationalise the observation made by Biot. He noticed that recrystallisation of the racemic sodium ammonium salt of tartaric acid gave two different crystals with mirror image shapes. The two crystals, dissolved in water, gave solutions that rotated the polarised light in opposite directions. Pasteur called the two “species” of tartrates *dextro* (+) and *levo* (-) based on their effects on polarised light.⁶ The structures of *dextro* and *levo* tartaric acids are reported in **Scheme 1.1**.⁷

The presence of n stereogenic centres in a molecule can give rise to a maximum of 2^n different molecular structures. **Scheme 1.3** illustrates the example of a compound with 2 stereogenic centres: 4 molecular structures can be drawn from all possible combinations of configurations, (R) or (S), around each stereocenter. The pairs A-B and C-D are pairs of *enantiomers*. On the other hand there is no relationship of specularity between compounds of the pair AB to those of the pair CD. The pairs A-B and C-D are *diastereoisomers*. Phenomena of degeneracy are possible when a chiral centre of the molecule carries the same three different substituents as another chiral centre. This situation is illustrated by the case of tartaric acid. Only three isomers of tartaric acid exist, one of which is called *meso* form and is not chiral due to the presence of a plane of symmetry in its structure. The structures of the isomers of tartaric acid are shown in **Scheme 1.1**.^{13, 14}



Scheme 1.3: possible stereoisomer of a generic molecule containing two asymmetric centres.

The microscopic reversible inversion of configuration of one enantiomer, leading to its mirror image, as shown in **Equation 1.1**,¹⁵ is called *enantiomerization*. *Racemisation* is the “macroscopic and statistical reaction of irreversible change of one enantiomer into the racemic form”^{16, 17} and can be represented as in **Equation 1.2**.¹⁵ The inversion of configuration of only one chiral centre in a molecule that contains two or more chiral centres is called *epimerization*.¹¹



In **Equations 1.1** and **1.2** $k_{\text{rac}} = 2 \cdot k_1$.

Usually racemisation is described as in **Equation 1.2**, leading to a first-order kinetic rate law. Racemisation can be followed over time by monitoring “signals”, such as the optical rotation, which are proportional to the difference in concentration of opposite

enantiomers. The link between k_1 and k_{rac} can be understood in two ways. First, every enantiomerisation event “racemises two molecules”. Alternatively, kinetic analysis of the simple process of uncatalysed enantiomerisation, as shown in **Equation 1.1**, allows a straightforward derivation. Enantiomerisation is a reversible first-order reaction with equal rate constants for the forward and the reverse processes, leading to a rate expression described by **Equation 1.3**,

$$\ln \left\{ \frac{[(+)\text{A}]_t - [(\text{+})\text{A}]_e}{[(+)\text{A}]_0 - [(\text{+})\text{A}]_e} \right\} = -2k_1t \quad \text{Equation 1.3}$$

where $[(+)\text{A}]_0$ is the concentration of $(+)\text{A}$ at time $t=0$, $[(+)\text{A}]_e$ is concentration of $(+)\text{A}$ at equilibrium and $[(+)\text{A}]_t$ is the concentration of $(+)\text{A}$ at time t .

Racemisation of $(+)\text{A}$ can be represented as in **Figure 1.1**. From the figure it can be seen that the term $\frac{[(+)\text{A}]_0 - [(\text{+})\text{A}]_e}{[(+)\text{A}]_t - [(\text{+})\text{A}]_e} = \frac{bc}{yz} = \frac{ac}{xz} = \frac{[(+)\text{A}]_t - [(-)\text{A}]_t}{[(+)\text{A}]_0} = \frac{\alpha_0}{\alpha_t}$ where α_t and α_0 are the optical activities at time t of reaction and at time $t=0$, respectively.

By substitution in **Equation 1.3**, the first-order kinetic rate expression shown in **Equation 1.4** is obtained.

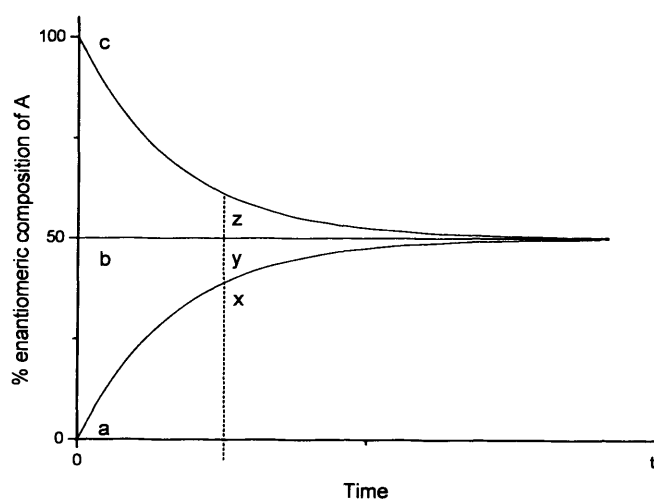


Figure 1.1: Schematic representation of racemisation of the generic chiral molecule $(+)\text{A}$.

$$\ln \left(\frac{\alpha_t}{\alpha_0} \right) = -2k_1t \quad \text{Equation 1.4}$$

Because $\ln(\alpha_t/\alpha_0)$ defines the extent of racemisation of the sample at time t , its time dependence could also be given by **Equation 1.5**.

$$\ln\left(\frac{\alpha_t}{\alpha_0}\right) = -k_{\text{rac}}t$$

Equation 1.5

Comparison of **Equations 1.4** and **1.5** shows that k_{rac} equals $2 k_1$.¹⁸

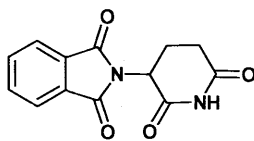
1.2. The problem of racemisation in drug development.

The development of new drugs with increased structural complexity not only implies more complex synthetic routes but leads to a parallel increased complexity in their reactivity, stability, and fate in the human body. The presence of a chiral center in a pharmaceutically active molecule is an aspect that deserves particular attention. Asymmetry is ubiquitous in nature and in biological systems. Biological macromolecules are rich in chiral centres of set configurations such as *L*-amino acids and *D*-sugars. In the complex “chiral” biological system, enantiomers may therefore experience phenomena of selective binding, absorption, enzyme or receptor interactions, leading to different biological responses.^{1, 19} Several optically active enantiomers of a variety of drugs have been found to racemise in the human body and frequently only one of the two enantiomers is active while the other may be inactive or even toxic. The case of thalidomide is a tragically famous example. Racemic thalidomide, used as a sedative and anti-nausea drug, was withdrawn from the market in 1961 due to its teratogenic effects.²⁰ It was later recognised that the molecule was configurationally not stable (*vide infra*), and the *S* (-)-enantiomer of the drug was proposed as being responsible for the teratogenic effects.²¹⁻²⁴ In 1992 the US Food and Drug Administration set forth precise guidelines regulating the marketing of new chiral drugs, accounting for the possibility of phenomena of racemisation and potential differences in the biological activity between opposite enantiomers.²⁵ It is therefore very important to know not only the pharmaceutical properties of both forms of chiral drugs but also the kinetics and mechanisms by which they may interconvert. The problem of racemisation of chiral drugs has been reviewed^{16, 22, 26} and its implications in drug development discussed, leading to the “enantiomer versus racemate debate”, examining advantages and disadvantages in the marketing of either of the two “forms” of a chiral drug. Testa *et al.* in particular discussed the relevance of the problem of racemisation in drug development with respect to the time scale of the process, distinguishing between pharmaceutical and pharmacological relevance. If the half life of a molecule, under

physiological conditions (37 °C, pH=7.4), is of the order of minutes or hours, *i.e.* lower than the time of residence of the drug in the body, the process has pharmaceutical relevance. Half lives of racemisation or epimerisation of the order of months or years are relevant from the pharmacological point of view, due to the implications in the process of manufacturing and storage of the drug.^{22, 26} Preliminary kinetic studies assessing the stereolability of potential drug candidates, under all relevant conditions, can therefore help orient medicinal chemists' decisions when dealing with the development of chiral drugs. The important implications of racemisation in drug design prompted many studies aiming at assessing the stereolability of different chiral drugs. The results of studies on the configurational stabilities of a few important biologically active chiral compounds are briefly described in the following paragraphs.

1.2.1. Some studies on the racemisation of drugs under various conditions

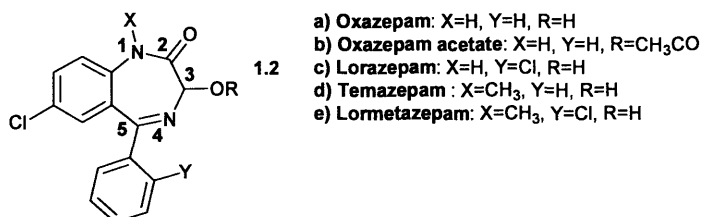
Knoche and Blaschke²⁴ reported the fast racemisation of thalidomide (structure **1.1** in **Scheme 1.4**) enantiomers in phosphate buffer 0.067 M, pH=7.4 at 37°C (approximate $t_{1/2}$ = 270 minutes) The reaction is accelerated by the addition of human serum albumin. Reist *et al.*²³ also studied the racemisation of thalidomide in phosphate buffers under various experimental conditions. The chiral inversion was found to be catalysed by hydroxyl ions, phosphate, albumin and amino acids. The pseudo-first-order rate constants of enantiomerisation, in buffered solutions at pH 7.4 and 37 °C, were found to increase linearly with phosphate buffer concentration and with the concentration of co-added fatty-acid free human serum albumin. Rate constants of enantiomerisation were close to zero in 0.1 M phosphate buffers at pH 2 and 3 and increased with buffer pH. Based on the experimental results, the authors proposed that chiral inversion occurred through a mechanism of electrophilic substitution of the asymmetric proton, catalysed by bases. The catalytic effect of human serum albumin was proposed to reside in the basic arginine and lysine residues of human serum albumin rather than in a single catalytic site of the protein.



1.1

Scheme 1.4: structure of thalidomide.

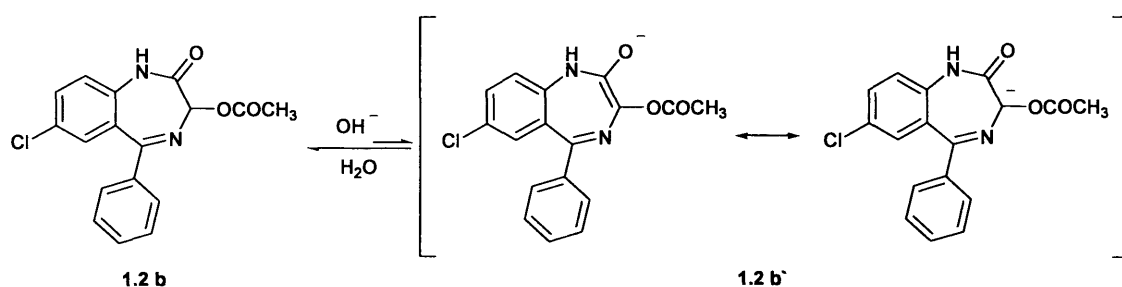
Oxazepam (structure **1.2 a**) in **Scheme 1.5**) is a drug which has been used as a sedative in its racemic form.²⁷ Testa reported an estimated half-life of 10 ± 5 minutes at room temperature and neutral pH for racemisation of oxazepam.²⁶ The kinetics of racemisation of oxazepam were studied by Aso *et al.*²⁷ in aqueous buffered solutions in the pH range between 0.5 and 13.3. The authors reported that no general-acid or general-base catalysis was observed for racemisation of **1.2 a**) in the pH range under study. pH-rate profiles showed the independence of the rates of racemisation on pH, in the neutral pH region (a “flat” region of the pH-rate profile was found between approximately pH=3 and 9). Rate constants increased with pH above pH=10, reaching a plateau value at pH=13. Slow racemisation was observed in the acidic pH range. Three different protonation states of oxazepam at different pH were reported in the paper, the proposed sites of protonation and deprotonation being the nitrogen in position 4 and the hydroxyl oxygen, respectively, according to previous studies (**Scheme 1.5**).



Scheme 1.5: structure of oxazepam and related compounds.

In the pH range under investigation racemisation of oxazepam was attributed to “spontaneous reaction of neutral oxazepam species in the neutral pH region” and hydroxide-catalysed or spontaneous racemisation of the deprotonated form of the molecule in the basic pH range. The kinetics of base-catalysed racemisation and hydrolysis of enantiomers of Oxazepam 3-acetate (structure **1.2b** in **Scheme 1.5**) were studied in buffers and in sodium hydroxide solutions, in the pH range 7.5-14, by Yang and Bao.²⁸ Kinetic traces were fitted to a first-order kinetics rate law. A half life of

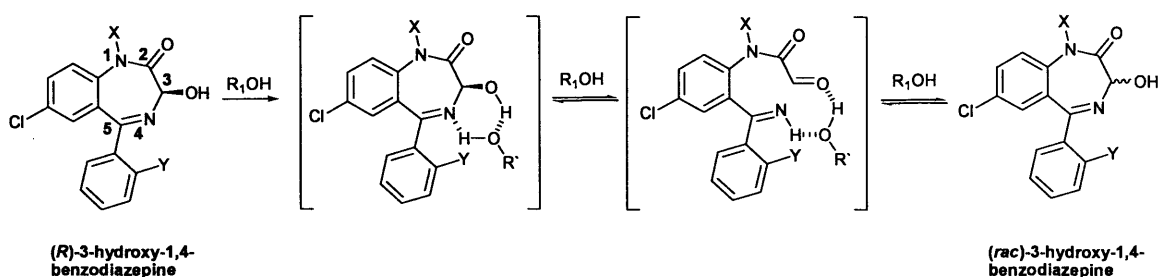
racemisation of 62.0 minutes, determined at 55 °C in a mixture of isopropanol and Robinson-Britton buffer²⁹ at pH 9.5 in the proportion 1:10 (v:v) was reported. Racemisation under similar conditions but with a Robinson-Britton buffer with a pH of 7.5 was observed but it appeared to be very slow (an estimated half life >1000 min was reported). The pH-rate profile showed a plateau at high pH, explained by the deprotonation of the NH group of **1.2b** in position 1 (Scheme 1.5), and consequent formation of a resonance-stabilised anion, which is not prone to racemisation. A pK_a of 10.5 was determined for ionisation of the NH group in position 1 of **1.2b**.³⁰ Racemisation was found to proceed with deuterium incorporation when carried out in deuterated media. The results were interpreted as evidence for a mechanism of racemisation involving formation of an intermediate enolate anion **1.2b'**, as shown in Scheme 1.6.



Scheme 1.6: mechanism of base-catalysed racemisation of Oxazepam 3-acetate **1.2b**, via enolate formation, as proposed by Aso *et al.*

The spontaneous racemisation of enantiomers of oxazepam and of other 3-hydroxy-1,4-benzodiazepines (structures **1.2a**, **1.2c**, **1.2d**, **1.2e** in Scheme 1.5), used as anxiolytic and hypnotic drugs, were studied by Yang³¹ in six different alcohols. Racemisation followed pseudo first-order kinetics. Primary and solvent kinetic isotope effects were determined for oxazepam (**1.2a**), using a labelled analogue of oxazepam, deuterated in the C3 position and deuterated solvents, respectively. No primary kinetic isotope effect was observed in any of the solvents investigated while a solvent kinetic isotope effect (k_{ROH}/k_{ROD}) of about 1.9 was found. It was concluded that OH bonds of solvent molecules but not the C3H bond of oxazepam were broken in the rate-determining step

of the reaction. Small negative entropies of activation were reported for the racemisation of oxazepam in methanol, ethanol and 2-propanol. Based on the reported experimental data, a mechanism as shown in **Scheme 1.7** was proposed for the spontaneous racemisation of 3-hydroxy-1,4-benzodiazepines in alcoholic solvents. The proposed mechanism involves an achiral imino aldehyde intermediate, where “hydrogen bonds resulting from solvation by protic solvents probably initiating the opening of the diazepine ring at C3-N4 bond”.



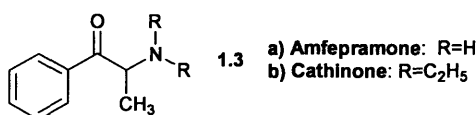
Scheme 1.7: mechanism of racemisation for enantiomers of 3-hydroxy-1,4-benzodiazepines in anhydrous alcoholic solvents (R_1OH), as proposed by Yang.

A mechanism involving an intermediate achiral imino aldehyde was also proposed by Stromar *et al.*³² for racemisation of 3-hydroxy and 3-acyloxy 1,4-benzodiazepines in aqueous media, at acidic pH.

Amfepramone or diethylpropion (structure **1.3a** in **Scheme 1.8**) is a sympathomimetic drug which has been used as an anorectic in the treatment of obesity³³. The configurational stability of the molecule and of its metabolite cathinone (Structure **1.3b** in **Scheme 1.8**) were assessed by Reist *et al.*³⁴ by H/D exchange studies in D_2O phosphate and hydroxylamine buffers, in a pD range between 2.34 and 7.53, at 37 or 50 °C. For both **1.3a** and **b**, the pseudo-first-order rate constants of H/D exchange increased with pD and, at a constant pD of 7.4 with buffer concentration. By analogy with other ketones, equal rate constants of racemisation and deuteration were assumed. An S_E1 mechanism was proposed for H/D exchange and racemisation of **1.3a** and **b**, involving general-base-catalysed proton abstraction from the chiral centre as rate-determining step. The intermediate enolates were proposed to be stabilised by the strong electron withdrawing effects of the protonated terminal amino groups of **1.3a** and **b**.³⁵ The racemisation of enantiomers of **1.3a** was also investigated by Mey³³ under different

experimental conditions. The pseudo-first-order rate constants of racemisation in phosphate buffers at 25 °C were reported to increase with pH and buffer concentration. The rates of racemisation increased with increasing temperature and decreased with increasing ionic strength. A rate constant of 0.0144 min⁻¹ was reported for racemisation in 0.2 M phosphate buffer, 0.53 I, at pH 7.4 and 25 °C.

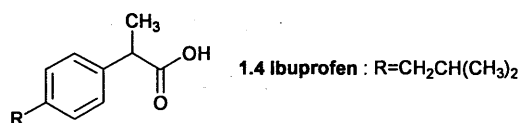
The addition of cyclodextrins to a 10 mM phosphate buffer with pH 6.7, was found to have small rate-retarding or rate-accelerating effects, depending on the nature of the cyclodextrins. A need for further investigations to explain the effects was mentioned. However, the relatively strong rate-retarding effect of sulfobutyl ether β-cyclodextrins was attributed to formation of a particularly stable complex of the cyclodextrin and **1.3a** due to electrostatic interactions between the sulfonic acid groups of the cyclodextrins and the basic groups of **1.3a**. The inclusion of amfepramone molecules in the complexes with cyclodextrins was proposed to retard the racemisation due to hindered attack by hydroxyl ions and other catalytic species present in solution.



Scheme 1.8: structures of amfepramone and cathinone.

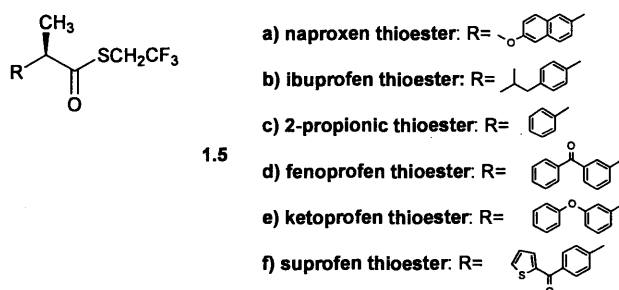
2-Arylpropionic acids are an important class of anti-inflammatory drugs whose therapeutic effect is mainly ascribed to the (*S*)-enantiomer.³⁶⁻³⁸ Ibuprofen, racemic 2-(4-isobutylphenyl) propionic acid (structure **1.4** in **Scheme 1.9**), is a commonly used example of this group of drugs. The racemisation of ibuprofen enantiomers was studied by Xie *et al.* in aqueous solutions of NaOH³⁹ and in mixed DMSO-NaOH solutions in the proportion 4:1 (v:v)³⁷, at 100 °C. At 30 °C racemisation was found to be slow: a decrease of enantiomeric excess from 78.9% to 78.7%, after 6 hours in a 1.25 M solution of NaOH was reported. Racemisation followed a first-order kinetic law and rate constants of racemisation were found to increase with NaOH concentration in both media, at 100 °C. The increase of the rate constants of racemisation was reported to be linear with NaOH concentration in the study conducted in the mixed medium containing 80% DMSO.³⁷ A mechanism of racemisation involving keto-enol tautomerism with formation of an intermediate enolate, catalysed by base, was proposed. A marked influence of organic co-solvents added to the solutions of NaOH was also reported (*vide infra*).³⁹ Although apparently not very prone to racemisation, the *R* enantiomers of

ibuprofen and, in general, of 2-arylpropionic acids are known to undergo chiral inversion *in vivo* through a stereospecific enzyme-mediated pathway.^{36, 40}

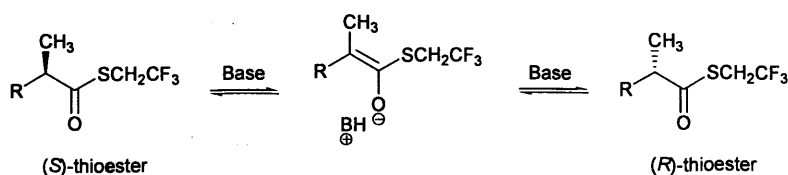


Scheme 1.9: structure of ibuprofen.

The racemisation of a series of (*S*)-profen-2,2,2-trifluoroethyl thioesters with different aromatic substituents on the chiral carbon (structures **1.5a-f** in **Scheme 1.10**), in isooctane with trioctylamine as base, was studied by Chen *et al.*³⁸ Racemisation followed first-order kinetics and interconversion rate constants increased linearly with trioctylamine concentration. The effect of different aryl substituents attached to the chiral carbon on the rates of racemisation was studied. A Hammett plot correlating the second-order rate constants of enantiomerisation with the σ values of the different aryl groups gave a Hammett ρ value of 3.58, suggesting build up of negative charge in the transition state. A mechanism of racemisation was proposed³⁸ involving rate-determining proton abstraction of the asymmetric proton by the base, with formation of an enolate intermediate forming a contact ion-pair with the protonated base, as in **Scheme 1.11**.

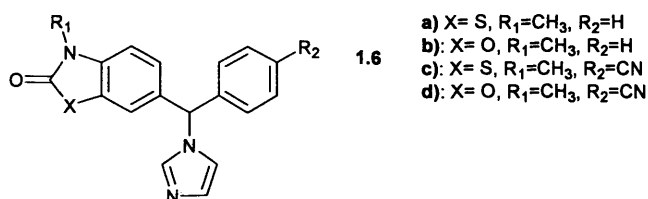


Scheme 1.10: structures of (*S*)-profen-2,2,2-trifluoroethyl thioesters studied by Chen *et al.*



Scheme 1.11: mechanism of racemisation of (*S*)-profen 2,2,2- trifluoroethyl thioesters catalysed by organic bases in apolar aprotic solvents, as proposed by Chen *et al.*

The kinetics of racemisation of a series of *N*-imidazole derivatives (structures **1.6a-d** in **Scheme 1.12**), potentially useful in the treatment of breast cancer, were studied by Danel *et al.*⁴¹ in organic solvents and in aqueous buffers. Solutions of **1.6a-d** in ethanol in the presence of acetic acid were configurationally stable. Only substrates **1.6c** and **d** were found to racemise in ethanolic solutions in the presence of triethylamine as catalyst and in buffers with pH 7.4 and 9.6. Pseudo-first-order rate constants of racemisation for **1.6c** and **d**, in ethanol in the presence of triethylamine, increased with increasing the concentration of base. Experiments carried out in phosphate buffer showed that rate constants of racemisation increased with increasing buffer pH. A mechanism of racemisation involving base-catalysed deprotonation at the chiral centre was proposed. The differences in configurational stability of **1.6a** and **1.6b** as compared to **1.6c** and **d** were explained in term of increased acidity of the latter compounds, due to the electron-withdrawing effect of the cyano substituents on the phenyl ring.



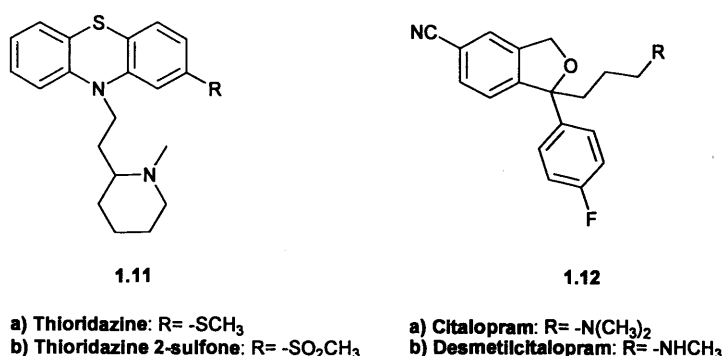
Scheme 1.12: structures of *N*-imidazole derivatives studied by Danel *et al.*

Thiazolidinediones are an important class of drugs used in the treatment of diabetes. The high configurational lability of the chiral thiazolidinedione **1.7**, whose structure is shown in **Scheme 1.13**, has been reported by Welch *et al.*⁴² Rapid racemisation was observed in different organic solvents and solvent mixtures. Rates of racemisation increased with the addition of triethylamine to the organic solvents while the addition of acetic acid showed a rate-depressing effect. Very short half-lives were reported in aqueous media and in plasma and addition of acid was reported to be ineffective in slowing down the process of racemisation in aqueous media.

configurationally stable over a period of study of 24 hours. The configurational stability of **1.10** was attributed to the presence of bulky substituents at the chiral centre, either hindering the approach of the base or inhibiting formation of the carbanion intermediate.

Thioridazine (structure **1.11a** in **Scheme 1.15**), a drug used for the treatment of psychiatric disorders, and the antidepressant citalopram (structure **1.12a** in **Scheme 1.15**) are examples of drugs whose activity was found to reside mainly in one of the enantiomers and which have been reported to be configurationally stable. The *R* and the *S* enantiomer are the active forms of thioridazine and citalopram, respectively.^{44, 45} The racemisation reactions of thioridazine and thioridazine 2-sulfone (structure **1.11b** in **Scheme 1.15**) in buffers and human plasma were investigated by De Gaitani *et al.*⁴⁵ No racemisation was observed for enantiomers of **1.11a** and **b** in human plasma, at temperatures up to 38 °C, over periods of 7 days for **1.11a** and 14 days for **1.11b**. Similarly, no racemisation was reported in 0.05 M phosphate buffers at pH 5, 7 and 8.5, at 4 °C, over the same periods of study.

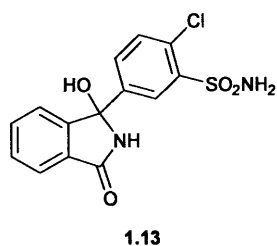
Information on the configurational stability of citalopram and its demethylated metabolite (structure **1.12b** in **Scheme 1.15**), under typical HPLC analysis working conditions, has been provided by Rochat *et al.*⁴⁴ No racemisation was observed in samples of enantiomers of **1.12a** and **b** stored at room temperature for 45 days in mixtures of hexane-isopropanol in the ratio 93.5:6.5 (v:v) containing 0.2% of diethylamine, or in toluene solutions for 2 hours at 60 °C.



Scheme 1.15: structures of thioridazine, citalopram and derivatives.

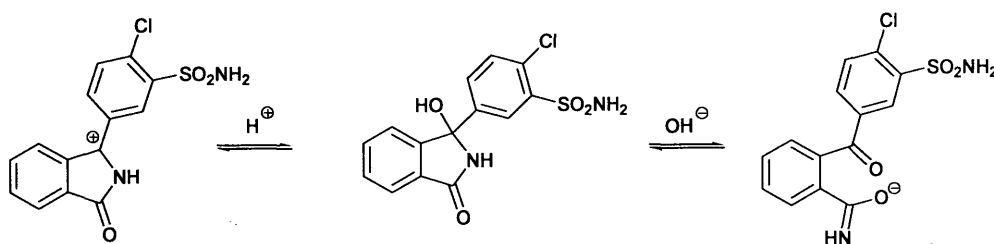
The configurational stability of chlortalidone, (structure **1.13** in **Scheme 1.16**), a diuretic and antihypertensive drug, has been investigated by Lamparter *et al.*⁴⁶ Rate

constants of racemisation of (+) chlortalidone in mixtures of aqueous buffer and dioxane at different pH values, at room temperature, were determined. A pH-rate profile with a minimum at a pH of 3 was obtained.



Scheme 1.16: structure of chlortalidone

Racemisation was proposed to proceed via formation of a carbocation at acidic pH and through a ring opening process at basic pH, as shown in **Scheme 1.17**. A retarding effect of liposomes on racemisation rates was also observed. The involvement of an intermediate carbocation, as shown in **Scheme 1.17**, was also proposed for the spontaneous racemisation of **1.13** in aqueous media, at room temperature, by Severin.⁴⁷



Scheme 1.17: mechanisms of acid-catalysed racemisation and base-catalysed ring-opening of chlortalidone as proposed by Lamparter *et al.*

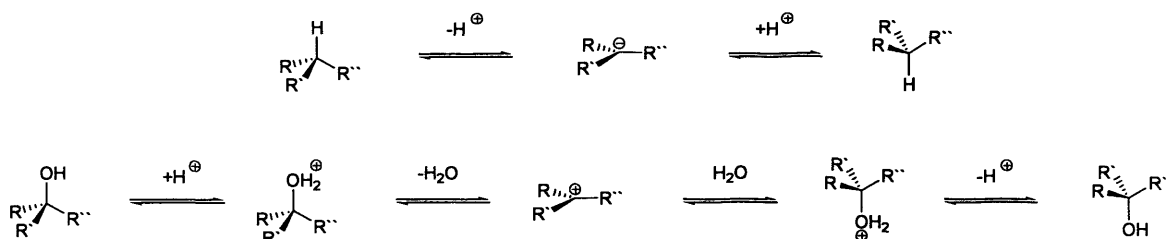
1.3. Structure and stereolability.

1.3.1. Chiral centres potentially liable to racemise.

Testa *et al.*²⁶, reviewing the literature on the stereolability of different chiral drugs, highlighted the fact that most configurationally unstable compounds were carbon acids

with general structure $R''R'CH$ where, often, one of the substituents attached to the chiral carbon was a carbonyl group. In case of carbon acids he therefore suggested the general possibility of base-catalysed racemisations, involving the corresponding carbanions as intermediates.

The presence of labile hydroxyl groups attached to chiral carbons was another structural motif related to configurational instability of molecules. In case of the presence of labile hydroxyl group, a mechanism involving acid catalysis and formation of an intermediate carbocationic species was suggested to be typical. Proposed mechanisms of racemisation for the two above mentioned classes of molecules are shown in **Scheme 1.18**.



Scheme 1.18: proposed mechanisms of racemisation for a generic carbon acid (**top**) and for a compound with a labile hydroxyl group attached to the chiral centre (**bottom**).

In case of carbon acids, two potential mechanisms of racemisation can be envisaged, as proposed by Testa *et al.*¹⁷ for the specific case of hydantoins (*vide infra*): 1) an S_E1 mechanism involving formation of a resonance-stabilised carbanion or 2) a concerted S_E2 pull-push mechanism. The two mechanisms can be distinguished by comparing the rate constants of racemisation with those of deuteration, as discussed in **Section 1.5**, provided phenomena of asymmetric solvation of carbanions can be excluded.⁴⁸

1.3.2. Stereolability and carbon acid acidity.

The possibility of relating the stereolability of chiral compounds to their chemical structures is a topic of great interest in drug development. We will focus our attention on the stereolability of carbon acids. Qualitative information about the factors affecting the stereolability of carbon acids can be obtained from the numerous studies present in the literature. Indeed, based on a collection of literature data on the racemisation of

several chiral drugs, Testa *et al.*^{22, 26} provided some guidelines for the prediction of the configurational stability of carbon acids with general structure R^*R^*RCH .

Table 1.1: List of functional groups affecting the configurational stability of carbon acids with general structure R^*R^*RCH .

Groups decreasing configurational stability (acid-strengthening groups)	Neutral groups	Groups increasing configurational stability (acid- weakening groups)
-COOR (strong)	-CH ₃	-COO ⁻
-CO-aryl (strong)	-CH ₂ CH ₃	-SO ₃ ⁻ (?) ^{a)}
-CONRR`		
-OH		
-Halogens (?) ^{a)}		
-Pseudohalogens (?) ^{a)}		
-NRR`		
-N = R		
-Aryl		
-CH ₂ -aryl		
-CH ₂ OH (?)		

a) Question marks indicate suspect cases

In Testa's papers a list of possible substituents at the chiral carbon of the generic carbon acid R^*R^*RCH are reported and classified as groups decreasing configurational stability, increasing configurational stability and neutral groups.⁴⁹ The classification is summarised in **Table 1.1**.

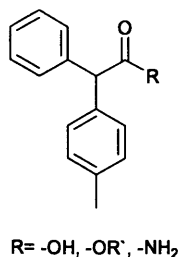
Testa pointed out that the racemisation of chiral compounds with the above shown structure was catalysed by hydroxide ion and bases and involved formation of the carbanion $R^*R^*RC^-$ as reaction intermediate.

According to Testa, for a centre to be configurationally unstable so as to be of concern from the pharmaceutical or pharmacological point of view, either of the two following structural conditions has to be met:

- 1) the presence of three carbanion-stabilizing groups directly attached to the chiral centre
- 2) the presence of two carbanion-stabilizing groups (of which one has to be strongly carbanion stabilising) and a neutral group directly attached to the chiral centre.

Wilson reviewed⁵⁰ experimental data from previous studies to help understand the effect of substituents on the stereolability of compounds of the form $R'RCHX$ where $X = -COR, -CN$ or $-NO_2$. The aim of the review was to give experimental evidence for the hypothesis of the equivalence of the processes of racemisation and tautomerisation for carbon acids with the mentioned structure. The author reported a classification of groups X , in order of increasing ability at inducing tautomeric change: $-COO^- < -CONH_2 < -COOH < -COOR < -COCl < -COR < -CN$. Wilson compared the ranking above with literature data from racemisation studies, and highlighted a parallel in the ability of the groups at promoting tautomeric change and racemisation. Wilson highlighted the unanimous opinion of several authors about the stabilising effect of the carboxylate group, the first substituent in the series. For example a study by Alhberg⁵¹ was mentioned, who found that neutralization of optically active α, α' -sulpho-di-*n*-butyric acid ($HOOCCH(C_2H_5)SO_2CH(C_2H_5)COOH$), to form the corresponding dicarboxylate, almost completely suppressed its racemisation. As far as substituents R' and R (in Wilson's notation) are concerned, if either of the two is an electron-withdrawing group, the stereolability of the molecule is invariably enhanced. Examples are reported illustrating the particularly strong destabilising effects of cyano and ammonium groups. Weaker effects were reported for halogens and the hydroxy group, for which the order $-Cl > -Br \gg -OH$, in terms of ability at favouring racemisation, was deduced based on studies of the stereolability of phenyl halogenoacetic esters. The effect of alkyl groups on the base-catalysed racemisation of acids with structure $SO_2(CHRCOOH)_2$ was also discussed by Wilson, citing a study by Ahlberg,⁵¹ suggesting the order $-CH_3 > -C_2H_5 > -CH(CH_3)_2$ for facilitation of racemisation. Finally the case of aryl groups, strong activating groups in prototropy, was treated. Wilson reported several studies demonstrating the ability of aryl groups at promoting racemisation. For example, Mc Kenzie and Wren observed that esters of the form $RCH(OH)COOR'$ were not generally prone to racemisation under basic conditions, unless R was a phenyl group.⁵² On the other hand, the phenyl group had to be directly

attached to a so-called “racemisable system” such as $-CH(OH)COOR$ ⁵² or $-CH(OH)NHR$ ⁵³, for a compound to be configurationally unstable. This observation is in line with the above-mentioned empirical “rules” reported by Testa *et al.*^{22, 26} for chiral stability. McKenzie *et al.* also observed particularly low configurational stability of optically active derivatives of phenyl-*p*-tolylacetic acid, whose structures are shown in **Scheme 1.19**, under the catalytic action of alkali.^{53, 54}



Scheme 1.19: general structure of the derivatives of phenyl-*p*-tolylacetic acid studied by McKenzie and co-workers.

As mention earlier, the potential stereolability of chiral compounds bearing a benzylic proton at the chiral centre was also predicted by Pepper *et al.*⁴³

Further examples of the effects of substituents at a chiral centre on its configurational stability are given in the study by Testa on the chiral inversion of 5-substituted hydantoins (*vide infra*).¹⁷

The ability of substituents at stabilising carbanions, i.e. increasing the acidity of carbon acids is therefore recognised as an important feature to take into consideration, when dealing with the racemisation of this class of compounds.

1.3.3. Quantitative studies on carbon acid acidity.

It has recently been proposed⁵⁵ that the stereolability of chiral α -substituted ketones could be predicted using the pK_a of these carbon acids. The pK_a themselves can be modulated by means of structural modifications. This hypothesis was successfully tested using two biologically active ketones.

The acidity of a carbon acid has both thermodynamic and kinetic implications and the kinetic acidity, measured by the rate at which a carbon acid donates protons to a base, can be correlated to its thermodynamic acidity.⁵⁶ Quantitative studies on the carbon acidities of several α -carbonyl carbon acids, in aqueous solution, were carried out by Richard *et al.*. The measurement of the rate constants of deprotonation by bases of

carbon acids allowed the evaluation of their pK_a through a rate-equilibrium relationship (**Equation 1.6**).

$$pK_a = pK_{aBH} + \log\left(\frac{k_{BH}}{k_B}\right) \quad \text{Equation 1.6}$$

In **Equation 1.6** pK_a is the equilibrium constant for ionisation of the carbon acid. pK_{aBH} is the pK_a of the conjugate acid is the base B , k_B and k_{BH} are the rate constant for deprotonation of the carbon acid by the base B to form the corresponding enolate and the rate constant for reprotonation of the free enolate by the conjugate acid of the base, BH , respectively.

A logarithmic plot of the rate constants for hydroxide-catalysed deprotonation (k_{OH^-}) of a series of neutral mono carbonyl compounds, statistically corrected for the number of acidic protons (p), versus their related statistically corrected pK_a values gave an excellent linear correlation. A linear rate-equilibrium correlation, shown in **Figure 1.2**, spanning a wide range of pK_a s was obtained from the combination of literature data and newly determined values. In **Figure 1.2** the rate equilibrium correlation for k_{HOH} , for the reverse protonation of the enolates of the carbon acids by solvent water, is also shown. Ketones, aldehydes, amides and esters⁵⁷⁻⁵⁹ were included in the rate-equilibrium correlations and quantitative information on the effect of substituents at the α -carbonyl carbon on the acidity of these classes of carbon acids was provided. Some reported pK_a values are listed in **Table 1.2**.

Equation 1.7 is the reported analytical expression describing the rate-equilibrium correlation shown in **Figure 1.2** where the value related to acetate anion has been excluded.

$$\log(k_{OH^-}/p) = 6.52 - 0.40 \cdot (pK_a + \log p) \quad \text{Equation 1.7}$$

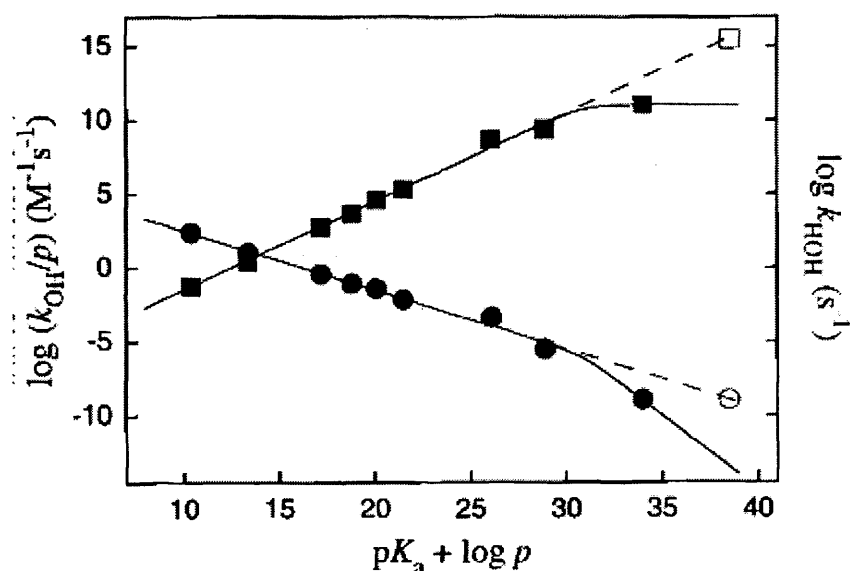


Figure 1.2: rate-equilibrium correlation for $\log(k_{OH^-}/p)$ for deprotonation by hydroxide ion of different α -carbonyl carbon acids (●) and for $\log k_{HOH}$ for the reverse protonation of the enolates of the same carbon acids by solvent water (■). The data points for the correlation between $\log(k_{OH^-}/p)$ and $pK_a + \log p$ (●), excluding the point at pK_a for acetate ion, are fitted to **Equation 1.7**. The dashed lines are obtained from extrapolations of the linear fits for $\log(k_{OH^-}/p)$ and $\log k_{HOH}$ “to the “impossible” values of $pK_a=38$ and $k_{HOH}=4 \cdot 10^{15} \text{ s}^{-1}$ for acetate anion”⁵⁹, values reported as open symbols in the graph. The graph has been reprinted with permission from reference⁵⁹ Copyright 2002, American Chemical Society.

Acetate anion, in fact, appeared to deviate from the correlation, causing a break in the linear fit. The downward break in the graph in **Figure 1.2** was attributed to a change in rate-determining step of reaction from the chemical step of proton transfer to solvent reorganisation. The rate of reprotonation of the particularly unstable enolate of the acetate anion was reported to be limited by the rate of reorganisation of solvent water molecules ($(k_{HOH})_{lim} = k_{reorg} \sim 10^{11} \text{ s}^{-1}$) to reach a “reactive position”.^{59, 60} Similarly, solvent reorganisation was demonstrated to be rate limiting for the hydroxide-ion-catalysed H/D exchange for acetonitrile.⁵⁹⁻⁶¹ No general-base catalysis of H/D exchange was observed and a primary kinetic isotope effect “not much larger than unity”⁶⁰ strongly supported the hypothesis of a mechanism of proton transfer where solvent reorganisation is rate limiting. The extrapolation of the linear correlation of k_{HOH} (■) in

Figure 1.2 shows that the “levelling” effect of rate-determining solvent reorganisation occurs for enolates of carbon acids with a pK_a of approximately 30.⁶⁰

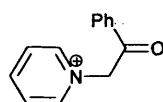
Table 1.2: Second order rate constants for deprotonation by hydroxide ion and pK_a for ionization in water of some α -carbonyl carbon acids, at 25°C and $I=1M$ (KCl), reported in papers by Richard *et al.*

Carbon acid	$k_{OH^-} / M^{-1}s^{-1}$	pK_a
$CH_3CHO^a)$	1.17	16.7
$CH_3COCH_3^a)$	0.22	19.3
$CH_3COOEt^a)$	$1.2 \cdot 10^{-3}$	25.6
$CH_3COSEt^a)$	0.02	21.0
$PhCH_2CHO^a)$	20	13.1
$Ph_2CHCHO^a)$	254	10.4
$CH_3CONH_2^b)$	$9.5 \cdot 10^{-6}$	28.4
$CH_3CONMe_2^b)$	$2.9 \cdot 10^{-6}$	29.4
$CH_3COO^-^b)$	$3.5 \cdot 10^{-9}$	~33.5

a) Data from reference⁵⁸

b) Data from reference⁵⁹

Richard *et al.* extended their studies on carbon acid acidities to the determination of the pK_a of amino acids and amino acids derivatives.^{62, 63} Important differences between neutral and cationic species were observed. The pK_a of the glycine zwitterion $^+NH_3CH_2COO^-$ and its derivatives, *viz.* *N*-protonated glycine methyl ester $^+NH_3CH_2COOMe$, betaine methyl ester, $^+Me_3NCH_2COOMe$, and betaine $^+Me_3NCH_2COO^-$, were determined. Glycine methyl ester and the betaine derivatives were used as “equivalents” of glycine where the ionization state is fixed and therefore not pH dependent, allowing an easier investigation of the effect of the ionisation state of glycine on its pK_a . In Table 1.3 the pK_a of glycine derivatives, of the cationic ketone 1.14 (Scheme 1.20) and their second-order rate constants for deprotonation by hydroxide ion are reported. Values for ethyl acetate are also reported for comparison.



1.14

Scheme 1.20: structure of the cationic ketone **1.14** included in the rate-equilibrium correlation shown in **Figure 1.3**, reported by Richard *et al*

Table 1.3: Second order rate constants for deprotonation by hydroxide ion and pK_a for ionization in water of ethyl acetate and glycine derivatives and **1.14**, at 25°C and $I=1M$ (KCl), determined by Richard *et al*.

Carbon acid	$k_{OH^-} / M^{-1}s^{-1}$	pK_a
CH_2COOEt	$1.2 \cdot 10^{-3}$	25.6
$^+NH_3CH_2COOMe$	4.1	21.0 ± 1.0
$^+Me_3NCH_2COOMe$	390	18.0 ± 1.0
$^+NH_3CH_2COO^-$	$4.5 \cdot 10^{-5}$	28.8 ± 0.5
$^+Me_3NCH_2COO^-$	$3.3 \cdot 10^{-4}$	27.3 ± 1.2
1.14	$1.8 \cdot 10^{-5}$	10.9

From the data in **Table 1.3** the acidifying effect of the $\alpha-NR_3^+$ (R=H, Me) groups is evident. The lower acidifying effect of the $\alpha-NH_3^+$ group as compared to the $\alpha-NMe_3^+$ was found to be in line with the polar effects of the groups as quantified by the inductive substituent constants σ_1 ,⁶⁴ which have been reported to be $\sigma_1 = 0.92$ and 0.60 for $\alpha-NMe_3^+$ and $\alpha-NH_3^+$, respectively.^{62,65} It was highlighted⁵⁹ that the same 4.6 units in pK_a difference between ethyl acetate and *N*-protonated glycine methyl ester is reflected in the pK_a difference between acetate anion (value reported in **Table 1.2**) and glycine zwitterions.

Positive deviations from the linear rate-equilibrium correlation for neutral carbon acids were observed for the cationic species $^+NH_3CH_2COOMe$ and $^+Me_3NCH_2COOMe$ as shown in **Figure 1.3**.

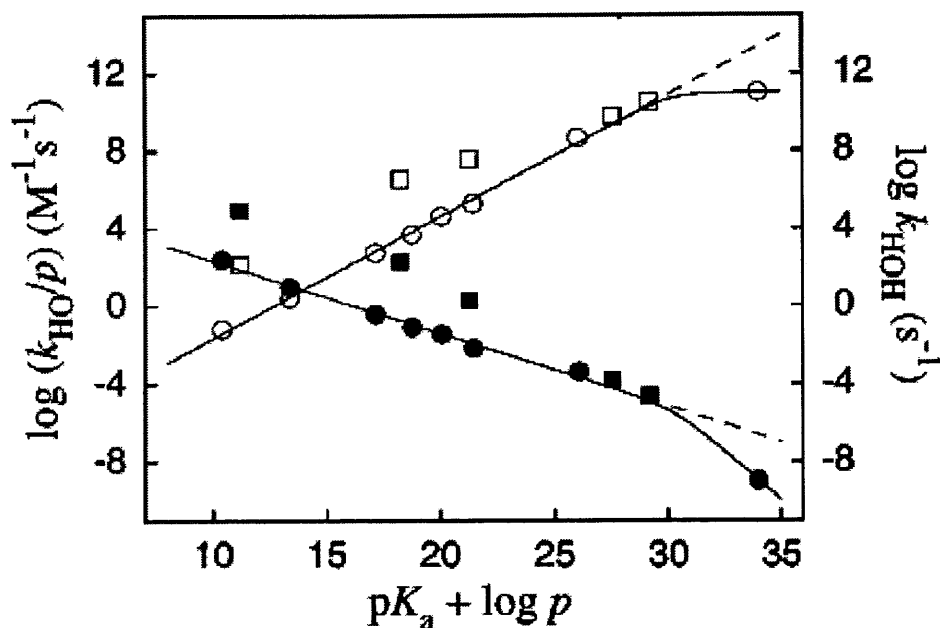


Figure 1.3: rate equilibrium correlation for $\log(k_{OH^-}/p)$ for deprotonation by hydroxide ion of different neutral aldehydes, ketones and esters (●) and for $\log k_{HOH}$ for the reverse protonation of the enolates of the same carbon acids by solvent water (○). (■) Data for deprotonation of amino acid derivatives and the cationic ketone **1.14**, shown in **Scheme 1.20**. (□) Data for the reprotonation of the enolates of amino acid derivatives and of ketone **1.14**, values reported as open symbols in the graph. The graph has been reprinted with permission from reference.^{59,62} Copyright 2000, American Chemical Society.

The very different values of k_{OH^-} for reactions with “similar thermodynamic driving force” were explained in term of smaller Marcus intrinsic barriers (Λ_1), for deprotonation of cationic carbon-acids as compared to neutral ones. The lower intrinsic barriers⁶⁰ (Λ_1 in **Figure 1.4**) for proton transfer due to cationic substituents on the α -carbonyl carbon are attributed to two different effects: 1) electrostatic interaction between hydroxide ion and the cationic α -NH₃⁺ groups on the carbon acids which stabilises the transition state for deprotonation and 2) a decreased resonance stabilisation of the enolate and a higher localisation of the negative charge on the carbonyl carbon due to the electron-withdrawing effects of the α -NMe₃⁺ and α -NH₃⁺ groups.⁶²

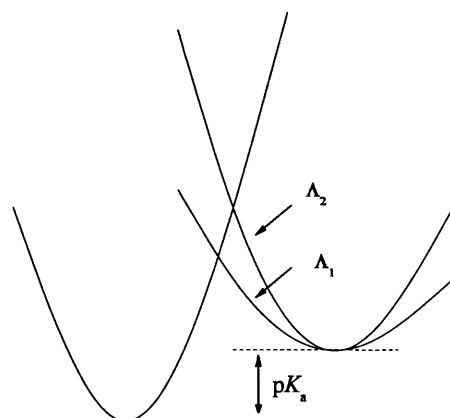
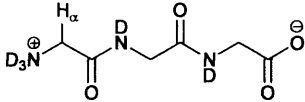
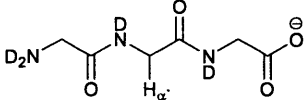


Figure 1.4: schematic representation of free-energy profiles for proton transfer reactions with different intrinsic barriers.

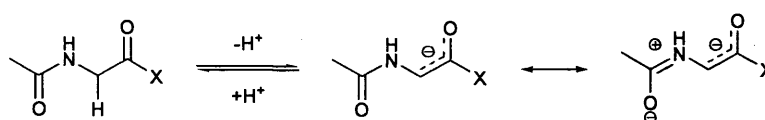
The good linear rate-equilibrium correlations for neutral and cationic α -carbonyl carbon acids allowed an estimate of the acidities of α -carbonyl protons in different glycine derivatives as well as in peptides.⁶⁶ The second-order rate constants for deprotonation of the carbon acids by deuterioxide ion were determined and, from these, pK_a values were obtained by interpolation or extrapolation from the previously determined linear correlations. Deprotonation at the α -amino carbon of protonated *N*-terminal amino acids were found to proceed much faster than deprotonation of the corresponding α -amino carbon of an internal amino acid, as illustrated by the data for the tripeptide glycylglycylglycine (**Table 1.4**). The observation confirms the strong acidifying effect of cationic α -NR₃⁺ groups. From the kinetic data obtained for glycylglycylglycine, it was estimated that the α -amino carbon of the *N*-terminal amino acid in a protein (such as H _{α} for glycylglycylglycine, **Table 1.4**) should undergo deprotonation approximately 130-fold faster than an α -amino carbon of an internal amino acid (like H _{α '} for glycylglycylglycine, in **Table 1.4**).

Table 1.4 Second-order rate constants for deprotonation by hydroxide ion and pK_a for ionization in water of different carbons in the tripeptide glycylglycylglycine, at 25 °C and an ionic strength (I) of 1 M (KCl), determined by Richard *et al.* (reported data refer to the protons named as H_α in the formulas).

Carbon acid ^{a)}	$k_{OH^-} / M^{-1}s^{-1}$	pK_a
	0.23	25.1
	$3.9 \cdot 10^{-4}$	25.9

a) The two protonated forms of glycylglycylglycine are reported to be the reactive species in the deuterium exchange reactions of the acidic protons of the *N*-terminal and of the internal amino acid of the tripeptide.⁶⁶

The study on glycine derivatives and peptides⁶⁶ also provided information on the effects of α -NHCOCH₃ and α -NH₃⁺ groups on the acidity of carbonyl compounds. The comparison of the pK_a of α -NHCOCH₃ and α -NH₃⁺ substituted carbon acids with the pK_a of their unsubstituted analogues, or of unsubstituted compounds of closely related structure, highlighted the similar acidifying effects of the α -NHCOCH₃ and α -NH₃⁺ groups. The ammonium group is more strongly electron-withdrawing than the NHCOCH₃ group and should therefore have a stronger stabilising effect on the negative charge of the enolate. The “extra stabilisation” provided by an α -NHCOCH₃ group was proposed to arise from an “adjustment of the structure and charge distribution of the α -amide group” leading to increased stabilising electrostatic interactions between opposite charges in the enolate, as shown in **Scheme 1.21**.



Scheme 1.21: stabilisation of the enolate of a generic α -carbonyl carbon acid by the α -NHCOCH₃ group as proposed by Richard *et al.*

In the absence of changes in rate determining step, Richard *et al.* showed that pK_a values for neutral or cationic α -carbonyl compounds can be obtained from their rate constants for hydroxide-catalysed deprotonation (k_{OH^-}), by interpolation or extrapolation of good linear rate-equilibrium correlations obtained by the authors.

1.4. The hydantoins ring in drug development

In this thesis the racemisation of 5-substituted hydantoins, chosen as model chiral compounds, has been investigated.

Hydantoins and related rings are contained in a number of drugs and drug-like molecules. The hypnotic properties of hydantoins have been known since 1916 when 5-ethyl-5-phenylhydantoin, known as Nirvanol, was introduced in therapy as a hypnotic drug with comparable activity but lower toxicity than phenobarbital. Nirvanol was also, later, used for the treatment of chorea.⁶⁷ One of the best known hydantoins used in medicine is 5,5-diphenylhydantoin, marketed under different trade names such as dilantin. Dilantin was first used in 1938 for the treatment of epilepsy and was also recommended in case of anoxia induced by high altitudes.⁶⁷ More recent pharmacological studies testify of a current keen interest in hydantoins and prove the importance of this class of compounds in drug discovery. 5,5-diphenylhydantoin is still used as anticonvulsant drug.⁶⁸ The anticonvulsant properties of 5,5-diphenylhydantoin have been proposed to reside in the ability of the molecule at acting as a sodium channel blocker.⁶⁹ Several studies relating the structure of hydantoins to their anticonvulsant activity are present in the literature, aiming both at the development of new anticonvulsant drugs and at elucidating the structure of the drug-binding site of the neuronal voltage-gated sodium channel.⁶⁸⁻⁷³ Local anaesthetics, some antiarrhythmic and anticonvulsant drugs such as 5,5-diphenylhydantoin are, in fact, now accepted to share a common binding site on the sodium channel protein complex. Structural information on the binding site of drugs of the sodium channel would improve future development of these important classes of therapeutic agents.⁷³

In addition to the use of hydantoins as hypnotic, anticonvulsant, anaesthetic and antiarrhythmic agents, the interest in the hydantoin ring in drug discovery appears to span a very wide range of therapeutic fields. Hydantoin derivatives showed interesting activities as androgen receptor antagonists⁷⁴ and as tissue selective androgen receptor

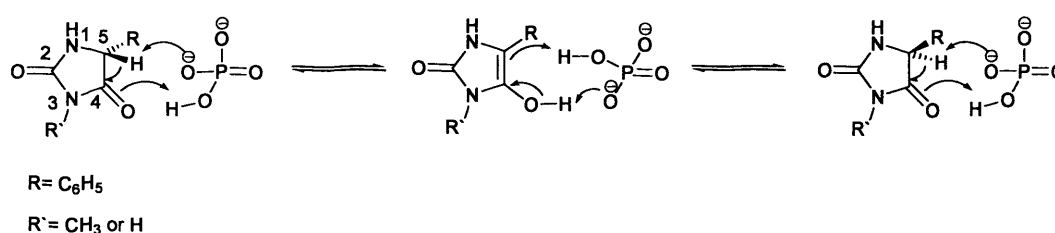
modulators⁷⁵ which makes them attractive prospective drugs for the treatment of prostate cancer⁷⁴ and other androgen-dependent disorders.⁷⁵ Further recent studies report on the activity of phenylmethylene hydantoins as inhibitors of the growth of some prostate⁷⁶ and lung⁷⁷ cancer cell lines. Diphenylhydantoin and other hydantoin derivatives have been proposed as prospective drugs for the treatment of HIV infection since they appeared to interfere with the entry of viral strains into the host cells.^{78, 79} Different 3,5-substituted hydantoins were proposed as interesting compounds with potential use for the treatment of rheumatoid arthritis^{80, 81} and pulmonary emphysema.⁸⁰ Literature studies reported affinity of 5,5'-diphenyl hydantoins⁸² and 5,5'-diphenyl thiohydantoins⁸³ for the human CB₁ cannabinoid receptor. The hydantoin ring has thus been proposed as an attractive scaffold for the development of a new class of compounds able to modulate the activity of the cannabinoid system, useful for the treatment of several diseases associated to disorders of this system. Tetrahydroisoquinoline-hydantoin derivatives have been suggested as potential sigma-1 receptor modulators, useful for the treatment of cocaine addiction and other dysfunctions associated with sigma-1 receptors.^{84, 85} Thiohydantoin derivatives have also been proposed as potential hypolipidemic agents.⁸⁶

1.5. The racemisation of hydantoins

In spite of the current keen interest in the hydantoin ring in drug design, different interpretations are reported in the literature on the mechanisms of racemisation of this class of compounds.

Dakin⁸⁷, as early as 1910, observed that optically active 5-substituted hydantoins racemised in alkaline solutions. The author proposed that the mechanism of racemisation involved a process of keto-enol tautomerism with formation of an intermediate planar enolate (**Scheme 1.22**). The configurational stability of the corresponding uramido acids of the hydantoins and of a 5,5-disubstituted hydantoin (structures **1.15** and **1.16** in **Scheme 1.22**), where similar keto-enol tautomerism is not possible, were given as evidence for the proposed mechanism. In further experiments Dakin tested the configurational stability of some proteins because of the similarity of their molecular structures with the groupings present in the hydantoin ring. Alkaline solutions of different proteins, at room temperature, showed a decrease in, but not a complete loss of, optical activity. The finding was explained with the hypothesis that

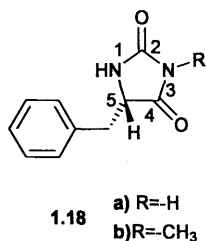
the authors proposed a mechanism as shown in **Scheme 1.24**, involving rate-determining proton abstraction by the dibasic form of the buffer. The mechanism involves a concerted exchange of protons between the divalent phosphate and the hydantoin, leading to a neutral enol as intermediate. The donation of the proton by water molecules, instead of by phosphate, is however not excluded. The reason for proposing a concerted mechanism is that the presence of an intermediate carbanion was considered unlikely by the authors since it should involve formation of a basic species in a medium where efficient proton donors such as water and phosphate molecules are present.



Scheme 1.24: proposed mechanism of phosphate catalysed racemisation of (*R*)-5-phenylhydantoin.

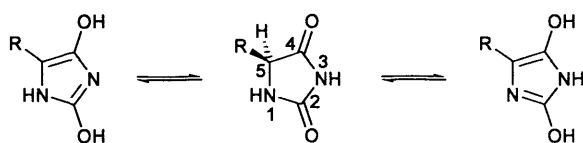
Lazarus⁸⁹ studied the racemisation of (*S*)-5-benzylhydantoin **1.18a** and (*S*)-*N*-methyl-5-benzylhydantoin **1.18b**, shown in **Scheme 1.25**, in aqueous buffers in a pH range between 6 and 14, at 37 °C. Racemisation was reported to be hydroxide- and buffer-catalysed. The kinetics of racemisation of (*S*)-5-benzylhydantoin were found to be complicated by the acidity of the proton in position 3 of the hydantoin ring. A pK_a of 8.65 ± 0.10 was reported for 5-benzylhydantoin. To distinguish between the kinetically equivalent processes of general-base catalysis acting on the protonated form of **1.18a** and general-acid catalysis acting on the deprotonated form, the kinetics of racemisation of (*S*)-*N*-methyl-5-benzylhydantoin **1.18b** were investigated. (*S*)-*N*-methyl-5-benzylhydantoin can be seen as an “equivalent” of the protonated form of (*S*)-5-benzylhydantoin. Evidence for hydroxide catalysis on protonated and deprotonated forms of **1.18a** was provided and these pathways come in addition to catalysis by phosphate, tris and carbonate buffers. The racemisation of **1.18b** was also found to be catalysed by hydroxide and buffers. Brønsted plots for racemisation of **1.18a** and **1.18b** gave values of β of 0.59 and 0.51, respectively. Based on the experimental data, a

mechanism of racemisation involving general-base catalysis acting on the protonated form of (*S*)-5-benzylhydantoin was proposed. A transition state was depicted with the proton in position 5 being halfway between the hydantoin and the buffer species.



Scheme 1.25: structures of (*S*)-5-benzylhydantoin **1.18a** and (*S*)-*N*-methyl-5-benzylhydantoin **1.18b**.

Bovarnick and Clarke⁹⁰ discussed the observations and conclusions reported by Dakin (briefly described earlier) about the mechanism of racemisation of 5-substituted hydantoins. According to the authors, Dakin overlooked the possibility of tautomerism involving the amide-imide system in the hydantoin ring and in peptides. Amide-imide tautomerism in the hydantoin ring (**Scheme 1.26**), was proposed to be likely.



Scheme 1.26: tautomerism in a generic 5-substituted hydantoin, as proposed by Bovarnick and Clarke.

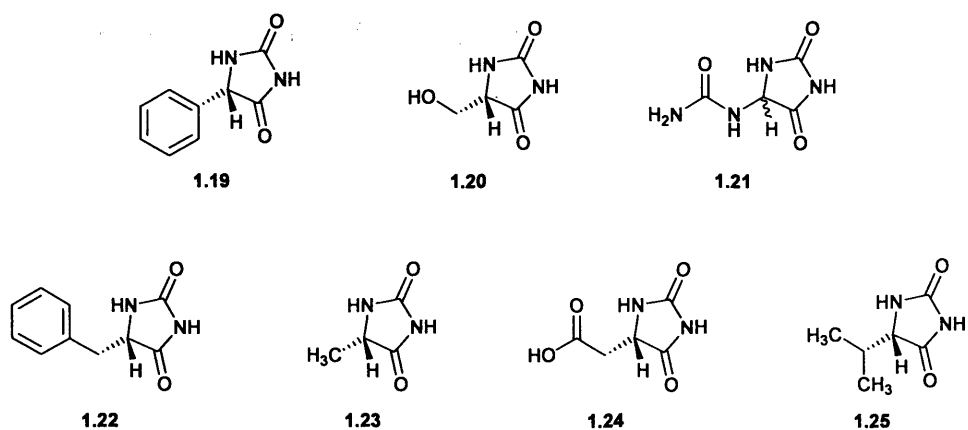
Assuming the described tautomerism was responsible for the racemisation of hydantoins, the authors argued that substitution of one or both the protons in positions 1 and 3 of the ring should retard and prevent racemisation, respectively. A series of optically active substituted hydantoins was therefore prepared and the racemisation reactions of these compounds in 0.02 N NaOH solutions in 95% ethanol, at 20-25 °C, were studied (**Table 1.5**). **Table 1.5** shows that racemisation could still occur in the 1, 3 substituted hydantoins and in some cases was even faster, for example in the case of 3-

phenyl-5-*p*-methoxybenzylhydantoin. The authors therefore proposed that ionisation of the hydrogen attached to the chiral centre should be the key step through which racemisation takes place. Racemisation should, therefore, be affected by the alkalinity of the medium and by the electron withdrawing ability of the substituents attached to the chiral centre.

Table 1.5: kinetic data reported by Bovarnick and Clarke on the racemisation of different substituted hydantoins in 0.02 N NaOH solutions in 95% ethanol.

Hydantoin	Molarity of hydantoin	Half Time/ hours
5- <i>p</i> -Hydroxybenzylhydantoin	0.0046	15
3-Phenyl-5- <i>p</i> -hydroxybenzylhydantoin	0.0222	2.5
1-Methyl-5- <i>p</i> -hydroxybenzylhydantoin	0.030	11.5
1-Methyl-3-phenyl-5- <i>p</i> -hydroxybenzylhydantoin	0.0287	0.5
5- <i>p</i> -Methoxybenzylhydantoin	0.0267	45
5- <i>p</i> -Methoxybenzylhydantoin	0.0046	9
3-Phenyl-5- <i>p</i> -methoxybenzylhydantoin	0.026	<0.1

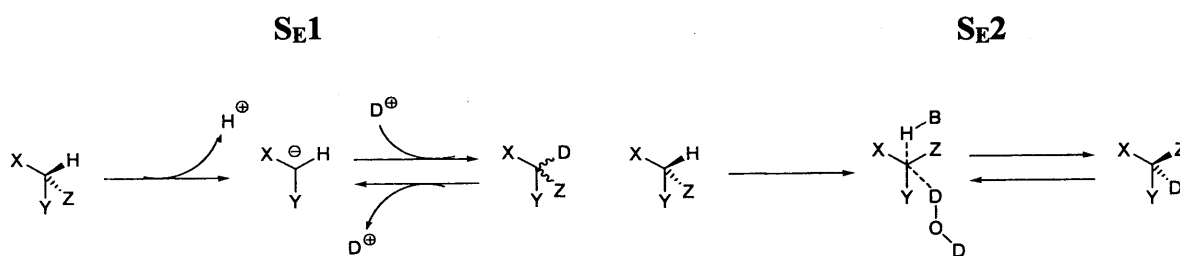
Testa *et al.*¹⁷ reported a study on the racemisation of a series of (*S*)-5-substituted hydantoins (**Scheme 1.27**), mainly aiming at elucidating the mechanisms of racemisation of this class of compounds. A concerted S_E2 pull-push mechanism was proposed, as opposed to a stepwise process involving formation of an intermediate carbanion. The two hypotheses and their “kinetic implications”, which will be discussed below, are illustrated in **Scheme 1.28**. Both H/D exchange and racemisation of the hydantoins were studied. Preliminary H/D exchange experiments on (*S*)-5-methylhydantoin (**1.23** in **Scheme 1.27**) in D₂O phosphate buffers with a pD of 7.4, at 37 °C, followed by ¹H NMR spectroscopy, showed general-base catalysis.



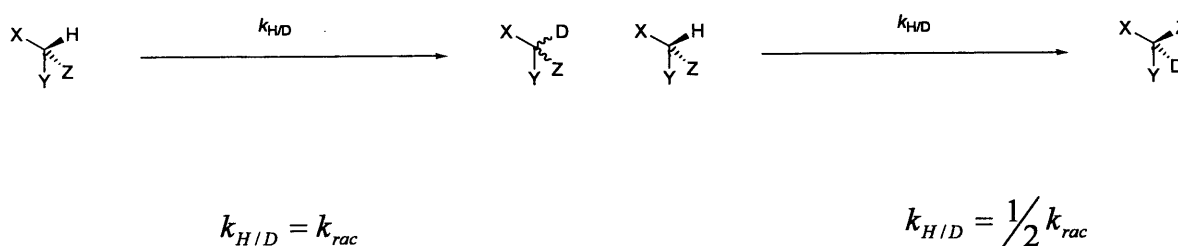
Scheme 1.27: structures of hydantoin, studied by Testa *et al.*

The kinetics of H/D exchange and racemisation of (*S*)-5-phenyl hydantoin **1.19** and (*S*)-5-benzylhydantoin **1.22** were studied at different temperatures in mixtures of D₂O phosphate buffer (pD=7.4, 0.1M, 0.22M) and d₆-DMSO in the ratio 1:1 (v:v). The racemisation was also followed in undeuterated media composed of H₂O phosphate buffer pH=7.4, 0.1M, 0.22M) and DMSO in the same ratio. A “modest solvent isotope effect” for racemisation was observed. Reported ratios of rate constants of racemisation in non-deuterated and deuterated media ($k_{\text{H}_2\text{O}}/k_{\text{D}_2\text{O}}$) were 1.13 ± 0.05 and 1.24 ± 0.08 for **1.19** and **1.22**, respectively.⁹¹ The activation energies for H/D exchange and for racemisation in deuterated and non-deuterated media were evaluated and, for both **1.19** and **1.22**, they appeared to be the same within experimental error.

Chemical Model



Kinetic Model



Scheme 1.28: comparison between S_E1 and S_E2 mechanisms for racemisation of 5-substituted hydantoins.

It was therefore concluded that H/D exchange and racemisation shared a common mechanism. For both hydantoins, **1.19** and **1.22**, the rate constants of deuteration were observed to be approximately half those of racemisation suggesting that racemisation proceeds through an S_E2 mechanism. In the alternative S_E1 mechanism, deuteration and racemisation should proceed at the same rate since the process involves an intermediate carbanion that can be captured with equal probability from each side. Faster rates of racemisation as compared to deuteration are consistent, on the other hand, with an S_E2 mechanism. In an S_E2 process each deuteration event is accompanied by inversion of configuration, and therefore two molecules of hydantoin are racemised per molecule undergoing deuteration, as shown in **Scheme 1.28**. In other words in an S_E2 mechanism the rate constants of deuteration are equal to the rate constant of enantiomerisation and therefore half those of racemisation, as described by the kinetic models in **Equations 1.1** and **1.2** on pages 3-4. Comparison of the rate constants for H/D exchange of **1.19-1.25**, in the mixed medium D₂O phosphate buffer (pD 7.4, 0.1M, 0.22M I) and d₆-

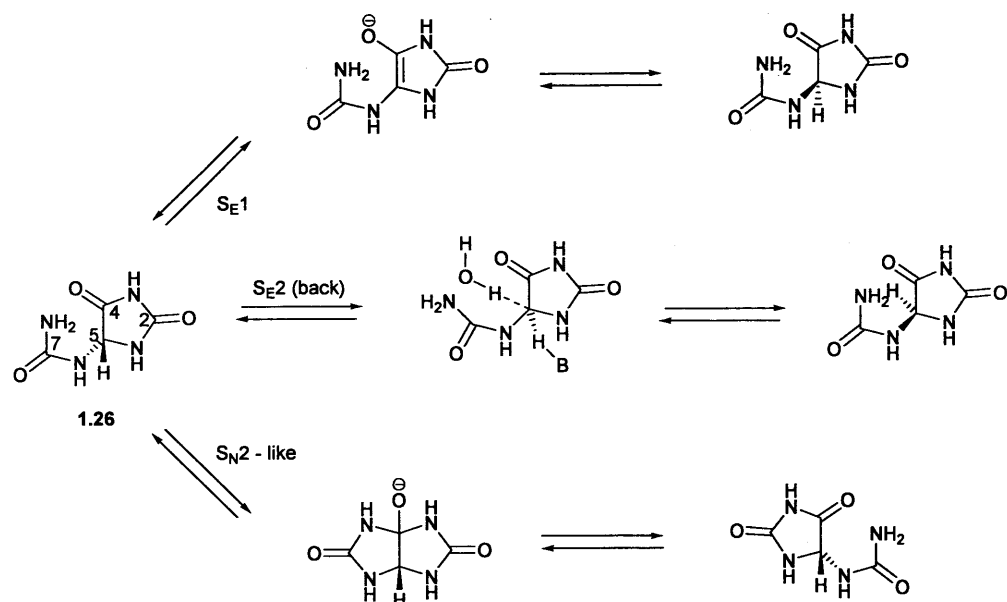
DMSO highlighted the marked effects of the substituents attached to the chiral centre on the stereolability of the hydantoins. Rate constants were found to increase with substituents attached to the chiral centre in the order $-\text{CH}(\text{CH}_3)_2 < -\text{CH}_2\text{COOH} < -\text{CH}_3 < -\text{PhCH}_2 < \text{-ureido} < -\text{CH}_2\text{OH} < \text{-phenyl}$, with a 1800-fold rate increase going from $-\text{CH}(\text{CH}_3)_2$ to $-\text{phenyl}$, as shown in **Table 1.6**.

Table 1.6: rate constants of H/D exchange for 5-substituted hydantoins in a mixture D_2O phosphate buffer at pD 7.4, 0.1M, 0.22 M *I* and d_6 -DMSO in a volume ratio of 1:1, at 50 °C.

Substrate	$k_{\text{H/D}}/\text{h}^{-1}$
1.19	11.3±1.9
1.20	0.280±0.055
1.21	0.118±0.006
1.22	0.060±0.004
1.23	0.033±0.001
1.24	0.017±0.001
1.25	0.0060±0.0007

No correlation was found between the rate constants of H/D exchange and either enthalpies of activation (ΔH^\ddagger) or entropies of activation (ΔS^\ddagger) alone. The relative stereolabilities of the hydantoins appeared to be determined by both the values of ΔH^\ddagger and ΔS^\ddagger . It was concluded that inductive and resonance effects, stabilising the anionic transition state and reflected in the ΔH^\ddagger term, can only partially explain the different reactivities of the hydantoins.

A later study by Kahn and Tipton⁹² on the racemisation of (*S*)-5-ureido-hydantoin, also called allantoin, (**1.26** in **Scheme 1.29**) in D_2O phosphate buffers suggested that three possible mechanisms of racemisation could be envisaged, among which the $\text{S}_{\text{E}2}$ mechanism proposed by Testa *et al.*,¹⁷ for racemisation of 5-substituted hydantoins.



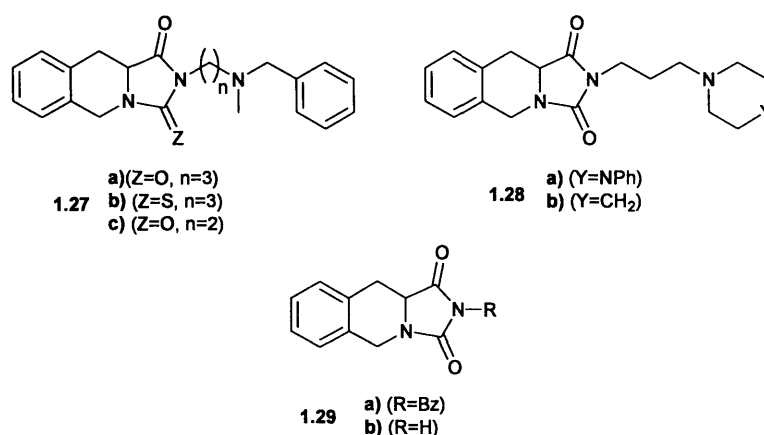
Scheme 1.29: proposed mechanisms for racemisation of allantoin.

Allantoin was found to racemise both via S_E mechanisms (no distinction was made between S_{E1} and S_{E2} in the paper and both hypothesis are shown in **Scheme 1.29**, as well as in the paper by Kahn and Tipton) and via an intramolecular process involving a bicyclic intermediate, as shown in **Scheme 1.29**. The S_E mechanism was studied by determining the rate constants of exchange of the proton attached to the chiral carbon. The intramolecular process, defined as an S_{N2} -like mechanism, was monitored using ^{13}C NMR spectroscopy, by measuring the rate of C2-C7 scrambling in analogues of allantoin whose carbons in position 2 and 7 had been labelled with ^{13}C . The “ S_{N2} -like” mechanism appeared to be the main pathway of racemisation. Both the S_E and the S_{N2} -like routes of racemisation followed pseudo-first-order kinetics, with the S_E mechanism being general-base catalysed, in agreement with Testa’s findings. The overall rates of racemisation, followed by CD spectroscopy, were found to be independent of buffer concentration, confirming that the “ S_{N2} -like” mechanism is the dominant pathway. Attempts at identifying the mechanism of the pathway where racemisation accompanied H/D exchange were unsuccessful.

Lee and Fang⁹³ studied the racemisation of (*R*)-5-phenylhydantoin and of (*R*)-5-(4-hydroxyphenyl) hydantoin in aqueous solution at pH values between 5.5 and 8.5 and at different temperatures. Racemisation followed a first-order kinetic law, with rate constants increasing with increasing pH and with increasing temperature. Based on

previous studies, a mechanism of racemisation involving keto-enol tautomerism was proposed. Slightly higher rates of racemisation were observed for (*R*)-5-(4-hydroxyphenyl) hydantoin as compared with (*R*)-5-phenylhydantoin; at pH 7.5 and 25 °C the half-lives for (*R*)-5-(4-hydroxyphenyl) hydantoin and (*R*)-5-phenylhydantoin are reported to be 191.9 and 209.8 minutes, respectively. The slightly higher rate constants of racemisation for (*R*)-5-(4-hydroxyphenyl) hydantoin were attributed to the electron-withdrawing effect of the hydroxyl substituent on the phenyl ring, increasing the stabilization of the enolate structure.

A recent study has been published by Cabordery *et al.*⁸⁴ on the racemisation of some tetrahydroisoquinoline hydantoins (tic-hydantoins), in ethanolic and aqueous media. The structures of the hydantoins are shown in **Scheme 1.30**.



Scheme 1.30: structures of the tetrahydroisoquinoline hydantoins studied by Cabordery *et al.*

Most kinetic experiments in aqueous media were performed in 75:25 (v:v) mixtures of phosphate buffers at pH 7.4 and ethanol, at different buffer concentrations. Preliminary experiments showed the higher stereolability of hydantoin **1.27b** as compared to **1.27a**. A linear increase of the first-order rate constant of racemisation with buffer concentration was observed for both **1.27a** and **1.27b**, suggesting general-base catalysis. The racemisation of **1.27b** was followed in mixed aqueous-ethanolic media where the pH of the buffers used were 2.5, to avoid the high rates of racemisation at higher pH values. The rate constants for racemisation of **1.27a** and **1.27b** were determined in non-deuterated and in deuterated buffered media, at 25 and 15 °C, respectively. The rate constants of H/D exchange of **1.27a** and **1.27b**, under the same experimental conditions as for racemisation studies, were also determined. Small solvent kinetic isotope effects

of approximately 1.5 were found for both hydantoins **1.27a** and **1.27b**, in accordance with results reported by Testa *et al.* in their study on 5-substituted hydantoins¹⁷ (*vide supra*). Almost equal rate constants for racemisation and deuteration were obtained for hydantoin **1.27a**. An S_E1 mechanism for racemisation of **1.27a** was therefore proposed, involving formation of a planar carbanion which is then non-stereospecifically reprotonated. On the contrary, for hydantoin **1.27b**, at pD=7.3, the rate constant of deuteration was found to be half that of racemisation suggesting that deuteration occurred with inversion of configuration. An S_E2 mechanism, as proposed by Testa¹⁷, is therefore proposed for hydantoin **1.27b**.⁹⁴ The rate constants for racemisation of hydantoins **1.27c**, **1.28a, b** and **1.29a**, determined in a 75:25 (v:v) mixture of phosphate buffers 0.33 mM with pH 7.4 and ethanol, at 25 °C, were found to be similar to those of **1.27a** (the reported half life is 28.8 hours), under identical conditions. Reported half lives for **1.27c**, **1.28a, b** and **1.29a**, were variable between 30 and 46 hours, suggesting a small influence of the nature of the side chain on the rate constants of racemisation. A slightly smaller rate constant of racemisation was reported for compound **1.29b** (half-life of 62 hours), with no substituent on the nitrogen in position 3 of the hydantoin ring. The authors highlight the analogy with results published by Bovarnick and Clarke⁹⁰ (*vide supra*) who reported an higher stereolability of 3-phenyl-5-p-methoxybenzylhydantoin as compared to 5-p-methoxybenzylhydantoin (**Table 1.5**).

From the results of the studies on the racemisation of 5-substituted hydantoins, briefly described in this section, it appears that the mechanism of racemisation of this class of compounds is still under discussion. An S_E1 mechanism is, in general, recognised for racemisation and H/D exchange of ketones.^{17, 95-97} We will mention here the kinetic studies by Wilson *et al.* on the model ketone 2-o-carboxybenzyl-1-indanone.^{95, 98} Bromination and racemisation of 2-o-carboxybenzyl-1-indanone were reported to proceed at the same rate with ionisation being the rate determining step of both processes.⁹⁵ A primary kinetic isotope effect k_H/k_D of 3.0 at 45 °C was observed for base-catalysed bromination of the ketone.⁹⁸ A stepwise mechanism involving a short lived enolate intermediate has also been proposed by Richard *et al.* for base-catalysed deuterium incorporation into a wide range of α -carbonyl carbon acids (*vide supra*).^{57, 58, 62, 66} S_E2 mechanisms are however proposed, in the literature, for racemisation of hydantoin derivatives, along with S_E1 pathways (*vide supra*).

1.6. Solvent effects on reactions of racemisation and H/D exchange.

1.6.1 Solvents and solvent properties

The crucial role of the solvent in chemical reactions has been noticed since the very early stages of chemical investigations but many aspects of “solvent effects” still remain beyond our quantitative understanding. Hence, correlations between solvent effects on reactions and physical properties of the solvents are, usually, not straightforward.

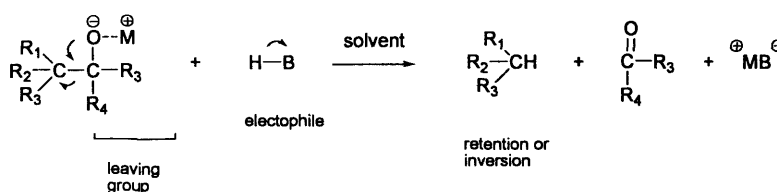
A comprehensive classification of solvents is not easy due to the diversity of physical and chemical properties within the wide range of organic and inorganic solvents.⁹⁹ However, extending a classification made by Parker,¹⁰⁰ solvents can be conveniently divided in three main groups.^{101, 102}

- a) Protic: this class include solvents that possess hydrogen atoms bound to electronegative atoms (OH, NH, *etc.*). Protic solvents usually have high dielectric constants ($\epsilon > 15$), are hydrogen-bond donors and are, therefore, good anion solvators. Water and alcohols belong to this class.
- b) Dipolar-aprotic: solvents of this class have no acidic protons but possess large dielectric constants ($\epsilon > 15$), and large dipole moments ($\mu > 8.3 \cdot 10^{-30}$ Cm)¹⁰¹. Dipolar-aprotic solvents are good electron-pair donors (EPD solvents) and therefore, good cation solvators through their lone pair of electrons. On the other hand their ability at solvating anions is poor (*vide infra*). Acetone, acetonitrile, DMSO are examples of dipolar aprotic solvents.
- c) Non-polar aprotic: this class is characterised by low dielectric constants ($\epsilon < 15$) and low dipole moments ($\mu < 8.3 \cdot 10^{-30}$ Cm)¹⁰¹. Solvents of this class do not have acidic protons and donor/acceptor properties and therefore show only weak interaction with the solute. Hydrocarbons, halocarbons and ethers are typical solvents of this class.

1.6.2. The effect of the medium on racemisation and H/D exchange reactions: examples from the published literature

Several literature studies testify to the effects that the reaction medium can have on the rate constants of racemisation and H/D exchange reactions of different chiral substrates. For example, in their study of the racemisation of ibuprofen (*vide supra*) Xie *et al.*³⁹

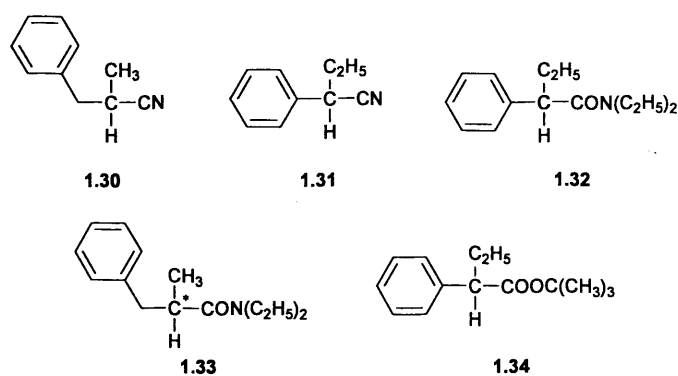
reported marked effects of the reaction medium on the rate constants of base-catalysed racemisation of the drug. Mixtures of organic solvents and aqueous 1.25 M NaOH in the proportion 5:2 (v:v) were investigated. Co-added glycol, ethanol and dimethylformamide were found to decrease the rate constant of racemisation while DMSO and dioxane showed a rate-increasing effect. No explanation was provided to explain the reported effects. Some investigations more specifically addressed the role of the medium on different aspects of reactions of racemisation and H/D exchange. We mention here a series of studies by Cram *et al.*¹⁰³⁻¹⁰⁸ on solvent effects on reactions of racemisation and H/D exchange of different substrates. The studies are particularly focused on the changes of stereochemical course of reaction induced by changes of the solvent. The authors carried out the studies on H/D exchange reactions based on interesting previous results obtained from investigations on base-catalysed electrophilic substitutions at saturated carbon of the type shown in **Scheme 1.31**. An example are the results of a study on base-catalysed electrophilic substitutions of a series of tertiary alcohols investigated by these authors which showed stereospecificity dependent on the reaction medium.¹⁰⁹



Scheme 1.31: generic scheme of base-catalysed electrophilic substitution at saturated carbon proceeding mainly with retention or inversion of configuration or with racemisation depending on the nature of the solvent.

High retention of configuration was observed in solvents of low ion dissociating power (e.g. *t*-butyl alcohol), racemisation was observed in solvents “of high dissociating power which are not proton donors” (e.g. DMSO) and inversion of configuration was found in protic polar solvents (e.g. diethylene glycol). The differences in the stereochemical course of reaction were explained in term of different reactive intermediates, viz. “carbanions or ion-pairs involving carbanions which capture protons from neighbouring molecules either before or after their solvent envelope becomes symmetric”. In low dissociating solvents (e.g. *t*-butyl alcohol), with metal alkoxides as bases, an intimate ion pair is formed with proton donors (electrophile) favourably orientated by the interaction with the metal cations. Reprotonation of the carbanion is, therefore, favoured

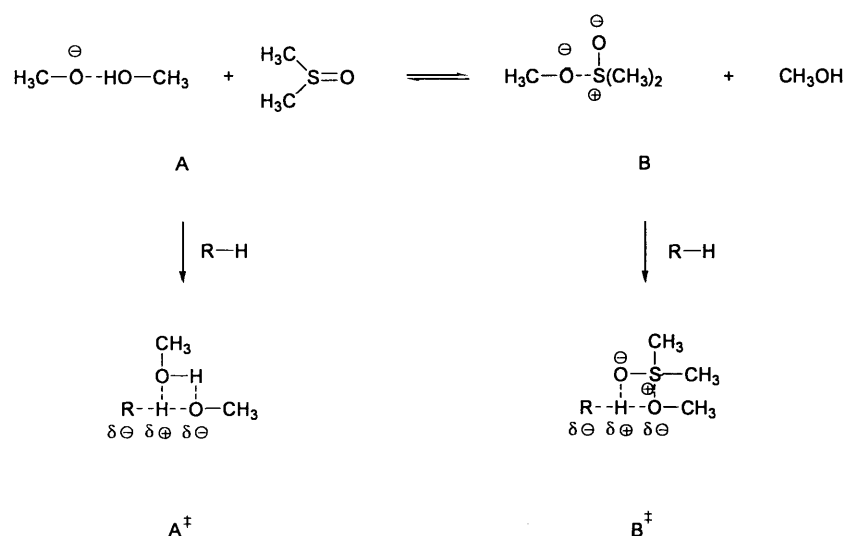
from the same side of the preceding carbon–hydrogen bond cleavage, with consequent retention of configuration. In dipolar aprotic solvents, the formed carbanion is sufficiently long lived to pass into a symmetrical solvent shell before reprotonation occurs, due to the low concentration of proton donors in the reaction medium. Racemisation occurs in this latter case. Finally, in solvents “of high dissociating power and good proton donors”, the species undergoing cleavage is proposed to be a solvent-separated ion pair. Reprotonation occurs more rapidly from the site opposite to the leaving group, due to the hindering effect of the latter. By analogy with the described electrophilic substitutions, the stereochemical course of H/D exchange reactions of different substrates has been studied and the experimental results explained with similar arguments.¹⁰³ Stereospecificity, when found, was explained in terms of intrinsic asymmetry of the “intermediate” carbanion (in particular in dissociating solvents) or with asymmetric solvation of otherwise symmetric carbanions.^{104, 105, 106} Base-catalysed H/D exchange for a particular series of carbon acids (**Scheme 1.32**) was found to proceed with complete racemisation irrespectively of the nature of the solvent. The lack of stereospecificity in the H/D exchange of the carbon acids **1.30-1.34** was argued to be in line with the hypothetical possibility for the mentioned species of existing in tautomeric, optically inactive forms. The tautomers were proposed as discrete reaction intermediates which, in a second stage, reform the more stable nitriles, amides and esters. This sequence invariably leads to racemisation.^{106, 107}



Scheme 1.32: structures of the carbon acids studied by Cram *et al.* undergoing H/D exchange with complete racemisation.

Cram *et al.*, in the above-mentioned paper on the H/D exchange of the carbon acids shown in **Scheme 1.32**, also reported one of the most striking examples of solvent effects on the rates of chemical reactions. The base-catalysed H/D exchange reaction of

2-methyl-3-phenylpropionitrile (compound **1.30** in **Scheme 1.32**) was found to increase by a factor of 10^9 by changing the solvent from methanol to DMSO.¹⁰⁷ The reaction, catalysed by metal alkoxides, was studied in pure methanol and in a series of mixtures of methanol and DMSO in various proportions.¹¹⁰ The solvation of methoxide ions in the different media was pointed out as an important factor affecting reaction rates. Methoxide ions can form hydrogen bonds with solvent molecules in methanol but not with the aprotic solvent DMSO. The absence of hydrogen bonding in DMSO leaves the anions less solvated and therefore more reactive. The authors explain the rate enhancement in terms of different specific solvation effects on ground state species and transition state, acting mainly at low and high concentrations of DMSO.



Scheme 1.33: interactions between solvents and reactants in the ground state and in the activated complex, for the methoxide-catalysed racemisation of 2-methyl-3-phenylpropionitrile **1.30**, in a mixed medium composed of methanol and DMSO.

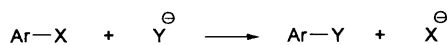
At low concentrations of DMSO the increase in rate constants is attributed to specific solvation of the transition state for deprotonation of the substrate RH by DMSO (transition state B^\ddagger in **Scheme 1.33**). Even if the low concentration of DMSO compared to methanol renders the equilibrium between A and B more favourable for A, the lower energy of B^\ddagger can compensate for the lower concentration of the ground state species in the reaction medium (its “statistic impairment”). In fact, in going from A to A^\ddagger , a strong hydrogen bond between a methoxide anion and a molecule of methanol is replaced by two weak hydrogen bonds between two molecules of methanol. On the other hand,

going from B to B[‡] involves exchanging a weak dipole-anion interaction for a strong hydrogen bond between a molecule of DMSO and one of methanol. At high concentration of DMSO, the rate-enhancing effect is mainly attributed to destabilisation of the ground state methoxide anion since, in this latter case, the equilibrium between A and B (**Scheme 1.33**) is favourably shifted toward B. The effect is accentuated by the fact that DMSO has a very good ability at hydrogen bonding with hydroxyl groups and therefore with methanol. The effect further reduces the concentration of “free” methanol molecules available for solvation of the methoxide anions. Similar rate increases are also reported by Cram *et al.* in studies on the *tert*-butoxide-catalysed racemisation of optically active 2-phenylbutane and 1-phenylmethoxyethane by passing from *tert*-butyl alcohol to dimethylsulfoxide as reaction medium.¹⁰⁸ The authors suggest that the rate increase observed in the base-catalysed racemisation of different substrates in DMSO, as compared to hydroxylic solvents, should be general for reactions subject to base-catalysis.¹⁰⁸ Similarly, Reichardt reports rate acceleration in dipolar aprotic solvents as a common feature of base-catalysed reactions.¹¹¹ A similar effect of increased basicity of anions as observed in DMSO is also reported for 1,4-dioxane, when added to a protic solvent. As also found for DMSO by Cram *et al.*¹⁰⁷, Reichardt¹¹² reports that when 1,4-dioxane is added to a protic solvent, donor-acceptor interactions between the two solvent species take place. The association between DMSO or 1,4-dioxane with the protic solvent thus decreases the concentration of molecules of the protic solvent available for solvation of a basic anion. This solvent association effect should therefore result in an increase in the concentration of “free” (i.e. not strongly solvated) anions in the reaction medium. We note, however, that only systems involving neutral acids and their anionic conjugate bases are discussed here. Reactions involving neutral bases (such as amines) and their cationic conjugate acids will be affected differently by solvents.

The above-mentioned study by Xie *et al.*³⁷ on the hydroxide-catalysed racemisation of ibuprofen enantiomers, conducted in a series of mixtures of water-DMSO, further testifies to the rate-increasing effect of DMSO on racemisation reactions. Under conditions of equal concentration of sodium hydroxide the rates of racemisation of ibuprofen were found to increase with the content of DMSO in the reaction medium.

It is also worth mentioning a paper by Miller and Parker¹¹³ on the effect of dipolar aprotic solvents on the rates of model bimolecular aromatic nucleophilic substitutions (S_NAr) (**Scheme 1.34**). For ion-dipole reactions, like the S_NAr shown in **Scheme 1.34**,

which involve dispersal of charge in going from reactants to transition state the Hughes Ingold rules¹¹⁴ predict a “small decrease” of rates with increasing ion-solvating ability of the medium.



Ar = a nitro substituted aromatic compound

Scheme 1.34: schematic representation of a generic nucleophilic aromatic substitution, involving a nitro substituted aromatic compound.

For the model S_NAr reactions under study the authors report rate constants in dipolar aprotic solvents 10⁵-fold higher than in protic solvents. Interesting conclusions about the nature and origin of ion solvation are reported, explaining the higher reaction rates in dipolar aprotic solvents. Differences in solvation affecting “the stability of the various components of the reaction” in protic and dipolar aprotic solvents are reported to play an important role in determining the relative reaction rates in the two classes of solvents. The effect is illustrated by the authors using the scheme reported in **Figure 1.5** which shows the free energy-reaction coordinate diagram for an S_NAr reaction in the specific case where Y⁻ is an azide anion and fluorine is the leaving group. The small azide ion is better solvated in protic solvents than in dipolar aprotic ones, with consequent higher reactivity in the latter case. On the other hand, it is suggested that the large polarisable intermediate complex (I.C. in **Figure 1.5**) and the structurally similar transition state should be better solvated in dipolar aprotic solvents than in protic ones. Stabilisation by hydrogen-bond formation should be more important for small anions, with little dispersal of charges. Conversely, large anions with more dispersed charge are better solvated by mutual polarizability interactions with dipolar aprotic solvents than by hydrogen bonding interactions.

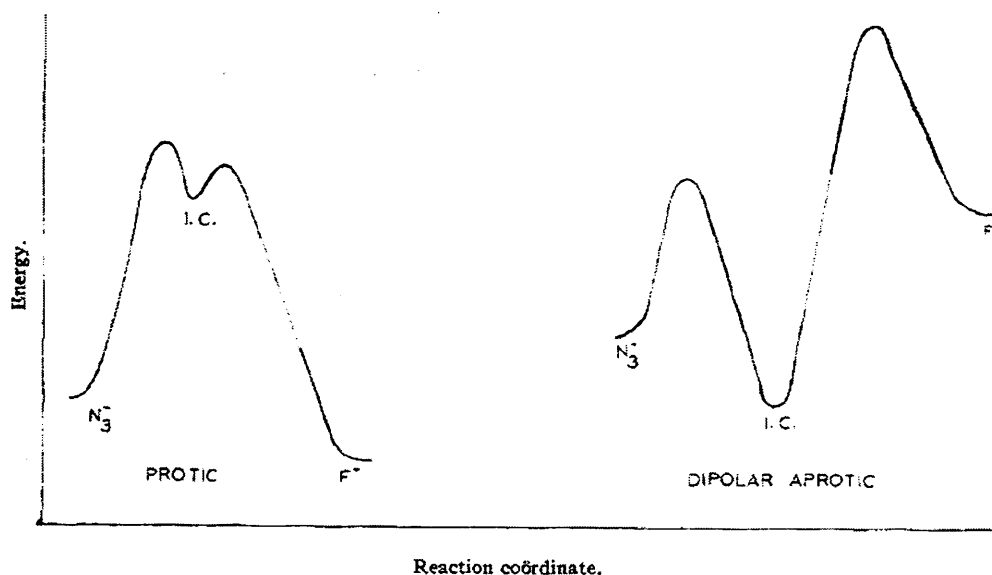


Figure 1.5: Energy reaction coordinate diagram for a model S_NAr reaction in protic (methanol) and dipolar aprotic (acetone, dimethylformamide) solvents. Energy levels are based on expected relative solvation energies of anionic participants. Figure and note reprinted and adapted with permission from reference ¹¹³ Copyright American Chemical Society 1961.

The authors highlight the fact that the rate increase in passing from polar to dipolar aprotic solvents should be general for anion-dipolar molecule reactions with a “relatively large, negatively charged, transition state”.

1.6.3. The effect of the medium on equilibria

We review in this section the results of studies on the effect of the reaction medium on acid-base equilibria. Since the kinetic experiments of H/D exchange and racemisation described in this thesis have been conducted in buffers in the presence and absence of co-solvents, studies of solvent effects on acid-base equilibria are interesting for our discussions since potential changes in pK_a of buffers may reflect marked influences on their effectiveness as general-base catalysts. Similarly solvent effects on the reactants' pK_a values will also lead to reactivity differences.

The pK_a values of different organic acids have been found to be different in different media. Water and DMSO have been particularly well studied from this point of view and pK_a values of several different organic acids have been reported to be higher in

DMSO as compared to the values determined in water.^{115, 116} Studies in the literature also report pK_a values of some organic acids in mixed aqueous media containing different amounts of DMSO¹¹⁷⁻¹²⁰ or d_6 -DMSO¹²⁰⁻¹²² co-added. Some of the studies^{121, 122} report very small values of ΔpK_a (approximately 0.2 units)¹²³ for acetic acid and propionic acid derivatives in mixtures of d_6 -DMSO and water containing up to 64 volume-% of d_6 -DMSO. Other studies, however, report larger ΔpK_a values (for example Baughman and Kreevoy report values of ΔpK_a for a series of organic acids ranging from 2 to 3 units between H_2O and a mixture of H_2O with 80 volume-% DMSO) and a linear^{117, 120} or almost linear¹¹⁸ increase of pK_a with increasing mole fraction of DMSO in the binary mixture H_2O -DMSO. Nevertheless, Ballash *et al.* suggested that there is no simple correlation between the two quantities based on their imperfect linear correlation between pK_a values and mole fraction of DMSO. Similarly, Mukerjee¹¹⁷ highlighted the fact that ΔpK_a values for different acids can be very different and therefore a simple model to predict the pK_a of different structures is not realistic. Higher pK_a values, as compared to those determined in pure water, are also reported for some acetic acid derivatives in binary mixtures water-ethanol¹²⁴ and for different acids in pure ethanol¹²⁵ and in methanol.¹²⁶ Increased pK_a values for acetic acid, as compared to the values in pure water, are also reported in binary mixtures water-dioxane.¹²⁷ As far as buffers are concerned, an interesting study by Mukerjee and Ostrow reports a linear increase in the measured pH values of phosphate buffer solutions in water with the amount of DMSO co-added.¹¹⁷

1.7. Aim of the thesis

The first part of the work described in this thesis has addressed the kinetics of racemisation of 5-substituted hydantoins in the attempt of shedding light on the controversial mechanistic aspects of the racemisation of this class of compounds. Some results reported in the literature have been confirmed, others refuted, and new data have been obtained. The second part of the work described in this thesis was focused on the development of suitable model compounds allowing relevant information by means of different analytical techniques to be obtained.

References

1. Smith, S. W., *Toxicological Sciences* **2009**, *110* (1), 4-30.
2. Vollhardt, P., *Chimica Organica*. Zanichelli Editore S.p.A.: Bologna, 1998; p 149.
3. Smith, M. B.; March, J., *March's Advanced Organic Chemistry*. Sixth ed.; WILEY-INTERSCIENCE: Hoboken, New Jersey, 2007; p 136-138.
4. From the latin term "*racemus*", which means "bunch of grapes".
5. Turner, E., *Elements of Chemistry*. Fifth ed.; Desilver, Thomas & Co.: Philadelphia, 1835; p 511-512.
6. Flack, H. D., *Acta Crystallographica Section A* **2009**, *65*, 371-389.
7. Vollhardt, P., *Chimica Organica*. Zanichelli Editore S.p.A.: Bologna, 1990; p 168.
8. Streitwieser, A.; Schaeffer, W. D., *Journal of the American Chemical Society* **1956**, *78* (21), 5597-5599.
9. Cahn, R. S.; Ingold, C. K.; Prelog, V., *Experientia* **1956**, *12* (3), 81-94.
10. The old D/L system introduced by Rosanoff is still used for amino acids. The system is based on the convention of assigning the configuration of chiral centres, by analogy with an arbitrarily chosen configuration of (+)-glyceraldehyde, used as a standard.
11. Moss, G. P., *Pure and Applied Chemistry* **1996**, *68* (12), 2193-2222.
12. On the contrary, some compounds are chiral and therefore exhibit optical activity even if they do not contain any asymmetric carbon atom. Most common examples are compounds where restricted rotation gives rise to perpendicular dissymmetric planes such as asymmetrical substituted biphenyl with prevented or restricted rotation around the single bond or some asymmetrically substituted cumulenes. Compounds can be chiral also by virtue of their helical structure.
13. Smith, M. B.; March, J., *March's Advanced Organic Chemistry*. Sixth ed.; WILEY-INTERSCIENCE: Hoboken, New Jersey, 2007; p 164-165.
14. Vollhardt, P., *Chimica Organica*. Zanichelli Editore S.p.A.: Bologna, 1998; p 163-170.
15. Maskill, H., *The Physical Basis of Organic Chemistry*. Oxford University Press: Oxford New York, 1990.

16. Ali, I.; Gupta, V. K.; Aboul-Enein, H. Y.; Singh, P.; Sharma, B., *Chirality* **2007**, *19* (6), 453-463.
17. Reist, M.; Carrupt, P. A.; Testa, B.; Lehmann, S.; Hansen, J. J., *Helvetica Chimica Acta* **1996**, *79* (3), 767-778.
18. Maskill, H., *The physical Basis of Organic Chemistry*. Oxford University Press: Oxford New York, 1990; p 278-282.
19. Caldwell, J., *Journal of Chromatography A* **1996**, *719* (1), 3-13.
20. Therapontos, C.; Erskine, L.; Gardner, E. R.; Figg, W. D.; Vargesson, N., *Proceedings of the National Academy of Sciences of the United States of America* **2009**, *106* (21), 8573-8578.
21. The enantioselectivity of the teratogenic properties of thalidomide is, however, controversial.
22. Testa, B.; Carrupt, P. A.; Gal, J., *Chirality* **1993**, *5* (3), 105-111.
23. Reist, M.; Carrupt, P. A.; Francotte, E.; Testa, B., *Chemical Research in Toxicology* **1998**, *11* (12), 1521-1528.
24. Knoche, B.; Blaschke, G., *Journal of Chromatography A* **1994**, *666* (1-2), 235-240.
25. U. S. Food and Drug Administration. Development of New Stereoisomeric Drugs(1992).<http://www.fda.gov/Drugs/GuidanceComplianceRegulatoryInformation/Guidances/ucm122883.htm> (accessed July 11 2011).
26. Reist, M.; Testa, B.; Carrupt, P. A., *Enantiomer* **1997**, *2* (3-4), 147-155.
27. Aso, Y.; Yoshioka, S.; Shibasaki, T.; Uchiyama, M., *Chemical & Pharmaceutical Bulletin* **1988**, *36* (5), 1834-1840.
28. Yang, S. K.; Bao, Z. P., *Chirality* **1994**, *6* (4), 321-328.
29. A mixed buffer containing borate, citrate, acetate and phosphate species.
30. Value determined by spectrophotometric titration in a mixture acetonitrile-buffer in the ratio 1:10 (v:v) at 23 °C.
31. Yang, S. K., *Enantiomer* **1998**, *3* (6), 485-490.
32. Stromar, M.; Sunjic, V.; Kovac, T.; Klasinc, L.; Kajfez, F., *Croatica Chemica Acta* **1974**, *46* (4), 265-274.
33. Mey, B.; Paulus, H.; Lamparter, E.; Blaschke, G., *Chirality* **1998**, *10* (4), 307-315.
34. Reist, M.; Christiansen, L. H.; Christoffersen, P.; Carrupt, P. A.; Testa, B., *Chirality* **1995**, *7* (6), 469-473.

35. pK_a values of 8.79 ± 0.017 and 8.37 ± 0.023 were reported for **1.3a** and **1.3b**, respectively.
36. Caldwell, J.; Hutt, A. J.; Fournelgigleux, S., *Biochemical Pharmacology* **1988**, *37* (1), 105-114.
37. Xie, Y. C.; Liu, H. Z.; Chen, J. Y., *International Journal of Pharmaceutics* **2000**, *196* (1), 21-26.
38. Chen, C. Y.; Chang, Y. S.; Lin, S. A.; Wen, H. I.; Cheng, Y. C.; Tsai, S. W., *Journal of Organic Chemistry* **2002**, *67* (10), 3323-3326.
39. Xie, Y. C.; Liu, H. Z.; Chen, J. Y., *Biotechnology Letters* **1998**, *20* (5), 455-458.
40. Knihinicki, R. D.; Williams, K. M.; Day, R. O., *Biochemical Pharmacology* **1989**, *38* (24), 4389-4395.
41. Danel, C.; Foulon, C.; Goossens, J.-F.; Bonte, J.-P.; Vaccher, C., *Tetrahedron-Asymmetry* **2006**, *17* (16), 2317-2321.
42. Welch, C. J.; Kress, M. H.; Beconi, M.; Mathre, D. J., *Chirality* **2003**, *15* (2), 143-147.
43. Pepper, C.; Smith, H. J.; Barrell, K. J.; Nicholls, P. J.; Hewlins, M. J. E., *Chirality* **1994**, *6* (5), 400-404.
44. Rochat, B.; Amey, M.; Vangelder, H.; Testa, B.; Baumann, P., *Chirality* **1995**, *7* (6), 389-395.
45. de Gaitani, C. M.; Martinez, A. S.; Bonato, P. S., *Chirality* **2003**, *15* (6), 479-485.
46. Lamparter, E.; Blaschke, G.; Schluter, J., *Chirality* **1993**, *5* (5), 370-374.
47. Severin, G., *Chirality* **1992**, *4* (4), 222-226.
48. Cram, D. J., *Fundamentals of Carbanion Chemistry*. Academic Press: New York and London, 1965; Vol. 4, p 85-105.
49. Gu, L.; Strickley, R. G., *Pharmaceutical Research* **1987**, *4* (5), 392-397.
50. Wilson, C. L., *Journal of the Chemical Society* **1934**, 98-99.
51. Ahlberg, R., *Berichte Der Deutschen Chemischen Gesellschaft* **1928**, *61*, 811-817.
52. McKenzie, A.; Wren, H., *Journal of the Chemical Society* **1920**, *117*, 680-690.
53. McKenzie, A.; Smith, I. A., *Journal of the Chemical Society* **1922**, *121*, 1348-1361.
54. McKenzie, A.; Widdows, S. T., *Journal of the Chemical Society* **1915**, *107*, 702-715.

55. Cirilli, R.; Costi, R.; Gasparini, F.; La Torre, F.; Pierini, M.; Siani, G., *Chirality* **2009**, *21* (1), 24-34.
56. Cram, D. J., *Fundamentals of Carbanion Chemistry*. Academic Press: New York and London, 1965; Vol. 4, p 1-20.
57. Amyes, T. L.; Richard, J. P., *Journal of the American Chemical Society* **1992**, *114* (26), 10297-10302.
58. Amyes, T. L.; Richard, J. P., *Journal of the American Chemical Society* **1996**, *118* (13), 3129-3141.
59. Richard, J. P.; Williams, G.; O'Donoghue, A. C.; Amyes, T. L., *Journal of the American Chemical Society* **2002**, *124* (12), 2957-2968.
60. Richard, J. P.; Amyes, T. L.; Toteva, M. M., *Accounts of Chemical Research* **2001**, *34* (12), 981-988.
61. Richard, J. P.; Williams, G.; Gao, J. L., *Journal of the American Chemical Society* **1999**, *121* (4), 715-726.
62. Rios, A.; Amyes, T. L.; Richard, J. P., *Journal of the American Chemical Society* **2000**, *122* (39), 9373-9385.
63. Williams, G.; Maziarz, E. P.; Amyes, T. L.; Wood, T. D.; Richard, J. P., *Biochemistry* **2003**, *42* (27), 8354-8361.
64. Hine, J., *Structural Effects on Equilibria in Organic Chemistry*. Wiley-Interscience: New York London Sydney Toronto, 1975; p 97-99.
65. Hine, J., *Structural Effects on Equilibria in Organic Chemistry*. Wiley-Interscience: New York London Sydney Toronto, 1975; p 98.
66. Rios, A.; Richard, J. P.; Amyes, T. L., *Journal of the American Chemical Society* **2002**, *124* (28), 8251-8259.
67. Ware, E., *Chemical Reviews* **1950**, *46* (3), 403-470.
68. Thenmozhiyal, J. C.; Wong, P. T. H.; Chui, W. K., *Journal of Medicinal Chemistry* **2004**, *47* (6), 1527-1535.
69. Brouillette, W. J.; Jestkov, V. P.; Brown, M. L.; Akhtar, M. S.; Delorey, T. M.; Brown, G. B., *Journal of Medicinal Chemistry* **1994**, *37* (20), 3289-3293.
70. Cortes, S.; Liao, Z. K.; Watson, D.; Kohn, H., *Journal of Medicinal Chemistry* **1985**, *28* (5), 601-606.
71. Brown, M. L.; Brown, G. B.; Brouillette, W. J., *Journal of Medicinal Chemistry* **1997**, *40* (4), 602-607.

72. Mehta, N. B.; Diuguid, C. A. R.; Soroko, F. E., *Journal of Medicinal Chemistry* **1981**, *24* (4), 465-468.
73. Zha, C. X.; Brown, G. B.; Brouillette, W. J., *Journal of Medicinal Chemistry* **2004**, *47* (26), 6519-6528.
74. Balog, A.; Salvati, M. E.; Shan, W. F.; Mathur, A.; Leith, L. W.; Wei, D. D.; Attar, R. M.; Geng, J. P.; Rizzo, C. A.; Wang, C. H.; Krystek, S. R.; Tokarski, J. S.; Hunt, J. T.; Gottardis, M.; Weinmann, R., *Bioorganic & Medicinal Chemistry Letters* **2004**, *14* (24), 6107-6111.
75. Zhang, D.; Xing, X. C.; Cuny, G. D., *Journal of Organic Chemistry* **2006**, *71* (4), 1750-1753.
76. Mudit, M.; Khanfar, M.; Muralidharan, A.; Thomas, S.; Shah, G. V.; van Soest, R. W. M.; El Sayed, K. A., *Bioorganic & Medicinal Chemistry* **2009**, *17* (4), 1731-1738.
77. Zuliani, V.; Carmi, C.; Rivara, M.; Fantini, M.; Lodola, A.; Vacondio, F.; Bordi, F.; Plazzi, P. V.; Cavazzoni, A.; Galetti, M.; Alfieri, R. R.; Petronini, P. G.; Mora, M., *European Journal of Medicinal Chemistry* **2009**, *44* (9), 3471-3479.
78. Kim, D.; Wang, L. P.; Caldwell, C. G.; Chen, P.; Finke, P. E.; Oates, B.; MacCoss, M.; Mills, S. G.; Malkowitz, L.; Gould, S. L.; DeMartino, J. A.; Springer, M. S.; Hazuda, D.; Miller, M.; Kessler, J.; Danzeisen, R.; Carver, G.; Carella, A.; Holmes, K.; Lineberger, J.; Schleif, W. A.; Emini, E. A., *Bioorganic & Medicinal Chemistry Letters* **2001**, *11* (24), 3099-3102.
79. Comber, R. N.; Reynolds, R. C.; Friedrich, J. D.; Manguikian, R. A.; Buckheit, R. W.; Truss, J. W.; Shannon, W. M.; Secrist, J. A., *Journal of Medicinal Chemistry* **1992**, *35* (19), 3567-3572.
80. Groutas, W. C.; Stanga, M. A.; Castrisos, J. C.; Schatz, E. J., *Journal of enzyme inhibition* **1990**, *3* (3), 237-243.
81. deLazslo, S. E.; Allen, E. E.; Li, B.; Ondeyka, D.; Rivero, R.; Malkowitz, L.; Molineaux, C.; Siciliano, S. J.; Springer, M. S.; Greenlee, W. J.; Mantlo, N., *Bioorganic & Medicinal Chemistry Letters* **1997**, *7* (2), 213-218.
82. Kanyonyo, M.; Govaerts, S. J.; Hermans, E.; Poupaert, J. H.; Lambert, D. M., *Bioorganic & Medicinal Chemistry Letters* **1999**, *9* (15), 2233-2236.
83. Muccioli, G. G.; Martin, D.; Scriba, G. K. E.; Poppitz, W.; Poupaert, J. H.; Wouters, J.; Lambert, D. M., *Journal of Medicinal Chemistry* **2005**, *48* (7), 2509-2517.

84. Cabordery, A.-C.; Toussaint, M.; Azaroual, N.; Bonte, J.-P.; Melnyk, P.; Vaccher, C.; Foulon, C., *Tetrahedron-Asymmetry* **2011**, *22* (2), 125-133.
85. Toussaint, M.; Mousset, D.; Foulon, C.; Jacquemard, U.; Vaccher, C.; Melnyk, P., *European Journal of Medicinal Chemistry* **2010**, *45* (1), 256-263.
86. Tompkins, J. E., *Journal of Medicinal Chemistry* **1986**, *29* (5), 855-859.
87. Dakin, H. D., *American Chemical Journal* **1910**, *44*, 48.
88. Dudley, K. H.; Bius, D. L., *Drug Metabolism and Disposition* **1976**, *4* (4), 340-348.
89. Lazarus, R. A., *Journal of Organic Chemistry* **1990**, *55* (15), 4755-4757.
90. Bovarnick, M.; Clarke, H. T., *Journal of the American Chemical Society* **1938**, *60*, 2426-2430.
91. The authors suggest that the small solvent kinetic isotope effect should support an S_E2 mechanism. However a comparison appears to be made with literature data reporting values of primary kinetic isotope effects.
92. Kahn, K.; Tipton, P. A., *Bioorganic Chemistry* **2000**, *28* (2), 62-72.
93. Lee, C. K.; Fan, C. H., *Enzyme and Microbial Technology* **1999**, *24* (10), 659-666.
94. The hypothesis however does not seem to be in line with the small reported solvent kinetic isotope effect of **1.27b**.
95. Hsu, S. K.; Wilson, C. L., *Journal of the Chemical Society* **1936**, 623-625.
96. Hsu, S. K.; Ingold, C. K.; Wilson, C. L., *Journal of the Chemical Society* **1938**, 78-81.
97. The equivalence of rates of bromination, racemisation and H/D exchange observed for ketones, lead to the conclusion that, for this class of compounds, ionisation should be the common rate determining step for all the three processes.
98. Wilson, C. L., *Journal of the Chemical Society* **1936**, 1550-1553.
99. Reichardt, C., *Solvents and Solvent Effects in Organic Chemistry*. Third ed.; WILEY VCH: Weinheim, 2003; p 57.
100. Parker, A. J., *Chemical Reviews* **1969**, *69* (1), 1-32.
101. Reichardt, C., *Solvents and Solvent Effects in Organic Chemistry*. Third ed.; WILEY VCH: Weinheim, 2003; p 82-84.
102. Isaacs, N. S., *Physical Organic Chemistry*. Pearson Education Limited: Harlow, UK, 1995; p 194.

103. Cram, D. J.; Kingsbury, C. C.; Rickborn, B., *Journal of the American Chemical Society* **1959**, *81* (21), 5835-5835.
104. Roitman, J. N.; Cram, D. J., *Journal of the American Chemical Society* **1971**, *93* (9), 2225-2231.
105. Cram, D. J.; Rickborn, B.; Kingsbury, C. A., *Journal of the American Chemical Society* **1961**, *83* (17), 3688-&.
106. Cram, D. J.; Nielsen, W. D.; Rickborn, B., *Journal of the American Chemical Society* **1960**, *82* (24), 6415-6416.
107. Cram, D. J.; Kingsbury, C. A.; Haberfie.P; Rickborn, B., *Journal of the American Chemical Society* **1961**, *83* (17), 3678-3687.
108. Cram, D. J.; Rickborn, B.; Knox, G. R., *Journal of the American Chemical Society* **1960**, *82* (24), 6412-6413.
109. Cram, D. J.; Mateos, J. L.; Hauck, F.; Langemann, A.; Kopecky, K. R.; Nielsen, W. D.; Allinger, J., *Journal of the American Chemical Society* **1959**, *81* (21), 5774-5784.
110. The authors exclude phenomena of ion pairing at the low concentrations of base employed and the metal alkoxides are considered fully dissociated in all the reaction mixtures under investigation.
111. Reichardt, C., *Solvents and Solvent Effects in Organic Chemistry*. Third ed.; WILEY VCH: Weinheim, 2003; p 259-262.
112. Reichardt, C., *Solvents and Solvent Effects in Organic Chemistry*. Third ed.; WILEY VCH: Weinheim, 2003; p 241-242.
113. Miller, J.; Parker, A. J., *Journal of the American Chemical Society* **1961**, *83* (1), 117-123.
114. Hughes, E. D.; Ingold, C. K., *Journal of the Chemical Society* **1935**, 244-255.
115. <http://www.chem.wisc.edu/areas/reich/pkatable>.
116. pK_a Data Compiled by R. Williams http://research.chem.psu.edu/brpgroup/pKa_compilation.pdf.
117. Mukerjee, P.; Ostrow, J. D., *Tetrahedron Letters* **1998**, *39* (5-6), 423-426.
118. Ballash, N. M.; Robertso.Eb; Sokolows.Md, *Transactions of the Faraday Society* **1970**, *66* (574), 2622-2628.
119. Baughman, E. H.; Kreevoy, M. M., *Journal of Physical Chemistry* **1974**, *78* (4), 421-423.

120. Vesala, A.; Saloma, E., *Acta Chemica Scandinavica Series a-Physical and Inorganic Chemistry* **1976**, 30 (4), 277-280.
121. Holmes, D. L.; Lightner, D. A., *Tetrahedron* **1995**, 51 (6), 1607-1622.
122. Holmes, D. L.; Lightner, D. A., *Tetrahedron* **1996**, 52 (15), 5319-5338.
123. ΔpK_a is defined as the difference of pK_a in the presence of d_6 -DMSO or DMSO co-added and the pK_a value in water alone.
124. Frohliche, J.; Gartska, R. A.; Irwin, H. W.; Steward, O. W., *Analytical Chemistry* **1968**, 40 (10), 1408-1411.
125. Reichardt, C., *Solvents and Solvent Effects in Organic Chemistry*. Third ed.; WILEY VCH: Weinheim, 2003; p 95.
126. Clare, B. W.; Cook, D.; Ko, E. C. F.; Mac, Y. C.; Parker, A. J., *Journal of the American Chemical Society* **1966**, 88 (9), 1911-1916.
127. Bates, R. G.; Pawlak, Z., *Journal of Solution Chemistry* **1976**, 5 (3), 213-222.

Chapter 2

The kinetics and mechanism of racemisation of (*S*)-5-benzylhydantoin and (*S*)-3-*N*-methyl-5-benzylhydantoin.

Abstract

The kinetics and mechanism of racemisation and H/D exchange of (*S*)-5-benzylhydantoin **2.1** and of (*S*)-3-*N*-methyl-5-benzylhydantoin **2.2** have been studied in D₂O- and H₂O-based buffers. Both processes are general-base catalysed. The kinetics of racemisation of (*S*)-5-benzylhydantoin is complicated by the acidity of the proton in position 3 of the hydantoin ring (**Scheme 2.3**). A method is presented allowing the analysis of the complex kinetics where the rate of racemisation depends on the protonation state of the molecule. A Brønsted plot for racemisation (*S*)-3-*N*-methyl-5-benzylhydantoin in aqueous buffers gave a value of β of approximately 0.6, suggesting a transition state of the rate-determining step of racemisation with the exchangeable proton being halfway between the asymmetric carbon and the base. No solvent kinetic isotope effect was detected for racemisation of the benzylhydantoins in phosphate buffers, while a primary kinetic isotope effect of approximately 3.5 for racemisation of (*S*)-5-benzylhydantoin was observed. Deuterium-labelled 5-benzylhydantoins have been synthesised which allowed us to obtain further stereochemical and mechanistic information on H/D exchange of the molecules in D₂O phosphate buffer. A mathematical expression describing the racemisation of a generic chiral molecule in a deuterated medium, following an S_E2 mechanism has been developed and experimental data have been fitted to the mentioned model. The expected ECD signal for a generic

kinetic trace for the mentioned model was also numerically simulated and compared to experimental kinetic traces.

Mathematical analyses, numerical simulations, comparison of rate constants of racemisation and H/D exchange, experimental kinetic isotope effects, and kinetic experiments carried out with deuterium labelled benzylyhdantoin all consistently support the S_E1 mechanism of racemisation and not the previously proposed S_E2 mechanism.

2.1. Introduction

Despite the keen interest in the hydantoin ring in drug design¹⁻¹⁹ and several studies in the literature on the racemisation of 5-substituted hydantoins^{17, 20-26} and closely related structures,^{27, 28} the mechanism of interconversion of opposite enantiomers of this class of compounds has not been unequivocally elucidated (see Chapter 1, **Sections 1.4** and **1.5**). The studies described in this Chapter aim to shed more light on the mechanism of racemisation of 5-substituted hydantoins, under experimental conditions mimicking physiological ones.

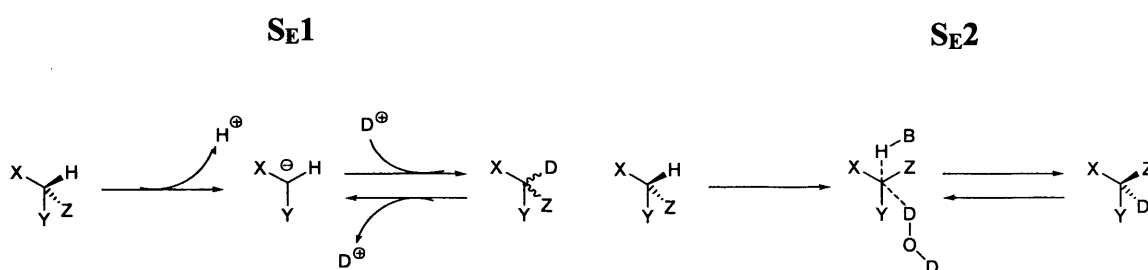
5-Benzylhydantoin and 3-*N*-methyl-5-benzylhydantoin were chosen as model compounds for our studies of the kinetics and mechanism of racemisation of 5-substituted hydantoins. This choice was based on the consideration that benzylyhdantoin allow for significant structural variation (also see Chapter 3), show convenient rates of racemisation and because of the presence of suitable UV-active functional groups in their structures, enabling easy detection by UV and ECD (electronic circular dichroism) spectroscopy.²⁹

As proposed by Testa *et al.*²³ and briefly discussed in Chapter 1, two main mechanistic pathways can be envisaged for the racemisation of 5-substituted hydantoins: the S_E1 and the S_E2 pathways, shown in **Scheme 2.1**.

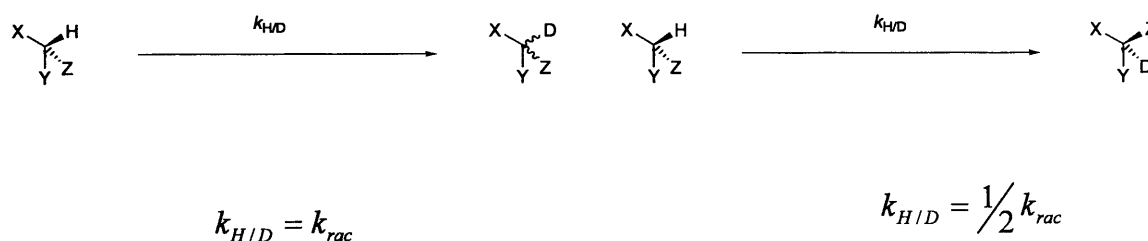
Testa *et al.*, in the above mentioned paper, suggested a general-base catalysed S_E2 mechanism for racemisation of 5-substituted hydantoins. (*S*)-5-benzylhydantoin and (*S*)-5-phenylhydantoin were used as model compounds. The kinetic experiments described in the paper were carried out in a mixed medium composed by 50% DMSO and 50% phosphate buffer. Both deuterated and non-deuterated solvents were used. A key

experiment, upon which the authors base their hypothesis of a concerted mechanism, is the comparison of the rate constants of racemisation (determined by HPLC) with those of deuteration (determined by H/D exchange experiments, carried out by ^1H NMR spectroscopy). Testa *et al.* reported rate constants of deuteration approximately half those of racemisation (k_{rac}). As described in **Scheme 2.1**, the finding suggests that deuteration ($k_{\text{H/D}}$) must proceed via inversion of configuration, in contrast with the hypothesis of planar intermediates which should lead to equal rate constants of racemisation and deuteration.

Chemical Model

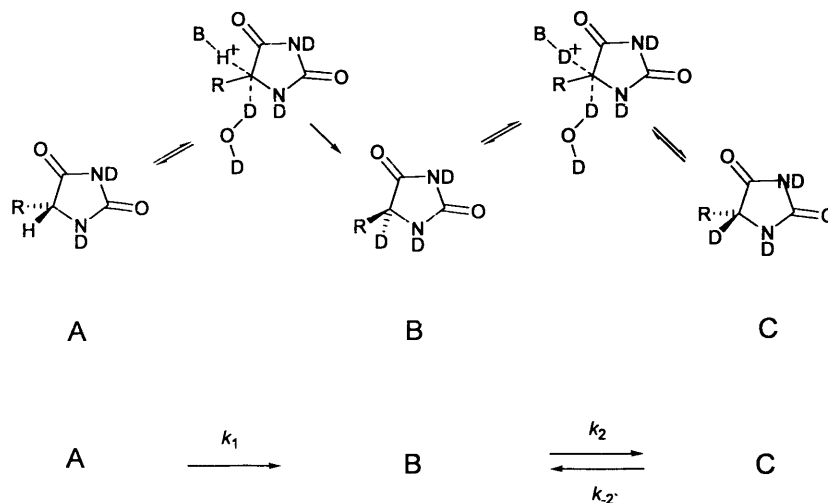


Kinetic Model



Scheme 2.1: comparison between S_E1 and S_E2 mechanisms for racemisation of 5-substituted hydantoins

Assuming an S_E2 mechanism, Testa *et al.* described the process of H/D exchange of 5-substituted hydantoins as shown in **Scheme 2.2**.

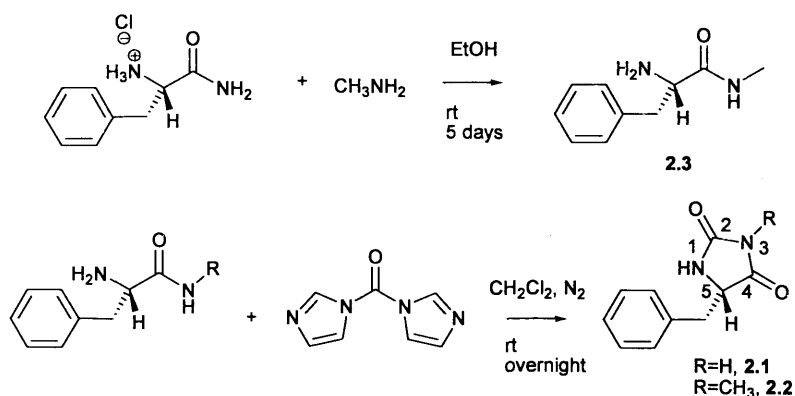


Scheme 2.2: proposed S_E2 mechanism for 5-substituted hydantoin and its schematic representation.

2.2. Syntheses

Optically active (*S*)-5-benzylhydantoin **2.1** was synthesised from the corresponding (*L*) amino acid amide using carbonyldiimidazole (CDI) as a coupling agent according to methods reported in the literature^{30,31} (**Scheme 2.3**).

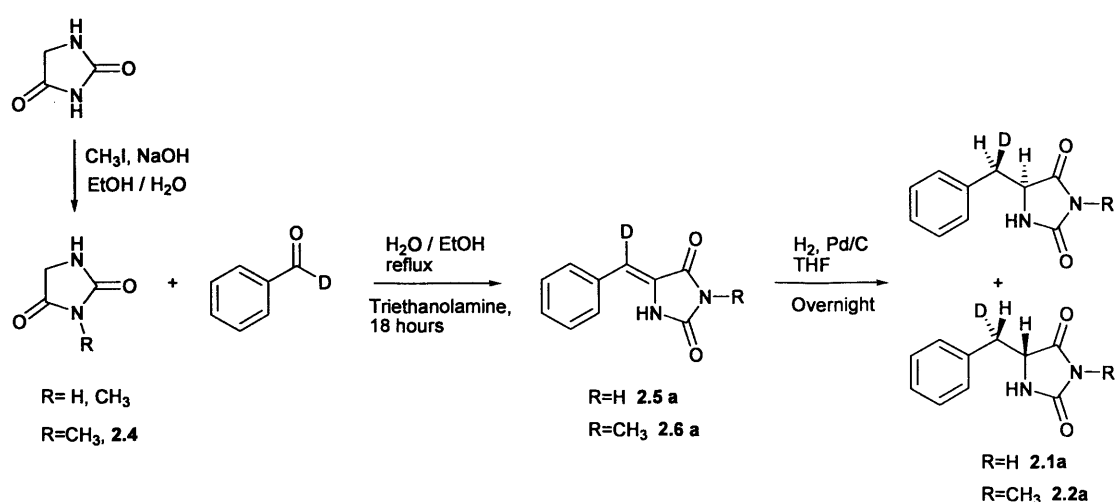
(*S*)-3-*N*-Methyl-5-benzylhydantoin **2.2** was synthesised from (*S*)-2-amino-*N*-methyl-3-phenylpropionamide **2.3** following the analogous synthetic route (**Scheme 2.3**). (*S*)-2-Amino-*N*-methyl-3-phenylpropionamide was prepared from the corresponding amino acid methyl ester hydrochloride and methylamine, according to literature methods.³¹ The reaction of (*S*)-2-amino-*N*-methyl-3-phenylpropionamide with carbonyldiimidazole afforded optically active (*S*)-3-*N*-methyl-5-benzylhydantoin **2.2**.



Scheme 2.3: syntheses of (*S*)-5-benzylhydantoin **2.1** and (*S*)-3-*N*-methyl-5-benzylhydantoin **2.2**

Though partial racemisation was observed during the syntheses, the enantiomeric excesses of the obtained 5-benzylhydantoins were found to be sufficient to enable kinetic studies of racemisation by means of CD spectroscopy; aqueous solutions of benzylhydantoins **2.1** and **2.2** exhibited strong negative Cotton effects in the CD spectra around 230 nm.

Deuterium-labelled 5-benzylhydantoin **2.1a** and 3-*N*-methyl-5-benzylhydantoin **2.2a** were synthesised following a synthetic route involving a condensation reaction followed by hydrogenation (Scheme 2.4). Reaction conditions were optimised using unlabelled starting materials.



Scheme 2.4: synthesis of 6-d-5-benzylhydantoin **2.1a** and 6-d-3-*N*-methyl-5-benzylhydantoin **2.2a**.

3-*N*-Methyl-hydantoin **2.4** was obtained by methylating hydantoin using iodomethane. Guidelines for the choice of experimental conditions were obtained from the literature.³² The Knoevenagel condensations of the hydantoins and benzaldehyde were carried out following a literature procedure.^{1, 10, 33, 34} Only the *Z* isomers of the intermediate benzylidenehydantoins were obtained. The configuration and three dimensional structure of benzylidenehydantoin was confirmed by X-ray crystallography (Figure 2.1).

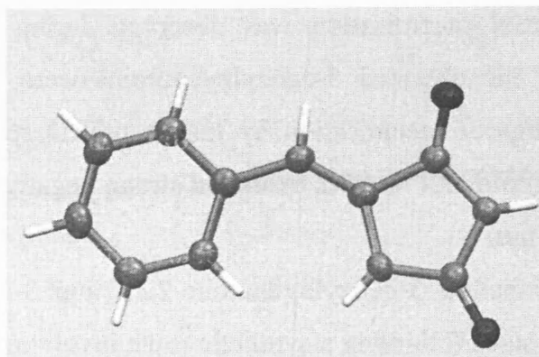
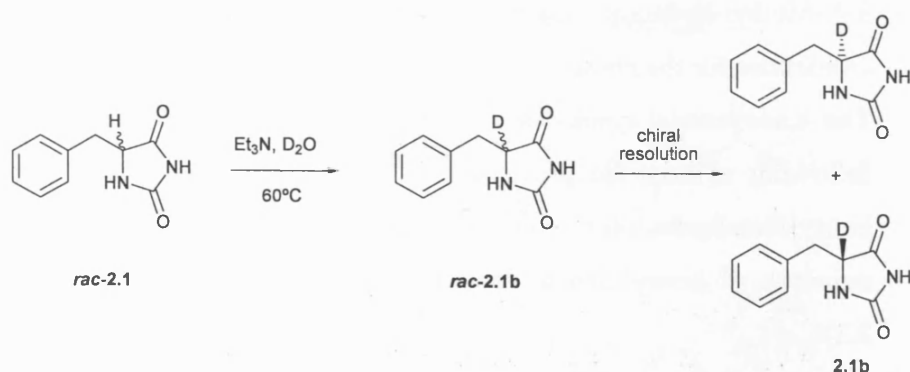


Figure 2.1: three dimensional structure of benzylidenehydantoin determined by X-ray crystallography.

Hydrogenations were carried out using THF as solvent and Pd/C as catalyst, as suggested in the literature.³⁵

The presence of single signals for the methylene protons in the ^1H NMR spectra of benzylidenehydantoins **2.1a** and **2.2a** indicates that only one pair of enantiomers was obtained, rather than a mixture of diastereoisomers. In **Figure 2.13, left** (*vide infra*), partial ^1H NMR spectra for **2.1a** (**top**) and **2.2a** (**bottom**) in D_2O are shown with the signals from the methylene protons labelled “2”.

The alternatively deuterium-labelled racemic 5-benzylhydantoin **rac-2.1b** was obtained from the corresponding racemic 5-benzylhydantoin **rac-2.1** upon base-catalysed exchange of the asymmetric proton with deuterium, as shown in **Scheme 2.5**. Single enantiomers of **2.1b** were then obtained upon resolution of the racemate by means of chiral HPLC.



Scheme 2.5: synthesis of enantiomers of 5-d-5-benzylhydantoin **2.1b**

2.3. Kinetic studies

2.3.1. Racemisation of (*S*)-5-benzylhydantoin in phosphate buffers

The racemisation of **2.1** in D₂O phosphate buffers at 1 M ionic strength was followed in real time by means of CD spectroscopy. Most kinetic data for the racemisation process were collected at 60 °C, the racemisation of **2.1** being conveniently fast at this temperature. In **Figure 2.2** typical kinetic traces obtained for racemisation of **2.1**, are shown. **Figure 2.2 (left)** shows the changes over time in the CD spectrum of **2.1** during racemisation in D₂O phosphate buffer, 0.5 M, 1 M *I* at pH** 7.2 and 60 °C. **Figure 2.2 (right)** shows only one trace.

Figure 2.3 (left) shows the decrease of the CD signals at 230 nm, during experiments of racemisation of **2.1** in D₂O phosphate buffers with different concentrations, as a function of time. The experimental data were found to be in good agreement with pseudo first-order kinetics (**Equation 2.1**).³⁶

$$\ln\left(\frac{S}{S_0}\right) = -k_{obs}t \quad \text{Equation 2.1}$$

with *S* the signal at time *t*, *S*₀ the signal at time *t*=0 and *k*_{obs} the observed rate constant.

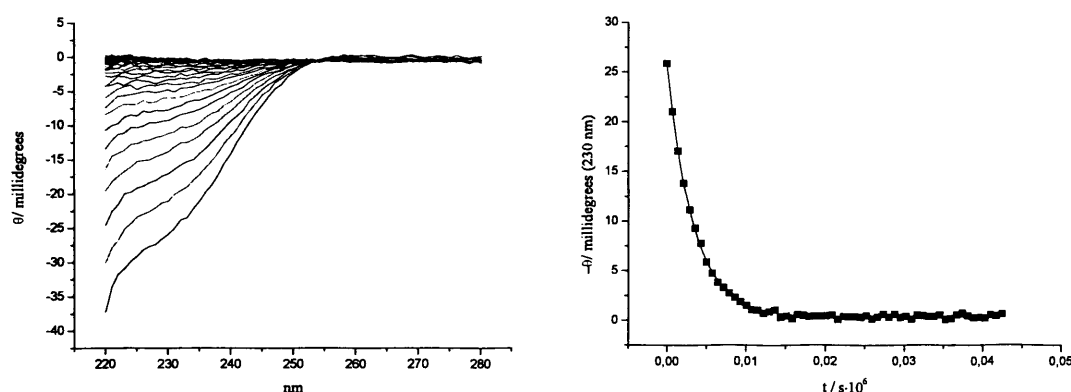


Figure 2.2: racemisation of (*S*)-5-benzylhydantoin at 60 °C in D₂O phosphate buffers, pH** 7.2, 0.5 M, 1 M *I*. **Left:** CD spectra of **2.1** recorded over time during racemisation **Right:** CD signal of **2.1** at 230 nm plotted as a function of reaction time (the line is the fit to pseudo-first-order kinetics).

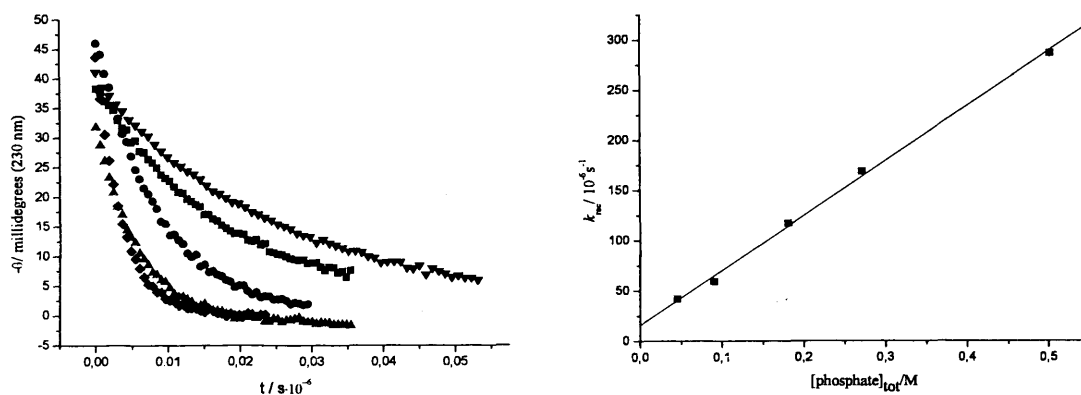


Figure 2.3: racemisation of (*S*)-5-benzylhydantoin at 60 °C in D₂O phosphate buffers, pH** 7.2, 1 M *I* (maintained with KCl), 0.5 M (◆), 0.27 M (▲), 0.18 M (●), 0.09 M (■) and 0.045 M (▼). **Left:** CD signal of 2.1 at 230 nm plotted as a function of reaction time. The lines are the fits to pseudo-first-order kinetics. **Right:** observed rate constant of racemisation as a function of buffer concentration.

Observed rate constants of racemisation (k_{rac}) were found to increase linearly with buffer concentration (**Figure 2.3**) which, taken together with the dependence on pH** of the rate constant (*vide infra*), suggests that racemisation is general-base catalysed. The dependence of the observed rate constants for racemisation on buffer concentration can be expressed as in **Equation 2.2**.

$$k_{rac} = k_0 + k_{OD^-}[OD^-] + k_{phosphate_{tot}}[phosphate_{tot}] \quad \text{Equation 2.2}$$

In **Equation 2.2** the term $k_{OD^-}[OD^-]$ is the rate constant for the combined non-catalysed and deuterioxide-catalysed processes and $k_{phosphate_{tot}}$ is the second-order rate constant for buffer-catalysed racemisation. The straight line fit to the experimental data for racemisation of 2.1 in D₂O phosphate buffers, 1 M *I* at pH** 7.2 and 60 °C, is given by **Equation 2.3**:

$$k_{rac} = (17.1 \pm 0.5) \cdot 10^{-6} s^{-1} + (542.2 \pm 2.5) \cdot 10^{-6} M^{-1} s^{-1} [phosphate_{tot}] \quad \text{Equation 2.3}$$

Equation 2.3 shows that, at approximately neutral pH** (pH** 7.2), the buffer species are the main catalysts for racemisation of 2.1 but a non-zero contribution to k_{rac} from the deuterioxide-catalysed and/or non-catalysed processes are also observed.

2.3.2. The effect of pH** on the rate constants of racemisation

The effect of pH** on the rate constants for racemisation of (*S*)-5-benzylhydantoin was investigated. **Figure 2.4** shows the rate constants of racemisation of **2.1**, in buffered D₂O solutions at different pH** values as a function of buffer concentration.

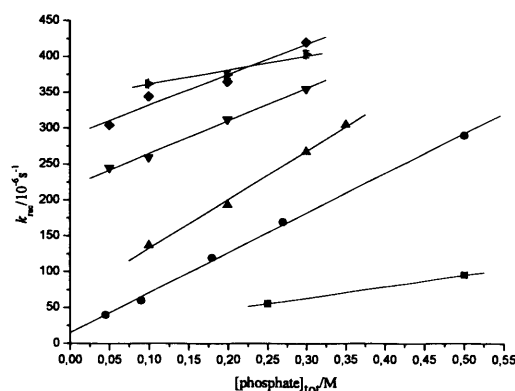


Figure 2.4: rate constants of racemisation of (*S*)-5-benzylhydantoin **2.1** as a function of total buffer concentration at pH** 11.0 (►), 10.0 (◆), 9.0 (▼), 8.0 (▲), 7.2 (●) and 6.0 (■), at 60 °C.

As shown by **Equation 2.3** and **Figure 2.4**, at neutral pH** the contribution from the term $k_0 + k_{OD^-}[OD^-]$ is small and buffer-catalysis dominates the kinetics of racemisation. At higher pH** the hydroxide-catalysed process becomes increasingly important, as expected, but $k_{\text{phosphate tot}}$ does not show the anticipated increase due to a higher concentration of basic form of the buffer (species DPO_4^{2-}) at higher pH**. In **Figure 2.5** the same pseudo-first-order rate constants of racemisation as reported in **Figure 2.4** are re-plotted as a function of the concentration of the basic component of the buffer. A decrease of the slopes with increasing pH** is observed.

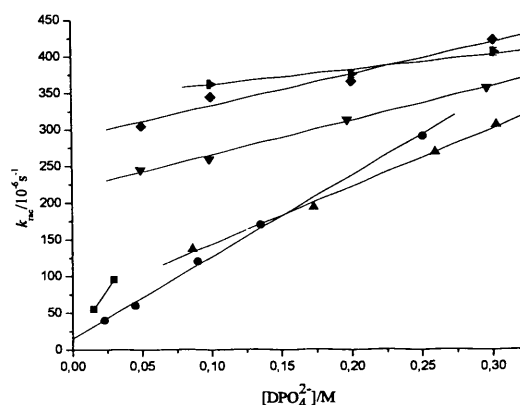


Figure 2.5: rate constants of racemisation of (*S*)-5-benzylhydantoin **2.1** as a function of the concentration of the species DPO_4^{2-} at pH** 11.0 (\blacktriangleright), 10.0 (\blacklozenge), 9.0 (\blacktriangledown), 8.0 (\blacktriangle), 7.2 (\bullet) and 6.0 (\blacksquare), at 60 °C.

The individual rate constants contributing to the overall observed pseudo-first order rate constants for racemisation of **2.1** as a function of pH** are displayed in **Figure 2.6**. In **Figure 2.6 (left)** the calculated values of the rate constants $k_{OD^-}[OD^-]$, obtained from the global fit of the experimental rates of racemisation to **Equation 2.4** (*vide infra*), are plotted as a function of pH**. Analogously, **Figure 2.6 (right)** shows the trends of the second-order rate constants for the buffer catalysed-racemisation of (*S*)-5-benzylhydantoin over the same range of pH**. The trends suggest the concurrent racemisation of two different chemical species in the reaction medium. Reversible changes in the UV (**Figure 2.7, left**) and CD spectra (**Figure 2.7, right**) of buffered D₂O solutions of **2.1** at different pH** were observed, consistent with different protonation states of the molecule at different pH**. The pK_a^{**} for the proton in position 3 of the (*S*)-5-benzylhydantoin was determined by spectrophotometric titration under the same experimental conditions as used for the racemisation experiments (D₂O phosphate buffers, 1 M I, 60 °C).

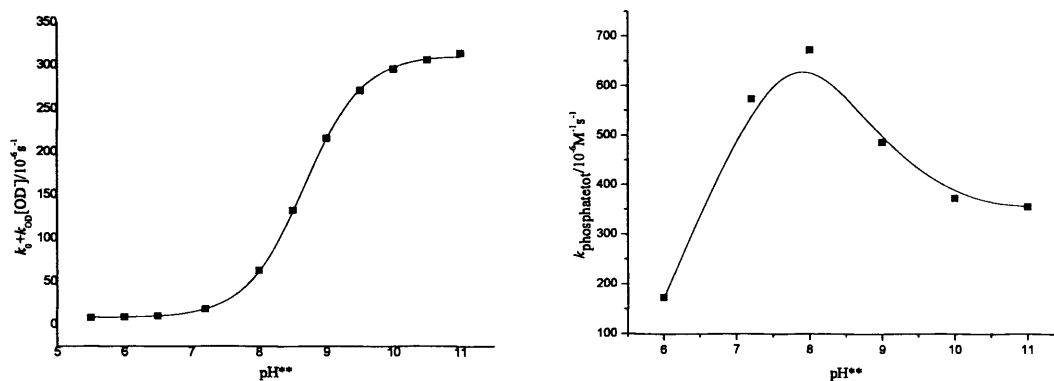


Figure 2.6: rate constants of racemisation of (*S*)-5-benzylhydantoin at zero buffer concentration (**left**) and rate constants for the buffer catalysed racemisation of (*S*)-5-benzylhydantoin (**right**) as a function of pH^{**} . Data points are fitted values obtained from the global fits of experimental kinetic data to **Equation 2.4** (*vide infra*). The solid line in the graph on the left is the fit of the data points to **Equation S1.1** (see Appendix 1) where the constants of racemisation of (*S*)-5-benzylhydantoin at zero buffer concentration were considered instead of the extinction coefficient ϵ . A kinetic pK_a of 8.67 ± 0.01 was obtained from the fit. The solid line in the graph on the right is drawn to guide the eye.

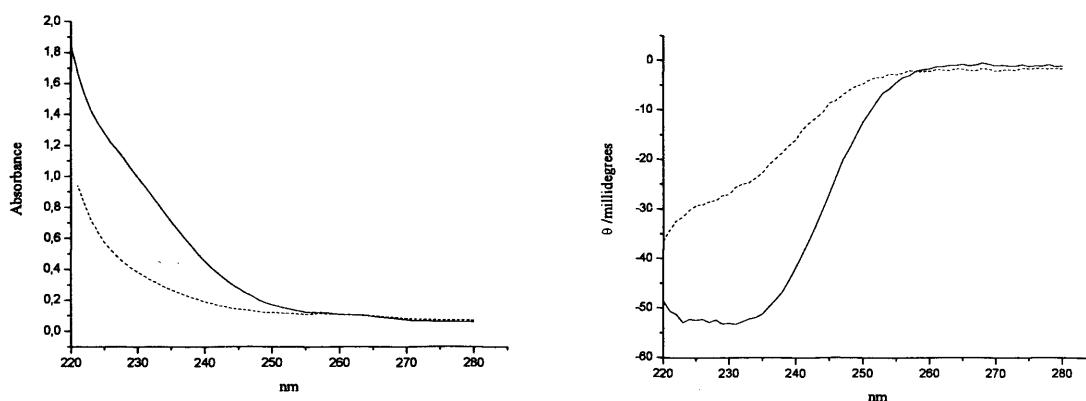
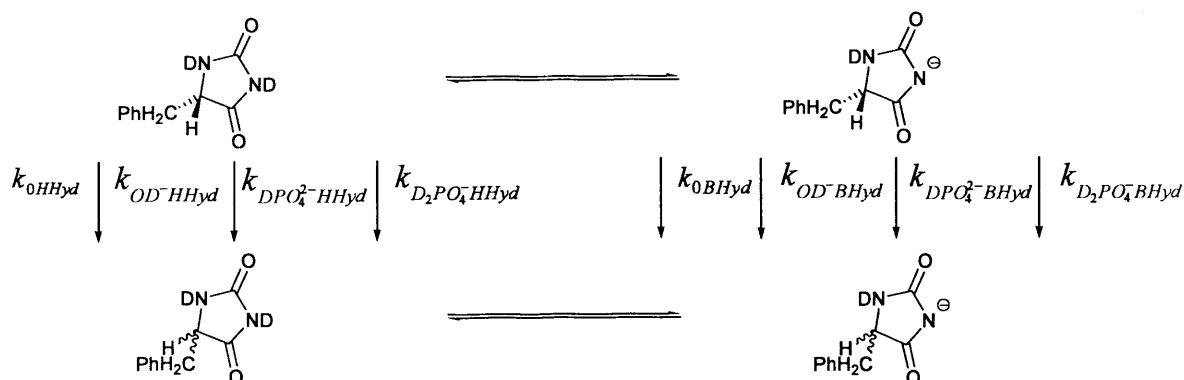


Figure 2.7: UV (**left**) and CD spectra (**right**) of (*S*) 5-benzylhydantoin at pH^{**} 9.0 (**solid lines**) and 7.2 (**dash lines**).

From the titration a pK_a^{**} value of 8.65 ± 0.06 was determined.³⁷ Our value of pK_a^{**} is consistent with the literature value of 8.65 ± 0.10 .²¹ As reported in the study by Lazarus *et al.*²¹ (also see Chapter 1), the protonation state of the molecule is an aspect that must be taken into consideration when studying the kinetics of racemisation of 5-

benzylhydantoin. An overall process as shown in **Scheme 2.6** can be envisaged for the racemisation of (*S*)-5-benzylhydantoin. The racemisation proceeds simultaneously on the protonated and deprotonated analogues of (*S*)-5-benzylhydantoin in a reaction medium where 4 different potential catalytic species are present.



Scheme 2.6: Proposed process of racemisation of (*S*)-5-benzylhydantoin

Equation 2.4 is the complete analytical expression describing the complex process.

$$k_{rac1} = \{k_{0BHyd} + k_{OD^-BHyd}[OD^-] + k_{D_2PO_4^-BHyd}[D_2PO_4^-] + k_{DPO_4^{2-}BHyd}[DPO_4^{2-}]\} \frac{[BHyd]}{[Hyd_{tot}]} +$$

$$+ \{k_{0HHyd} + k_{OD^-HHyd}[OD^-] + k_{D_2PO_4^-HHyd}[D_2PO_4^-] + k_{DPO_4^{2-}HHyd}[DPO_4^{2-}]\} \frac{[HHyd]}{[Hyd_{tot}]}$$

Equation 2.4

In Equation 2.4 k_{0BHyd} and k_{0HHyd} are the rate constants for the uncatalysed racemisation of deprotonated (*Bhyd*) and protonated (*HHyd*) hydantoin **2.1**, k_{OD^-BHyd} and k_{OD^-HHyd} are the catalytic rate constants for the deuterioxide-catalysed racemisation of the deprotonated and protonated hydantoin, $k_{D_2PO_4^-BHyd}$ and $k_{D_2PO_4^-HHyd}$ are the rate constants for racemisation with the monobasic form of the buffer acting as a catalyst on deprotonated and protonated hydantoin, respectively, and $k_{DPO_4^{2-}BHyd}$ and $k_{DPO_4^{2-}HHyd}$ are the rate constants of racemisation with the dibasic form of the buffer acting as a catalyst

on deprotonated and protonated hydantoin, respectively. Finally, $\frac{[BHyd]}{[Hyd_{tot}]}$ and

$\frac{[HHyd]}{[Hyd_{tot}]}$ are the fractions of the deprotonated and the protonated form of **2.1** present in

the reaction mixture at a given pH**.

The use of **Equation 2.4** for data analysis is not straightforward; many variables are involved and several of the individual contributions to the overall observed rate constant are kinetically equivalent.

2.3.3. Racemisation of (*S*)-3-*N*-methyl-5-benzylhydantoin in phosphate buffers

To overcome the problem of deprotonation of **2.1** and simplify the kinetic system, the 3-*N*-methyl analogue of (*S*)-5-benzylhydantoin (compound **2.2** in **Scheme 2.3**) was synthesised and its racemisation studied under the same experimental conditions as for **2.1**. Kinetic experiments were carried out in D₂O phosphate buffers at pH** 6.0, 7.2, 8.0, 9.0 and 10.0. However the kinetic experiments carried out at pH** 10.0 appeared to be irreproducible (Appendix 1) and were not included in the fits described in the following sections. The reason of the poor reproducibility of the data is unclear. UV spectra of **2.2** during racemisation experiments did not show evident changes and there is therefore no clear support for the hypothesis of structural modification, such as hydrolysis of **2.2**, over time but neither can the possibility be unambiguously excluded. The results of the kinetic experiments of racemisation of **2.2** are summarised in **Figure 2.8 (left)** where the observed rate constants for racemisation of **2.2** are plotted as a function of buffer concentration. Similarly, **Figure 2.8 (right)** shows the rate constants for racemisation of **2.1** plotted as a function of buffer concentration.

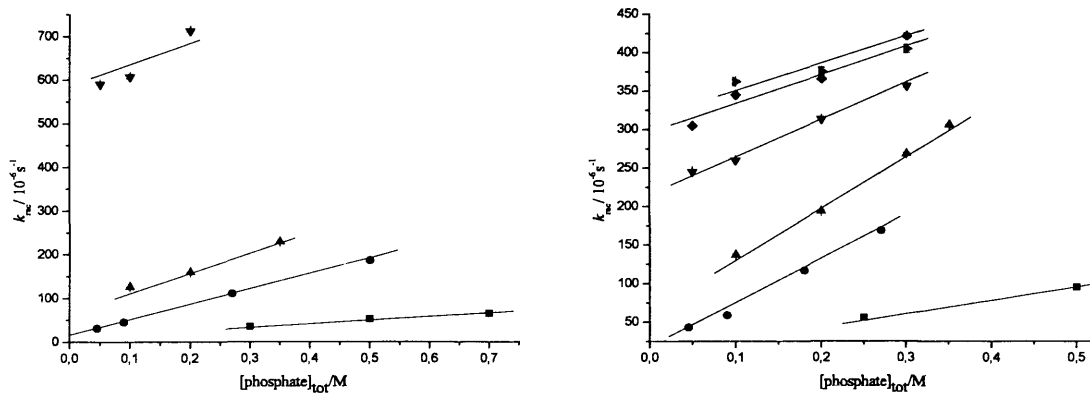


Figure 2.8: rate constants of racemisation of (*S*)-3-*N*-methyl-5-benzylhydantoin (**left**) and of (*S*)-5-benzylhydantoin (**right**) as a function of total buffer concentration at pH** 6.0 (■), 7.2 (●), 8.0 (▲), 9.0 (▼), 10.0 (◆) and 11.0 (►). Lines are global fits to **Equations 2.4** (**right**) and **2.5** (**left**) (*vide infra*).

Figure 2.8 (**left**) shows a steady increase of the slopes of the rate constants of racemisation of **2.2** with increasing pH**, in contrast with the trend observed for (*S*)-5-benzylhydantoin shown in **Figure 2.8** (**right**). Please note that **Figure 2.4** shows the same data analysed in terms of individual straight line fits, whereas the straight line fits in **Figure 2.8** are global fits to **Equations 2.4** (**Figure 2.8** (**right**)) and **Equations 2.5** (**Figure 2.8** (**left**)) (*vide infra*).

Figure 2.9 shows the calculated values of the rate constants $k_0+k_{OD^-}[\text{OD}^-]$ and of the second-order rate constants for the buffer-catalysed racemisation ($k_{\text{phosphate tot}}$) of **2.2** obtained from the straight line fits shown in **Figure 2.8**, **left**, as a function of pH**.

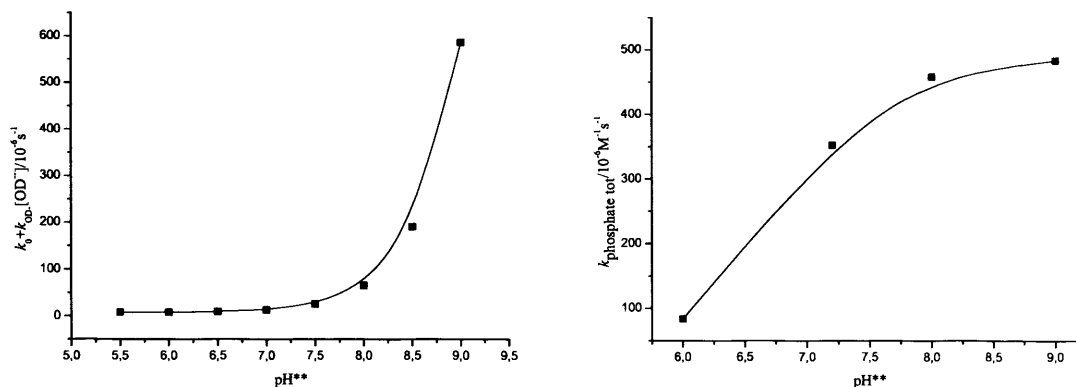


Figure 2.9: rate constants of racemisation of (*S*)-3-*N*-methyl-5-benzylhydantoin at zero buffer concentration (**left**) and rate constants for the buffer catalysed racemisation of (*S*)-3-methyl-5-benzylhydantoin (**right**), as a function of pH**. Data points are fitted values obtained from the global fits of the experimental kinetic data to **Equations 2.5**. Lines are drawn to guide the eye.

Figure 2.9 shows the steady increase of the terms $k_0 + k_{OD^-}[OD^-]$ and of $k_{\text{phosphate tot}}$ for **2.2** with increasing pH**, as opposed to the trends obtained for **2.1**, shown in **Figure 2.6**.

Equation 2.5 is the complete analytical expression describing the phosphate-catalysed racemisation of **2.2**.

$$k_{rac2} = k_0 + k_{OD^-}[OD^-] + k_{D_2PO_4^-}[D_2PO_4^-] + k_{DPO_4^{2-}}[DPO_4^{2-}] \quad \text{Equation 2.5}$$

In **Equation 2.5**, k_0 is the rate constant for the uncatalysed racemisation of (*S*)-3-*N*-methyl-5-benzylhydantoin, k_{OD^-} is the catalytic rate constant for deuteroxide-catalysed racemisation, $k_{D_2PO_4^-}$ and $k_{DPO_4^{2-}}$ are the catalytic rate constants for racemisation of **2.2** catalysed by the monobasic and dibasic form of the buffer, respectively. **Equation 2.5** is essentially identical to **Equation 2.4**, but without the terms corresponding to the deprotonated form of the hydantoin.

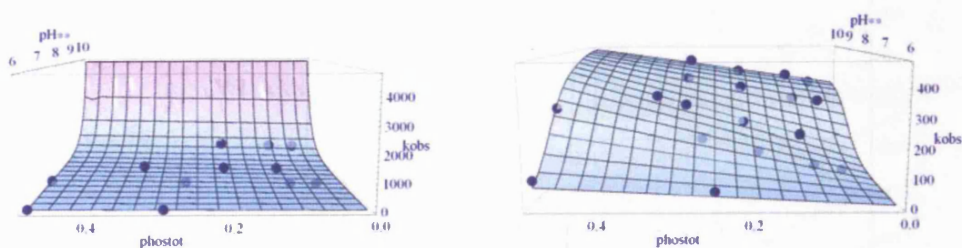


Figure 2.10: **Left:** three-dimensional fit of the rate constants of racemisation of (*S*)-3-*N*-methyl-5-benzylhydantoin **2.2** in D₂O phosphate buffers at different pHs** and 60 °C. **Right:** three-dimensional fit of the rate constants of racemisation of (*S*)-5-benzylhydantoin **2.1** in D₂O phosphate buffers at different pHs** and 60 °C where the rate constants for the protonated species of **2.1** were substituted with the corresponding rates obtained from the global fit for **2.2**.

The obtained kinetic data for racemisation of **2.1** and **2.2** at all pH** were simultaneously analysed in terms of **Equations 2.4** and **2.5**, respectively, by means of the program Mathematica. The global fit by Mathematica not only afforded a more accurate fit to the data at each pH**, but also allowed us to estimate the contribution of each catalytic species present in the buffer solution to the observed rate constants of racemisation. In the following discussion we will firstly describe the results obtained for the simpler case of racemisation of **2.2**, and secondly we will treat the more complex kinetics for racemisation of **2.1**.

The three-dimensional (global) fit of the rate constants of racemisation of **2.2** to **Equation 2.5** is shown in **Figure 2.10 (left)**. The fitted rate constants for individual catalytic species present in the buffer solutions are reported in **Table 2.1**.

Table 2.1: Rate constants for catalysis by individual species present in the buffer solutions ^{a)} in the racemisation of (*S*)-3-*N*-methyl-5-benzylhydantoin at 60 °C.

Rate constant	$k/10^{-6}$
k_0	$7 \pm 5 \text{ s}^{-1}$
k_{OD^-}	$(1.7 \pm 0.5) \times 10^7 \text{ s}^{-1} \text{M}^{-1}$
$k_{\text{D}_2\text{PO}_4^-}$	$21 \pm 14 \text{ s}^{-1} \text{M}^{-1}$
$k_{\text{DPO}_4^{2-}}$	$(4.9 \pm 0.3) \times 10^2 \text{ s}^{-1} \text{M}^{-1}$

a) D₂O phosphate buffers, pH** 7.2, 1 M I

Table 2.1 shows that the main catalytic species for racemisation of **2.2** are the deuterioxide anion and the dibasic form of the buffer (DPO_4^{2-}) while little contribution is made by reactions involving the solvent or the monobasic form of the buffer (D_2PO_4^-). As mentioned earlier, the kinetic data related to racemisation of **2.2** at pH** 10.0 were not included in the three-dimensional fit described in this section. The introduction of the data points in the fits did not lead to significant differences in the rate constants reported in **Table 2.1**, however the fitted values were affected by larger errors. The same analysis was carried out for **2.1** but did not lead to equally satisfactory estimates for all the dependent parameters in **Equation 2.4**. In particular the catalytic rate constants relating to the racemisation of the deprotonated form of **2.1** were affected by big errors.

Hydantoins **2.1** and **2.2** are structurally very similar and their exchangeable protons in their ¹H NMR spectra have similar chemical shifts of $\delta=4.24$ and 4.16 ppm, respectively (in CDCl₃). The similar chemical shifts suggest similar local (electronic) environments. It therefore appeared reasonable to approximate the catalytic rate constants for racemisation of the protonated form of (*S*)-5-benzylhydantoin using the corresponding rate constants for (*S*)-3-*N*-methyl-5-benzylhydantoin at the same pH**, as also suggested by Lazarus.²¹

The substitution of the rate constants obtained for (*S*)-3-*N*-methyl-5-benzylhydantoin in the three-dimensional fit of the rate constant of racemisation of (*S*)-5-benzylhydantoin greatly simplified the system, affording a better evaluation of the individual catalytic constants for the deprotonated form of (*S*)-5-benzylhydantoin. **Figure 2.10 (right)**

shows the three-dimensional fit of the rate constants of racemisation of (*S*)-5-benzylhydantoin where the described substitution was made. The related catalytic rate constants are listed in **Table 2.2**.

Table 2.2: Estimates for the rate constants for individual catalytic species present in the buffer solutions^{a)} acting on deprotonated (*S*)-5-benzylhydantoin (BHyd) at 60 °C.

Rate constant	$k/10^{-6}$
k_0	$51 \pm 10 \text{ s}^{-1}$
k_{OD^-}	$(2.8 \pm 5.0) \cdot 10^3 \text{ s}^{-1} \text{M}^{-1}$
$k_{\text{D}_2\text{PO}_4^-}$	$(2.3 \pm 0.1) \cdot 10^4 \text{ s}^{-1} \text{M}^{-1}$
$k_{\text{DPO}_4^{2-}}$	$(3.4 \pm 0.6) \cdot 10^2 \text{ s}^{-1} \text{M}^{-1}$

a) D₂O phosphate buffers, pH** 7.2, 1 M I

The monobasic form of the buffer appears to be the main catalytic species for the racemisation of deprotonated **2.1**. This finding suggests the possibility of general-acid catalysis in the racemisation of the basic form of (*S*)-5-benzylhydantoin. Three scenarios can be envisaged to account for general-acid catalysis³⁸:

- Reactions involving rate-determining proton transfer to the substrate
- Equilibrium protonation followed by rate-determining deprotonation of another site of the molecule.
- Catalysis through hydrogen bonding

The second hypothesis is particularly interesting. It would in fact suggest a mechanism of racemisation involving the equilibrium re-protonation of **2.1** followed by racemisation through rate-limiting de-protonation. Such a mechanism should, however, be accounted for already in **Equation 2.4** as general-base catalysed reaction of the protonated form of **2.1**. The general-acid catalysis for reaction of the deprotonated form of **2.1** may therefore simply represent the difference in reactivity between **2.1** and **2.2**. If this is the case, then reaction of deprotonated **2.1** is not subject to general-acid or general-base catalysis. The term k_{OD^-} in **Table 2.2** is affected by a big error and does not allow us to draw unequivocal conclusions about the importance of this term on the

overall rate constant of racemisation of the deprotonated form of **2.1**. However an estimate can be made of the contribution of the term k_{OD^-} on the deprotonated form of **2.1**. The maximum value that can be obtained for k_{OD^-} from the data reported in **Table 2.2** is approximately $(8 \cdot 10^3) \cdot 10^{-6} \text{ s}^{-1} \text{ M}^{-1}$. At pH** 11.0 the concentration of the catalytic species OD^- can be estimated to be $3.5 \cdot 10^{-3} \text{ mol dm}^{-3}$ (see Appendix 1). An estimated value of $28 \cdot 10^{-6} \text{ s}^{-1}$ for the term $k_{OD^-} \cdot [OD^-]$ can be therefore calculated. At pH** 11.0 **2.1** is almost completely deprotonated (considering a pK_a^{**} of 8.65 the fraction of **2.1** in the deprotonated form can be calculated as 0.996). The contribution of the term $k_{OD^-} \cdot [OD^-]$ on the overall solvent and hydroxide catalysed racemisation of **2.1** at pH** 11.0 can be therefore estimated as $(28 \cdot 10^{-6}) \cdot 0.996 \text{ s}^{-1} \sim 28 \cdot 10^{-6} \text{ s}^{-1}$. Similarly, the contribution of the term $k_0 + k_{OD^-} [OD^-]$ for the protonated form of **2.1** (0.004 %, at pH** 11.0) can be estimated as approximately $262 \cdot 10^{-6} \text{ s}^{-1}$. The value of $262 \cdot 10^{-6} \text{ s}^{-1}$ can be calculated using the fitted values of k_0 and k_{OD^-} for **2.2** (**Table 2.1**) as estimates of the analogous terms for the protonated form of **2.1**. Finally, from the intercept of the straight-line fit of the experimental rate-constants for racemisation of **2.1** at pH** 11.0 a value of $342 \cdot 10^{-6} \text{ s}^{-1}$ can be obtained for the overall term $k_0 + k_{OD^-} [OD^-]$, for solvent and hydroxide catalysis for both protonated and deprotonated **2.1**. The estimated value of approximately $28 \cdot 10^{-6} \text{ s}^{-1}$ for the term $k_{OD^-} [OD^-]$ for the deprotonated form of **2.1** is therefore small compared to the term $k_0 + k_{OD^-} [OD^-]$ for protonated **2.1** and to the value of $342 \cdot 10^{-6} \text{ s}^{-1}$ obtained for the overall term $k_0 + k_{OD^-} [OD^-]$ for racemisation of **2.1**, at pH** 11.0 at 60 °C in D_2O . On the other hand, a small increase of slope is observed in the pH** rate profiles in **Figure 2.6, left** at pH** above 9, which also suggests only a small contribution for catalysis by deuteroxide ions on the deprotonated form of **2.1**. Catalysis by hydroxide ions on the deprotonated form of (*S*)-5 benzylhydantoin has also been reported by Lazarus.²¹

2.3.4. H/D exchange of (*S*)-5-benzylhydantoin

Kinetic experiments probing H/D exchange for **2.1** in D_2O phosphate buffers were carried out by means of 1H NMR spectroscopy. Pseudo-first-order rate constants for H/D exchange were obtained by following the decrease of the area of the 1H NMR peak corresponding to the exchangeable proton of **2.1** over time. H/D exchange experiments were carried out at 25 and 37 °C. No kinetic data for H/D exchange at 60 °C could be collected since, at this temperature, the residual water peak in the 1H NMR spectrum of

2.1 partially overlaps the signal of the exchangeable proton of the hydantoin, making the integration of the latter impossible. An additional problem with the use of ^1H NMR spectroscopy for our kinetic studies was the low solubility of **2.1** in D_2O , which made the collection of accurate kinetic data by ^1H NMR spectroscopy more difficult than by means of CD spectroscopy, for which lower concentrations are required. Kinetic traces from H/D exchange experiments for **2.1** carried out at 37 and 25 °C are shown in Figures 2.11 and 2.12, respectively.

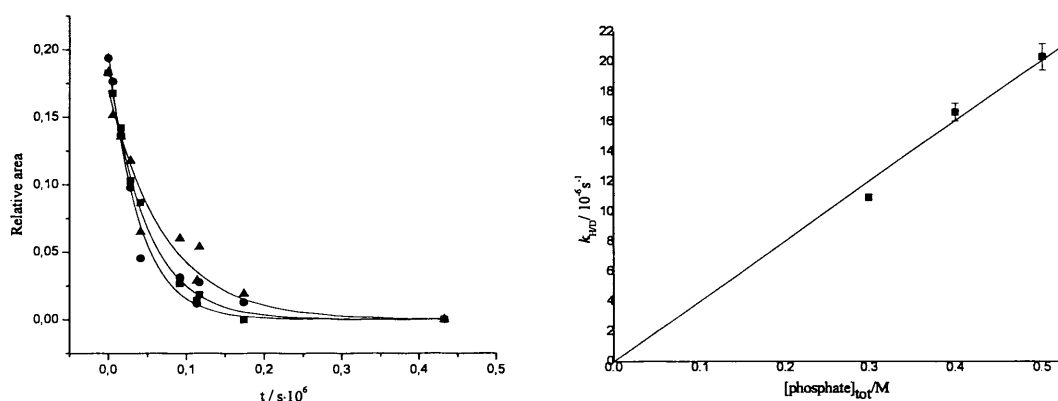


Figure 2.11: H/D exchange of (*S*)-5-benzylhydantoin **2.1** at 37 °C in D_2O phosphate buffers, pH** 7.2, 1 M I, 0.5 M (■), 0.4 M (●) and 0.3 M (▲). **Left:** relative area of the peak of the asymmetric proton in the ^1H NMR spectrum of **2.1** plotted as a function of reaction time. The relative area at each time of the reaction is defined as Area (asymmetric proton)/Area (protons of the phenyl ring). The peak area of the multiplet from the protons of the phenyl ring of **2.1** was set as 1 and used as an internal standard in each ^1H NMR spectrum. The lines are fits to pseudo-first-order kinetics with the final area set to zero. **Right:** observed rate constants of H/D exchange as a function of buffer concentration (the straight linear fit has been forced through the origin as, otherwise, a negative intercept would be obtained. The standard deviation for the linear fit forced through the origin is 0.87849 while a linear fit not forced through the origin gave the value of 0.81241. From the ratio of the squares of the two standard deviation, an $F_{(2,1)}$ value of 1.17 was obtained, lower than the tabulated value $F_{(2,1)}=199$, for a 1- tailed 95% confidence level³⁹. It can be concluded that forcing the straight line through the origin does not lead to a statistically significant reduction of the quality of the fit and the approximation is therefore acceptable.

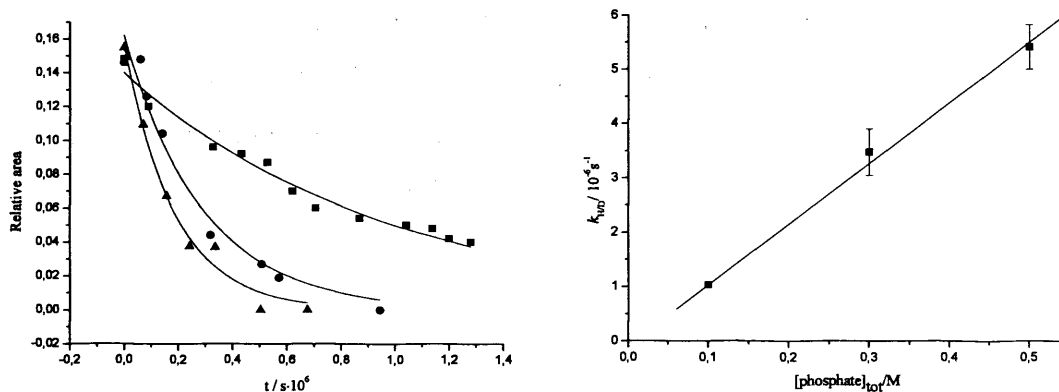


Figure 2.12: H/D exchange of (*S*)-5-benzylhydantoin **2.1** at 25 °C in D₂O phosphate buffers, pH* 7.2, 1 M *I*, 0.5 M (▲), 0.3 M (●) and 0.1 M (■). **Left:** relative area of the peak of the asymmetric proton in the ¹H NMR spectrum of **2.1** plotted as a function of reaction time. The relative area at each time of the reaction is defined as Area (asymmetric proton)/Area (protons of the phenyl ring). The peak area of the multiplet from the protons of the phenyl ring of **2.1** was set as 1 and used as an internal standard in each ¹H NMR spectrum. The lines are fits to pseudo -first-order kinetics with the final area set to zero. **Right:** observed rate constant of H/D exchange as a function of buffer concentration.

As shown in **Figures 2.11 (right) and 2.12 (right)**, general-base catalysis, observed for racemisation of **2.1**, was confirmed in H/D exchange experiments.

Table 2.3 shows the second-order rate constants for buffer-catalysed H/D exchange of **2.1** in D₂O phosphate buffers of 1 M *I* at pH** 7.2, at 37 and 25 °C and the corresponding rate constants for the combined uncatalysed and deuterioxide-catalysed H/D exchange reactions.

Table 2.3: rate constants for buffer-catalysed and for the combined uncatalysed and deuterioxide-catalysed H/D exchange of **2.1** in D₂O phosphate buffers, 1 M *I*, pH ** 7.2, at 37 and 25 °C.

Temperature / °C	$k_{\text{phosphate tot}} / 10^{-6} \text{ s}^{-1} \text{ M}^{-1}$	$k_0 + k_{\text{OD}^-} [\text{OD}^-] / 10^{-6} \text{ s}^{-1}$
37	38.5±20.6 ^{a)}	0 ^{b)}
25	11.4±0.7 ^{a)}	-0.1±0.1 ^{a)}

a) Standard errors from linear fitting performed by means of the program Origin.

b) The straight line fit has been forced through the origin.

2.4. Mechanistic aspects

2.4.1. The comparison of the rate constants of racemisation and H/D exchange of (*S*)-5-benzylhydantoin in phosphate buffers

As mentioned in the introduction of this Chapter, the comparison of the rate constants of racemisation with rate constants of H/D exchange allows stereochemical and mechanistic information to be obtained. Rate constants for racemisation of (*S*)-5-benzylhydantoin were compared with rate constants for H/D exchange in D₂O phosphate buffers, at 25 °C, under several conditions (**Table 2.4**).

Table 2.4: comparison of rate constants for racemisation and H/D exchange of (*S*)-5-benzylhydantoin **2.1** in D₂O phosphate buffers, 1 M *I*, at 25 °C.

[phosphate] / M	pH*	$k_{\text{rac}} / 10^{-6} \text{ s}^{-1}$	$k_{\text{H/D}} / 10^{-6} \text{ s}^{-1}$	$k_{\text{rac}} / k_{\text{H/D}}$
0.5	7.2	$6.28 \pm 0.08^{\text{a)}$	$5.42 \pm 0.41^{\text{a)}$	$1.2 \pm 0.1^{\text{c)}$
0.1	7.2	$1.30 \pm 0.02^{\text{a)b)}$	$1.03 \pm 0.05^{\text{a)}$	$1.3 \pm 0.1^{\text{c)}$
0.3	9.0	$8.79 \pm 0.25^{\text{a)}$	$6.69 \pm 0.29^{\text{a)}$	$1.3 \pm 0.1^{\text{c)}$

a) Errors from nonlinear least squares fitting performed by means of the program Origin based on the Levenberg-Marquardt (LM) algorithm.

b) Rate constant determined in H₂O phosphate buffer 0.1 M, 1 M *I*.

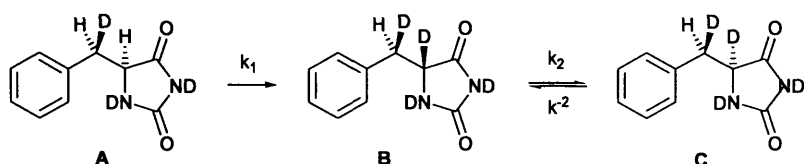
c) Errors calculated as uncertainties on functions of several variables.⁴⁰

The differences between rate constants for H/D exchange and racemisation are small, *viz.* up to a factor of 1.3. Testa *et al.*²³ reported values for $k_{\text{rac}}/k_{\text{H/D}}$ varying from 1.4 to 1.7 for 5-benzylhydantoin, although these values are for experiments under different experimental conditions (D₂O phosphate buffer, pD 7.4, 0.1 M, 0.22 M *I*, in a mixture with d₆-DMSO in the proportion 1:1 (v:v), at a series of temperatures between 50 and 80 °C).

Our ratios of $k_{\text{rac}}/k_{\text{H/D}}$ are close to unity, supporting an S_E1 rather than an S_E2 mechanism. Our experimental values $k_{\text{rac}}/k_{\text{H/D}}$ are similar to those reported by Caborderly¹⁷ for racemisation of a model tetrahydroisoquinoline hydantoin, as mentioned in Chapter 1.

2.4.2. The H/D exchange of deuterium-labelled 5-benzylhydantoins 2.1a and 2.2a.

For a better insight in the mechanistic aspects of the racemisation of 5-benzylhydantoins, deuterium-labelled 5-benzylhydantoin **2.1a** and deuterium-labelled 3-*N*-methyl-5-benzylhydantoin **2.2a** were synthesised and their H/D exchange reaction was studied by ^1H NMR spectroscopy. In the following discussion we will refer to 5-benzylhydantoin for descriptive convenience but the same considerations apply to 3-*N*-methyl-5-benzylhydantoin **2.2a**. If we assume an $\text{S}_{\text{E}}2$ mechanism for the racemisation of 5-benzylhydantoin and for the related H/D exchange reaction, then the “racemisation” of **2.1a** carried out in D_2O can be described as in **Scheme 2.7**. The scheme is analogous to **Scheme 2.2** but with the structures of A, B and C explicitly drawn. For convenience, only one of the “enantiomers” of A has been drawn.



Scheme 2.7: $\text{S}_{\text{E}}2$ mechanism for racemisation of 6-d-5-benzylhydantoin **2.1a**.

During the first irreversible step in **Scheme 2.7**, H/D exchange of A according to the $\text{S}_{\text{E}}2$ mechanism should give rise to the initial appearance of B followed by its decrease as a result of the second reversible step equilibrating diastereoisomers B and C. If racemisation occurs via an $\text{S}_{\text{E}}1$ mechanism, however, B and C should appear at the same rate and no temporary excess of B should be detected. Structures B and C should be distinguishable by ^1H NMR spectroscopy because they are diastereoisomers.

H/D exchange experiments on **2.1a** and **2.2a** were carried out in D_2O phosphate buffers at $\text{pH}^* 7.2$. **Figure 2.13 (top)** shows the NMR spectra of **2.1a** at the beginning (**left**) and at the end (**right**) of the H/D exchange experiment. The disappearance of the peak corresponding to the proton attached to the chiral centre in A (signal 1 in **Figure 2.13, left**) is observed during the kinetic experiments along with the appearance and growth of a peak attributed to diastereoisomer B (signal 2” in **Figure 2.13, right**).

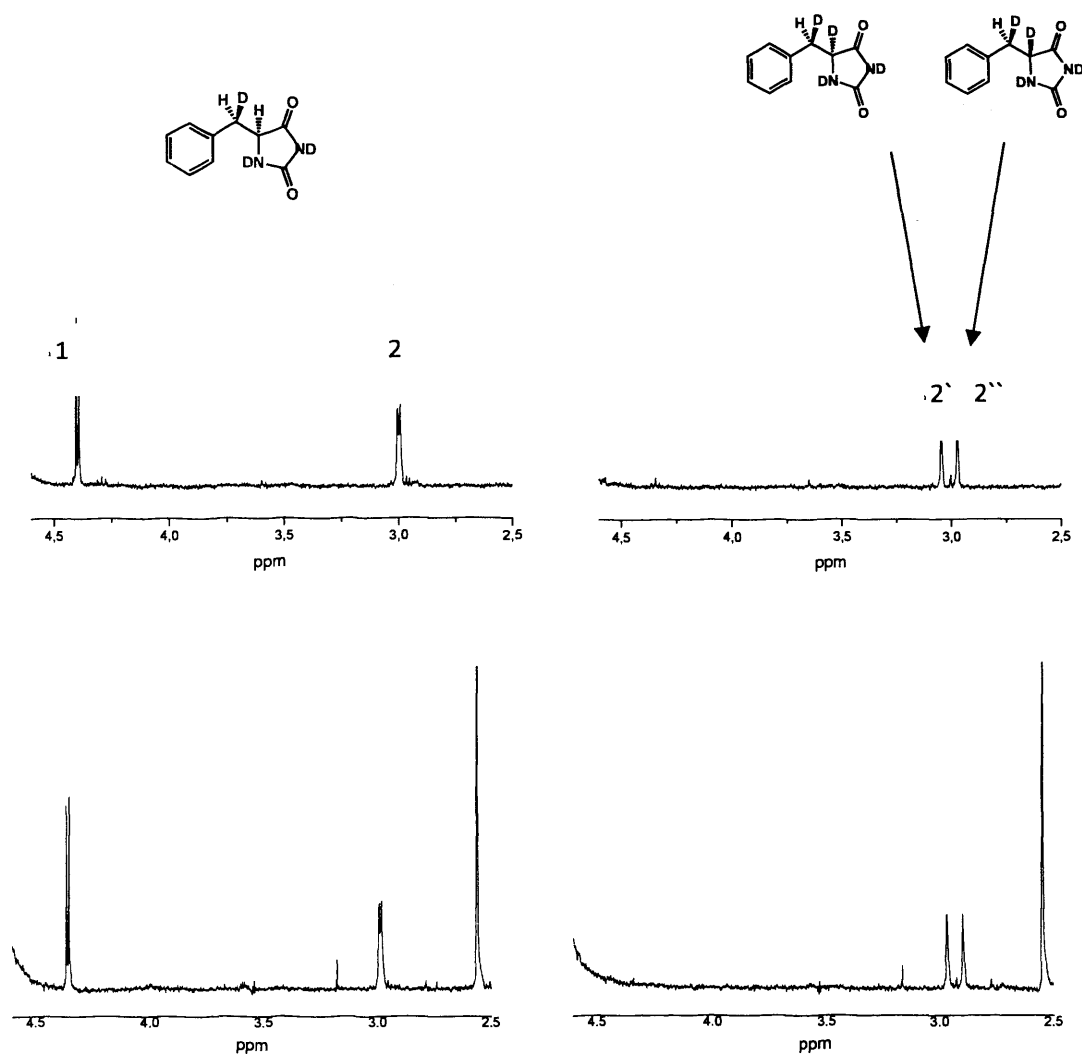


Figure 2.13 top: partial ^1H NMR spectra for **2.1a** at the beginning (**left**) and end (**right**) of a H/D exchange experiment carried out at 25 °C in D_2O phosphate buffer pH* 7.2, 0.5 M, 1 M I; **bottom:** partial ^1H NMR spectra of **2.2a** at the beginning (**left**) and end (**right**) of a H/D exchange experiment carried out at 25 °C in D_2O phosphate buffer pH* 7.2, 0.5 M, 1 M I.

The ^1H NMR signals for the methylene proton in **A** (signal 2), and for the methylene proton in **C** (signal 2'), have very similar chemical shifts and could not be resolved during the intermediate stages of the H/D experiment when species **A** and **C** are present simultaneously in the reaction mixture. H/D exchange experiments conducted on **2.2a** led to similar observations, as shown in **Figure 2.13 bottom, left and right**.

Figure 2.14 shows the integrals of peaks 1, 2+2' and 2'' as a function of time for H/D exchange experiments carried out on **2.1a** and **2.2a**, respectively. The fits describing the change over time of the area integral of the exchangeable protons of **2.1a** and **2.2a**, shown with squares (■) in **Figure 2.14**, gave the rate constants of H/D exchange for

2.1a (left) and **2.2a (right)**, respectively. The rate constant of H/D exchange for the deuterium-labelled compounds (for **2.1a** $k_{\text{H/D}}$ equals $(5.25 \pm 0.21) \cdot 10^{-6} \text{ s}^{-1}$, and for **2.2a** $k_{\text{H/D}}$ equals $(3.38 \pm 0.11) \cdot 10^{-6} \text{ s}^{-1}$) were consistent with the corresponding rate constants for H/D exchange of the unlabelled analogues under the same experimental conditions (**2.1** $k_{\text{H/D}} = (5.42 \pm 0.41) \cdot 10^{-6} \text{ s}^{-1}$, **2.2** $k_{\text{H/D}} = (3.36 \pm 0.16) \cdot 10^{-6} \text{ s}^{-1}$).

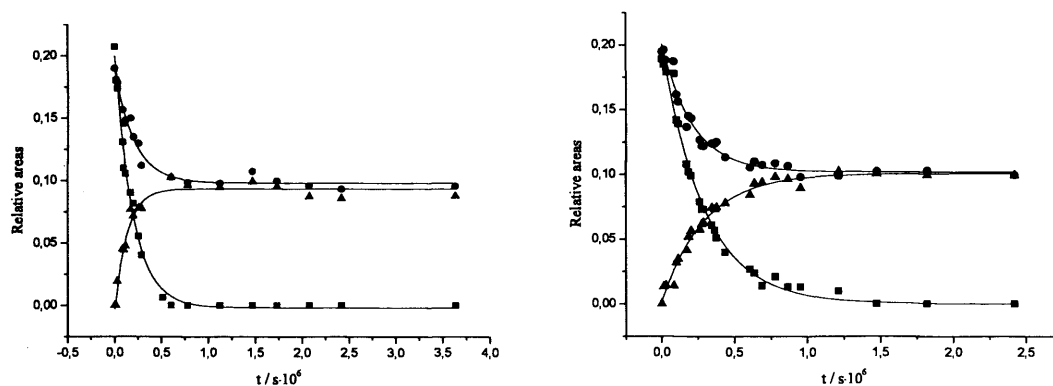


Figure 2.14: relative areas of peaks 1 (■), 2+2' (●) and 2'' (▲) as a function of time during H/D exchange of 6-d-5-benzylhydantoin **2.1a** (left) and during H/D exchange of 6-d-3-N-methyl-5-benzylhydantoin **2.2a** (right), at 25 °C in D₂O phosphate buffer pH* 7.2, 0.5 M, 1 M I. Lines are fits to first-order kinetics.

Traces 2'' (▲) show the change in concentration of species **B** over time during the H/D exchange experiments. For both hydantoins, no sign of an excess of **B** was observed at any stage of the reaction, or in any of the kinetic experiments, suggesting an S_E1 mechanism for racemisation of **2.1** and **2.2** under the tested experimental conditions.

2.4.3. Brønsted correlation for base-catalysed racemisation of 5-benzylhydantoins.

The effect of the base strength of the buffer on the rate constants of racemisation of **2.2** was investigated by studying the racemisation of **2.2** in acetate, TRIS, phosphate and borate buffers. The rate constants of racemisation were found to be markedly influenced by the base strength of the catalyst. Second-order rate constants for buffer-catalysed racemisations of **2.2** were determined at 60 °C by means of CD spectroscopy in acetate ($\text{p}K_{\text{a}}^{25\text{ °C}}=4.62$, $\text{p}K_{\text{a}}^{60\text{ °C}}=4.65$), TRIS ($\text{p}K_{\text{a}}^{25\text{ °C}}=8.08$, $\text{p}K_{\text{a}}^{60\text{ °C}}=7.06$), and borate ($\text{p}K_{\text{a}}^{25\text{ °C}}=9.2$, $\text{p}K_{\text{a}}^{60\text{ °C}}=8.96$) aqueous buffers at pH^{25 °C} 5.0, 8.1 and 9.3, respectively.⁴¹

The second-order rate constants for buffer-catalysed racemisation of **2.2** in the different buffers are listed in **Table 2.5**.

Table 2.5: Second-order rate constants for buffer catalysed racemisation ($k_{\text{buffer, basic component}}$) of **2.2** in aqueous buffers with 1 M I, at 60 °C, pH^{25 °C} 5.0 (acetate buffer), 8.1 (TRIS buffer), 9.3 (borate buffer) and pH** 7.2 (phosphate buffer)^{b)}.

Buffer	$k_{\text{buffer, basic component}} / \text{s}^{-1} \cdot \text{M}^{-1} \cdot 10^{-6}$
Acetate	10.3±1.8 ^{a) c)}
Phosphate ^{b)}	479.0±9.6 ^{a) c)}
Tris	910.5±6.2 ^{a) c)}
Borate	4382±107 ^{a) c)}

- a) Errors from non-linear least squares fitting performed by means of the program Origin using the Levenberg-Marquardt (LM) algorithm.
 b) Data related to D₂O phosphate buffers, see note ⁴¹.
 c) Rate constants are corrected for the fraction of the buffer in the basic form, considering pK_a values for the buffers, at 25 °C.

A Brønsted plot for racemisation of **2.2** at 60 °C was constructed (**Figure 2.15**). Two fits are reported in **Figure 2.15**, obtained by using literature values of pK_a of the buffers determined at either 25 or 60 °C.⁴²⁻⁴⁵ The values of β obtained from linear fits of the two sets of data are 0.57 ± 0.08 when pK_a values at 25 °C are used, and 0.59 ± 0.08 when pK_a values at 60 °C are considered. A small difference is obtained and the two values are within error margins. The β value of approximately 0.6 confirms general-base catalysis and reveals a transition state where the exchangeable proton in position 5 of (*S*)-3-*N*-methyl-5-benzylhydantoin is approximately halfway between the base (basic form of the buffers) and the chiral carbon of the hydantoin, as was also proposed by Lazarus.²¹ The experimental value of β is consistent with the literature²¹ value of 0.51. The strong similarities between **2.1** and **2.2**, as apparent from the previous experiments (*vide supra*), suggest that a similar conclusion can safely be drawn for **2.1**. Very similar β values for racemisation of **2.1** and **2.2** are also reported in the literature for catalysis by phosphate, TRIS, carbonate and hydroxide.²¹

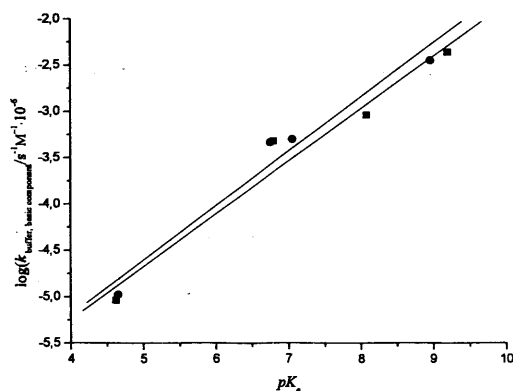


Figure 2.15: Brønsted plot for base-catalysed racemisation of **2.2** in aqueous buffers at 60 °C using pK_a values determined at 25 °C (■) and at 60 °C (●).⁴¹

The fact that general-base catalysis by borate buffer fits the same trend as the other buffers is interesting, because borate is not a “conventional” Brønsted base.⁴⁶

2.4.4. Kinetic isotope effects for racemisation of **2.1** and **2.2**

The kinetic experiments described so far suggest an S_E1 mechanism for base-catalysed racemisation of hydantoins **2.1** and **2.2** in aqueous media. In order to obtain additional information on the mechanistic aspects of racemisation of benzylhydantoins **2.1** and **2.2**, the solvent and primary kinetic isotope effects on the reaction were determined.

2.4.4.1. The solvent kinetic isotope effect

Rate constants for racemisation of **2.1** and **2.2** were determined in aqueous and D₂O phosphate buffers with equal buffer concentration and buffer ratios (Table 2.6).

Table 2.6: rate constants of racemisation of (*S*)-5-benzylhydantoin and (*S*)-3-*N*-methyl-5-benzylhydantoin in D₂O and H₂O phosphate buffers ^{a)}, 0.25 M, 0.5 M *I*, at 60 °C

Substrate	H ₂ O phosphate buffer	D ₂ O phosphate buffer
	$k_{\text{rac}}/10^{-6} \text{ s}^{-1}$	$k_{\text{rac}}/10^{-6} \text{ s}^{-1}$
2.1	167.3±1.3 ^{b)}	175.0±0.2 ^{b)}
2.2	114.4±0.5 ^{c)}	112.9±0.4 ^{c)}

- a) Buffers prepared by weighing separately potassium dihydrogen phosphate and potassium monohydrogen phosphate in the desired molar ratio and dissolving them in D₂O and H₂O, respectively. The measurement of the pH** and pH^{25 °C} of the above described solutions gave values pH** (D₂O) = 7.3 and pH^{25 °C} (H₂O) = 7.2.
- b) Errors from non-linear least squares fitting performed by means of the program Origin using the Levenberg-Marquardt (LM) algorithm.
- c) Errors from weighted averages of 2 or more analytical determinations.

Table 2.6 shows small differences between the rate constants of racemisation determined in deuterated and not deuterated media. As mentioned in Chapter 1, modest solvent kinetic isotope effects ($k_{\text{H}_2\text{O}}/k_{\text{D}_2\text{O}}$) of 1.13±0.05 and 1.24±0.08 were reported by Testa *et al.*²³ for racemisation of (*S*)-5-phenylhydantoin and (*S*)-5-benzylhydantoin, respectively, in a 50/50 (v/v) mixture of phosphate buffer and DMSO. Similarly, Cabordery *et al.*¹⁷ investigated the racemisation of tetrahydroisoquinoline hydantoins and reported a solvent kinetic isotope effect ($k_{\text{H}_2\text{O}}/k_{\text{D}_2\text{O}}$) of approximately 1.5 in a 75/25 (v/v) mixture of phosphate buffer and ethanol. In an S_E2 mechanism the breaking of the C-H bond in the transition state should be concerted with the donation of a proton or deuteron by a molecule of solvent or by a molecule of phosphate. The H₂O or D₂O molecules should, therefore, act both as solvent and reactants. The absence of a normal solvent kinetic isotope effect observed here, on the other hand, suggests no involvement of solvent molecules (as proton donors) in the rate-determining step of the reaction. In fact, for hydantoin **2.1** a small inverse solvent kinetic isotope effect is found. This inverse solvent kinetic isotope effect is attributed to the higher extent of deprotonation of **2.1** in H₂O as compared to D₂O, as usual (see Appendix 1).

As shown before, the rate constant of racemisation of the deprotonated species of **2.1** is negligible as compared to the rate constant of racemisation of the protonated form of **2.1**. The slightly larger fraction of the “non-racemising” deprotonated form of **2.1** in light water should lead to an overall slower racemisation of **2.1** in this solvent. This hypothesis is supported by the absence of an inverse solvent isotope effect for

racemisation of (*S*)-3-*N*-methyl-5-benzylhydantoin **2.2**, where deprotonation cannot occur.

2.4.4.2. The primary kinetic isotope effect

From the Brønsted plot (*vide supra*), a value of β of approximately 0.6 for racemisation of **2.2** was obtained, which suggests a symmetric and “stiff” activated complex where the exchangeable proton is halfway between the substrate and the base. A high primary kinetic isotope effect is anticipated for such a transition state.⁴⁷ (See Appendix 1).

In order to confirm this anticipated kinetic isotope effect, the rate constants for racemisation of (*S*)-5-benzylhydantoin **2.1** and of (*S*)-5-d-5-benzylhydantoin **2.1b** were measured both in non-deuterated and deuterated phosphate buffers at 60 °C (Table 2.7).

Table 2.7: rate constants of racemisation of **2.1** and **2.1b** in D₂O and H₂O phosphate buffers, 0.5 M, 1 M I, pH** or pH^{25 °C} 7.2^{a)}, at 60 °C and related primary kinetic isotope effects.

Phosphate buffer	$k_{\text{rac}}/10^{-6} \text{ s}^{-1}$		Ratio
	2.1b	2.1	
H ₂ O	76.9±0.7 ^{b)}	284.5±1.7 ^{b)}	3.70±0.04 ^{c)}
D ₂ O	85.8±0.9 ^{b)}	288.4±1.1 ^{b)}	3.36±0.04 ^{c)}

a) Buffers prepared by dissolving potassium dihydrogen phosphate in D₂O and adjusting the pH** or pH^{25 °C} of the solution with KOH

b) Errors from weighted averages of 2 or more determinations.⁴⁸

c) Errors calculated as uncertainties on functions of several variables.⁴⁰

A mean primary kinetic isotope effect of approximately 3.5 was found. As mentioned in Chapter 1, a similar primary kinetic isotope effect of 3.0 at 45 °C was reported by Wilson for base-catalysed bromination, and therefore racemisation,⁴⁹ of 2-*o*-carboxybenzyl-1-indanone⁵⁰ for which an S_E1 mechanism of racemisation is accepted. Bromination and racemisation of this ketone share the same rate-determining step, viz. anion formation.

2.4.5. Kinetic consequences of racemisation of (S)-5-benzylhydantoins 2.1 and 2.2 by the S_E1 and S_E2 mechanisms.

Scheme 2.2 by Testa *et al.*²³ describes the process of racemisation of a generic 5-substituted hydantoin carried out in D₂O. Good fits to pseudo first-order kinetics were obtained in all our kinetic experiments of racemisation carried out in deuterated buffers. However, if D₂O is the reaction medium and if there is a kinetic isotope effect on the rates of racemisation then a first-order kinetic law, strictly speaking, is not a correct kinetic model for the process.

Indeed, the transformation described in **Scheme 2.2** leads to a complex rate law. By definition, the steady state approximation cannot be used to simplify the analysis since we assume a temporary accumulation of B in the reaction medium during the reaction. Mathematical manipulations (see Appendix 1) to obtain a simple expression for the observable CD signal (A-B+C, *vide infra*) as a function of the rate constants k_1 , k_2 and k_2' (where $k_2 = k_2'$), lead to an inhomogeneous first-order equation with a general solution (**Equation 2.6**). **Equation 2.6** describes the trend of the CD signal during the racemisation of a generic chiral molecule *A* via an S_E2 mechanism, assuming the process is carried out in D₂O.

$$A - B + C = A_0 \cdot \left\{ -\frac{2}{2k_2 - k_1} \left[(k_1 - k_2) \cdot e^{-k_1 t} - \frac{k_1}{2} \cdot e^{-2k_2 t} \right] \right\} \quad \text{Equation 2.6}$$

Equation 2.6 predicts a temporary enantiomeric excess of the hydantoin with configuration opposite to that of the starting compound (Species B in **Scheme 2.2**), if $k_2 < k_1$. Technically the temporary excess of B over A and C is not a true enantiomeric excess because A and B are not strictly enantiomers as a result of the H/D exchange.

The temporary enantiomeric excess may be detected by studying the racemisation by means of analytical techniques enabling both a real time study of the process and the detection of the enantiomeric excess of one of the enantiomers in a mixture of the two. This effect should be, in principle, detectable by following the racemisation by means of circular dichroism (ECD).

In the process as shown in **Scheme 2.2**, the CD signal is proportional to $[A]-[B]+[C]$, at any time of the reaction. $[A]$, $[B]$ and $[C]$ are the concentrations of the species A, B and C respectively. The expected change in the CD signal over time during a process of racemisation following the S_E2 mechanism can therefore be mathematically simulated. Simulations (see **Figure 2.16**) show that, for a ratio of the rate constants k_2 and k_1 of 0.29 (that is considering a mean isotope effect of 3.5, obtained from our experimental values reported in **Table 2.7**), the predicted temporary enantiomeric excess of the opposite pseudo-enantiomer should be experimentally detectable by CD spectroscopy (See also Appendix 1).

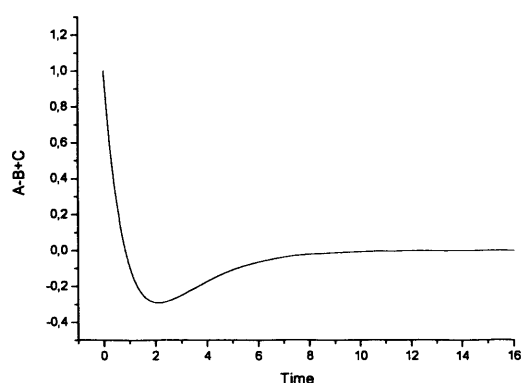


Figure 2.16: expected ECD signal plotted as a function of time in a simulated racemisation process with a value $k_2/k_1 = 0.29$, corresponding to our experimental primary kinetic isotope effect of 3.5. The time scale of the x axis is in arbitrary units.

No such effect was observed in any of our kinetic experiments of racemisation followed by ECD, as shown in **Figure 2.2** which reports a typical kinetic trace.

Equation 2.6 was used to fit simulated data with set values of the ratio k_2/k_1 : very good fits were obtained and the fitted values of k_1 and k_2 were in excellent agreement with the set ratios (see Appendix 1). Although no temporary enantiomeric excess was observed, we used **Equation 2.6** to fit experimental data obtained from racemisation experiments of (*S*)-5-benzylhydantoin **2.1** conducted at 60 °C and 25 °C. The fits are shown in **Figure 2.17**; the fits of the same data to the first-order kinetic law (**Equation 2.7**) are reported as well, for comparison.

$$A - B + C = A_0 e^{-k_{obs} t} \quad \text{Equation 2.7}$$

The obtained fitted values of k_1 , k_2 , and k_{obs} are reported in **Table 2.8**

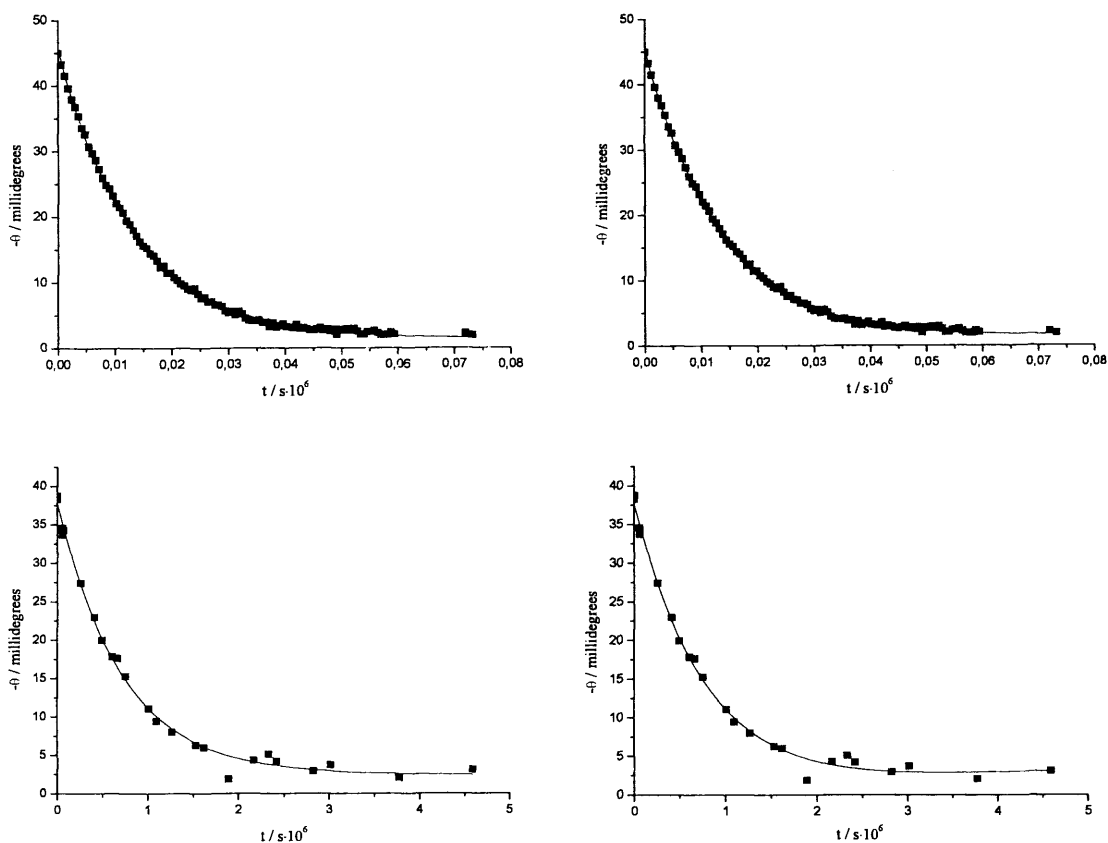


Figure 2.17: Fits of experimental data from racemisation experiments of **2.1** in D₂O phosphate buffer 0.1 M, pH** 7.2, 0.2 M *I* at 60 °C by **Equation 2.6** (top left) and **Equation 2.7** (top right) and at 25 °C by **Equation 2.6** (bottom left) and **Equation 2.7** (bottom right)

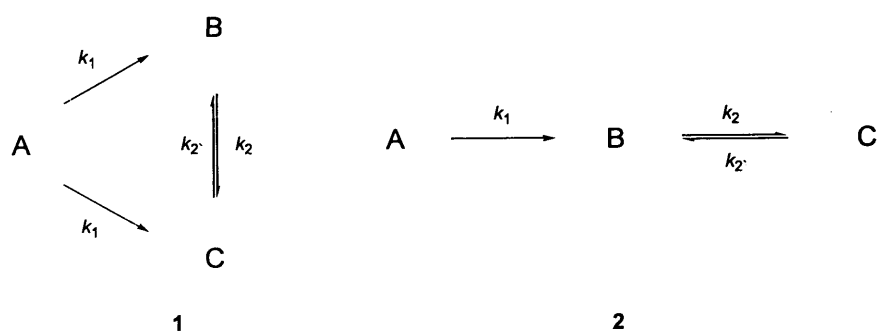
k_1 is the rate constant of enantiomerisation of the starting material, (*S*)-5-benzylhydantoin, while k_2 is the rate constant of enantiomerisation of an hypothetically labelled analogue of **2.1**, where the proton in position 5 of the hydantoin ring has been replaced by a deuterium. The fit of the data obtained from experiments of racemisation of **2.1** to **Equation 2.6** therefore indirectly provide an estimate of the primary kinetic isotope effect for the racemisation of a generic chiral molecule **2.1** in a deuterated medium, if the mechanism of reaction is S_E2. Small differences between the fitted values of k_2 and k_1 were obtained (mean ratio $k_2/k_1 = 0.9$) suggesting either a small primary kinetic isotope effect in the reaction, which is not consistent with our experimental primary kinetic isotope effect (*vide supra*), or an S_E1 mechanism.

Table 2.8: values of k_{obs} , k_1 and k_2 as defined in **Equations 2.6** and **2.7** for racemisation of (*S*)-5-benzylhydantoin **2.1** in D₂O phosphate buffer, pH** 7.2, 0.1 M, 0.2 M I, from fits of experimental data.

	$T / ^\circ\text{C}$	$k_{\text{obs}} / 10^{-6} \text{ s}^{-1}$	$k_1 / 10^{-6} \text{ s}^{-1}$	$k_2 / 10^{-6} \text{ s}^{-1}$
Equation	25	$1.40 \pm 0.06^{\text{a}}$		
2.7	60	$75.60 \pm 0.58^{\text{a}}$		
Equation	25		$0.69 \pm 0.03^{\text{a}}$	$0.61 \pm 0.05^{\text{a}}$
2.6	60		$37.36 \pm 0.24^{\text{a}}$	$34.57 \pm 0.44^{\text{a}}$

a) Errors from nonlinear least squares fitting performed by means of the program Origin based on the Levenberg-Marquardt (LM) algorithm.

As mentioned in Section 2.4.2, the use of labelled benzylhydantoins **2.1a** and **2.2a** for kinetic experiments of H/D exchange affords additional information as compared to the use of the unlabelled analogues **2.1** and **2.2**. In fact, the appearance of the species B in **Scheme 2.7** can be followed over time (by monitoring the appearance and growth of the area of peak 2'' in **Figure 2.13**) together with the simultaneous disappearance of A (by monitoring the decrease of the area of peak 1 in **Figures 2.13 left**). The change over time of the area of the third signal in the ¹H NMR spectra is complex since it "contains" the non resolved peaks 2 (from the methylene proton of A) and 2' (from the methylene proton of C, the deuterated analogue of A with the same configuration around the chiral centre). These three kinetic traces, shown in **Figure 2.14**, were analysed simultaneously (using Mathematica) in terms of the three rate constants k_1 , k_2 and k_2' , assuming an S_E2 mechanism for racemisation as shown in **Schemes 2.8, right**. The fit of the kinetic data for **2.2a**, shown in **Figure 2.14, right** gave a value for k_1 of $3.38 \cdot 10^{-6} \text{ s}^{-1}$ and similar values for k_2 and k_2' of approximately $13 \cdot 10^{-6} \text{ s}^{-1}$. The estimated values for the rate constants k_2 and k_2' are not consistent with our experimental primary kinetic isotope effect. In fact the high values of k_2 and k_2' , in comparison with the value of k_1 , suggest a very rapid equilibration between B and C, consistent with a model as shown in **Scheme 2.8 left**, where B and C are simultaneously formed. This model is in fact in line with an S_E1 process of racemisation.



Scheme 2.8: **Left:** schematic representation of mechanism 1, proposed for racemisation of **2.1a** and **2.2a**. **Right:** mechanism 2, describing the racemisation of a generic chiral compound, in D₂O, following a hypothetical S_E2 mechanism.

If k_2 and k_2' are much bigger than k_1 , mechanism 2 in **Scheme 2.8, left** becomes equivalent to mechanism 1 (**Scheme 2.8, right**).

2.5. Conclusions

Kinetic experiments of racemisation and H/D exchange of (*S*)-5-benzylhydantoin and (*S*)-3-*N*-methyl-5-benzylhydantoin, in both D₂O and aqueous buffers, gave evidence for pseudo-first-order kinetics and general-base catalysis. The kinetics of racemisation of 5-benzylhydantoin was found to be complicated by the acidity of the proton in position 3 of the hydantoin ring, in agreement with the literature.²¹ The basic form of the buffer is the main catalytic species in the racemisation of **2.2** and in the racemisation of the protonated form of **2.1**. The deprotonated form of **2.1** appeared to be less prone to racemise. The lower stereolability of deprotonated (*S*)-5-benzylhydantoin is explained by the presence of the negative charge inhibiting the abstraction of a second proton from the molecule, as also proposed by Lazarus²¹ and by Dudley and Bius.²² Similar rate constants for racemisation and H/D exchange of **2.1** in D₂O phosphate buffers, under identical experimental conditions, were found indicating that racemisation proceeds via an S_E1 mechanism.

Isotopically labelled 5-benzylhydantoin **2.1a** and 3-*N*-methyl-5-benzylhydantoin **2.2a** were synthesised. Kinetic experiments of H/D exchange of **2.1a** and **2.2a** enabled the monitoring over time of the concentration of the species with opposite configuration to

the starting material, species B in **Scheme 2.7**, during H/D exchange experiments. No temporary excess of the above mentioned species was detected at any stage of the H/D exchange experiments. A β value of 0.6 was obtained for racemisation of **2.2**, confirming general-base catalysis and revealing a symmetric activated complex for racemisation with the exchangeable proton halfway between the base and the molecule of hydantoin. Solvent and primary kinetic isotope effects for racemisation of **2.1** were determined. No normal solvent kinetic isotope effect was detected while the reaction revealed a mean primary kinetic isotope effect of 3.5. All experimental findings suggest a stepwise mechanism (S_E1) as the most likely mechanistic route for base catalysed racemisation of benzyhydantoin **2.1** and **2.2**, in purely aqueous media. Finally, a mathematical model for a generic S_E2 process of racemisation in D_2O was developed and experimental data of racemisation have been analysed in terms of this equation. No primary isotope effect was predicted by the fits of experimental data to the mentioned rate law. The finding confirms that the racemisation of **2.1** and **2.2** proceeds via an S_E1 mechanism.

2.6. Experimental Part 1

Materials

All solvents, drying agents, inorganic acids and bases were Laboratory Reagent Grade and were purchased from Fisher Scientific. All dry solvents were dried using an MB SPS-800 solvent purification system. All materials were used without further purification. (*S*)-2-amino-3-phenylpropanamide, (*S*)-methyl-2-amino-3-phenylpropanoate hydrochloride, methylamine (33% dry solution in ethanol), iodomethane, triethanolamine, 1d-benzaldehyde and palladium on activated carbon (5 weight %), were from Sigma-Aldrich. Carbonyldiimidazole (CDI), hydantoin, and benzaldehyde, were from Alfa-Aesar.

Chromathography

Filtrations were carried out on medium fast speed filter paper or on celite kieselgur, white (general purpose grade). Celite was from Fisher Scientific. Separations by HPLC were carried out on an Agilent HPLC system 1200 series equipped with a 1200 Series quaternary pump, a 1200 Series diode array detector, a 1200 Series vacuum degasser and a 1200 Series preparative autosampler. HPLC grade solvents were purchased from Fisher Scientific.

NMR Spectroscopy

^1H NMR spectra were recorded on a Bruker AVANCE 400 or a Bruker AVANCE 500 spectrometer at 400 or 500 MHz, respectively. ^{13}C NMR spectra were recorded on the same instruments as ^1H NMR spectra, at ^{13}C resonance frequencies of 101 MHz (Bruker AVANCE 400) and 126 MHz (Bruker AVANCE 500). Coupling constants are reported in hertz (Hz). Chemical shifts are reported in parts per million (δ) and are referenced to the residual ^1H and ^{13}C signal of the NMR solvent used in ^1H NMR and ^{13}C NMR spectra, respectively. Dimethylsulfoxide- d_6 , acetone- d_6 , chloroform- d or D_2O were used as reported in the individual sections. Dimethylsulfoxide- d_6 (D 99.9%) was purchased from Cambridge Isotope Laboratories, Inc, chloroform- d ($\text{H}_2\text{O}<0.01\%$, 99.80 %D) was from EURISO-TOP, deuterium oxide (99.9%) was obtained from Fluorochem.

Mass spectrometry

Molecular masses were determined from high resolution mass spectra (HRMS). The spectra were recorded on a Waters GCT Premier XE GCMS spectrometer. EI (electron impact) was used as ionisation method.

IR spectroscopy

IR spectra were recorded on a Varian Excalibur Spectrometer (FTS 7000) equipped with a SensIR ATR accessory (attenuated total reflectance Fourier transform infrared (ATR FT-IR) spectra) and a Deuterated Tri-Glycine Sulfate (DTGS) detector.

Melting points

Melting points were recorded on a Stuart Melting point SMP11. Thermometers were Brannan LO-tox with a temperature range 0-300 °C and divisions of 1 °C.

Polarimetry

Specific optical activities were determined by means of an Optical Activity Ltd. AA-1000 polarimeter in a 5.00 cm path length glass cell. D refers to the D line of the emission spectrum of sodium ($\lambda=589$ nm). Approximate optical purities were calculated based on literature values of specific optical activities of enantiopure compounds, when available. Solvent and concentration (expressed in g/100 ml) of the solutions used for the measurements are reported in the individual sections.

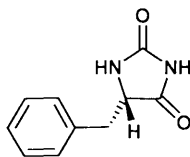
Methods

Two general methods were used to prepare more than one compound.

Method 2.1: synthesis of (*Z*)-5-benzylideneimidazolidine-2,4-diones 2.5, 2.6, 2.5a, 2.6a: (*Z*)-5-benzylideneimidazolidine-2,4-diones, precursor of the unlabelled racemic benzylhydantoins *rac*-2.1, *rac*-2.2, and of deuterium-labelled benzylhydantoins **1a** and **2a** were prepared by condensation of hydantoin or *N*-methylhydantoin with unlabelled or deuterium-labelled benzaldehyde. Hydantoin or *N*-methylhydantoin was dissolved in water (10 ml per gram of hydantoin) in a round bottom flask at 70 °C with stirring. The pH was adjusted to 7 with few drops of a saturated solution of NaHCO₃. Triethanolamine was added to the solution of hydantoin. A solution of aldehyde in ethanol (3 ml per gram of aldehyde), was then added dropwise and the temperature rose to reflux. The reaction mixture was kept under reflux for approximately 24 hours. The mixture was then allowed to cool down and the products were recovered by filtration. The solid products were washed with a mixture of ethanol and water (1:5) and recrystallised from ethanol.

Method 2.2: Hydrogenations: hydrogenations were carried out in a Parr 5500 Series Compact reactor connected to a hydrogen generator PGH₂600 and equipped with a Parr 4836 Controller (supplied by Scientific and Medical Products, ltd). The starting materials (*Z*)-5-benzylideneimidazolidine-2,4-diones were dissolved in dry THF and transferred in the vessel of the hydrogenation reactor. Pd/C (0.25 grams per gram of starting material) was added and the reaction chamber was sealed and pressurised with hydrogen up to 3 bars. The mixtures were allowed to react overnight under vigorous stirring. The reaction mixtures were then filtered under vacuum over a layer of celite and the products were recovered as pure, white solids upon evaporation of the solvent.

Synthesis of (*S*)-5-benzylimidazolidine-2,4-dione 2.1



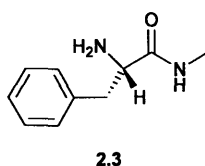
2.1

A suspension of (*S*)-2-amino-3-phenylpropanamide (0.50 g, 3.33 mmol) in dry CH₂Cl₂ (10 ml) in a sealed round bottom flask under nitrogen atmosphere was prepared. A solution of carbonyldiimidazole (0.81 g, 4.99 mmol) in dry CH₂Cl₂ (5 ml) was prepared in the same way. The solution of CDI was added by cannula to the suspension of (*S*)-2-amino-3-phenylpropanamide. The reaction mixture, kept under nitrogen atmosphere, was stirred overnight at room temperature. The hydantoin was found to precipitate from the reaction mixture. The precipitate was filtered, washed with water and high vacuum dried.

(*S*)-5-benzylimidazolidine-2,4-dione: yield 59%, M.p. 178-182 °C (literature values: 174-175 °C when recrystallised from EtOH; 179-180 °C, with partial melting at 174-175 °C when crystallised from water;²³ 173 °C;²¹ 182 °C;²⁹ 171-172 °C³⁰); HRMS m/z (EI⁺) = 190.0741, C₁₀H₁₀N₂O₂⁺ requires 190.0742; ¹H NMR (400 MHz CDCl₃): δ 7.55 (br s, 1H, CONHCO), δ 7.30-7.11 (m, 5H, C₆H₅), δ 5.28 (br s, 1H, CHNH), δ 4.24 (ddd J = 9.4, 3.8, 1.0 Hz, 1H, CH_AH_BCH), δ 3.23 (dd J = 13.9, 3.8 Hz, 1H,

CHCH_AH_B), δ 2.80 (dd, $J=13.9, 9.4$ Hz, 1H, CHCH_AH_B); ¹³C NMR (100 MHz, CDCl₃): δ 175.6 (CHCONH), δ 157.5 (NHCONH), δ 136.0 (C Ar), δ 130.1 (CH Ar), δ 128.5 (CH Ar), δ 127.0 (CH Ar), δ 58.8 (CH), δ 36.7 (CH₂). IR (neat): $\nu_{\max}=1759, 1688$ cm⁻¹ (C=O), $[\alpha]_D^{25} = -67^\circ$ (0.33 g/100 ml in EtOH) (literature value: $[\alpha]_D^{24} = -103^\circ$ (1.04 g/100ml in EtOH)²³; -93.7° (1 g/100 ml in acetone)²¹) optical purity=65%.

Synthesis of (S)-2-amino-N-methyl-3-phenylpropanamide 2.3

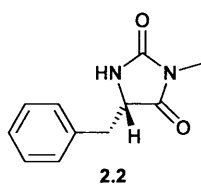


4 ml (32.45 mmoles) of a 33% dry solution of methylamine in ethanol (4.0 ml) was added to (S)-methyl 2-amino-3-phenylpropanoate hydrochloride (1.00 g, 4.64 mmoles), and the mixture was stirred at room temperature for five days. A 4 M solution of sodium carbonate was then added and the mixture was extracted with chloroform. The combined organic extracts were dried over anhydrous Na₂SO₄. The product was recovered as a light-yellow solid upon evaporation of the solvent and used in the next reaction without any further purification.

(S)-2-amino-N-methyl-3-phenylpropanamide: yield 87%, M.p. 58-60 °C (crystallised from CH₂Cl₂/Hexane) (Reported as a colourless oil in the literature⁵¹); HRMS m/z (EI⁺): molecular peak not detected, visible peak in LRMS at m/z (EI⁺)=120 consistent with M⁺-CONH₂⁵²); ¹H NMR (400 MHz D₂O): δ 7.29-7.06 (m, 5H, C₆H₅), δ 3.45 (dd appears as t, $J_{\text{mean}}=7.1$ Hz, 1H, CH₂CH), δ 2.82-2.72 (m, 2 H, CHCH_ACH_B), δ 2.49 (s, 3H, CH₃); ¹H NMR (400 MHz CDCl₃): δ 7.28-7.10 (m, 6H, C₆H₅ + NH), δ 3.56 (dd, $J=9.5, 4.0$ Hz, 1H, CH_ACH_BCH), δ 3.22 (dd $J=13.7, 4.2$ Hz, 1H, CHCH_ACH_B), δ 2.74 (d, $J=5.1$ Hz, 3H, CH₃), 2.62 (dd $J=13.7, 9.5$ Hz, 1H CHCH_ACH_B), δ 1.65 (br s, 2H, NH₂) (Appendix 1); ¹³C NMR (100 MHz, D₂O): δ 177.1 (CHCONH), δ 137.5 (C Ar),

δ 129.6 (CH Ar), δ 128.9 (CH Ar), δ 127.2 (CH Ar), δ 56.6 (CH), δ 41.0 (CH₂), 25.9 (CH₃); IR (neat): ν_{\max} = 1648 cm⁻¹ (C=O), $[\alpha]_D^{24}$ = -92° (crystallised from CH₂Cl₂/Hexane, 0.47 g/100 ml in chloroform) (literature value: $[\alpha]_D^{24}$ = -6.8° (1.1 g/100 ml in chloroform)⁵¹).

Synthesis of (*S*)-5-benzyl-3-methylimidazolidine-2,4-dione **2.2**

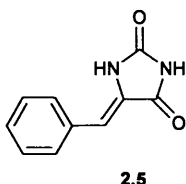


A solution of (*S*)-2-amino-*N*-methyl-3-phenylpropanamide **2.3** (1.10 g, 6.17 mmoles) in dry CH₂Cl₂ (25 ml) in a sealed round bottom flask under nitrogen atmosphere was prepared. A solution of CDI (1.50 g, 9.26 mmoles) in dry CH₂Cl₂ (25 ml) was prepared in the same way. The solution of amide was added by cannula to the CDI solution. The reaction mixture, kept under nitrogen atmosphere, was stirred overnight at room temperature. The solution was washed three times with acidified water (pH=2). The organic layer was then dried over anhydrous Na₂SO₄, filtered and concentrated. The product was purified by column chromatography on silica gel using CH₂Cl₂/ethyl acetate (80:20).

(*S*)-5-benzyl-3-methylimidazolidine-2,4-dione: yield 86%, M.p. 165-170 °C (literature value: 166-167 °C²¹); HRMS *m/z* (EI⁺) = 204.0894, C₁₁H₁₂N₂O₂⁺ requires 204.0899; ¹H NMR (400 MHz CDCl₃): δ 7.28-7.11 (m, 5H, C₆H₅), δ 5.73 (br s, 1H, NH), δ 4.16 (ddd, *J*=9.2, 3.7, 0.8 Hz, 1H, CH_AH_BCH), δ 3.21 (dd, *J*=13.9, 3.7 Hz, 1H, CHCH_AH_B), δ 2.88 (s, 3H, CH₃), δ 2.75 (dd, *J*=13.9, 9.2 Hz, 1H, CHCH_AH_B); ¹³C NMR (100 MHz, CDCl₃): δ 173.8 (CHCONCH₃), δ 157.9 (NHCONCH₃), δ 135.7 (C Ar), δ 129.6 (CH Ar), δ 129.2 (CH Ar), δ 127.8 (CH Ar), δ 59.0 (CH), δ 38.3 (CH₂), 24.9 (CH₃); IR (neat): ν_{\max} = 1752, 1706 cm⁻¹ (C=O), $[\alpha]_D^{24}$ = -64° (0.47 g/100 ml in

acetone) (literature value: $[\alpha]_D^{24} = -113^\circ$ (1.0 g/100ml in acetone²¹, $[\alpha]_D^{22.3} = -86.5^\circ$ (1.0 g/100 ml in acetone³¹); approximate optical purity=56%.

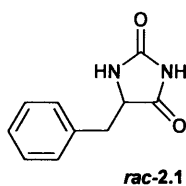
Synthesis of (*Z*)-5-benzylideneimidazolidine-2,4-dione **2.5**



Method 2.1 was followed. Amounts used: hydantoin: 1.00 g (10 mmoles), triethanolamine: 1.3 ml (10 mmoles), benzaldehyde: 1.1 ml (10 mmoles).

(*Z*)-5-benzylideneimidazolidine-2,4-dione: yield 43 %, M.p. 214-221 °C (crystallised from EtOH) (literature value: 220-224°C¹), HRMS m/z (EI^+) = 188.0584, ($C_{10}H_8N_2O_2^+$ requires 188.0586); 1H NMR (400 MHz d_6 -DMSO): δ 10.8 (br s, 1H, CNHCO), δ 7.68-7.27 (m, 5H, C_6H_5), δ 6.41 (s, 1H, CH); ^{13}C NMR (100 MHz, d_6 -DMSO): δ 165.9 (CCONH), δ 156.1 (NHCONH), δ 133.3 (C Ar), δ 129.7 (CH Ar), δ 129.1 (CH Ar), δ 128.7 (CH Ar), δ 128.3 (CHCCO), δ 108.6 (CH); IR (neat): $\nu_{max} = 1766, 1706\text{ cm}^{-1}$ (C=O), 1653 cm^{-1} (C=C).

Synthesis of racemic 5-benzylimidazolidine-2,4-dione *rac*-2.1



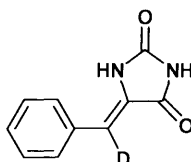
Method 2.2 was followed. (*Z*)-5-benzylideneimidazolidine-2,4-dione **2.5**: 0.22 g (1.17 mmoles) dissolved in 25 ml of dry THF.

5-benzylimidazolidine-2,4-dione: yield 98 %, M.p. 190-192 °C (literature value for racemic 5-benzylhydantoin = 185-186 °C³⁰); 1H NMR (400 MHz d_6 -DMSO): δ 10.50



(br s, 1H, CONHCO), δ 7.99 (br s, 1H, CHNH), δ 7.37-7.20 (m, 5H, C₆H₅), δ 4.39 (ddd appears as td, J=5.0, 0.9 Hz, 1H, CHCH_AH_B), δ 3.04-2.93 (m, 2H, CHCH_AH_B).

Synthesis of (*Z*)-5-(deutero(phenyl)methylene)imidazolidine-2,4-dione 2.5a

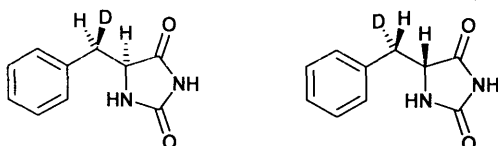


2.5a

Method 2.1 was followed. Hydantoin: 0.50 g (5.0 mmoles), triethanolamine: 0.66 ml (5.0 mmoles) 1d-benzaldehyde: 0.51 ml (5.0 mmoles).

(*Z*)-5-(deutero(phenyl)methylene)imidazolidine-2,4-dione: yield 36%, M.p. 222-226 °C (crystallised from EtOH); HRMS m/z (EI⁺) = 189.0643, (C₁₀H₇DN₂O₂⁺ requires 189.0649); ¹H NMR (400 MHz d₆-DMSO): δ 10.8 (br s, 1H, CNHCO), δ 7.66-7.27 (m, 5H, C₆H₅); ¹³C NMR (126 MHz) d₆-DMSO): δ 165.5 (CCONH), δ 155.6 (NHCONH), δ 132.8 (C Ar), δ 129.3 (CH Ar), δ 128.7 (CH Ar), δ 128.3 (CH Ar), δ 127.9 (CHCCO);⁵³ IR (neat): ν_{\max} = 1759, 1702 cm⁻¹ (C=O), 1648 cm⁻¹ (C=C).

Synthesis of 5-(deutero(phenyl)methyl)imidazolidine-2,4-dione 2.1a

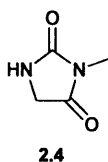


2.1a

Method 2.2 was followed. (*Z*)-5-(deutero(phenyl)methylene)imidazolidine-2,4-dione **2.5a**: 0.17 g (0.90 mmoles) dissolved in 20 ml of dry THF. The compound was obtained as a single diastereoisomer.

5-(deutero(phenyl)methyl)imidazolidine-2,4-dione: yield 94%, M.p. 188-190 °C, HRMS m/z (EI^+) = 191.0800 ($C_{10}H_9DN_2O_2^+$ requires 191.0805); 1H NMR (400 MHz d_6 -DMSO): δ 10.43 (br s, 1H, CONHCO), δ 7.93 (br s, 1H, CHNH), δ 7.30-7.15 (m, 5H, C_6H_5), δ 4.32 (d, $J=4.8$, 1H, CHCDH), δ 2.91 (d, $J=4.5$, 1H, CHCDH); ^{13}C NMR (126 MHz, d_6 -DMSO): δ 175.1 (CHCONH), δ 157.1 (NHCONH), δ 135.7 (C Ar), δ 129.7 (CH Ar), δ 128.0 (CH Ar), δ 126.6 (CH Ar), δ 58.3 (CH), δ 36.1 (t, $J=19.5$, CHD); IR (neat): ν_{max} = 1760, 1696 cm^{-1} (C=O).

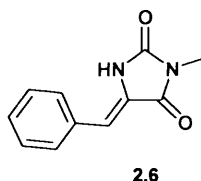
Synthesis of 3-methylimidazolidine-2,4-dione 2.4



A suspension of hydantoin (5.0 g, 50 mmoles) in 60 ml of ethanol was prepared in a round bottom flask with a condenser. 2.0 g (50 mmoles) of sodium hydroxide were dissolved in 45 ml of water. The solution of sodium hydroxide was added to the suspension of hydantoin and the mixture was stirred until a clear solution was obtained. Iodomethane (6.2 ml, 100 mmoles) was added drop wise. The reaction mixture was stirred, at room temperature, overnight. The pH of the solution was adjusted to 6 by means of aqueous HCl. The solution was then concentrated to a final volume of 30 ml and extracted with chloroform. The combined organic layers were dried over anhydrous Na_2SO_4 , filtered and concentrated to yield 3-methylimidazolidine-2,4-dione as a white solid. The product was used in the next synthetic steps without any further purification.

3-methylimidazolidine-2,4-dione: yield 33 %, M.p. 164-168 °C, HRMS m/z (EI^+) = 114.0425, ($C_4H_6DN_2O_2^+$ requires 114.0429); 1H NMR (400 MHz d_6 -DMSO): δ 8.08 (brs, 1H, NH), δ 3.95 (s, 2H, CH_2), δ 2.87 (s, 3H, CH_3); ^{13}C NMR (100 MHz, d_6 -DMSO): δ 172.5 (CH_2CONCH_3), δ 158.2 (NHCON CH_3), δ 46.3 (CH_2), δ 42.3 (CH_3); IR (neat): ν_{max} = 1774, 1746 cm^{-1} (C=O).

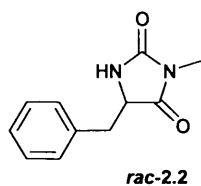
Synthesis of (*Z*)-5-benzylidene-3-methylimidazolidine-2,4-dione **2.6**



Method 2.1 was followed. 3-methylimidazolidine-2,4-dione **2.4**: 0.5 g (4.4 mmol), triethanolamine: 0.6 ml (4.4 mmol), benzaldehyde: 0.5 ml (4.4 mmol).

(*Z*)-5-benzylidene-3-methylimidazolidine-2,4-dione: yield 29 %, M.p. 220-224 °C (crystallised from EtOH), HRMS m/z (EI^+) = 202.0744, ($C_{11}H_{10}N_2O_2^+$ requires 202.0742); 1H NMR (400 MHz d_6 -DMSO): δ 10.8 (brs, 1H, CNHCO), δ 7.68-7.27 (m, 5H, C_6H_5), δ 6.54 (s, 1H, CH), δ 2.98 (s, 3H, CH_3); ^{13}C NMR (100 MHz, DMSO): δ 164.7 (C=O), δ 155.8 (NHCO), δ 133.1 (C Ar), δ 129.8 (CH Ar), δ 129.2 (CH Ar), δ 128.9 (CH Ar), δ 127.1 (CHCO), δ 109.6 (CH), δ 24.7 (CH_3) IR (neat): ν_{max} = 1746, 1701 cm^{-1} (C=O), 1648 cm^{-1} (C=C).

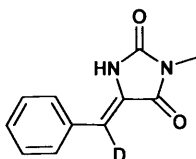
Synthesis of racemic 5-benzyl-3-methylimidazolidine-2,4-dione *rac*-**2.2**



Method 2.2 was followed. (*Z*)-5-benzylidene-3-methylimidazolidine-2,4-dione **2.6**: 0.20 g (0.98 mmol) dissolved in 20 ml of THF.

5-benzyl-3-methylimidazolidine-2,4-dione: yield 99 %, M.p. 127-129 °C. The expected signals were observed in the 1H NMR spectrum.

Synthesis of (Z)-5-(deutero(phenyl)methylene)-3-methylimidazolidine-2,4-dione 2.6a

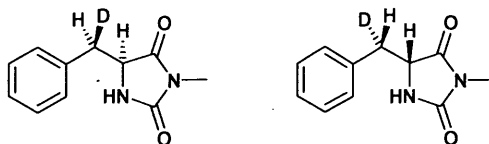


2.6a

Method 2.1 was followed. 3-methylimidazolidine-2,4-dione **2.4**: 0.45 g (3.9 mmoles), triethanolamine: 0.53 ml (3.9 mmoles), 1d-benzaldehyde: 0.4 ml (3.9 mmoles).

(Z)-5-(deutero(phenyl)methylene)-3-methylimidazolidine-2,4-dione: yield 39%, M.p. 203-206°C (crystallised from EtOH), HRMS m/z (EI^+) = 203.0804, ($C_{11}H_9DN_2O_2^+$ requires 203.0804); 1H NMR (400 MHz d_6 -DMSO): δ 10.8 (brs, 1H, CNHCO), δ 7.70-7.26 (m, 5H, C_6H_5), δ 2.96 (s, 3H, CH_3). ^{13}C NMR (100 MHz, d_6 -DMSO): δ 164.7 (C=O), δ 155.8 (NHCONCH₃), δ 133.1 (C Ar), δ 129.8 (CH Ar), δ 129.2 (CH Ar), δ 128.9 (CH Ar), δ 127.1 (CDCCO), δ 24.7 (CH_3);⁵⁴ IR (neat): ν_{max} = 1752, 1701 cm^{-1} (C=O), 1645 cm^{-1} (C=C).

Synthesis of 5-(deutero(phenyl)methyl)-3-methylimidazolidine-2,4-dione 2.2a



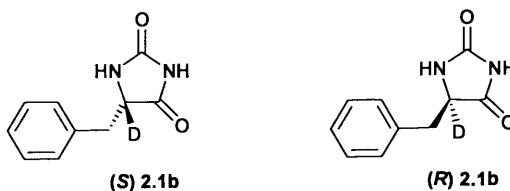
2.2a

Method 2.2 was followed. (Z)-5-(deutero(phenyl)methylene)-3-methylimidazolidine-2,4-dione **2.6a**: 0.2 g (0.98 mmoles) dissolved in 20 ml of THF. The compound was obtained as a single diastereoisomer.

5-(deutero(phenyl)methyl)-3-methylimidazolidine-2,4-dione: yield 97%, M.p. 126-128 °C, HRMS m/z (EI^+) = 205.0960, ($C_{11}H_{11}DN_2O_2^+$ requires 205.0962), 1H NMR (400 MHz d_6 -DMSO): δ 8.21 (brs, 1H, CHNH), δ 7.30-7.11 (m, 5H, C_6H_5), δ 4.36 (dd, $J=4.9, 1.0$ Hz, 1H, CHCDH), δ 2.96 (d, $J=4.8$, 1H, CHCDH), δ 2.65 (s, 3H, CH_3).

^{13}C NMR (126 MHz, d_6 -DMSO): δ 173.6 (CHCONCH₃), δ 156.7 (NHCONCH₃), δ 135.49 (C Ar), δ 129.5 (CH Ar), δ 128.0 (CH Ar), δ 126.7 (CH Ar), δ 57.2 (CH), δ 36.2 (t, J=16 Hz, CHD), δ 23.8 (CH₃); IR (neat): ν_{max} = 1773, 1691 cm^{-1} (C=O).

Synthesis of (S)- and (R)-5-deutero-5-benzylimidazolidine-2,4-dione (S) 2.1b and (R) 2.1b



A solution of racemic 5-benzylimidazolidine-2,4-dione, *rac*-2.1, (0.05 g, 0.26 mmoles) in D₂O (65 ml) was prepared. The pH was adjusted to 8 with few drops of triethylamine and the solution was stirred for 2 days at 60 °C in a stoppered round bottom flask. The solvent was evaporated and the solid high vacuum dried. 30 mg of the product were dissolved in 12 ml of methanol. The solution of racemate was resolved by HPLC on a chiral 25X4.6 mm Astec Chirobiotic T column. Only partial resolution of the two enantiomers could be achieved, the best experimental conditions being 100% methanol as mobile phase with a flow rate of 1 ml/min, run time of 8 minutes and UV detection at 230 nm. The individual HPLC fractions were concentrated and high vacuum dried. First eluting enantiomer (elution time: 4.1 min): (*R*)-5-deutero-5-benzylimidazolidine-2,4-dione: approximate optical purity=41%; Second eluting enantiomer (elution time: 4.5 min): (*S*)-5d-5-benzylimidazolidine-2,4-dione: approximate optical purity=32%.⁵⁵

(*S*)-5-deutero-5-benzylimidazolidine-2,4-dione: HRMS m/z (EI⁺)=191.0804, C₁₀H₉DN₂O₂⁺ requires 191.0805); ^1H NMR (400 MHz MeOD): δ 7.21-7.06 (m, 5H, C₆H₅), δ 2.99 (d J=14.1 Hz, 1H, CDCH_AH_B), δ 2.90 (d, J=14.1 Hz, 1H, CDCH_AH_B); ^{13}C NMR (100 MHz, CDCl₃): δ 176.0 (CDCONH), δ 158.4 (NHCONH), δ 135.3 (C Ar), δ 129.4 (CH Ar), δ 128.1 (CH Ar), δ 126.7 (CH Ar), δ 59.1 (t, J=22.7 Hz, CD), δ 36.7 (CH₂). IR (neat): ν_{max} = 1776, 1688 cm^{-1} (C=O).

2.7. Experimental Part 2

Materials

Potassium chloride (analytical grade) and acetic acid (analytical grade) were from Fluka. Potassium hydroxide (analytical grade) was from Fisher Scientific. Potassium dihydrogen phosphate (crystallised) was from VWR. Dipotassium hydrogen phosphate anhydrous was from Fisher Scientific. Deuterium oxide (99.9%) was purchased from Fluorochem. Potassium tetraborate tetrahydrate (99.5%) was from Alfa Aesar. Potassium acetate (99+%) was from Aldrich. Tris-(hydroxymethyl)-aminomethane (molecular biology grade, >99.9%) was purchased from Melford. The water used for the preparation of solutions was demineralised by means of a water purification system Purelab Option from Elga.

Apparatus

Materials were weighed on an analytical balance Fisher Brand PS-100 (Max 100 g, $d=0.1$ mg). Volumes of solutions were measured by means of Gilson or Eppendorf Research micropipettes. pH measurements were carried out, at room temperature, using a HANNA INSTRUMENTS pH 210 pH meter. The pH meter was calibrated before each measurement with certified traceable to NIST buffers at pH 7.00 ± 0.01 (at 25 °C) (from Fisher), pH 10.01 ± 0.02 (at 25 °C) (from Fisher) and pH 4.00 ± 0.01 (at 25 °C) (from Reagecon). Reported values are uncorrected. Values are reported as pH** indicating the reading of the pH meter. Thermostatic water baths Subaqua 12 (temperature stability ± 0.2 °C) or Julabo MB-5 Heating Circulator (temperature stability ± 0.2 °C) were used to control the temperature of solutions in kinetic experiments with timescales longer than three days. Kinetic experiments of racemisation were carried out on a Chirascan CD spectrometer equipped with a temperature-controlled sample holder for circular dichroism (temperature stability: ± 0.02 °C), in 1.00 cm path length quartz cuvettes, unless otherwise stated. Kinetic experiments of H/D exchange were carried out on a Bruker AVANCE 400 spectrometer at 400 MHz. Pulse interval (D1): 1 s, pulse width (pw): 10.75 μ s, acquisition time (at): 3.42 s.

Preparation of solutions

D₂O phosphate buffers pH** 6.0, 7.2, 8.0, 9.0, 10.0, 11.0, 2 M *I* and H₂O phosphate buffer pH** 7.2, 1 M, 2 M *I* were prepared by dissolving dihydrogen phosphate in D₂O and H₂O, respectively, and by adjusting the pH to the desired value with KOH. D₂O and H₂O phosphate buffers 0.5 M, 1 M *I*, were prepared by weighing separately potassium dihydrogen phosphate and potassium monohydrogen phosphate in the desired molar ratio and dissolving them in D₂O and H₂O, respectively.⁵⁶ The measurement of the pH** of the above described solutions gave values pH** (D₂O) = 7.33 and pH^{25 °C} (H₂O) = 7.24. For D₂O phosphate buffers, after preparation of the solutions, as described above, the solvent was evaporated and replenished 3 times with fresh D₂O, to guarantee the exchange with deuterons and removal of the protons from the non-deuterated inorganic materials used to prepare the solutions. D₂O phosphate solutions at pH** 9.0, 10.0 and 11.0 are, technically, not phosphate buffers since the pH is more than 1 units higher than the p*K*_a of the conjugate acid-base pair *KH*₂*PO*₄ / *K*₂*HPO*₄. However, no significant change of pH** was detected during kinetic experiments even in the presence of reduced buffer capacity. D₂O phosphate solutions at pH** 9.0, 10.0 and 11.0 should be, more correctly, regarded as solutions of catalyst of racemisation. Water acetate buffers pH^{25 °C} 5.0, 2 M *I* were prepared by mixing acetic acid and potassium acetate in the desired molar ratio and by adding water to the final desired total buffer concentrations. Water borate buffers pH^{25 °C} 9.3, 2 M *I* were prepared by dissolving the desired amount of potassium tetraborate tetrahydrate in water. No pH adjustment was made. Water TRIS buffers pH^{25 °C} 8.1, 2 M *I*: water solutions of Tris-(hydroxymethyl)-aminomethane were prepared and the pH was adjusted to the desired value with HCl. Potassium chloride was used to adjust the ionic strength of all buffer solutions.

Stock solutions of hydantoins were prepared by dissolving the solid hydantoins in D₂O or H₂O for the use in kinetic experiments carried out in deuterated and non-deuterated media, respectively. The solutions were prepared in plastic eppendorfs which were kept, overnight, under continuous rotation at a speed of 20 rpm by means of a Stuart Tube rotator SB2. The solutions were then centrifuged for 8 minutes at 13.3 rpm on a Jencons-pls Spectrafuge 24.D centrifuge. The clear supernatant was transferred in a new eppendorf and an amount of fresh solvent, equivalent to 1/10 of the total volume of solution, was added to the solutions, to avoid precipitation.

Kinetic studies

The reaction media for the CD experiments were prepared by mixing buffer solutions, D₂O, and the stock solutions of hydantoins in suitable proportions to obtain final solutions with the desired ionic strength, and concentrations of buffer and of hydantoin. Typical final concentrations of hydantoins were 0.4 mmolar for hydantoins **2.1** and **2.1b**, 0.9 mmolar for hydantoin **2.2**. Kinetic experiment of racemisation of **2.1** in D₂O 0.5 M phosphate buffer at 1 M ionic strength at different concentrations of the hydantoin showed the independence, within experimental errors, of the rate constants of racemisation on the concentration of hydantoin (See Appendix 1).

Solvents and stock solutions were mixed immediately before the start of the kinetic experiments, to minimise the time lag between the beginning of the reaction and the acquisition of the kinetic data. CD experiments at 60 °C were carried out in 1 cm quartz cuvettes housed in the thermostated sample holder of the spectrometer, unless otherwise stated. CD spectra were automatically recorded at set time intervals which were chosen based on the timescale of the reaction. In the kinetic experiments at 25 °C, the temperature was controlled by housing the solutions in thermostatic water baths. CD spectra were recorded at set time intervals. The decreases of the CD signals at 230 nm (for hydantoins **2.1** and **2.1b**) or 240 nm (for hydantoin **2.2**) were followed over time.

Kinetic experiments of racemisation for (*S*) 5-benzylhydantoin **2.1**, at different concentrations of substrate were carried out by mixing stock solution of buffer and stock solution of hydantoin in different proportion to give the desired final concentrations of buffer and hydantoin. The experiment at 100% volume (*S*)-5-benzylhydantoin, was carried out by dissolving the hydantoin directly in the buffer mixture. Experiments were carried out in 1 cm path length (5 and 10% volume of substrate) or 1 mm path length (50 and 100% volume of substrate), quartz cuvettes.

The reaction media for the kinetic experiments of H/D exchange were prepared by mixing equal volumes of stock solutions of buffers and stock solutions of hydantoins, to give the desired final concentrations of buffer and ionic strength. The choice of the final concentrations of hydantoins was limited by their solubilities in D₂O. Typical final concentrations were 2 mM for hydantoins **2.1**, **2.1a** and **2.1b** and 5 mM for hydantoins **2.2** and **2.2a**. Solvents and stock solutions were mixed immediately before the start of the kinetic experiments. Reaction mixtures were transferred in NMR tubes which were

housed in thermostatic water baths. ^1H NMR spectra were taken at set time intervals chosen depending on the time scale of the H/D exchange reaction. The NMR tubes were not thermostated during the time of acquisition of the ^1H NMR spectra.

Rate constants of H/D exchange were obtained by following the decrease of the relative area integral of the exchangeable protons of the hydantoins, over time. In all experiments, the ^1H NMR signal from the phenyl ring of the benzylhydantoins, was used as internal standard to evaluate the integrals of the ^1H NMR peaks of the exchangeable protons of **2.1** and **2.2** and of the exchangeable protons and methylene protons of **2.1a** and **2.2a**. Spectral processing and integrations of ^1H NMR signals were carried out by means of the program SpinWorks 2.5.5.

The rate constants for all kinetic experiments were obtained by fitting experimental data-points to first-order kinetics or to the kinetic model described by **Equation 2.6**, by means of the computer program Origin. The three-dimensional fits of the experimental rate constants for racemisation of **2.1** and **2.2**, at different pH** and buffer concentrations were carried out by means of the program “Mathematica”. The data analysis for the H/D exchange experiments of compounds **2.2a**, described in **Section 2.4.5** was also carried out by means of the program “Mathematica”.

pK_a measurements of 2.1

The UV spectra of **2.1** were recorded in D₂O phosphate buffers at different pH**, at 60 °C, in 1 cm quartz cuvettes, using a Jasco UV-VIS V-650 Spectrometer. Four titrations were performed using buffered solutions of **2.1** with concentrations of the hydantoin variable between 0.2 and 0.5 mM. The extinction coefficients (ϵ) of **2.1** at 230 nm were plotted as a function of pH**. The pK_a** was obtained from the fit of the data points to a sigmoidal curve.

Acknowledgments

I thank Dr Lavinia Onel for deriving **Equation 2.6**, which is the analytical solution of the kinetic model describing a hypothetical process of racemisation following an S_E2 mechanism and for the data analysis for hydantoins **2.1a** and **2.2a**. Dr Rob Richardson

is gratefully acknowledged for help in the synthesis lab, in particular with the use of the hydrogenation reactor and useful discussions. I thank Prof. Guy Lloyd-Jones for suggesting the use of deuterium-labelled **2.1a** and **2.2a**. Dr Benson Kariuki is acknowledged for the determination of the X-ray structure of **2.5**. Dave Walker and Robin Hicks are acknowledged for recording high resolution mass spectra.

References

1. Thenmozhiyal, J. C.; Wong, P. T. H.; Chui, W. K., *Journal of Medicinal Chemistry* **2004**, *47* (6), 1527-1535.
2. Brouillette, W. J.; Jestkov, V. P.; Brown, M. L.; Akhtar, M. S.; Delorey, T. M.; Brown, G. B., *Journal of Medicinal Chemistry* **1994**, *37* (20), 3289-3293.
3. Cortes, S.; Liao, Z. K.; Watson, D.; Kohn, H., *Journal of Medicinal Chemistry* **1985**, *28* (5), 601-606.
4. Brown, M. L.; Brown, G. B.; Brouillette, W. J., *Journal of Medicinal Chemistry* **1997**, *40* (4), 602-607.
5. Mehta, N. B.; Diuguid, C. A. R.; Soroko, F. E., *Journal of Medicinal Chemistry* **1981**, *24* (4), 465-468.
6. Zha, C. X.; Brown, G. B.; Brouillette, W. J., *Journal of Medicinal Chemistry* **2004**, *47* (26), 6519-6528.
7. Balog, A.; Salvati, M. E.; Shan, W. F.; Mathur, A.; Leith, L. W.; Wei, D. D.; Attar, R. M.; Geng, J. P.; Rizzo, C. A.; Wang, C. H.; Krystek, S. R.; Tokarski, J. S.; Hunt, J. T.; Gottardis, M.; Weinmann, R., *Bioorganic & Medicinal Chemistry Letters* **2004**, *14* (24), 6107-6111.
8. Zhang, X.; Allan, G. F.; Sbriscia, T.; Linton, O.; Lundeen, S. G.; Sui, Z., *Bioorganic & Medicinal Chemistry Letters* **2006**, *16* (22), 5763-5766.
9. Mudit, M.; Khanfar, M.; Muralidharan, A.; Thomas, S.; Shah, G. V.; van Soest, R. W. M.; El Sayed, K. A., *Bioorganic & Medicinal Chemistry* **2009**, *17* (8), 3216-3217.
10. Zuliani, V.; Carmi, C.; Rivara, M.; Fantini, M.; Lodola, A.; Vacondio, F.; Bordi, F.; Plazzi, P. V.; Cavazzoni, A.; Galetti, M.; Alfieri, R. R.; Petronini, P. G.; Mora, M., *European Journal of Medicinal Chemistry* **2009**, *44* (9), 3471-3479.

11. Kim, D.; Wang, L. P.; Caldwell, C. G.; Chen, P.; Finke, P. E.; Oates, B.; MacCoss, M.; Mills, S. G.; Malkowitz, L.; Gould, S. L.; DeMartino, J. A.; Springer, M. S.; Hazuda, D.; Miller, M.; Kessler, J.; Danzeisen, R.; Carver, G.; Carella, A.; Holmes, K.; Lineberger, J.; Schleif, W. A.; Emini, E. A., *Bioorganic & Medicinal Chemistry Letters* **2001**, *11* (24), 3099-3102.
12. Comber, R. N.; Reynolds, R. C.; Friedrich, J. D.; Manguikian, R. A.; Buckheit, R. W.; Truss, J. W.; Shannon, W. M.; Secrist, J. A., *Journal of Medicinal Chemistry* **1992**, *35* (19), 3567-3572.
13. Groutas, W. C.; Stanga, M. A.; Castrisos, J. C.; Schatz, E. J., *Journal of enzyme inhibition* **1990**, *3* (3), 237-43.
14. deLaszlo, S. E.; Allen, E. E.; Li, B.; Ondeyka, D.; Rivero, R.; Malkowitz, L.; Molineaux, C.; Siciliano, S. J.; Springer, M. S.; Greenlee, W. J.; Mantlo, N., *Bioorganic & Medicinal Chemistry Letters* **1997**, *7* (2), 213-218.
15. Kanyonyo, M.; Govaerts, S. J.; Hermans, E.; Poupaert, J. H.; Lambert, D. M., *Bioorganic & Medicinal Chemistry Letters* **1999**, *9* (15), 2233-2236.
16. Muccioli, G. G.; Martin, D.; Scriba, G. K. E.; Poppitz, W.; Poupaert, J. H.; Wouters, J.; Lambert, D. M., *Journal of Medicinal Chemistry* **2005**, *48* (7), 2509-2517.
17. Cabordery, A.-C.; Toussaint, M.; Azaroual, N.; Bonte, J.-P.; Melnyk, P.; Vaccher, C.; Foulon, C., *Tetrahedron-Asymmetry* **2011**, *22* (2), 125-133.
18. Toussaint, M.; Mousset, D.; Foulon, C.; Jacquemard, U.; Vaccher, C.; Melnyk, P., *European Journal of Medicinal Chemistry* **2010**, *45* (1), 256-263.
19. Tompkins, J. E., *Journal of Medicinal Chemistry* **1986**, *29* (5), 855-859.
20. Bovarnick, M.; Clarke, H. T., *Journal of the American Chemical Society* **1938**, *60*, 2426-2430.
21. Lazarus, R. A., *Journal of Organic Chemistry* **1990**, *55* (15), 4755-4757.
22. Dudley, K. H.; Bius, D. L., *Drug Metabolism and Disposition* **1976**, *4* (4), 340-348.
23. Reist, M.; Carrupt, P. A.; Testa, B.; Lehmann, S.; Hansen, J. J., *Helvetica Chimica Acta* **1996**, *79* (3), 767-778.
24. Kahn, K.; Tipton, P. A., *Bioorganic Chemistry* **2000**, *28* (2), 62-72.
25. Dakin, H. D., *American Chemical Journal* **1910**, *44*, 48.
26. Lee, C. K.; Fan, C. H., *Enzyme and Microbial Technology* **1999**, *24* (10), 659-666.

27. Pepper, C.; Smith, H. J.; Barrell, K. J.; Nicholls, P. J.; Hewlins, M. J. E., *Chirality* **1994**, *6* (5), 400-404.
28. Welch, C. J.; Kress, M. H.; Beconi, M.; Mathre, D. J., *Chirality* **2003**, *15* (2), 143-147.
29. Suzuki, T.; Igarashi, K.; Hase, K.; Tuzimura, K., *Agricultural and Biological Chemistry* **1973**, *37* (2), 411-416.
30. Yamaguchi, J.; Harada, M.; Kondo, T.; Noda, T.; Suyama, T., *Chemistry Letters* **2003**, *32* (4), 372-373.
31. Zhang, D.; Xing, X. C.; Cuny, G. D., *Journal of Organic Chemistry* **2006**, *71* (4), 1750-1753.
32. Akeng'a, T. O.; Read, R. W., *South African Journal of Chemistry-Suid-Afrikaanse Tydskrif Vir Chemie* **2007**, *60*, 11-16.
33. Mudit, M.; Khanfar, M.; Muralidharan, A.; Thomas, S.; Shah, G. V.; van Soest, R. W. M.; El Sayed, K. A., *Bioorganic & Medicinal Chemistry* **2009**, *17* (4), 1731-1738.
34. Mudit, M.; Khanfar, M.; Muralidharan, A.; Thomas, S.; Shah, G. V.; van Soest, R. W. M.; El Sayed, K. A., *Bioorganic & Medicinal Chemistry* **2009**, *17* (8), 3216-3217.
35. From SciFinder search: Takuma, Y.; Watanabe, N., (Mitsubishi Chemical Corp., Japan). Jpn. Kokai Tokkyo Koho (2001), 5pp. CODEN: JKXXAF JP 2001158775 A 20010612 Patent written in Japanese. Application JP 2000-149256 20000522.
36. Maskill, H., *The physical Basis of Organic Chemistry*. Oxford University Press: Oxford New York, 1990; p 278-282.
37. The pH values used in the titration was the conventional pH** defined as described in the experimental section, which was routinely used in all the experiments described in this thesis.
38. Maskill, H., *The Physical Basis of Organic Chemistry*. Oxford University Press: Oxford New York, 1990; p 327-335.
39. http://instruct.uwo.ca/geog/500/f_test.htm. (accessed 14 April 1012).
40. Taylor, J., *An introduction to error analysis The study of uncertainties in physical measurements*. Second ed.; University Science Books: Sausalito, California, 1997; p 73-77.

41. The value for the second-order rate constants for buffer catalysed racemisations of **2.2** in D₂O phosphate buffer has also been included. Considering the small solvent kinetic isotope effect observed for racemisation of (*S*)-5-benzylhydantoins **2.1** and **2.2**, the approximation was considered appropriate.
42. Fukada, H.; Takahashi, K., *Proteins-Structure Function and Genetics* **1998**, *33* (2), 159-166.
43. Ramette, R. W.; Culberson, C. H.; Bates, R. G., *Analytical Chemistry* **1977**, *49* (6), 867-870.
44. Good, N. E.; Winget, G. D.; Winter, W.; Connolly, T. N.; Izawa, S.; Singh, R. M. M., *Biochemistry* **1965**, *5* ((2)), 467-477.
45. Bates, R. G., *Journal of Research of the National Bureau of Standards Section a-Physics and Chemistry* **1962**, *66* (2), 179-&.
46. Silvestroni, P., *Fondamenti di Chimica*. 10th ed.; Masson Editoriale Veschi: Milano, 1996; p 711.
47. Anslyn, E. V.; Dougherty, D. A., *Modern Physical Organic Chemistry*. University Science Books: Sausalito, California, 2006; p 421.
48. Taylor, J. R., *An introduction to Error Analysis The study of uncertainties in physical measurements*. Second ed.; University Science Books: Sausalito, California, 1997; p 174-177.
49. Hsu, S. K.; Wilson, C. L., *Journal of the Chemical Society* **1936**, 623-625.
50. Wilson, C. L., *Journal of the Chemical Society* **1936**, 1550-1553.
51. Ojima, I.; Chen, H. J. C.; Qiu, X. G., *Tetrahedron* **1988**, *44* (17), 5307-5318.
52. Kasai, T.; Furukawa, K.; Sakamura, S., *Journal of the Faculty of Agriculture Hokkaido University* **1979**, *59* (3), 279-283.
53. The ¹³C NMR signal (CD), corresponding to the peak at δ 108.6 (CH), in the ¹³C NMR spectrum of the unlabelled analogue, **2.5**, appears to be very weak and not clearly distinguishable from noise.
54. The ¹³C NMR signal (CD), corresponding to the peak at δ 109.6 (CH), in the ¹³C-NMR spectrum of the unlabelled analogue, **2.6**, appears to be very weak and not clearly distinguishable from noise.
55. Absolute configurations and approximate optical purity of enantioenriched samples of (*S*) and (*R*) 5d-5-benzylimidazolidine-2,4-dione were **2.1b** obtained by comparing their respective CD spectra to CD spectra of (*S*) 5-benzylimidazolidine-2,4-

dione 2.1, used as a reference. It was assumed that CD and UV spectra were unaffected by the isotopic substitution.

56. The buffers prepared by weighing separately the basic and acidic forms of phosphate were used in the experiments for the determination of solvent kinetic isotope effects, to obtain the same buffer ratios in H₂O and D₂O. Unless otherwise stated, the other experiments were carried out in buffers prepared by dissolving potassium dihydrogen phosphate in D₂O and adjusting the pH* to the desired value with KOH.

Chapter 3

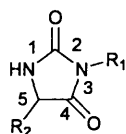
The effect of structural modifications on the kinetics and mechanism of racemisation of 5-substituted hydantoins.

Abstract

A series of hydantoins with different substituents in positions 3 and 5 has been synthesised and their configurational stability has been assessed by means of H/D exchange and racemisation experiments in phosphate buffers. H/D exchange and racemisation follow pseudo-first-order kinetics. General-base catalysis was observed for racemisation of the compounds obtained in optically active forms. Structural modifications in both positions 5 and 3 affect the rate constants of H/D exchange and racemisation. A mechanism involving intramolecular facilitation of racemisation by cationic functional groups is proposed for two 3-substituted hydantoins, one containing an alkyl chain with terminal protonated amino group and the other carrying an ammonium group as substituent. The possibility of intramolecular base-catalysis for racemisation of a model hydantoin containing a pyridyl group in its structure was also explored but no evidence was found supporting such catalysis. The solvent and primary kinetic isotope effects were determined for racemisation of (*S*)-5-substituted hydantoins carrying a pyridyl group and an *N*-methyl-pyrrolyl group. The significant primary kinetic isotope effects along with the absence of solvent kinetic isotope effects support an S_E1 mechanism for racemisation of the two hydantoins, as was also proposed in Chapter 2 for racemisation of (*S*)-5-benzylhydantoin.

3.1. Introduction

The possibility of correlating the structure of a chiral compound to its configurational stability is an important goal for medicinal and physical chemists. The study of structure-reactivity relationships is a classic technique used in physical chemistry to obtain information on reaction mechanisms¹ and, as far as the problem of chiral stability is concerned, an important starting point for a rationalisation of the phenomenon of chiral inversion. Several studies are present in the literature reporting compilations of data on the effect of structural variations on the configurational stability of different chiral compounds (see Chapter 1). The vast majority of the studies focus their attention on the variation of substituents directly attached to the chiral centre, since inductive and resonance effects are expected to be strongest if the reaction centre is directly involved. In the present chapter we present the effects of several structural modifications in positions 3 and 5 of the hydantoin ring (**Scheme 3.1**) on the rate constant of racemisation and H/D exchange. Modifications in position 3, relatively far from the chiral centre, were initially introduced in an attempt to obtain a model benzylhydantoin with a better water solubility than benzylhydantoin **3.1** (**Scheme 3.2**), with minimum alteration of its reactivity. It will be shown that not all of the substituents investigated appeared to fulfil both the desired requirements of increased water solubility and negligible effect on reactivity.



Scheme 3.1: the hydantoin ring

The substituents around the asymmetric carbon of chiral molecules with general structure $R^1R^2R^3CH$ are known to play a crucial role in the stabilisation or destabilisation of the chiral centre, in these carbon acids. Most studies present in the literature aimed at rationalising the phenomenon of racemisation, as mentioned in Chapter 1, focus their attention on the nature of substituents around the chiral centre and on their effects on the lability of the exchangeable proton.²⁻⁶

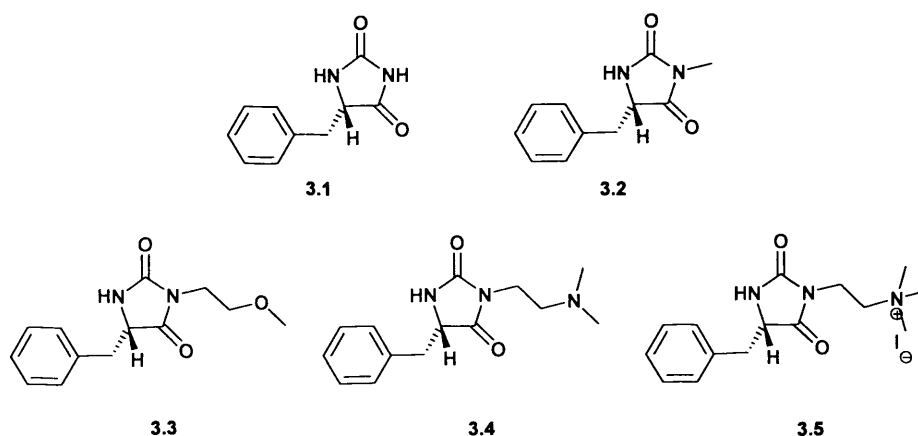
As also mentioned in Chapter 1, based on a collection of literature data on the racemisation of several chiral drugs Testa *et al.*^{4,5} provided guidelines for the prediction

of the configurational stability of carbon acids with general structure R^*R^*CH . In Testa's papers configurational stability is linked to the nature of substituents, classified as groups decreasing or increasing configurational stability and neutral groups, in the generic carbon acid R^*R^*CH . A similar approach was adopted by Wilson³ in a study aimed at establishing links between structure and configurational stability of compounds of the form R^*CHX where $X = -COR, -CN$ or NO_2 (Chapter 1). The importance of the ability of substituents at stabilising carbanions, i.e. increasing the acidity of carbon acids, has been highlighted in the literature as an important factor affecting the configurational stability of carbon acids. In Chapter 1 studies have been mentioned reporting on correlations between pK_a and rate constants of deprotonation by bases of a wide range of α -carbonyl carbon acids.⁶⁻¹¹

3.2. Structural modifications in position 3

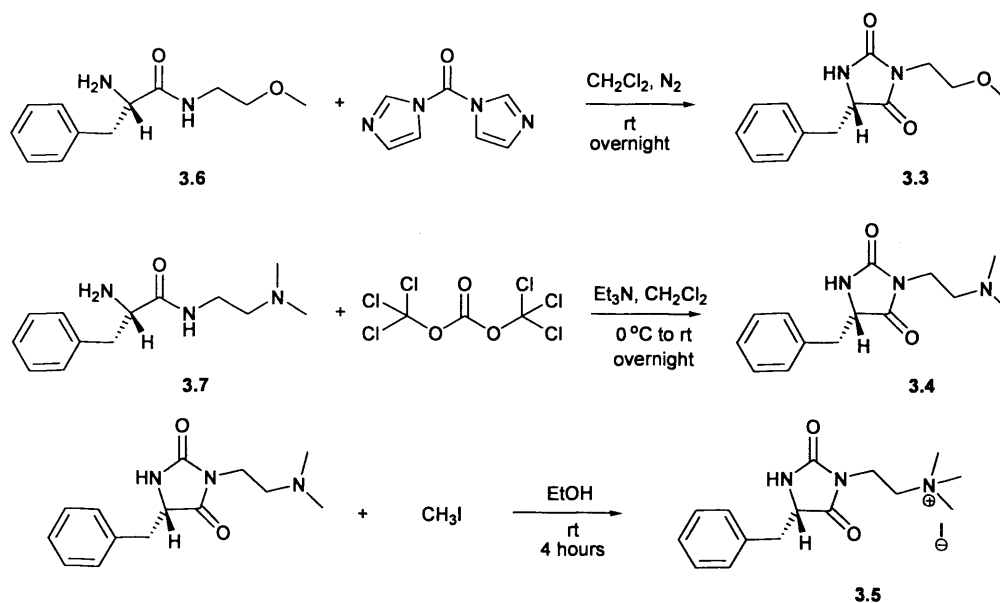
3.2.1. Syntheses

The introduction of polar groups in position 3 of the hydantoin ring appeared to be a convenient structural modification to obtain model (*S*)-5-benzylhydantoins with increased solubility in water. **Scheme 3.2** shows the structures of the (*S*)-3-*N*-substituted-5-benzyl hydantoins **3.3-3.5** that we have synthesised. In hydantoins **3.3-3.5** the substituents are not directly attached to the chiral centre, hence little change in the rate constants of racemisation was expected compared to benzylhydantoins **3.1** and **3.2**, whose structures are also shown in **Scheme 3.2**. As for compound **3.2**, the substitution of the hydrogen in position 3 with an alkyl group allowed to circumvent complications of the kinetics of racemisation arising from the presence of an acidic proton in the substrate (see Chapter 2). Compound **3.4** was initially synthesised simply as a reaction intermediate to prepare compound **3.5** but its racemisation and H/D exchange were investigated anyway.



Scheme 3.2: structures of (*S*)-5-benzylhydantoin **3.1**, (*S*)-3-*N*-methyl-5-benzylhydantoin **3.2** and of (*S*)-3-*N*-substituted-5-benzylhydantoin with increased water solubility **3.3-3.5**.

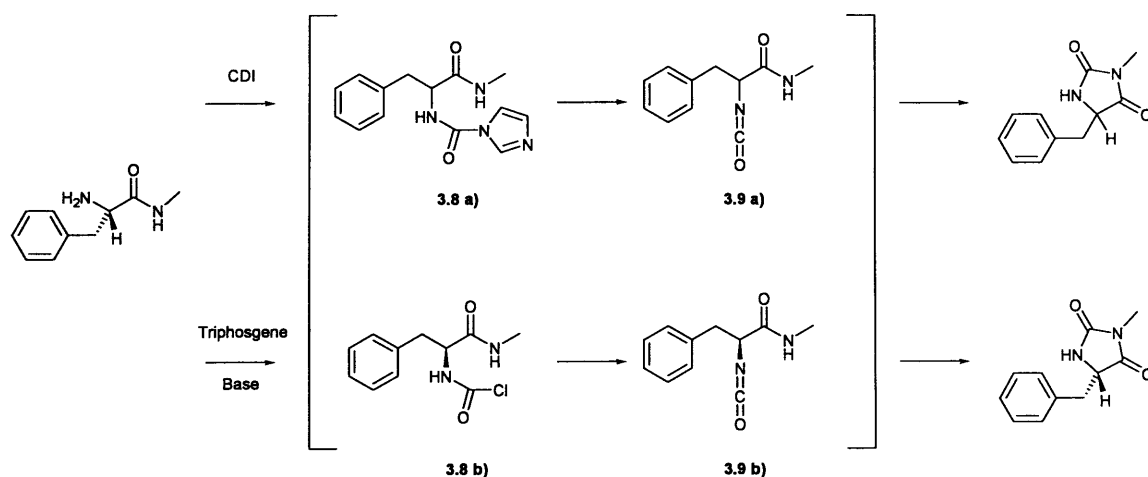
Hydantoins **3.3-3.5** were synthesised following the same synthetic route as used for (*S*)-3-*N*-methyl-5-benzylhydantoin **3.2** (Chapter 2), with a few modifications (**Scheme 3.3**). Aminoacid amide intermediates **3.6** and **3.7** were prepared from the corresponding alkyl amines and the common starting material *L*-phenylalanine methyl ester which was obtained by treatment of the corresponding hydrochloride salt with a saturated solution of Na_2CO_3 to free the amino group. Ring closures, to give optically active hydantoins **3.3** and **3.4**, were carried out by means of CDI and triphosgene, respectively. Compound **3.5** was obtained through methylation of **3.4** using methyl iodide.



Scheme 3.3: synthesis of (*S*)-3-*N*-substituted-5-benzylhydantoins **3.3-3.5**.

Unfortunately, the use of CDI in the synthesis of **3.4** led to its complete racemisation. Partial racemisation during the synthesis of (*S*)-3-*N*-methyl-5-benzylhydantoin from the α -amino amide and CDI has been reported by Zhang *et al.* while no racemisation was observed by these authors when triphosgene was used instead of CDI.¹²

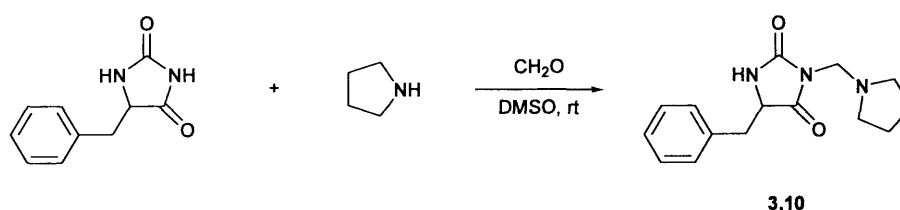
The mechanism of cyclization of α -amino amides with CDI and triphosgene, proposed by Zhang *et al.*, is shown in **Scheme 3.4**. The process involves the formation of intermediates **3.8 a)** and **3.8 b)** when using CDI and triphosgene, respectively. Intermediates **3.8 a)** and **3.8 b)** generate isocyanates **3.9 a)** and **3.9 b)** whose cyclizations give the product hydantoin with or without racemisation. Structures similar to **3.9 b)** and amino acid isocyanates are known not to racemise in the presence of bases.^{13, 14} The authors therefore attribute the racemisation during the synthesis with CDI to the intermediate imidazole carbamate **3.8 a)**. We think that racemisation of the product hydantoin during the synthesis should also be considered alongside the racemisation of reaction intermediate **3.8 a)**. During the reaction of α -amino amides with CDI, imidazole is formed as a leaving group, which has been reported¹⁵ to be a better catalyst for the racemisation of 5-phenylhydantoin than phosphate. The use of triphosgene avoids the generation of basic leaving groups and intermediates, thus allowing control over the process of racemisation during synthesis by reducing the concentration of bases and controlling the pH of the reaction medium.



Scheme 3.4: proposed mechanism for the cyclization of (*S*)-2-amino-*N*-methyl-3-phenylpropanamide by means of CDI and triphosgene to give racemic or enantioenriched (*S*)-*N*-methyl-5-benzylhydantoin **3.2**.

The higher stereolability of **3.4** (*vide infra*) as compared to hydantoins **3.1-3.3** and the presence of the amino group in the alkyl chain, potentially acting as additional catalyst of racemisation, could explain the complete racemisation of **3.4** during its synthesis when CDI was used. Although we assume that racemisation was not avoided completely, the use of triphosgene yielded (*S*)-5-benzylhydantoin **3.4** with a suitable enantiomeric excess to allow the study of its racemisation by means of ECD.

Racemic 5-benzyl-3-*N*-(pyrrolidin-1-ylmethyl) hydantoin **3.10** was prepared following published literature methods. Racemic 5-benzylhydantoin was obtained by condensation of hydantoin and benzaldehyde as described in Chapter 2.¹⁶⁻¹⁹ Racemic 5-benzylhydantoin was then coupled with pyrrolidine via a Mannich reaction (**Scheme 3.5**).²⁰



Scheme 3.5: synthesis of racemic 5-benzyl-3-*N*-(pyrrolidin-1-ylmethyl) hydantoin **3.10**.

3.2.2. Kinetic studies

The racemisation and H/D exchange reactions of hydantoins **3.3-3.5** were investigated under the same experimental conditions as used for compounds **3.1** and **3.2** (Chapter 2). Good fits of the experimental data to first-order kinetics were obtained in all cases (Appendix 2).

In **Figure 3.1**, the rate constants of racemisation for compounds **3.3**, **3.4** and **3.5** in D_2O phosphate buffers at 1 M *I* and 60 °C are reported as a function of buffer concentration. The rate constants of racemisation for compounds **3.1** and **3.2** are reported as well, for comparison. The linear increase of the rate constants with increasing buffer concentration suggests general-base catalysis for racemisation of compounds **3.3-3.5**, as was observed for benzylhydantoins **3.1** and **3.2**.

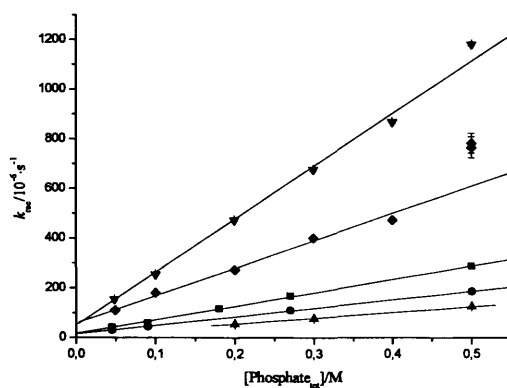


Figure 3.1: Rate constants of racemisation in D₂O phosphate buffers, pH** 7.2, 1 M *I* kept constant with KCl, at 60 °C of compounds 3.1 (■), 3.2 (●), 3.3 (▲), 3.4 (▼) and 3.5 (◆), as a function of buffer concentration.

We note that **Figure 3.1** shows that the observed rate constant for racemisation of 3.5 in D₂O phosphate buffer at a buffer concentration of 0.5 M deviates from the linear fit and that the observed rate constant is reproducible. A similar deviation may be occurring for 3.4 as well. Currently, we have no fully satisfactory explanation for this result.²¹

In **Table 3.1** the second-order rate constants for buffer-catalysed racemisation of hydantoins 3.1-3.5 and the corresponding pseudo-first-order rate constants for the combined uncatalysed and deuterioxide-catalysed processes are reported. For all hydantoins, under our experimental conditions, the main catalyst of racemisation is the phosphate buffer while the solvent-catalysed and deuterioxide-catalysed reactions are relatively unimportant.

Small differences in rate constants are observed for compounds 3.1-3.3, while the buffer-catalysed racemisation of 3.5 and, in particular, 3.4 are considerably faster.

Table 3.1: rate constants for buffer-catalysed and for the combined uncatalysed and deuteroxide catalysed racemisation of 5-benzylhydantoins **3.1-3.5** in D₂O phosphate buffers, 1 M I, kept constant with KCl, pH ** 7.2, at 60 °C.

Substrate	$k_{\text{phosphate tot}} / 10^{-6} \text{ s}^{-1} \cdot \text{M}^{-1}$	$k_0 + k_{\text{OD}^-}[\text{OD}^-] / 10^{-6} \text{ s}^{-1}$
3.1	542.2±2.5 ^{a)}	17.7±0.5 ^{a)}
3.2	342.6±0.9 ^{a)}	15.1 ±0.1 ^{a)}
3.3	231.2±1.7 ^{a)}	8.6±0.5 ^{a)}
3.4	2127±9 ^{a)}	51.1±0.8 ^{a)}
3.5	1106±19 ^{a)}	58.3±2.8 ^{a)}

a) Errors from linear fitting performed by means of the program Origin.

Similarly, 5-benzylhydantoins **3.4** and **3.5** were found to undergo faster H/D exchange as compared to substrates **3.1-3.3**. Pseudo-first-order rate constants of H/D exchange for hydantoins **3.1-3.5** in phosphate buffered D₂O, at 25 °C, are reported in **Table 3.2**.

Table 3.2: rate constants for H/D exchange of 5-benzylhydantoins in D₂O phosphate buffers, 0.5 M, 1 M I, kept constant with KCl, pH * 7.2, at 25 °C

Substrate	$k_{\text{H/D}} / 10^{-6} \text{ s}^{-1}$
3.1	5.42±0.41 ^{a)}
3.2	3.37±0.11 ^{b)}
3.3	2.11±0.01 ^{a)}
3.4	25.08±0.23 ^{a)}
3.5	12.38±0.23 ^{a)}

a) Errors from non-linear least squares fitting performed by means of the program Origin using the Levenberg-Marquardt (LM) algorithm.

b) Errors from weighted averages²² of 2 or more analytical determinations.

Comparison of the rate constants of racemisation with the rate constants of H/D exchange in principle allow the mechanism of racemisation to be identified (see Chapter 1). Unfortunately, in this case the data in **Tables 3.1** and **3.2** cannot be compared since

data were collected at two different temperatures. As was the case in Chapter 2 for hydantoin **3.1**, no kinetic data of H/D exchange at 60 °C could be collected due to a shift of the residual water peak in the ^1H NMR spectra of benzylhydantoins toward the signal of the exchangeable protons of the compounds, making the integration of the latter impossible.

Compound **3.4** was initially synthesised simply as a reaction intermediate (*vide supra*) and we thought that the presence of the amino group on the alkyl chain would likely complicate the kinetics of racemisation and render it potentially dependent on the protonation state of the molecule. Therefore, the racemisation of **3.4** in D_2O phosphate buffers at 1 M I , was studied at three different pH^{**} values, viz. 7.2, 6.0 and 8.0. In **Figure 3.2** the rate constants of racemisation of **3.4** are plotted as a function of total buffer concentration.

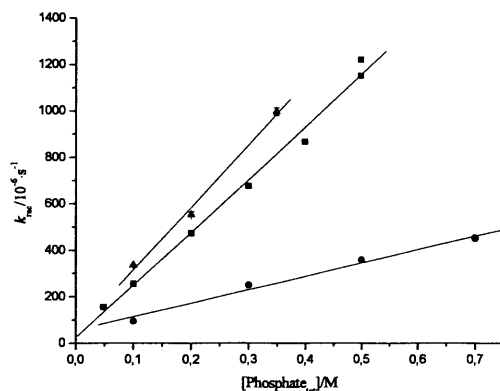


Figure 3.2: observed rate constants of racemisation for compound **3.4** in D_2O phosphate buffers 1 M I , kept constant with KCl, as a function of total buffer concentration at pH^{**} 6.0 (●), pH^{**} 7.2 (■) and pH^{**} 8.0 (▲), at 60 °C.

Figure 3.2 shows a steady increase of the slopes of the linear fits of the rate constants for racemisation of **3.4** as a function of buffer concentration with increasing the pH^{**} of the medium.

In **Figure 3.3** the rate constants for the combined uncatalysed and deuterioxide-catalysed racemisation, $k_0+k_{\text{OD}}[\text{OD}^-]$, and the catalytic rate constants for racemisation catalysed by the dibasic form of the buffer $k_{\text{DPO}_4^{2-}}$, as obtained from the linear fits in **Figure 3.2** are reported as a function of pH^{**} .

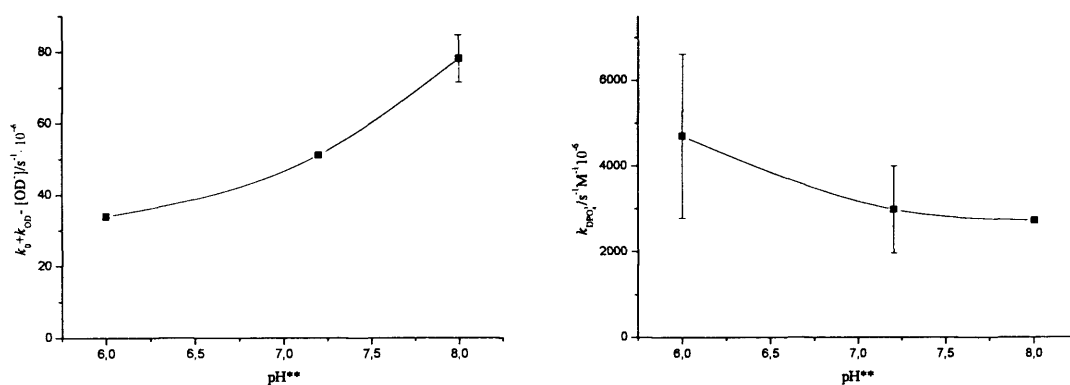


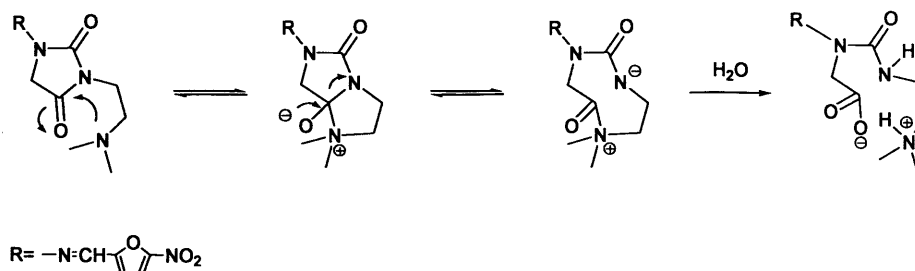
Figure 3.3: individual catalytic rate constants for racemisation of **3.4**, in D_2O phosphate buffers 1 M I , kept constant with KCl , at $60\text{ }^\circ C$ plotted as a function of pH^{**} . **Left:** rate constants for the combined uncatalysed and deuterioxide-catalysed racemisation. **Right:** second-order catalytic constants for racemisation catalysed by the dibasic form of the buffer $k_{DPO_4^{2-}}$.

As shown in **Figure 3.3 left**, the term $k_0 + k_{OD} [OD]$ for the combined uncatalysed and deuterioxide-catalysed racemisation, seems to show a steady increase with increasing pH^{**} . The catalytic rate constants for racemisation catalysed by the dibasic form of the buffer $k_{DPO_4^{2-}}$ (**Figure 3.3 right**) does not vary with pH^{**} within the (fairly big) error margins. The big error margins, the limited number of data points and the width of the pH^{**} interval does not allow definitive conclusions to be drawn about the protonation states of **3.4** in the reaction media investigated and their effect on the observed kinetics. The racemisation of **3.4** at higher pH^{**} values was not investigated due to stability issues, which further hinder interpretation of the pH^{**} dependence of $k_{DPO_4^{2-}}$. Evidence of the presence of **3.4** in different protonation states with different configurational stability cannot be derived from the data shown in **Figure 3.3**.

In fact, complications in addition to the possibility of different protonation states arose during the study of the racemisation of **3.4**. Hydantoin **3.4** was found to undergo rapid racemisation by CD spectroscopy and rapid H/D exchange by 1H NMR spectroscopy in D_2O , in the absence of added catalyst (and hence in the absence of buffer). The pH^* of the D_2O solution of **3.4** in the NMR tube was 9.78. Notably, after virtually complete

H/D exchange, the appearance of new peaks was observed in the NMR spectrum, suggesting structural changes in the molecule in addition to H/D exchange.

3-*N*-Aminoalkyl hydantoin with structures similar to **3.4** have been reported to hydrolyse easily in water via a nucleophilic attack by the terminal nitrogen atom on the carbonyl carbon in position 4, as shown in **Scheme 3.6**.²³



Scheme 3.6: proposed mechanism for hydrolysis of 3-(2-*N,N*-dimethylaminoethyl)-1-(5-nitrofurfurilideneamino) hydantoin.

The degradation of **3.4** in D₂O was followed by ¹H NMR spectroscopy. **Figure 3.4** reports three example ¹H NMR spectra for **3.4** in a D₂O solution, stored at 37 °C between experiments, and these spectra show clear changes. At the beginning of the experiment (*t*=0) the ¹H NMR spectrum shows only the peaks of the starting material. After 6 days the appearance of three new peaks was clearly observable in the ¹H NMR spectrum, viz. a singlet at δ=2.53 ppm, a doublet at δ=2.67 ppm with *J*=14.0 Hz and a triplet at δ=2.81 ppm with *J*=5.9 Hz. The ratio of the integrals for the new peaks was, consistently, 3 : 0.5 : 1 (singlet at δ=2.53 ppm : doublet at δ=2.67 ppm : apparent triplet at δ=2.81 ppm) in all the ¹H NMR spectra recorded during the experiment. The change in shape and an analysis of the integrals for the multiplet at δ=3.27-3.06 ppm and for the doublet at δ=2.98 ppm of the exchanged starting material suggested the appearance of two new signals in these regions of the spectrum. An increased complexity of the signals in the aromatic region, with the appearance of new peaks overlapping the peaks for the starting materials, was also observed. The area integrals of the singlet at 2.00 ppm and of the multiplet at 1.98-1.80 ppm of the starting material showed a decrease over time; the ratio of the areas being consistently 3:1 in all the ¹H NMR spectra recorded throughout the experiment. These observations clearly support the hypothesis

of degradation of hydantoin **3.4** over time with concurrent formation of a single new compound with a closely related structure, consistent with the hydrolysed hydantoin (see Appendix 2). In spite of the described complications in the kinetics of racemisation of hydantoin **3.4**, good fits to first-order kinetics were obtained both for racemisation and H/D exchange experiments. No changes were observed in the ^1H NMR spectra of **3.4** in phosphate buffered D_2O at pH^* 6.0 and 7.2, during the H/D exchange experiments. Some signs of the beginning of hydrolysis were observed in the very late stages of the H/D exchange experiments at pH^* 8.0 and in non-buffered D_2O solutions of **3.4**. However, in these latter cases, the effect of hydrolysis on the measured rate constants of racemisation appears negligible and within experimental error. As far as racemisation experiments are concerned, no evident change was detected in the UV spectra of **3.4** during kinetic experiments of racemisation, which further demonstrate the stability of the molecule over the time of racemisation experiments and supports the validity of our kinetic data.

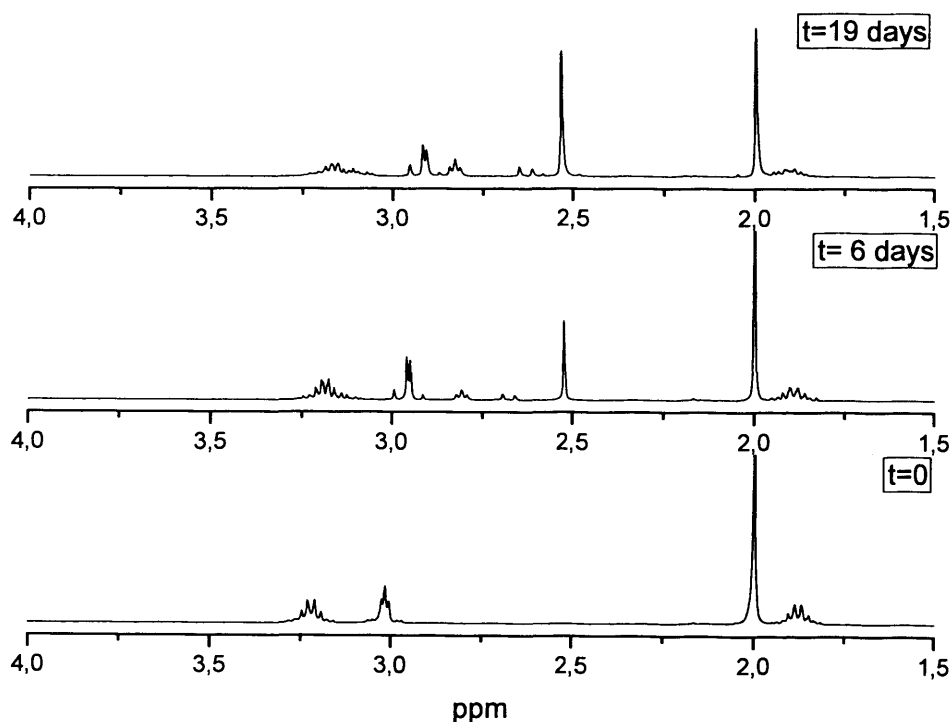


Figure 3.4: representative ^1H NMR spectra at 400 MHz, in the region between 4.0 and 1.5 ppm, of a D_2O solution of **3.4** stored at 37 °C, at time $t=0$ (bottom), after 6 days (middle) and after 19 days (top).

3.2.3. Activation parameters for racemisation of 3.2, 3.3 and 3.5

The temperature dependence of the rate constants of racemisation of hydantoins 3.2, 3.3 and 3.5 in D₂O phosphate buffer at pH** 7.2 was investigated and the activation parameters of racemisation were determined, according to the Eyring equation (Equation 3.1).²⁴

$$\ln\left(\frac{k \cdot h}{k_B \cdot T}\right) = -\frac{\Delta H^\ddagger}{R \cdot T} + \frac{\Delta S^\ddagger}{R} \quad \text{Equation 3.1}$$

Where k is the rate constant for DPO_4^{2-} -catalysed racemisation²⁵ (in $s^{-1} M^{-1}$), h is Planck's constant, k_B is the Boltzmann constant, R is the gas constant and T is the absolute temperature (in K).

Rate constants of racemisation were found to increase with an increase in the temperature. Figure 3.5 shows the Eyring plots for phosphate-catalysed racemisation of 3.2, 3.3 and 3.5.

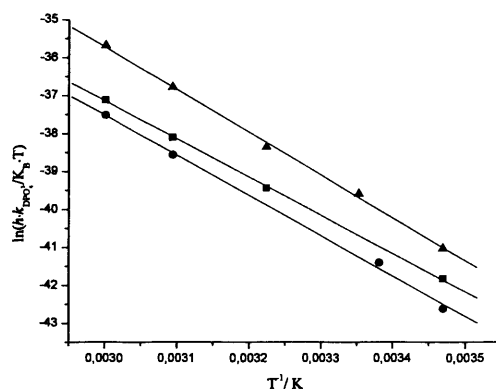


Figure 3.5: Eyring plots for racemisation of hydantoins 3.2 (■), 3.3 (●) and 3.5 (▲) in D₂O phosphate buffer 1 M I, kept constant with KCl, pH** 7.2.

Table 3.3 summarises the experimental values of enthalpy and entropy of activation for **3.2**, **3.3** and **3.5**.

Table 3.3: activation parameters for base-catalysed racemisation of (*S*)-5-benzylhydantoin **3.1**^a, **3.2**, **3.3** and **3.5** in D₂O phosphate buffer pH** 7.2, 1 M *I* kept constant with KCl.

Substrate	$\Delta H^\ddagger / \text{kcal mol}^{-1}$	$\Delta S^\ddagger / \text{e.u.}$
3.1 ^a	22.53±0.60 ^a	-10.3±0.4 ^a
3.2	20.0±0.2 ^b	-13.9±0.7 ^b
3.3	21.0±0.7 ^b	-11.5±2.4 ^b
3.5	22.4±0.5 ^b	-3.9±1.5 ^b

a) Literature value for activation parameters of deuteration in D₂O phosphate buffer, pD 7.4 / DMSO 1:1 (v/v).²

b) Errors from linear fitting performed by means of the program Origin.

All hydantoins show similar enthalpies of activation, close to the literature value for deuteration of (*S*)-5-benzylhydantoin **3.1**, also reported in **Table 3.3**.² Unfortunately, the comparison of the enthalpies of activation for compounds **3.2**, **3.3** and **3.5** with the values reported in the literature for **3.1** is, strictly, not correct. The literature data for H/D exchange of **3.1** were, in fact, determined in a solvent mixture composed of 50% d₆-DMSO and 50% D₂O phosphate buffer while our experimental values relate to racemisation experiments carried out in a purely aqueous medium. Moreover it appears from the paper by Testa *et al.*² that no correction has been made to account for the fact that catalysis is only by the basic component of the buffer, and this incorrect choice of the catalyst concentration will have affected the term ΔS^\ddagger . The comparison here is therefore intended to provide just qualitative information.

If we compare the entropies of activation we find similarities between compounds **3.2** and **3.3** while a less negative value is found for **3.5**.

The entropy of activation of a reaction is a complex term. It has been defined as a “probability or geometrical term”²⁶ and it can be described, in a very approximate manner, as the difference in what can be called “molecular order” between starting material and transition state in a generic chemical reaction.²⁷ A negative entropy of activation is found in those reactions where translational, vibrational or rotational

degrees of freedom are lost when passing from starting material to activated complex. Solvation is also an important factor which can significantly affect the value of ΔS^\ddagger . The complex nature of ΔS^\ddagger of a reaction makes its interpretation difficult; however comparison of values of ΔS^\ddagger appears to be reasonable within the context of the same, or strongly related, chemical reaction.^{26,27}

In a simple model of phosphate-catalysed racemisation of hydantoins, the chemical species potentially involved in the rate-determining step of reaction are a molecule of hydantoin, the catalyst (here dibasic phosphate) and molecules of D₂O. Catalyst and solvent are the same in all racemisation reactions compared here. We can therefore exclude any contribution from these species alone to the differences in the reaction profile of the investigated hydantoins. Any difference in the activation parameters of racemisation should therefore be attributed to differences in the structures of the hydantoins.

During the process of racemisation a CH bond is partially broken in the transition state with consequent formation of a partial negative charge on the carbon atom upon going from reactant to activated complex. In case of the racemisation of neutral hydantoins **3.1-3.3**, this corresponds to a net build up of charge upon going from reactants to activated complexes. In the case of the positively charged compound **3.5**, the developing negative charge is formed in the presence of the cationic substituent. The positive charge can be imagined to contribute intramolecularly to stabilisation of the formation of the partial negative charge in **3.5**, while for the neutral molecules, this role can only be played by the solvent water. Solvation will be accompanied by an “entropic penalty” due to the creation of a local shell of “structured” water molecules, oriented by the developing negative charge of the activated complex. In the case of compound **3.5**, an ammonium salt, solvation effects are already important in the reactants due to the positive charge of the ammonium group. Therefore, in the case of **3.5**, the “movement” along the reaction profile from reactants to activated complex involves passing from a charged species to a formally neutral one. This explanation could be worded alternatively by stating that the positive charge on the ammonium group could compete with the solvent at stabilising the developing negative charge in the transition state. Therefore, in the racemisation of **3.5**, contrary to substrates **3.1-3.3**, solvation effects should be more important in the reactant than in the activated complex, with a consequent smaller entropic loss while going from the reactant state to the transition

state. As will be discussed later in this chapter (Section 3.2.4), an effect of intramolecular stabilisation of the activated complex could be hypothesised for the racemisation of **3.5**.

3.2.4. Mechanistic considerations

3.2.4.1. The possible mechanisms of intramolecular participation of the cationic groups in the racemisation of **3.4 and **3.5****

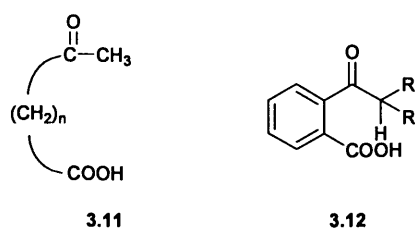
Racemisation and H/D exchange experiments described in Section 3.2.2 highlight the higher stereolability of benzyldantoin **3.4** and **3.5** as compared to substrates **3.1-3.3**. This observation, taken together with the fast hydrolysis of hydantoin **3.4**, due to intramolecular nucleophilic participation of the terminal amino group, prompted us to consider the possibility of similar effects of intramolecular participation also in the process of racemisation of **3.4** and **3.5**.

A list of typical participating functional groups and of the modes in which neighbouring groups often participate in reaction is reported by Isaacs.²⁸ Typical participating groups are those with unshared pairs of electrons (O, N, S, P and halogen) or π -electrons (alkenes or arene groups). The types of participation include nucleophilic participation, electrophilic participation (*i.e.* intramolecular proton transfer), intramolecular acid and base catalysis by neighbouring groups through solvent molecules.

A few examples are present in the literature of intramolecular catalysis in processes involving racemisation or keto-enol tautomerism. Among those it is worth mentioning the detailed study by Kahn *et al.*²⁹ on the racemisation of allantoin (5-ureidohydantoin), whose results have been briefly summarised in Chapter 1. Three different mechanisms for the racemisation of allantoin are envisaged in the paper, among which the S_E2 mechanism proposed by Testa *et al.*² for racemisation of 5-substituted hydantoins. Allantoin was found to racemise both via an S_E1 or S_E2 mechanisms (no distinction is made between the two in Kahn's paper) and via an intramolecular process involving a bicyclic intermediate (see Chapter 1). Similarly, racemisation of **3.4** and **3.5** may

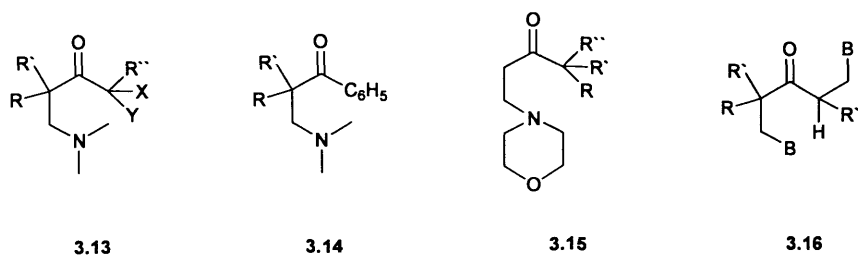
proceed via an alternative pathway involving the terminal amino or ammonium groups in **3.4** and **3.5**.

Bell and Fluendy³⁰ and Harper and Bender³¹ propose intramolecular general-base and/or general acid catalysis in enolization of ketones **3.11**³⁰ and **3.12**³¹ (**Scheme 3.7**). Although the model compounds studied in these papers are achiral, the investigations are interesting in our discussion since it is well established that enolisable chiral ketones racemise via an S_E1 mechanism and rates of enolisation equal those of racemisation.^{3, 32-35} Similar intramolecular catalysis may therefore be occurring in the racemisation of **3.4** and **3.5** as well.



Scheme 3.7: general structures of the model ketones studied by Bell and Fluendy (**3.11**) and by Harper and Bender (**3.12**)

Work by Coward and Bruice³⁶ evaluates the possibility of concerted general-base general-acid catalysis on enolisation of a series of β -amino ketones. The structures of the ketones investigated are reported in **Scheme 3.8**. Even if no evidence was found for concerted general-base general-acid catalysis for the diamino ketones, evidence is given for intramolecular participation by the terminal amino groups in the enolisation of the ketones under study. Similarly, the terminal amino and ammonium groups may be participating in the racemisation of **3.4** and **3.5**, respectively.



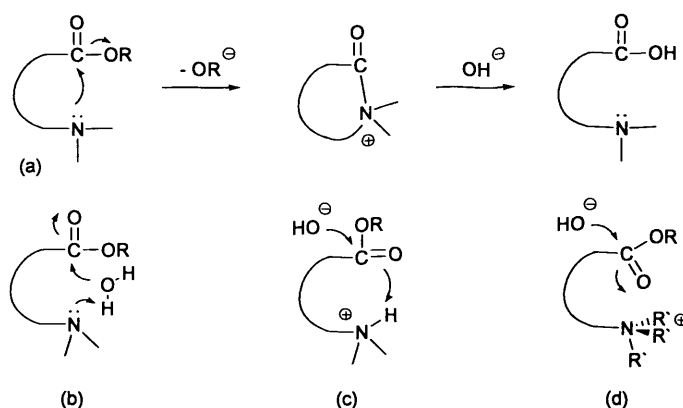
R, R', R'' = H or CH₃ or C₂H₅

Y, X = H or CH₃

B = N(CH₃)₂ or

Scheme 3.8: general structures of the β -amino ketones studied by Coward and Bruice

As mentioned before and illustrated by some of the above cited examples, the amino and ammonium functional groups present in hydantoins **3.4** and **3.5**, respectively, are typical participating groups in intramolecular processes.^{37, 38}



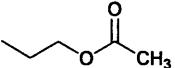
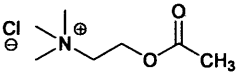
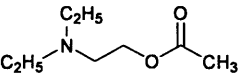
Scheme 3.9: proposed mechanisms available to the amino group for intramolecular facilitation of ester hydrolysis

The mechanisms for intramolecular facilitation by the amino group were summarised by Bruice³⁸ for the case of ester hydrolysis, as shown in **Scheme 3.9** for a) intramolecular nucleophilic catalysis, b) intramolecular general-base catalysis, c) intramolecular general-acid, specific-base catalysis and d) electrostatic facilitation by either a protonated tertiary amine or by an ammonium group. Similar mechanisms may be acting in the racemisation of hydantoins **3.4** and **3.5**.

We note that Path d) is the only possible mechanism for intramolecular facilitation by a neighbouring quaternary ammonium group, and because both **3.4** and **3.5** show a

remarkable rate-enhancement, this mechanism is of immediate interest. Mechanism d) has been proposed in several studies³⁹⁻⁴¹ to explain unusually high rates of hydrolysis of esters containing a β -dimethylethylamino or a β -trimethylammonium group in a favourable position for electrostatic interaction as shown in **Scheme 3.9**. Zaslowsky *et al.*³⁹, in particular, compare the rate constant for hydroxide-catalysed hydrolysis of ethyl acetate, acetylcholine and β -diethylamino acetate hydrochloride, in the pH range 5.5-8.4 at 50-65 °C (**Table 3.4**). The observed higher rate constants for hydrolysis of β -diethylamino acetate hydrochloride are explained in terms of a higher accelerating effect when the positive charge is carried by a labile proton, rather than by a quaternary ammonium, due to a reduced shielding of the electrostatic charge in the former case.⁴²

Table 3.4: rate constants for hydroxide-catalysed hydrolysis of different acetate esters at 60 °C (Data reported by Zaslowsky *et al.*)

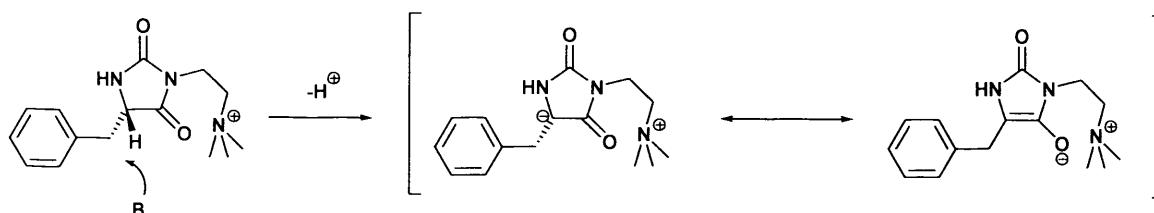
Substrate	$k / \text{M}^{-1} \text{sec}^{-1}$
	1.11
	28.21
	516.1

The “acidifying effects” of α -NR₃⁺ (R = Me, H) substituents on carbon acidity has been reported by Richard *et al.*⁹ As mentioned in Chapter 1, Richard *et al.* reported a correlation between the rate constants of hydroxide-catalysed deprotonation of some neutral aldehydes, ketones and esters, to form the corresponding enolates, and determined the acidity of the α -carbonyl proton in these carbon acids.⁷

The analogous rate-equilibrium correlation was investigated by Richard *et al.* for a different class of carbon acids, *viz.* the amino acid glycine zwitterion ⁺NH₃CH₂COO⁻ and its derivatives *viz.* *N*-protonated glycine methyl ester (⁺NH₃CH₂COOMe), betaine methyl ester, (⁺Me₃NCH₂COOMe), and betaine (⁺Me₃NCH₂COO⁻). Observed rate

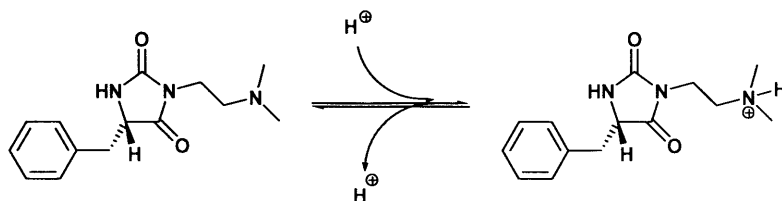
constants for deprotonation of the species $^+NH_3CH_2COOMe$ and $^+Me_3NCH_2COOMe$ by deuteroxide ion (k_{OD^-}) were respectively 6.0 ± 0.2 and $570 \pm 40 \text{ M}^{-1}\text{s}^{-1}$, significantly higher than the values of k_{OD^-} for the formally neutral analogues $^+NH_3CH_2COO^-$ and $^+Me_3NCH_2COO^-$ for which values of $(8.9 \pm 0.3) \cdot 10^{-5}$ and $(6.6 \pm 0.1) \cdot 10^{-4} \text{ M}^{-1}\text{s}^{-1}$, respectively, are reported. Positive deviations from the rate equilibrium correlation reported for neutral carbon acids were obtained for the cationic ester derivatives *N*-protonated glycine methyl ester and betaine methyl ester.⁹ Similar positive deviations were also found for cationic amides.¹⁰ The introduction of a cationic substituent on the α -carbonyl carbon of a carbon acid, therefore, leads to a much higher rate constant of deprotonation than is found for neutral carbon acids with the same pK_a . These reported “activating” effects of cationic groups are interesting, even if in our model hydantoins the cationic substituents are not in α -position with respect of the site of deprotonation of the molecule. The large increase of k_{OD^-} ($> 10^5$) for cationic carbon acids, as compared to their neutral analogues, observed by Richard, is due to the direct attachment of the quaternary ammonium groups to the sites of deprotonation of the molecules. In case of our substrates **3.4** and **3.5**, the quaternary groups are further removed from the site of deprotonation, hence a smaller effect is observed.

In analogy with the above-cited literature data, the higher rate constant of racemisation observed for **3.5** could be explained in term of intramolecular facilitation of deprotonation of **3.5** by the ammonium group. The positive charge on the ammonium group of **3.5** can stabilise, via a through-space electrostatic interaction, a developing negative charge on the asymmetric carbon, partly delocalised by resonance on the carbonyl oxygen as shown in **Scheme 3.10**. This stabilising effect of the terminal ammonium group would explain the increased carbon acid acidity of **3.5**, relative to hydantoins **3.1**, **3.2** and **3.3**.



Scheme 3.10: proposed intramolecular stabilisation of the hypothetical carbanion formed by deprotonation of the asymmetric carbon of **3.5** by a generic base, B.

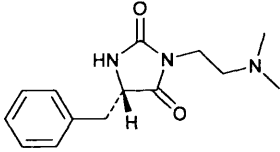
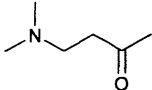
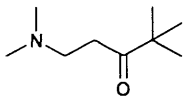
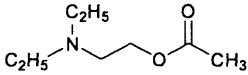
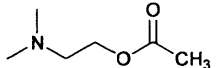
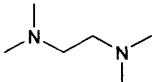
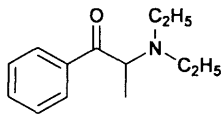
We mentioned before the possibility of different protonation states for hydantoin **3.4**, depending on the pH of the reaction medium, according to the equilibrium shown in **Scheme 3.11**.



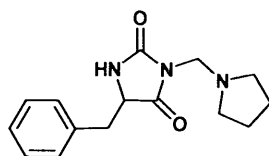
Scheme 3.11: equilibrium protonation of hydantoin **3.4**

Attempts were made to measure the pK_a^* of compound **3.4** by means of spectrophotometric and NMR titrations but no satisfactory pH profile could be obtained (see Appendix 2). In **Table 3.5** the pK_a value of **3.4**, predicted using the ACD/I-Lab Web service (ACD/pKa 12.0) is reported together with selected experimental pK_a s of compounds with structures similar to **3.4**. From **Table 3.5**, we can deduce that, under the experimental conditions chosen in our kinetic study (phosphate buffered D_2O at pH* 7.2), hydantoin **3.4** should be mainly in the protonated state. A pK_a value of 8.95 ± 0.28 can also explain the trend of the rate constants of racemisation of **3.4** shown in **Figures 3.2** and **3.3**. In the pH** range 6-8 the protonated form of **3.4** should be the major species in the reaction medium. The chemical species present in neutral D_2O solutions of hydantoins **3.4** and **3.5** are, therefore, effectively very similar to the former bearing a positive charge by virtue of an equilibrium protonation while the latter bears a stable positive charge in the same position due to its intrinsic nature. The same mechanism as proposed for hydantoin **3.5** (**Scheme 3.10**) is therefore likely to occur also in the case of **3.4**, under the experimental conditions investigated.

Table 3.5: pK_a values for different chemical substrates containing a dimethylaminoethyl or diethylaminoethyl moiety in their structure.

Substrate	pK_a
	8.95 ± 0.28^{43}
	ca. 9.5^{36}
	9.49^{36}
	8.2^{39}
	8.3^{41}
	8.6^{44}
	8.79 ± 0.023^{45}

An important factor affecting the effectiveness of intramolecular catalysis is the distance between the reacting and catalysing group. The possibility of formation of a 5- or 6-membered cyclic transition states appears to be a particularly favourable condition in intramolecularly catalysed processes.^{23, 29-31, 36} To check the feasibility of the mechanism described in **Scheme 3.10**, racemic 5-benzyl-3-*N*-(pyrrolidin-1-ylmethyl) hydantoin **3.10**, was prepared (**Scheme 3.12**).



3.10

Scheme 3.12: structure of racemic 5-benzyl-3-*N*-(pyrrolidin-1-ylmethyl) hydantoin **3.10**.

In compound **3.10**, a possible electrostatic interaction between the protonated pyrrolidinium group and the carbonyl oxygen should be less sterically favourable than for compounds **3.4** and **3.5**. The pK_a for **3.10**, predicted using the ACD/I-Lab Web service (ACD/pKa 12.0), is 8.37 ± 0.70 ⁴³ and therefore, as was the case for hydantoin **3.4**, **3.10** is expected to be mainly in its protonated form at pH* 7.2. Kinetic experiments of H/D exchange of **3.10** in D₂O phosphate buffer, 0.5 M, 1 M I, at pH* 7.2 were carried out and a rate constant (k) of $(6.45 \pm 0.25) 10^{-6} \text{ s}^{-1}$ was obtained.⁴⁶ If we compare this value with the rate constant for H/D exchange of **3.4** in Table 3.2, we notice the higher configurational stability of **3.10** as compared to **3.4**, in spite of the presence of an amino group in the side chain. The rate constants for H/D exchange of **3.10** are, in fact, very similar to those of **3.1**, under identical experimental conditions. The result supports the above-described hypothesis of intramolecular phenomena being responsible for the lower configurational stability of compounds **3.4** and **3.5** as compared to benzylhydantoins **3.1-3.3**.

3.2.4.2. The slight rate-depressing effect of alkyl groups

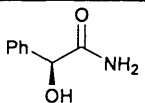
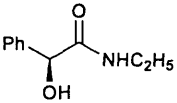
Scrutiny of the kinetic data in Tables 3.2 and 3.8 (*vide infra*), ignoring compounds **3.4** and **3.5** where intramolecular processes appear to be involved, shows that all 3-*N*-alkyl hydantoins show slightly lower rates of proton-deuterium exchange than their unsubstituted counterparts. The observed rate-depressing effect appears to be enhanced by the substitution of the 3-*N*-hydrogen with a methoxyethyl group (hydantoin **3.3**). In hydantoin **3.3** the nitrogen in position 3 is attached to a secondary carbon, instead of a primary one, as is the case in 3-*N*-methylhydantoins. Wilson³ reports data collected by Ahlberg⁴⁷ illustrating the effect of different alkyl groups on the rates of base-catalysed racemisation of compounds of the form $SO_2(CH_2R)COOH$. The data are summarised in Table 3.6.

Table 3.6: substituent (*R*) effect on half - lives of base catalysed racemisation of compounds with structure $SO_2(CHRCOOH)_2$, under comparable conditions (data reported by Wilson from original paper by Ahlberg).

R	-CH ₃	-C ₂ H ₅	-CH(CH ₃) ₂
Half-life / hours	1.3	2.75	50

The order of facilitation of racemisation $-CH_3 > -C_2H_5 > -CH(CH_3)_2$ is clear. The study by Testa² on the racemisation of 5-substituted hydantoins reports data (see Chapter 1) consistent with Ahlberg's observation: (*S*)-5-isopropylhydantoin undergoes H/D exchange approximately 5 times more slowly than (*S*)-5-methylhydantoin, under identical conditions. The reported observations are interesting, even if they cannot be directly compared with our experimental data, mainly due to the fact that the alkyl groups in the compounds studied by Ahlberg and Testa are directly attached to the chiral centre. Both studies seem to suggest a parallel between stereolability and relative ability of different alkyl substituents at stabilising carbanions.

Table 3.7: half-lives for base-catalysed racemisation of *L*-mandelamide and *L*-mandeloethylamide in 0.077 N ethyl-alcoholic alkali, at "ordinary temperature" (Data reported by Wilson from original paper by McKenzie).

Substrate	$t_{1/2}$ /days
	4
	25

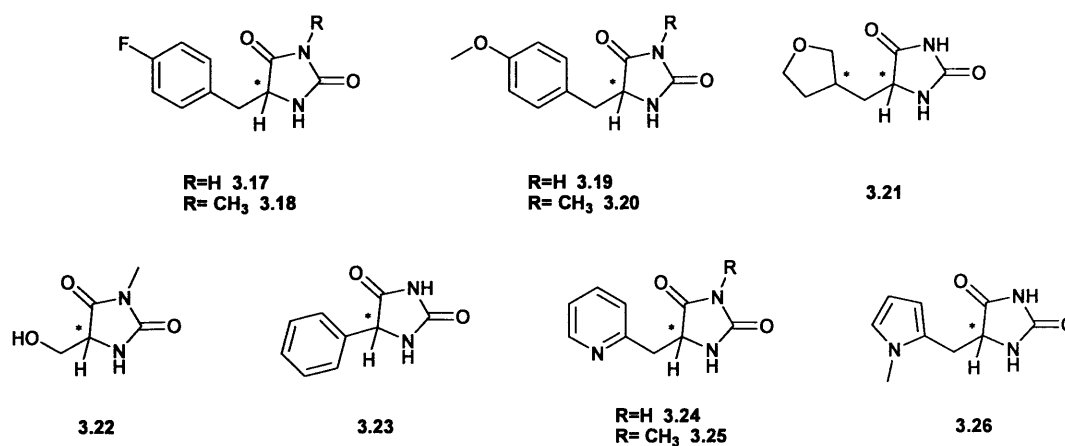
More relevant to our discussion are data reported by McKenzie⁴⁸ who observed effects on rates of racemisation due to the introduction of an alkyl group in a position relatively far from the chiral center. The model compounds studied by McKenzie are *L*-mandelamide and *L*-mandeloethylamide. The structures of *L*-mandelamide and *L*-

mandeloethylamide are reported in **Table 3.7** together with the corresponding half-lives of base-catalysed racemisation, under identical experimental conditions.

The analogy between the couple *L*-mandelamide and *L*-mandeloethylamide and the couple hydantoin and 3-*N*-alkyl hydantoin is apparent. The shared common pattern $R_1R_2CHCONR_3R_4$, with R_4 the alkyl group whose effect is investigated attached to the nitrogen in β position to the chiral centre seems to suggest a similar effect of alkyl substituents R_5 on the configurational stability of the two classes of compounds.

3.3. Structural modifications in position 5

Further structural variations of model compound **3.1** were made by substituting the benzyl group in position 5 with different aromatic and aliphatic groups (**Scheme 3.13**). All the 5-substituted hydantoin in **Scheme 3.13** were obtained as racemic mixtures either due to the use of racemic starting materials or because, where enantiopure starting materials were employed, racemisation during synthesis could not be avoided.

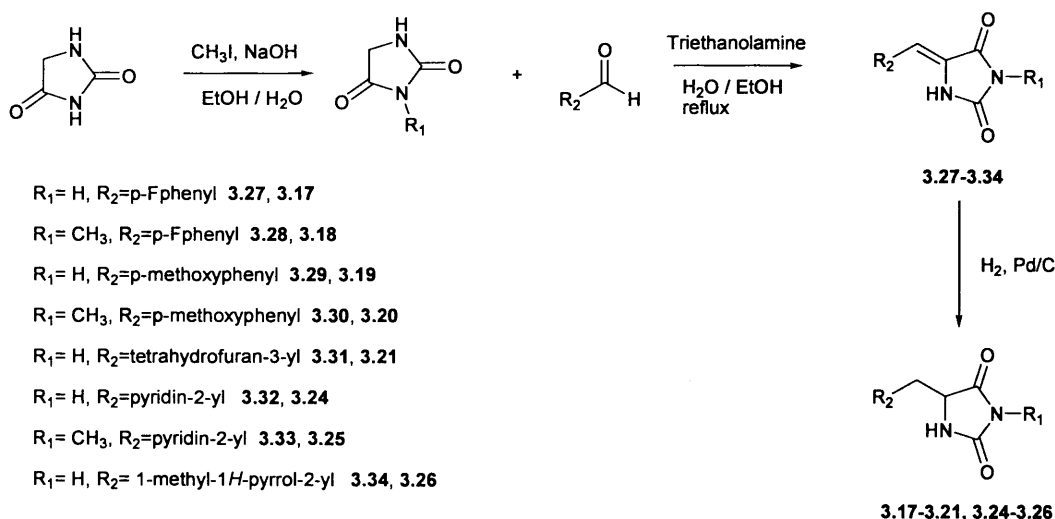


Scheme 3.13: Structures of racemic model 5-substituted-hydantoin. The chiral centres are highlighted.

3.3.1. Syntheses

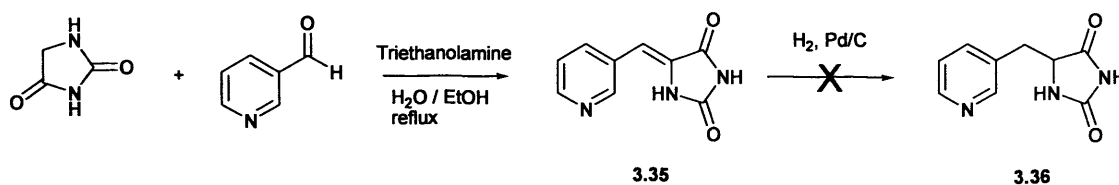
The synthesis of hydantoins **3.17-3.21** and **3.24-3.26** is shown in **Scheme 3.14**. Hydantoins **3.17-3.21** and **3.24-3.26** were obtained via a Knoevenagel condensation of hydantoin (for compounds **3.17**, **3.19**, **3.21**, **3.24** and **3.26**) or 3-*N*-methylhydantoin (for compounds **3.18**, **3.20** and **3.25**) with appropriate aldehydes, followed by catalytic hydrogenation.

3-*N*-methylhydantoin was obtained by the methylation of hydantoin with iodomethane, in the presence of sodium hydroxide, using a literature procedure with some modifications.^{49, 50} The Knoevenagel condensation was carried out following literature procedures.¹⁶⁻¹⁹ Solvent and catalyst in the hydrogenation step were chosen based on available literature information.⁵¹ Hydantoin **3.21** (**Scheme 3.13**) was obtained as a mixture of diastereoisomers in an approximately 1:1 diastereomeric ratio.



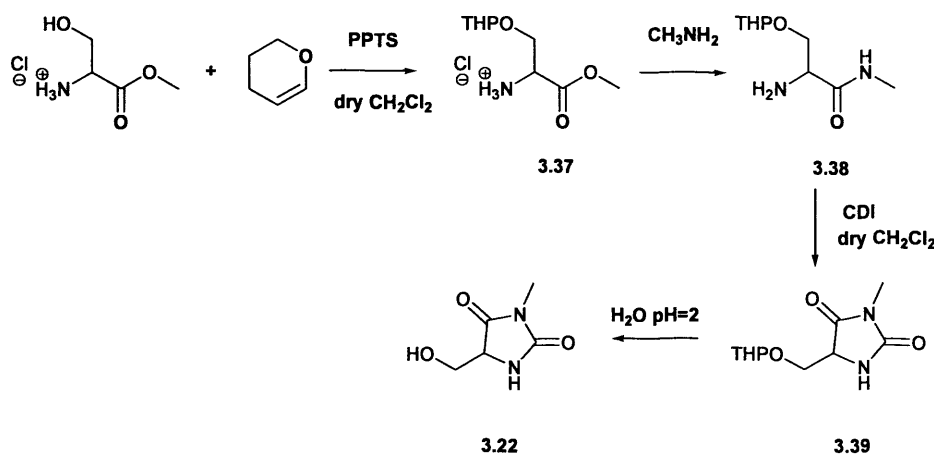
Scheme 3.14: synthesis of racemic 5-substituted-hydantoins **3.17-3.21** and **3.24-3.26**

Attempts at preparing the pyridine-containing hydantoin **3.36** (**Scheme 3.15**) proved unsuccessful. Condensation of hydantoin with 3-pyridinecarboxaldehyde gave intermediate **3.35** with very poor solubility in common organic solvents. As a result of the poor solubility, **3.35** could not be hydrogenated by means of the our routine hydrogenation procedure (**Scheme 3.15**).⁵²



Scheme 3.15: attempted synthesis of 5-substituted-hydantoin 3.36

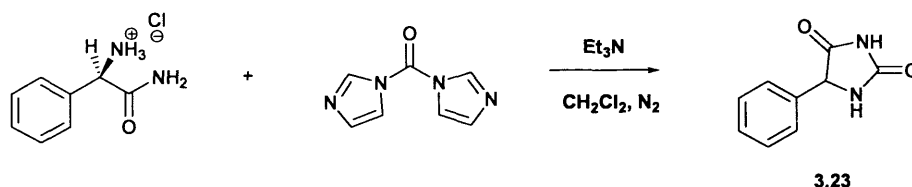
3-*N*-methyl-serine hydantoin **3.22** was prepared as shown in **Scheme 3.16**. Literature procedures⁵³ with some modifications were followed. The THP protection of 2-amino-3-hydroxypropanoate hydrochloride was carried out by reaction with 3,4-dihydro-2H-pyran in the presence of pyridinium *p*-toluenesulfonate (PPTS), as catalyst. The same procedure as used for the synthesis of **3.2** (Chapter 2) was used in the following synthetic steps, *viz.* reaction of the THP-protected amino acid methyl ester hydrochloride with methylamine¹² and subsequent cyclization of the obtained amino amide by means of CDI.¹² Deprotection, accomplished by stirring an acidic aqueous solution of the product of cyclization (**3.39**), gave 3-*N*-methyl-serine hydantoin **3.22** which was then purified by HPLC.



Scheme 3.16: synthesis of racemic 3-*N*-methyl-serine hydantoin **3.22**

Attempts were made to prepare optically active phenylhydantoin **3.23** from commercially available (*R*)-phenyl glycine amide hydrochloride. Unfortunately, using CDI, racemisation during synthesis could not be avoided. The use of triphosgene as

coupling agent, which had allowed us to obtain enantio-enriched benzylhydantoin **3.4** (*vide supra*), gave racemic phenylhydantoin in very poor yield. Best yields were obtained using CDI as the coupling agent and an equimolar amount of triethylamine (**Scheme 3.17**), *i.e.* following the synthetic procedure routinely used in this work to prepare hydantoin from the corresponding amino amides.



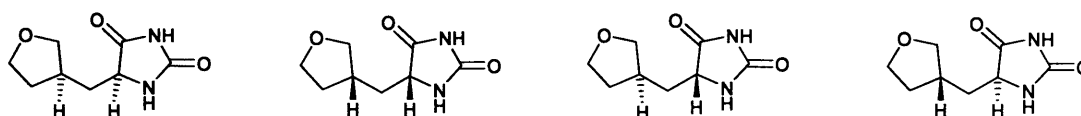
Scheme 3.17: synthesis of 5-phenylhydantoin **3.23**

3.3.2. Kinetic studies

To explore the effect of substituents on position 5 of the hydantoin, the H/D exchange reaction of hydantoin **3.17-3.26** was investigated in D₂O phosphate buffer pH* 7.2, 0.5 M, 1 M *I*, at 25 °C. Overall good fits of the experimental data to first-order kinetics were obtained. The fits for compounds **3.17-3.20** were less accurate due to the poor solubility of the hydantoin in D₂O (see Appendix 2).

The kinetic data are reported in **Table 3.8**. Rate constants of H/D exchange for 5-benzylhydantoin **3.1** and 3-*N*-methyl-5-benzylhydantoin **3.2** (see Chapter 2) are reported for ease of comparison.

The kinetic analysis of the H/D exchange of **3.21** is complicated by two factors. Firstly, two chiral centres are present in the molecule, as highlighted in **Scheme 3.13**. However, only the chiral centre on the hydantoin ring is configurationally unstable, as predicted by Testa^{4, 5} (see Chapter 1), and here experimentally confirmed by ¹H NMR spectroscopy during H/D exchange experiments. A further complication arises from the fact that hydantoin **3.21** was obtained as an epimeric mixture. Both enantiomers of two different chemical species (**Scheme 3.18**) are therefore present in the reaction medium during experiments of H/D exchange.



Scheme 3.18: species present in the epimeric mixture of **3.21**

The rate constant for H/D exchange of **3.21** reported in **Table 3.8** should therefore be considered a mean value of the individual rate constants of the two epimers. We note, however, that analysis of the ^1H NMR spectra of **3.21** during H/D exchange experiments suggests approximately equal rate constants of deuteration for the two epimers. (See Appendix 2).

Table 3.8 shows the particularly high rate constants of H/D exchange of phenylhydantoin **3.23**, as compared to the other hydantoins in the series. This result is in agreement with Testa's findings² and with several other studies demonstrating the strong destabilising effect of the phenyl group on chiral centres of a wide range of carbon acids.

The much higher rate constant of H/D exchange of phenylhydantoin, as compared to other hydantoins, is attributed to formation of a resonance stabilised intermediate carbanion. All the other hydantoins in **Table 3.8** show much lower rate constants of H/D exchange.

Table 3.8: rate constants for H/D exchange of 5-substituted hydantoins in D₂O phosphate buffers, 0.5 M, 1 M I, kept constant with KCl, pH * 7.2, at 25 °C

Substrate	$k_{\text{HD}} / 10^{-6} \text{ s}^{-1}$
3.1	5.42±0.41 ^{a)}
3.2	3.37±0.11 ^{b)}
3.17	6.75±0.55 ^{a)}
3.18	3.05±0.16 ^{b)}
3.19	4.42±0.30 ^{b)}
3.20	2.46±0.13 ^{b)}
3.21	11.11±0.15 ^{b)}
3.22	21.22±0.27 ^{b)}
3.23	408.0±13.2 ^{a)c)}
3.24	9.29±0.38 ^{a)d)}
3.25	3.28±0.39 ^{a)d)}
3.26	6.00±0.22 ^{a)e)}

- a) Errors from non-linear least squares fitting performed by means of the program Origin using the Levenberg-Marquardt (LM) algorithm.
- b) Errors from weighted averages²² of 2 or more analytical determinations.
- c) Rate constant determined in D₂O phosphate 0.1 M, 1 M I.
- d) Data collected by Daniela Milan⁵⁴
- e) Data collected by Rhys Williams⁵⁵

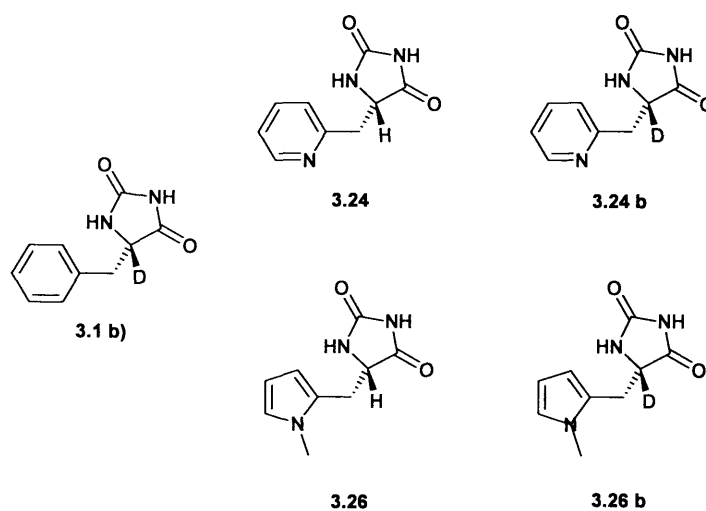
Compound **3.24** was synthesised in order to investigate the possibility of intramolecular catalysis of racemisation. The replacement of the phenyl ring in **3.1** with a pyridyl ring in **3.24** produces an approximate two-fold increase in the rate constant of H/D exchange. Similarly, the experimental rate constants of racemisation (*vide infra*) in D₂O phosphate buffer 0.5 M, 1 M I with pH** 7.2, at 60 °C for **3.1** and **3.24**⁵² were $k_{\text{rac}} = (288.4 \pm 1.1) \cdot 10^{-6} \text{ s}^{-1}$ and $k_{\text{rac}} = (498.8 \pm 6.1) \cdot 10^{-6} \text{ s}^{-1}$, respectively, i.e. a similar approximate two-fold increase. Similarly, the second-order rate constants for buffer-

catalysed racemisation ($k_{\text{phosphate tot}}$) in D₂O phosphate buffers at 1 M *I* at pH** 7.2 and 60 °C were $k_{\text{phosphate tot}} = (542.2 \pm 2.5) \cdot 10^{-6} \text{ s}^{-1} \text{ M}^{-1}$ and $k_{\text{phosphate tot}} = (906.4 \pm 22.7) \cdot 10^{-6} \text{ s}^{-1} \text{ M}^{-1}$ for **3.1** and **3.24**⁵², respectively. A p*K*_a value of 5.97 is reported in the literature⁵⁶ for 2-methyl and 2-ethyl pyridine. We therefore assume a similar p*K*_a value for protonation of the pyridine ring in hydantoin **3.24**. Under the experimental conditions chosen in our kinetic studies (buffered D₂O with pH** 7.2) the pyridine ring in **3.24** is therefore expected to be mainly deprotonated. The pyridine ring could therefore, at least in principle, act as an additional catalyst for racemisation acting via an intramolecular pathway. Considering the Brønsted β value of 0.59 for racemisation of (*S*)-5-benzylhydantoin (see Chapter 2 and reference⁵⁷) a local effective concentration of catalytic pyridyl groups of 10 M,⁵⁸ and a p*K*_a value of 5.97 for protonation of the pyridyl group of **3.24**, a rate constant for intramolecular catalysis of racemisation by the pyridyl group of $960 \cdot 10^{-6} \text{ s}^{-1}$ was estimated. The linear fit of the experimental rate constants of racemisation of **3.24** in D₂O phosphate buffers at 60 °C plotted as a function of buffer concentration gave a rate constant for the reaction not catalysed by buffer of $(41.1 \pm 6.6) \cdot 10^{-6} \text{ s}^{-1}$. This value should include the contributions to racemisation from all catalytic species present in solution, apart from the buffer, and therefore also the contribution for hypothetical intramolecular catalysis by the pyridyl substituent. The comparison of the experimental value of $(41.1 \pm 6.6) \cdot 10^{-6} \text{ s}^{-1}$ with the estimated value of $960 \cdot 10^{-6} \text{ s}^{-1}$ for catalysis via hypothetical intramolecular catalysis of racemisation by the pyridyl groups appears to exclude this hypothesis, or at least highlights that intramolecular catalysis is not efficient.

A very small difference in configurational stability is observed when the phenyl ring of **3.1** is replaced with an *N*-methyl-pyrrolyl group (compound **3.26**). The observed rate constants for racemisation of **3.26**⁵⁵ in D₂O 0.5 M phosphate buffer, 1 M *I* at pH** 7.2, at 60 °C (k_{rac}) and the second-order rate constant for buffer catalysed racemisation ($k_{\text{phosphate tot}}$) in D₂O phosphate buffers were $k_{\text{rac}} = (303.5 \pm 1.1) \cdot 10^{-6} \text{ s}^{-1}$ and $k_{\text{phosphate tot}} = (579.1 \pm 50.1) \cdot 10^{-6} \text{ s}^{-1} \text{ M}^{-1}$, respectively. These rate constants are similar in value to the corresponding values found for **3.1** (*vide supra* and Table 3.9). Hydantoin **3.26** contains an *N*-methyl pyrrole in its structure. A p*K*_a of ca. -10 is reported in the literature⁵⁹ for protonation of pyrrole at nitrogen. The very weak basicity of pyrrole indicates the impossibility of the *N*-methyl pyrrolyl moiety in **3.26** to act as an efficient

intramolecular catalyst for racemisation. Indeed hydantoins **3.1** and **3.26** show equal configurational stabilities.

The primary and solvent kinetic isotope effects were determined for racemisation of compounds **3.24**⁵² and **3.26**.⁵⁵ Enantio-enriched samples of (*S*)-**3.24** and (*S*)-**3.26** (**Scheme 3.19**) were obtained by chiral resolution of the racemates by means of HPLC. The deuterated analogues of (*S*)-**3.24** and (*S*)-**3.26**, (*S*)-**3.24b** and (*S*)-**3.26b** were also prepared following a procedure^{52, 54, 55} analogous to that described in Chapter 2 for the synthesis of (*S*)-5-d-5-benzylhydantoin **3.1b** whose structure is also shown in **Scheme 3.19**. The rate constants for racemisation of (*S*)-**3.24** and (*S*)-**3.24b**, and of (*S*)-**3.26** and (*S*)-**3.26b**, determined in deuterated and non-deuterated phosphate buffers 0.5M, 1 M *I* with pH** 7.2 or pH^{25 °C} 7.2, at 60 °C are reported in **Table 3.8**.



Scheme 3.19: structure of (*S*)-5-d-5-benzyl hydantoin **3.1 b** and of (*S*)-5-substituted hydantoins **3.24** and **3.26** and related labelled analogues **3.24 b** and **3.26 b**.

As shown in **Table 3.9**, no detectable solvent kinetic isotope effects were observed for racemisation of (*S*)-**3.24** and (*S*)-**3.26** while significant primary kinetic isotope effects were detected. The data are consistent with those reported in Chapter 2 for racemisation of (*S*)-5-benzylhydantoin under the same experimental conditions. As discussed in Chapter 2 for (*S*)-5-benzylhydantoin, the significant primary kinetic isotope effects and the absence of normal solvent kinetic isotope effects indicate an S_E1 mechanism for racemisation of (*S*)-**3.24** and (*S*)-**3.26**, as for **3.1**.

Table 3.9: rate constants for racemisation of **3.24** and **3.24 b**^{a)} and of **3.26** and **3.26 b**^{b)} in D₂O and H₂O phosphate buffers, 0.5 M, 1 M I, kept constant with KCl, pH** or pH^{25 °C} 7.2^{c)}, at 60 °C and related primary kinetic isotope effects.

Phosphate buffer	$k_{\text{rac}} / 10^{-6} \text{ s}^{-1}$		Ratio
	3.24	3.24b	
H ₂ O	494±16 ^{d)}	--	--
D ₂ O	498.8±6.1 ^{d)}	150.5±4.9 ^{d)}	3.3±0.1 ^{e)}
Phosphate buffer	$k_{\text{rac}} / 10^{-6} \text{ s}^{-1}$		Ratio
	3.26	3.26b	
H ₂ O	208±10 ^{d)}	--	--
D ₂ O	303.5±5.3 ^{d)}	61.9±7.2 ^{d)}	4.9±0.6 ^{e)}

- a) Kinetic data for racemisation of **3.24** have been collected by Julia Kennedy⁵²
- b) Kinetic data for racemisation of **3.26** have been collected by Rhys Williams⁵⁵.
- c) Buffers prepared by dissolving potassium dihydrogen phosphate in D₂O and adjusting the pH** or pH^{25 °C} of the solution with KOH
- d) Errors from non-linear least squares fitting performed by means of the program Origin using the Levenberg-Marquardt (LM) algorithm.
- e) Errors calculated as uncertainties on functions of several variables.⁶⁰

3.4. Conclusions

Structural modifications were introduced in positions 3 and 5 of the hydantoin ring and the effect of these modifications on configurational stability was investigated. The introduction of polar substituents in the 3 position of the hydantoin ring yielded model 5-benzylhydantoins with improved water solubility (water solubilities are approximately 50 mM for model hydantoins **3.3** and **3.5**, 4 mM for hydantoin **3.1** and 10 mM for **3.2**). Hydantoins **3.3** and **3.5** also have increased solubility in common organic solvents. Structural modifications in position 5 afforded model hydantoins with excellent solubility in water (e.g. compounds **3.21**, **3.22**, and **3.24-3.26**) The introduction of marked structural changes directly in position 5 led to the strongest effects on configurational stability (e.g. compound **3.23**). Less marked, but nevertheless

evident effects were observed when structural modification was introduced in position β with respect to the chiral centre (e.g. compounds **3.21**, **3.22**, **3.24**, **3.25**). Small differences in the rate constants of H/D in further positions (e.g. compounds **3.17-3.20**) or upon replacement of the phenyl ring in **3.1** with an *N*-methyl-pyrrolyl group (e.g. compound **3.26**) were observed.

Some of the structural modifications in position 3 of the hydantoin ring led to remarkably big changes in the rate constants of racemisation, even if the site of differentiation involved positions far from the chiral centre. The hypothesis of intramolecular facilitation has been proposed to explain unusually high rates of racemisation and H/D exchange of 3 substituted benzylhydantoins **3.4** and **3.5**, containing amino and ammonium groups. The positive charges on the ammonium group of **3.5** and on the protonated amino group of **3.4** could stabilise, via through-space electrostatic interactions, the developing negative charges on the asymmetric carbons of **3.5** and **3.4**, respectively. Literature and experimental data supporting the hypothesis of intramolecular facilitation of H/D exchange for **3.4** and **3.5** are reported. The possibility of intramolecular base-catalysis of racemisation has been investigated by comparing the configurational stability of the model compound **3.26**, containing a pyridyl substituent in its structure, with that of (*S*)-5-benzylhydantoin **3.1**. The small value of the intercept of the straight line fit obtained by plotting the rate constants of racemisation of **3.26** against the concentration of the buffer excludes the hypothesis of efficient intramolecular general-base catalysis in this compound. Marked primary kinetic isotope effects and the absence of solvent kinetic isotope effects were observed for racemisation of hydantoins **3.24** and **3.26**, as for hydantoin **3.1**. The finding indicates an S_E1 mechanism for racemisation of the two compounds, as was also found for racemisation of hydantoin **3.1** (Chapter2).

3.5. Experimental Part 1

Materials

All solvents, drying agents, inorganic acids and bases were Laboratory Reagent Grade and were purchased from Fisher Scientific unless otherwise stated. All dry solvents were dried using an MB SPS-800 solvent purification system. All materials were used without further purification. (*S*)-methyl-2-amino-3-phenylpropanoate, 3-methoxypropan-1-amine, *N,N*-dimethylethane-1,2-diamine, triethylamine, iodomethane, triethanolamine, palladium on activated carbon (5 weight %), 3,4-dihydro-2H-pyran, tetrahydrofuran-3-carboxaldehyde, formaldehyde (37% solution in water) and (*R*)-2-amino-2-phenyl acetamide hydrochloride were from Sigma-Aldrich. Carbonyldiimidazole, hydantoin, 4-methoxy-benzaldehyde, 4-fluoro-benzaldehyde, (*DL*)-Serine methyl ester hydrochloride and pyrrolidine were from Alfa-Aesar. Triphosgene and pyridinium 4-toluenesulfonate were from Acros Organics.

Chromatography

Column chromatography purifications were carried out on Silica 60 Å, particle size 35-70 micron or Florosil, 60-100 mesh. Filtrations were carried out on medium fast speed filter paper or on celite kieselgur, white (general purpose grade), unless otherwise stated. Silica and celite were from Fisher Scientific. Florosil was obtained from Alfa Aesar. Separations by HPLC were carried out on an Agilent HPLC system 1200 series equipped with a 1200 Series quaternary pump, a 1200 Series diode array detector, a 1200 Series vacuum degasser and a 1200 Series preparative autosampler. HPLC grade solvents were purchased from Fisher Scientific.

NMR Spectroscopy

¹H NMR spectra were recorded on a Bruker AVANCE 400 or a Bruker AVANCE 500 spectrometers at 400 or 500 MHz respectively. ¹³C NMR spectra were recorded on the same instruments as ¹H NMR spectra, at ¹³C resonance frequencies of 101 MHz (Bruker

AVANCE 400) and 126 MHz (Bruker AVANCE 500). Coupling constants are reported in hertz (Hz). Chemical shifts are reported in parts per million (δ) and are referenced to the residual ^1H and ^{13}C signal of the NMR solvent used in ^1H NMR and ^{13}C NMR spectra, respectively. Dimethylsulfoxide- d_6 (D 99.9%) was purchased from Cambridge Isotope Laboratories, inc, chloroform- d ($\text{H}_2\text{O} < 0.01\%$, 99.80 %D), acetone- d_6 ($\text{H}_2\text{O} + \text{D}_2\text{O} < 0.02\%$, 99.80 %D) and methanol- d_4 ($\text{HOD} + \text{D}_2\text{O} < 0.03\%$) were from EURISO-TOP, Deuterium oxide (99.9%) was obtained from Fluorochem.

Mass spectrometry

Molecular masses were determined from high resolution mass spectra (HRMS). The spectra were recorded on a Waters GCT Premier XE GCMS spectrometer. EI (electron impact) was used as ionisation method, unless otherwise stated. Molecular masses could not be determined for molecules where fragmentations could not be avoided. Fragment masses of particular diagnostic relevance are reported instead, when they were detected.

IR spectroscopy

IR spectra were recorded on a Varian Excalibur Spectrometer (FTS 7000) equipped with a SensIR ATR accessory (attenuated total reflectance Fourier transform infrared (ATR FT-IR) spectra), a Deuterated Tri-Glycine Sulfate (DTGS) detector and a liquid nitrogen cooled Cryogenic Mercury Cadmium Telluride (MCT) detector. A CaF_2 cell, 100 μm path length, was used for spectra in D_2O solution.

Melting points

Melting points were recorded on a Stuart Melting point SMP11. Thermometers were Brannan LO-tox with temperature range 0-300 $^\circ\text{C}$, division 1 $^\circ\text{C}$.

Polarimetry

Specific optical activities $[\alpha]_D^T$ were determined by means of an Optical Activity Ltd. AA-1000 polarimeter in a 5.00 cm path length glass cell. D refers to the D line of the emission spectrum of sodium ($\lambda=589$ nm). Approximate optical purities were calculated based on literature values of specific optical activities of enantiopure compounds, when available. Solvent and concentration (expressed in g/100 ml) of the solutions used for the measurements are reported in the individual sections.

Methods

General methods were used to prepare more than one compound.

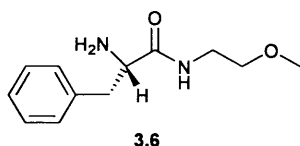
Method 3.1: synthesis of α -amino amides 3.6 and 3.7: (*S*)-methyl-2-amino-3-phenylpropanoate hydrochloride was stirred for five minutes with a 4 M solution of sodium carbonate in a round bottom flask. The mixture was extracted with chloroform, the combined organic extracts were dried over anhydrous Na_2SO_4 and the solvent evaporated. (*S*)-methyl-2-amino-3-phenylpropanoate was recovered as yellow oil (yield: 95%). Dry methanol and the alkylamines were added to (*S*)-methyl-2-amino-3-phenylpropanoate and the reaction mixtures were stirred at room temperature for five days. Solvent and residual amines were then evaporated.

Method 3.2: Synthesis of (*Z*)-5-benzylideneimidazolidine-2,4-diones 3.27-3.30 and (*Z*)-5-((tetrahydrofuran-3-yl) methylene) imidazolidine-2,4-dione 3.31: hydantoin (compounds 3.27, 3.29, 3.31) or *N*-methylhydantoin (compounds 3.28 and 3.30) was dissolved in water (10 ml per gram of hydantoin) in a round bottom flask at 70 °C with stirring. The pH was adjusted to 7 with few drops of a saturated solution of NaHCO_3 . Triethanolamine was added to the solution of hydantoin. A solution of aldehyde in ethanol (3 ml per gram of aldehyde), was then added dropwise and the temperature raised to reflux. The reaction mixture was kept under reflux for approximately 24 hours. The mixture was then allowed to cool down and the product recovered by filtration or

by extraction (compound **3.31**). When solid products were obtained, they were washed with a mixture of ethanol and water (1:5) and recrystallised.

Method 3.3: hydrogenations: hydrogenations were carried out in a Parr 5500 Series Compact reactor connected to a Hydrogen generator PGH₂600 and equipped with a Parr 4836 Controller (supplied by Scientific and Medical Products, Ltd). The starting materials were dissolved in dry THF or dioxane and transferred in the vessel of the hydrogenation reactor. Pd/C (0.25 grams per gram of starting material) was added and the reaction chamber was sealed and pressurised with hydrogen up to 3 bars. The mixtures were allowed to react overnight under vigorous stirring. The reaction mixtures were then filtered under vacuum over a layer of celite and the products were recovered as pure, white solids upon evaporation of the solvent.

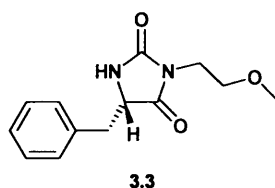
Synthesis of (*S*)-2-amino-*N*-(2-methoxyethyl)-3-phenylpropanamide **3.6**



Method 3.1 was followed. (*S*)-methyl 2-amino-3-phenylpropanoate: 0.48 g (2.68 mmoles), 3-methoxypropan-1-amine: 1.61 ml (18.7 mmoles) in 3 ml of dry methanol. The product was recovered as a light-yellow oil and used in the next reaction without any further purification.

(*S*)-2-amino-*N*-(2-methoxyethyl)-3-phenylpropanamide: yield 90%; ¹H NMR (400 MHz CDCl₃): δ 7.40 (brs, 1H, NH), δ 7.29-7.10 (m, 5H, C₆H₅), δ 3.64 (dd, J=9.7, 4.1 Hz, 1H, CH_AH_BCH), δ 3.38-3.35 (m, 4H, CH₂CH₂), δ 3.26 (s, 3H, CH₃), δ 3.19 (dd, J=13.9, 4.6 Hz 1H, CH_AH_BCH), δ 2.71 (dd, J=13.8, 9.0 Hz 1H, CH_AH_BCH); ¹³C NMR (100 MHz, D₂O): δ 174.6 (CHCONH), δ 138.3 (C Ar), δ 129.7 (CH Ar), δ 129.1 (CH Ar), δ 127.2 (CH Ar), δ 71.6 (CH₂CH₂O), δ 59.2 (OCH₃), δ 56.9 (CH), δ 41.4 (CH₂CH), δ 39.3(CH₂NH); IR (neat): ν_{max}= 1647 cm⁻¹ (C=O), [α]_D²⁵ = -65° (1.52 g/100ml in chloroform).

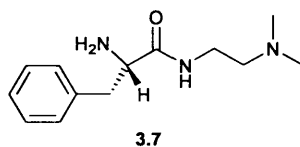
Synthesis of (*S*)-5-benzyl-3-(2-methoxyethyl)-imidazolidine-2,4-dione 3.3



A solution of (*S*)-2-amino-*N*-(2-methoxyethyl)-3-phenylpropanamide **3.6** (0.54 g, 2.42 mmoles) in dry CH₂Cl₂ (5 ml), in a sealed round bottom flask under nitrogen atmosphere was prepared. A solution of CDI (0.59 g, 3.63 mmoles) in dry CH₂Cl₂ (10 ml) was prepared in the same way. The solution of CDI was added by cannula to the solution of amide. The reaction mixture, kept under nitrogen atmosphere, was stirred overnight at room temperature. The solution was washed three times with acidified water (pH 2). The organic layers were then dried over anhydrous Na₂SO₄, filtered and concentrated. The product was purified by column chromatography on silica gel using CH₂Cl₂/ethyl acetate (80:20) to yield a white solid.

(*S*)-5-benzyl-3-(2-methoxyethyl)imidazolidine-2,4-dione: yield 70%, M.p. 65-70°C, HRMS *m/z* (EI⁺)=249.1242, (C₁₃H₁₆N₂O₃⁺ requires 249.1239); ¹H NMR (400 MHz CDCl₃): δ 7.30-7.06 (m, 5H, C₆H₅), δ 5.52 (br s, 1H, NH), δ 4.19 (ddd, J=9.2, 3.8, 1.1 Hz, 1H, CH_AH_BCH), δ 3.64-3.52 (m, 2H, CH₂CH₂O), δ 3.46-3.36 (m, 2H, CH₂CH₂O), δ 3.27-3.19 (m, 3+1 H, CH₃ + CHCH_AH_B), δ 2.77 (dd J=13.9, 9.0 Hz, 1H, CHCH_AH_B); ¹³C NMR (100 MHz, CDCl₃): δ 173.5 (CHCONCH₂), δ 157.3 (NHCONCH₂), δ 135.8 (C Ar), δ 129.6 (CH Ar), δ 129.3 (CH Ar), δ 127.9 (CH Ar), δ 69.2 (CH₂CH₂O), δ 59.1 (OCH₃), δ 58.8 (CH), δ 38.4 and 38.3 (CH₂N and CH₂CH); IR (neat): ν_{max}= 1773, 1710 cm⁻¹ (C=O), [α]_D²⁰ = -98° (0.55 g/100ml in chloroform).

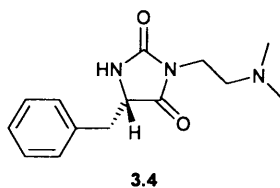
Synthesis of (*S*)-2-amino-*N*-(2-(dimethylamino)ethyl)-3-phenylpropanamide **3.7**



Method 3.1 was followed. (*S*)-methyl 2-amino-3-phenylpropanoate: 0.50 g (2.8 mmoles), *N,N*-dimethylethane-1,2-diamine (2.13 ml, 19.5 mmoles), 2 ml of dry methanol. The product was recovered as a yellow oil and used in the next reaction without any further purification.

(*S*)-2-amino-*N*-(2-(dimethylamino)ethyl)-3-phenylpropanamide: yield 80%; ^1H NMR (400 MHz CDCl_3): δ 7.30 (brs, 1H, NH), δ 7.27-7.13 (m, 5H, C_6H_5), δ 3.52 (dd, $J=9.2$, 4.3 Hz, 1H, $\text{CH}_\text{A}\text{H}_\text{B}\text{CH}$), δ 3.26 (m, 2H, NHCH_2CH_2), δ 3.17 (dd, $J=13.6$, 4.3, 1H, $\text{CH}_\text{A}\text{H}_\text{B}\text{CH}$), δ 2.64 (dd, $J=13.6$, 9.2 Hz, 1H, $\text{CH}_\text{A}\text{H}_\text{B}\text{CH}$), δ 2.34-2.28 (m, 2H, $\text{NHCH}_2\text{CH}_2\text{N}$), δ 2.13 (s, 6H, CH_3); ^{13}C NMR (100 MHz, CDCl_3): δ 174.8 (CHCONH), 138.5 (C Ar), δ 129.7 (CH Ar), δ 129.1 (CH Ar), 127.2 (CH Ar), δ 58.4 ($\text{CH}_2\text{N}(\text{CH}_3)_2$), δ 57.1 (CH_2CH), δ 45.6 ($\text{N}(\text{CH}_3)_2$), δ 41.6 (CH_2CH), δ 36.9 (CH_2NH); IR (neat): $\nu_{\text{max}} = 1651 \text{ cm}^{-1}$ (C=O), $[\alpha]_{\text{D}}^{25} = -48^\circ$ (2.38 g/100ml in chloroform).

Synthesis of (*S*)-5-benzyl-3-(2-(dimethylamino)ethyl)imidazolidine-2,4-dione **3.4**

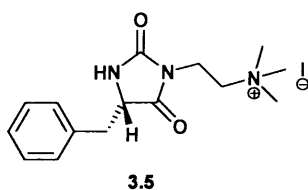


A solution of (*S*)-2-amino-*N*-(2-(dimethylamino)ethyl)-3-phenylpropanamide **3.7** (0.52 g, 2.2 mmoles) in dry CH_2Cl_2 (3 ml), in a sealed round bottom flask under nitrogen atmosphere was prepared. A solution of triphosgene (0.26 g, 0.88 mmoles) in dry CH_2Cl_2 (4 ml) was prepared in the same way. Triethylamine (0.74 ml, 5.3 mmoles) was added to the solution of amide and the solution was cooled with an ice bath. The

solution of triphosgene was added by cannula to the cold solution of amide and the mixture, kept under nitrogen atmosphere, was allowed to reach the room temperature and react overnight with stirring. The solution was washed three times with water. The organic layer was then dried over anhydrous Na₂SO₄, filtered and concentrated. The product was purified by column chromatography on silica gel using a gradient CH₂Cl₂/ethyl acetate/methanol (from 40:20:0 to 40:20:20) to yield a white solid.

(S)-5-benzyl-3-(2-(dimethylamino)ethyl)imidazolidine-2,4-dione: yield 55%, M.p. 105-107 °C, HRMS *m/z* (EI⁺)=261.1472, (C₁₅H₂₂N₃O₂⁺ requires 261.1477); ¹H NMR (500 MHz CDCl₃): δ 7.28-7.10 (m, 5H, C₆H₅), δ 5.77 (br s, 1H, NH), δ 4.17 (dd, J=8.6, 3.4 Hz, 1H, CH_AH_BCH), δ 3.49 (t, J=6.4 Hz, 2H, CONCH₂CH₂), δ 3.18 (dd, J=14.0, 3.4 Hz, 1H, CHCH_AH_B), δ 2.77 (dd, J=14.0, 8.7 Hz, 1H, CHCH_AH_B), δ 2.37 (t, J=6.7, 2H, CH₂CH₂N(CH₃)₂), δ 2.18 (s, 6 H, N(CH₃)₂); ¹³C NMR (100 MHz, CDCl₃): δ 173.8, (CHCONCH₂), δ 157.6 (NHCONCH₂), δ 135.8 (C Ar), δ 129.7 (CH Ar), δ 129.2 (CH Ar), δ 127.7 (CH Ar), δ 58.7 (CH), δ 56.7 (CH₂N(CH₃)₂), δ 45.7 (N(CH₃)₂), δ 38.3 (CH₂CH), δ 36.7 (CH₂NCO); IR (neat): ν_{max}= 1773, 1710 cm⁻¹ (C=O), [α]_D^r = -132° (0.44 g /100 ml in chloroform).

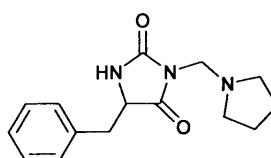
Synthesis of *(S)*-2-(4-benzyl-2,5-dioxoimidazolidin-1-yl)-*N,N,N*-trimethylethanaminium iodide 3.5



(S)-5-benzyl-3-(2-(dimethylamino)ethyl)imidazolidine-2,4-dione **3.4** (0.27 g, 1.0 mmoles) was dissolved in ethanol (6 ml) in a round bottom flask. Iodomethane (0.13 ml, 2.0 mmoles) was added dropwise to the solution and the reaction mixture was stirred for 5 hours at room temperature. The product was found to precipitate from the reaction mixture and it was recovered by filtration as a white solid.

(*S*)-2-(4-benzyl-2,5-dioximidazolidin-1-yl)-*N,N,N*-trimethylethanaminium iodide: yield 76%, M.p. 220-225°C, HRMS m/z (EI^+)=276.1715, ($C_{15}H_{22}N_3O_2^+$ requires 276.1712); 1H NMR (400 MHz, D_2O): δ 7.30-7.02 (m, 5H, C_6H_5), δ 4.46 (t, $J=4.0$ Hz, 1H, CH_2CH), δ 3.71-3.51 (m, 2H, NCH_2CH_2), δ 3.05 (d, $J=4.2$, 2H, CH_2CH), δ 2.92-2.72 (m, 9+2 H, $N(CH_3)_3$ + $CH_2N(CH_3)_3$); ^{13}C NMR (100 MHz, D_2O): δ 175.8 ($CHCONCH_2$), δ 157.7 ($NHCONCH_2$), δ 134.4 (C Ar), δ 130.5 (CH Ar), δ 129.0 (CH Ar), δ 128.0 (CH Ar), δ 62.3 ($CH_2N(CH_3)_3$), δ 58.4 (CH), δ 53.3 ($N(CH_3)_3$), δ 36.0 (CH_2CH), δ 32.3 (CH_2NCO); IR (solution D_2O): ν_{max} = 1763, 1705 cm^{-1} (C=O), $[\alpha]_D^{25} = -38^\circ$ (0.41 g/100 ml in water).

Synthesis of 5-benzyl-3-(pyrrolidin-1-ylmethyl)imidazolidine-2,4-dione **3.10**



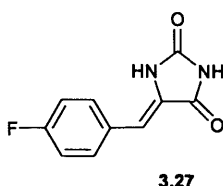
3.10

Racemic 5-benzylimidazolidine-2,4-dione (*rac*-**2.1**, prepared, as described in Chapter 2, following **method 2.2**), (0.3 g, 1.6 mmol) was dissolved in DMSO (6 ml) in a round bottom flask with a stopper and pyrrolidine (0.12 ml, 1.4 mmol) was added. 0.15 ml (2.1 mmol) of formaldehyde (solution 37% in water) were added and the solution was stirred, at room temperature, for 20 hours. The solution was concentrated to an approximate volume of 2 ml. Water (ca. 2 ml) was added and the mixture was kept in the fridge for 7 days to aid crystal formation. The product was recovered by filtration as a white solid. The crystals were washed with 3 ml of a mixture of water and ethanol (5:1).

5-benzyl-3-(pyrrolidin-1-ylmethyl)imidazolidine-2,4-dione: yield 15 %, M.p. 156-163 °C, HRMS m/z (EI^+)=273.1485, ($C_{15}H_{19}N_3O_2^+$ requires 273.1477); 1H NMR (400 MHz $CDCl_3$): δ 7.28-7.10 (m, 5H, C_6H_5), δ 5.83 (br s, 1H, NH), δ 4.42 (d, $J=13.4$, 1H, NCH_AH_BN), δ 4.37 (d, $J=13.3$, 1H, NCH_AH_BN), δ 4.23 (ddd, $J=7.7, 4.0, 1.0$ Hz, CH_ACH_BCH), δ 3.18 (dd, $J=14.1, 3.9$ Hz, 1H, CH_ACH_BCH), δ 2.86 (dd, $J=14.0, 7.6$ Hz, 1H, CH_ACH_BCH), δ 2.47-2.34 (m, 4H, CH_2NCH_2), δ 1.65-1.51 (m, 4 H, $CH_2CH_2CH_2CH_2$); ^{13}C NMR (100 MHz, d_6 -DMSO): δ 174.7 ($CHCONCH_2$),

δ 157.6 (NHCONCH₂), δ 135.3 (C Ar) δ 130.3 (CH Ar), δ 128.4 (CH Ar), δ 127.0 (CH Ar), δ 57.5 (CH), δ 54.7 (NCH₂N), δ 49.4 (2C, CH₂NCH₂), δ 36.4 (CHCH₂), δ 23.3 (2C, CH₂CH₂CH₂CH₂); IR (neat): ν_{\max} = 1752, 1691 cm⁻¹ (C=O).

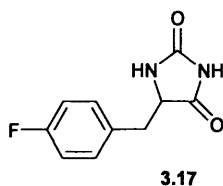
Synthesis of 5-(4-fluorobenzyl)imidazolidine-2,4-dione 3.27



Method 3.2 was followed. Hydantoin: 4.0 g (40 mmoles), triethanolamine: 5.3 ml (40 mmoles), 4-fluorobenzaldehyde (4.3 ml, 40 mmoles). The solvent of crystallisation was: ethanol/2-propanol (10:1).

(Z)-5-(4-fluorobenzylidene) imidazolidine-2,4-dione: yield 26 %, M.p. 262-266 °C (crystallised from EtOH/2-propanol) (literature value: 260-262 °C¹⁸), HRMS m/z (EI⁺) = 206.0491, (C₁₀H₇FN₂O₂⁺ requires 206.0492; ¹H NMR (400 MHz, d₆-DMSO): δ 10.9 (br s, 1H, CNHCO), δ 7.71-7.61 (m, 2H, 2 x CHC(CH) Ar), δ 7.27-7.17 (m, 2H, 2 x CHCF Ar), δ 6.42 (s, 1H, CH); ¹³C NMR (100 MHz, d₆-DMSO): δ 165.8 (CCONH), δ 162.2 (d, J=247.3 Hz, CF Ar), δ 156.1 (NHCONH), δ 131.9 (d, J=8.3 Hz, CH Ar), δ 129.9 (d, J=3.0 Hz, C Ar), δ 128.1 (NHCCO), δ 116.1 (d, J=21.0 Hz, CH Ar), δ 107.6 (CH); IR (neat): ν_{\max} = 1765, 1729 cm⁻¹ (C=O), 1662 cm⁻¹ (C=C).

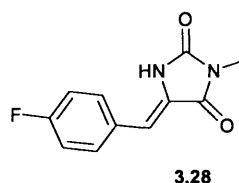
Synthesis of 5-(4-fluorobenzyl)imidazolidine-2,4-dione 3.17



Method 3.3 was followed. *(Z)*-5-(4-fluorobenzylidene) imidazolidine-2,4-dione **3.27**: 0.30 g (1.45 mmoles) dissolved in 30 ml of THF.

5-(4-fluorobenzyl)imidazolidine-2,4-dione: yield 99 %, M.p. 198-204 °C, HRMS m/z (EI^+) = 208.0644, ($C_{10}H_9FN_2O_2^+$ requires 208.0648); 1H NMR (400 MHz d_6 -DMSO): δ 10.52 (br s, 1H, CONHCO), δ 7.99 (br s, 1H, CHNH), δ 7.25-7.12 (m, 4H, Ar), δ 4.39 (t, $J=4.8$ Hz, 1H, CH), δ 2.98 (m, 2H, CH_2); ^{13}C NMR (100 MHz, d_6 -DMSO): δ 175.6 (CHCONH), δ 161.6 (d, $J=242.5$ Hz, CF Ar), δ 157.5 (NHCONH), δ 132.1 (C Ar), δ 131.9 (d, $J=8.16$ Hz, CH Ar), δ 115.2 (d, $J=31.3$ Hz, CH Ar), δ 58.7 (CH), δ 35.8 (CH_2); IR (neat): $\nu_{max}=1756, 1699\text{ cm}^{-1}$ (C=O).

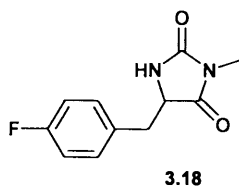
Synthesis of (*Z*)-5-(4-fluorobenzylidene)-3-methylimidazolidine-2,4-dione 3.28



Method 3.2 was followed. 3-methylimidazolidine-2,4-dione: 0.80 g (7.0 mmoles), triethanolamine: 0.9 ml (7.0 mmoles), 4-fluorobenzaldehyde: 0.75 ml (7.0 mmoles). The solvent of crystallisation was ethanol/2-propanol (10:1).

(Z)-5-(4-fluorobenzylidene)-3-methylimidazolidine-2,4-dione: yield 58 %, M.p. 258-264 °C (crystallised from EtOH/2-propanol), HRMS m/z (EI^+) = 220.0643, ($C_{11}H_9FN_2O_2^+$ requires 220.0648); 1H NMR (400 MHz d_6 -DMSO): δ 10.8 (br s, 1H, CNHCO), δ 7.74-7.63 (m, 2H, 2 x $CHC(CH)$ Ar), δ 7.29-7.17 (m, 2H, 2 x $CHCF$ Ar), δ 6.54 (s, 1H, CH), δ 2.96 (s, 3H, CH_3); ^{13}C NMR (100 MHz, d_6 -DMSO): δ 164.6 (C $CONCH_3$), δ 162.2 (d, $J=247.4$ Hz, CF Ar), δ 155.8 (NH $CONCH_3$), δ 132.1 (d, $J=8.5$ Hz CH Ar), δ 129.8 (d, $J=3.6$ C Ar), δ 126.7 (NHCCO), δ 116.1 (d, $J=21.8$ Hz CH Ar), δ 108.51 (CH), δ 24.7 (CH_3); IR (neat): $\nu_{max}=1748, 1701\text{ cm}^{-1}$ (C=O), 1647 cm^{-1} (C=C).

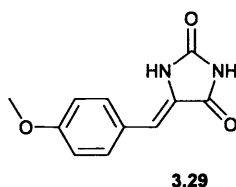
Synthesis of (*Z*)-5-(4-fluorobenzylidene)-3-methylimidazolidine-2,4-dione 3.18



Method 3.3 was followed. (Z)-5-(4-fluorobenzylidene)-3-methylimidazolidine-2,4-dione **3.28**: 0.3 g (1.36 mmol) dissolved in 30 ml of THF.

5-(4-fluorobenzyl)-3-methylimidazolidine-2,4-dione: yield 90 %, M.p. 148-151 °C, HRMS m/z (EI^+) 222.0802, ($C_{11}H_{11}FN_2O_2^+$ requires 222.0802); 1H NMR (400 MHz d_6 -DMSO): δ 8.26 (br s, 1H, CHNH), δ 7.36-7.04 (m, 4H, Ar), δ 4.40 (t, $J=5.0$ Hz, 1H, CH), δ 3.10-2.89 (m, 2H, CH_2), δ 2.70 (s, 3H, CH_3); ^{13}C NMR (100 MHz, d_6 -DMSO): δ 173.9 (CHCON CH_3), δ 161.0 (d, $J=245.3$ Hz, CF Ar), δ 157.1 (NHCON CH_3), δ 132.0 (C Ar), δ 131.8 (d, $J=7.4$ Hz, CH Ar), δ 115.2 (d, $J=21.3$ Hz, CH Ar), δ 57.6 (CH), δ 36.0 (CH_2), δ 24.2 (CH_3); IR (neat): ν_{max} = 1756, 1686 cm^{-1} (C=O).

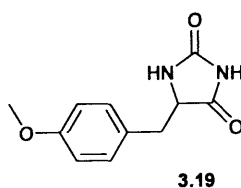
Synthesis of (Z)-5-(4-methoxybenzylidene)imidazolidine-2,4-dione **3.29**



Method 3.2 was followed. Hydantoin: 6.00 g (60 mmol), triethanolamine: 8.0 ml (60 mmol), 4-methoxyaldehyde: 7.3 ml (60 mmol).

(Z)-5-(4-methoxybenzylidene)imidazolidine-2,4-dione: yield 23 %, M.p. 250-256 °C (crystallised from EtOH) (literature value: 243-245 °C¹⁸), HRMS m/z (EI^+) = 218.0688, ($C_{11}H_{10}N_2O_3^+$ requires 218.0691); 1H NMR (400 MHz d_6 -DMSO): δ 10.5 (br s, 1H, CNHCO), δ 7.59 (d, $J=8.6$ Hz, 2H, 2xCHC(CH) Ar), δ 6.96 (d, $J=8.6$ Hz, 2H, 2xCHC(O) Ar), δ 6.39 (s, 1H, CH), δ 3.79 (s, 3H, CH_3); ^{13}C NMR (100 MHz, d_6 -DMSO): δ 165.9 (CCONH), δ 159.7 (C(O) Ar), δ 156.0 (NHCONH), δ 131.4 (CH Ar), δ 126.4, 125.8 (CHCCH Ar and NHCCO), δ 114.7 (CH Ar), δ 109.0 (CH), δ 55.6 (CH_3); IR (neat): ν_{max} = 1751, 1707 cm^{-1} (C=O), 1647 cm^{-1} (C=C).

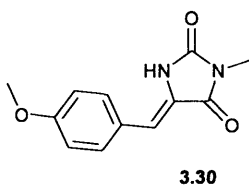
Synthesis of 5-(4-methoxybenzyl)imidazolidine-2,4-dione 3.19



Method 3.3 was followed. (*Z*)-5-(4-methoxybenzylidene)imidazolidine-2,4-dione **3.29**: 0.30 g (1.36 mmol) dissolved in 45 ml of dioxane.

5-(4-methoxybenzyl)imidazolidine-2,4-dione: yield 99 %, M.p. 170-176 °C (literature value for (*S*)-5-(4-methoxybenzyl)imidazolidine-2,4-dione 171-173 °C recrystallised from water⁶¹), HRMS m/z (EI^+) = 220.0840, ($C_{11}H_{12}N_2O_3^+$ requires 220.0848); 1H NMR (400 MHz d_6 -DMSO): δ 10.46 (br s, 1H, CONHCO), δ 7.96 (br s, 1H, CHNH), δ 7.15 (d, $J=8.6$ Hz, 2H, 2xCHC(CH₂) Ar), δ 6.89 (d, $J=8.6$ Hz, 2H, 2xCHC(O) Ar), δ 4.33 (t, $J=4.9$ Hz, 1H, CH), δ 3.77 (s, 3H, CH₃), δ 2.92 (d, $J=4.8$ Hz, 2H, CH₂); ^{13}C NMR (100 MHz, d_6 -DMSO): δ 175.6 (CHCONH), δ 158.4 (C(O) Ar), δ 157.5 (NHCONH), δ 131.2 (CH Ar), δ 127.6 (CCH₂ Ar), δ 113.8 (CH Ar), δ 58.9 (CH), δ 55.3 (CH₃), δ 35.8 (CH₂); IR (neat): ν_{max} = 1758, 1698 cm^{-1} (C=O).

Synthesis of (*Z*)-5-(4-methoxybenzylidene)-3-methylimidazolidine-2,4-dione 3.30



Method 3.2 was followed. 3-methylimidazolidine-2,4-dione: 0.50 g (4.4 mmol), triethanolamine: 0.6 ml (4.4 mmol), *p*-methoxyaldehyde: 0.5 ml (4.4 mmol).

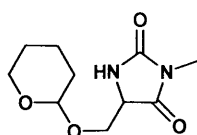
(*Z*)-5-(4-methoxybenzylidene)-3-methylimidazolidine-2,4-dione: yield 47 %, M.p. 216-220 °C (crystallised from EtOH), HRMS m/z (EI^+) = 232.0844, ($C_{12}H_{12}N_2O_3^+$ requires 232.0848); 1H NMR (400 MHz d_6 -DMSO): δ 10.7 (br s, 1H, CNHCO), δ 7.61 (d, $J=9.0$ Hz, 2H, 2xCHC(CH) Ar), δ 6.96 (d, $J=9.0$ Hz, 2H, 2xCHC(O) Ar), δ 6.51 (s, 1H, CH),

A suspension of D/L methyl 2-amino-3-hydroxypropanoate hydrochloride (1.50 g, 9.6 mmoles) and pyridinium 4-toluenesulfonate (0.12 g, 0.48 mmoles) in 30 ml of dry dichloromethane was prepared in a round bottom flask with a stopper. 3,4-dihydro-2H-pyran (1.3 ml, 14.5 mmoles) was added and the mixture was stirred overnight. The reaction mixture was filtered on silica with little methanol. The solvent was then evaporated and **3.37** was recovered as yellow oil (the signals in the ^1H NMR spectrum of the crude of the reaction are reported). A 33% solution of methylamine in ethanol (8 ml, 64 mmoles) was added to the same flask and the solution was stirred for 5 days. 5 ml of a 4 M solution of sodium carbonate were added. The mixture was stirred for 2 minutes and then extracted with chloroform. The combined organic extracts were dried over anhydrous Na_2SO_4 and the solvent evaporated. The crude of the reaction was purified by column chromatography on fluorosil (gradient dichloromethane : ethyl acetate : methanol from 80:20:0 to 80:20:20) to yield a diastereomeric mixture of two amides **3.38** as yellow oil.

2-amino-3-(5,6-dihydro-2H-pyran-2-yloxy)-N-methylpropanamide yield 34%. ^1H NMR of the crude intermediate **3.37** (400 MHz, d_6 -DMSO): mixture of 2 diastereoisomers (2 sets of signals only partly resolved), signals attributable to starting material are also present: δ 5.64 (br s 1H, OH starting material), δ 4.66-4.60, 6.60-4.55 (2 m, 2xH, OCHO), δ 4.38-4.33, 4.33-4.29 (2 m, 2xH, $\text{CH}_A\text{H}_B\text{CH}$), δ 4.10 (t, $J=4.1$ Hz, 1H, CH_2CH starting material), δ 4.05-3.96 (m, 2xH, $\text{OCH}_A\text{H}_B\text{CH}_2$), δ 3.84-3.70 (m, 2xH, $\text{CH}_A\text{H}_B\text{CH} + 2 \times 3\text{H}$, $\text{OCH}_3 + 2\text{H}$, CH_2CH starting material + 3H, OCH_3 starting material), δ 3.64-3.55 (m, 2xH, $\text{CH}_A\text{H}_B\text{CH}$), δ 3.48-3.41 (m, 2xH, $\text{OCH}_A\text{H}_B\text{CH}_2$), δ 1.82-1.33 (m, 2x6H, $\text{CH}_2\text{CH}_2\text{CH}_2\text{CH}$); ^1H NMR (400 MHz d_6 -DMSO) of *2-amino-3-(5,6-dihydro-2H-pyran-2-yloxy)-N-methylpropanamide* **3.38**: mixture of 2 diastereoisomers (2 sets of signals only partly resolved) δ 8.00-7.82 (br s, 2 x 1H, NH), δ 4.60 (t, $J= 3.3$, 2x1H, OCHO), δ 3.83-3.70 (m, 2x1H, $\text{OCH}_A\text{H}_B\text{CH}_2$), δ 3.67 (dd, $J=10$, $J=6$ Hz 2x1H $\text{NH}_2\text{CHCH}_A\text{H}_B$), δ 3.58–3.31 (m, 2x1H $\text{NH}_2\text{CHCH}_A\text{H}_B + 2 \times 1\text{H}$, $\text{OCH}_A\text{H}_B\text{CH}_2 + 2 \times 1\text{H}$, $\text{NH}_2\text{CHCH}_A\text{H}_B$), δ 2.67, 2.65 (2xs, 2x3H, CH_3), 1.95-1.39 (m, 2x(2+6H), $\text{CH}_2\text{CH}_2\text{CH}_2$); ^{13}C NMR (100 MHz, d_6 -DMSO: δ 173.1 (2 x CO), δ 98.5, 98.1 (2xOCHO), δ 70.3, 70.1 (2x CH_2CHNH_2), δ 61.5 (2x OCH_2CH_2), δ 55.1 (2x

CHCO), δ 30.5 (2xCH₂CHO), δ 25.8 (2xNCH₃), δ 25.4 (2xOCH₂CH₂), δ 19.4 (2xCHC
H₂CH₂); IR (neat): ν_{\max} = 1648 cm⁻¹ (C=O).

Synthesis of 3-methyl-5-((tetrahydro-2H-pyran-2-yloxy)methyl)imidazolidine-2,4-dione **3.39**



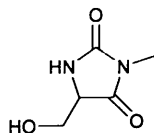
3.39

A solution of **3.38** (0.34 g, 1.66 mmol) in dry CH₂Cl₂ (6 ml) was prepared in a sealed round bottom flask, under nitrogen atmosphere. A solution of carbonyldiimidazole (0.40 g, 2.48 mmol) in dry CH₂Cl₂ (5 ml) was prepared in the same way. The solution of carbonyldiimidazole was added by cannula to the solution of **3.38** and the mixture, kept under nitrogen atmosphere, was let react overnight with stirring. The solution was washed three times with acidic water till neutral pH. The organic layer was then dried over anhydrous Na₂SO₄, filtered and concentrated. The product was purified by column chromatography on fluorosil (gradient dichloromethane /methanol from 100:0 to 80:20). **3.39** was obtained as white solid.

3-methyl-5-((tetrahydro-2H-pyran-2-yloxy)methyl)imidazolidine-2,4-dione: yield 46%, M.p. 92-96 °C, HRMS m/z (ESI and APCI)=molecular peak not detectable (visible peak at 126.04 as for serine hydantoin); ¹H NMR (400 MHz d₆-DMSO): mixture of 2 diastereoisomers (2 sets of signal only partly resolved), δ 8.37, 8.30 (2xs, 2x1H, NH), δ 4.66, 4.62 (2xt, J_{mean} =3.0 Hz, 2x1H, OCHO), δ 4.33-4.27 (m, 2x1H, CH_AH_BCHNH), δ 3.88 (2xdd, J =10.5, 2.8 Hz, 2x1H, NHCHCH_AH_B), δ 3.84-3.73 (m, 2x1H CH₂CH_AH_BO), δ 3.64, 3.60 (2xdd, J =10.6, 4.6 Hz, 2x1H, NHCHCH_AH_B), δ 3.53-3.33 (m, 2x1H, CH₂CH_AH_BO + 2x3H, NCH₃), δ 1.76-1.41 (m, 2x6H, CH₂CH₂CH₂CH); ¹³C NMR (100 MHz, d₆-DMSO): δ 173.1, 173.0 (2x CHCONCH₃), δ 157.9, 157.7 (2x NHCONCH₃), δ 98.6, 97.9 (2x OCHO), δ 66.1, 65.3 (2x CH₂CHNH), δ 61.7, 61.2 (2x CH₂CH₂O), δ 57.8, 57.6 (2x CH₂CHNH), δ 30.4, 30.3 (2x

CH₂CH₂CH), δ 25.3 (2x OCH₂CH₂CH₂), δ 24.4 (2x NCH₃), δ 19.2, 18.9 (2x CH₂CH₂CH); IR (neat): ν_{\max} = 1756, 1695 cm⁻¹ (C=O).

Synthesis of 5-(hydroxymethyl)-3-methylimidazolidine-2,4-dione 3.22

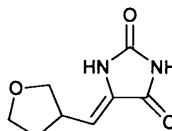


3.22

3.39 (0.09 g, 0.32 mmol) was dissolved in water (5 ml). Few drops of dilute HCl were added to a final pH 2. The solution was stirred overnight, diluted with 20 ml of deionised water and purified by means of HPLC on a 150x4.6 mm Zorbax Eclipse XDB-C18 column (Agilent Technologies). Mobile phase: gradient from 95% water - 5% acetonitrile to 100% acetonitrile, flow rate: 1 ml/min. Detection: 230 nm, elution time = 1.8 min. The combined HPLC fractions were concentrated and high vacuum dried. The product was recovered as a white solid.

5-(hydroxymethyl)-3-methylimidazolidine-2,4-dione: yield 87%, M.p. 121-125 °C, HRMS m/z (EI⁺) = 126.0429, (C₅H₈N₂O₃⁺ requires 144.1286, M⁺ - H₂O requires 126.0429); ¹H NMR (400 MHz, D₂O): δ 4.24 (t, J=3.0 Hz, 1H, CH), δ 3.87 (dd, 1H, J=12.2, 3.1 Hz, CH_AH_BCH), δ 3.81 (dd, J=12.3, 2.8 Hz, 1H, CH_AH_BCH), δ 2.9 (s, 3H, NCH₃); ¹³C NMR (100 MHz, d₆-DMSO): δ 173.4 (CHCONCH₃), δ 157.9 (NHCONCH₃), δ 60.2 (CH₂), δ 59.5 (CH), δ 24.3 (NCH₃); IR (neat): ν_{\max} = 1768, 1719 cm⁻¹ (C=O).

Synthesis of (Z)-5-((tetrahydrofuran-3-yl)methylene)imidazolidine-2,4-dione 3.31

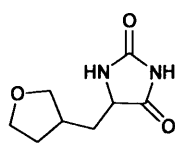


3.31

Method 3.2 was followed. Hydantoin: 4.0 g (40.0 mmoles), triethanolamine: 5.3 ml (40.0 mmoles), tetrahydrofuran-3-carboxaldehyde (50 weight % in H₂O): 7.5 ml (40.0 mmoles). No precipitate was observed at the end of the reaction. The reaction mixture was extracted with chloroform. The combined organic layers were concentrated and high vacuum dried. The product was purified by column chromatography on silica gel (dichloromethane:ethyl acetate=1:2).

(Z)-5-((tetrahydrofuran-3-yl)methylene)imidazolidine-2,4-dione: yield 4% M.p. 152-162 °C, HRMS *m/z* (EI⁺) =182.0694, (C₈H₁₀N₂O₃⁺ requires 182.0691); ¹H NMR (400 MHz D₂O): δ 5.71 (d, J=10.4 Hz, 1H, CCH), δ 3.88-3.80 (m, 2H, CHCH_AH_BO + CH₂CH_AH_BO), δ 3.74 (ddd appears as q, J_{mean} =7.7, 1H, CH₂CH_AH_BO), δ 3.45 (dd, J=8.5, 6.8 Hz, 1 H, CHCH_AH_BO), δ 3.1-3.0 (m, 1 H, CH₂CH), δ 2.19-2.07 (m, 1H, CHCH_AH_BCH₂), δ 1.78-1.66 (m, 1H, CHCH_AH_BCH₂); ¹³C NMR (100 MHz, d₆-DMSO): δ 166.6 (CCONH), δ 156.8 (NHCONH), δ 133.2 (CCH), δ 117.1 (CCH), δ 72.1 (OCH₂CH), δ 68.3 (OCH₂CH₂), δ 37.2 (CH₂CHCH₂), δ 32.4 (CHCH₂CH₂); IR (neat): ν_{max} = 1718 cm⁻¹ (br, C=O), 1683 cm⁻¹ (C=C).

Synthesis of 5-((tetrahydrofuran-3-yl)methyl)imidazolidine-2,4-dione **3.21**



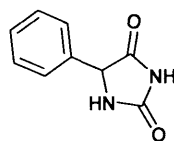
3.21

Method 3.3 was followed. (*Z*)-5-((tetrahydrofuran-3-yl)methylene) imidazolidine-2,4-dione **25**: 0.28 g, (1.51 mmoles) dissolved in 35 ml THF. The product was obtained as a mixture of diastereoisomers.

5-((tetrahydrofuran-3-yl)methyl)imidazolidine-2,4-dione: yield 42 %, M.p. 122-126 °C, HRMS *m/z* (EI⁺) =184.0847, (C₈H₁₂N₂O₃⁺ requires 184.0848); ¹H NMR (400 MHz acetone-d₆): diastereomeric mixture (approximate diastereomeric ratio 1:1): 2 sets of signal only partly resolved): δ 9.48 (br s, 2x1H, CONHCO), δ 7.05, 6.99 (2xs, 2x1H, CHNHCO), δ 4.05-3.98 (m, 2x1H, COCHCH₂), δ 3.77-3.70 (m, 2x1H, CHCH_AH_BO), δ

3.69-3.60 (m, 2x1H, CH₂CH_AH_BO), δ 3.57-3.49 (m, 2x1H, CH₂CH_AH_BO), δ 3.21 (t, J=7.7 Hz) and δ 3.17 (t, J=8.0 Hz) (2x1H, CHCH_AH_BO), δ 2.35-2.20 (m, 2x1H, CH₂CHCH₂O), δ 2.01-1.88 (m, 2x1 H, CHCH_AH_BCH₂ overlapped to acetone residual peak), δ 1.82-1.57 (m, 2x2H, CHCH_AH_BCH), δ 1.50-1.37 (m, 2x1H, CHCH_AH_BCH₂); ¹³C NMR (100 MHz, acetone-d₆): δ 175.2, 175.1 (2x CHCONH), δ 157.0, 156.9 (2x NHCONH), δ 72.7, 72.4 (2x OCH₂CH), δ 67.1, 67.0 (2x OCH₂CH₂), δ 57.5 (2x COCHCH₂), δ 35.7, 35.6 (2x CH₂CHCH₂), δ 35.2 (2x CHCH₂CH), δ 32.4, 31.2 (2x CH₂CH₂CH); IR (neat): ν_{max} = 1768, 1719 cm⁻¹ (C=O).

Synthesis (*R*)-5-phenylimidazolidine-2,4-dione **3.23**



3.23

A suspensions of (*R*)-2-amino 2 phenyl acetamide hydrochloride (0.20 g, 1.05 mmoles) in dry CH₂Cl₂ (10 ml) in a sealed round bottom flask under nitrogen atmosphere was prepared. A solution of CDI (0.26 g, 1.57 mmoles) in dry CH₂Cl₂ (5ml) was prepared in the same way. Triethylamine (0.15 ml, 1.05 mmoles) was added to the suspension of (*R*)-2-amino-2-phenyl acetamide hydrochloride. The solution of CDI was added by cannula to the suspension of the amino acid amide hydrochloride. The reaction mixture, kept under nitrogen atmosphere, was stirred for 4 hours. The hydantoin was recovered after evaporation of the solvent and treatment with little water to favour crystal formation. The solid product was washed with CH₂Cl₂ and water and high vacuum dried. The product was recovered in racemic form.

5-phenylimidazolidine-2,4-dione: yield 54%, M.p. 163-170°C (Literature value: 173-174 °C recrystallised from water, (*S*) enantiomer²) HRMS (m/z = 176.0587, (C₉H₈N₂O₂⁺ requires 176.0586); ¹H NMR (400 MHz, CDCl₃): δ 7.72 (brs, 1H, CONHCO), δ 7.44–7.32 (m, 5H, C₆H₅), δ 5.74 (br s, 1H, CHNH), δ 5.12 (s, 1H, CH); ¹³C NMR (100 MHz, CDCl₃): δ 174.6 (CHCONH), δ 157.88 (NHCONH), δ 136.39 (C

Ar), δ 129.03 (CH Ar) δ 128.62 (CH Ar) δ 127.06 (CH Ar) δ 61.54 (CH); IR (neat): ν_{\max} = 1774, 1718 cm^{-1} (C=O). $[\alpha]_D^{25} = 0^\circ$ (0.45 g/100ml in EtOH).

3.6. Experimental Part 2

Materials

Potassium chloride (analytical grade) was from Fluka. Potassium hydroxide (analytical grade) was from Fisher Scientific. Potassium dihydrogen phosphate (crystallised) was from VWR. Deuterium oxide (99.9%) was purchased from Fluorochem.

Apparatus

Materials were weighed on an analytical balance Fisher Brand PS-100 (Max 100 g, $d=0.1\text{mg}$). Volumes of solutions were measured by means of Gilson or Eppendorf Research micropipettes. pH measurements were carried out, at room temperature, using a HANNA INSTRUMENTS pH 210 pH meter. The pH meter was calibrated before each measurement with certified traceable to NIST buffers at pH 7.00 ± 0.01 (at 25 °C) (from Fisher), pH 10.01 ± 0.02 (at 25 °C) (from Fisher) and pH 4.00 ± 0.01 (at 25 °C) (from Reagecon). Reported values are uncorrected. Values are reported as pH** indicating the reading of the pH meter at room temperature. Thermostatic water baths Subaqua 12 (temperature stability ± 0.2 °C) or Julabo MB-5 Heating Circulator (temperature stability ± 0.2 °C) were used to control the temperature of solutions in kinetic experiments with timescales longer than three days. Kinetic experiments of racemisation were carried out on a Chirascan CD spectrometer equipped with a Temperature-Controlled Sample Holder for circular dichroism (temperature stability: ± 0.02 °C), in 1.00 cm path length quartz cuvettes. Kinetic experiments of H/D exchange were carried out on a Bruker AVANCE 400 or a Bruker AVANCE 500 spectrometers at 400 (pulse interval (D1): 1 s, , pulse width (pw):10.75 μs , acquisition time (at): 3.42 s) or 500 MHz (pulse interval (D1): 1 s, , pulse width (pw):12.00 μs , acquisition time (at): 5.45 s), respectively.

Preparation of solutions

Stock solutions of D₂O phosphate buffers were prepared by dissolving potassium dihydrogen phosphate in D₂O and adjusting the pH** of the solution with KOH, to give final buffers with the desired concentrations and pH**. Potassium chloride was used to adjust the ionic strength of the buffer solutions. After preparation of the buffers, as described above, the solvent was evaporated and replenished 3 times with fresh D₂O, to guarantee the exchange with deuterons and removal of the protons from the non deuterated inorganic materials used to prepare the solutions.

Stock solutions of hydantoins were prepared by dissolving the solid hydantoins in D₂O. In all cases except for hydantoins **3.4**, **3.21** and **3.22**, the solutions were prepared in plastic eppendorfs which were kept, overnight, under continuous rotation at a speed of 20 rpm by means of a Stuart Tube rotator SB2. The solutions were then centrifuged for 8 minutes at 13.3 rpm on a Jencons-pls Spectrafuge 24.D centrifuge. The clear supernatant was transferred in a new eppendorf and an amount of fresh solvent, equivalent to approximately 1/10 of the total volume of solution, was added to the saturated solution, to avoid precipitation. Solution of hydantoins **3.4**, **3.21** and **3.22** were obtained by dissolving the desired amounts of hydantoins with stirring for 10 minutes.

Kinetic experiments

The reaction media for the CD experiments were prepared by mixing buffer solutions, D₂O, and the stock solutions of hydantoins in suitable proportions to obtain final solutions with the desired ionic strength, concentration of buffer and concentration of hydantoin. Typical final concentrations of hydantoins were 0.7 mM for hydantoin **3.3**, 0.3 mM for hydantoin **3.4** and 0.1 mM for hydantoin **3.5**. Solvents and stock solutions were mixed immediately before the start of the kinetic experiments, to minimise the time lag between the beginning of the reaction and the acquisition of the kinetic data. CD experiments at 60 °C, 50 °C and some experiments at 37 °C, with a timescale lower than three days, were carried out in the quartz cuvettes housed in the thermostated sample holder of the spectrometer. CD spectra were automatically recorded at set time intervals which were chosen based on the timescale of the reaction. In the kinetic

experiments at 15, 25 and 37 °C, whose timescale was ranging from a week to three months, the temperature was controlled by housing the solutions in thermostatic water baths and CD spectra were recorded at set time intervals. The decreases of the CD signals, typically at 235 or 240 nm, were followed over time.

The reaction media for the kinetic experiments of H/D exchange were prepared by mixing equal volumes of stock solutions of buffers and stock solutions of hydantoins, to give the desired final concentrations of buffer and ionic strength. The choice of the final concentrations of hydantoins was limited by their solubilities in D₂O. Typical final concentrations were variable between 2 and 5 mM for hydantoins **3.1**, **3.2**, **3.10**, **3.17-3.20** and **3.23**, from 25 to 27 mM for hydantoins **3.3**, **3.4** and **3.5** and 60 mM for hydantoins **3.21** and **3.22**. Solvents and stock solutions were mixed immediately before the start of the kinetic experiments. Reaction mixtures were transferred in NMR tubes which were housed in thermostatic water baths. ¹H NMR spectra were taken at set time intervals chosen depending on the time scale of the H/D exchange reaction. Except for the kinetic experiments for 5-phenylhydantoin (carried out on a Bruker AVANCE 500 spectrometer), whose H/D exchange was particularly fast, the NMR tubes were not thermostated during the time of acquisition of the ¹H NMR spectra. H/D exchange experiments for phenylhydantoin **3.23** at 25 °C were carried out on a Bruker AVANCE 500 spectrometer at 500 MHz. The temperature was controlled by a Bruker BVT 3000 digital controller (temperature stability ±0.2 °C). Spectra were taken every 5 minutes. Pseudo first-order rate constants of H/D exchange were obtained by following over time the decrease of the relative area integrals of the exchangeable protons of the hydantoins. The ¹H NMR signal from the phenyl ring (compounds **3.1-3.5**, **3.10**, **3.23** and **3.17-3.20**) or from stable alkyl groups of the hydantoins (compounds **3.21** and **3.22**) were used as internal standards to evaluate the integrals of the NMR peaks of exchangeable protons. Spectral processing and integrations of NMR signals were carried out by means of the program SpinWorks 2.5.5.

Rate constants for all kinetic experiments were obtained by fitting experimental data points to first-order kinetics, by means of the computer program Origin.

Solubility tests

The solubilities of hydantoins were determined gravimetrically. The water was evaporated from exactly measured volumes of saturated solutions of hydantoins, and the residue was weighed on an analytical balance.

Acknowledgments

I would like to acknowledge Prof. Barry Carpenter for his useful group-meeting comments leading to the discussion reported in Section 3.2.3. Dr Robert Richardson is gratefully acknowledged for kind help and discussions on spectral analyses reported in this Chapter. I thank Daniela Milan, Julia Kennedy and Rhys Williams for their work on this project leading to the synthesis of hydantoins 3.24-3.26 and 3.24b, 3.26b and related kinetic experiments. I would also like to thank Dr Rob Jenkins for technical support with the NMR experiments of H/D exchange for compound 3.23 and Dave Walker and Robin Hicks for recording high resolution mass spectra.

References

1. Anslyn, E. V.; Dougherty, D. A., *Modern Physical Organic Chemistry*. University Science Books: Sausalito, California, 2006; p 441-445.
2. Reist, M.; Carrupt, P. A.; Testa, B.; Lehmann, S.; Hansen, J. J., *Helvetica Chimica Acta* **1996**, 79 (3), 767-778.
3. Wilson, C. L., *Journal of the Chemical Society* **1934**, 98-99.
4. Reist, M.; Testa, B.; Carrupt, P. A., *Enantiomer* **1997**, 2 (3-4), 147-155.
5. Testa, B.; Carrupt, P. A.; Gal, J., *Chirality* **1993**, 5 (3), 105-111.

6. Cirilli, R.; Costi, R.; Gasparrini, F.; La Torre, F.; Pierini, M.; Siani, G., *Chirality* **2009**, *21* (1), 24-34.
7. Amyes, T. L.; Richard, J. P., *Journal of the American Chemical Society* **1996**, *118* (13), 3129-3141.
8. Richard, J. P.; Williams, G.; O'Donoghue, A. C.; Amyes, T. L., *Journal of the American Chemical Society* **2002**, *124* (12), 2957-2968.
9. Rios, A.; Amyes, T. L.; Richard, J. P., *Journal of the American Chemical Society* **2000**, *122* (39), 9373-9385.
10. Rios, A.; Richard, J. P.; Amyes, T. L., *Journal of the American Chemical Society* **2002**, *124* (28), 8251-8259.
11. Williams, G.; Maziarz, E. P.; Amyes, T. L.; Wood, T. D.; Richard, J. P., *Biochemistry* **2003**, *42* (27), 8354-8361.
12. Zhang, D.; Xing, X. C.; Cuny, G. D., *Journal of Organic Chemistry* **2006**, *71* (4), 1750-1753.
13. Nowick, J. S.; Powell, N. A.; Nguyen, T. M.; Noronha, G., *Journal of Organic Chemistry* **1992**, *57* (26), 7364-7366.
14. Nowick, J. S.; Holmes, D. L.; Noronha, G.; Smith, E. M.; Nguyen, T. M.; Huang, S. L., *Journal of Organic Chemistry* **1996**, *61* (11), 3929-3934.
15. Dudley, K. H.; Bius, D. L., *Drug Metabolism and Disposition* **1976**, *4* (4), 340-348.
16. Mudit, M.; Khanfar, M.; Muralidharan, A.; Thomas, S.; Shah, G. V.; van Soest, R. W. M.; El Sayed, K. A., *Bioorganic & Medicinal Chemistry* **2009**, *17* (4), 1731-1738.
17. Mudit, M.; Khanfar, M.; Muralidharan, A.; Thomas, S.; Shah, G. V.; van Soest, R. W. M.; El Sayed, K. A., *Bioorganic & Medicinal Chemistry* **2009**, *17* (8), 3216-3217.
18. Thenmozhiyal, J. C.; Wong, P. T. H.; Chui, W. K., *Journal of Medicinal Chemistry* **2004**, *47* (6), 1527-1535.
19. Zuliani, V.; Carmi, C.; Rivara, M.; Fantini, M.; Lodola, A.; Vacondio, F.; Bordi, F.; Plazzi, P. V.; Cavazzoni, A.; Galetti, M.; Alfieri, R. R.; Petronini, P. G.; Mora, M., *European Journal of Medicinal Chemistry* **2009**, *44* (9), 3471-3479.
20. Zha, C. X.; Brown, G. B.; Brouillette, W. J., *Journal of Medicinal Chemistry* **2004**, *47* (26), 6519-6528.

21. Instrumental imprecision arising from the high rates of racemisation together with a smaller CD signal of compound **3.5** as compared to compounds **3.1-3.4** could be hypothesised. The weaker CD signals of **3.5** can be due to its smaller enantiomeric excess as compared to hydantoins **3.1-3.4**, leading to a smaller signal to noise ratio. The ease of racemisation of **3.5** and, most importantly, of its precursor **3.4** strongly supports further partial racemisation of **3.5** during the last step of its synthesis, involving the methylation of **3.4**. The instrumental limit is, however, only an hypothesis for the odd experimental result. The possibility for the reaction being second order in phosphate could also be envisaged. However further investigations are needed to confirm the hypothesis.
22. Taylor, J. R., *An introduction to Error Analysis The study of uncertainties in physical measurements*. Second ed.; University Science Books: Sausalito, California, 1997; p 174-177.
23. Spencer, C. F., *Journal of Heterocyclic Chemistry* **1973**, *10* (4), 455-457.
24. Maskill, H., *The Physical Basis of Organic Chemistry*. Oxford University Press: Oxford New York, 1990; p 247.
25. Under the experimental conditions (buffer 0.5 M, pH** 7.2), the basic form of the buffer was found to be the main catalyst for the racemisation of benzylhydantoins **3.1** and **3.2** (see Chapter 2) and the approximation $k_{\text{obs}} \sim k_{\text{HPO}_4^{2-}} \cdot [\text{HPO}_4^{2-}]$ could be made. By analogy and considering that, at neutral pH the racemisation of hydantoins **3.1-3.5** is in practice completely catalysed by phosphate buffer, the same approximation appeared to be reasonable for hydantoins **3.3** and **3.5**.
26. Maskill, H., *The Physical Basis of Organic Chemistry*. Oxford University Press: Oxford New York, 1990; p 253-260.
27. Anslyn, E. V.; Dougherty, D. A., *Modern Physical Organic Chemistry*. University Science Books: Sausalito, California, 2006; p 372.
28. Isaacs, N. S., *Physical Organic Chemistry*. Longman Scientific & Technical: 1995; p 643-667.
29. Kahn, K.; Tipton, P. A., *Bioorganic Chemistry* **2000**, *28* (2), 62-72.
30. Bell, R. P.; Fluendy, M. A. D., *Transactions of the Faraday Society* **1963**, *59* (487), 1623-1630.
31. Harper, E. T.; Bender, M. L., *Journal of the American Chemical Society* **1965**, *87* (24), 5625-5632.

32. Ingold, C. K.; Wilson, C. L., *Journal of the Chemical Society* **1934**, 93-97.
33. Ingold, C. K.; Wilson, C. L., *Journal of the Chemical Society* **1934**, 773-777.
34. Hsu, S. K.; Wilson, C. L., *Journal of the Chemical Society* **1936**, 623-625.
35. Hsu, S. K.; Ingold, C. K.; Wilson, C. L., *Journal of the Chemical Society* **1938**, 78-81.
36. Coward, J. K.; Bruice, T. C., *Journal of the American Chemical Society* **1969**, *91* (19), 5339-5345.
37. Isaacs, N., *Physical Organic Chemistry*. Longman Scientific & Technical: 1995; p 647.
38. Bruice, T. C.; Benkovic, S. J., *Bioorganic Mechanisms*. First ed.; W. A. Benjamin, Inc: New York Amsterdam, 1966; Vol. I, p 134-145.
39. Zaslowsky, J. A.; Fisher, E., *Journal of Physical Chemistry* **1963**, *67* (5), 959-961.
40. Holland, G. F.; Durant, R. C.; Friess, S. L.; Witkop, B., *Journal of the American Chemical Society* **1958**, *80* (22), 6031-6035.
41. Davis, W.; Ross, W. C. J., *Journal of the Chemical Society* **1950**, (NOV), 3056-3062.
42. In spite of the ability of quaternary ammonium groups at facilitating ester hydrolysis, solutions of **3.5** in D₂O and in D₂O phosphate buffers with pH* 7.2 were found to be stable.
43. The predicted value of pK_a was obtained using the ACD/I-Lab Web service (ACD/pK_a 12.0).
44. Dahlen, A.; Hilmersson, G., *Journal of the American Chemical Society* **2005**, *127* (23), 8340-8347.
45. Mey, B.; Paulus, H.; Lamparter, E.; Blaschke, G., *Chirality* **1998**, *10* (4), 307-315.
46. Error from weighted average of 3 analytical determinations.
47. Ahlberg, R., *Berichte Der Deutschen Chemischen Gesellschaft* **1928**, *61*, 811-817.
48. McKenzie, A.; Smith, I. A., *Journal of the Chemical Society* **1922**, *121*, 1348-1361.
49. Khan, A.; Marson, C. M.; Porter, R. A., *Synthetic Communications* **2001**, *31* (11), 1753-1764.

50. Akeng'a, T. O.; Read, R. W., *South African Journal of Chemistry-Suid-Afrikaanse Tydskrif Vir Chemie* **2007**, *60*, 11-16.
51. From SciFinder search: Takuma, Y.; Watanabe, N., (Mitsubishi Chemical Corp., Japan). Jpn. Kokai Tokkyo Koho (2001), 5pp. CODEN: JKXXAF JP 2001158775 A 20010612 Patent written in Japanese. Application JP 2000-149256 20000522.
52. Kennedy, J., CD spectroscopy as analytical means for the study of mechanisms of racemisation of hydantoins. Cardiff University: Cardiff, 2011.
53. Asahina, Y.; Takei, M.; Kimura, T.; Fukuda, Y., *Journal of Medicinal Chemistry* **2008**, *51* (11), 3238-3249.
54. Milan, D., Kinetics and computational studies of the mechanism of racemisation and H/D exchange of substituted hydantoins in aqueous, mixed-aqueous and non-aqueous solvents. Cardiff University: Cardiff, 2011.
55. Williams, R., Kinetics of racemisation of a substituted hydantoin pyrrole. Cardiff University: Cardiff, 2011.
56. pK_a Data Compiled by R. Williams http://research.chem.psu.edu/brpgrp/pKa_compilation.pdf.
57. Lazarus, R. A., *Journal of Organic Chemistry* **1990**, *55* (15), 4755-4757.
58. Misuraca, M. C.; Grecu, T.; Freixa, Z.; Garavini, V.; Hunter, C. A.; van Leeuwen, P. W. N. M.; Dolores Segarra-Maset, M.; Turegat, S. M., *Journal of Organic Chemistry* **2011**, *76* (8), 2723-2732.
59. Katritzky, A. R., *Handbook of Heterocyclic Chemistry*. Pergamon Press: Oxford New York Toronto Sydney Frankfurt, 1985; p 250.
60. Taylor, J., *An introduction to error analysis*. University Science Books: Sausalito, California, 1997; p 73-77.
61. Bovarnick, M.; Clarke, H. T., *Journal of the American Chemical Society* **1938**, *60*, 2426-2430.

Chapter 4

The effect of cosolvents on the racemisation of substituted hydantoins in aqueous solutions

Abstract

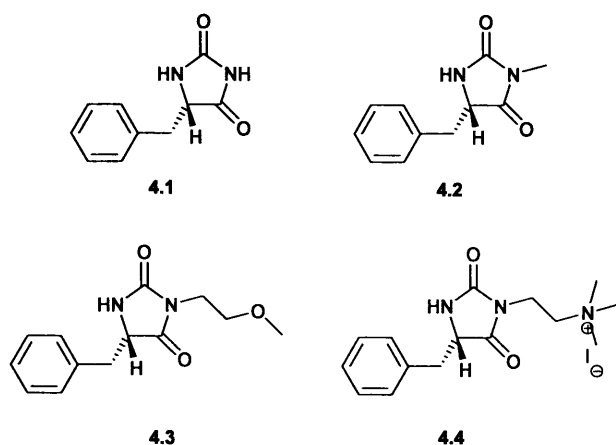
We report on the effect of added co-solvents on the phosphate-catalysed racemisation and H/D exchange reactions of a series of 5-benzylhydantoins (**Scheme 4.1**). The effects of added dimethyl sulfoxide (DMSO), 2-propanol, trifluoroethanol, and dioxane were investigated. The rate constants for racemisation and H/D exchange of neutral hydantoins **4.1-4.3** were found to increase in the presence of increasing amounts of added DMSO. Added trifluoroethanol similarly increased the rate constants for racemisation and H/D exchange, but to a lesser extent than DMSO. 2-Propanol and dioxane showed a rate-depressing effect. The rate constants for racemisation and H/D exchange of cationic hydantoin **4.4** were found to be increased by the addition of all of the co-solvents under investigation, with dioxane showing the strongest rate-accelerating effect. The absence of significant solvent kinetic isotope effects for the racemisation of all hydantoins in the presence and in the absence of added co-solvents supports an S_E1 mechanism for racemisation of all model hydantoins in all the mixed media investigated. No evidence was found for changes in the stereochemical course of the H/D exchange of **4.1** in mixed media containing d_6 -DMSO and d_8 -2-propanol as co-solvent, as compared to H/D exchange in pure D_2O phosphate buffers. In the mixed media, as in pure buffers (Chapter 2), approximately equal rate constants for racemisation (k_{rac}) and H/D exchange ($k_{H/D}$) were observed.

4.1. Introduction

As mentioned in Chapter 3, a major practical problem in the study of (*S*)-5-benzylhydantoin **4.1** and, to a lesser extent, (*S*)-3-*N*-methyl-5-benzylhydantoin **4.2** (**Scheme 4.1**) as model compounds for kinetic studies of racemisation is their poor solubility in water. Although the poor water solubility is not a problem when UV and CD spectroscopy are used, detection limits become important in less sensitive techniques such as NMR or IR spectroscopy, where higher concentrations are required. The addition of a co-solvent can help address the solubility problem and this strategy has been used in previous studies. For example, all kinetic experiments described in the paper on the racemisation of hydantoins by Testa *et al.*¹, often cited in this thesis, were conducted in mixed media composed of 50 volume-% phosphate buffers and 50 volume-% DMSO. In light of the difference between our mechanistic conclusions in aqueous solutions and Testa's conclusions in water-DMSO mixtures, we decided to conduct kinetic studies in the presence of DMSO to both improve the solubility of hydantoins **4.1** and **4.2** and to investigate possible changes in the process of racemisation and H/D exchange of our model hydantoins, induced by changes in the reaction medium.

Marked effects on the rate constants of H/D exchange of **4.1** and **4.2**, due to the addition of DMSO, were found. This observation prompted us to extend our studies to further co-solvents and to the racemisation and H/D exchange of hydantoins **4.1**, **4.2**, **4.3** and **4.4** (**Scheme 4.1**).

Co-solvents could not be added in every proportion to the buffer solutions because of mixing problems and, eventually, precipitation of buffer components. Under the experimental conditions typically used in the kinetic experiments described in this thesis (phosphate buffers with 1 M *I*), 25 % was the maximum volume of co-solvent that could be added to the buffer. Kinetic experiments at higher concentrations of co-solvents were possible only in the presence of lower buffer concentrations and ionic strengths. The kinetic experiments described in this thesis were typically conducted in buffers at 1 M ionic strength while mixtures containing 50 volume-% DMSO and 50 volume-% phosphate buffers at 0.2 M ionic strength were the typical reaction media in the experiments carried out by Testa.¹



Scheme 4.1: structures of model hydantoin whose racemisation and H/D exchange reactions have been studied in mixed media composed of phosphate buffer with added organic co-solvent.

4.2. DMSO, 2-propanol, trifluoroethanol, and dioxane as co-solvents: a few characteristics

As mentioned in Chapter 1, the reaction medium is an important factor in homogeneous chemical reactions. The reaction medium can have dramatic effects on rates, equilibria and the stereochemical course of reactions. In Chapter 1 the main results of selected published studies on the effect of the solvent on racemisation and H/D exchange reactions of different carbon acids have been summarised.

Correlations between solvent effects on reactions and physical properties of the solvents are, usually, not straightforward for example because selective solvation can take place in solvent mixtures.² Nevertheless, we have listed selected solvent properties for the co-solvents used in the kinetic experiments described in this chapter (**Table 4.1**). Dielectric constant, dipole moment and the $E_T(30)$ value are properties commonly used to characterise a solvent in term of its “polarity”. The term “polarity” in itself is ambiguous but can loosely be defined, using Isaacs’ description³ as “the degree to which a solvent is capable of solvating and stabilising charges”. Many solvation scales have been proposed: some are based on physical properties (such as the dielectric constant), others are empirical scales based on solvent-sensitive reaction rates or based on spectroscopic properties.

In **Table 4.1** the bulk property ϵ (dielectric constant) and the empirical parameters $E_T(30)$ ⁴ and π^* ⁵ give indications about the polarity of the solvent. The parameters α and β ⁵

evaluate the hydrogen-bond donor (HBD) acidity and hydrogen-bond acceptor (HBA) basicity of the solvent.

Table 4.1: solvent properties of selected solvents, based on different solvation scales.

Solvent property	Water	TFE	2-propanol	DMSO	1,4-dioxane
$\mu \cdot 10^{30}$ ^{a)}	6.07	--	5.54	13.0	1.50
ϵ ^{b)}	78.4	26.7	19.9	46.7	2.2
E_T (30) ^{c)}	63.1	59.5	48.6	45.0	36.0
π^* ^{d)}	1.09	0.73	0.48	1.00 ^{e)}	0.45
α ^{d)}	1.17	1.51	0.76	0	0
β ^{d)}	0.47	0.00	0.84	0.76	0.37

a) Dipole moment in Coulombmeter (Cm) taken from reference ⁶

b) Dielectric constants taken from reference ⁷

c) Transition energy at 25°C for the long-wavelength absorption band of a standard pyridinium-*N*-phenoxide betaine dye. Values in kcal·mol⁻¹, taken from reference ⁷

d) Kamlet and Taft's solvatochromic parameters taken from reference ⁸

e) Scale reference

In **Table 4.2** dielectric constants and E_T (30) values for selected binary mixtures water-2-propanol and water-1,4-dioxane are also reported for compositions similar to the mixtures used in our kinetic experiments.

Table 4.2: properties of selected binary mixtures of water and 2-propanol and of water and dioxane.

2-propanol			1,4-dioxane		
%	$\epsilon^a)$	$E_T^b)$	%	$\epsilon^c)$	$E_T^b)$
20	65.72	--	14.7	57.60	--
25	--	57.6	20	--	58.6
30	58.40	--	30	45.35	57.1
--	--	--	81.1	8.90	--
100	18.62	48.7	100	--	36.0

a) Values in Coulomb meter determined at 20 °C, mixture compositions are expressed in weight %⁹

b) Values at 25 °C, calculated as $E_T [\text{kcal} \cdot \text{mol}^{-1}] = 2.859 \cdot 10^{-3} \cdot \frac{1}{\lambda} [\text{cm}^{-1}]$. Equation and values of λ published by Dimroth and Reichardt¹⁰, mixture compositions are expressed in volume %.

c) Values determined at 50 °C, mixture compositions are expressed in weight %¹¹

The data in **Table 4.2** provide some useful indicative information since the physical properties of a binary solvent mixture often vary in a non linear fashion with its composition.

4.3. Kinetic studies

4.3.1. The effect of d_6 -DMSO and d_8 -2-propanol on the kinetics of H/D exchange and racemisation of (*S*)-5-benzylhydantoins

4.3.1.1. Kinetic studies in the presence of 33% added co-solvent

In order to increase the solubility of hydantoins **4.1** and **4.2** in the buffer solutions co-solvents were added and the effect of these co-solvents on H/D exchange of **4.1** and **4.2** was studied in D₂O phosphate buffers. Drawing on the paper by Testa *et al.*, and considering its ability at increasing the solubility of 5-benzylhydantoin **4.1**¹², d_6 -DMSO was selected first. Mixing problems and precipitation were encountered upon the addition of d_6 -DMSO to our usual phosphate buffers.

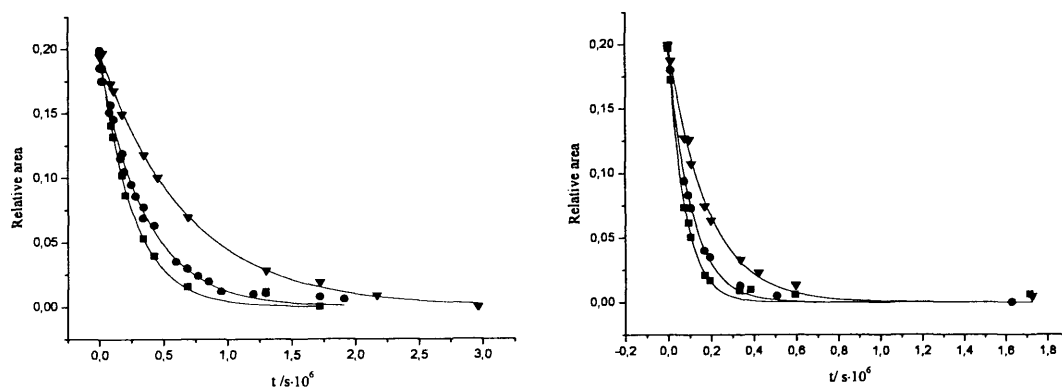


Figure 4.1: Kinetic traces for H/D exchange experiments of 5-benzylhydantoin **4.1** in mixtures of D₂O phosphate buffers pH** 7.2, 1 M *I* (33 volume-%) and 1:1 (v:v) mixture D₂O-d₆-DMSO (67 volume-%). The concentrations of buffers are: 0.3 M (■), 0.2 M (●) and 0.1M (▼). **Left:** kinetic traces of experiments carried out at 25 °C. **Right:** kinetic traces of experiments carried out at 37°C. The relative areas of the peaks of the asymmetric proton in the NMR spectra of **4.1** are plotted as a function of time. The solid lines are the fits to pseudo first-order kinetics.

Buffer concentrations and ionic strength were adjusted depending on the percent volume of d₆-DMSO co-added, to obtain homogeneous and stable solutions.

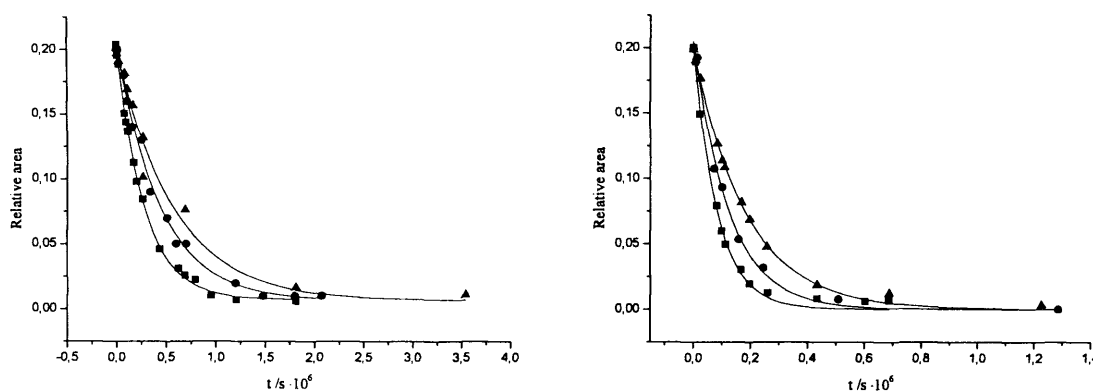


Figure 4.2: Kinetic traces for H/D exchange experiments of 3-*N*-methyl-5-benzylhydantoin **4.2** in mixtures of D₂O phosphate buffers pH** 7.2, 1 M *I* (33 volume-%) and 1:1 (v:v) mixture D₂O-d₆-DMSO (67 volume-%). The concentrations of buffers are: 0.3 M (■), 0.2 M (●) and 0.1 M (▼). **Left:** kinetic traces of experiments carried out at 25 °C. **Right:** kinetic traces of experiments carried out at 37 °C. The relative area of the peaks of the asymmetric proton in the NMR spectra of **4.2** is plotted as a function of time. The solid lines are the fits to pseudo first-order kinetics.

Reaction mixtures containing 33 volume-percent of phosphate buffers at 1 M ionic strength and 33 volume-percent d_6 -DMSO co-added with the remaining 33 percent being D_2O appeared to be suitably stable reaction media.

The kinetics for H/D exchange of **4.1** and **4.2** in the described mixtures at different buffer concentrations were used (**Figures 4.1** and **4.2**).

Figures 4.1 and **4.2** show that the experimental data follows first-order kinetics. The pseudo-first-order rate constants for H/D exchange were plotted as a function of buffer concentration (**Figure 4.3**). **Figure 4.3** shows a linear increase of the rate constants with increasing buffer concentration, suggesting general-base catalysis for the H/D exchange of **4.1** and **4.2** in D_2O phosphate buffers with 33 percent volume of d_6 -DMSO co-added.

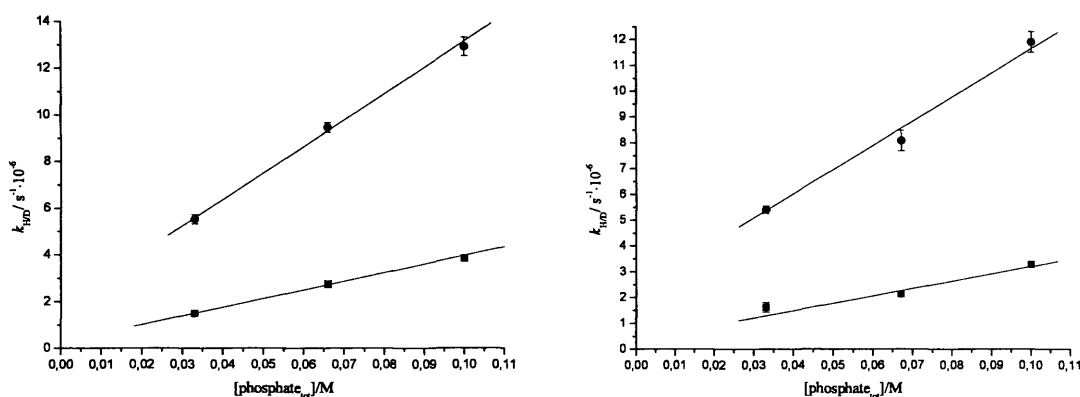


Figure 4.3: Left: observed rate constant of H/D exchange of 5-benzylhydantoin **4.1** (left) and **4.2** (right), as a function of total buffer concentration in mixtures of D_2O phosphate buffers pH** 7.2, and d_6 -DMSO (33 volume-%), at 25 °C (■) and at 37 °C (●). The solid lines are the fits of the experimental points to straight lines.

Slopes and intercepts of the straight line fits in **Figure 4.3** represent the terms $k_0 + k_{OD^-} [OD^-]$ (rate constant for the combined non-catalysed and deuteroxide-catalysed H/D exchange) and $k_{\text{phosphate tot}}$ (second-order rate constant for the phosphate-catalysed process), respectively, according to the general expression

$$k_{H/D} = k_0 + k_{OD^-} [OD^-] + k_{\text{phosphate tot}} \cdot [\text{phosphate}_{\text{tot}}]$$

Table 4.3: rate constants for buffer-catalysed and for the combined non-catalysed and deuterioxide-catalysed H/D exchange of **4.1** and **4.2** in mixtures of D₂O phosphate buffers pH** 7.2, and d₆-DMSO (33 volume-%), at 37 and 25 °C.

Substrate	Temperature / °C	$k_{\text{phosphate tot}} / 10^{-6} \text{ M}^{-1} \text{ s}^{-1}$	$k_0 + k_{\text{OD}}[\text{OD}] / 10^{-6} \text{ s}^{-1}$
4.1	37	113.2±6.0 ^{a)}	1.86 ±0.36 ^{a)}
	25	37.1±1.3 ^{a)}	0.27 ±0.06 ^{a)}
4.2	37	93.7±5.9 ^{a)}	2.28±0.29 ^{a)}
	25	28.5±2.8 ^{a)}	0.36±0.23 ^{a)}

a) Standard errors from linear fitting performed by means of the program Origin.

In **Table 4.3** the second-order rate constants for buffer-catalysed H/D exchange of **4.1** and **4.2** in mixtures of D₂O phosphate buffers pH** 7.2, in the presence of added d₆-DMSO (33 volume-%), at 25 °C and at 37 °C and the corresponding pseudo-first-order rate constants for the combined uncatalysed and deuterioxide-catalysed processes are reported.

A major drawback of the use of DMSO as co-solvent is its high UV cut-off value (268 nm).¹³ The high UV cut-off of DMSO resulted in the total coverage of the region where the ECD absorption of 5-benzylhydantoins is localised, preventing the use of ECD spectroscopy for kinetic studies of racemisation. We therefore decided to extend our investigation to d₈-2-propanol, because of its ability to increase the solubility of benzylhydantoin **4.1** and its low UV cut-off wavelength (205 nm).¹³ Similar reaction mixtures as those containing d₆-DMSO as co-solvent were prepared using d₈-2-propanol. The observed rate constants for H/D exchange of **4.1** and **4.2**, in the presence of d₈-2-propanol, were found to be lower than those obtained when d₆-DMSO was used as co-solvent, under otherwise identical experimental conditions. In **Table 4.4** the rate constants for H/D exchange of **4.1** and **4.2** in D₂O phosphate buffer at pH** 7.2, with and without the addition of d₆-DMSO or d₈-2-propanol are reported. The rate constants for H/D exchange in D₂O phosphate buffers with the same total buffer concentration as for the mixed media are also reported, for comparison.

Table 4.4: rate constants of H/D exchange ($k_{\text{H/D}}$) for 5-benzylhydantoin **4.1** and 3-*N*-methyl-5-benzylhydantoin **4.2** in reaction media composed of D₂O phosphate buffer pH** 7.2, 0.2 M, 1 M I (33%) and D₂O or in D₂O phosphate buffer pH** 7.2, 0.2 M, 1 M I (33%) and a 1:1 (v:v) mixture of D₂O- deuterated co-solvent (67%), at 37 °C.

Substrate	$k_{\text{H/D}}/10^{-6}\text{s}^{-1}$		
	No cosolvent	d ₆ -DMSO	d ₈ -2-propanol
4.1	2.66±0.18 ^{a)}	9.47±0.21 ^{a)}	1.80±0.07 ^{a)}
4.2	2.19±0.12 ^{a)}	8.08±0.40 ^{a)}	1.65±0.10 ^{a)}

a) Errors from non-linear least squares fitting performed by means of the program Origin using the Levenberg-Marquardt (LM) algorithm

The addition of d₆-DMSO accelerates the H/D exchange of **4.1** and **4.2** while 2-propanol shows a rate-depressing effect. The rate-accelerating effect of DMSO co-added to protic solvents on racemisation of different substrates has been reported before in the literature (see Chapter 1)¹⁴⁻¹⁷ and is considered a general phenomenon in base-catalysed reactions.¹⁸ This rate-enhancing effect of DMSO is typically explained in terms of increased basicity of anions in dipolar-aprotic solvents due to their lesser extent of solvation compared to protic solvents, as mentioned in Chapter 1. On the other hand, solvation effects on the transition state for proton abstraction should also be considered. As mention in Chapter 1, Cram *et al.*¹⁶ attribute the higher rate constants of base-catalysed racemisation of 2-methyl-3-phenylpropionitrile in methanol, at “low concentration” of added DMSO to “specific solvation by dimethyl sulfoxide of the transition state for proton abstraction”. Similarly, the higher rate constants for reactions involving “large polarizable anionic transition states” in dipolar aprotic solvents compared to protic ones are attributed by Miller and Parker to stabilising dipole-dipole interactions between solvent and transition state. (see Chapter 1).¹⁹ Similar effects may explain the rate-accelerating effect of d₆-DMSO observed in our kinetic experiments. Less clear is the rate-depressing effect of d₈-2-propanol. Published studies on the effect of added co-solvents on the p*K*_a of organic acids (*vide infra*) seem to suggest that added 2-propanol should increase the basicity of the anionic catalytic species of the buffer, as was the case for DMSO. An increase in the rate constants for H/D exchange with the addition of 2-propanol is therefore expected, which is in contrast to the experimental observations. However, effects of solvation on the neutral ground state hydantoins and

on the transition state of the reaction should also be taken into consideration. Phenomena of preferential solvation of the neutral hydantoins by the organic solvent in the mixed reaction media can be hypothesised. Preferential solvation of the neutral hydantoins by 2-propanol may hinder the approach of the basic anions, slowing down the reaction. Relative differences of solvation between the neutral hydantoin and the transition state in pure buffer and in the mixture buffer-2-propanol may therefore explain the rate-retarding effect of added 2-propanol to the buffer. The latter effect may outcompete the effect of increased basicity of the anionic catalytic species, leading to an overall rate-depressing effect of added 2-propanol (*vide infra*).

4.3.1.2. Kinetic studies in the presence of 25% added co-solvent

The observed effects of adding co-solvents to the buffer on the rate constants of H/D exchange of **4.1** and **4.2** prompted further investigation of the effects of the reaction medium on the racemisation and H/D exchange reactions of hydantoins. The study was extended to benzylhydantoins **4.3** and **4.4**. Kinetic experiments were carried out in mixed media under experimental conditions similar to those routinely used in the investigations described in this thesis. The experiments described in this section were carried out in mixed media containing 25 volume-% of co-solvent. The effects of co-solvents on the stereolability of the model hydantoins were investigated, when possible, by means of CD spectroscopy, at 60 °C. The effect of co-added d_6 -DMSO was investigated by means of ^1H NMR spectroscopy by comparing the rate constants of H/D exchange of the hydantoins at 25 °C, in the absence and presence of added co-solvent. In **Table 4.5** the rate constants of H/D exchange and racemisation for benzylhydantoins **4.1-4.4**, in D_2O phosphate buffer at pH** 7.2, with and without d_6 -DMSO or d_8 -2-propanol are reported.

Table 4.5: rate constants for H/D exchange ($k_{\text{H/D}}$) at 25 °C and rate constants for racemisation (k_{rac}) at 60 °C for 5-benzylhydantoins **4.1-4.4** in mixed media containing 50 volume-% of D₂O phosphate buffer, pH* or pH** 7.2, 1 M, 2 M *I* and 50 volume-% of D₂O or of a mixture 1:1 (v:v) D₂O – d₆-DMSO or D₂O – d₈-2-propanol (d₈-IP) to give a total 25 volume-% of co-solvent in the mixture.

Hydantoin	$k_{\text{H/D}} / 10^{-6} \text{ s}^{-1}$ (at 25 °C) ^{a)}			$k_{\text{rac}} / 10^{-6} \text{ s}^{-1}$ (at 60 °C) ^{a)}	
	No cosolvent	25% d ₆ -DMSO	25% d ₈ -IP	No cosolvent	25% d ₈ -IP
4.1	5.42±0.41	7.80±0.28	3.75±0.18	288.4±1.1 ^{b)}	173.5±1.4
4.2	3.37±0.11 ^{b)}	7.09±0.17	--	186.7±0.8	95.5±0.6
4.3	2.11±0.01	3.49±0.02	--	125.4±0.5	53.1±0.5
4.4	12.38±0.23	31.76±0.80 ^{b)}	--	775.4±29.1 ^{b)}	959.8±26.2

a) Errors from non-linear least squares fitting performed by means of the program Origin using the Levenberg-Marquardt (LM) algorithm

b) Errors from weighted averages of 2 or more analytical determinations.²⁰

In all kinetic experiments conducted in the presence of added d₆-DMSO or d₈-2-propanol, good fits to first-order kinetics were obtained.

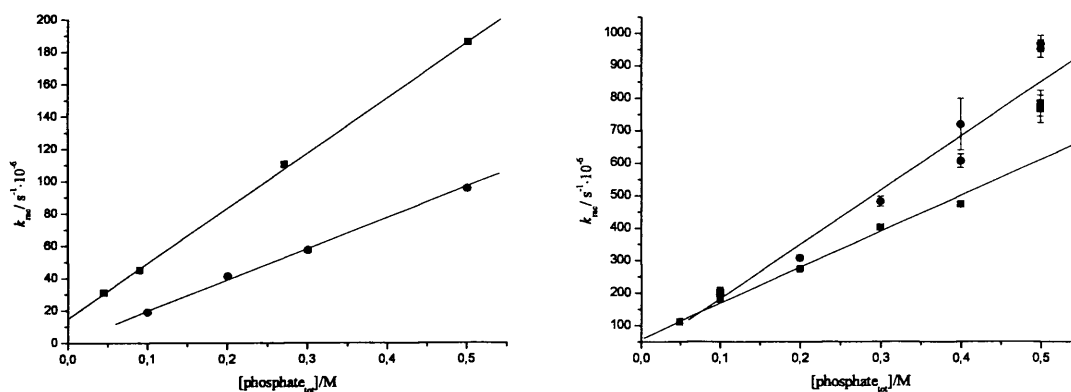


Figure 4.4: rate constants for racemisation of **4.2** (left) and **4.4** (right), as a function of total buffer concentration in mixtures composed of 50 volume-% of D₂O phosphate buffers, pH** 7.2, 2 M *I* and 50 volume-% of a mixture D₂O-d₈-2-propanol 1:1 (v:v), to give a total 25% of d₈-2-propanol co-added (●) or 50% D₂O, i.e. no added cosolvent (■).

Added d₆-DMSO showed a rate-increasing effect on the H/D exchange reactions for all hydantoins, confirming the results observed for H/D exchange of hydantoins **4.1** and

4.2, in mixed media containing 33 volume-% of the co-solvent added to the buffer (Section 4.3.1.1).

On the contrary, the addition of d_8 -2-propanol slows down the processes of racemisation of the uncharged hydantoins **4.1-4.3**, while a rate increase was observed for the cationic hydantoin **4.4**.

In **Figure 4.4**, the rate constants for racemisation of the neutral hydantoin **4.2** and for racemisation of the cationic hydantoin **4.4**, in D_2O phosphate buffers at constant pH^{**} 7.2, with and without added d_8 -2-propanol, are plotted as a function of total buffer concentration. In both cases the rate constants of racemisation increased with increasing buffer concentration, suggesting general-base catalysis as also observed in the absence of co-solvents (Chapter 3).

A plot of the observed rate constants for racemisation of (*S*)-3-*N*-methyl-5-benzylhydantoin **4.2** in D_2O phosphate buffers with 25% d_8 -2-propanol co-added gave a good fit to straight lines (Figure 4.4 left). From the intercept and slope of the straight line fit of the rate constants for racemisation of **4.2** values of $k_0 + k_{OD^-}[OD^-]$ and $k_{\text{phosphate tot}}$ were obtained (Table 4.6).

Table 4.6: rate constants for buffer-catalysed H/D exchange of **4.2** and for the combined non-catalysed and deuteroxide-catalysed H/D exchange of **4.2** in mixtures composed of 50 volume-% of D_2O phosphate buffers, pH^{**} 7.2, 2 M *I* and 50 volume-% of mixture D_2O - d_8 -2-propanol 1:1 (v:v) (25% of d_8 -2-propanol) or 50% D_2O (0% d_8 -2-propanol).

Cosolvent /% (v:v)	$k_{\text{phosphate tot}} / 10^{-6} \text{ s}^{-1} \text{ M}^{-1}$	$k_0 + k_{OD^-}[OD^-] / 10^{-6} \text{ s}^{-1}$
0	342.6±0.9 ^{a)}	15.13±0.11 ^{a)}
25	193.5±1.4 ^{a)}	0.31 ±0.27 ^{a)}

a) Errors from linear fitting performed by means of the program Origin.

When d_8 -2-propanol is added to the buffer, the term $k_0 + k_{OD^-}[OD^-]$ is almost completely suppressed and the second-order rate constant for the buffer-catalysed racemisation ($k_{\text{phosphate tot}}$) is reduced by one half.

Less straightforward behaviour is observed in case of hydantoin **4.4**; a linear fit does not seem to be suitable to describe the trend in the rate constants for racemisation of **4.4** as a function of buffer concentration in the presence of d_8 -2-propanol added to the buffer

(Figure 4.4 - right). Similarly, in the absence of any co-solvent the point at the highest buffer concentration (0.5 M) was found to deviate from the linear fit (Chapter 3). A polynomial fit appeared to better reproduce the variation in k_{rac} with increasing buffer concentration. However, the origin of the observed increase in k_{rac} at higher buffer concentration is currently unclear (see Appendix 3). Nevertheless, even if the dependence of the rate constants of racemisation of 4.4 on buffer concentration is not simple, the rate enhancing effect of added 2-propanol is clear.

4.3.2. Solvent kinetic isotope effects in mixed media

In Chapter 2 we reported very small differences between the rate constants of racemisation of 4.1 and 4.2 in kinetic experiments conducted in deuterated and non-deuterated buffers. This observation suggested no direct involvement of the solvent in the rate-determining step of the reaction, in agreement with the conclusion that racemisation and H/D exchange occur *via* the $S_{\text{E}}1$ mechanism. To explore whether the mechanism of racemisation and H/D exchange remain the same in the presence of added co-solvents, kinetic experiments of racemisation were carried out in the presence of 25% co-solvent added to the buffer, in deuterated and non-deuterated media.

Considering the opposite effects of d_6 -DMSO and d_8 -2-propanol on the rate constants for H/D exchange of 4.1-4.4, the effects of two additional co-solvents, viz. dioxane and trifluoroethanol, were also tested. The kinetic data have been summarised in Table 4.7. Table 4.7 illustrates the effect of added 1,4-dioxane and trifluoroethanol on the rate constants for racemisation of hydantoins 4.1-4.4. The rate constant of racemisation in the absence of any co-solvent added to the buffer are also reported, for comparison. As observed in the case of 2-propanol, the addition of 1,4-dioxane also has a rate-depressing effect on racemisation of hydantoins 4.1-4.3 while a marked rate-increasing effect was found for hydantoin 4.4. Trifluoroethanol has a slight accelerating effect on the racemisation of all hydantoins, however the effect seems to be small and further data are needed to allow interpretation of the results.

Table 4.7: rate constants for racemisation of hydantoins **4.1-4.4**, at 60 °C, in mixtures composed of 50 volume-% of H₂O and D₂O phosphate buffers ^{a)}, 0.5 M, 1 M / and 50 volume-% of H₂O or mixtures 1:1 (v:v) of H₂O-non-deuterated co-solvent and D₂O or mixtures 1:1 (v:v) of D₂O-deuterated co-solvent, respectively, to give a total concentration of co-solvent of 25 volume-% (v:v).

H ₂ O buffer (pH ^{25 °C} 7.2) ^{a)}				
Hydantoin	$k_{rac} / s^{-1} \cdot 10^{-6}$			
	no cosolvent	2-propanol	trifluoroethanol	dioxane
4.1	167.3±1.3 ^{b)}	129.9±1.0 ^{b)}	208.0±1.8 ^{b)}	134.8±1.5 ^{b)}
4.2	114.5±0.5 ^{c)}	76.3±0.7 ^{b)}	128.7±1.0 ^{c)}	89.3±0.4 ^{b)}
4.3	78.4±0.6 ^{b)}	48.8±0.2 ^{b)}	95.5±0.3 ^{b)}	57.6±0.2 ^{b)}
4.4	524.1±13.4 ^{b)}	808.5±14.7 ^{c)}	676.2±30.1 ^{b)}	947.8±29.6 ^{b)}

D ₂ O buffer (pH ^{**} 7.3) ^{a)}				
Hydantoin	$k_{rac} / s^{-1} \cdot 10^{-6}$			
	no cosolvent	d ₈ -2-propanol	Trifluoroethan (Od)ol	dioxane
4.1	175.0±1.5 ^{b)}	134.8±1.9 ^{b)}	191.4±2.4 ^{b)}	140.5±1.2 ^{b)}
4.2	112.8±0.4 ^{c)}	77.4±0.4 ^{b)}	107.3±0.6 ^{c)}	86.7±0.6 ^{b)}
4.3	77.0±0.3 ^{b)}	46.7±0.1 ^{b)}	82.5±0.3 ^{b)}	56.1±0.3 ^{b)}
4.4	539.7±15.1 ^{b)}	896.9±15.5 ^{c)}	615.4±17.0 ^{b)}	968.8±21.6 ^{b)}

a) Buffers were prepared by mixing dihydrogen potassium phosphate and monohydrogen potassium phosphate to give final solutions with the desired buffer ratio.

b) Errors from non-linear least-squares fitting performed by means of the program Origin using the Levenberg-Marquardt (LM) algorithm.^c

c) Errors from weighted averages of 2 or more analytical determinations.²⁰

For all model hydantoins, the rate constants of racemisation in deuterated and non-deuterated media are similar, both in the presence and absence of organic co-solvents added to the buffer. The absence of a significant normal solvent kinetic isotope effect supports an S_E1 mechanism of racemisation for all the hydantoins under investigation both in the presence and in the absence of added co-solvent to the phosphate buffer.

4.3.3. The effect of added co-solvents on pK_a

It is known that co-solvents affect pK_as (see Chapter 1) of acids. In order to explore typical effects we recorded the readings of the pH-meter for buffer mixtures containing 25 volume-% of co-solvents. Values of pH* or pH in D₂O phosphate buffer (DB) and H₂O phosphate buffer (HB) with and without 25 volume-% of trifluoroethanol (TFE), 2-

propanol (IP), dioxane (DIOX) or dimethyl sulfoxide (DMSO) co added, are reported in **Table 4.8**.

Table 4.8: pH meter readings for phosphate buffers with 25 percent volume of co-solvent added (total buffer concentration 0.25 M).^{a)}

	DB ^{b)}	HB ^{c)}	HB/TFE ^{d)}	HB/IP ^{e)}	HB/DIOX ^{f)}	HB/DMSO ^{g)}
pH*(pH)	7.33	7.24	7.32	7.78	7.91	8.28

- a) The electrode was calibrated using aqueous reference buffers, the reported values must therefore be considered only indicative
- b) D₂O phosphate buffer
- c) H₂O phosphate buffer
- d) H₂O phosphate buffer with 25% (v:v) trifluoroethanol co-added
- e) H₂O phosphate buffer with 25% (v:v) 2-propanol co-added
- f) H₂O phosphate buffer with 25% (v:v) 1,4-dioxane co-added
- g) H₂O phosphate buffer with 25% (v:v) DMSO co-added

Table 4.8 shows that in all cases, except for trifluoroethanol co-added, the reading of the pH meter appeared to be higher in the presence of a co-solvent, in particular when DMSO was used a co-solvent, in agreement with findings by Mukerjee.²¹

4.3.4. Medium effects and the stereochemical course of H/D exchange of (*S*)-5-benzylhydantoin 4.1.

To confirm our conclusion from the solvent kinetic isotope effects that racemisation should proceed via an S_E1 mechanism,²² kinetic experiments on the H/D exchange reaction of (*S*)-5-benzylhydantoin 4.1 were carried out to investigate the possibility of changes in the stereochemical course of the reaction, induced by changes in the reaction medium. Reaction media with several different compositions were tested.

Table 4.9: comparison of rate constants for racemisation (k_{rac}) and for H/D exchange ($k_{H/D}$) of (*S*)-5-benzylhydantoin (**4.1**) in mixed media composed of D₂O phosphate buffers and organic co-solvents, in different proportions, at 25 °C.

Reaction medium		Rate constants / s ⁻¹ ·10 ⁻⁶		
buffer	co-solvent mixture	k_{rac} ^{a)}	$k_{H/D}$ ^{a)}	Ratio ^{b)}
pH** 7.2, 1 M, 2 M <i>I</i> (50%)	D ₂ O-d ₈ -2-propanol 4:1 (50%)	5.93±0.19	5.37±0.44	1.1±0.1
pH** 7.2, 1 M, 2 M <i>I</i> (50%)	D ₂ O-d ₈ -2-propanol 1:1 (50%)	3.72±0.09	3.76±0.19	1.0±0.1
pH** 7.2, 0.1 M, 1 M <i>I</i> (33%)	D ₂ O-d ₆ -DMSO 1:1 (67%)	1.79±0.07	1.49±0.03	1.2±0.1
pH** 7.2, 0.2 M, 1 M <i>I</i> (33%)	D ₂ O-d ₆ -DMSO 1:1 (67%)	2.95±0.28	2.74±0.04 ^{c)}	1.1±0.1
pH** 7.1, 0.1 M, 0.22 M <i>I</i> (50%)	d ₆ DMSO (50%)	3.39±0.39	2.92±0.08	1.2±0.1

a) Errors from non-linear least squares fitting performed by means of the program Origin using the Levenberg-Marquardt (LM) algorithm.

b) Errors calculated as uncertainties on functions of several variables.²³

c) Errors from weighted averages of 2 or more analytical determinations.²⁰

Racemisation and H/D exchange of **4.1** were studied in D₂O phosphate buffers, with d₆-DMSO or d₈-2-propanol co-added, under identical conditions and the observed rate constants were compared. The racemisation of **4.1** in the presence of d₆-DMSO could not be followed by ECD, due to the high UV-cut off value of the co-solvent, the reaction was therefore followed polarimetrically. Results are presented in **Table 4.9**.

Under all the experimental conditions studied, the rate constants for racemisation are approximately equal to those for H/D exchange. Similar results were obtained in kinetic experiments carried out in D₂O phosphate buffer without any co-solvent added (Chapter 2). We therefore conclude that there is no evidence for changes in the stereochemical course of H/D exchange of **4.1**.

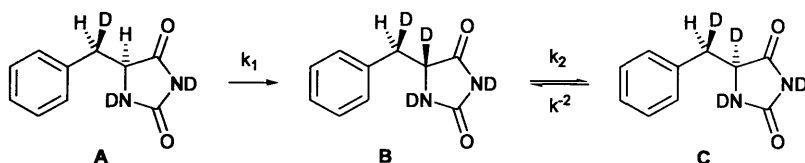
The H/D exchange of deuterium labelled 5-benzylhydantoin **4.1a** (**Scheme 4.2**) was studied in a 1:1 (v:v) mixture of D₂O phosphate buffer, pH* 7.1, 0.1 M, 0.2 *I* and d₆-DMSO, to confirm the S_E1 mechanism for racemisation of **4.1** as concluded from the data reported in **Table 4.9** (see Chapter 2), in all of the reaction media investigated.



Scheme 4.2: structure of deuterium labelled hydantoin **4.1a**.

If we assume an S_E2 mechanism for the racemisation of 5-benzylhydantoin and for the related H/D exchange reaction, then the “racemisation” of **4.1a** carried out in a deuterated medium can be described as in **Scheme 4.3**. The same scheme was used, in Chapter 2, to describe the racemisation of **4.1a** in D_2O . For convenience, only one of the “enantiomers” of A has been drawn.

As described in Chapter 2, monitoring the appearance and growth of a peak attributed to the species B (**Scheme 4.3**) during H/D exchange of **4.1a** by 1H NMR spectroscopy over time provides insight in the stereochemical course of the reaction in D_2O phosphate buffer.



Scheme 4.3: H/D exchange of **4.1a**, following a hypothetical S_E2 mechanism.

Unfortunately, in the mixture D_2O phosphate buffer and d_6 -DMSO, the signal of the methylene proton of B partly overlaps the signal of the methylene proton of the starting material A (see Appendix 3). Attempts of deconvoluting the peaks did not prove successful.

4.4. Discussion

The analysis of solvent effects on chemical reactions is typically complicated by multiple factors potentially affecting different aspects of the reaction under study. For

example, the bulk properties of the solvent are often not sufficient to fully explain solvent effects on chemical reactions.²⁴ The use of a binary mixture of solvents introduces further complications in the system, such as preferential solvation.²

The reaction media used in the kinetic experiments described in this chapter (aqueous or D₂O phosphate buffers in mixtures with organic solvents) are complex systems where two solvent species are present together with the different chemical species, i.e. the reactant and the buffer components.

A key issue here is that a change of the solvent can affect acid-base equilibria through differences in the solvation of ions. For the buffers, the potential changes in pK_a in combination with the Brønsted relationship mean that different reaction media can greatly affect their effectiveness as base catalysts. The analogous Brønsted relationship for the reactants suggests that solvent effects on the reactant's pK_a will also lead to reactivity differences.

4.4.1. The effect of co-solvents on the rate constants of racemisation and H/D exchange of neutral benzylhydantoins.

Possible explanations for the rate-enhancing effect of DMSO and the rate-depressing effect of 2-propanol on the H/D exchange of hydantoins **4.1** and **4.2** have been anticipated in section 4.3.1.1. As mentioned in Chapter 1, the accelerating effect of DMSO on the base-catalysed racemisation of chiral molecules in organic and aqueous media has been reported in previous studies.¹⁴⁻¹⁷ The effect is typically attributed to the poor ability of DMSO at solvating anions, therefore improving the effectiveness of the base as a catalyst (*vide supra*). The increased basicity of anions in dipolar aprotic solvents, as compared to protic solvents, due to the poor ability of dipolar aprotic solvents at solvating anions is documented in the literature.^{16, 18, 19, 25}

The “activating effect” of DMSO on the basicity of anions is therefore probably the simplest explanation for the higher rates of racemisation observed for hydantoins **4.1-4.4** in the presence of DMSO. On the other hand contributions from phenomena of “specific solvation by dimethyl sulfoxide of the transition state for proton abstraction” as proposed by Cram *et al.*¹⁶ or to dipolar interactions between DMSO and a “large

polarizable anionic transition state”, as described by Miller and Parker (see Chapter 1)¹⁹ may also play a role in the observed rate-enhancing effect.

Less clear is the origin of the rate-retarding effect of dioxane and 2-propanol on the racemisation of neutral hydantoins 4.1-4.3. As mentioned in Chapter 4, not just DMSO but also other solvents, such as ethanol and dioxane, tend to increase the pK_a of organic acids and a similar effect may be envisaged for phosphate in our buffer mixtures.^{21, 26-33}

Therefore, an increased basicity of anions with consequent increased rate constants of base-catalysed racemisation may also be expected when 2-propanol and dioxane are added to the buffer. In the specific case of dioxane, an activating effect on basic anions similar to, although weaker than, that of DMSO is reported in the literature (Chapter 1).³⁴ In reality, the rate constants of racemisation and H/D exchange of neutral hydantoins are lower in the mixed media containing dioxane and 2-propanol than in pure buffers. The lower dielectric constant of 2-propanol and, in particular, dioxane as compared to water would also support the hypothesis of ion-pair formation, which could explain the lower rate constants in the presence of the co-solvents.³⁵ However the dielectric constants of binary mixtures water/dioxane and water/2-propanol with contents of co-solvent similar to the buffer mixtures used in our experiments are still higher than 40 (see Table 4.2) which, according to Reichardt,³⁶ is not sufficient for extensive ion pair formation. The observed decreased rate constants of racemisation therefore suggests that such anion-solvation effects are counterbalanced by other, more important, effects involving differences in solvation of the reactant hydantoins or the transition state of reaction in mixed media as compared to pure buffers. Phenomena of preferential solvation of the hydantoins by the organic co-solvents, hindering the approach of the phosphate molecules and, therefore, slowing down the process of racemisation can be envisaged, as mentioned earlier for the case of 2-propanol.

The good ability of 2-propanol and dioxane at solubilising the hydantoins, taken together with the low polarity of the solvents support the hypothesis. Similar to 2-propanol and dioxane, DMSO shows a good ability at solubilising the hydantoins, however it is more polar than 2-propanol and dioxane. In addition, as mentioned in Chapter 1, when DMSO is added to a protic solvent, donor-acceptor interactions between the two solvent species can take place. The mentioned effects seem to render the hypothesis of phenomena of preferential solvation of the hydantoins in mixed media containing DMSO less likely than in mixtures buffer-dioxane or buffer-2-propanol. Finally while DMSO should have a good stabilising effect on the transition state for

proton abstraction (*vide supra*), the lower polarities of 2-propanol and 1,4 dioxane should render them less “good” at solvating “large polarizable anionic transition states”. A relative lower stabilization of the transition state of reaction, as compared to the neutral ground state hydantoins in the mixed media containing 2-propanol or dioxane than in pure buffers, could therefore explain the rate depressing effects of the two co-solvents.

4.4.2. The effect of co-solvents on the rate constants of racemisation and H/D exchange of the cationic hydantoin 4.4.

In case of the cationic hydantoin 4.4, the rate constants of racemisation are increased by the addition of all of the organic co-solvents investigated. In case of DMSO, the increased effectiveness of phosphate anions as basic catalyst could play a role in the rate increase, as it did for the neutral hydantoins 4.1-4.3. In Chapter 3 we proposed that the higher rate constants of racemisation and H/D exchange of hydantoin 4.4, as compared to hydantoins 4.1-4.3, could be due to intramolecular facilitation of deprotonation of 4.4 by the ammonium group. It was proposed that the positive charge on the ammonium group of 4.4 could stabilise, via a through-space electrostatic interaction, a developing negative charge on the asymmetric carbon. The binary mixtures containing 2-propanol and 1,4-dioxane have a lower dielectric constants than pure water and should be less effective at solvating charged species in solution. A lower dielectric constant and a lesser extent of solvation of the ammonium group in the binary mixtures could be responsible for more favourable intramolecular electrostatic interactions in the mixed media, leading to an increase in the observed rate constant of racemisation.

4.4.3. The solvent kinetic isotope effect for racemisation and the comparison of the rate constants of racemisation and H/D exchange in mixed media: mechanistic implications.

Kinetic experiments of racemisation of hydantoins 4.1-4.4, conducted in deuterated and non-deuterated media, in the presence of co-solvents as well as in pure buffer, gave similar rate constants of racemisation. This absence of a solvent kinetic isotope effect suggests no direct participation of the solvent as a reactant in the rate-determining step of the process of racemisation in all cases, supporting the hypothesis of an S_E1

mechanism as proposed in Chapter 2 for the racemisation of **4.1** and **4.2** in purely aqueous media. Similarly, the ratios of the rate constants of racemisation and H/D exchange for **4.1** in several different binary mixtures containing d₈-2-propanol and d₆-DMSO were found to be approximately 1. This finding also supports the hypothesis of an S_E1 mechanism for racemisation of **4.1** under all experimental conditions investigated.

4.5. Conclusions

Kinetic studies of H/D exchange and racemisation for hydantoins **4.1-4.4** in binary mixtures of phosphate buffer with added organic co-solvents were carried out. The rate constants were found to be affected by the addition of co-solvents. DMSO has an accelerating effect on the racemisation and H/D exchange of all of the model hydantoins. This result is in line with literature data reporting increased rate constants of racemisation for different chiral compounds in the presence of DMSO as co-solvent. The effect is attributed to the poor ability of DMSO at solvating basic anions, rendering them more effective general-base catalysts. The addition of 1,4-dioxane and 2-propanol to the buffer was found to have a rate-depressing effect on racemisation of neutral hydantoins **4.1-4.3**. Different hypotheses have been proposed to explain the finding, however no definitive explanation can be given at this stage. Contrary to the neutral hydantoins **4.1-4.3**, for cationic hydantoin **4.4** the addition of 2-propanol or dioxane to the buffer led to an increase of the rate constants of racemisation. Notably, the biggest rate increase was observed for the addition of the apolar cosolvent 1,4-dioxane. This finding is tentatively interpreted as support for the hypothesis of a mechanism of racemisation for **4.4** involving intramolecular facilitation by the ammonium group (see Chapter 3).

The rate constants for racemisation and H/D exchange of (*S*)-5-benzylhydantoin **4.1** were compared for selected different reaction media containing d₈-2-propanol and d₆-DMSO as co-solvents. Racemisation and H/D exchange were found to proceed approximately at the same rates, as observed in pure aqueous media. Kinetic experiments of racemisation for hydantoins **4.1-4.4** were also carried out in binary deuterated and non-deuterated media. The rates were found to be approximately the same, i.e. there is no solvent kinetic isotope effect as was also observed in the absence

of any added organic cosolvent. These findings support an S_E1 mechanism of racemisation for the model hydantoins in the binary mixtures investigated, as proposed for the racemisation of **4.1** and **4.2** in purely aqueous buffers in Chapter 2 and of hydantoins **3.24** and **3.26** (Chapter 3).³⁷⁻³⁹

4.6. Experimental

Materials

Potassium chloride (analytical grade) was from Fluka. Potassium hydroxide (analytical grade) was from Fisher Scientific. Potassium dihydrogen phosphate (crystallised) was from VWR. Dipotassium hydrogen phosphate (anhydrous) was from Fisher Scientific. Deuterium oxide (99.9%) was purchased from Fluorochem. 2-Propanol (HPLC grade) was purchased from Fisher Scientific. 2-Propanol- d_8 (99% isotopic), 2,2,2-trifluoro ethanol (NMR grade, >99.5%) and 1,4 dioxane (99+%) were from Alfa Aesar. 2,2,2-Trifluoroethanol(d) (99 atom % D) was from Aldrich. Methyl sulfoxide (99.85%, extra pure) was from Acros Organics. Dimethylsulfoxide- d_6 (D 99.9%) was purchased from Cambridge Isotope Laboratories, Inc. The water used for the preparation of H_2O phosphate buffers was demineralised by means of a water purification system Purelab Option from Elga. Hydantoins **4.1-4.4** and **4.1a** were synthesised as described in Chapters 2 and 3.

Apparatus

Materials were weighed on an analytical balance Fisher Brand PS-100 (Max 100 gr, $d=0.1$ mg). Where needed, accurate volumes of aqueous and D_2O solutions were delivered by means of Gilson or Eppendorf Research micropipettes. Volumes of organic co-solvent, except for dimethylsulfoxide and dimethylsulfoxide- d_6 , were dispensed by means of microsyringes. pH measurements were carried out, at room temperature, using a HANNA INSTRUMENTS pH 210 pH meter. The pH meter was calibrated before each measurement with certified buffers traceable to NIST standards at pH 7.00 ± 0.01 (at 25 °C) (from Fisher), pH 10.01 ± 0.02 (at 25 °C) (from Fisher) and pH 4.00 ± 0.01 (at 25 °C) (from Reagecon). Reported pH values are uncorrected. Values reported as pH**

represent the reading of the pH meter for a D₂O-based solution not used at 25 °C. Thermostatic water baths Subaqua 12 (temperature stability ±0.2°C) or Julabo MB-5 Heating Circulator (temperature stability ±0.2°C) were used to control the temperature of solutions in kinetic experiments with timescales longer than three days. Kinetic experiments of racemisation, except when d₆-DMSO was used as a co-solvent, were carried out on a Chirascan CD spectrometer equipped with a temperature-controlled sample holder (temperature stability: ± 0.02°C), in 1.00 cm or 0.5 cm path length quartz cuvettes. Kinetic experiments of racemisation in the presence of d₆-DMSO were carried out by means of an Optical Activity Ltd. AA-1000 polarimeter in a 5.00 cm path length glass cell. Kinetic experiments of H/D exchange were carried out on a Bruker AVANCE 400 spectrometer at 400 MHz (for ¹H). Pulse interval (D1): 1 s, pulse width (pw):10.75 µs, acquisition time (at): 3.42 s.

Preparation of solutions

Unless otherwise stated, stock solutions of D₂O phosphate buffers were prepared by dissolving potassium dihydrogen phosphate in D₂O and adjusting the pH** of the solution using KOH to give final buffers at the desired concentrations and pH**. D₂O and H₂O phosphate buffers at 0.5 M and 1 M ionic strength were prepared by weighing separately potassium dihydrogen phosphate and potassium monohydrogen phosphate in the desired molar ratio and dissolving them in D₂O and H₂O, respectively.⁴⁰ The measurement of the pH^{25 °C} or pH** of the above described solutions gave values pH* (D₂O) = 7.33 and pH^{25 °C} (H₂O) = 7.24. For D₂O phosphate buffers, after preparation of the solutions as described above, the solvent was evaporated and replenished 3 times with fresh D₂O, to guarantee the full exchange with deuterons and removal of the protons from the non-deuterated inorganic materials used to prepare the solutions. Potassium chloride was used to adjust the ionic strength of all buffer solutions.

Stock solutions of hydantoins for racemisation experiments carried out by CD spectroscopy were prepared in plastic eppendorfs which were kept, overnight, under continuous rotation at a speed of 20 rpm by means of a Stuart Tube rotator SB2. The solutions were then centrifuged for 8 minutes at 13.3 rpm on a Jencons-pls Spectrafuge 24.D centrifuge. The clear supernatant was transferred to a new eppendorf and an amount of fresh solvent, equivalent to 1/10th of the total volume of solution, was added

to the solutions to ensure concentrations below the solubility limits of the hydantoins to avoid precipitation. Unless otherwise stated, stock solutions of hydantoins for H/D exchange experiments carried out by ^1H NMR spectroscopy and solutions for racemisation experiments followed polarimetrically were prepared by dissolving the solid hydantoins directly in mixtures of D_2O and deuterated co-solvents in the desired volumetric ratios.

Kinetic studies

The reaction media for the CD experiments in mixed deuterated media were prepared by mixing D_2O phosphate buffers, deuterated co-solvents, D_2O , and stock solutions of hydantoins in D_2O to give desired final concentrations of buffer, hydantoin and the required volume of co-solvent. The same procedure was followed for CD experiments carried out in non-deuterated media where H_2O , H_2O buffers, non-deuterated co-solvents and solutions of hydantoins in H_2O were used. Typical final concentrations of hydantoins were the same as for kinetic experiments performed in purely aqueous media, described in Chapters 2 and 3, viz. 0.4 mM for hydantoin **4.1**, 0.9 mM for hydantoin **4.2**, 0.7 mM for hydantoin **4.3**, and 0.1 mM for hydantoin **4.4**. Solvents and stock solutions were mixed immediately before the start of the kinetic experiments to minimise the time lag between the beginning of the reaction and the acquisition of the kinetic data. CD experiments at 60 °C were carried out in quartz cuvettes housed in the thermostated sample holder of the spectrometer. CD spectra were automatically recorded at set time intervals which were chosen based on the timescale of the reaction. For longer experiments at 25 °C, the temperature of the cuvettes between recording CD spectra was controlled by storing the solutions in thermostatic water baths and recording CD spectra at set time intervals. For all cases, the decreases of the CD signals at 230, 235 or 240 nm were followed over time.

The reaction media for the kinetic experiments of H/D exchange were prepared by mixing the desired volumes of stock solutions of D_2O phosphate buffers with stock solutions of the hydantoins in mixed deuterated media to give the desired final concentrations of buffer and the desired volume percentage of co-solvent. For the kinetic experiments for **4.1**, carried out in mixtures of D_2O phosphate buffers and d_6 -DMSO in a 1:1 volumetric ratio, the solid hydantoin was dissolved directly in the reaction mixture. In the H/D exchange experiments for hydantoins **4.1** and **4.2** in the

presence of d_6 -DMSO (50 volume-% and 33 volume-%) typical concentrations of hydantoins **4.1** and **4.2** were approximately 25 mM. For the H/D exchange experiments for hydantoins **4.1-4.4** in the presence of 25% co-solvent, typical final, total concentrations of hydantoins in the reaction medium were 10 mM for hydantoins **4.1** and **4.2** and 30 mM for hydantoins **4.3** and **4.4**. The required stock solutions were mixed immediately before the start of the kinetic experiments. Reaction mixtures were transferred to NMR tubes which were stored in thermostatic water baths during the time of the kinetic experiments. ^1H NMR spectra were recorded at set time intervals chosen depending on the time scale of the H/D exchange reaction. The NMR tubes were not thermostated during the time of acquisition of the ^1H NMR spectra. H/D exchange was monitored by following the decrease of the area integral of the exchangeable protons of the hydantoins over time. In all experiments, the ^1H NMR signal from the phenyl ring of the benzylhydantoins was used as internal standard to evaluate the integrals of the ^1H NMR peaks of exchangeable protons. Spectral processing and integrations of NMR signals were carried out by means of the program SpinWorks 2.5.5.

The reaction media for kinetic experiments of racemisation of **4.1** in the presence of DMSO, which was followed polarimetrically, were the same as those used for H/D exchange experiments followed by ^1H NMR spectroscopy. Solutions were stored at constant temperature by means of thermostated water baths. Aliquots of the solutions were taken at set time intervals and the optical rotation (α) of the solution was measured.

Rate constants for all kinetic experiments were obtained by fitting experimental data points to a first-order kinetics rate law, by means of the computer program Origin.

Solubility tests

Solubilities of hydantoins were determined gravimetrically. The solvent was evaporated from exactly measured volumes of saturated solutions of hydantoins in the mixed media. The residue was then weighed on an analytical balance.

References

1. Reist, M.; Carrupt, P. A.; Testa, B.; Lehmann, S.; Hansen, J. J., *Helvetica Chimica Acta* **1996**, 79 (3), 767-778.
2. Reichardt, C., *Solvents and Solvent Effects in Organic Chemistry*. Third ed.; WILEY VCH: Weinheim, 2003; p 38-42.
3. Isaacs, N. S., *Physical Organic Chemistry*. 1995; p 199.
4. Reichardt, C., *Solvents and Solvent Effects in Organic Chemistry*. Third ed.; WILEY VCH: Weinheim, 2003; p 416.
5. Reichardt, C., *Solvents and Solvent Effects in Organic Chemistry*. Third ed.; WILEY VCH: Weinheim, 2003; p 431.
6. Reichardt, C., *Solvents and Solvent Effects in Organic Chemistry*. Third ed.; WILEY VCH: Weinheim, 2003; p 472-475.
7. Isaacs, N. S., *Physical Organic Chemistry*. Pearson Education Limited: Harlow, UK, 1995; p 203-204.
8. Reichardt, C., *Solvents and Solvent Effects in Organic Chemistry*. Third ed.; WILEY VCH: Weinheim, 2003; p 433.
9. Akerlof, G., *Journal of the American Chemical Society* **1932**, 54, 4125-4139.
10. Dimroth, K.; Reichard.C, *Zeitschrift Fur Analytische Chemie Fresenius* **1966**, 215 (5), 344-350.
11. Leong, T. H.; Dunn, L. A., *Journal of Physical Chemistry* **1972**, 76 (16), 2294-2298.
12. Solubility tests of **4.1** in a 1:1 (v:v) mixture of H₂O-DMSO, at room temperature, gave a mean value of 107 mM. Solubility tests of **4.1** in H₂O with the addition of 33% (v:v) and 25% (v:v) DMSO or 2-propanol gave approximate values of 50 and 30 mM, respectively.
13. Jackson, B. <http://macro.lsu.edu/HowTo/solvents/UV%20Cutoff.htm>.
14. Xie, Y. C.; Liu, H. Z.; Chen, J. Y., *Biotechnology Letters* **1998**, 20 (5), 455-458.
15. Xie, Y. C.; Liu, H. Z.; Chen, J. Y., *International Journal of Pharmaceutics* **2000**, 196 (1), 21-26.
16. Cram, D. J.; Kingsbury, C. A.; Haberfie.P; Rickborn, B., *Journal of the American Chemical Society* **1961**, 83 (17), 3678-3687.

17. Cram, D. J.; Rickborn, B.; Knox, G. R., *Journal of the American Chemical Society* **1960**, *82* (24), 6412-6413.
18. Reichardt, C., *Solvents and Solvent Effects in Organic Chemistry*. Third ed.; WILEY VCH: Weinheim, 2003; p 259-262.
19. Miller, J.; Parker, A. J., *Journal of the American Chemical Society* **1961**, *83* (1), 117-123.
20. Taylor, J. R., *An introduction to Error Analysis The study of uncertainties in physical measurements*. Second ed.; University Science Books: Sausalito, California, 1997; p 174-177.
21. Mukerjee, P.; Ostrow, J. D., *Tetrahedron Letters* **1998**, *39* (5-6), 423-426.
22. The comparison of the rate constants of H/D exchange and racemisation can provide mechanistic information, in the absence of phenomena of preferential solvation.
23. Taylor, J., *An introduction to error analysis The study of uncertainties in physical measurements*. Second ed.; University Science Books: Sausalito, California, 1997; p 73-77.
24. Reichardt, C., *Solvents and Solvent Effects in Organic Chemistry*. Third ed.; Wiley VCH Weinheim, 2003; p 218.
25. Parker, A. J., *Chemical Reviews* **1969**, *69* (1), 1-32.
26. Ballash, N. M.; Robertso.Eb; Sokolows.Md, *Transactions of the Faraday Society* **1970**, *66* (574), 2622-2628.
27. Baughman, E. H.; Kreevoy, M. M., *Journal of Physical Chemistry* **1974**, *78* (4), 421-423.
28. Vesala, A.; Saloma, E., *Acta Chemica Scandinavica Series a-Physical and Inorganic Chemistry* **1976**, *30* (4), 277-280.
29. Holmes, D. L.; Lightner, D. A., *Tetrahedron* **1995**, *51* (6), 1607-1622.
30. Holmes, D. L.; Lightner, D. A., *Tetrahedron* **1996**, *52* (15), 5319-5338.
31. Reichardt, C., *Solvents and Solvent Effects in Organic Chemistry*. Third ed.; WILEY VCH: Weinheim, 2003; p 97.
32. Clare, B. W.; Cook, D.; Ko, E. C. F.; Mac, Y. C.; Parker, A. J., *Journal of the American Chemical Society* **1966**, *88* (9), 1911-1916.
33. Bates, R. G.; Pawlak, Z., *Journal of Solution Chemistry* **1976**, *5* (3), 213-222.
34. Reichardt, C., *Solvents and Solvent Effects in Organic Chemistry*. Third ed.; WILEY VCH: Weinheim, 2003; p 241-242.

35. Reichardt, C., *Solvents and Solvent Effects in Organic Chemistry*. Third ed.; WILEY VCH: Weinheim, 2003; p 262-263.
36. Reichardt, C., *Solvents and Solvent Effects in Organic Chemistry*. Third ed.; WILEY VCH: Weinheim, 2003; p 48.
37. Milan, D., Kinetics and computational studies of the mechanism of racemisation and H/D exchange of substituted hydantoins in aqueous, mixed-aqueous and non-aqueous solvents. Cardiff University: Cardiff, 2011.
38. Kennedy, J., CD spectroscopy as analytical means for the study of mechanisms of racemisation of hydantoins. Cardiff University: Cardiff, 2011.
39. Williams, R., Kinetics of racemisation of a substituted hydantoin pyrrole. Cardiff University: Cardiff, 2011.
40. The buffers prepared by weighing separately the basic and acidic forms of phosphate were used in the experiments for the determination of solvent kinetic isotope effects, to obtain the same buffer ratios in H₂O and D₂O. All the other experiments were carried out in buffers prepared by dissolving potassium dihydrogen phosphate in D₂O and adjusting the pH* to the desired value with KOH.

Chapter 5

Exploring the use of IR and VCD spectroscopy for the study of reaction mechanisms involving stereogenic centres.

Abstract

We present the results of exploratory studies aimed at evaluating potential and limitations of vibrational circular dichroism (VCD) and infrared (IR) spectroscopy for kinetic and mechanistic studies of reactions involving chiral compounds. The first section of the chapter describes calculation approaches for VCD spectra of a selection of small, relatively flexible, chiral molecules including our model compound 5-benzylhydantoin. A general method for predicting VCD spectra of flexible chiral molecules is described. The VCD spectra of selected synthetic intermediates of interest to AstraZeneca containing two chiral centres, one of which created by isotopic substitution, were also calculated. Couples of diastereoisomers differing only by the configuration at the chiral centre generated by isotopic labelling showed different calculated VCD spectra, even though these spectra are not mirror images. The findings suggest the possibility of discriminating between all members of a family of diastereoisomers using VCD spectroscopy by comparing the calculated with the experimental VCD spectra. The second part of the chapter addresses the practical aspects of recording IR and VCD spectra in aqueous solutions for mechanistic studies of racemisation of 5-substituted hydantoins. Our preliminary experiments did not prove successful. Instrumentation difficulties were encountered in recording experimental VCD spectra and in the detection of the CD bands in the IR spectra of deuterium labelled 5-benzylhydantoin and 3-*N*-methyl-5-benzylhydantoin as predicted by DFT

calculations. The final section of the chapter reports the IR spectra of 5 model 5-benzylhydantoins recorded in D₂O solution. In spite of the strong absorption of the solvent, the IR bands for the stretching modes of the carbonyl groups of the molecules could be detected. An attempted correlation between vibrational frequencies of the carbonyl stretching modes and the stereolability of the model hydantoins did not lead to satisfactory results.

5.1. The potentials of Vibrational Circular Dichroism (VCD) spectroscopy

5.1.1. The VCD technique

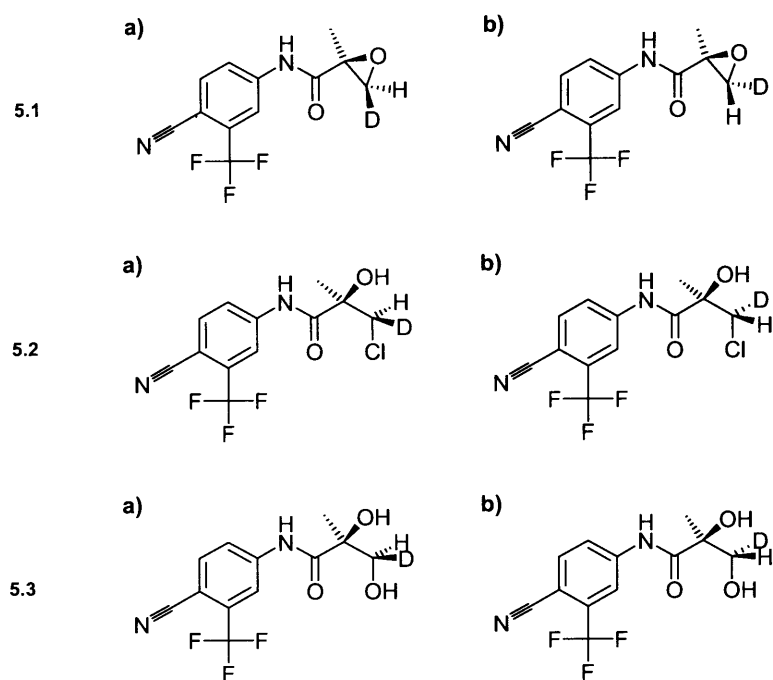
Vibrational Circular Dichroism (VCD) spectroscopy is a relatively recently developed spectroscopic technique useful for the study of chirality. The first commercial dedicated FTIR VCD spectrometer was marketed in 1997 by the company Bio Tools, in Illinois.¹ VCD spectroscopy can be seen as an extension of ECD (Electronic Circular Dichroism) spectroscopy from the UV-visible region, where electronic transitions occur, into the mid-IR or near-IR regions where vibrational transitions occur. VCD spectroscopy is therefore a potentially powerful means for detection of chirality, able to give access to information not available by means of any other analytical technique.¹⁻⁴ Indeed, VCD allows the assignment of absolute configuration of chiral molecules in solution by comparison of the experimental spectrum with the spectra predicted by means of *ab initio* quantum chemical calculations (*vide infra*). For flexible molecules in solution, experimental VCD spectra reflect the conformational populations over the various conformations. Calculated VCD spectra can similarly be constructed as Boltzmann-population-weighted composites of the calculated spectra of all lowest energy conformers of the molecule. Comparison between predicted and experimental spectra therefore allows conformational analysis. VCD spectroscopy can, in fact, resolve conformers that exist for as little as picoseconds, since typical vibrational periods are shorter than 1 picosecond.² VCD spectroscopy has been successfully used to study supramolecular structures of perfluorinated carbon chains,⁵ proteins⁶ and protein-oligosaccharide complexes⁷.

5.1.2 Calculated VCD spectra

5.1.2.1. Prediction of VCD spectra of model chiral molecules.

VCD spectra of chiral molecules can be predicted by means of quantum mechanical calculations carried out by dedicated software such as Gaussian.⁸⁻¹⁰ Comparison of calculated and experimental VCD spectra is a useful tool enabling the determination of absolute configuration of chiral molecules in solution. The VCD technique can, therefore, be potentially useful for the establishment of the stereochemical course and the mechanism of chemical reactions involving chiral centres. The technique can be extended because, as mentioned in Chapter 1, a molecule can be chiral simply by virtue of isotopic substitution. Isotopic labelling is, therefore, a very useful tool enabling the creation of “new” chiral centres in strategic positions of molecules and, as a consequence, allowing the widening of the potential applications of the VCD technique. Of particular interest here is the possibility of monitoring the stereochemical course of reactions by creating a chiral centre by means of isotopic labelling, for example using structures such as shown in **Scheme 5.1**. Structures **5.1-5.3** contain two chiral centres, one of which has been created by means of isotopic labelling.

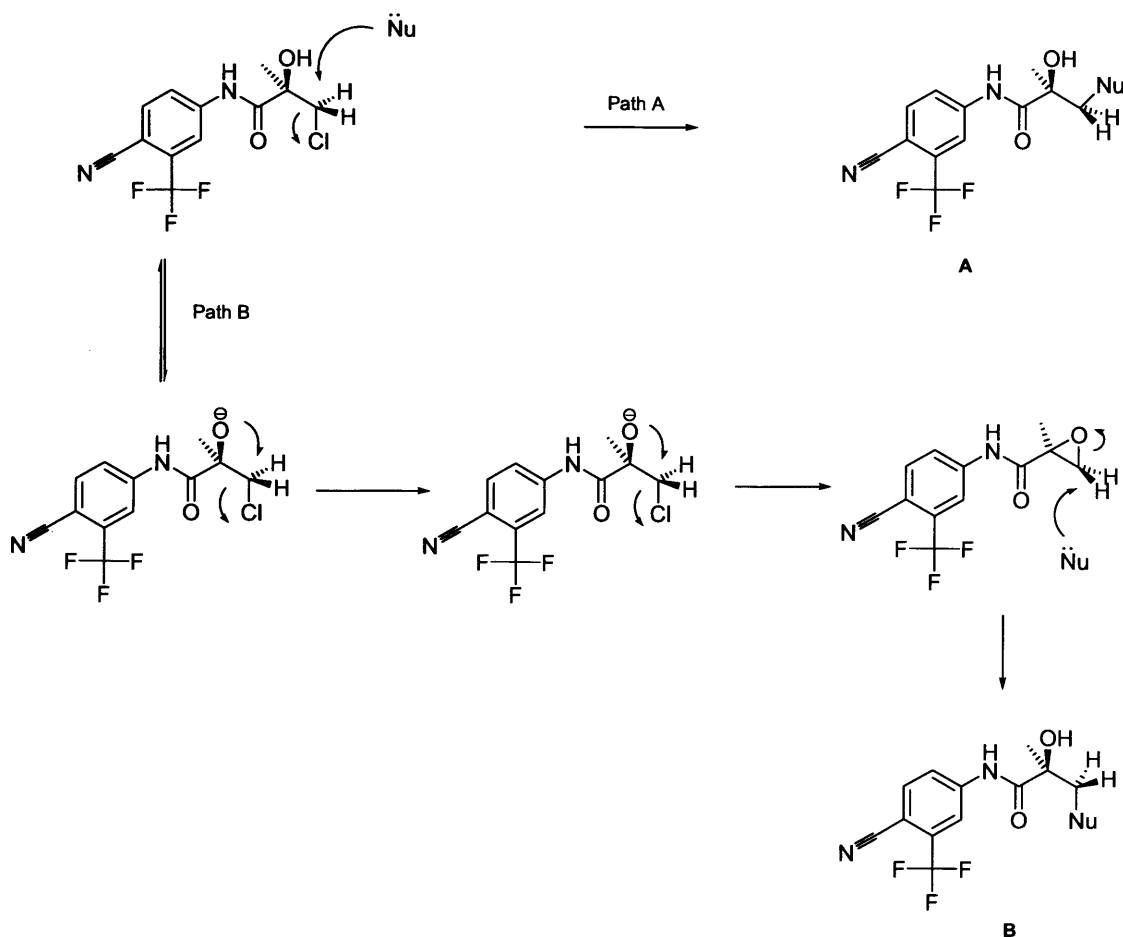
The VCD spectra of several molecules of interest to AstraZeneca (**Scheme 5.1**)¹¹ were calculated by DFT methods to investigate the possibility of using VCD to discriminate between compounds **5.1 a)** and **5.1 b)**, between **5.2 a)** and **5.2 b)** and between **5.3 a)** and **5.3 b)**. Being able to distinguish between these structures is important for the elucidation of the mechanism of a synthetic step in the preparation of bicalutamide, an important drug used in the treatment of hormone-dependent cancer.



Scheme 5.1: structures of molecules of interest of AstraZeneca whose VCD spectra have been calculated.

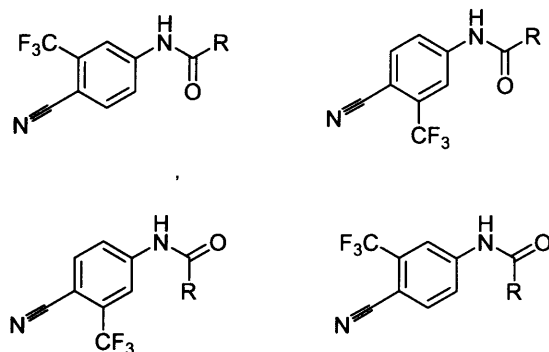
Bicalutamide can be synthesised from an appropriate halohydrin or an epoxide. In principle, when the halohydrin is used as starting material two possible reaction mechanisms can be envisaged: the “direct displacement of chloride by the nucleophile” (Nu) (path A in **Scheme 5.2**) or a mechanism involving the epoxide as reaction intermediate (path B in **Scheme 5.2**). A study carried out by HPLC¹¹ showed that the reaction in **Scheme 5.2** proceeds via path B. In fact, the “epoxide-opening reaction” was found to be slower than its expected rate of formation from the halohydrin.

If unlabelled starting materials are used, path A and B lead to non-distinguishable products (A=B). However if labelled analogues of the halohydrin (such as **5.2a**) or **b**) were used, path A and path B should lead to products A and B with opposite configuration at the chiral carbon bearing the deuterium. In fact, while path A involves an S_N2 reaction leading to a single inversion of configuration at the mentioned chiral centre, path B involves a double inversion and therefore retention of configuration. To explore whether such a system is amenable to mechanistic study by VCD, the structures shown in **Scheme 5.1** were chosen as models for our calculations.



Scheme 5.2: schematic representation of the possible mechanisms of formation of bicalutamide from a halohydrin precursor.

The predictions of the VCD spectra of the structures in **Scheme 5.1** were carried out in two slightly different ways. In a preliminary study a manual conformational search was used and only four conformers of the molecules under study were considered (**Scheme 5.3**)



Scheme 5.3: general representation of the four different conformers whose structures were used to obtain the input geometries for the DFT calculations.

The spectra were Boltzmann averaged over those conformations that were significantly populated.¹² In practice this meant that the number of conformations used for the calculations was reduced to one or two, depending on the molecule, because other conformations were too high in energy to be significantly populated. In a second investigation, conducted at AstraZeneca, the conformational search was carried out by means of MM (Molecular Mechanics) methods using the MMFF94 force field¹³, with Monte Carlo sampling of the conformations. More conformations were considered in this case, leading to a more accurate sampling of the conformers which is expected² to lead to a more accurate prediction of the VCD spectra.

In both cases, the essential steps can be summarised as follows:

1. Conformational search.¹⁴
2. Geometry optimization and calculation of the energy of the conformers with MM energies within 10 kcal/mole from the lowest energy conformer by means of DFT methods.^{14, 15} In the preliminary work, carried out with a manual conformational sampling, the energy of four selected conformers was calculated by means of DFT methods.
3. Calculations of VCD absorptions for both enantiomers of the compounds for the populated conformations.
4. Construction of the weighted averaged spectra.

As mentioned before, in the part of the work conducted at AstraZeneca, conformational searches were carried out by means of Force Field methods.^{16, 17}

Different Force Fields were checked for their ability to reproduce the relative energies calculated by DFT methods. **Table 5.1** shows the result of conformational searches for epoxide **5.1** in **Scheme 51**, carried out by means of different force fields (FF). The FF energies of the different conformers are compared to those calculated by DFT methods.

Table 5.1: comparison of the energy for different conformers of compound **5.1** evaluated by different Force Fields and calculated by DFT.

Force Field	Conformer	Force Field Energy (kcal/mole) ^{a)}	DFT ΔG (kcal/mol) ^{a)}
MMFF94	EpoxideMMFF_1	0.00	0.29
	EpoxideMMFF_2	0.06	0.00
	EpoxideMMFF_3	6.82	6.73
	EpoxideMMFF_4	6.87	0.44
OPLS 2005	EpoxideAOPLS2005_1	0.00	0.40
	EpoxideAOPLS2005_2	0.01	0.20
	EpoxideAOPLS2005_3	1.42	0.23
	EpoxideAOPLS2005_4	3.34	0.62
	EpoxideAOPLS2005_5	3.61	0.18
	EpoxideAOPLS2005_6	5.56	0.60
	EpoxideAOPLS2005_7	5.92	0.00
	EpoxideAOPLS2005_8	8.20	0.57
	EpoxideAOPLS2005_9	8.23	6.62
OPLS 2001	EpoxideAOPLS2001_1	0.00	0.02
	EpoxideAOPLS2001_2	0.00	0.31
	EpoxideAOPLS2001_3	0.02	6.43
	EpoxideAOPLS2001_4	3.21	6.16
	EpoxideAOPLS2001_5	4.56	0.00
	EpoxideAOPLS2001_6	4.61	0.38
OPLS	EpoxideAOPLS_1	0.00	0.54
	EpoxideAOPLS_2	0.26	0.31
	EpoxideAOPLS_3	0.33	0.60
	EpoxideAOPLS_4	0.48	0.00
	EpoxideAOPLS_5	2.11	0.36
Amber	Epoxideamber_1	0.00	0.00
	Epoxideamber_2	0.13	0.32
	Epoxideamber_3	2.06	0.30
	Epoxideamber_4	3.80	0.29
	Epoxideamber_5	4.00	0.22
	Epoxideamber_6	8.09	7.10
	Epoxideamber_7	8.46	0.31

^{a)} Values of potential energies are relative to those of the lowest energy conformer.

None of the FF seemed to be able to accurately reproduce the order of energies evaluated by Density Functional Theory (DFT). However, some of the conformers were found more than once within the same conformational search or in conformational searches carried out with different force fields. These findings seem to indicate a good conformational search could be performed with Force Field methods. However, the poor energies calculated by the force fields seem to exclude, in principle, the possibility of neglecting conformations which are high in energy according to FF results. The geometries obtained from the conformational searches were therefore used as starting input geometries for further optimisation by means of DFT calculations. The optimised geometries obtained from DFT calculations were used as input geometries for the calculation of VCD spectra of the labelled analogues of the compounds under investigation (**Scheme 5.1**). The energies of different conformers from the DFT calculations were used to calculate the Boltzmann population for each conformer at 25 °C. VCD frequencies and intensities for the labelled compounds were then obtained from DFT calculations for those conformations with a population above 2%.

DFT calculations were carried out with the functional and basis set B3PW91/6-31G+(d, p), according to indications reported in the literature. Typically the hybrid functional B3PW91 and B3LYP and a 6-31G (d) basis set are used, with similar good accuracy at predicting VCD spectra.^{2, 3, 8, 9}

The VCD spectra were constructed by generating Lorentzian band shapes centred on the calculated VCD intensities and by Boltzmann averaging the spectra over all conformers. A program in Matlab was prepared that allowed the simultaneous weighted averaging of the spectra and the visualization of the final calculated VCD spectrum.

The Boltzmann populations for each conformer, required for averaging the spectra, were calculated according to **Equation 5.1**.^{2, 18}

$$\frac{N_i}{N} = \frac{g_i \cdot e^{-\Delta G_i/kT}}{\sum_j g_j \cdot e^{-\Delta G_j/kT}} \quad \text{Equation 5.1}$$

Where N_i is the number of molecules in the i^{th} conformation, N is total number of molecules, g_i is the degeneracy of energy level i , ΔG_i is the energy difference between the i^{th} conformer and the most stable conformer, k is Boltzmann's constant and T is the temperature (in K).

To shape the bands **Equation 5.2** was used.^{8, 9}

$$\Delta\epsilon(\bar{\nu}) = \frac{32\pi^3 N}{3000hc(2.303)} \bar{\nu} \sum_i R_i f_i(\bar{\nu}, \bar{\nu}_i)$$

$$f_i(\bar{\nu}, \bar{\nu}_i) = \frac{1}{\pi\gamma_i} \frac{\gamma_i}{(\bar{\nu} - \bar{\nu}_i)^2 + \gamma_i^2}$$

Equation 5.2

$\bar{\nu}_i, R_i$ = excitation frequencies, rotational strengths

γ_i = half - width at half - height

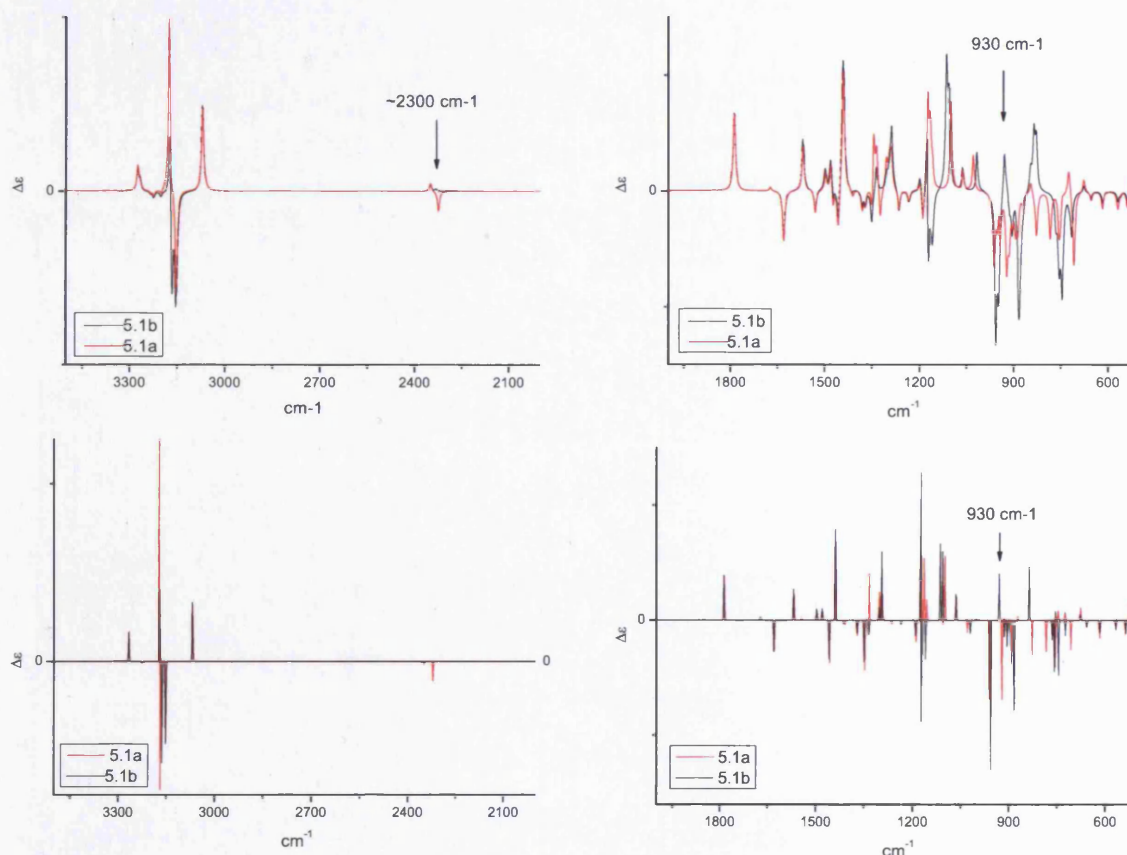


Figure 5.1: calculated VCD spectra for both diastereoisomers of labelled compound **5.1a** (red traces) and **5.1b** (black traces), in the regions between 4000 and 2000 cm^{-1} (**left**) and between 1900 and 600 cm^{-1} (**right**). **Top spectra:** weighted average over two conformations (conformational searches carried out with different force fields, leading to the same results) using Lorentzian band shapes. **Bottom spectra:** single conformer, not optimised band shapes. VCD bands from vibrational modes of the CD bond, with potential diagnostic importance for distinguishing between the two diastereoisomers of **5.1**, are highlighted in the spectra.

The calculated VCD spectra for both diastereoisomers of the labelled molecules under investigation are displayed in **Figures 5.1, 5.2 and 5.3 (top)**. The spectra of the same molecules, obtained from DFT calculations with a manual conformational search are

shown as well (**Figures 5.1, 5.2 and 5.3 - bottom spectra**). The shape of the bands has not been optimised in the latter case.

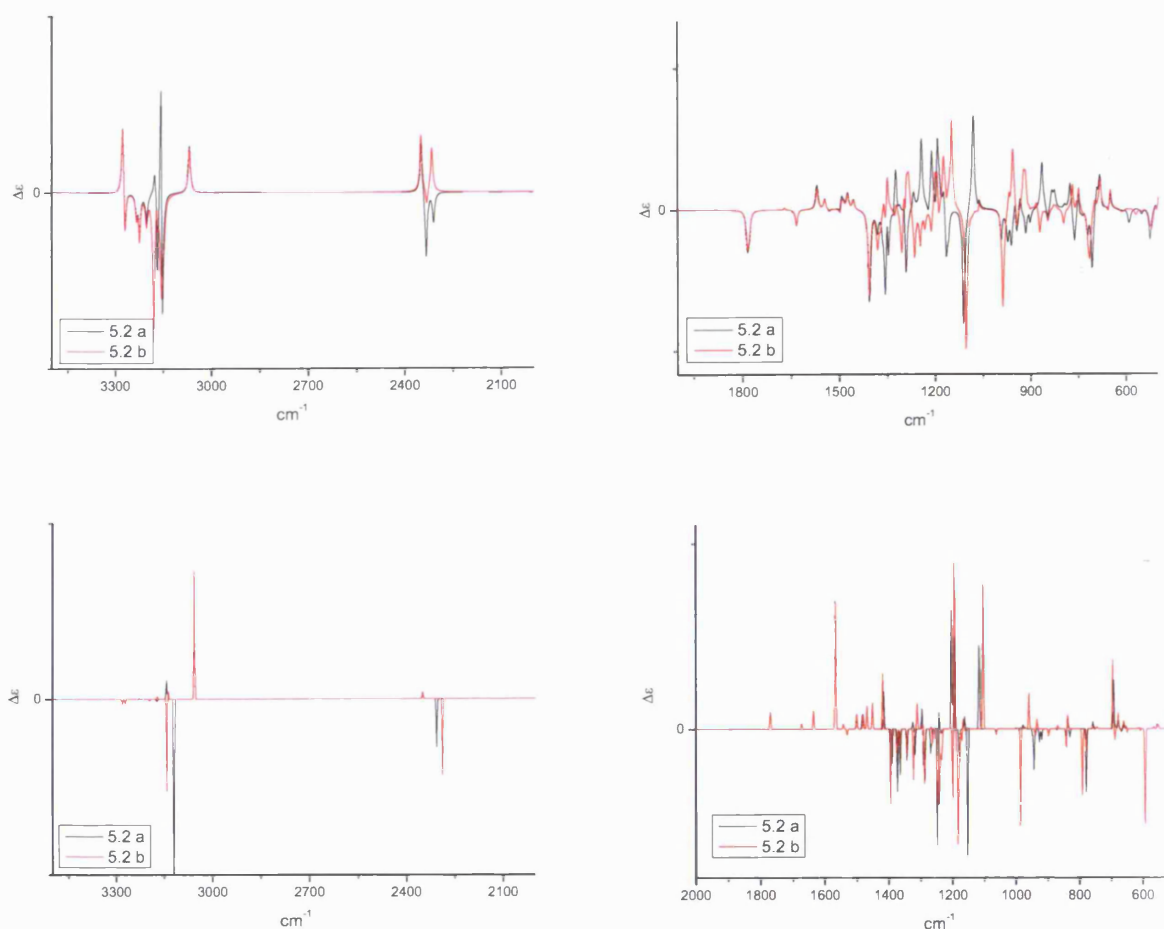


Figure 5.2: calculated VCD spectra for labelled compound **5.2 a** (black trace) and **5.2 b** (red traces), in the regions between 4000 and 2000 cm^{-1} (**left**) and between 1900 and 600 cm^{-1} (**right**). **Top spectra:** weighted average over 5 conformations (Force Field MMFF94), Lorentzian band shapes **Bottom spectra:** weighted average over 2 conformations, not optimised band shapes.

In the reported spectra, VCD bands from vibrational modes of the CD bond or CH bond at the chiral centre, with potential diagnostic importance for distinguishing between the two members of couples of diastereoisomers are indicated with arrows, when they were clearly detected, as in **Figure 5.1** and **Figure 5.3 (top spectra)**.

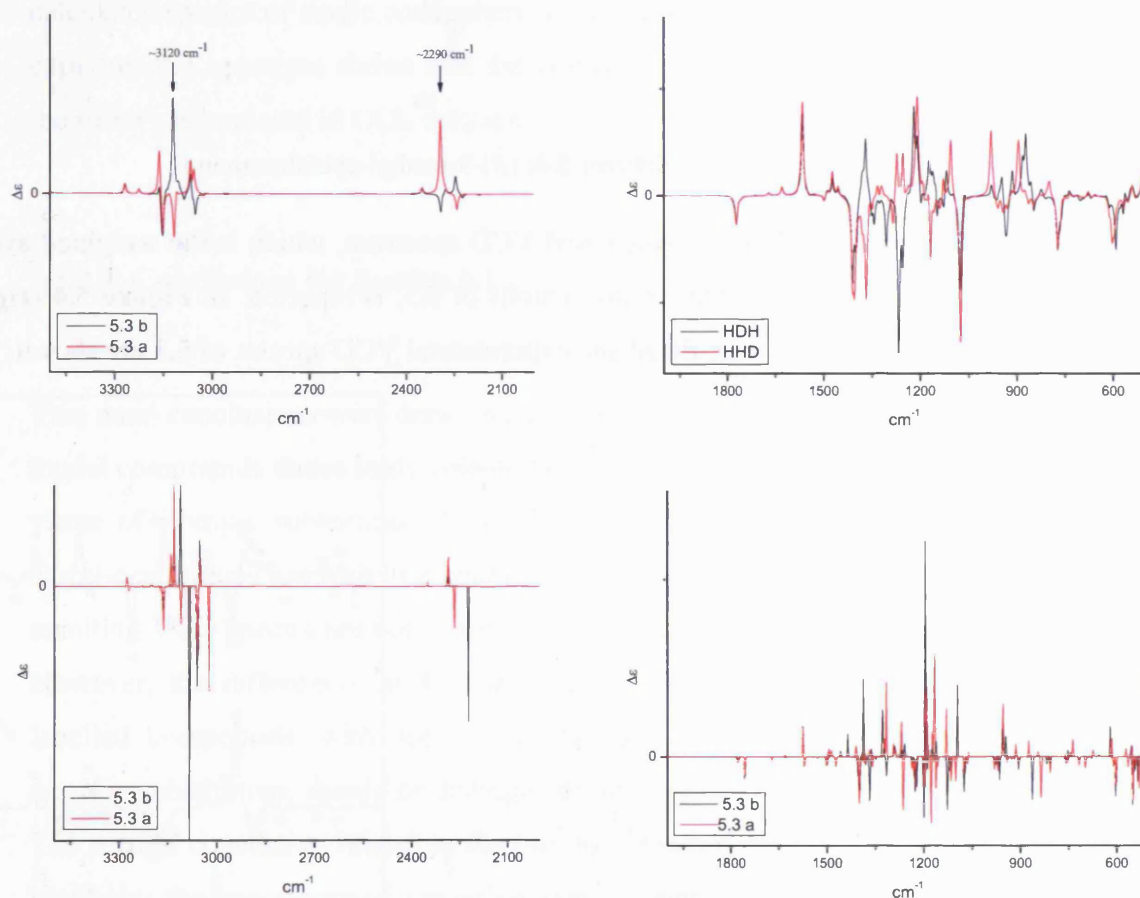
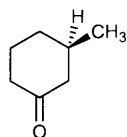


Figure 5.3: calculated VCD spectra for labelled compound **5.3 a** (red traces) and **5.3 b** (black traces), in the regions between 4000 and 2000 cm^{-1} (left) and between 1900 and 600 cm^{-1} (right). **Top spectra:** weighted average over 14 conformations (Force Field MMFF94) using Lorentzian band shapes. **Bottom spectra:** weighted average over 2 conformations, not optimised band shapes.

5.1.2.2. Testing the performance of the method for the prediction of VCD spectra.

To test our method for predicting VCD spectra, the VCD spectrum of a simple model compound, (*R*)-3-methyl-cyclohexanone (**Scheme 5.4**) was calculated¹⁹ and the calculated spectrum was compared with experimental and calculated spectra reported in the literature.³



5.4

Scheme 5.4: (*R*)-3-methyl-cyclohexanone.

In **Figure 5.4 (left)** the calculated VCD spectrum, which is the weighted average over the equatorial and axial conformations of **5.3**, is reported. In **Figure 5.4 (right)**, taken from reference 3, calculated and experimental VCD spectra of **5.3** are shown.

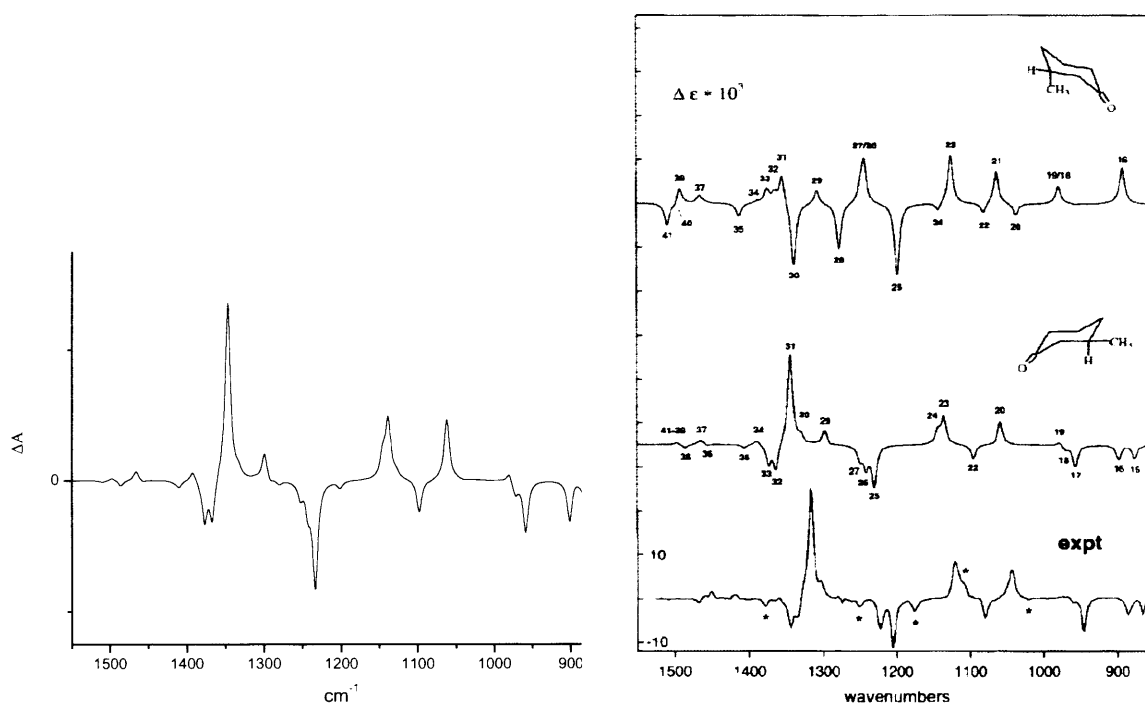


Figure 5.4: **Left:** calculated VCD spectrum of (*R*)-3-methyl-cyclohexanone **5.3** (DFT calculations carried out with the functional and basis set B3LYP-6-31G*. The spectrum is the Boltzmann-population-weighted-average over the equatorial and axial conformations. **Right:** literature calculated spectra of the single conformers of **5.3** (DFT calculations carried out with the functional B3PW92 and TZ2P basis set) and experimental VCD spectrum in CCl₄ solution. The literature spectra have been reprinted with permission from reference 3, Copyright 2000, John Wiley and Sons.

The calculated spectrum in **Figure 5.4 left** is in good qualitative accordance with the experimental VCD spectrum (**Figure 5.4, right, bottom**) allowing for a small, expected, overestimate of the frequencies, which is attributed to calculational errors and

anharmonicity^{8, 10, 20}. The comparison of the averaged spectrum (**Figure 5.4, left**) with calculated spectra of single conformers (**Figure 5.4, right, middle and top**) and with the experimental spectrum shows that the equatorial conformation is the most stable and therefore predominant in CCl₄ solution.

5.1.2.3. Conclusions for Section 5.1.2

Two main conclusions were drawn from the investigations described in this section. The model compounds under study contain two chiral centres, one of which is chiral only by virtue of isotopic substitution. Since the result of inverting the configuration at one chiral centre does not lead to a couple of enantiomers but to two diastereoisomers, the resulting VCD spectra are not expected to be (and were not found to be) mirror images. However, the differences in the calculated VCD spectra suggest that diastereomeric labelled compounds, with opposite configuration at one chiral centre generated by isotopic substitution, should be distinguishable by means of VCD spectroscopy.

The second conclusion relates to the method for calculating accurate VCD spectra and highlights the importance of a good sampling of the different possible conformers of the molecule under study. For the case of compound **5.1 (Scheme 5.1)** only 2 main conformers were found by means of different force fields. VCD spectra calculated with or without an automated conformational search (**Figure 5.1 Top** and **Figure 5.1 Bottom**, respectively) displayed essentially the same main VCD bands. Bigger differences between the two methods were found for compounds **5.2** and **5.3** for which a higher number of populated conformations were found.

In **Figure 5.5** calculated spectra for several populated single conformers of compound **5.3b** are reported as examples. As can be seen, different conformers of the same molecule result in quite different calculated spectra.

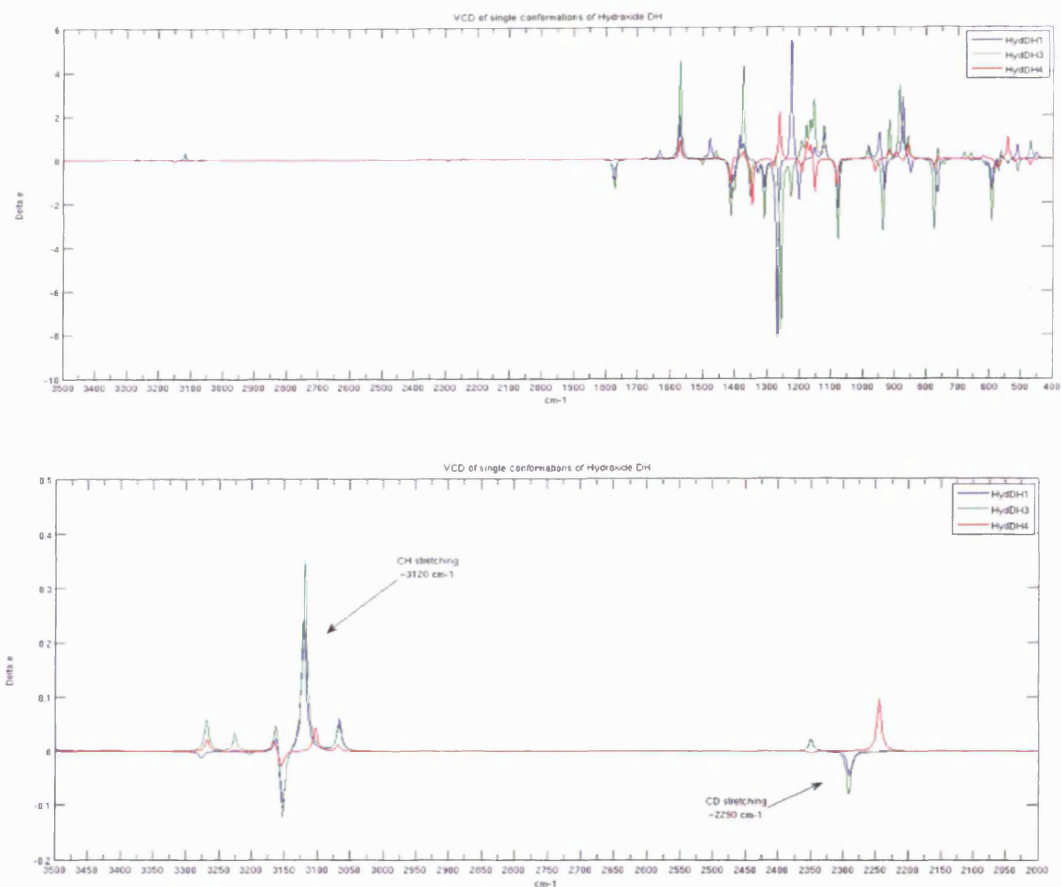


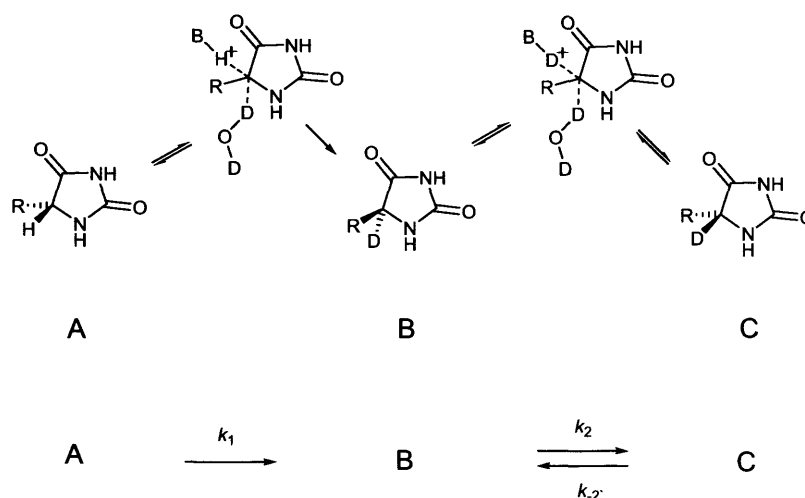
Figure 5.5: calculated VCD spectra of selected single conformers of compound **5.3b** (**top**) and zoom of the same spectra in the region between 3500 and 2000 cm^{-1} . The bands related to stretching modes of CH and CD bonds at the chiral centre are highlighted. (**bottom**). Spectra elaborated by means of Matlab.

An accurate calculation of a VCD spectrum therefore appears to be increasingly laborious with the increase in complexity and flexibility of the molecule under study, due to the increased number of conformations to be taken into account. Therefore, it is important to be able to rely on computer programs allowing accurate sampling of the conformational space and quick elaboration of large amounts of data. The Matlab program developed for this specific purpose is a very useful tool for the kind of calculations described in this section.

5.1.3. The use of VCD spectroscopy for kinetic and mechanistic studies of racemisation of 5-substituted hydantoins

5.1.3.1 Kinetic considerations regarding expected signals

In Chapter 2 the possibility of an S_E2 mechanism for racemisation of 5-substituted hydantoins, as proposed in the literature²¹, was discussed. A schematic representation of the base-catalysed racemisation of 5-substituted hydantoins in D_2O , if the racemisation were to occur via the S_E2 mechanism, was reported in Chapter 2 and is repeated below (**Scheme 5.5**) for convenience.



Scheme 5.5: proposed S_E2 mechanism for 5-substituted hydantoins and its schematic representation.

Mathematical simulations showed that, for small differences between the rate constants k_2 and k_1 (See **Scheme 5.5**) the temporary enantiomeric excess of species B over the combination of species A and C is expected to be small and, therefore, experimentally hardly detectable by ECD. On the other hand, the temporary enantiomeric excess of the species B over species C should be sufficiently high to be detectable by VCD spectroscopy. The reaction, if proceeding via the S_E2 mechanism, could therefore be followed effectively by monitoring the appearance and subsequent disappearance of the VCD signals arising from vibrational modes of the C-D bonds of the hydantoins undergoing racemisation and concomitant H/D exchange. Calculations of VCD spectra

of enantiomers of 5-d-5-benzylhydantoin **5.5b** (Scheme 5.6) (*vide infra*) predict the presence of mirror-image absorption bands at 2250 cm^{-1} for the stretching vibration of the CD bonds in the molecules. Values for the primary kinetic isotope effect $k_{\text{H}}/k_{\text{D}}$ of approximately 3.5 were found for racemisation of three (*S*)-5-substituted hydantoins (see Chapters 2 and 3), i.e. values for the ratio k_2/k_1 of about 0.3. Under these conditions, the hypothetical temporary enantiomeric excess of species B should be detectable both by means of ECD and VCD spectroscopy as illustrated by simulated ECD and VCD signals (which are proportional to A-B+C and B-C, respectively) for a primary kinetic isotope effects of 3.5 (Figure 5.6, left and right, respectively). Simulated data shows that a significant temporary enantiomeric excess of B over C should even be observable by following the racemisation by VCD spectroscopy if the ratio k_2/k_1 were equal to 1, when ECD spectroscopy is expected to be “blind” (see Appendix 4).

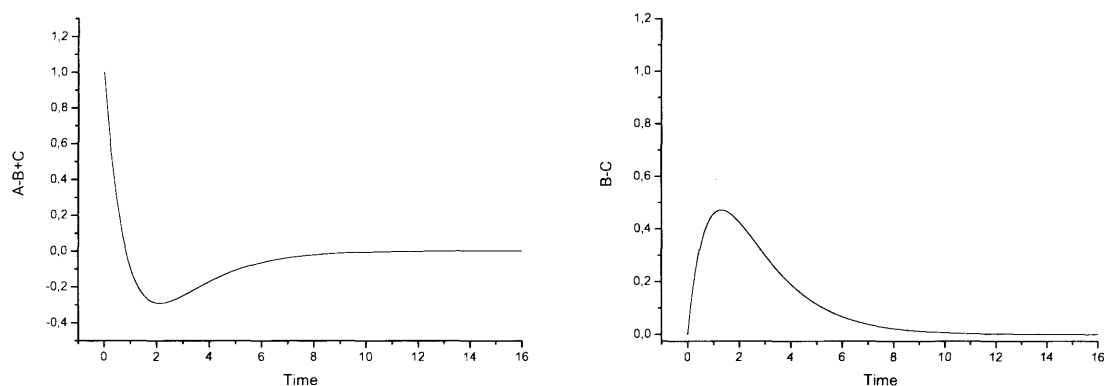


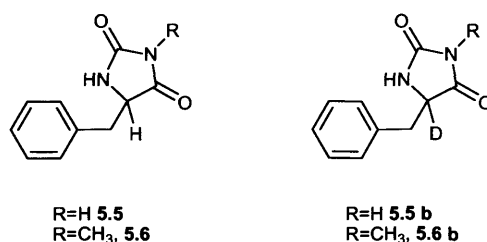
Figure 5.6: expected ECD (left) and VCD (right) signals plotted as a function of time in a simulated $S_{\text{E}}2$ racemisation in D_2O as a function of time for a value of the ratio k_2/k_1 of 0.29, corresponding to our experimental primary kinetic isotope effect of 3.5. The time scale of the x-axis is in arbitrary units.

The simulations in Figure 5.6 show that the hypothetical temporary enantiomeric excess of species B in the process of racemisation shown in Scheme 5.5, could in principle be detected by following the racemisation by means of VCD spectroscopy, as well as by means of ECD spectroscopy.

In principle, IR spectroscopy could also be used as an alternative to ^1H NMR spectroscopy for kinetic studies of H/D exchange, by following the appearance of the CD stretching band in the IR spectrum over time.

5.1.3.2. Calculated IR and VCD spectra for 5-benzylhydantoin

The VCD spectra of both enantiomers of our model compound 5-benzylhydantoin **5.5** and its deuterated analogue 5-d-5-benzylhydantoin **5.5b** (Scheme 5.6) were calculated to investigate the possibility of using VCD spectroscopy for kinetic studies of racemisation and H/D exchange. The IR spectra of **5.5** and **5.5b** were calculated as well. The method described in Section 5.1.2 was again used for the calculations.



Scheme 5.6: structures of 5-benzylhydantoin **5.5**, 3-*N*-methyl-5-benzylhydantoin **5.6** and related deuterium-labelled compounds **5.5b** and **5.6b**.

The conformational search was carried out using the force field MMFF94 and the DFT calculations were carried out with the functional and basis set B3PW91/6-31G+(d, p). The calculated IR spectra of 5-benzylhydantoin **5.5** and 5-d-5-benzylhydantoin **5.5b** are shown in Figure 5.7.

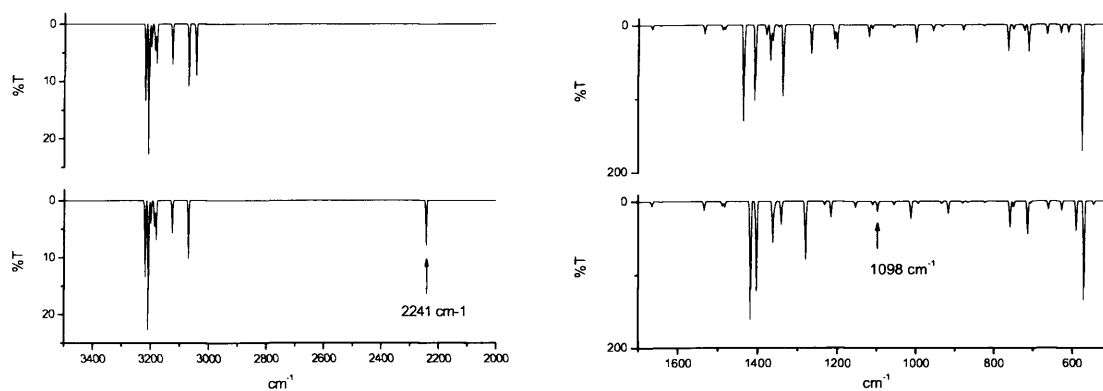


Figure 5.7: partial calculated IR spectra of 5-benzylhydantoin **5.5** (**top**) and 5-d-5-benzylhydantoin **5.5b** (**bottom**) in the region between 3400 and 2000 cm^{-1} (**left**) and the region between 1600 and 600 cm^{-1} (**right**). Vibrational modes of the CD bond, in the spectra of **5.5b** (**bottom**) are highlighted.

Figure 5.7 shows partial calculated IR spectra in the stretching region (**left**) and in the fingerprint region (**right**) of unlabelled hydantoin **5.5** (**top** spectra) and its deuterated analogue **5.5b** (**bottom** spectra). Vibrational modes of the CD bond, in the spectra of **5.5b**, in **Figure 5.7, bottom**, are highlighted.

Similarly, the VCD spectra of the (*R*)- and (*S*)-enantiomers of 5-benzylhydantoin **5.5** was calculated (**Figure 5.8**)

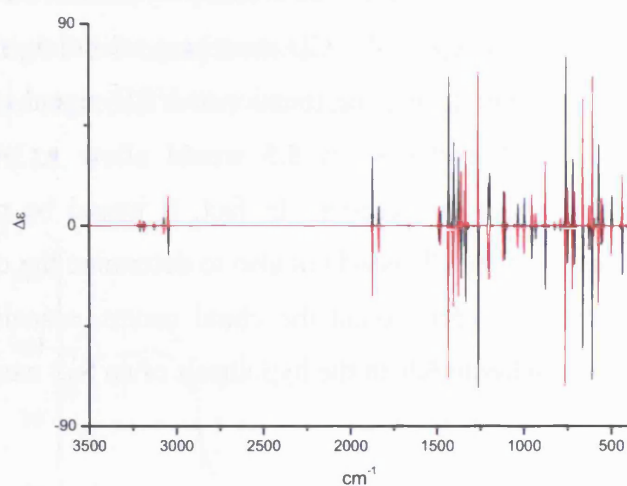


Figure 5.8: calculated VCD spectra of (*S*)-5-benzylhydantoin (**S**)-5.5 (black trace) and (*R*)-5-benzylhydantoin (**R**)-5.5 (red trace). The spectra are weighed averages over three conformations (Force Field MMFF94).

As expected, the VCD spectra for (*S*) and (*R*) **5.5** were found to be mirror images.

Finally, the VCD spectra for the (*R*)- and (*S*)-enantiomers of 5-d-5-benzylhydantoin **5.5b** were calculated (**Figure 5.9**).

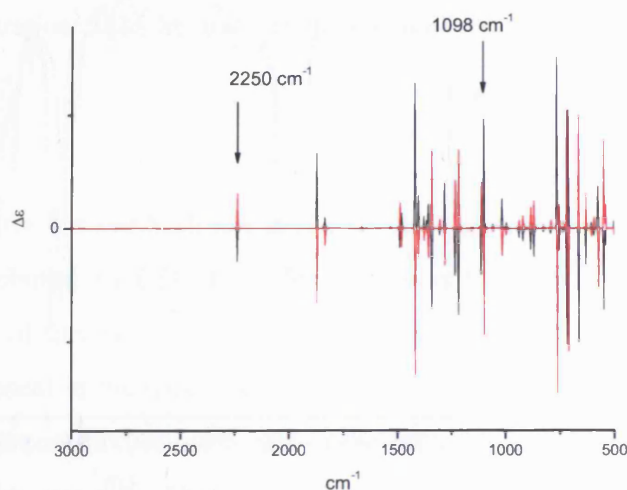


Figure 5.9: partial calculated VCD spectra of (*S*)-5-d-5-benzylhydantoin (**S**)-5.5b (black trace) and (*R*)-5-d-5-benzylhydantoin (**R**)-5.5b (red trace). The spectra are weighed averages over three conformations (Force Field MMFF94). Vibrational modes of the CD bond, are highlighted.

The calculated VCD spectra of 5-benzylhydantoin **5.5b** display well resolved, weak signals corresponding to the CD stretching vibration at 2250 cm^{-1} . The possibility of detecting and monitoring the mentioned VCD signal of **5.5b** in real time, during the process of H/D exchange of **5.5** would allow to obtain unequivocal mechanistic information about the reaction. In fact, it would be possible not only to detect the “appearance” of the CD bond but also to determine the change over time of the absolute configuration of **5.5b** around the chiral centre, essentially allowing the detection of species B in **Scheme 5.5**, in the hypothesis of an S_E2 mechanism of racemisation.

5.1.3.3 Experimental IR spectra for 5-benzylhydantoin and 3-*N*-methyl-5-benzylhydantoin

As a preliminary study, the IR spectra of (*S*)-5-benzylhydantoin (**S**)-**5.5** and of racemic 5-d-5-benzylhydantoin *rac*-**5.5b** (**Scheme 5.6**) in CHCl_3 were recorded. In **Figure 5.10** sections of the IR spectra of CHCl_3 solutions of (**S**)-**5.5** and *rac*-**5.5b** are shown.

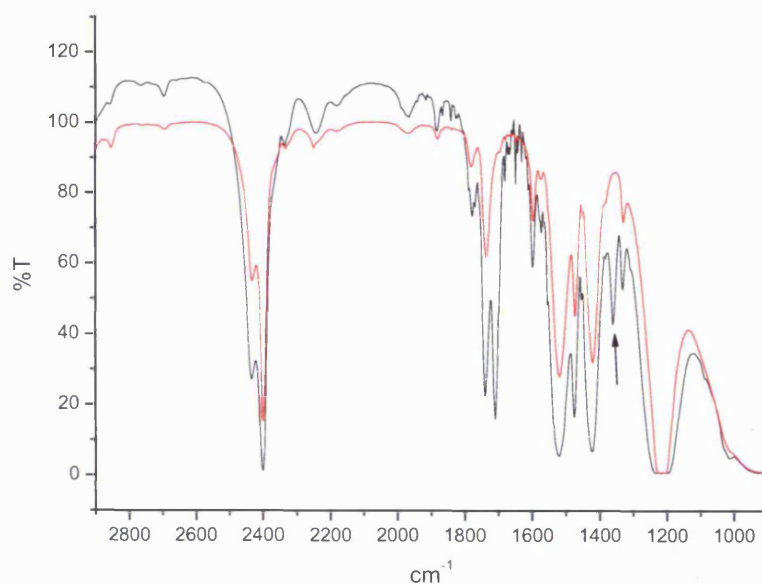


Figure 5.10: IR spectra of CHCl_3 solutions of (*S*)-5-benzylhydantoin (**S**)-**5.5** (black traces) and racemic 5-benzylhydantoin *rac*-**5.5b** (red traces) in the region between 2800 and 1000 cm^{-1} .

IR spectra of (*S*)-3-*N*-methyl-5-benzylhydantoin (**S**)-5.6 and its racemic deuterated analogue 3-*N*-methyl-5-d-5-benzylhydantoin *rac*-5.6b (Scheme 5.6), in CHCl₃ solutions, were also recorded under identical experimental conditions.²² Spectra are reported in Figure 5.11.

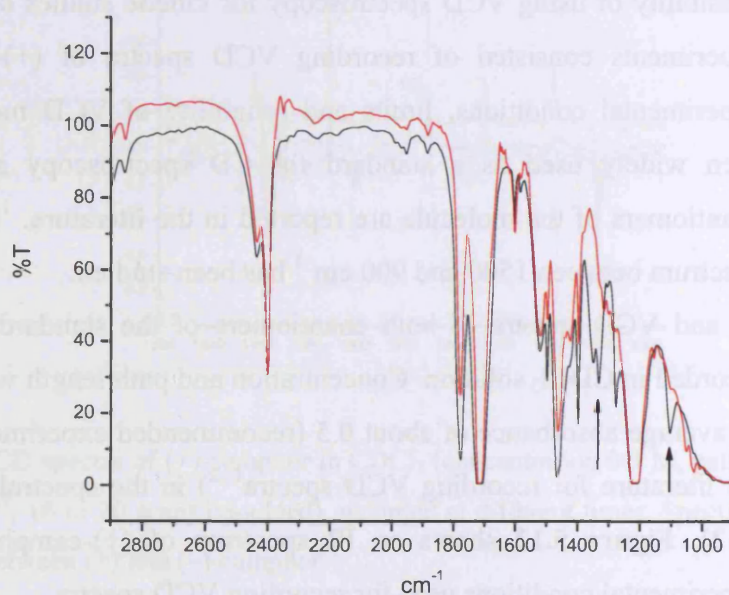


Figure 5.11: IR spectra of CHCl₃ solutions of (*S*)-3-*N*-methyl-5-benzylhydantoin (**S**)-5.6 (black traces) and its racemic deuterated analogue *rac*-5.6b (red traces) in the region between 2800 and 1000 cm⁻¹ (concentrations 0.24 M, path length 150 μm, resolution 4 cm⁻¹, 10000 scans co-added).

Neither in the spectra for *rac*-5.5b nor in the spectra for *rac*-5.6b were bands observed that could be attributed to CD stretching vibrational modes. An inspection of the fingerprint regions of the spectra of *rac*-5.5b and *rac*-5.6b similarly did not identify IR absorptions not present in the spectra of the respective non-deuterated analogues (**S**)-5.5 and (**S**)-5.6. On the contrary, some bands in the fingerprint regions of (**S**)-5.5 and (**S**)-5.6, highlighted with arrows in Figures 5.10 and 5.11, seem to be absent in the spectra of *rac*-5.5b and *rac*-5.6b. The IR bands for both stretching and bending vibrational modes of the CD bonds in *rac*-5.5b and *rac*-5.6b, appear to be very weak and could not be detected under our experimental conditions.

5.1.3.4. Recording VCD spectra: the VCD spectrum of the standard compound (+)-camphor

Attempts were made to record experimental VCD spectra in order to evaluate the possibility of using VCD spectroscopy for kinetic studies of racemisation. Preliminary experiments consisted of recording VCD spectra of (+)- and (-)-camphor to test experimental conditions, limits and reliability of VCD measurements. Camphor has been widely used as a standard for CD spectroscopy and VCD spectra of both enantiomers of the molecule are reported in the literature.^{1, 4, 9, 10, 23} The region of the spectrum between 1500 and 900 cm^{-1} has been studied.

IR and VCD spectra of both enantiomers of the standard compound camphor were recorded in CDCl_3 solution. Concentration and path length were adjusted so as to obtain an average absorbance of about 0.5 (recommended experimental conditions reported in the literature for recording VCD spectra^{1, 2}) in the spectral region of interest (**Figure 5.12**). **Figure 5.12** shows an IR spectrum of (+)-camphor recorded under typical experimental conditions used for recording VCD spectra.

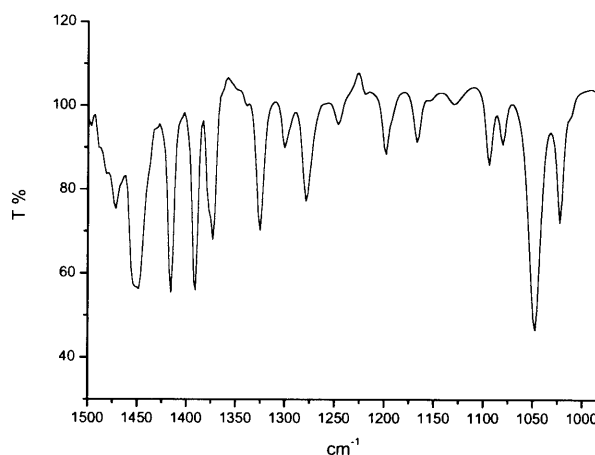


Figure 5.12: IR spectrum of (+)-camphor in CDCl_3 (concentration 0.3 M, path length 100 μm , resolution 4 cm^{-1} , 16 scans co-added)

For the VCD experiments, different instrumental settings were checked. A major but anticipated problem in recording VCD spectra was recording good baselines. Subtraction of the VCD spectrum of the solvent alone did not yield good spectra. Better baselines were obtained by recording the VCD spectra of both enantiomers of camphor,

as suggested in the literature.² Baseline corrected spectra were obtained as one half of the difference of the VCD spectra of (+)- and (-)-camphor. **Figure 5.13** shows typical experimental VCD spectra of (+)-camphor.

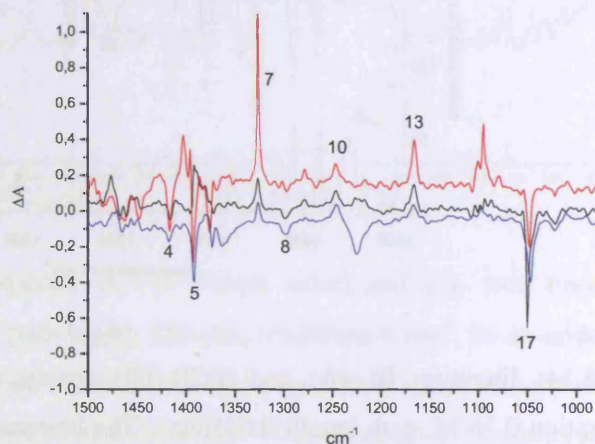


Figure 5.13: VCD spectra of (+)-camphor in CDCl_3 (concentration 0.3 M, path length 100 μm , resolution 4 cm^{-1} , 16 or 20 scans co-added), recorded at different times. Spectra are one half of the difference between (+) and (-)-camphor.

Recorded spectra were compared with spectra of (+)-camphor reported in the literature. Our experimental spectra were in reasonable qualitative agreement with those reported in the literature (**Figure 5.14**). In particular, it was possible to find a correspondence between several bands in the experimental spectra (**Figure 5.13**) and the literature spectrum reported in **Figure 5.14**. Corresponding bands are highlighted in our experimental spectra using the same numbers as were used in the literature.

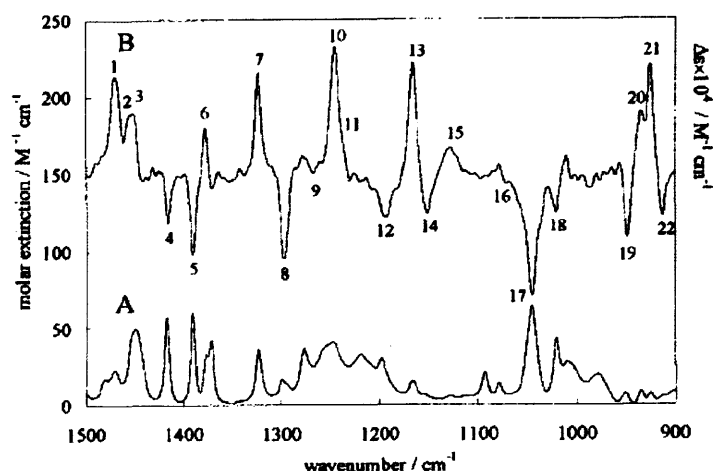


Figure 5.14: literature IR (A) and VCD (B) spectra of (+)-camphor in CCl_4 solution (concentration 0.36 M, path length 0.095mm). The literature spectra have been reprinted with permission from reference²³, Copyright 2006, John Wiley and Sons.

In spite of an overall reasonable qualitative agreement with spectra published in the literature, only the strongest bands were found in all of our experimental VCD spectra. As shown in **Figure 5.13**, the intensity of the VCD absorptions was not well reproducible. In addition, some of the characteristic absorptions of the VCD spectrum of (+)-camphor could not be unambiguously assigned in all spectra. Moreover, the correction of the baseline, obtained by plotting one half of the difference of the VCD spectra of (+)- and (-)-camphor, did not give equally good baselines in all measurement. We next explored the possibility of using the racemate to record VCD baseline spectra because this would enable recording VCD spectra without the need of both enantiomers of the compound under study. For several datasets, the baseline correction was performed by subtraction of the VCD spectrum of a 1:1 mixture of (+)- and (-)-camphor (essentially a racemic mixture of camphor), from the VCD spectra of enantiopure samples of (+)- and (-)-camphor. Examples of spectra corrected using the above described method are shown in **Figure 5.15, right**. Spectra obtained as half of the difference between (+)- and (-)-camphor are reported as well in **Figure 5.15, left**, for comparison.

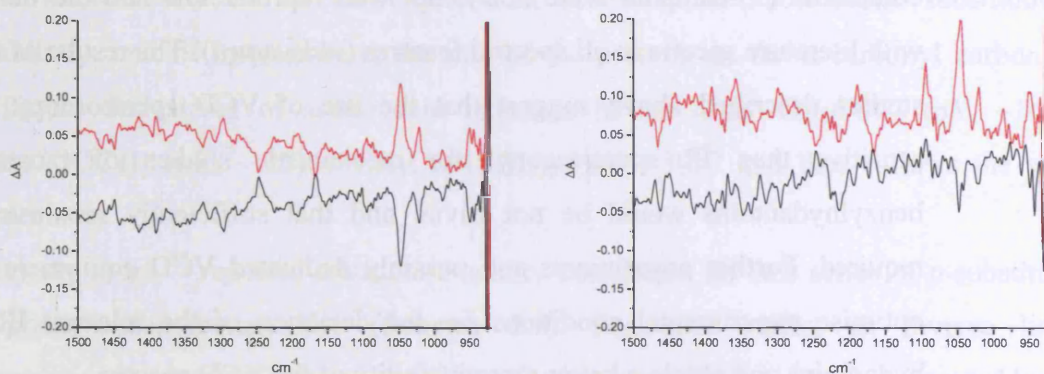


Figure 5.15: VCD spectra of (+)- (black trace) and (-)- (red trace) camphor in CDCl_3 (concentration 0.6 M, path length 150 μm , resolution 4 cm^{-1} , 16 co-added scans). **Left:** spectra were obtained as one half of the difference of individual spectra of opposite enantiomers. **Right:** spectra were obtained by subtraction of the VCD spectrum of racemic camphor from the spectra of (+)- and (-)-camphor.

The use of the racemate for the correction of the baseline allowed an improvement of the quality of the baseline, as compared to the uncorrected spectra. The quality of the VCD spectrum of (-)-camphor in **Figure 5.15, right** is comparable with the average quality of the spectra obtained as one half of the difference of the spectra of opposite enantiomers. The spectrum of (+)-camphor is more noisy and the characteristic band at 1047 cm^{-1} is weaker and less clearly distinguishable, reflecting the poor reproducibility of the measurement.

The described difficulties encountered in the recording of good quality VCD spectra may be due to limitations of the spectrometer. A dedicated VCD spectrometer may probably give spectra of better quality and reproducibility.

5.1.3.5. Conclusions for section 5.1.3

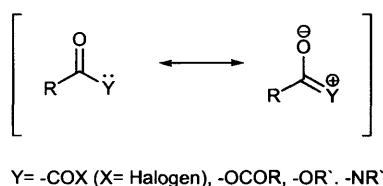
VCD spectroscopy is a potentially very useful tool for the elucidation of the mechanism of racemisation of 5-benzylhydantoin. Calculated VCD spectra of enantiomers of 5-d-5-benzylhydantoin **5.5b** exhibit a well resolved absorption at 2250 cm^{-1} for the stretching of the “chiral” C-D bond. However, it was not possible to detect absorption bands attributable to C-D vibrational modes in preliminary experimental IR spectra of the deuterated analogues of 5-benzylhydantoin *rac*-**5.5b** and 3-*N*-methyl-5-benzylhydantoin *rac*-**5.6b**. Moreover, experimental VCD spectra of the standard

compound (+)-camphor were noisy, not well reproducible and did not compare well with literature spectra in all spectral features (*vide supra*). The results of the preliminary studies described above suggest that the use of VCD spectroscopy, which is less sensitive than IR spectroscopy, for mechanistic studies of racemisation of 5-benzylhydantoins would be not trivial and that sufficiently sensitive equipment is required. Further experiments and possibly dedicated VCD equipment are needed to optimise experimental conditions for the detection of the relevant IR bands of the hydantoins and obtain a better reproducibility of the VCD spectra.

5.2. Structure-acidity correlations by IR Spectroscopy

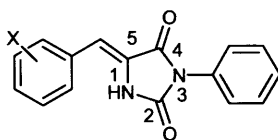
5.2.1. Literature correlation analyses using infrared spectral data

The frequency of the carbonyl stretching of carboxylic acid derivatives has been used a probe to evaluate the relative reactivity of this class of compounds toward nucleophiles.²⁴ For a generic carboxylic acid derivative resonance structures can be drawn as shown in **Scheme 5.7**.



Scheme 5.7: resonance structures of a generic carboxylic acid derivative

The degree of delocalization of the unshared pair of electrons of the substituents Y onto the carbonyl oxygen determines the order of reactivity of the species and is reflected in the frequency of the carbonyl stretching. A higher degree of delocalization results in a lower degree of double bond character of the carbonyl bond, with consequent decrease of its stretching frequency. On the other hand, electron-withdrawing effects of the substituent Y oppose the described resonance effect, causing an increase of the carbonyl frequency. The frequency of the carbonyl stretching in carboxylic acid derivatives decreases in the order: acyl chloride > anhydride > ester > amide. This order reflects the



X = H, -2-CH₃, 4-CH₃, 4-CH(CH₃)₂, 2, 4, 6-(CH₃)₃, 4-CN, 4-CF₃,
 4-N(CH₃)₂, 3-NO₂, 3-OCH₃, 4-OCH₂C₆H₅, 4-SCH₃, 2-Cl, 3-Cl,
 4-Cl, 2-Br, 3-Br, 4-Br, 2, 4-Cl₂

Scheme 5.9 series of 5-arylidene-3-phenylhydantoin investigated in the correlation study by Kleinpeter *et al.*²⁶

$$\overline{\nu(C=O)} = (7.50 \pm 0.37) \cdot \Sigma\sigma(X) + 1749.8 \quad \text{Equation 5.3}$$

where $\Sigma\sigma(X) = \sigma(X_1) + \sigma(X_2) + \sigma(X_3)$

In the same study a second linear relationship is reported that correlates the arithmetic means of the wave numbers of the symmetric and asymmetric stretching modes of the carbonyl ($\overline{\nu(C=O)}$) with the pK_a of the NH proton in position 1 of the hydantoin ring (defined as pK_s in the paper). The relationship is expressed by **Equation 5.4**.

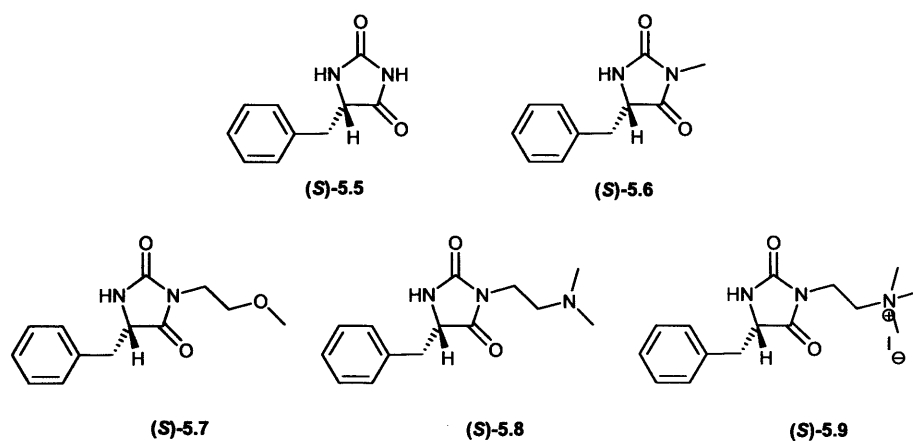
$$\overline{\nu(C=O)} = -(5.27 \pm 0.54) \cdot pK_s + 1809.2 \quad \text{Equation 5.4}$$

The negative slope in **Equation 5.4** suggests that an increased acidity of the NH proton is associated with higher frequencies of the carbonyl stretching. The finding is in agreement with **Equation 5.3**, that associate higher Hammett constants σ with higher values of $\overline{\nu(C=O)}$.

5.2.2 Correlation analysis for 5-benzylhydantoins

In Chapter 3 we reported on the effect of structural modifications on the stereolability of several 5-substituted hydantoins. In particular it was observed that, within the series of 3-substituted 5-benzylhydantoins, shown in **Scheme 5.10**, hydantoins (*S*)-5.8 and (*S*)-5.9 showed particularly high rate constants of racemisation and H/D exchange.

The following experiments were undertaken in an attempt of correlating the higher stereolability of (*S*)-5.8 and (*S*)-5.9 to an increased carbon acid acidity, with respect to the other hydantoins of the series.



Scheme 5.10 structures of (*S*)-5-benzylhydantoins (*S*)-5.5-(*S*)-5.9.

The IR spectra of our model benzylhydantoins (*S*)-5.5, (*S*)-5.6, (*S*)-5.7, (*S*)-5.8 and (*S*)-5.9, were recorded in D₂O and the wavenumbers of the IR absorption bands corresponding to the C=O stretching vibration were measured (**Figure 5.16**).

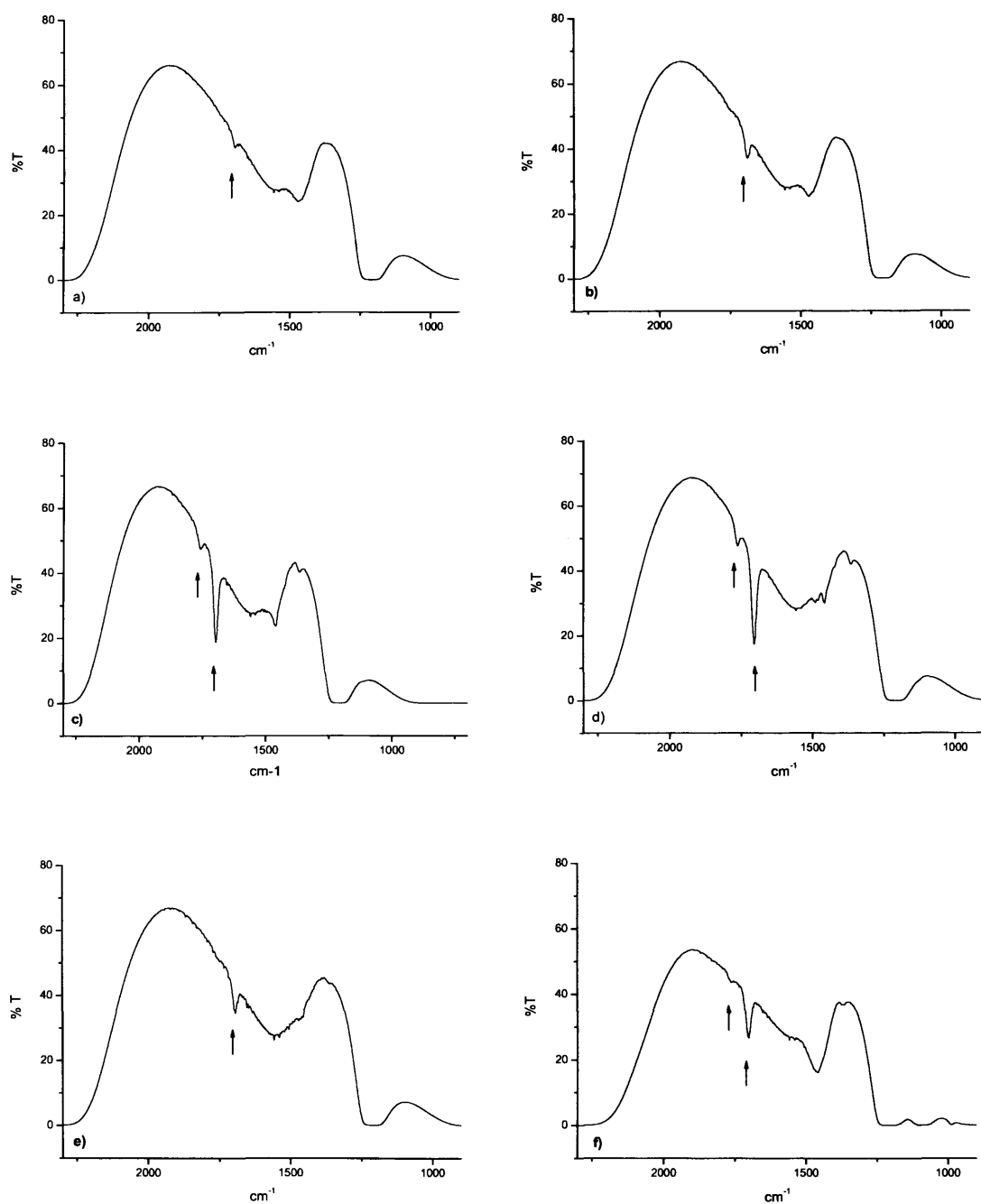


Figure 5.16: IR spectra of saturated solutions of 5-benzylhydantoin (**(S)**-5.5 (a)), (**(S)**-5.6 (b)), (**(S)**-5.7 (c)) and (**(S)**-5.9 (d)) in D₂O. Figures e) and f) show the IR spectra of (**(S)**-5.8 in D₂O and in D₂O phosphate buffer pH** 7.2, 1M, 2M *I*, respectively. Spectra were recorded with a pathlength of 50 μm, 16 scans co-added, at a resolution of 2 cm⁻¹. The arrows indicate the bands related to the carbonyl stretching vibrations.

The stretching vibrations of the carbonyl functionality of the hydantoins appear in the IR spectrum as two bands, which have been attributed to the symmetric and asymmetric stretching vibrations.²⁶ By comparison with other cyclic 1,3- and 1,2-dicarbonyl compounds, the bands at higher wave numbers and less intensity have been attributed to the symmetric stretching, $\nu_{symm}(C=O)$ while the more intensive bands at lower wave numbers have been attributed to the asymmetric stretching mode $\nu_{asymm}(C=O)$. Only the strongest IR bands, at lower wavenumbers, could be detected for all the hydantoins under study, due to the low solubility of the hydantoins in D₂O and strong absorptions of the solvent, partially covering the signals.

In Table 5.2 the asymmetric vibrational frequencies for the stretching vibrations of the carbonyl for hydantoins (S)-5.5-(S)-5.9 are reported.

Table 5.2: IR frequencies for the carbonyl stretching vibrations in hydantoins (S)-5.5-(S)-5.9 determined in D₂O solutions.

Hydantoin	$\nu_{symm}(C=O)/\text{cm}^{-1}$	$\nu_{asymm}(C=O)/\text{cm}^{-1}$
(S)-5.5	--	1696
(S)-5.6	--	1690
(S)-5.7	1756.8	1696
(S)-5.8	--	1696 ^{b)} – 1701 ^{a), b)}
(S)-5.9	1763.6	1705

a) Frequency measured in the IR spectrum of a solution of (S)-5.8 in D₂O phosphate buffer, 1M, 2M I, pH** 7.2.

b) Data from spectra recorded on Jasco FT-IR 660 Plus spectrometric and on a Varian Excalibur Spectrometer (FTS 7000).

To investigate whether a correlation exists between stereolability and carbonyl stretching frequencies, the second-order rate constants of racemisation for hydantoins (S)-5.5-(S)-5.9 were plotted as a function of $\nu_{asymm}(C=O)$ (Figure 5.17).

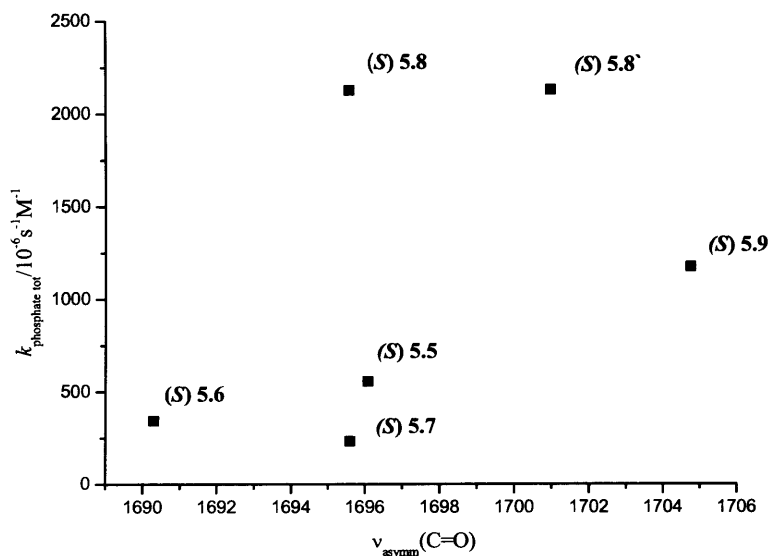


Figure 5.17: Second order rate constants of racemisation for hydantoins **(S)-5.5-(S)-5.9** plotted as a function of $\nu_{\text{asymm}}(\text{C}=\text{O})$. Data points are labelled with the related compound number. Two data points are reported for hydantoin **(S)-5.8**: for data point **(S)-5.8** and **(S)-5.8'**, values of $\nu_{\text{asymm}}(\text{C}=\text{O})$ from IR spectra of hydantoin **(S)-5.8** recorded in D_2O and in D_2O phosphate buffer, 1M, 2M I, $\text{pH}^* 7.2$, were used, respectively.

Figure 5.17 shows no correlation between the second-order rate constants of racemisation for hydantoins and $\nu_{\text{asymm}}(\text{C}=\text{O})$.

As discussed in Chapter 3 under the experimental conditions hydantoin **(S)-5.8** is likely to be mainly in the protonated state. We also invoked intramolecular catalysis by the terminal ammonium group of **(S)-5.9** and by the protonated terminal amino group of **(S)-5.8** to explain the higher rate constants of racemisation of hydantoins **(S)-5.8** and **(S)-5.9** as compared to those of hydantoins **(S)-5.5-(S)-5.7**.

In order to account for possible effects arising from differences in the protonation state of **(S)-5.8**, both on spectral data and rate constants of racemisation, we recorded the IR spectrum of **(S)-5.8** in buffered D_2O at $\text{pH}^* 7.2$. A shift to higher frequency (1701 cm^{-1}) of the IR band for the asymmetric stretching of the carbonyl of **(S)-5.8** was observed. The corresponding data point is indicated with **(S)-5.8'** in **Figure 5.17**. Even if a satisfactory correlation was still not established, the value of $\nu_{\text{asymm}}(\text{C}=\text{O})$ from the IR spectrum of **(S)-5.8** recorded in buffered D_2O solution is in better agreement with a

qualitative trend of the data that seems to associate higher values of $\nu_{asym}(C=O)$ to higher rate constants of racemisation. This trend also conforms to correlation studies on hydantoin derivatives reported in the literature (See Section 5.2.1).

5.3 Conclusion

In this chapter we reported preliminary experiments aimed at evaluating the potentials of VCD and IR spectroscopy in the study of the mechanism of reactions involving stereogenic centres. A method has been presented which allows the prediction of the VCD spectra of “flexible” chiral molecule for which the possibility of different conformations should be considered. Preliminary experiments have been presented aimed at finding suitable experimental conditions for the recording of experimental VCD spectra. Enantiomers of the model compound camphor has been used. The recorded spectra, although in overall qualitative agreement with literature spectra were noisy and not well reproducible. IR spectra of 5-benzylhydantoin **5.5**, 3-*N*-methyl-5-benzylhydantoin **5.6** and their deuterated analogues **5.5b** and **5.6b** were recorded. Unfortunately, it was not possible to detect the IR bands from vibrational modes of CD bonds in the deuterated hydantoins, potentially important in view of mechanistic studies of racemisation and H/D exchange. Further experiments and possibly dedicated VCD equipment are needed for the use of IR and VCD spectroscopy for mechanistic studies as envisaged in this chapter. Finally preliminary experiments aimed at searching a correlation between stereolability and vibrational frequencies of the carbonyl stretching modes of model hydantoins has been described. Satisfactory results were not obtained.

5.4. Experimental

Calculations of VCD and IR spectra

Conformational searches were carried out by means of the program MacroModel. The force field MMFF 94 was mainly used. Conformational searches were carried out within 10 kcal/mole with Monte Carlo sampling of the conformations, 100 steps per

rotatable bond. The DFT calculations were carried out by means of the Gaussian03 program, using the functional and basis set B3PW91/6-31G + (d, p). Elaborations of the VCD spectra with Lorentzian band shapes were carried out by means of the program MATLAB.

Experimental IR and VCD spectra

Apparatus

VCD and some of the IR spectra were recorded on a Varian Excalibur Spectrometer (FTS 7000) equipped with a liquid nitrogen cooled Cryogenic Mercury Cadmium Telluride (MCT) detector and a single modulation setup. The IR spectra described in Section 5.2.2 were recorded on a Jasco FT-IR 660 Plus spectrometer, unless otherwise stated. For VCD spectra and IR spectra in CDCl₃ and CHCl₃ solution, a liquid sample cell with variable path length and KBr windows was used. A liquid cell with CaF₂ windows, with Teflon spacers to define the optical path length, was used to record spectra in D₂O solutions.

Materials

Dimethylsulfoxide-d₆ (D 99.9%) was purchased from Cambridge Isotope Laboratories, inc, chloroform-d (H₂O<0.01%, 99.80 %D) was from EURISO-TOP, deuterium oxide (99.9%) was obtained from Fluorochem, CHCl₃ was from Fisher Scientific. (+)-Camphor, kindly provided by Dr. I. Fallis, and (-)-camphor were from Aldrich. Hydantoins (*S*)-5-benzylimidazolidine-2,4-dione (**S**-5.5), (*S*)-5-benzyl-3-methylimidazolidine-2,4-dione (**S**-5.6), (*S*)-5-benzyl-3-(2-methoxyethyl)-imidazolidine-2,4-dione (**S**-5.7), (*S*)-5-benzyl-3-(2-(dimethylamino)ethyl)imidazolidine-2,4-dione (**S**-5.8) and (*S*)-2-(4-benzyl-2,5 dioxoimidazolidin-1-yl)-*N,N,N*-trimethylethanaminium iodide (**S**-5.9) were prepared as described in Chapters 2 and 3. Deuterium-labeled hydantoins *rac*-5.5b and *rac*-5.6b were recovered from solutions in D₂O phosphate buffers used in H/D exchange kinetic experiments, after complete deuteration of the

substrates. The procedure used for recovery of *rac*-5.5b was as follow: the solution of *rac*-5.5b in D₂O phosphate buffer was concentrated and the deuterated hydantoin was recovered by filtration. The solid was washed three times with D₂O and high vacuum dried. In case of hydantoin *rac*-5.6b, the solution in D₂O phosphate buffer was concentrated to a small volume and quickly extracted with chloroform. The combined organic extracts were concentrated. The solid obtained was washed with a little D₂O, filtered and high vacuum dried. Structures were confirmed by ¹H NMR spectroscopy.

VCD and IR spectra

VCD spectra and the IR spectra described in section 5.1.3.3 and 5.1.3.4 were recorded on a Varian Excalibur Spectrometer (FTS 7000) equipped with a liquid nitrogen cooled Cryogenic MCT detector. The sample chamber was purged with nitrogen for 5 to 10 minutes after placing the cell in the sample holder and during spectral acquisitions. A TGS region filter ($< 2000 \text{ cm}^{-1}$) was used for the recording of VCD spectra of (+)- and (-)- camphor. IR spectra of the solution samples were recorded before the acquisition of VCD spectra and concentration and path length were adjusted in order to obtain IR spectra with an average transmission of approximately 30% in the spectral window of interest. Typical concentrations were 0.3 or 0.6 M, and optimal path lengths were found between 100 and 150 μm . Resolutions of 4 or 8 cm^{-1} were used for most experiments. VCD spectra of individual enantiomers were obtained from 16 to 25 co-added spectra. Baseline-corrected VCD spectra were obtained as one half of the difference between the VCD spectra of individual enantiomers or by subtracting the VCD spectrum of a racemic mixture of the compound under study from the spectrum of a single enantiomer. The IR spectra described in section 5.2.2. were recorded on a Jasco FT-IR spectrometer in a cell with a pathlength of 50 μm , at a resolution of 2 cm^{-1} with 16 scans co-added. The IR spectrum of (*S*)-5.8 in D₂O solution, recorded on the Jasco FT-IR spectrometer, was also recorded on the Varian FTIR Spectrometer, giving the same value for the frequency of the carbonyl stretching of (*S*)-5.8 as found in the previous experiment.

Acknowledgments

I thank Dr Andrew Leach, Dr Simone Tomasi, Dr Martin Packer (all at AstraZeneca) for their kind and valuable help with the development of the method for calculating VCD spectra described in **Section 5.1.** and Dr Nabil Asaad who inspired the work. I would also like to thank Dr Larry Goldman and Dr Robert Richardson, from Cardiff University, for precious help with the calculations carried out at Cardiff University. I acknowledge AstraZeneca and Cardiff University for making available computational facilities and time.

References

1. Nafie, L. A., *Business Briefing:Pharma Outsourcing* **2004**, 1-4.
2. Freedman, T. B.; Cao, X. L.; Dukor, R. K.; Nafie, L. A., *Chirality* **2003**, *15* (9), 743-758.
3. Stephens, P. J.; Davlin, F. J., *Chirality* **2000**, *12* (4), 172-179.
4. Kellenbach, E. R.; Dukor, R. K.; Nafie, L. A., *Spectroscopy Europe* **2007**, *19* (4), 15-18.
5. Monde, K.; Miura, N.; Hashimoto, M.; Taniguchi, T.; Inabe, T., *Journal of the American Chemical Society* **2006**, *128* (18), 6000-6001.
6. Keiderling, T. A., *Current Opinion in Chemical Biology* **2002**, *6* (5), 682-688.
7. Rudd, T. R.; Nichols, R. J.; Yates, E. A., *Journal of the American Chemical Society* **2008**, *130* (7), 2138-+.
8. Devlin, F. J.; Stephens, P. J.; Cheeseman, J. R.; Frisch, M. J., *Journal of Physical Chemistry A* **1997**, *101* (51), 9912-9924.
9. Devlin, F. J.; Stephens, P. J.; Cheeseman, J. R.; Frisch, M. J., *Journal of Physical Chemistry A* **1997**, *101* (35), 6322-6333.
10. Devlin, F. J.; Stephens, P. J.; Cheeseman, J. R.; Frisch, M. J., *Journal of the American Chemical Society* **1996**, *118* (26), 6327-6328.
11. Asaad, N.; Fillery, S., *Organic & Biomolecular Chemistry* **2009**, *7* (4), 678-686.

12. Only one (for compound **5.1**) or two (for compounds **5.2** and **5.3**) conformers were found to be populated with the population of the other conformers being below 0.001%..
13. Halgren, T. A., *Journal of Computational Chemistry* **1996**, *17* (5-6), 490-519.
14. Conformational searches, geometry optimisations and calculations of the energies, by means of DFT methods, for different conformers were carried out on non labelled analogues of the structures shown in **Scheme 5.1**.
15. Jensen, F., *Introduction to Computational Chemistry*. John Wiley & Sons: Chichester New York Weinheim Brisbane Singapore Toronto, 1999; p 177-194.
16. Jensen, F., *Introduction to Computational Chemistry*. John Wiley & Sons: Chichester New York Weinheim Brisbane Singapore Toronto, 1999; p 6-52.
17. The foundation of Force Field Methods or Molecular Mechanics (MM) is the observation that molecules tend to be composed of units (called “atom types”) which are structurally similar. MM methods can be seen as a generalisation and improvement of the usual ball and stick models of molecules, using the “atom types” as building blocks. FF methods bypass the solution of the Schrodinger equation by writing the energy as a parametric function of the internal coordinates of the molecule. They therefore enable a quick construction of the potential energy surface corresponding to different conformations of the molecule and a first rough evaluation of energy minima corresponding to stable conformers. The basis of Density Functional Theory (DFT), on the contrary, relies on the fact that the ground-state electronic energy of a set molecular structure can be correlated to the electron density, through appropriate functional.
18. Chiorboli, P., *Fondamenti di Chimica*. Second ed.; Unione Tipografico-Editrice Torinese: Torino, 1991; p 519.
19. The calculations were carried out by Dr Simone Tomasi from AstraZeneca.
20. Finley, J. W.; Stephens, P. J., *Theochem-Journal of Molecular Structure* **1995**, *357* (3), 225-235.
21. Reist, M.; Carrupt, P. A.; Testa, B.; Lehmann, S.; Hansen, J. J., *Helvetica Chimica Acta* **1996**, *79* (3), 767-778.
22. The better solubility of **5.6** and **5.6b** in CHCl₃ as compared to **5.5** and **5.5b** makes the formers more suitable for studies by means of analytical techniques, such as IR or VCD spectroscopy, where relatively high concentrations are needed.
23. Morita, H. E.; Kodama, T. S.; Tanaka, T., *Chirality* **2006**, *18* (10), 783-789.

24. Vollhardt, P., *Chimica Organica*. Zanichelli Editore S.p.A.: Bologna, 1998; p 790-794.
25. Perjessy, A.; Fabian, W. M. F.; Parik, P.; Ludwig, M.; Loos, D.; Sustekova, Z., *Molecules* **2004**, *9* (4), 213-222.
26. Kleinpeter, E.; Klod, S.; Perjessy, A.; Samalikova, M.; Synderlata, K.; Sustekova, Z., *Journal of Molecular Structure* **2003**, *645* (1), 17-27.

Chapter 6

Epilogue

6.1. Conclusions

This thesis describes studies on the processes of racemisation and H/D exchange of 5-substituted hydantoins, carried out mainly by means of CD and NMR spectroscopy. Studies in the literature report controversial conclusions about the mechanism of racemisation of 5-substituted hydantoins¹⁻⁸ and both S_E1 and S_E2 mechanisms have been proposed.

We focused on two model compounds, viz. (*S*)-5-benzylhydantoin and (*S*)-3-*N*-methyl-5-benzylhydantoin. Detailed kinetic studies of racemisation and H/D exchange of these two model hydantoins provided a coherent set of findings. First, reactions were found to follow pseudo-first-order kinetics and were general-base catalysed. Second, the ratio of the rate constants of racemisation and H/D exchange of (*S*)-5-benzylhydantoin are consistently equal under the experimental conditions where both rate constants were evaluated. Third, primary kinetic isotope effects are significant, while solvent kinetic isotope effects are negligible. Fourth, deuterium labelled hydantoins for which the process of H/D exchange and racemisation leads to the formation of diastereoisomers indicated immediate racemisation rather than inversion upon H/D exchange. Fifth, mathematical analyses and numerical simulations show that the observed first-order kinetics cannot be in agreement with a mechanism in which the first deuteration step also leads to inversion of the chiral centre. All these observations support the S_E1

mechanism for the racemisation of substituted hydantoins and most are incompatible with the S_E2 mechanism.

A series of 5-substituted hydantoins was also synthesised, addressing the low water solubility of (*S*)-5-benzylhydantoin and (*S*)-3-*N*-methyl-5-benzylhydantoin, therefore allowing kinetic studies by means of analytical techniques less sensitive than CD spectroscopy, such as IR or VCD spectroscopy. Some of the structural modifications gave rise to unexpected differences in the stereolability of the substrates. In particular hydantoins containing a protonated amino or an ammonium group showed increased stereolability. This finding was attributed to intramolecular facilitation of racemisation by the positive charge. For two 5-substituted hydantoins the primary and solvent kinetic isotope effects on racemisation were also determined with results again supporting an S_E1 mechanism of racemisation.

The experiments described in Chapter 4 of this thesis focused on the effect of the solvent on racemisation and H/D exchange of a series of 5-benzylhydantoins. DMSO added to phosphate buffers showed a marked rate-increasing effect for all of the substrates under study. Co-added 2-propanol and dioxane showed rate-decreasing effects on the racemisation and H/D exchange of neutral hydantoins and a rate-increasing effect on racemisation and H/D exchange of a cationic hydantoin. Solvent effects on the basicity of anionic catalysts and phenomena of preferential solvation were proposed as important factors affecting the rate constants in mixed media.

Finally, in Chapter 5, we have described preliminary experiments aimed at assessing potentials and limitations of VCD and IR spectroscopy for kinetic and mechanistic studies of racemisation.

6.2. Future work

A recent paper by Cabordery² reports an S_E1 mechanism of racemisation for a series of substituted hydantoins while an S_E2 mechanism is proposed for substituted 2-thiohydantoins. The finding is interesting because it suggests that the introduction of a thioamide has a significant effect on the racemisation reaction. Future work could therefore aim to confirm this finding. A Knoevenagel condensation of 2-thiohydantoin with appropriate aldehydes followed by a catalytic hydrogenation, as described in this thesis for preparing some of our model hydantoins (see Chapters 2 and

3) may be used to prepare the required substrates. The determination of primary and solvent kinetic isotope effects, together with studies of H/D exchange using suitable deuterium-labelled substrates (see Chapter 2) might help shed light on the mechanism of racemisation of these thiohydantoins.

Regarding the effects of co-solvents on racemisation reactions, further experiments are needed for a better insight into these. In particular further investigations should be addressing the question of the non-linear dependence of the rate constants of racemisation of a model cationic hydantoin in mixed media with the concentration of co-added 2-propanol (see Chapter 4).

It would be interesting to obtain information about the carbon acid acidity of 5-substituted hydantoins as described by Richardt *et al.* for several classes of different carbon acids (see Chapter 1).⁹⁻¹⁴

Further work may also be focussed on finding suitable experimental conditions allowing the use of VCD and IR spectroscopy for kinetic studies of racemisation of 5-substituted hydantoins. Substituted hydantoins with increased water solubility and not too high rate constants of racemisation, such as hydantoins 3.24 and 3.25, described in Chapter 3 of this thesis, may be used as model compounds for this purpose.

References

1. Reist, M.; Carrupt, P. A.; Testa, B.; Lehmann, S.; Hansen, J. J., *Helvetica Chimica Acta* **1996**, *79* (3), 767-778.
2. Caborder, A.-C.; Toussaint, M.; Azaroual, N.; Bonte, J.-P.; Melnyk, P.; Vaccher, C.; Foulon, C., *Tetrahedron-Asymmetry* **2011**, *22* (2), 125-133.
3. Lazarus, R. A., *Journal of Organic Chemistry* **1990**, *55* (15), 4755-4757.
4. Kahn, K.; Tipton, P. A., *Bioorganic Chemistry* **2000**, *28* (2), 62-72.
5. Dudley, K. H.; Bius, D. L., *Drug Metabolism and Disposition* **1976**, *4* (4), 340-348.
6. Bovarnick, M.; Clarke, H. T., *Journal of the American Chemical Society* **1938**, *60*, 2426-2430.
7. Dakin, H. D., *American Chemical Journal* **1910**, *44*, 48.
8. Lee, C. K.; Fan, C. H., *Enzyme and Microbial Technology* **1999**, *24* (10), 659-666.

9. Amyes, T. L.; Richard, J. P., *Journal of the American Chemical Society* **1992**, *114* (26), 10297-10302.
10. Amyes, T. L.; Richard, J. P., *Journal of the American Chemical Society* **1996**, *118* (13), 3129-3141.
11. Richard, J. P.; Williams, G.; O'Donoghue, A. C.; Amyes, T. L., *Journal of the American Chemical Society* **2002**, *124* (12), 2957-2968.
12. Rios, A.; Amyes, T. L.; Richard, J. P., *Journal of the American Chemical Society* **2000**, *122* (39), 9373-9385.
13. Williams, G.; Maziarz, E. P.; Amyes, T. L.; Wood, T. D.; Richard, J. P., *Biochemistry* **2003**, *42* (27), 8354-8361.
14. Rios, A.; Richard, J. P.; Amyes, T. L., *Journal of the American Chemical Society* **2002**, *124* (28), 8251-8259.

Appendices

for

The mechanism of racemisation of 5-substituted hydantoins in aqueous solution

Stefania Narduolo

**A thesis submitted for Degree of Doctor of Philosophy
School of Chemistry
Cardiff University**

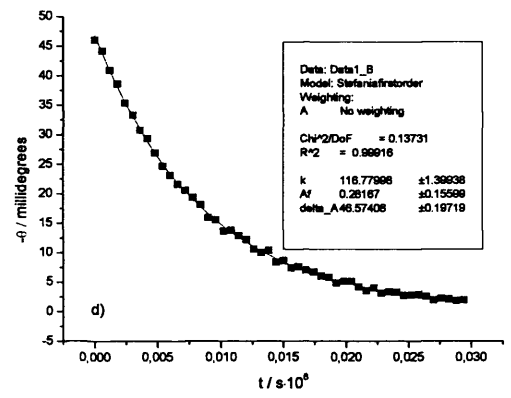
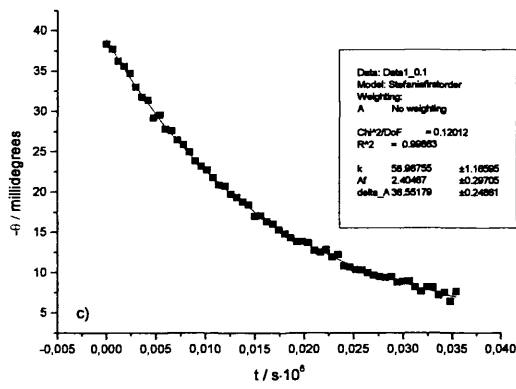
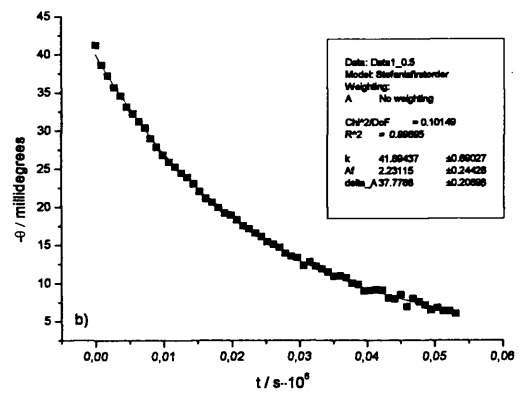
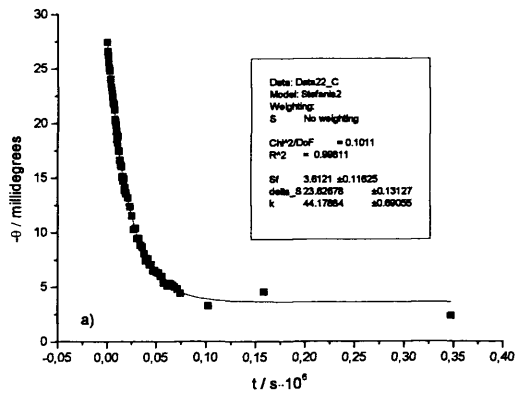
December 2011

Appendix 1

This Appendix is for Chapter 2

The kinetics and mechanism of racemisation of (*S*)-5-benzylhydantoin and (*S*)-3-*N*-methyl-5-benzylhydantoin

A.1.1 Kinetic traces for racemisation of 2.1 in D₂O phosphate buffers, pH 7.2, 1 M I, at 60 °C**



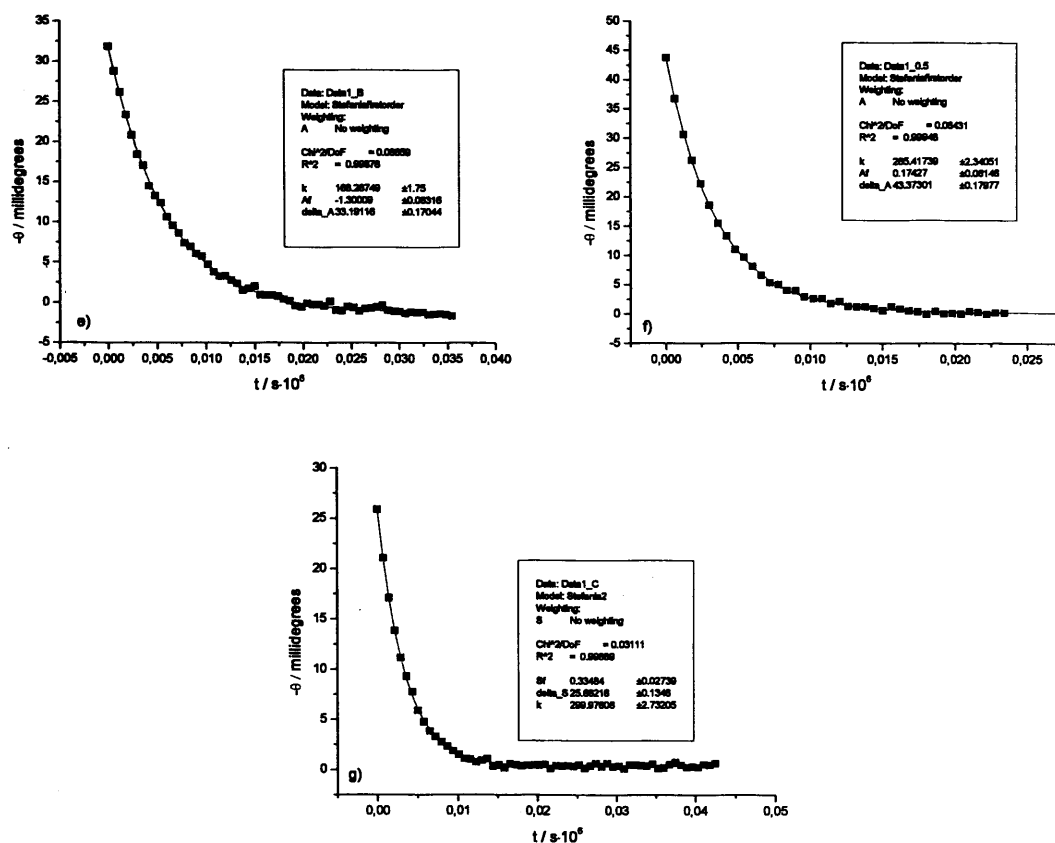


Figure S1.1a-g: racemisation of (S)-5-benzylhydantoin 2.1 at 60 °C in D₂O phosphate buffers, pH** 7.2, 1 M / a), b) 0.045 M, c) 0.09 M, d) 0.18 M, e) 0.27 M f), g) 0.5 M. The CD signals of 2.1 at 230 nm are plotted as a function of reaction time. The squares (■) are the experimental points, the solid lines are the fits to first-order kinetics.

A.1.2 Kinetic traces for racemisation of 2.1 in D₂O phosphate buffers, pH 8.0, 1 M I, at 60 °C**

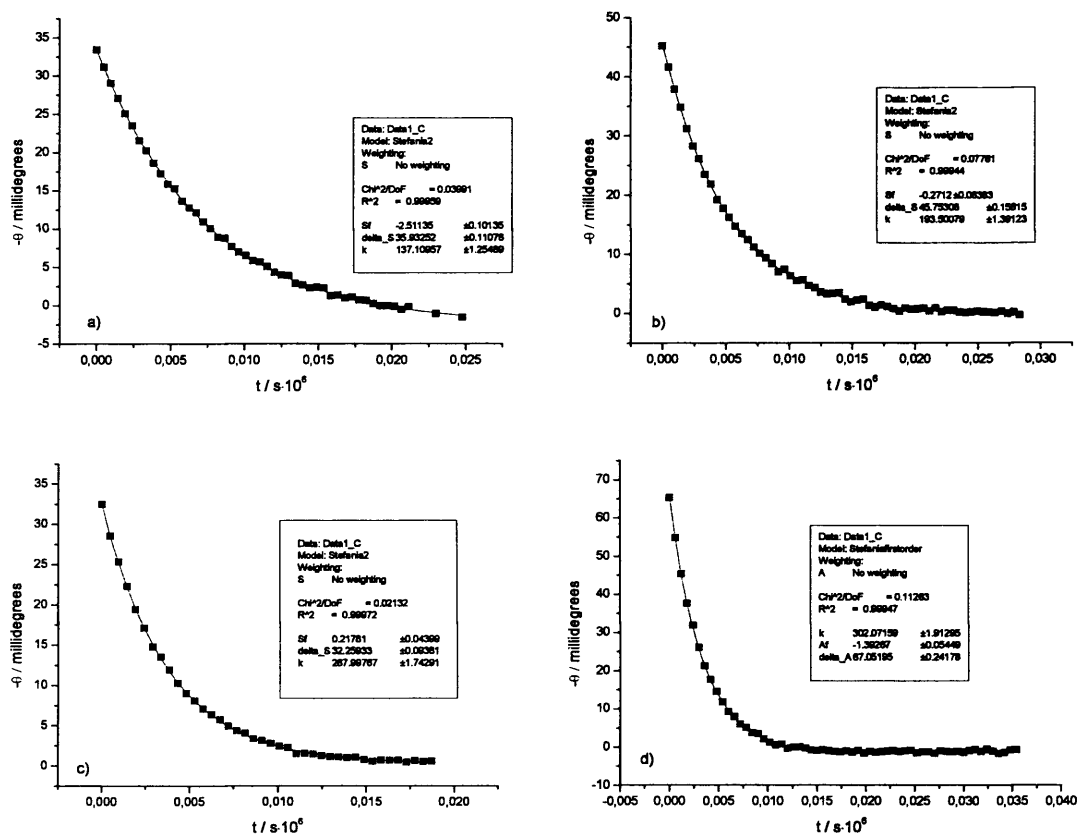


Figure S1.2a-d: racemisation of (S)-5-benzylhydantoin 2.1 at 60 °C in D₂O phosphate buffers, pH** 8.0, 1 M I / a) 0.1 M, b) 0.2 M, c) 0.3 M, d) 0.35 M. The CD signals of 2.1 at 230 nm are plotted as a function of reaction time. The squares (■) are the experimental points, the solid lines are the fits to first-order kinetics.

A.1.3 Kinetic traces for racemisation of 2.1 in D₂O phosphate buffers, pH 9.0, 1 M I, at 60 °C**

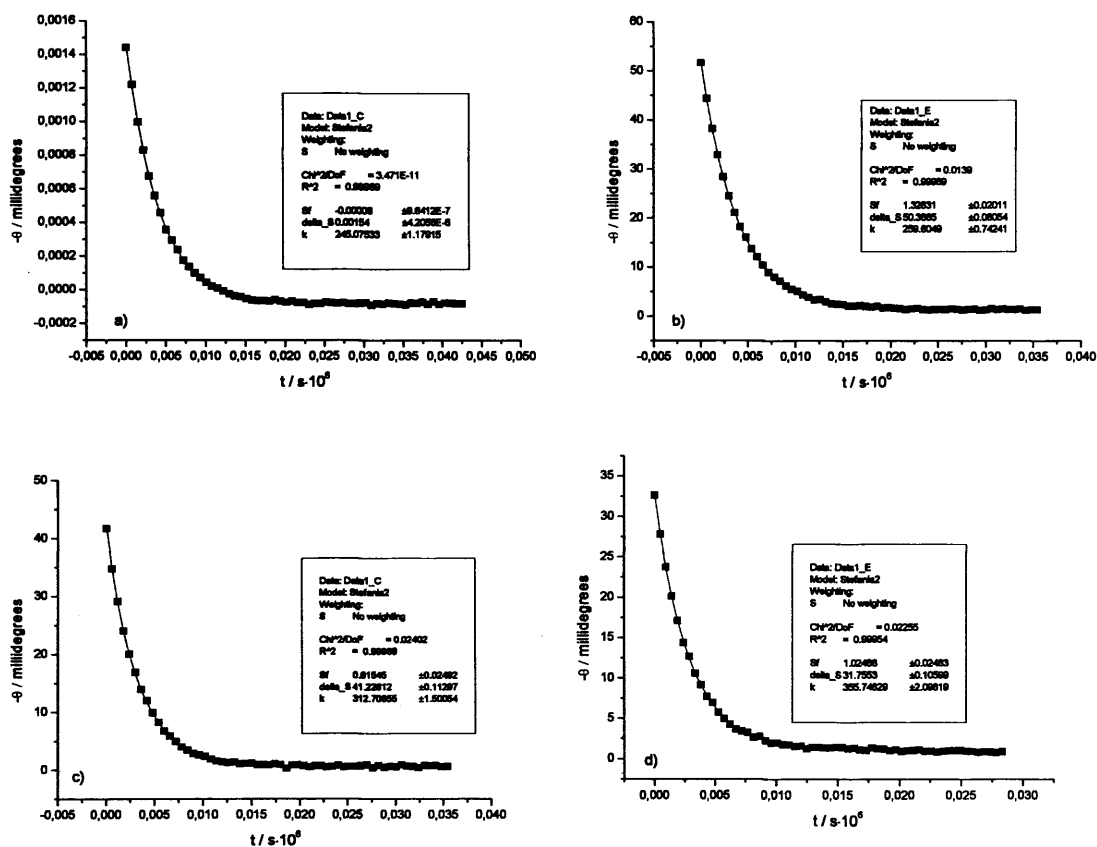


Figure S1.3a-d: racemisation of (S)-5-benzylhydantoin 2.1 at 60 °C in D₂O phosphate buffers, pH** 9.0, 1 M I / a) 0.05 b) 0.1 M, c) 0.2 M, d) 0.3 M. The CD signals of 2.1 at 240 nm are plotted as a function of reaction time. The squares (■) are the experimental points, the solid lines are the fits to first-order kinetics.

A.1.4 Kinetic traces for racemisation of 2.1 in D₂O phosphate buffers, pH 10.0, 1 M I, at 60 °C**

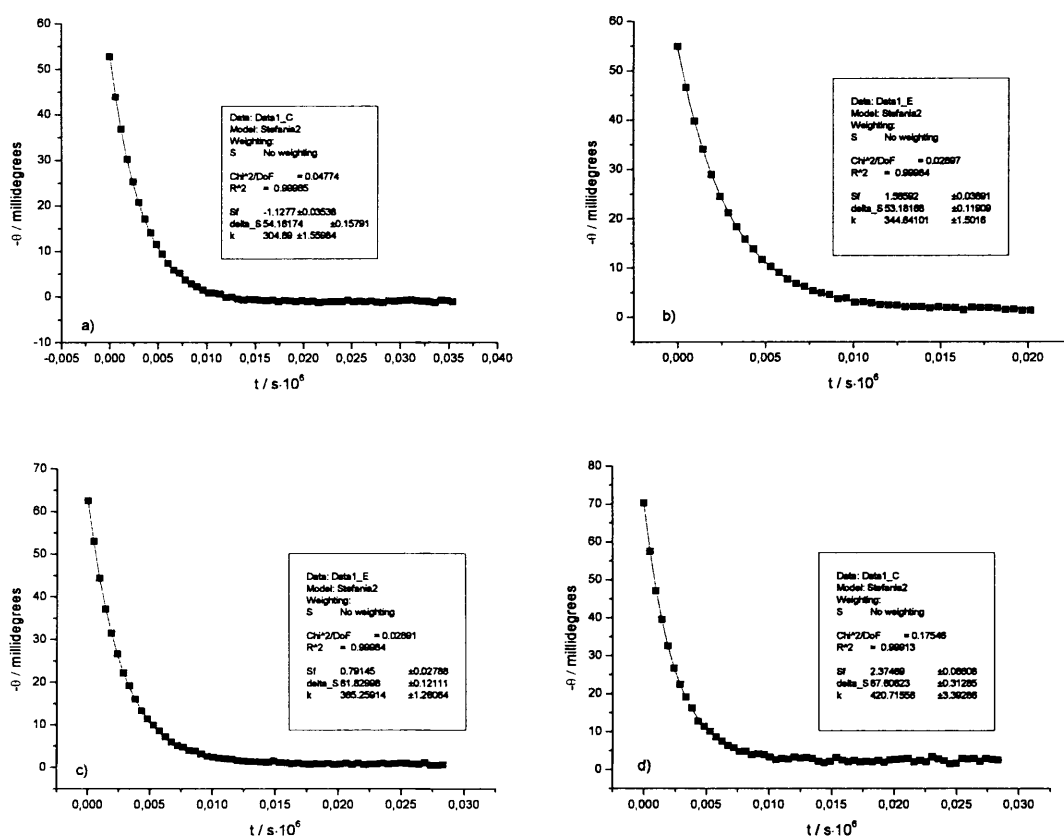


Figure S1.4a-d: racemisation of (*S*)-5-benzylhydantoin **2.1** at 60 °C in D₂O phosphate buffers, pH** 10.0, 1 M I a) 0.05 b) 0.1 M, c) 0.2 M, d) 0.3 M. The CD signals of **2.1** at 240 nm are plotted as a function of reaction time. The squares (■) are the experimental points, the solid lines are the fits to first-order kinetics.

A.1.5 Kinetic traces for racemisation of 2.1 in D₂O phosphate buffers, pH 11.0, 1 M I, at 60 °C**

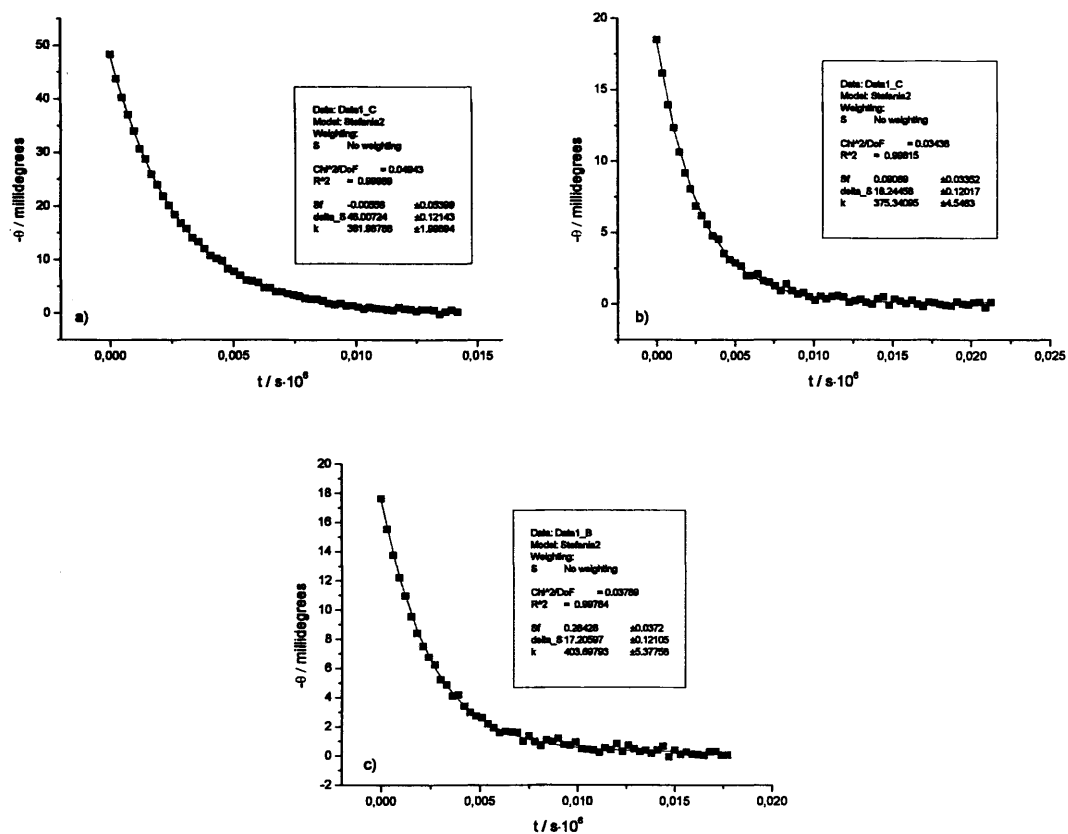


Figure S1.5a-c: racemisation of (S)-5-benzylhydantoin 2.1 at 60 °C in D₂O phosphate buffers, pH** 11.0, 1 M I a) 0.1 b) 0.2 M, c) 0.3 M. The CD signals of 2.1 at 240 nm (a) and 245 nm (b) and c) are plotted as a function of reaction time. The squares (■) are the experimental points, the solid lines are the fits to first-order kinetics.

A.1.6 Kinetic traces for racemisation of 2.1 in D₂O phosphate buffers, pH 6.0, 1M I, at 60 °C**

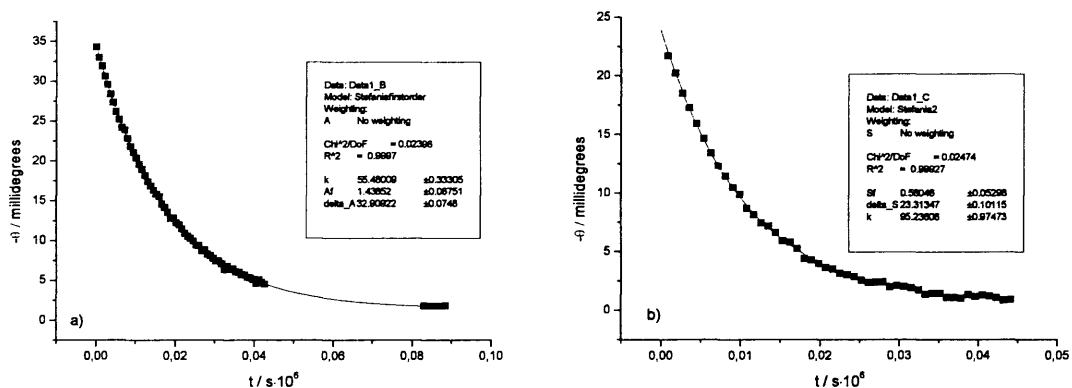


Figure S1.6a, b: racemisation of (*S*)-5-benzylhydantoin **2.1** at 60 °C in D₂O phosphate buffers, pH** 6.0, 1 M I, **a)** 0.25 M and **b)** 0.5 M. The CD signals of **2.1** at 230 nm are plotted as a function of reaction time. The squares (■) are the experimental points, the solid lines are the fits to first-order kinetics.

A.1.7 Kinetic traces for racemisation of 2.2 in D₂O phosphate buffers, pH 7.2, 1 M I, at 60 °C**

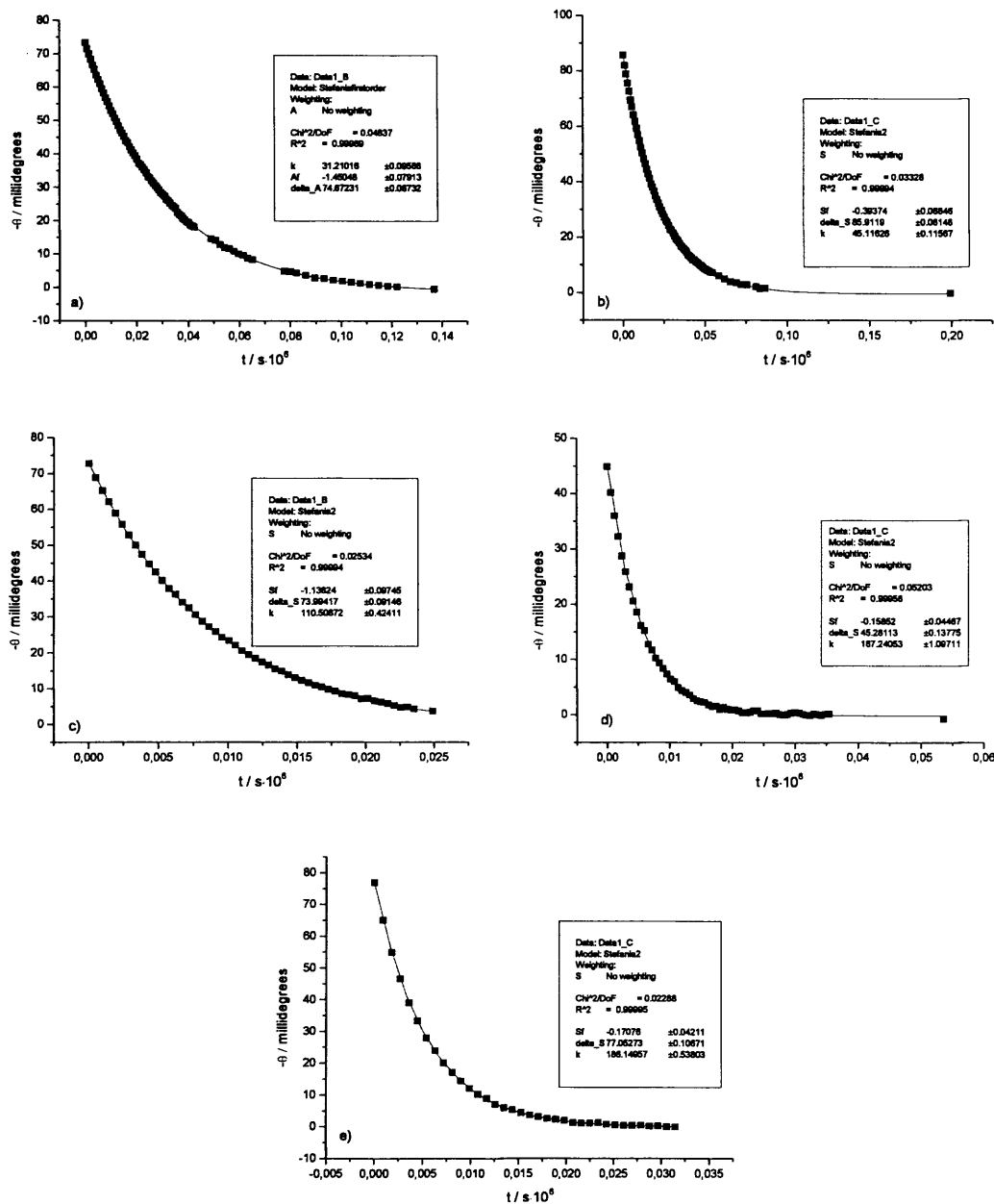


Figure S1.7a-e: racemisation of (S)-3-N-methyl-5-benzylhydantoin 2.2 at 60 °C in D₂O phosphate buffers, pH** 7.2, 1 M I, a) 0.045 M and b) 0.09 M, c) 0.27 M, d), e) 0.5 M. The CD signals of 2.2 at 235 nm are plotted as a function of reaction time. The squares (■) are the experimental points, the solid lines are the fits to first-order kinetics.

A.1.8 Kinetic traces for racemisation of 2.2 in D₂O phosphate buffers, pH 8.0, 1 M I, at 60 °C**

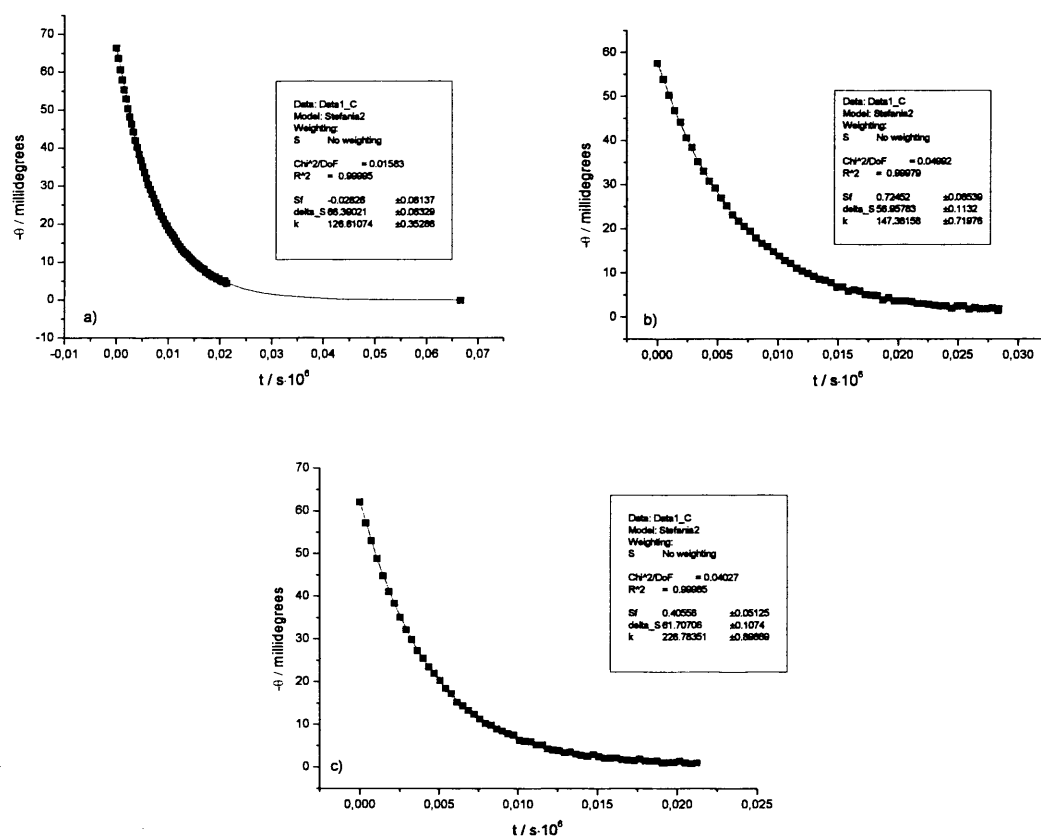


Figure S1.8a-c: racemisation of (*S*)-3-*N*-methyl-5-benzylhydantoin **2.2** at 60 °C in D₂O phosphate buffers, pH** 8.0, 1 M I, a) 0.1 M and b) 0.2 M, c) 0.35 M. The CD signals of **2.2** at 235 nm are plotted as a function of reaction time. The squares (■) are the experimental points, the solid lines are the fits to first-order kinetics.

A.1.9 Kinetic traces for racemisation of 2.2 in D₂O phosphate buffers, pH 9.0, 1 M I, at 60 °C**

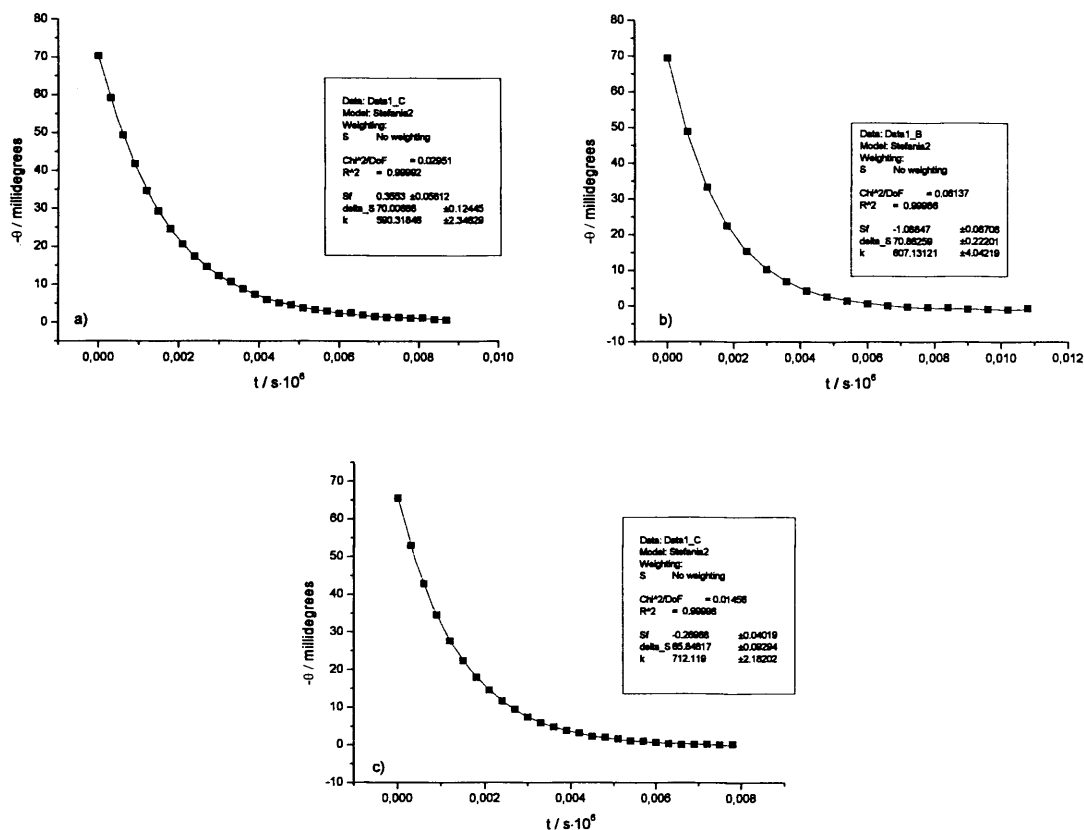


Figure S1.9a-c: racemisation of (S)-3-N-methyl-5-benzylhydantoin 2.2 at 60 °C in D₂O phosphate buffers, pH** 9.0, 1 M I, a) 0.05 M and b) 0.1 M, c) 0.2 M. The CD signals of 2.2 at 235 nm are plotted as a function of reaction time. The squares (■) are the experimental points, the solid lines are the fits to first-order kinetics.

A.1.10 Kinetic traces for racemisation of 2.2 in D₂O phosphate buffers, pH 6.0, 1 M I, at 60 °C**

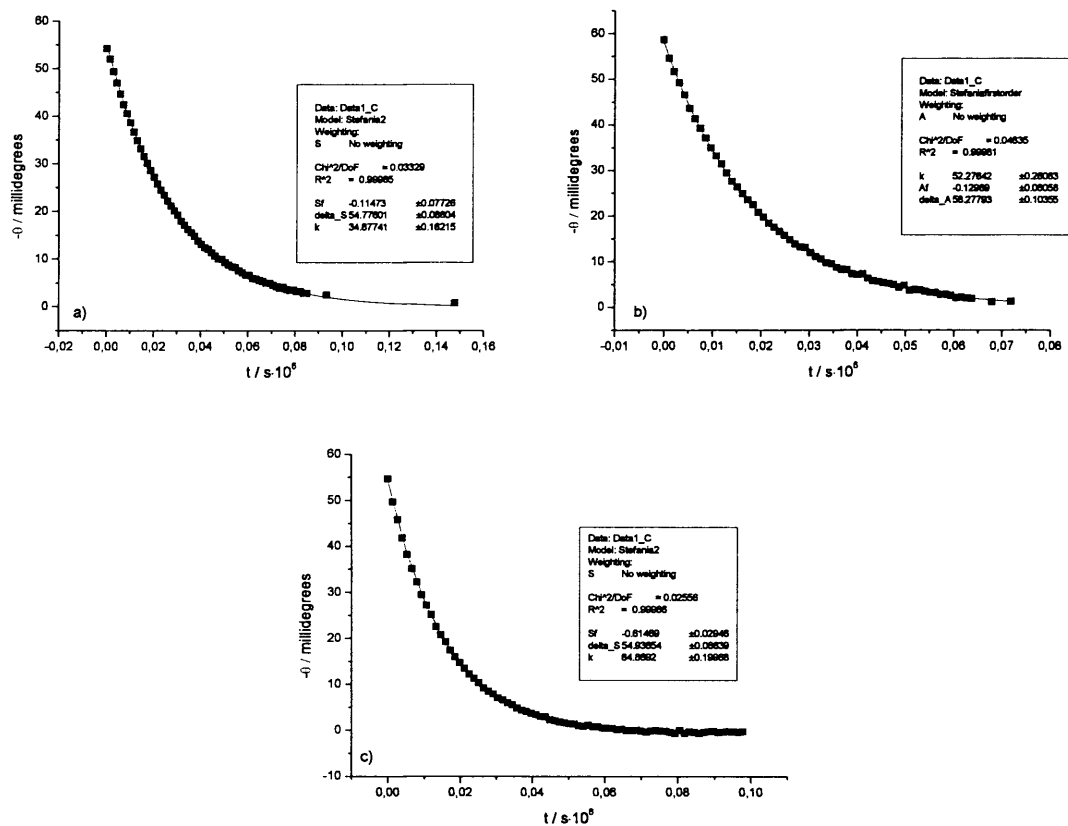


Figure S1.10a-c: racemisation of (S)-3-N-methyl-5-benzylhydantoin at 60 °C in D₂O phosphate buffers, pH** 6.0, 1 M I, a) 0.3 M and b) 0.5 M, c) 0.7 M. The CD signals of 2.2 at 235 nm are plotted as a function of reaction time. The squares (■) are the experimental points, the solid lines are the fits to pseudo first-order kinetics.

A.1.11 Kinetic traces for racemisation of 2.1 in phosphate buffers, pH* 7.2, 1 M I, at 25 °C

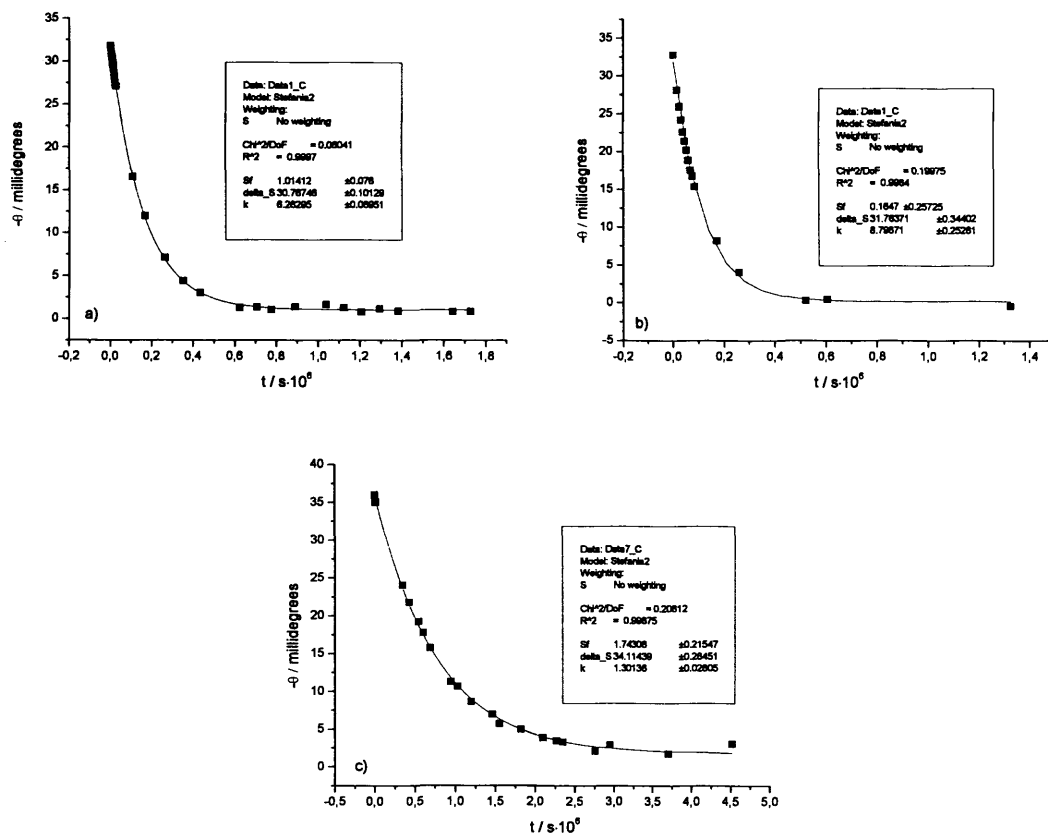


Figure S1.11a-c: racemisation of (*S*)-5-benzylhydantoin **2.1** at 25 °C **a)** in D₂O phosphate buffer, pH* 7.2, 0.5 M, 1 M I; **b)** in D₂O phosphate buffer, pH* 9.0, 0.3 M, 1 M I; **c)** in H₂O phosphate buffer, pH* 7.2, 0.5 M, 1 M I. The CD signals of **2.1** at 230 nm are plotted as a function of reaction time. The squares (■) are the experimental points, the solid lines are the fits to first-order kinetics.

A.1.12 Determination of the pK_a^{**} of 2.1 in D_2O , at 60 °C

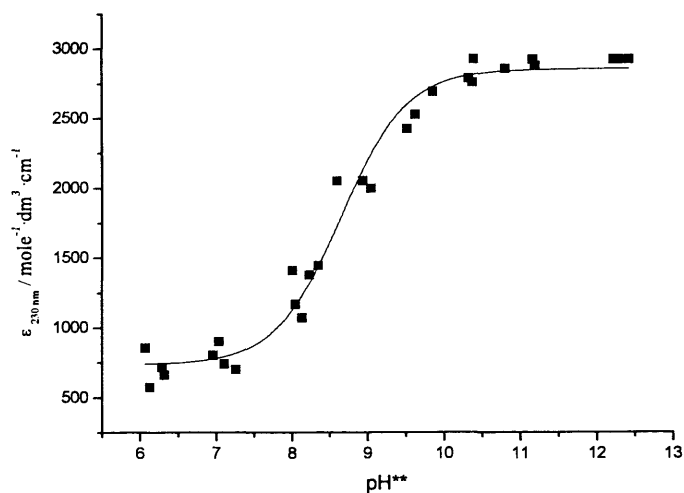


Figure S1.12: plot for the titration of 2.1 in D_2O phosphate buffers at 60 °C. The solid line is the fit of the experimental data-points to **Equation S1.1**

$$\epsilon = \frac{1}{1+10^{(pH-pK_a)}} \cdot \epsilon_a + \frac{10^{(pH-pK_a)}}{1+10^{(pH-pK_a)}} \cdot \epsilon_b \quad \text{Equation S1.1}$$

Where ϵ_{obs} is the observed extinction coefficient at each pH^{**} , at 60 °C, ϵ_a and ϵ_b are the extinction coefficient for protonated and deprotonated 2.1, respectively.

A.1.13 Kinetic traces for racemisation of (S)-5-benzylhydantoin 2.1 and (S)-3-N-methyl-5-benzylhydantoin 2.2 in D₂O and H₂O phosphate buffers, 0.25 M, 0.5 M I

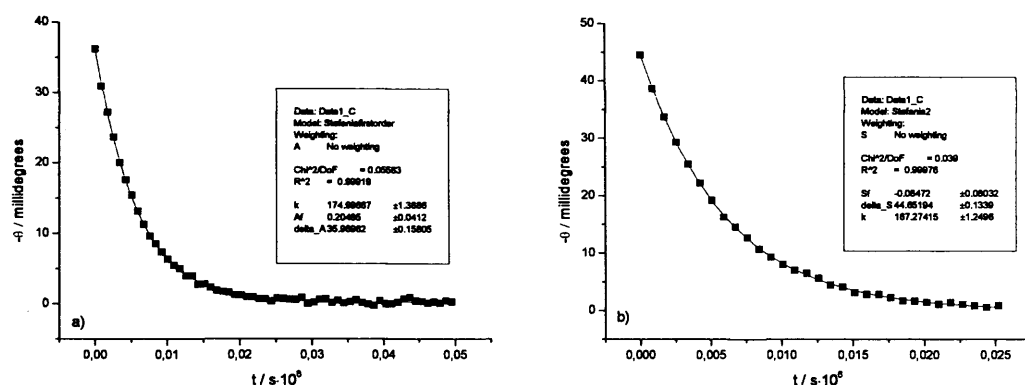


Figure S1.13: racemisation of 2.1, at 60 °C **a)** in D₂O phosphate buffer pH** 7.3, 0.25 M, 0.5 M I, and **b)** in H₂O phosphate buffer pH^{25 °C} 7.2, 0.25 M, 0.5 M I. The CD signals of 2.1 at 230 nm are plotted as a function of reaction time. The squares (■) are the experimental points, the solid lines are the fits to first-order kinetics.

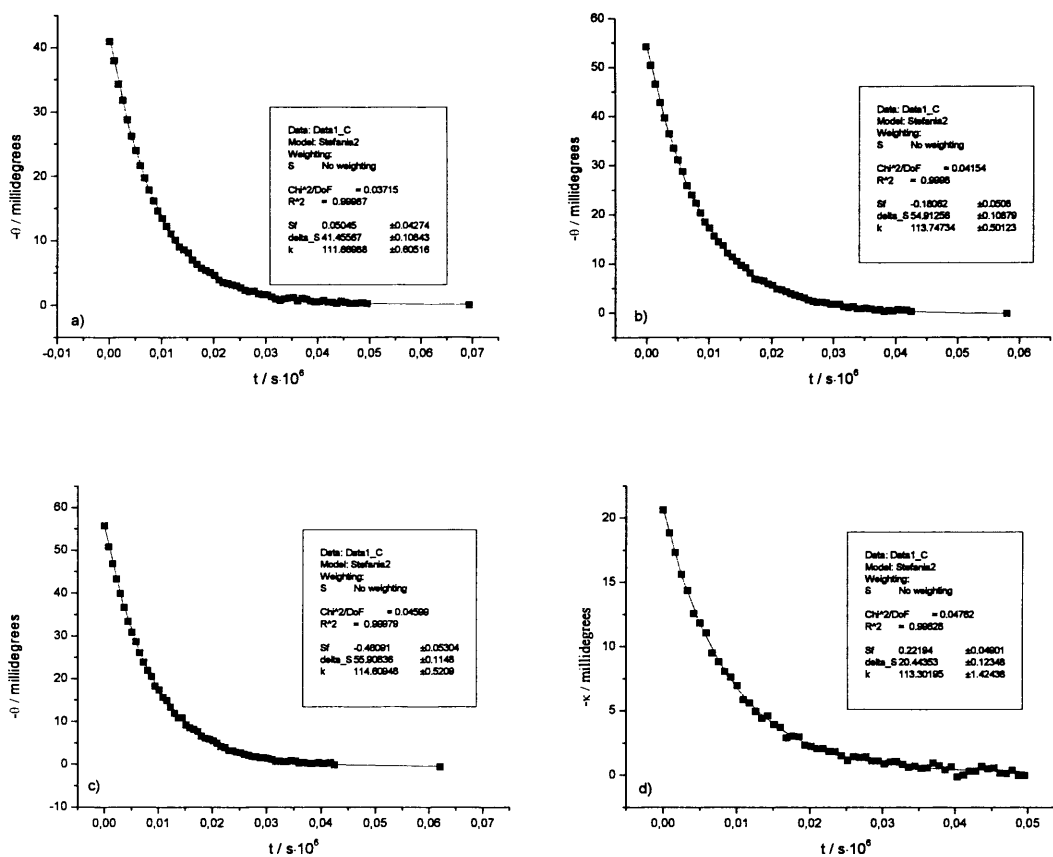


Figure S1.14 : racemisation of 2.2, at 60 °C a), b) in D₂O phosphate buffer pH** 7.3, 0.25 M, 0.5 M *I*, and c), d) in H₂O phosphate buffer pH²⁵ °C 7.2, 0.25 M, 0.5 M *I*. The CD signals of 2.2 at 240 nm are plotted as a function of reaction time. The squares (■) are the experimental points, the solid lines are the fits to first-order kinetics.

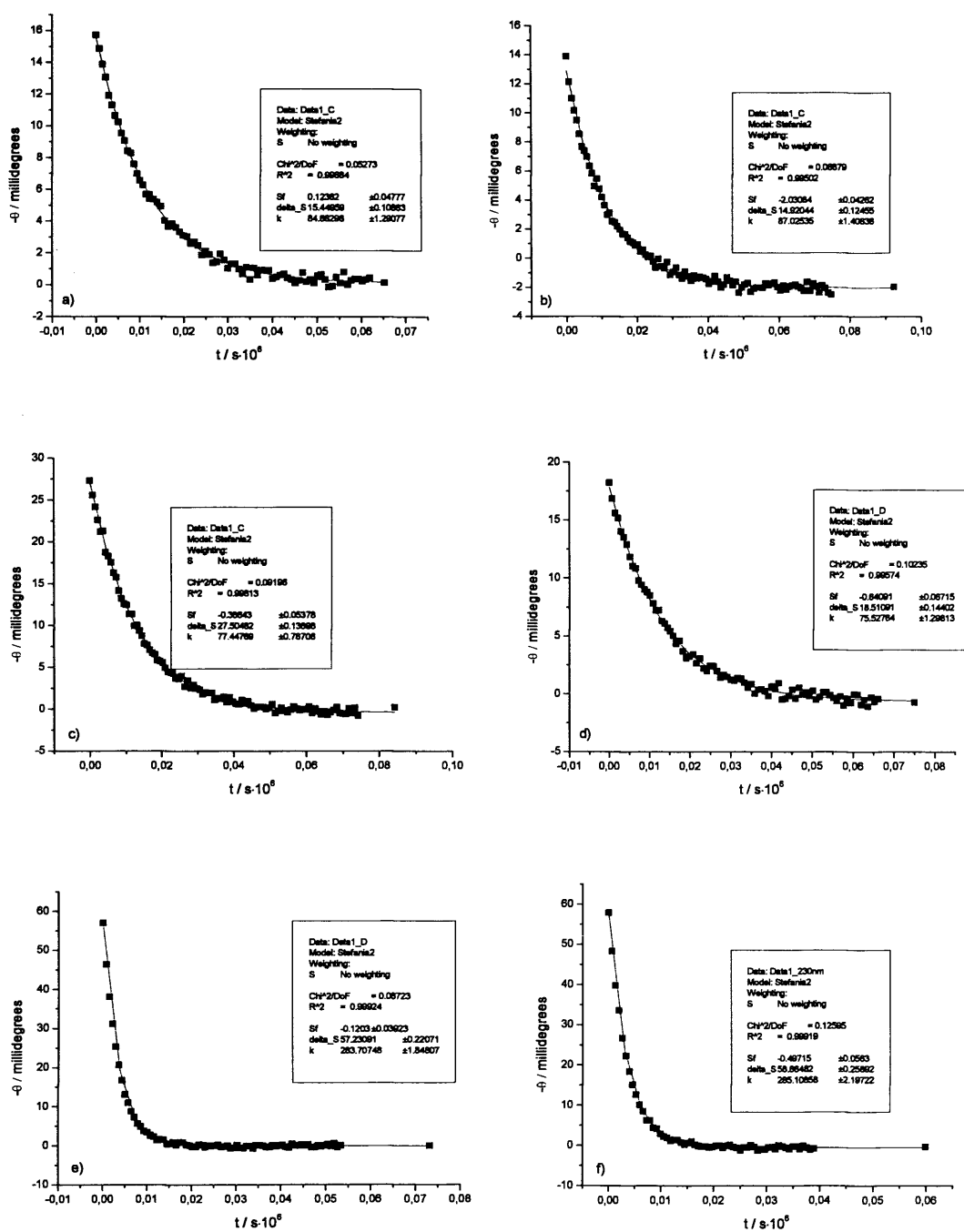


Figure S1.15: racemisation of (*S*)-5-d-5-benzylhydantoin **2.1b** in D₂O phosphate buffers, pH^{**} 7.2, 0.5 M, 1M I (a) and b)) and H₂O phosphate buffers, pH^{25 °C} 7.2, 0.5 M, 1M I (c) and d)) and racemisation of (*S*)-5-benzylhydantoin **2.1** in H₂O phosphate buffer, pH^{25 °C} 7.2, 0.5 M, 1M I, at 60 °C (e), f)). The CD signals of **2.1b** at 235 nm (a), c), d)), or 230 nm (b)) and the CD signals of **2.1** at 230 nm (e), f)) are plotted as a function of reaction time. The squares (■) are the experimental points, the solid lines are the fits to first-order kinetics.

A.1.14 Kinetic data used for the construction of the Brønsted plot for racemisation of 2.2.

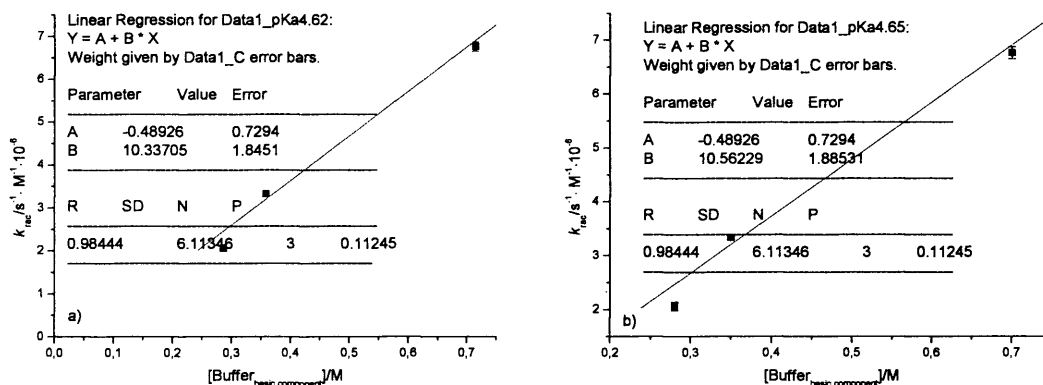


Figure S1.16 : rate constants of racemisation of 2.2, in H_2O acetate buffers, $\text{pH}^{25^\circ\text{C}} 5.0$, 1 M I, at 60°C plotted as a function of basic buffer component considering values of pK_a of a) 4.62 and b) 4.65.

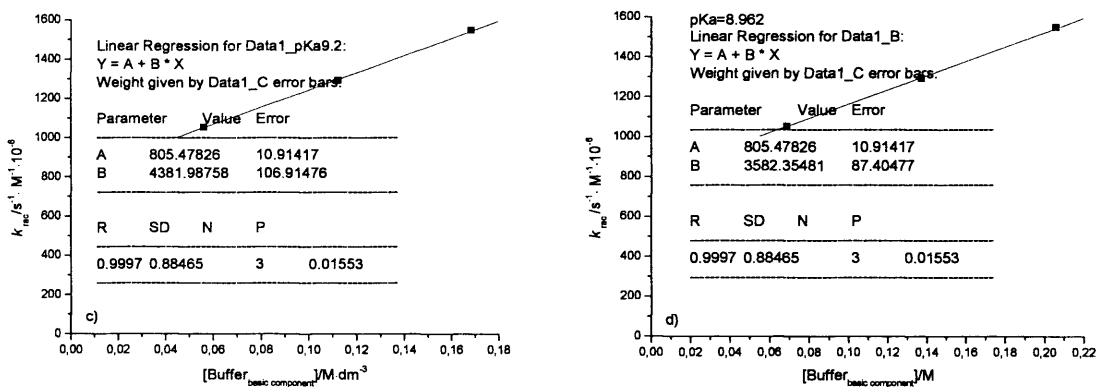


Figure S1.17 : rate constants of racemisation of 2.2, in H_2O phosphate buffers, $\text{pH}^{25^\circ\text{C}} 9.3$, 1 M I, at 60°C plotted as a function of basic buffer component considering values of pK_a of c) 9.2 and d) 8.962.

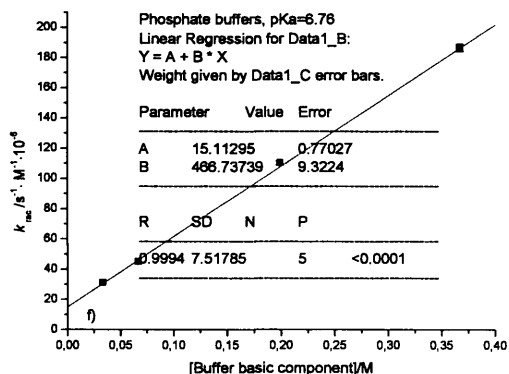
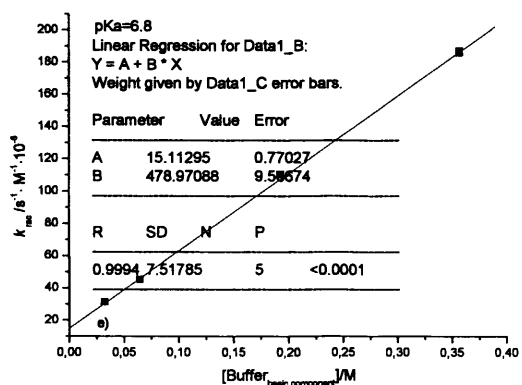


Figure S1.18 : rate constants of racemisation of **2.2**, in at D₂O phosphate buffers, pH** 7.2, 1 M I, at 60 °C plotted as a function of basic buffer component considering values of pK_a of e) 6.8 and f) 6.76.

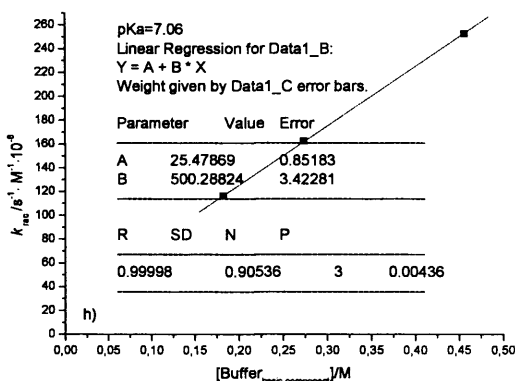
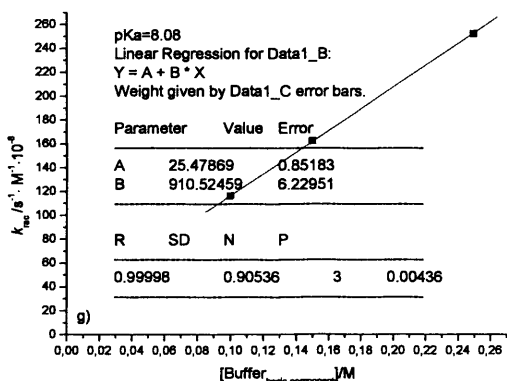


Figure S1.19 : rate constants of racemisation of **2.2**, in at H₂O TRIS buffers, pH^{25 °C} 8.1, 1 M I, at 60 °C plotted as a function of basic buffer component considering values of pK_a of g) 8.08 and h) 7.06.

A1.15. Primary kinetic isotope effects

For a kinetic isotope effect to be big and therefore easily detectable, a significant difference of zero point energies between reactants and transition state should be present while passing from a not labelled substrate, where a C-H bond is broken, to a labelled one, where a C-D bond is broken. In a situation of a proton transfer as described in **Scheme 2.2**, the important vibrational mode, that should contribute to a hypothetical primary isotope effect, is the symmetric stretch that forms at the transition state. For a

reaction such as racemisation of benzylhydantoins, with a transition state where the proton is halfway between the base and the hydantoin, the frequencies of the symmetric stretch in the activated complex, centred around the exchangeable proton, should display very little dependence upon the nature of the isotope. On the other end a significant difference in vibrational frequencies of stretching between deuterated and not deuterated reactants are expected. In practice, the molecule should “travel” along the reaction coordinate, from a “steep” to a “shallow” potential energy well on the energy surface. Significant primary kinetic isotope effects are expected in the described situation.¹

A1.16. Conversion factors for pH and p*K*_a in H₂O and D₂O

Typically the concentration of deuterons in a D₂O solution (pD) is correlated to the more familiar pH through the simple relation shown in **Equation S1.2**.^{2,3}

$$pD = pH + 0.4 \qquad \text{Equation S 1.2}$$

The p*K*_a value of phosphate in D₂O is, similarly, shifted by a factor of 0.5 as compared to the value in H₂O. The traditional conversion from p*K*_a (D) to p*K*_a (H) is shown in **Equation S1.3**.⁴

$$pKa(D) = pKa(H) + 0.5 \qquad \text{Equation S 1.3}$$

The two corrections described above essentially cancel out. On the other end, the molar ratio between protonated and deprotonated forms of **2.1** in solution are similarly affected by the shift in p*K*_a of **2.1** in D₂O as compared to H₂O. This p*K*_a shift turns into a slightly higher concentration of deprotonated form of **2.1** in H₂O as compared to D₂O.

A.1.17. Derivation of Equation 2.6

$$\frac{dA}{dt} = -k_1 A \qquad A = A_0 \cdot e^{-k_1 t}$$

$$\frac{dB}{dt} = k_1 A_0 \cdot e^{-k_1 t} - k_2 B + k_2 C \qquad 1$$

$$A_0 = A + B + C \qquad C = A_0 - A - B = A_0 - A_0 \cdot e^{-k_1 t} - B \qquad 2$$

By substituting 2 in 1

$$\frac{dB}{dt} = k_1 A_0 \cdot e^{-k_1 t} - k_2 B + k_2 A_0 - A_0 \cdot k_2 \cdot e^{-k_1 t} - k_2 B$$

$$\frac{dB}{dt} = A_0 (k_1 - k_2) \cdot e^{-k_1 t} - (k_2 + k_2) \cdot B + k_2 A_0$$

$$\frac{dB}{dt} + (k_2 + k_2) \cdot B = A_0 (k_1 - k_2) \cdot e^{-k_1 t} + k_2 A_0$$

$$\frac{dB}{dt} + (k_2 + k_2) \cdot \left[B - \frac{k_2 \cdot A_0}{k_2 + k_2} \right] = A_0 (k_1 - k_2) \cdot e^{-k_1 t}$$

This equation has the form of the inhomogeneous **Equation S1.4**

$$\frac{dy}{dt} + (k_2 + k_2) \cdot y = A_0 (k_1 + k_2) \cdot e^{-k_1 t} \qquad \text{Equation S1.4}$$

where $y = B - \frac{k_2 A_0}{k_2 + k_2}$ and $\frac{dy}{dt} = \frac{dB}{dt}$

General solution of **Equation S 1.4** is

$$y = \alpha \cdot e^{-k_1 t} + \beta \cdot e^{-(k_2 + k_2) \cdot t} \text{ where } \alpha, \beta \text{ are constants}$$

$$\alpha = \frac{A_0 (k_1 - k_2)}{k_2 + k_2 - k_1}$$

At $t = 0$ $B_0 = 0$

$$y_0 = -\frac{k_2 \cdot A_0}{k_2 + k_2} = \frac{A_0 (k_1 - k_2)}{k_2 + k_2 - k_1} \cdot e^{-k_1 t} + \beta \cdot e^{-(k_2 + k_2) \cdot t}$$

For $t = 0$

$$y_0 = -\frac{k_2 \cdot A_0}{k_2 + k_2} = \frac{A_0(k_1 - k_2)}{k_2 + k_2 - k_1} + \beta$$

$$\beta = -A_0 \cdot \left(\frac{k_2}{k_2 + k_2} + \frac{k_1 - k_2}{k_2 + k_2 - k_1} \right) \text{ or } \beta = -A_0 \cdot \left[\frac{k_1 k_2}{(k_2 + k_2) \cdot (k_2 + k_2 - k_1)} \right]$$

$$B = y + \frac{k_2 \cdot A_0}{k_2 + k_2} = \frac{A_0(k_1 - k_2)}{k_2 + k_2 - k_1} \cdot e^{-k_1 t} - \frac{A_0 k_1 k_2}{(k_2 + k_2) \cdot (k_2 + k_2 - k_1)} \cdot e^{-(k_2 + k_2) \cdot t} + \frac{k_2 \cdot A_0}{k_2 + k_2}$$

$A_0 = A + B + C$ so $A + C = A_0 - B$, by subtracting B from each term and by substitution, the analytical expression of $A + C - B$, proportional to the CD signal, is obtained:

$$\begin{aligned} A + C - B &= A_0 - B - B = A_0 - 2B = \\ &= A_0 \cdot \left\{ -2 \cdot \left[\frac{k_1 - k_2}{k_2 + k_2 - k_1} \cdot e^{-k_1 t} - \frac{k_1 k_2}{(k_2 + k_2)(k_2 + k_2 - k_1)} \cdot e^{-(k_2 + k_2) \cdot t} + \frac{k_2 \cdot A_0}{k_2 + k_2} \right] \right\} \end{aligned}$$

Since $k_2 = k_2$ we can simplify the expression to

$$A - B + C = A_0 \cdot \left\{ -\frac{2}{2k_2 - k_1} \left[(k_1 - k_2) \cdot e^{-k_1 t} - \frac{k_1}{2} \cdot e^{-2k_2 t} \right] \right\} \quad \text{Equation 2.6}$$

A1.18. Example of fit of simulated data to Equation 2.6

Equation 2.6 fits well the simulated ECD signal and accurately reproduces the k_2/k_1 ratio. Figure S1.20 shows an example of fit where k_2/k_1 has been set to be 0.7. The obtained fitted value for k_2/k_1 is 0.6975

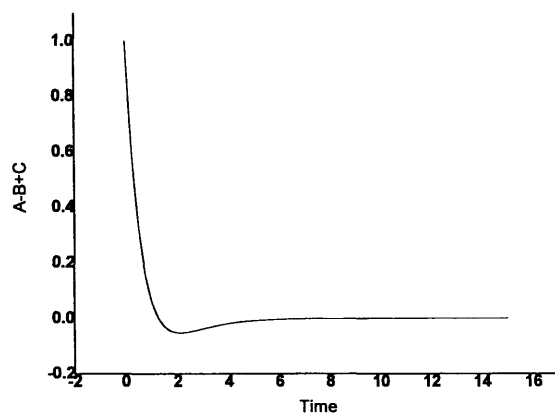


Figure S1.20: fit of the simulated ECD signal for $k_2/k_1=0.7$ to Equation 2.6.

A1.19. Examples of simulated CD signals for hypothetical S_E2 racemisation of generic molecules in deuterated media, assuming values for the ratio k_2/k_1 close to unity

Simulations in **Figure S1.21** show that, for values of the ratio of rate constants k_2 and k_1 near unity, the resulting temporary enantiomeric excess of the species B (**Scheme 2.2**) is expected to be small and, therefore hardly experimentally detectable by ECD.

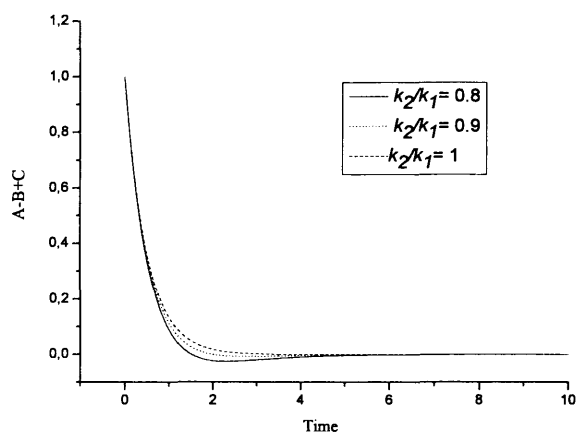


Figure S1.21: expected ECD signal plotted as a function of time in a simulated racemisation process for different values of the ratio k_2/k_1 . The time scale of the x axis is in arbitrary units.

A.1.20. Effect of substrate concentration on the rate constants of racemisation of 2.1.

The possible effect of substrate concentration on the rate constants of racemisation of 5-substituted hydantoins was investigated by carrying out racemisation experiments for (S)-5-benzylhydantoin **2.1** in D₂O phosphate buffer 0.5 M, 1 M I, pH** 7.2 at different substrate concentrations (**Figure S1.22**). The observed rate constants of racemisation appeared to be independent on the concentration of **2.1**. The linear fit of the data gave a straight line parallel to the x axis and intercept equal to $(289.2 \pm 1.5) 10^{-6} \text{ s}^{-1}$.

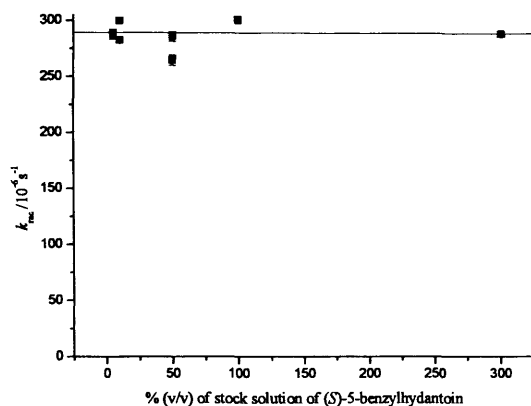


Figure S1.22: rate constants of racemisation of (*S*)-5-benzylhydantoin in D₂O phosphate buffer (0.5 M, 1 M I, pH** 7.2) as a function of substrate concentrations, with substrate concentrations expressed in terms of percent volume of a saturated stock solution of substrate in the reaction mixture, at 60 °C.

A.1.21 Partial ¹H NMR spectra of (*S*)-2-amino-*N*-methyl-3-phenylpropanamide 2.3 in D₂O and CDCl₃

Figure S1.23 shows partial ¹H NMR spectra of 2.3 in CDCl₃ and D₂O. In the latter solvent, the peaks corresponding to the diastereotopic (B and C) protons are not well resolved and a big roof effect is present making it appear as a multiplet. This effect appears to be typical for all amino acid amides and hydantoins described in this thesis. Marked roof effects and poor resolution of the peaks corresponding to the diastereotopic protons are also typically observed in ¹H NMR spectra in d₆-DMSO.

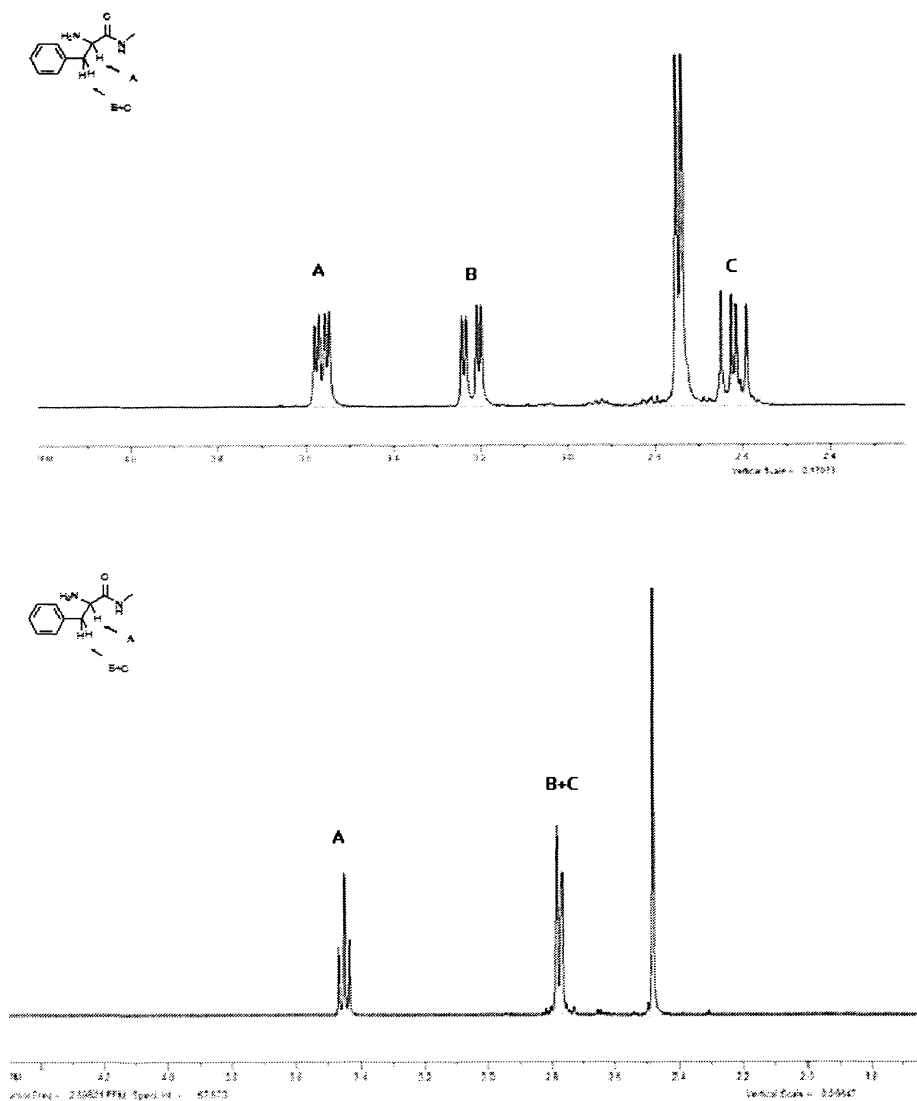


Figure S1.23: partial ¹H NMR spectra of 2.3 in CDCl₃ (top) and in D₂O (bottom)

A.1.22 Kinetic data for racemisation of 2.2 in D₂O phosphate buffers, pH 10.0 not included in the fits described in Chapter 2.**

Rate constants of racemisation of 2.2 in D₂O phosphate buffers at pH**10.0 showed a very poor reproducibility. The results of different kinetic experiments of racemisation are reported in **Figure S1.24**. A big scatter of the data points can be observed.

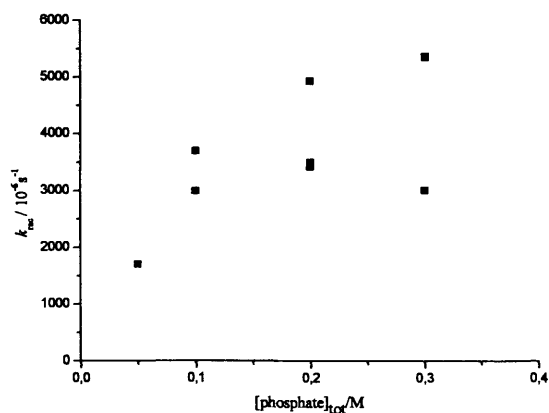


Figure S1.24: rate constants of racemisation of **2.2** as a function of total buffer concentration at pH** 10.0.

Figure S1.25 (a) shows a typical kinetic trace for racemisation of **2.2** in D₂O phosphate buffer 0.2 M, 1 M I, at pH** 10.0 at 60 °C. The UV spectra of **2.2** recorded over time during the same kinetic experiment are shown in **Figure S1.25 (b)**.

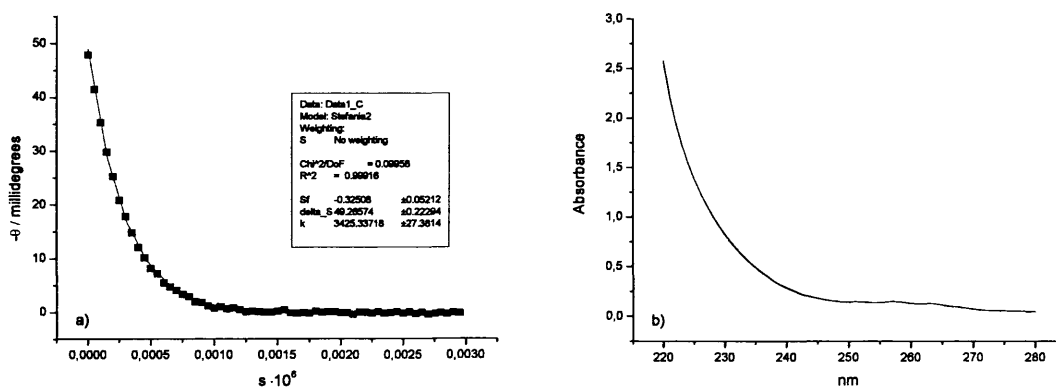


Figure S1.25: racemisation of **2.2** in D₂O phosphate buffers, pH** 10.0, 0.2 M, 1 M I, at 60 °C. **a)** the CD signals of **2.2** is plotted as a function of reaction time. The squares (■) are the experimental points, the solid line is the fit to pseudo-first-order kinetics. **b)** UV spectra of **2.2** recorded over time during the kinetic experiment shown in **a)**.

A.1.23 Estimated concentration of the catalytic species OD⁻ in a D₂O solution of potassium phosphate with pH** 11.0, at 60 °C

The concentration of the catalytic species OD⁻ in a D₂O solution of potassium phosphate with pH** 11.0, at 60 °C was estimated to be 3.5·10⁻³ mol dm⁻³. The value was obtained by assuming a value of 4.19 for $\log\left(\frac{[HPO_4^{2-}]}{[H_2PO_4^-]}\right)$ in D₂O, at 60 °C. The value of 4.19 was

obtained from the Enderson-Hasselback equation, (Equation S1.5) assuming a pK_a of 6.81⁵ for the second ionisation of potassium phosphate at 25 °C, in H₂O and a pH of 11.0. The calculated buffer ratio was assumed to remain the same in D₂O, at 60 °C. Then corrections of the pK_a for the second ionisation of potassium phosphate were introduced to account for the temperature of 60 °C (pK_a=6.76)⁵ and for the medium, D₂O, using Equation S 1.3. The corrected value of pK_a and the approximate value of 4.19 for the buffer ratio were then substituted in the Enderson-Hasselback equation and an approximate value of pD was obtained. From the estimated value of pD and the ionic product of D₂O, at 60 °C ($K_{w(D_2O,60^\circ C)} = 10^{-13.918}$)⁶, the approximate concentration of the species OD⁻ in a D₂O solution of potassium phosphate with pH** 11.0, at 60 °C was calculated, using Equations S1.6 and S1.7.

$$pH = pK_a + \log\left(\frac{[DPO_4^{2-}]}{[D_2PO_4^-]}\right) \quad \text{Equation S1.5}$$

$$pD + pOD = pK_{w(D_2O,60^\circ C)} \quad \text{Equation S1.6}$$

$$pOD = -\log[OD^-] \quad \text{Equation S1.7}$$

References

1. Anslyn, E. V.; Dougherty, D. A., *Modern Physical Organic Chemistry*. University Science Books: Sausalito, California, 2006; p 421.
2. Glasoe, P. K.; Long, F. A., *Journal of Physical Chemistry* **1960**, *64* (1), 188-190.
3. Li, N. C.; Tang, P.; Mathur, R., *Journal of Physical Chemistry* **1961**, *65* (6), 1074-1076.
4. Glasoe, P. K.; Ebersson, L., *Journal of Physical Chemistry* **1964**, *68* (6), 1560-1562.
5. pK_a s for phosphate from Fukada, H.; Takahashi, K., *Proteins-Structure Function and Genetics* 1998, *33* (2), 159-166
6. K_w for D_2O at 60 °C from "Handbook of Chemistry and Physics", 74th edition, 1993 1994, CRC Press, David R. Lide Editor-in-Chief, p.8-48

Appendix 2

This Appendix is for Chapter 3

**The effect of structural modifications on the kinetics
and mechanism of racemisation of 5-substituted
hydantoins.**

A2.1.: Kinetic traces for racemisation of hydantoin 3.2 in D₂O phosphate buffers, pH** 7.2

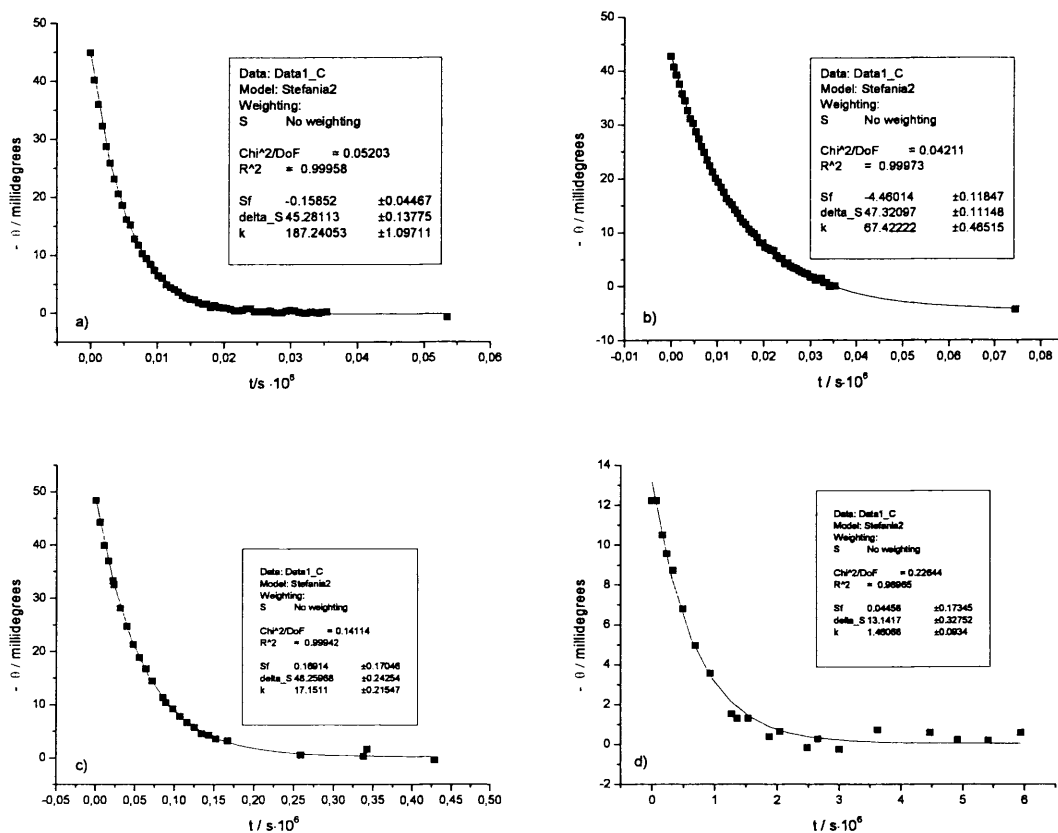


Figure S2.1a-d: racemisation of 3.2 in D₂O phosphate buffer, pH** 7.2, 0.5 M, 1M *I* a) at 60 °C, b) at 50 °C, c) at 37 °C, c) at 15 °C. The CD signals of 3.2 at 235 nm (a) - c)) or 240 nm (d)) are plotted as a function of reaction time. The squares (■) are the experimental data points, the solid lines are the fits to pseudo first-order kinetics.

A2.2.: Kinetic traces for racemisation of hydantoin 3.3 in D₂O phosphate buffers, pH** 7.2

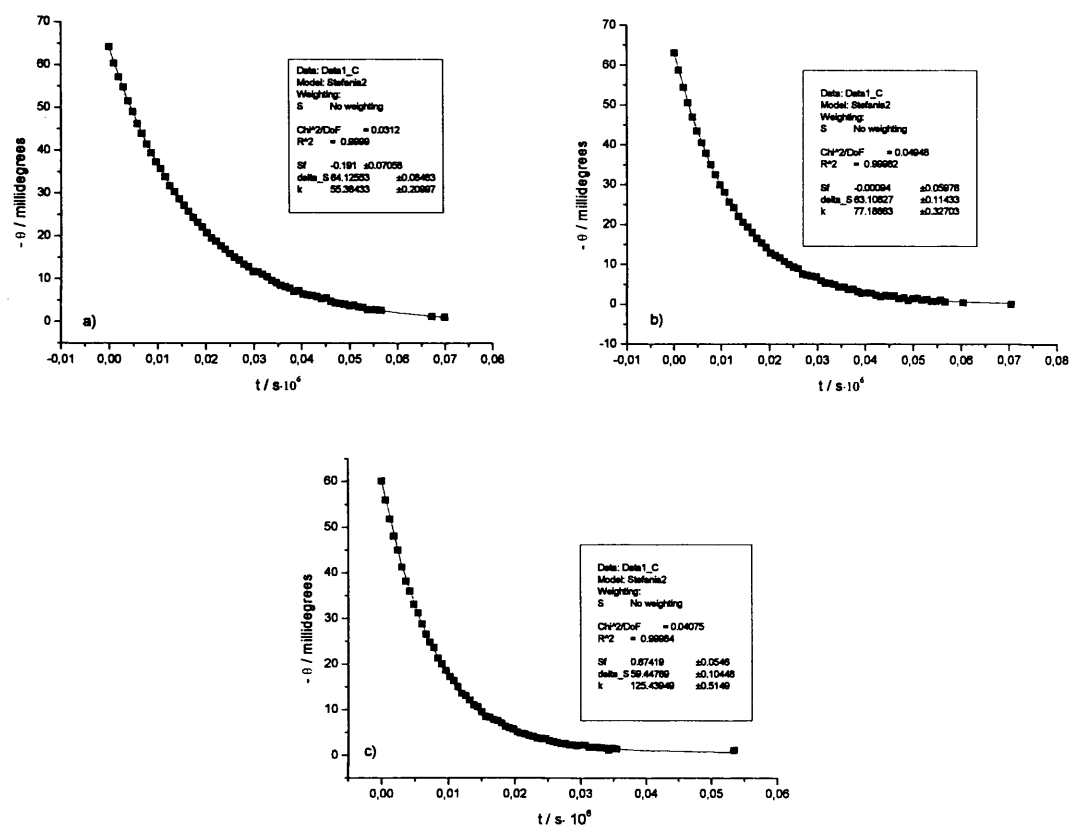


Figure S2.2a-c: racemisation of 3.3, at 60 °C in D₂O phosphate buffers, pH** 7.2, 1M / a) 0.2 M, b) 0.3 M, c) 0.5 M. The CD signals of 3.3 at 235 nm are plotted as a function of reaction time. The squares (■) are the experimental data points, the solid lines are the fits to pseudo first-order kinetics.

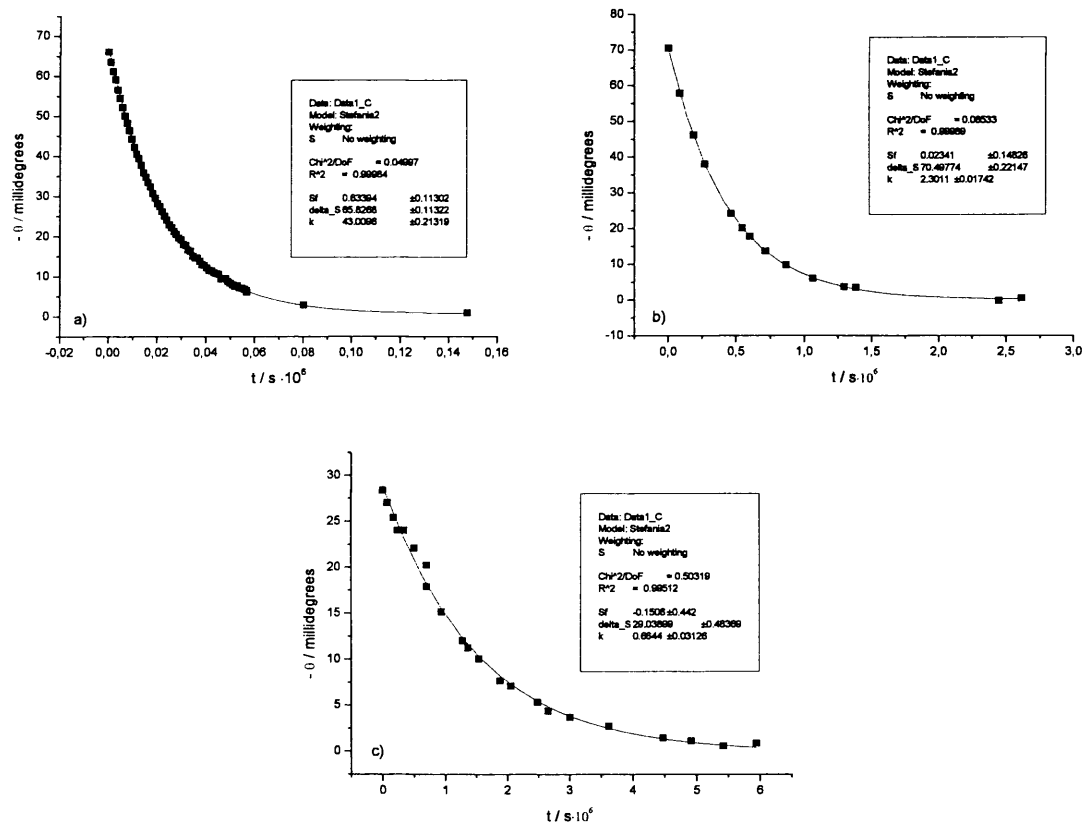


Figure S2.3a-c: racemisation of 3.3 in D₂O phosphate buffer, pH** 7.2, 0.5 M, 1M *I* a) at 50 °C, b) at 22.5 °C, c) at 15 °C. The CD signals of 3.3 at 235 nm (a), b)) or 240 nm (c)) are plotted as a function of reaction time. The squares (■) are the experimental data points, the solid lines are the fits to pseudo first-order kinetics.

A2.3.: Kinetic traces for racemisation of hydantoin 3.4 in D₂O phosphate buffers, pH 6.0, at 60 °C**

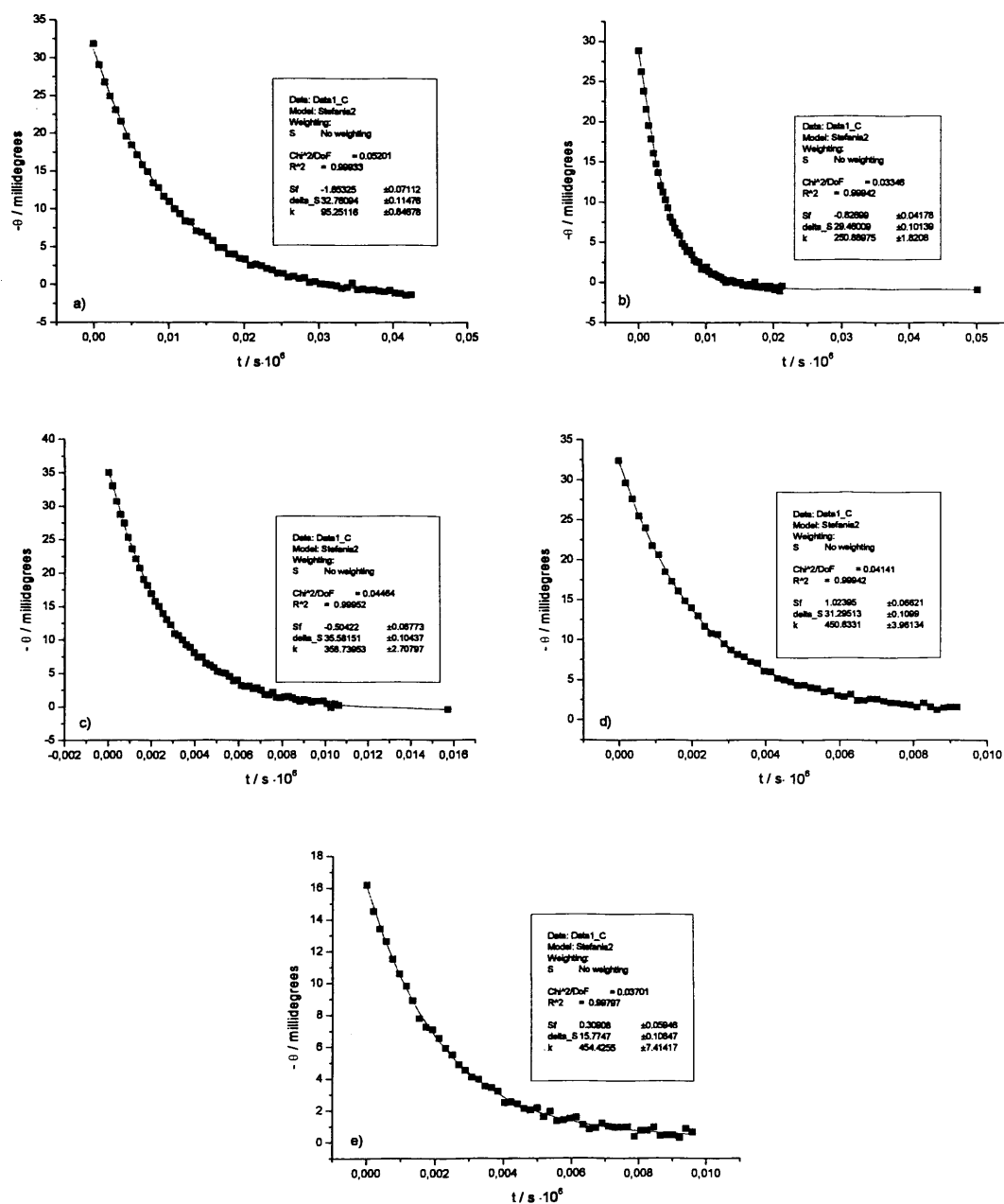
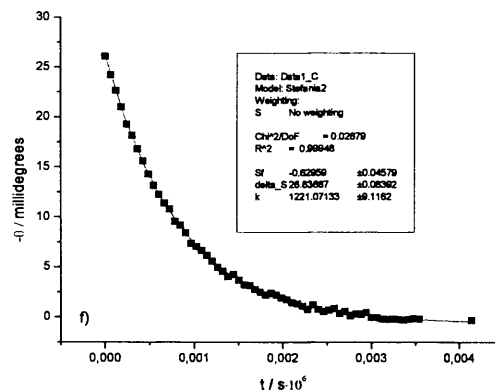
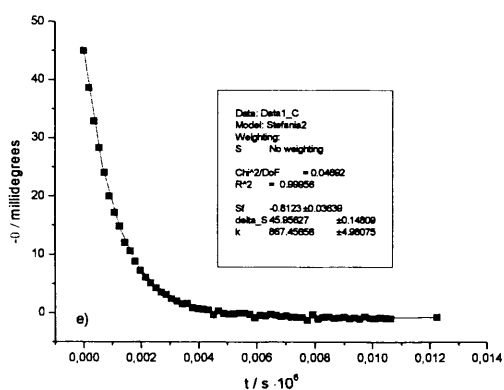
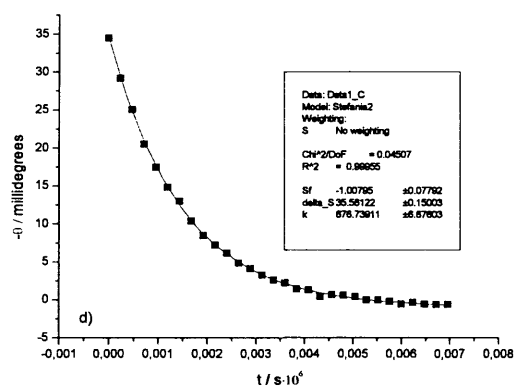
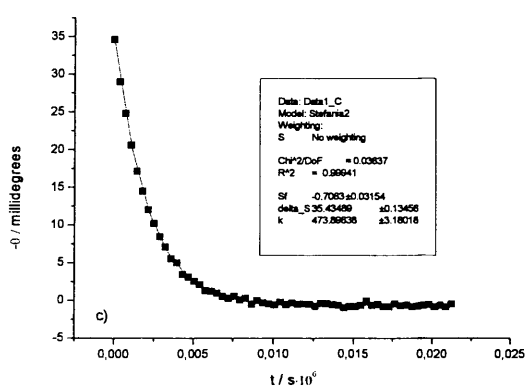
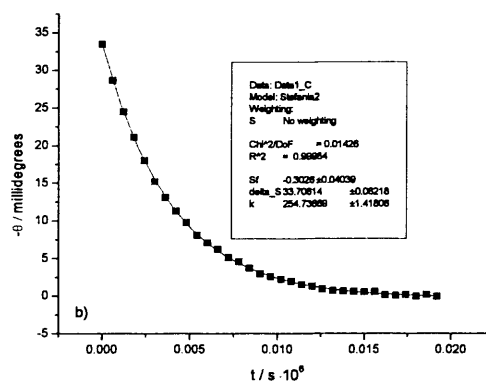
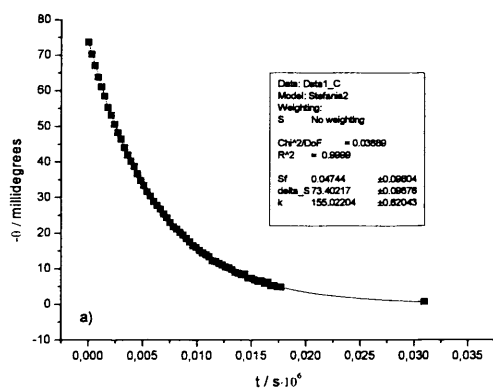


Figure S2.4a-e: racemisation of 3.4, at 60 °C in D₂O phosphate buffers, pH** 6.0, 1M / a) 0.1 M b) 0.3 M c) 0.5 M, c), d) 0.7 M. The CD signals of 3.4 at 235 nm are plotted as a function of reaction time. The squares (■) are the experimental data points, the solid lines are the fits to pseudo first-order kinetics.

A2.4.: Kinetic traces for racemisation of hydantoin 3.4 in D₂O phosphate buffers, pH** 7.2, at 60 °C



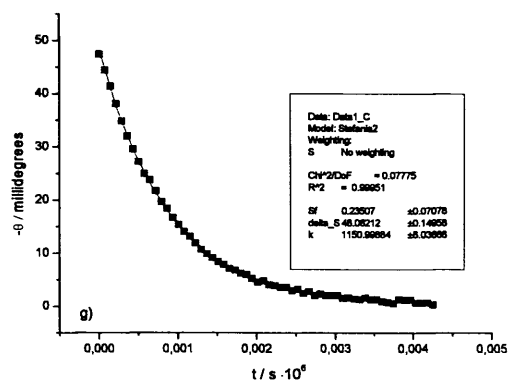
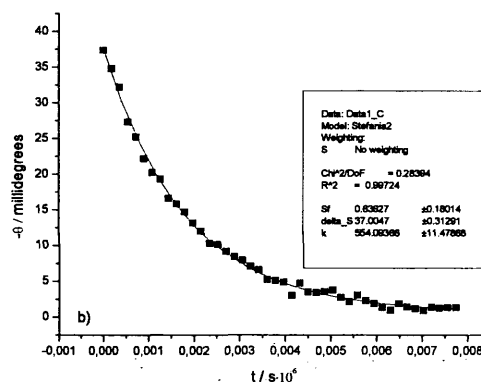
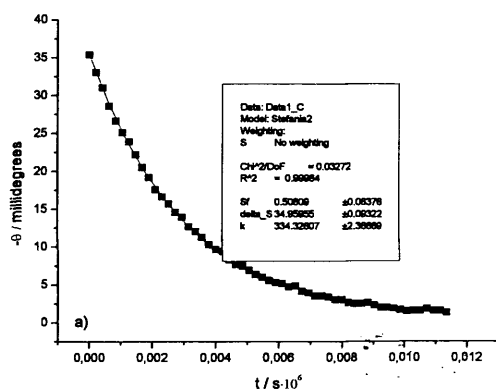


Figure S2.5a-g: racemisation of 3.4, at 60 °C in D₂O phosphate buffers, pH** 7.2, 1M I a) 0.048 M, b) 0.1 M, c) 0.2 M, d) 0.3 M, e) 0.4 M, f), g) 0.5 M. The CD signals of 3.4 at 235 nm are plotted as a function of reaction time. The squares (■) are the experimental data points, the solid lines are the fits to pseudo first-order kinetics.

A2.5.: Kinetic traces for racemisation of hydantoin 3.4 in D₂O phosphate buffers, pH 8.0, at 60 °C**



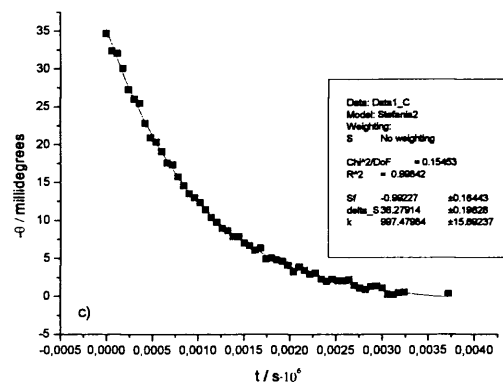
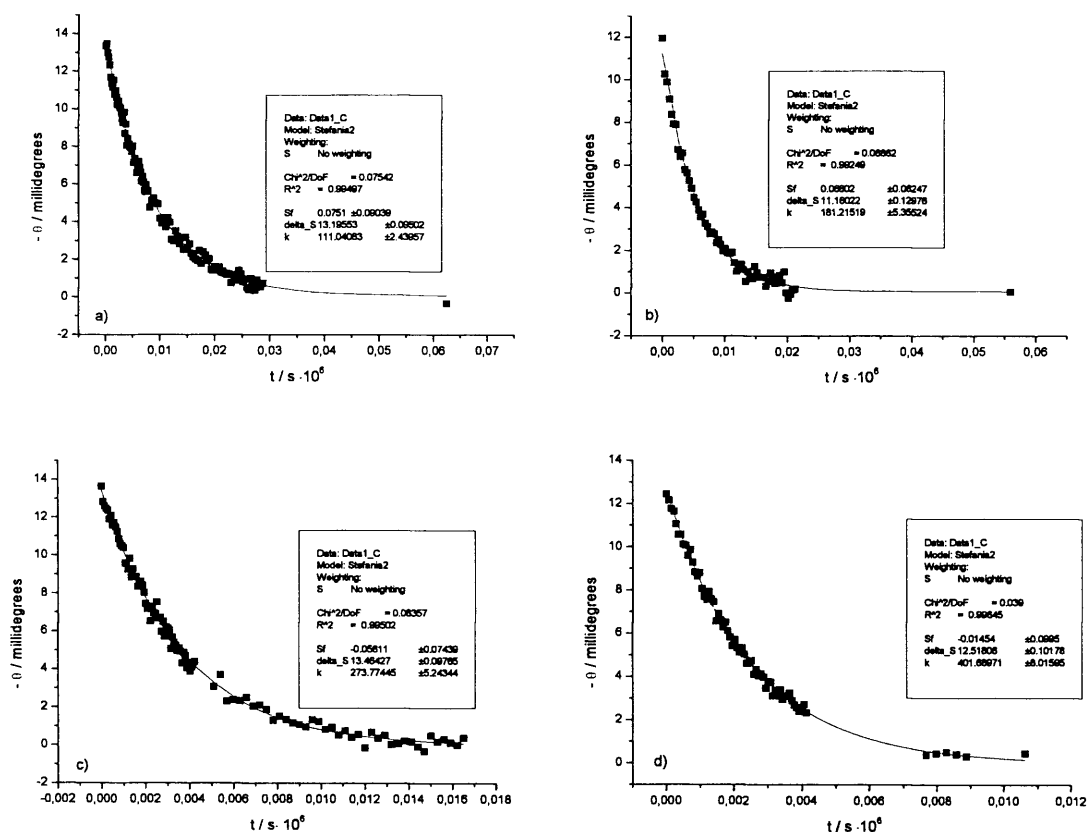


Figure S2.6a-c: racemisation of 3.4, at 60 °C in D₂O phosphate buffers, pH** 8.0, 1M / a) 0.1 M, b) 0.2 M, c) 0.35 M. The CD signals of 3.4 at 235 nm are plotted as a function of reaction time. The squares (■) are the experimental data points, the solid lines are the fits to pseudo first-order kinetics.

A2.6.: Kinetic traces for racemisation of hydantoin 3.5 in D₂O phosphate buffers, pH 7.2.**



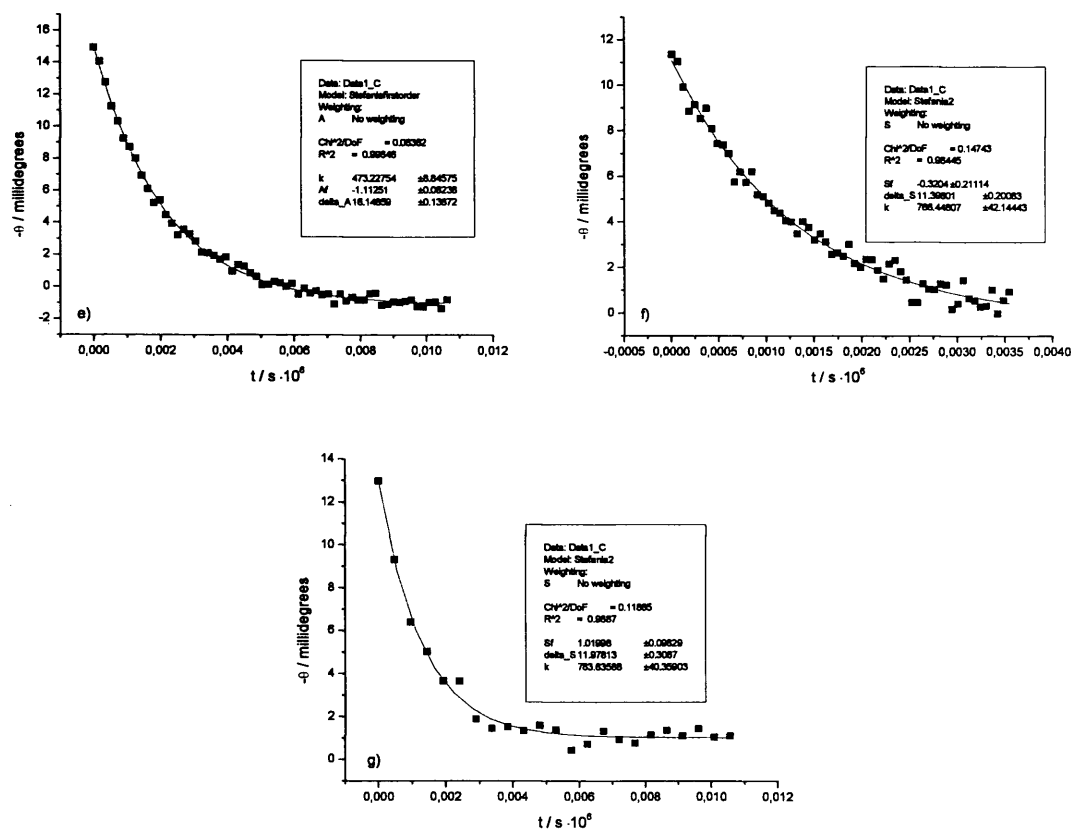


Figure S2.7a-g: racemisation of 3.5, at 60 °C in D₂O phosphate buffers, pH** 7.2, 1M I a) 0.049 M, b) 0.1 M, c) 0.2 M, d) 0.3 M, e) 0.4 M, f), g) 0.5 M. The CD signals of 3.5 at 240 nm are plotted as a function of reaction time. The squares (■) are the experimental data data points, the solid lines are the fits to pseudo first-order kinetics.

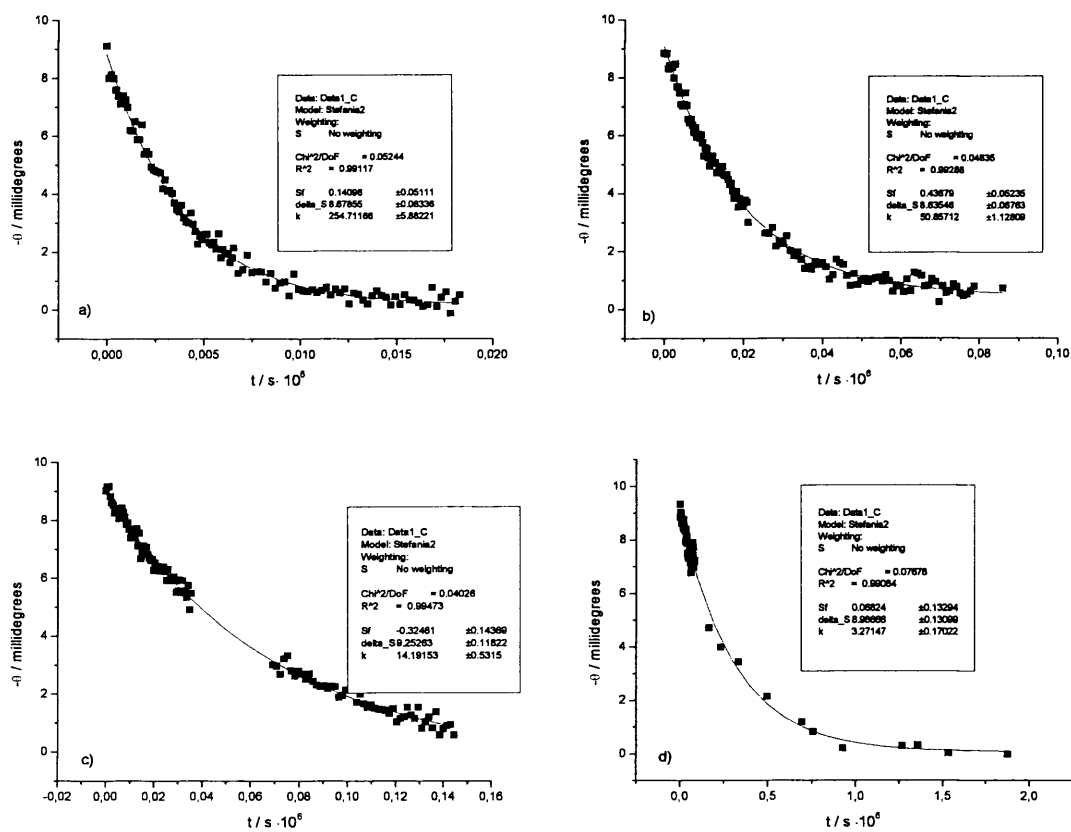
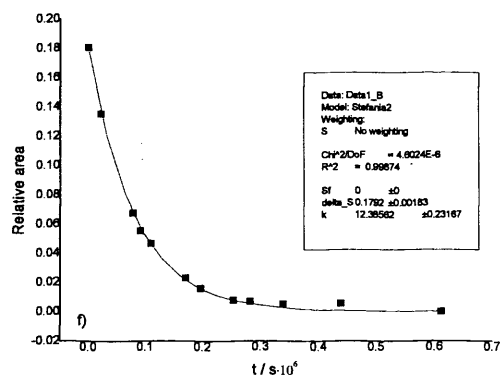
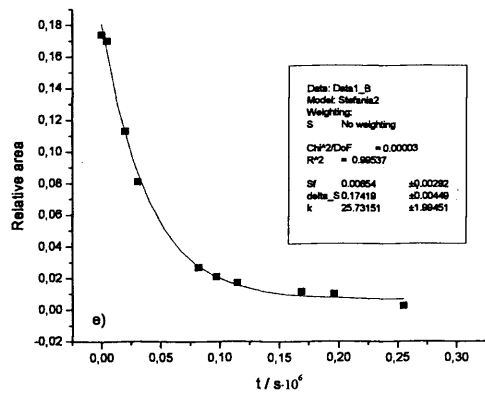
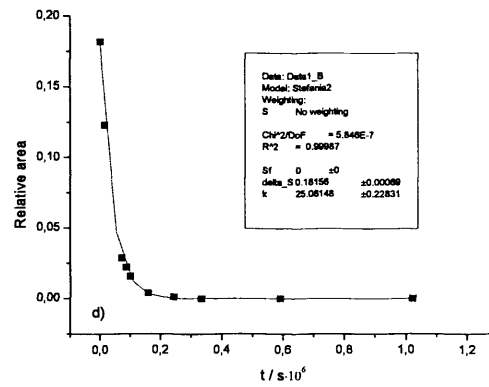
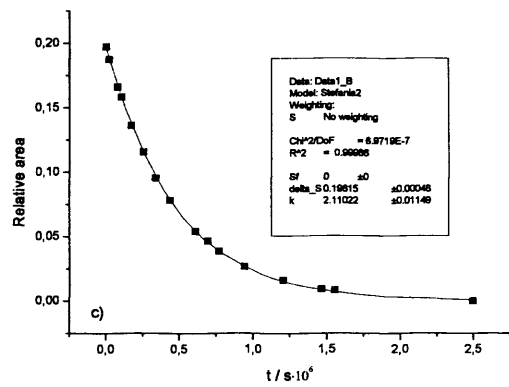
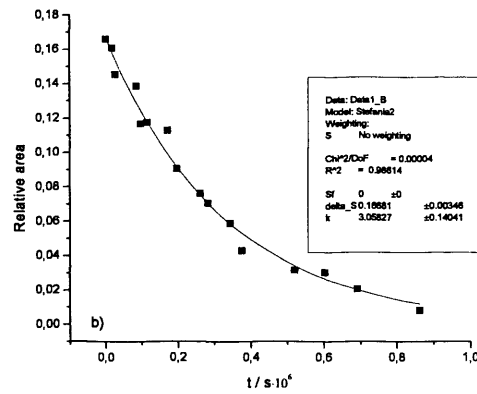
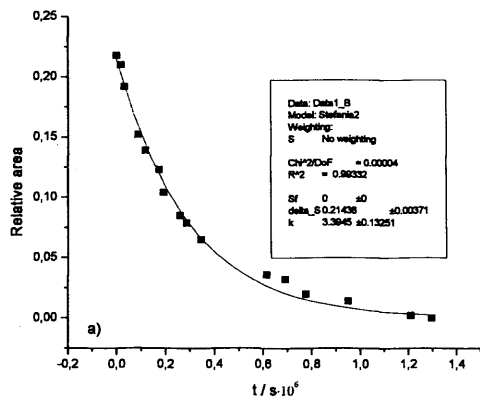


Figure S2.8a-d: racemisation of 3.5 in D₂O phosphate buffer, pH** 7.2, 0.5 M, 1M *I* a) at 50 °C, b) at 37 °C, c) 25 °C, d) 15 °C. The CD signals of 3.5 at 240 are plotted as a function of reaction time. The squares (■) are the experimental data points, the solid lines are the fits to pseudo first-order kinetics.

A2.7.: Kinetic traces for H/D exchange of 3-, 5-substituted hydantoin in D₂O phosphate buffer, pH* 7.2, 0.5 M, 1M I, at 25 °C.



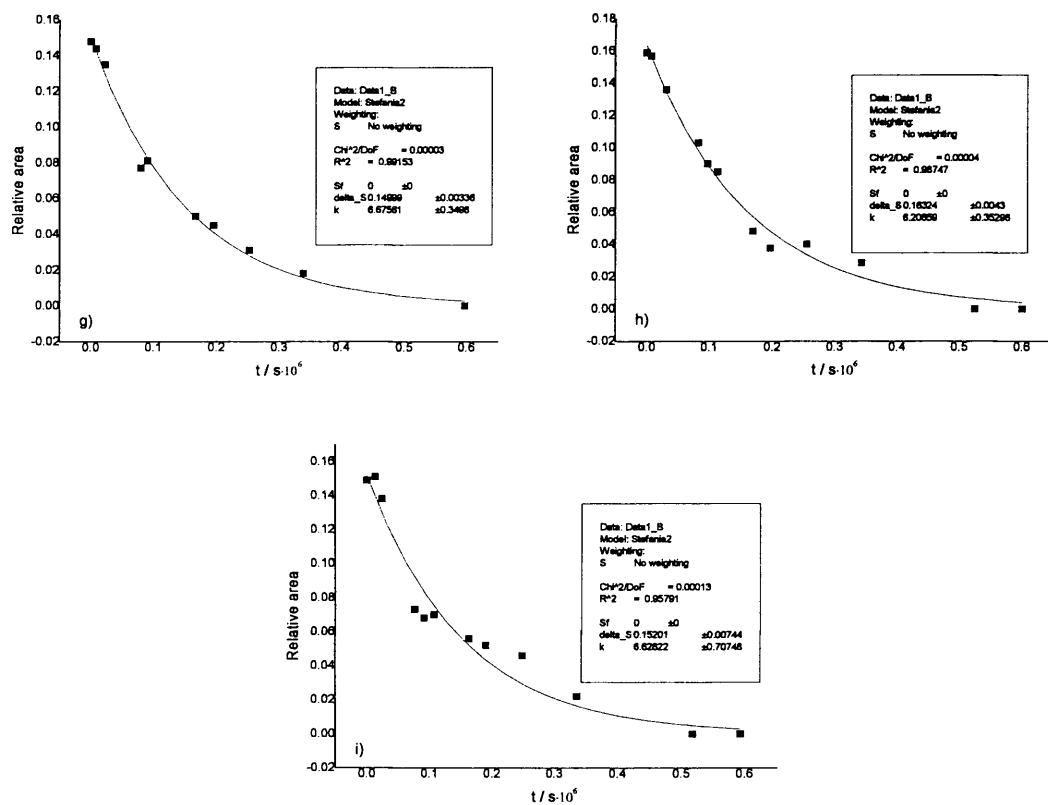


Figure S2.9a-i: H/D exchange of hydantoin a), b) 3.2, c) 3.3, d), e) 3.4, f) 3.5, g)-i) 3.10 at 25°C in D₂O phosphate buffer, pH* 7.2, 0.5 M, 1M *I*. The relative area integral of the peaks of the asymmetric protons in the ^1H NMR spectra of the hydantoin are plotted as a function of time. The squares (■) are the experimental data points, the solid lines are the fits to pseudo first-order kinetics.

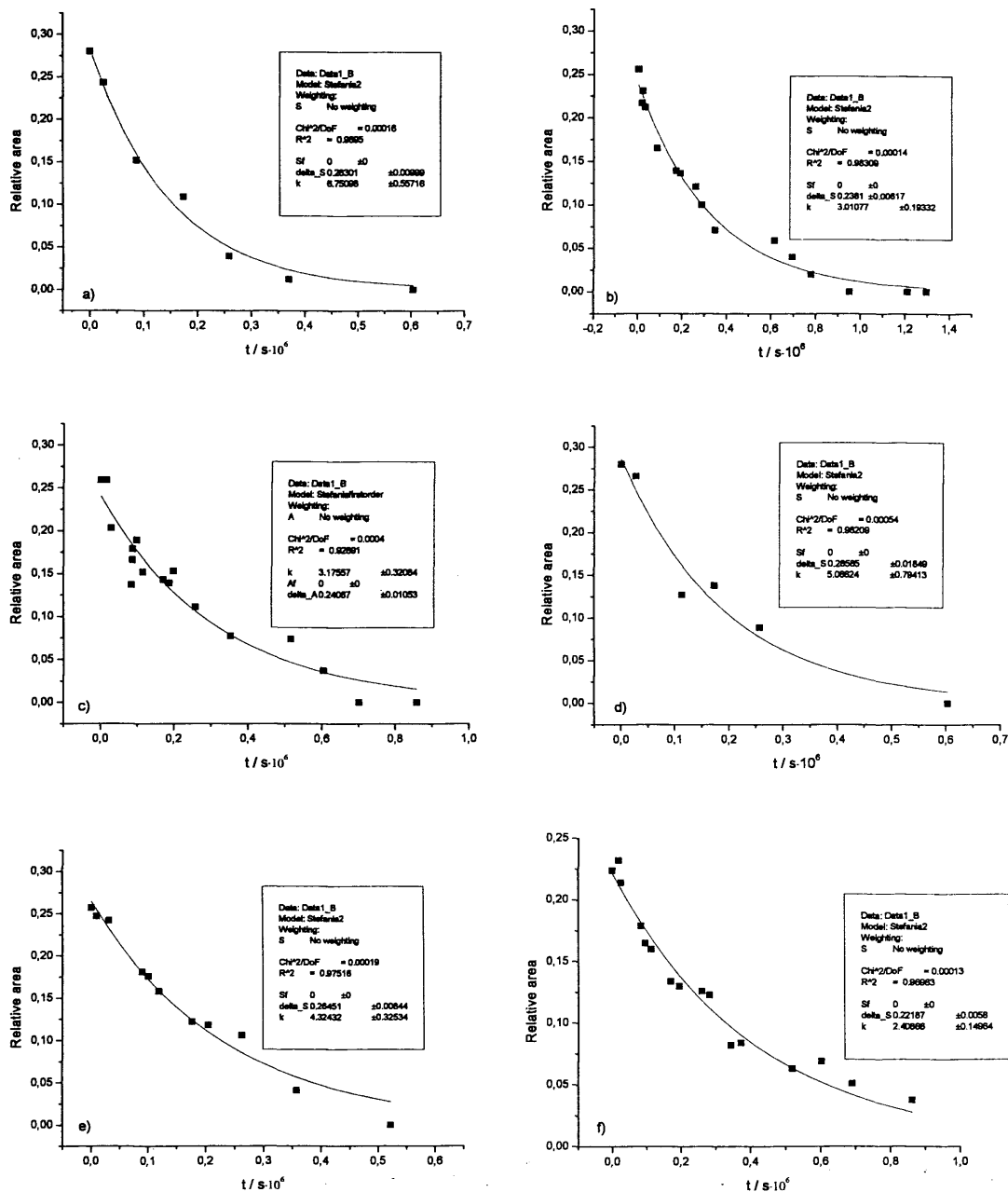


Figure S2.10 a-f: H/D exchange of hydantoin a) 3.17 b), c) 3.18, d), e) 3.19 d), f) 3.20 at 25°C in D₂O phosphate buffer, pH* 7.2, 0.5 M, 1M *I*. The relative area integral of the peaks of the asymmetric protons in the ¹H NMR spectra of the hydantoin are plotted as a function of time. The squares (■) are the experimental data points, the solid lines are the fits to pseudo first-order kinetics.

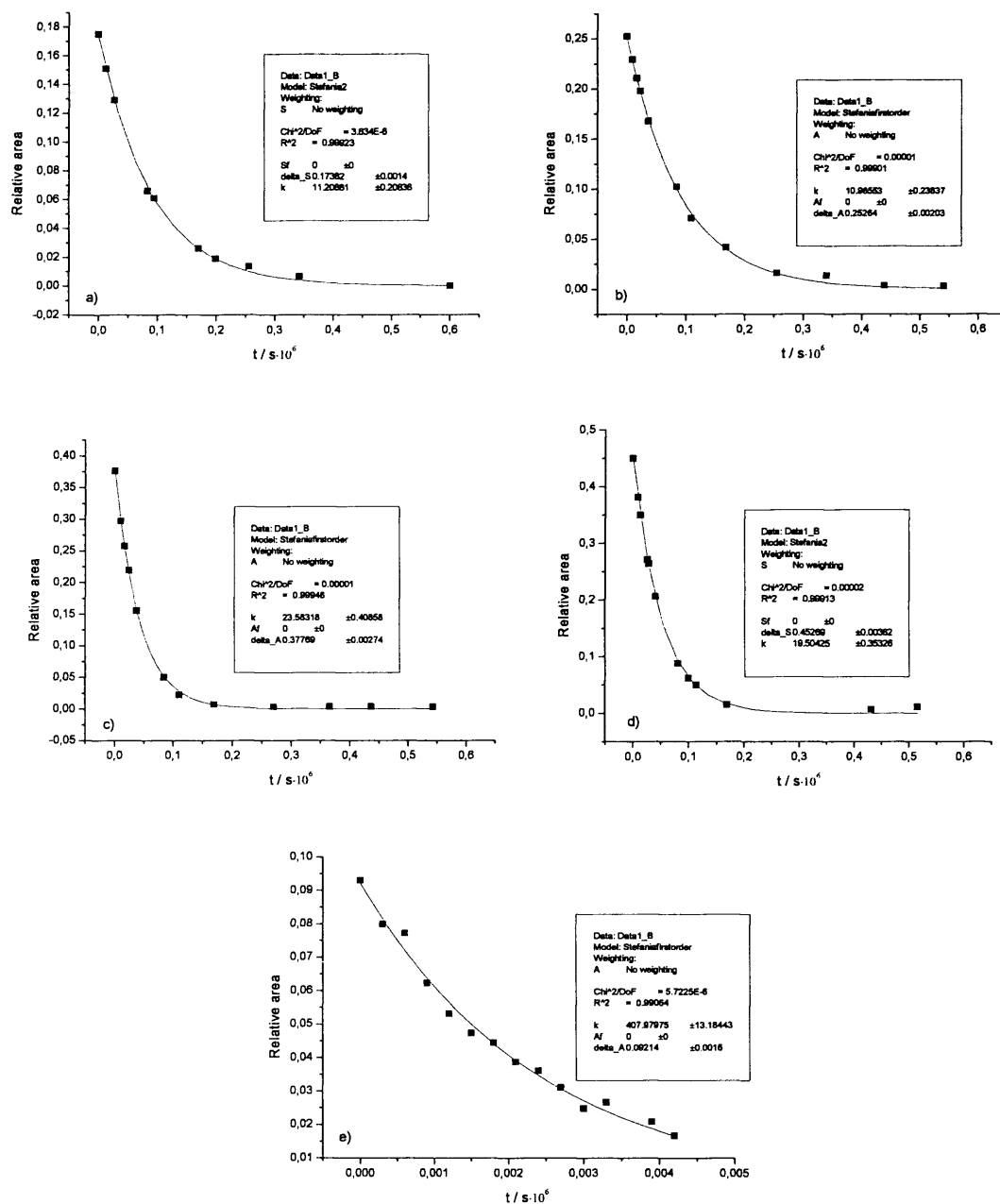
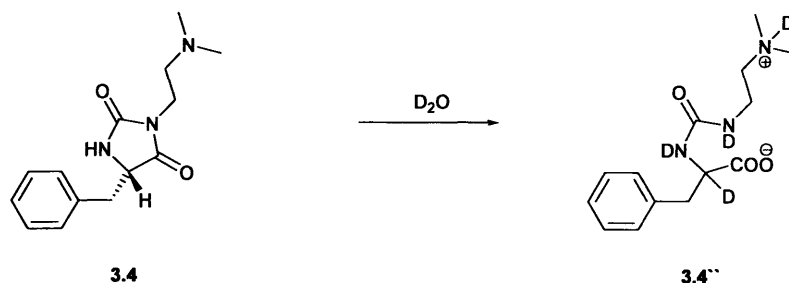


Figure S2.11 a-e: H/D exchange of hydantoin a), b) 3.21 c), d) 3.22, e) 3.23 at 25°C in D₂O phosphate buffer, pH* 7.2, 0.5 M, 1M I. The relative area integral of the peaks of the asymmetric protons in the ¹H NMR spectra of the hydantoin is plotted as a function of time. The squares (■) are the experimental data points, the solid lines are the fits to pseudo first-order kinetics.

A2.8.: Assignment of the signals in the ^1H NMR spectrum of a D_2O solution of partially hydrolysed hydantoin **3.4 (spectrum recorded at $t=6$ days, shown in Figure 3.4)**



Scheme S2.1: hydrolysis of hydantoin **3.4** in D_2O

^1H NMR (400 MHz, D_2O): δ 7.21-7.00 (m, 5H, C_6H_5 of exchanged **3.4** + 5H, C_6H_5 of **3.4''**), δ 3.27-3.06 (m, 2H, $\text{CONCH}_2\text{CH}_2$ of exchanged **3.4** + 2H $\text{CONDCH}_2\text{CH}_2$ of **3.4''**), δ 2.98 (d, $J=14.1$, 1H $\text{CH}_\text{A}\text{H}_\text{B}\text{CD}$) of exchanged **3.4** + d, $J=14.1$, 1H $\text{CH}_\text{A}\text{H}_\text{B}\text{CD}$ of **3.4''**), δ 2.93 (d, $J=14.3$, 1H, $\text{CH}_\text{A}\text{H}_\text{B}\text{CD}$ of exchanged **3.4**), δ 2.81 (t, $J=5.9$ Hz, 2H, $\text{CH}_2\text{ND}(\text{CH}_3)_2$ of **3.4''**), δ 2.67 (d, $J=14.0$, 1H, $\text{CH}_\text{A}\text{H}_\text{B}\text{CH}$ of **3.4''**), $\delta=2.53$ (s, 6H, $\text{N}(\text{CH}_3)_2$ of **3.4''**), 2.00 (s, 6H, $\text{N}(\text{CH}_3)_2$ of exchanged **3.4**), δ 1.98-1.80 (m, 2H, $\text{CH}_2\text{N}(\text{CH}_3)_2$ of exchanged **3.4**).

A2.9.: Attempted titration of hydantoin **3.4 by means of ^1H NMR spectroscopy.**

Figure S2.12 shows the attempted titration of **3.4**, by means of ^1H NMR spectroscopy. The NMR tubes were prepared by mixing equal volumes of D_2O phosphate buffers 0.2 M, 1M *I* with different pH^* values and a saturated stock solution of **3.4** in D_2O . The final pH^* of the solution was measured by means of a pH meter equipped with a micro pH probe. The NMR tubes were stored in a water bath at 25 °C for approximately 4 minutes before recording the ^1H NMR spectra. The ^1H NMR spectra were also acquired under conditions of temperature control. The values of the chemical shift of the singlet from the protons of the CH_3 groups of **3.4** (protons 1, in Scheme S2.2) were plotted as a function of the final pH^* of the buffered solutions of hydantoin.

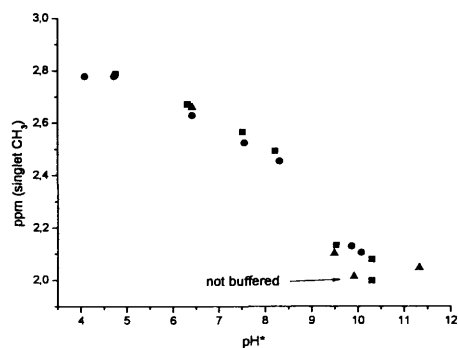
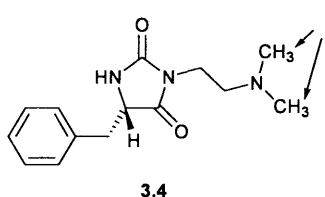


Figure S2.12: attempted titration of **3.4** by means of ^1H NMR spectroscopy. The values of the chemical shift of the singlet from the protons of the CH_3 groups of **3.4** (protons 1, in Scheme S2.2) are plotted as a function of the final pH^* of the buffered solutions of hydantoin. A data point related to a non buffered D_2O solution of **3.4** is also reported in the plot. Data points reported with different symbols relate to different datasets.



Scheme S2.2: structure of **3.4**. The arrows show the protons whose signals in ^1H NMR spectra in buffered D_2O , appear as a singlet with pH -dependent chemical shift.

A2.10.: Analysis of ^1H NMR spectra in an experiment of buffer-catalysed H/D exchange of **10**.

In **Figure S2.13** the ^1H NMR signal related to the exchangeable protons of the mixture of epimers A and B of **3.21** are reported at the start, during, and at the end of a H/D exchange experiment. Even if overlapped, two signals, related to the two epimers, can be distinguished in **Figure S2.13**: a triplet on the right and a doublet of doublets on the left. The different multiplicity is expected, considering the different dihedral angles between the exchangeable proton and the two vicinal, diastereotopic protons, in the different epimers. In **Figure S2.13** the purple line, relating to the spectrum recorded at time $t=0$, has been scaled by 0.28, so as to allow for the overlap of the triplet with the

same signal in the spectrum recorded after 26 hours ($t=26$ h, blue line), when some exchange had taken place. This rescaling allowed the use of the triplet as a reference. At time $t=26$ h the doublet of doublet on the left cannot be perfectly overlapped with the same signal at time $t=0$, showing a slightly slower decay of the doublet of doublets, as compared to the triplet. The observation suggests slightly different rates of deuteration for the two epimers of **3.21**. The difference, however, appears to be very small, probably within experimental errors if independent experiments were carried out with pure samples of single diastereoisomers.

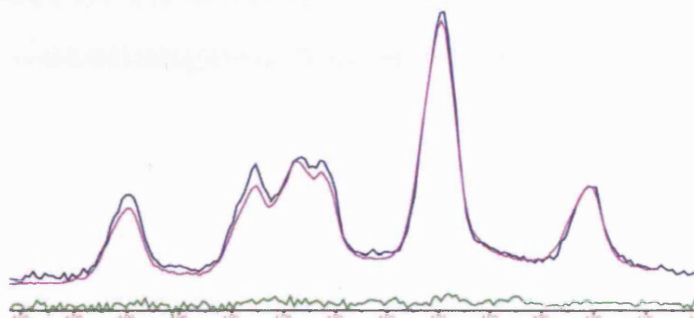


Figure S2.13: signals of the exchangeable protons in ^1H NMR spectra at 400 MHz of a solution of **3.21** in D_2O phosphate buffer 0.5M, 1M I at pH^* 7.2, stored at 25 °C. The purple line applies to the spectrum recorded at the beginning of the kinetic experiment ($t=0$) and it is scaled by 0.28. The blue and green lines are parts of the spectra recorded at time $t=26$ h and at time $t=239$ h, respectively. The spectra recorded at times $t=29$ h and $t=239$ h are unmodified.

A2.11.: HPLC traces for O-THP protected 3-*N*-methyl-5-serine hydantoin 3.39 and 3-*N*-methyl-5-serine hydantoin 3.22.

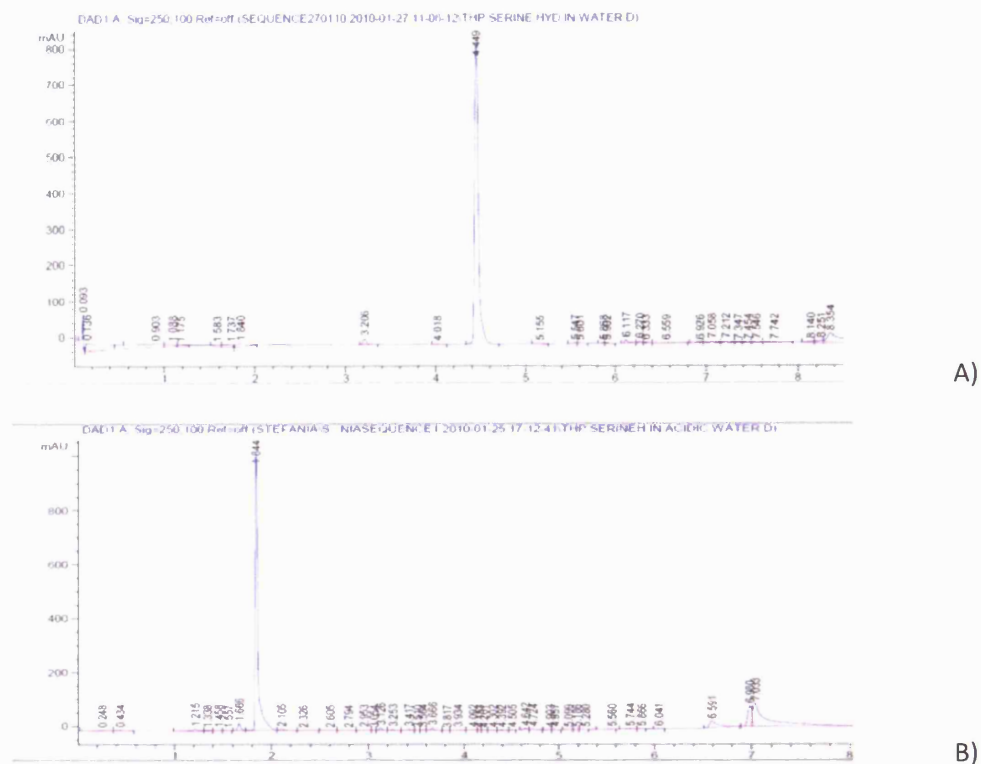


Figure S2.14: HPLC traces for O-THP protected 3-*N*-methyl-5-serine hydantoin **3.39** (trace **A**) and 3-*N*-methyl-5-serine hydantoin **3.22** (trace **B**).

Appendix 3

This Appendix is for Chapter 4

**The effect of co-solvents on racemisation and H/D
exchange of 5-benzylhydantoins**

A.3.1 Kinetic traces for racemisation of hydantoins 4.1-4.4 in mixed media containing 50 percent volume of D₂O phosphate buffer, pH 7.2, 1M, 2M *I* and 50 percent volume of a mixture 1:1 (v:v) D₂O – d₈-2-propanol.**

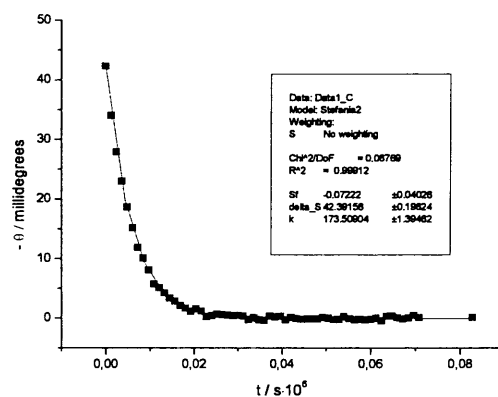


Figure S3.1: racemisation of **4.1** at 60 °C in a mixed medium containing 50 percent volume of D₂O phosphate buffer, pH** 7.2, 1 M, 2M *I* and 50 volume-% of a mixture 1:1 (v:v) D₂O –d₈-2-propanol. The CD signal of **4.1** at 230 nm is plotted as a function of reaction time. The squares (■) are the experimental points, the solid lines are the fits to pseudo first-order kinetics.

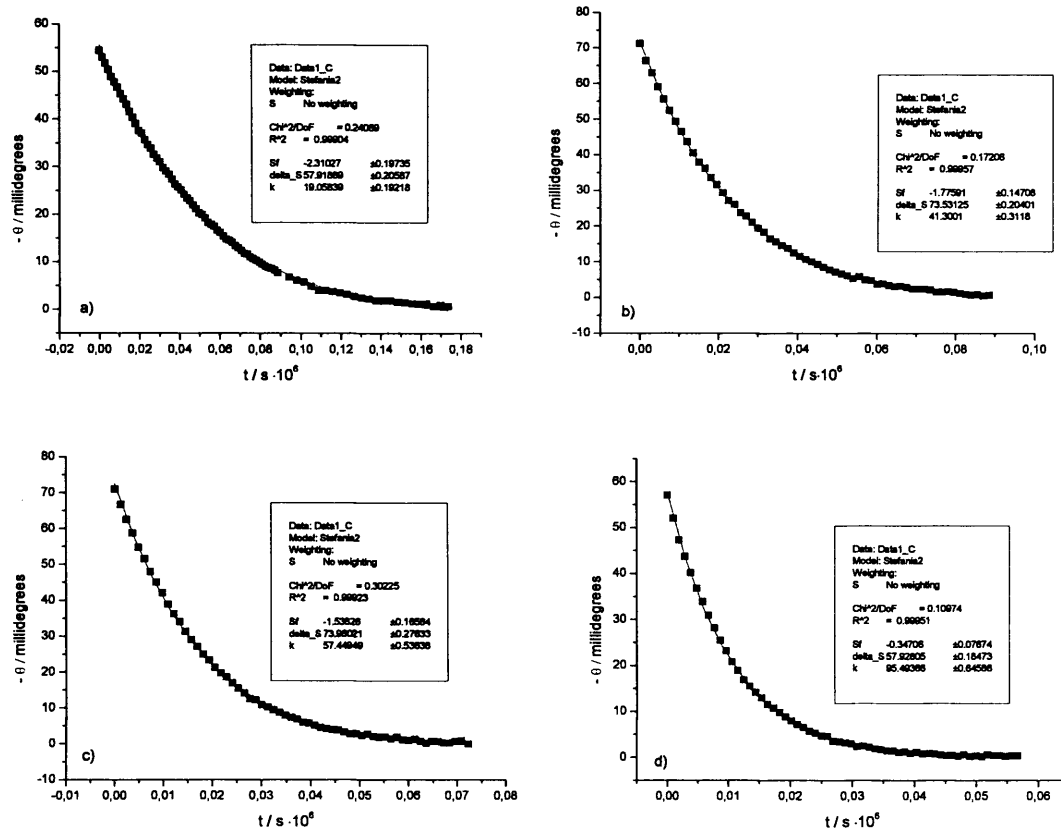


Figure S3.2 a-d: racemisation of 4.2 at 60 °C in mixed media containing 50 percent volume of D₂O phosphate buffers, pH** 7.2, 2M I and 50 volume-% of a mixture 1:1 (v:v) D₂O – d₈-2-propanol. Buffer concentrations are a) 0.1 M, b) 0.2 M, c) 0.3 M, d) 0.5 M. The CD signals of 4.2 at 235 nm are plotted as a function of reaction time. The squares (■) are the experimental points, the solid lines are the fits to pseudo first-order kinetics.

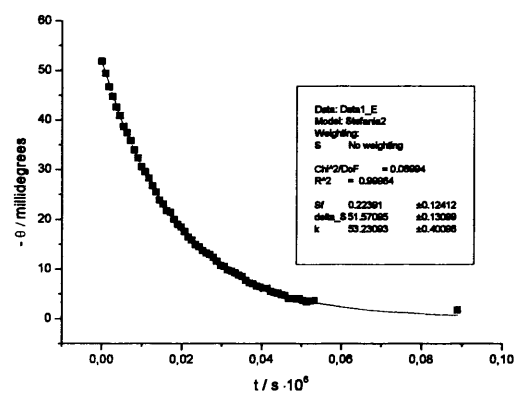
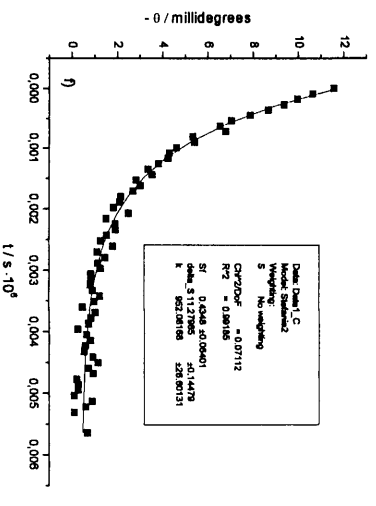
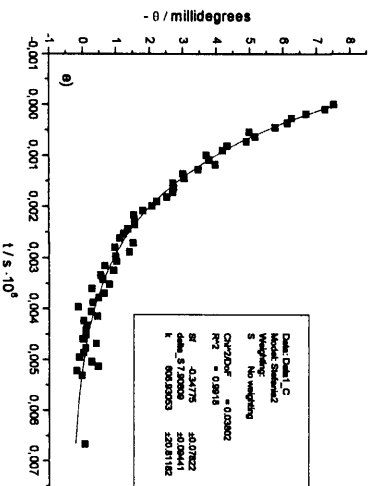
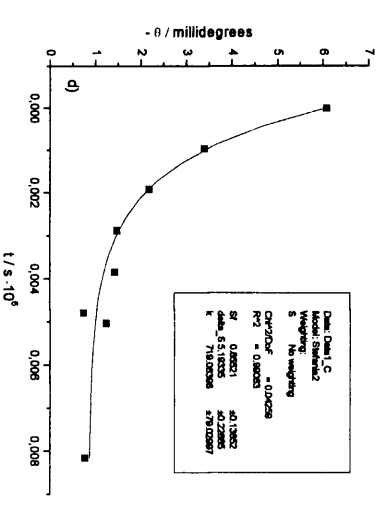
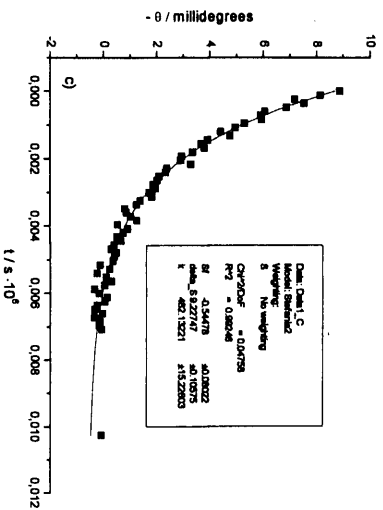
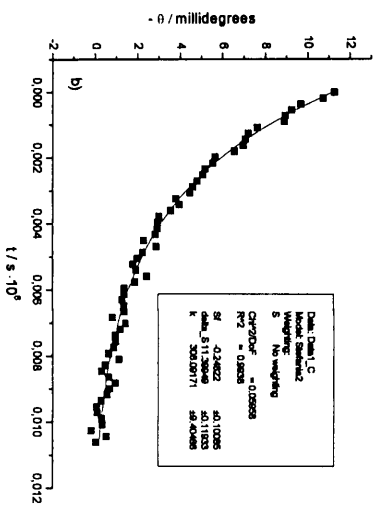
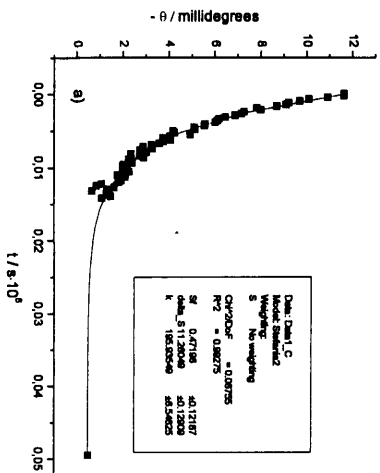


Figure S3.3: racemisation of **4.3** at 60 °C in a mixed medium containing 50 percent volume of D₂O phosphate buffer, pH** 7.2, 1M, 2M *I* and 50 percent volume of a mixture 1:1 (v:v) D₂O – d₈-2-propanol. The CD signal of **4.3** at 235 nm is plotted as a function of reaction time. The squares (■) are the experimental points, the solid lines are the fits to pseudo first-order kinetics.



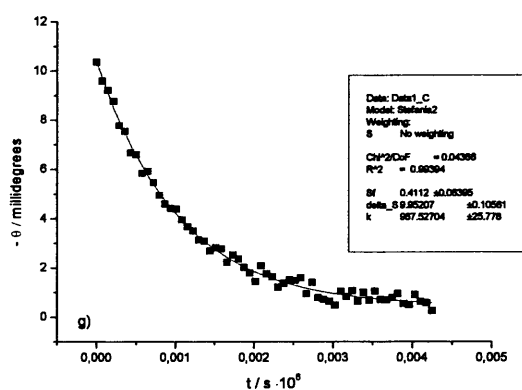
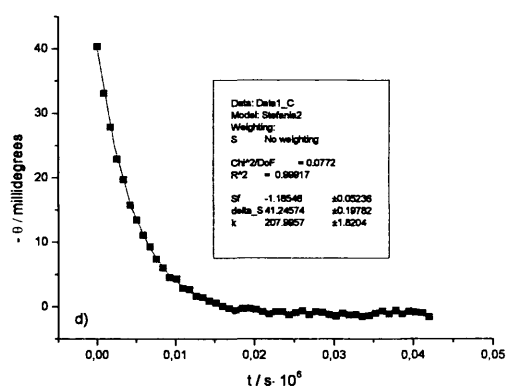
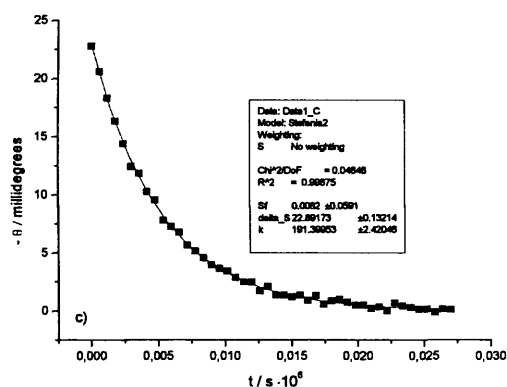
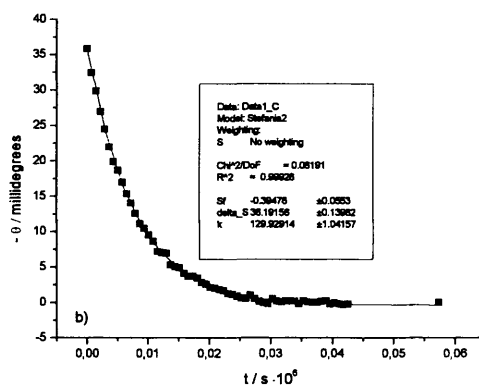
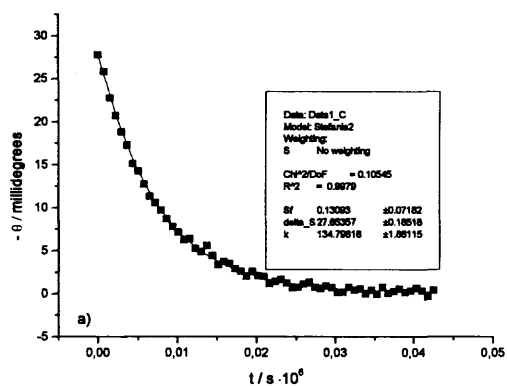


Figure S3.4 a-g: racemisation of **4.4** at 60 °C in mixed media containing 50 percent volume of D₂O phosphate buffers, pH** 7.2, 2M *I* and 50 percent volume of a mixture 1:1 (v:v) D₂O –d₈-2-propanol. Buffer concentrations are **a)** 0.1 M, **b)** 0.2 M, **c)** 0.3 M, **d), e)** 0.4 M **f), g)** 0.5 M. The CD signals of **4.4** at 240 nm (**a-f**) and 245 nm (**g**) are plotted as a function of reaction time. The squares (■) are the experimental points, the solid lines are the fits to pseudo first-order kinetics.

A.3.2 Kinetic traces for racemisation of hydantoin 4.1 and 4.2 in D₂O and H₂O phosphate buffers, in the presence of co-solvents and of 4.3 and 4.4 in D₂O and H₂O phosphate buffers, with and without co-solvents.



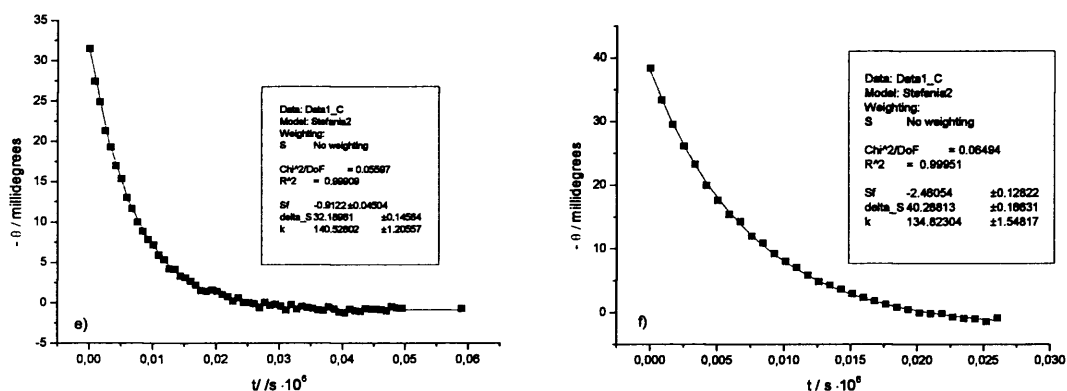
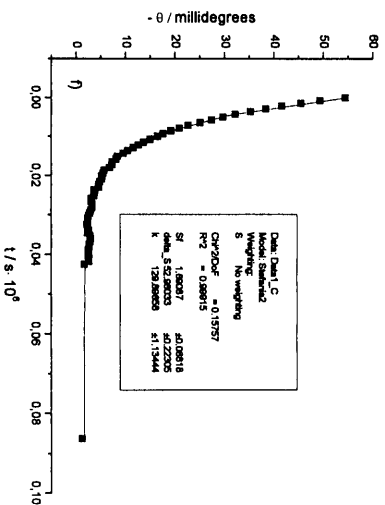
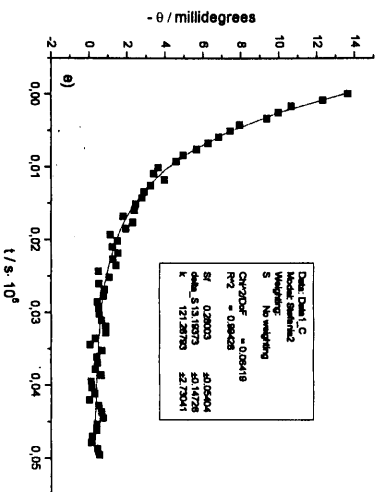
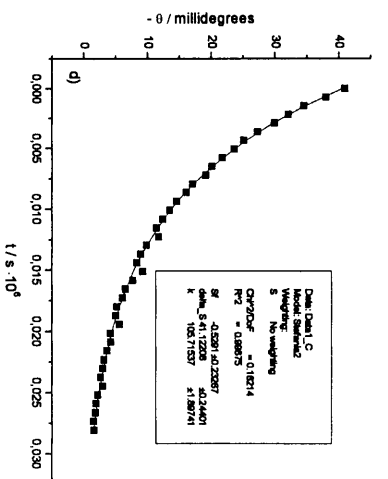
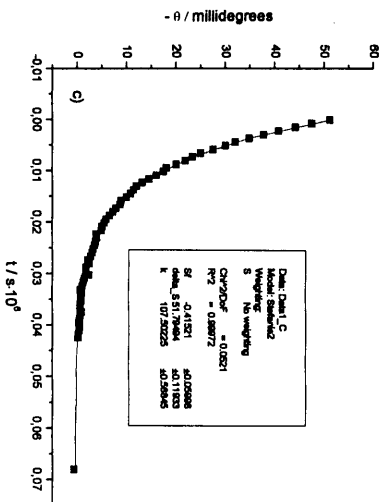
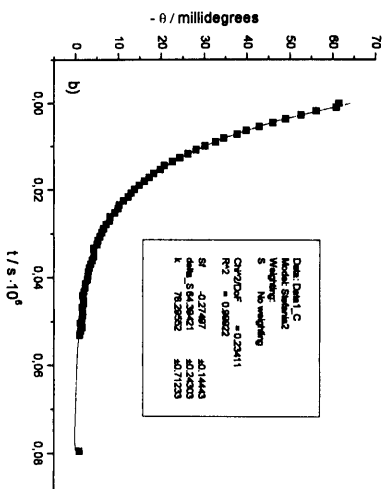
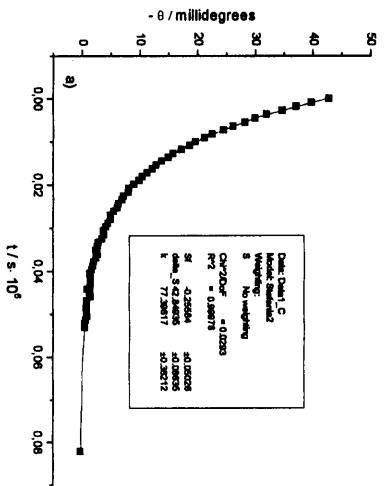


Figure S3.5 a-f : racemisation of **4.1**, at 60 °C in mixed media containing 50 percent volume of phosphate buffers, and 50 percent volume of mixtures 1:1 (v:v) D₂O or H₂O – co-solvent. **a)** D₂O phosphate buffer pH** 7.3, 0.5 M, 1M *I*, co-solvent: d_g-2-propanol **b)** H₂O phosphate buffer pH^{25 °C} 7.2, 0.5M, 1M *I*, co-solvent: 2-propanol **c)** in D₂O phosphate buffer pH** 7.3, 0.5 M, 1M *I*, co-solvent: trifluoroethan(Od)ol, **d)** H₂O phosphate buffer pH^{25 °C} 7.2, 0.5 M, 1M *I*, co-solvent: trifluoroethanol, **e)** D₂O phosphate buffer pH** 7.3, 0.5M, 1M *I*, co-solvent: dioxane, **d)** H₂O phosphate buffer pH^{25 °C}, 0.5M, 1M *I*, co-solvent: dioxane. The CD signals of **4.1** at 230 nm are plotted as a function of reaction time. The squares (■) are the experimental points, the solid lines are the fits to pseudo first-order kinetics.



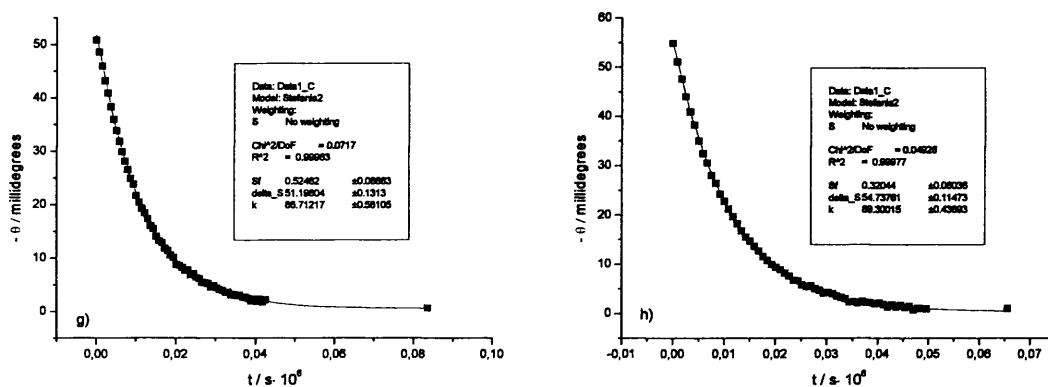
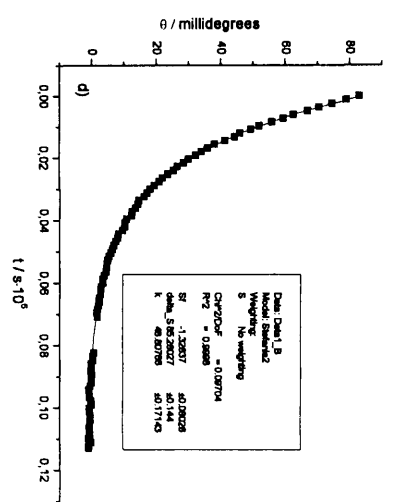
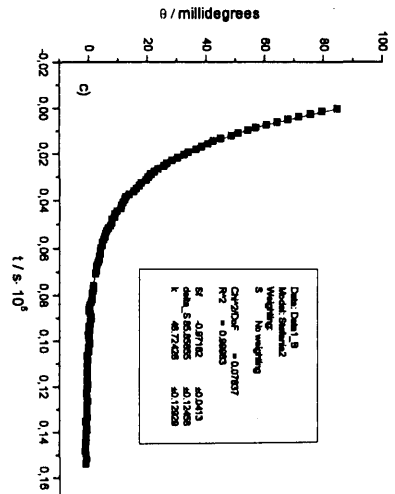
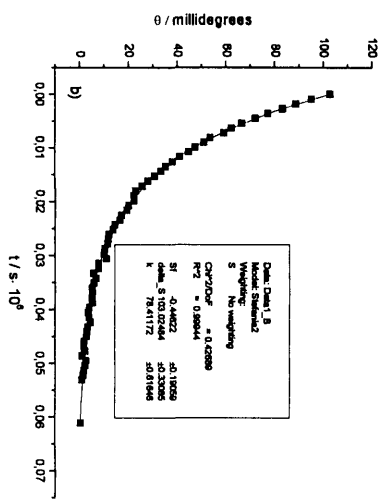
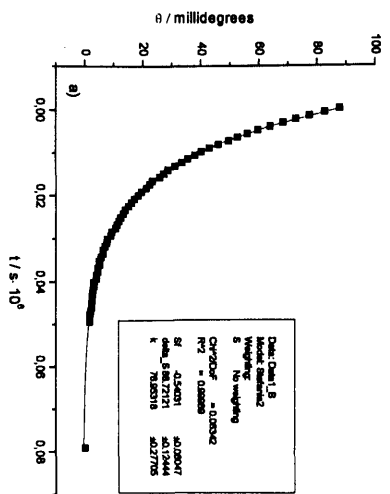


Figure S3.6 a-h : racemisation of 4.2, at 60 °C in mixed media containing 50 percent volume of phosphate buffers, and 50 percent volume of mixtures 1:1 (v:v) D₂O or H₂O – co-solvent. **a)** D₂O phosphate buffer pH** 7.3, 0.5M, 1M *I*, co-solvent: d₈-2-propanol **b)** H₂O phosphate buffer pH^{25 °C} 7.2, 0.5M, 1M *I*, co-solvent: 2-propanol **c), d)** D₂O phosphate buffer pH** 7.3, 0.5 M, 1M *I*, co-solvent: trifluoroethan(Od)ol, **e), f)** H₂O phosphate buffer pH^{25 °C} 7.2, 0.5M, 1M *I*, co-solvent: trifluoroethanol, **g)** D₂O phosphate buffer pH** 7.3, 0.5M, 1M *I*, co-solvent: dioxane, **h)** H₂O phosphate buffer pH^{25 °C}, 0.5 M, 1M *I*, co-solvent: dioxane. The CD signals of 4.2 at 240 nm are plotted as a function of reaction time. The squares (■) are the experimental points, the solid lines are the fits to pseudo first-order kinetics.



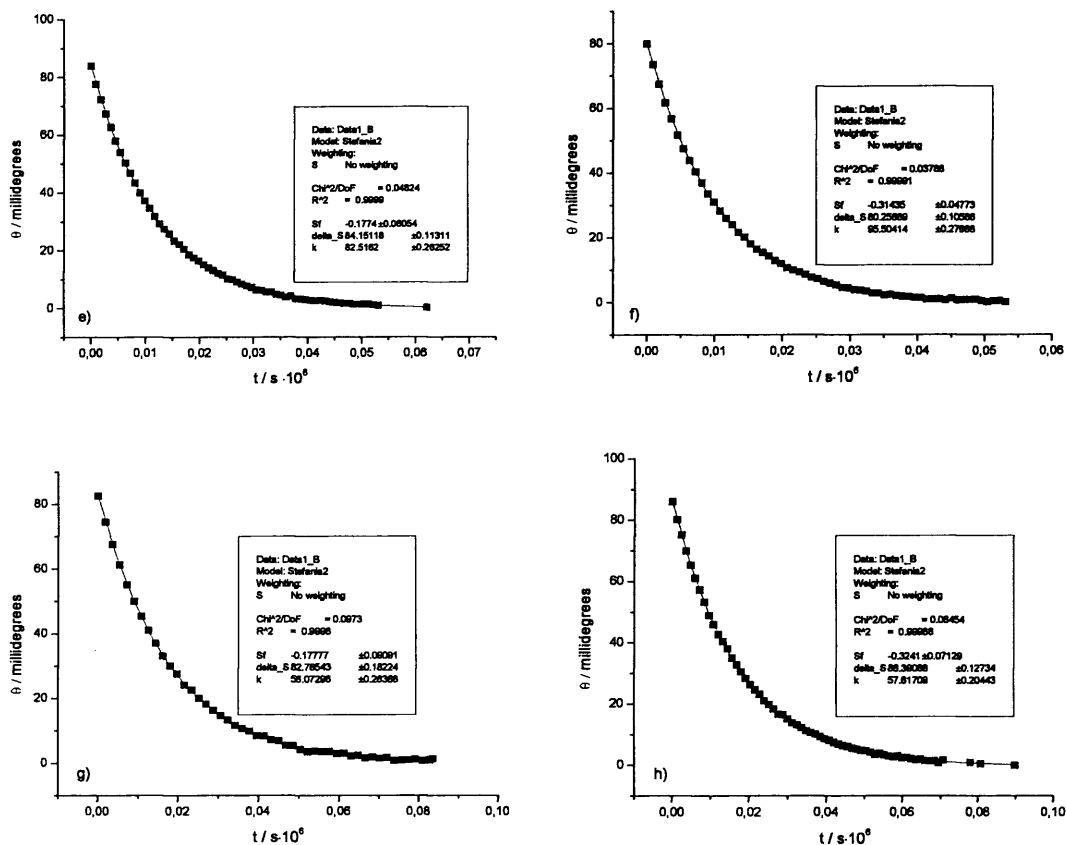
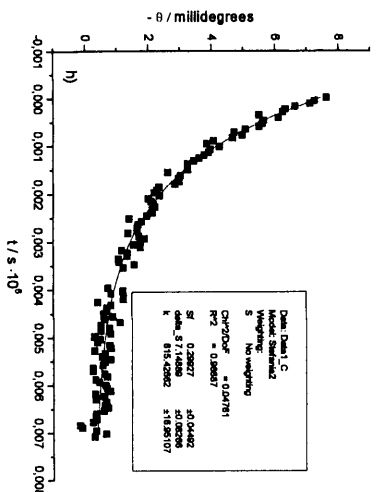
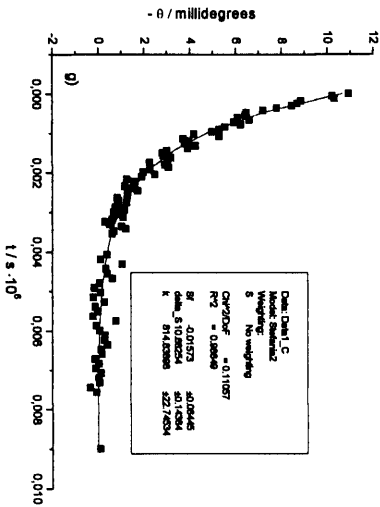
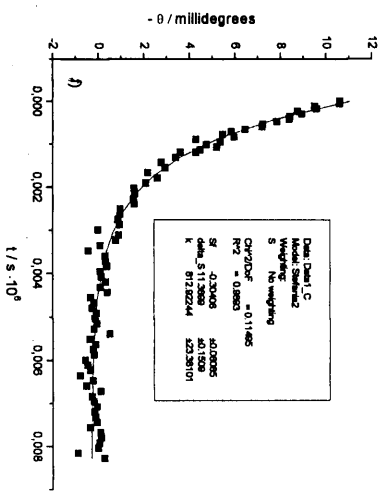
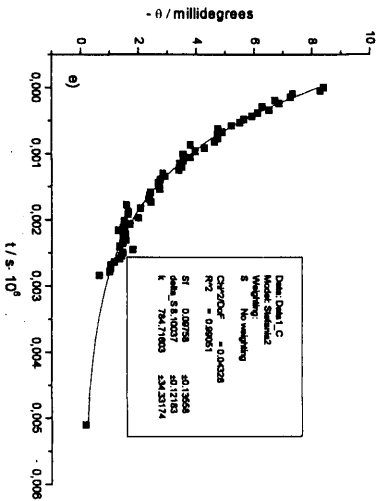
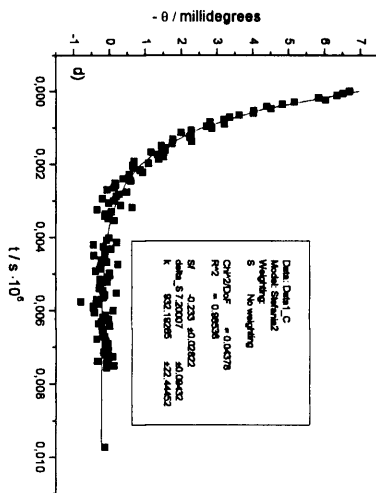
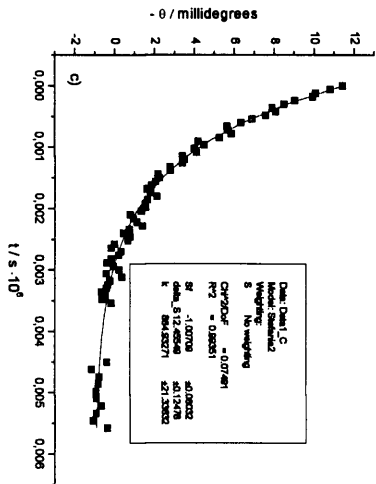
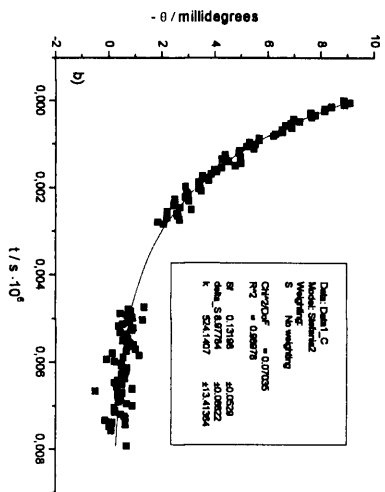
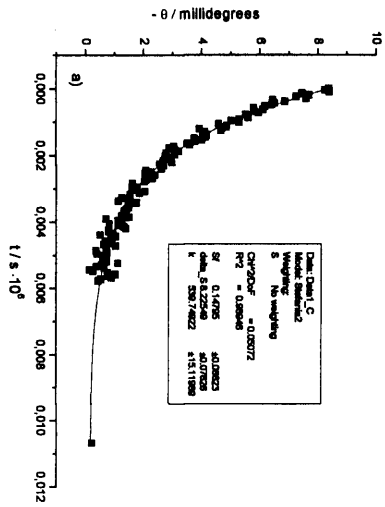


Figure S3.7a-h : racemisation of (R)-4.3, at 60 °C in mixed media containing 50 percent volume of phosphate buffers, and 50 percent volume of D₂O or H₂O (no co-solvent) or of mixtures 1:1 (v:v) D₂O or H₂O – co-solvent. **a)** D₂O phosphate buffer pH** 7.3, 0.5M, 1 M I, no co-solvent **b)** in H₂O phosphate buffer pH^{25 °C} 7.2, 0.5M, 1M I, no co-solvent **c)** D₂O phosphate buffer pH** 7.3, 0.5M I, 1M I, co-solvent: d₈-2-propanol **d)** H₂O phosphate buffer pH^{25 °C} 7.2, 0.5M, 1 M I, co-solvent: 2-propanol **e)** D₂O phosphate buffer pH** 7.3, 0.5 M, 1 MI, co-solvent: trifluoroethan(Od)ol, **f)** H₂O phosphate buffer pH^{25 °C} 7.2, 0.5 M, 1M I, co-solvent: trifluoroethanol, **g)** D₂O phosphate buffer pH** 7.3, 0.5M, 1M I, co-solvent: dioxane, **h)** H₂O phosphate buffer pH^{25 °C} 7.2, 0.5 M, 1 M I, co-solvent: dioxane. The CD signals of (R)-4.3 at 235 nm are plotted as a function of reaction time. The squares (■) are the experimental points, the solid lines are the fits to pseudo first-order kinetics.



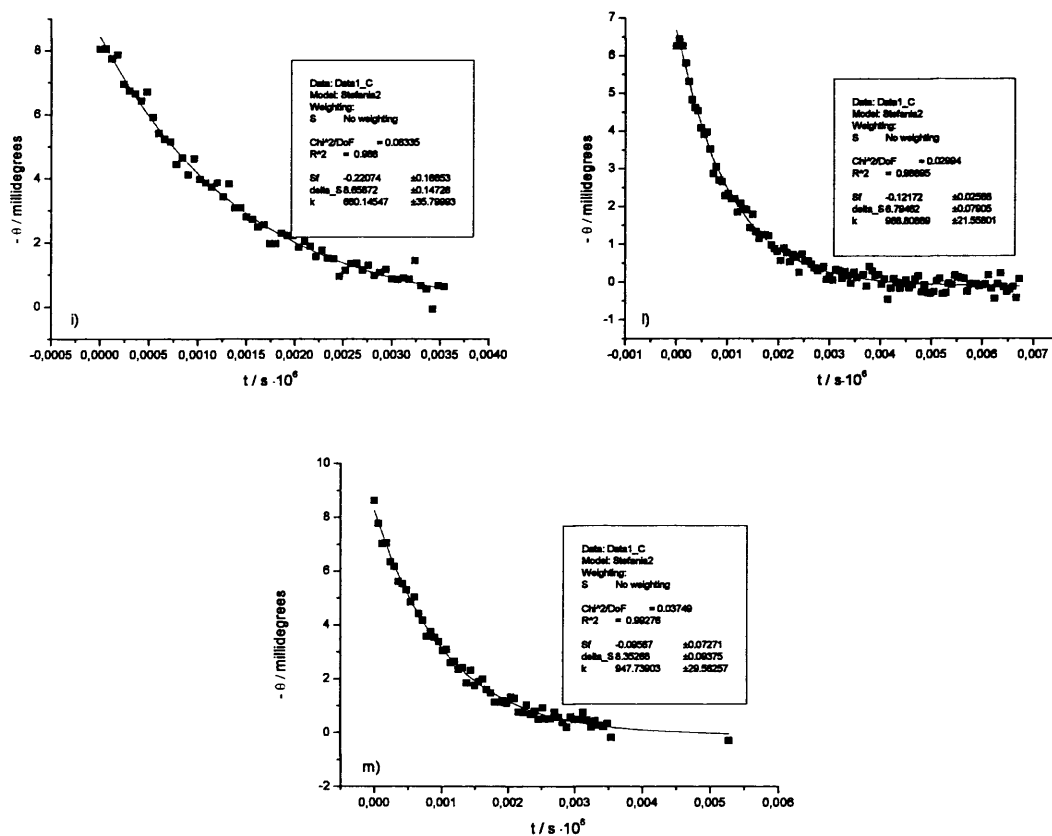


Figure S3.8 a-m: racemisation of 4.4, at 60 °C in mixed media containing 50 percent volume of phosphate buffers, and 50 percent volume of D₂O or H₂O (no co-solvent) or of mixtures 1:1 (v:v) D₂O or H₂O – co-solvent. **a)** D₂O phosphate buffer pH** 7.3, 0.5M, 1 M *I*, no co-solvent **b)** H₂O phosphate buffer pH^{25 °C} 7.2, 0.5 M, 1 M *I*, no co-solvent **c), d)** D₂O phosphate buffer pH** 7.3, 0.5M, 1M *I*, co-solvent: d₈-2-propanol **e), f), g)** H₂O phosphate buffer pH^{25 °C} 7.2, 0.5M, 1M *I*, co-solvent: 2-propanol **h)** D₂O phosphate buffer pH** 7.3, 0.5M, 1M *I*, co-solvent: trifluoroethan(Od)ol, **i)** H₂O phosphate buffer pH^{25 °C} 7.2, 0.5M, 1M *I*, co-solvent: trifluoroethanol, **l)** D₂O phosphate buffer pH** 7.3, 0.5M, 1 M *I*, co-solvent: dioxane, **m)** H₂O phosphate buffer pH^{25 °C} 7.2, 0.5M, 1 M *I*, co-solvent: dioxane. The CD signals of 4.4 at 240 nm are plotted as a function of reaction time. The squares (\blacksquare) are the experimental points, the solid lines are the fits to pseudo first-order kinetics.

A.3.3 Kinetic traces for H/D exchange of hydantoins 4.1 and 4.2 in D₂O phosphate buffers pH 7.2, with and without 33 percent volume of d₈-2-propanol or d₆-DMSO as co-solvents.**

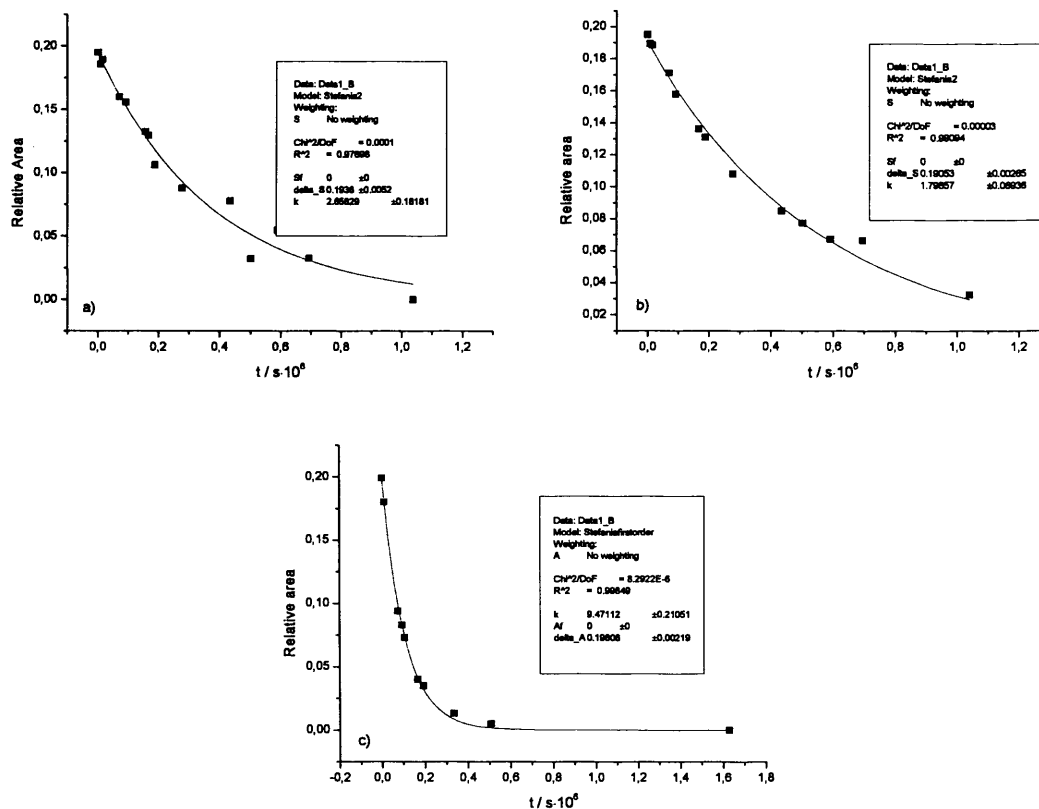


Figure S3.9 a-c : H/D exchange of 4.1, at 37°C in media containing a) D₂O phosphate buffer pH** 7.2, 0.2 M, 1M I (33 volume-%) and D₂O (67 volume-%), b) D₂O phosphate buffer pH** 7.2, 0.2 M, 1M I (33 volume-%) and 1:1 (v:v) mixture D₂O-d₈-2-propanol (67 volume-%) and c) D₂O phosphate buffer pH** 7.2, 0.2 M, 1M I (33 volume-%) and 1:1 (v:v) mixture D₂O-d₆-DMSO (67 volume-%). The relative area integrals of the peak of the asymmetric proton in the ¹H NMR spectra of 4.1 are plotted as a function of time. The squares (■) are the experimental points, the solid lines are the fits to pseudo first-order kinetics.

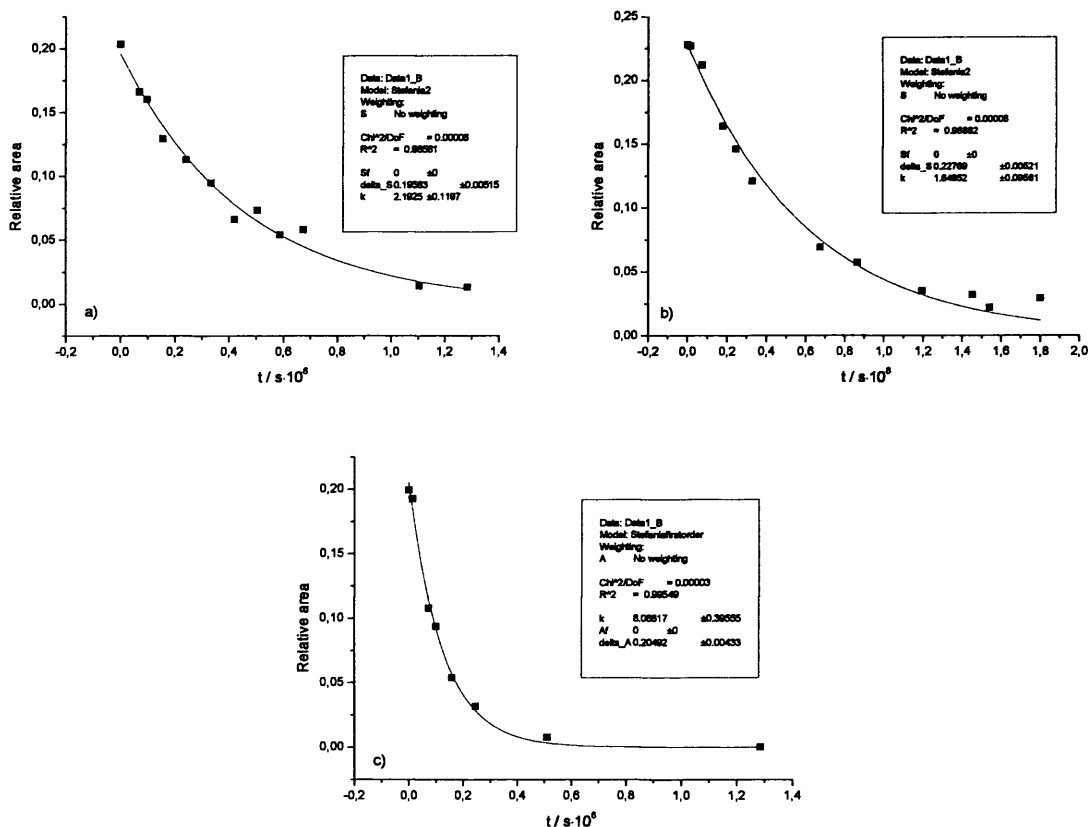
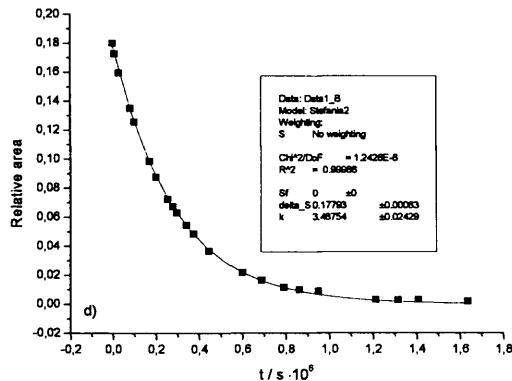
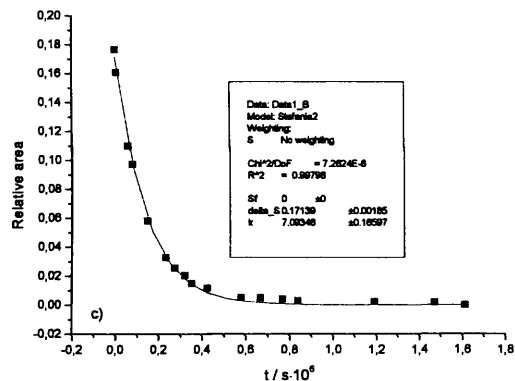
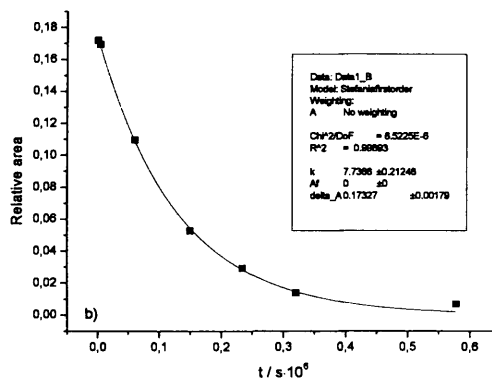
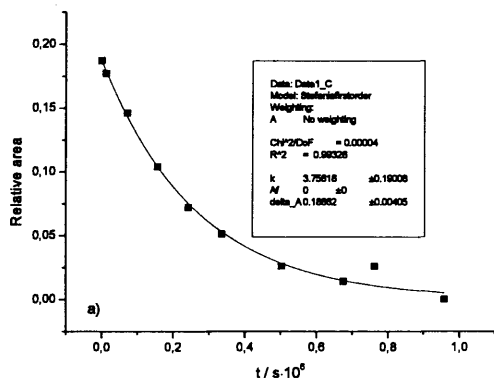


Figure S3.10 a-c : H/D exchange of **4.2**, at 37 °C in media containing **a)** D₂O phosphate buffer pH** 7.2, 0.2 M, 1M *I* (33 volume-%) and D₂O (67 volume-%), **b)** D₂O phosphate buffer pH** 7.2, 0.2 M, 1M *I* (33 volume-%) and 1:1 (v:v) mixture D₂O-d₈-2-propanol (67 volume-%) and **c)** D₂O phosphate buffer pH** 7.2, 0.2 M, 1M *I* (33 volume-%) and 1:1 (v:v) mixture D₂O-d₆-DMSO (67 volume-%). The relative area integrals of the peak of the asymmetric proton in the ¹H NMR spectra of **4.2** are plotted as a function of time. The squares (■) are the experimental points, the solid lines are the fits to pseudo first-order kinetics.

A.3.4 Kinetic traces for H/D exchange of hydantoins 4.1-4.4 and 4.2 in mixed media containing 50 percent volume of D₂O phosphate buffer, pH* 7.2, 1M, 2M I and 50 percent volume of mixtures 1:1 (v:v) D₂O – d₆-DMSO or D₂O –d₈-2-propanol.



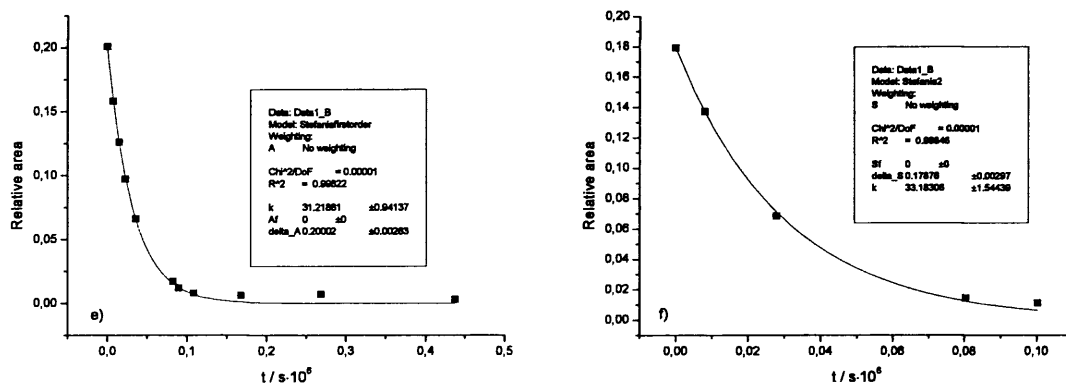
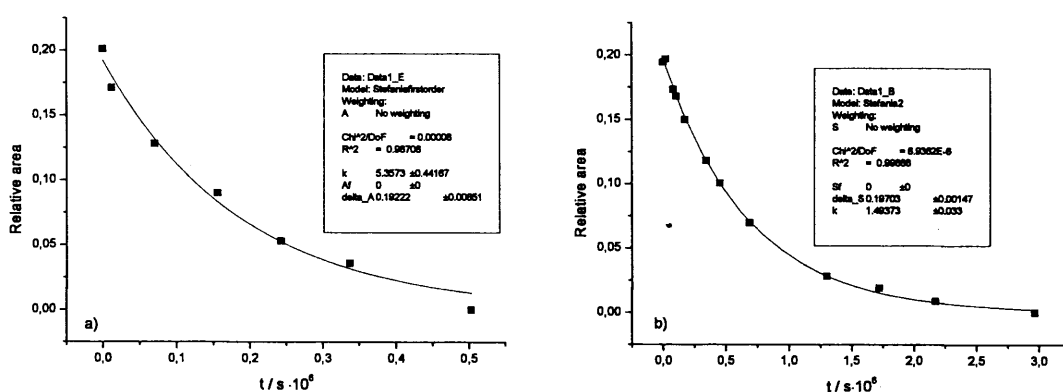


Figure S3.11 a-f: H/D exchange of 4.1-4.4 at 25 °C in mixed media containing 50 percent volume of D₂O phosphate buffer, pH* 7.2, 1 M, 2M I and 50 percent volume of mixtures 1:1 (v:v) D₂O – co-solvent a) H/D exchange of 4.1 with d₈-2-propanol as co-solvent, b) H/D exchange of 4.1 with d₆-DMSO as co-solvent, c) H/D exchange of 4.2 with d₆-DMSO as co-solvent, d) H/D exchange of 4.3 with d₆-DMSO as co-solvent, e), f) H/D exchange of 4.4 with d₆-DMSO as co-solvent. The area integrals of the peak of the asymmetric proton in the ¹H NMR spectra of the hydantoin are plotted as a function of time. The squares (■) are the experimental points, the solid lines are the fits to pseudo first-order kinetics.

A.3.5 Kinetic traces for H/D exchange of hydantoin 4.1, at 25 °C in mixed media with different compositions containing D₂O phosphate buffers and d₆-DMSO or d₈-2-propanol as co-solvents.



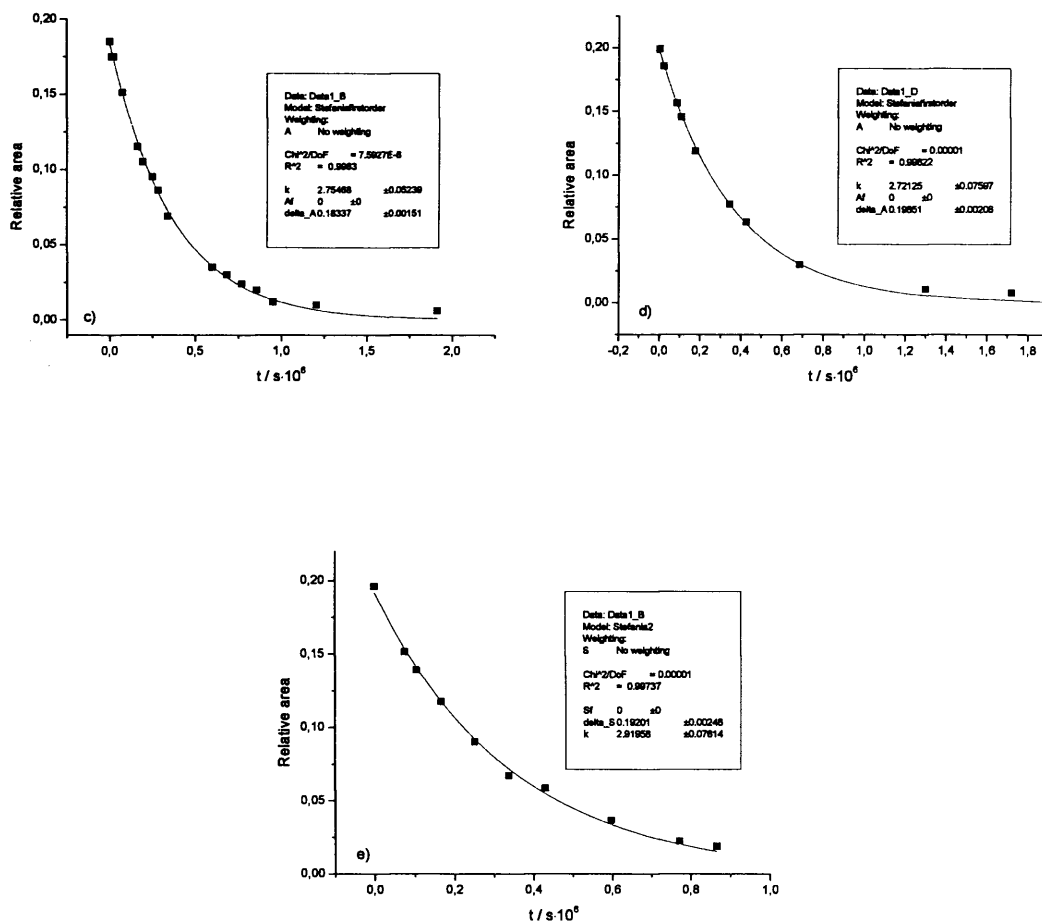
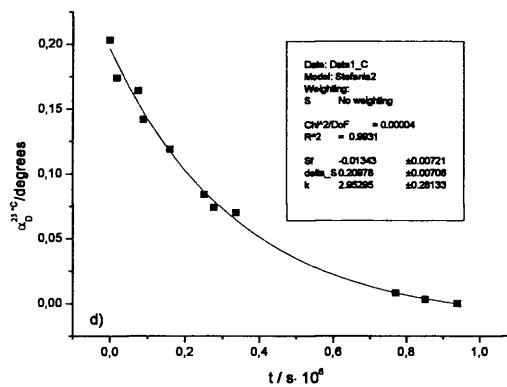
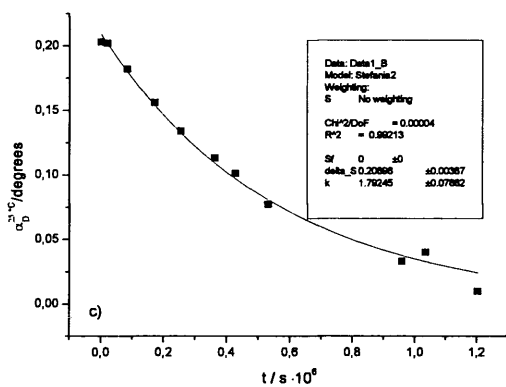
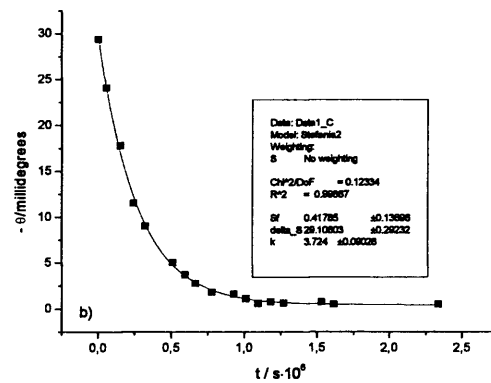
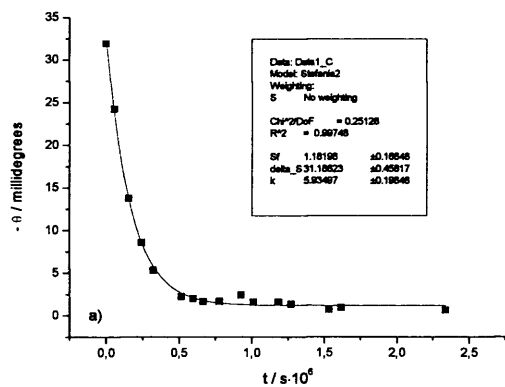


Figure S3.12 a-c: H/D exchange of 4.1, at 25 °C in mixed media containing a) D₂O phosphate buffer pH* 7.2, 1M, 2M I (50 volume-%) and D₂O-d₈-isopropanol 4:1 (50 volume-%), b) D₂O phosphate buffer pH* 7.2, 0.1M, 1M I (33 volume-%) and D₂O-d₆-DMSO 1:1 (67 volume-%) c), d) D₂O phosphate buffer pH* 7.2, 0.2M, 1M I (33 volume-%) and D₂O-d₆-DMSO 1:1 (67 volume-%) e) D₂O phosphate buffer pH* 7.0, 0.1M, 0.2 M I (50 volume-%) and d₆-DMSO (50 volume-%). The area integrals of the peak of the asymmetric proton in the ^1H NMR spectra of 4.1 are plotted as a function of time. The squares (■) are the experimental points, the solid lines are the fits to pseudo first-order kinetics.

A.3.6 Kinetic traces for racemisation of hydantoin 4.1, at 25 °C in mixed media with different compositions containing D₂O phosphate buffers and d₆-DMSO or d₈-2-propanol as co-solvents.



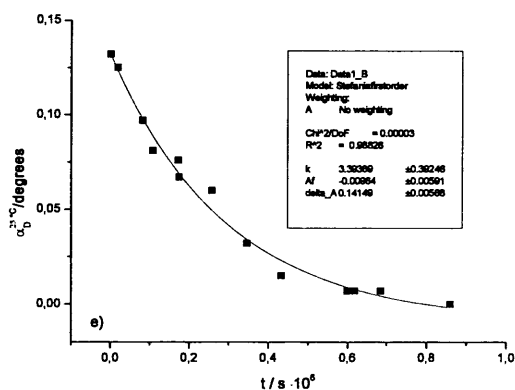


Figure S3.13 a-e: racemisation of **4.1**, at 25 °C in mixed media containing **a)** D₂O phosphate buffer pH* 7.2, 1M, 2M *I* (50 volume-%) and D₂O-d₈-isopropanol 4:1 (50 volume-%), **b)** D₂O phosphate buffer pH* 7.2, 1M, 2M *I* (50 volume-%) and D₂O-d₈-isopropanol 1:1 (50 volume-%), **c)** D₂O phosphate buffer pH* 7.2, 0.1M, 1M *I* (33 volume-%) and D₂O-d₆-DMSO 1:1 (67 volume-%) **d)** D₂O phosphate buffer pH* 7.2, 0.2M, 1M *I* (33 volume-%) and D₂O-d₆-DMSO 1:1 (67 volume-%) **e)** D₂O phosphate buffer pH* 7.1, 0.1M, 0.2 M *I* (50 volume-%) and d₆-DMSO (50 volume-%). The CD signal at 230 nm (**a**) and **b**)) and the optical rotation (**c**), **d**), and **e**)) of **4.1** are plotted as a function of time. The squares (■) are the experimental points, the solid lines are the fits to pseudo first-order kinetics.

A.3.7: Partial ¹H NMR spectra showing the change over time of the methylene protons of **4.1a** during a H/D experiment carried out in a mixed medium containing 50 percent d₆-DMSO added to the D₂O phosphate buffer.

Figure S3.14 shows the changes over time in the region of the spectrum corresponding to the ¹H NMR signal of the methylene proton of **4.1a**, during a H/D exchange experiment in a mixture D₂O phosphate buffer, pH* 7.0, 0.1M, 0.22 M *I* and d₆-DMSO in the ratio 1:1 (v:v), at 25 °C. At time t=0, only the doublet corresponding to the methylene proton of the starting material, species A, is visible. As the H/D exchange proceeds, the growth of a peak, overlapped to the doublet from species A, can be noticed. The new peak can be attributed to the methylene proton of the species B and C (see **Scheme 4.3**).

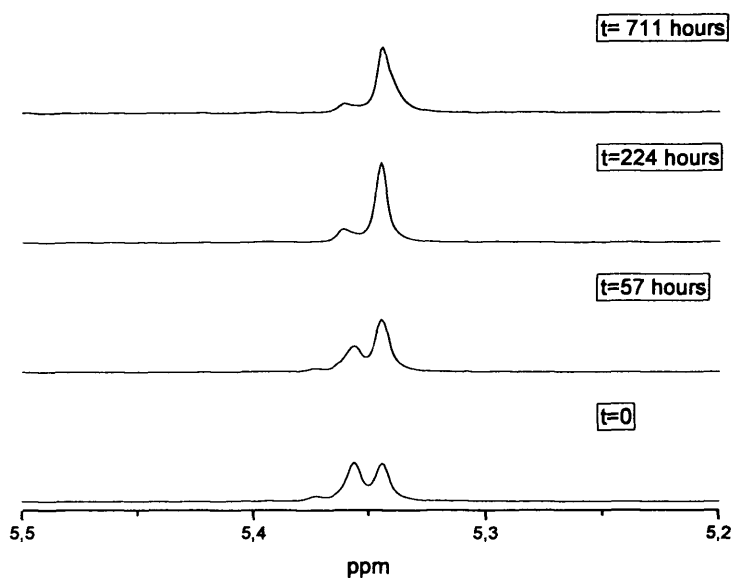


Figure S3.14: representative partial ^1H NMR spectra at 400 MHz, in the region between 5.5 and 5.2 ppm, during a H/D experiment of **4.1a** in a mixture of D_2O phosphate buffer, $\text{pH}^* 7.1$, 0.1M, 0.2 M *I* and d_6 -DMSO in the ratio 1:1 (v:v), at 25 °C. The spectra show the changes over time of the signal of the methylene proton of **4.1a**. Reported spectra were taken at the beginning of the reaction: $t=0$ (**bottom**), after 57 and 224 hours (**middle**) and after 711 hours (**top**).

A.3.8: Fit attempts of experimental data from racemisation experiments for hydantoin 4.4 carried out in buffered D_2O media containing a 25 percent volume of d_8 -2-propanol co-added.

Figure S3.15, left shows the linear fit of experimental rate constant of racemisation of **4.4** determined in buffered D_2O media containing 25volume-% of d_8 -2propanol co-added, plotted as a function of buffer concentration. In **Figure S3.15, right** the residuals from the fit, expressed as difference between experimental and fitted values are also reported as a function of buffer concentration. There seems to be a “pattern” in the plot of the residuals as a function of buffer concentration, suggesting that a linear fit is probably not suitable to fully reproduce the process behind the variation in k_{rac} with increasing buffer concentration.

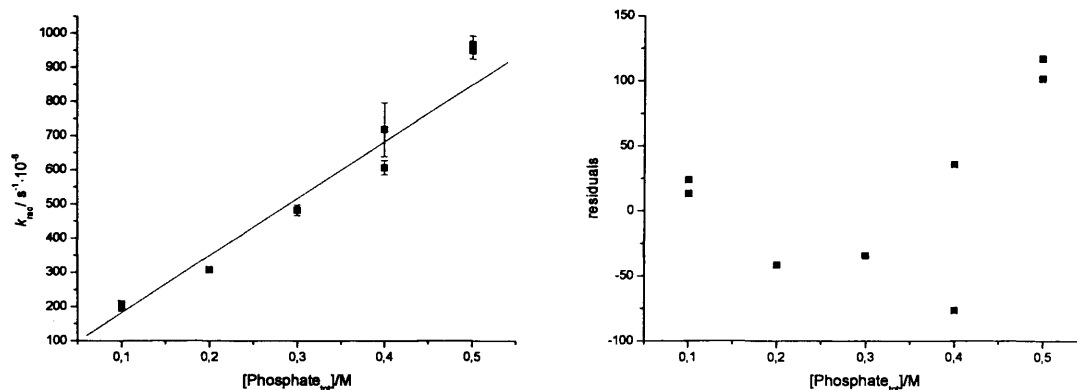


Figure S3.15 Left: linear fit (solid line) of experimental rate constants of racemisation of 4.4 (■), as a function of total buffer concentration in mixtures composed of 50 percent volume of D₂O phosphate buffers, pH** 7.2, 2M *I* and 50 percent volume of mixture D₂O-d₈-isopropanol 1:1 (v:v), to give a total 25 volume-% of d₈-isopropanol co-added. **Right:** residuals values obtained from the fit, plotted as a function of total buffer concentration. Experiments were carried out at 60°C.

Equation S3.1 is the analytical expression of the straight line fit shown in **Figure S 3.15**.

$$y = (16 \pm 29) + (1668 \pm 141) \cdot x$$

Equation S 3.1

$$R^2 = 0.958$$

Figure S3.16, left shows the polinomial fit of the same experimental data shown in **Figure S3.15**. In **Figure S3.16, right** the residuals from the fit, expressed as differences between experimental and fitted values, are also reported as a function of buffer concentration. The plot of the residuals as a function of buffer concentration gives a series of scattered points, consistent with random errors affecting the measurements. The finding seems to suggest that the model better reproduces the trend of the experimental data. However, the origin of the observed trend is currently unclear and further investigations are needed.

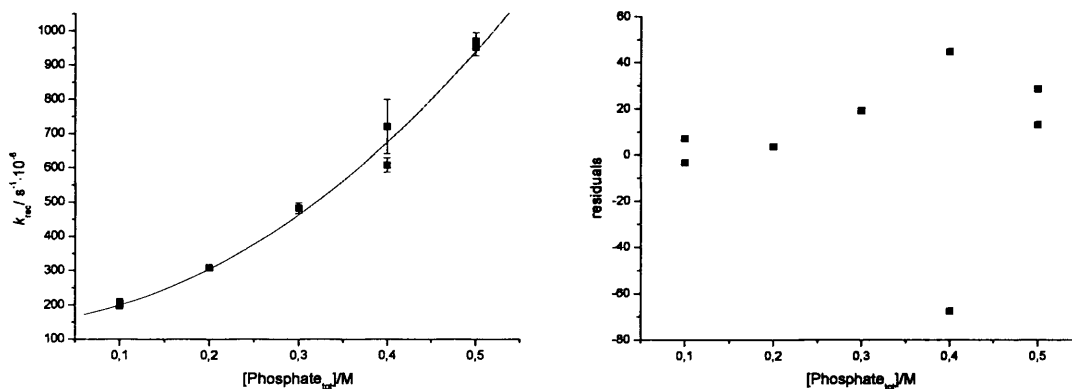


Figure S.3.16 Left: polynomial fit (solid line) of experimental rate constants of racemisation of 4.4 (■), as a function of total buffer concentration in mixtures composed of 50 percent volume of D₂O phosphate buffers, pH** 7.2, 2M *I* and 50 percent mixture D₂O-d₈-isopropanol 1:1 (v:v), to give a total 25volume-% of d₈-isopropanol co-added. Right: residuals values obtained from the fit, plotted as a function of total buffer concentration. Experiments were carried out at 60°C.

Equation S3.2 is the analytical expression of the polynomial fit shown in **Figure S 3.16**.

$$y = (147 \pm 30) + (255 \pm 303) \cdot x + (2658 \pm 556) \cdot x^2 \quad \text{Equation S3.2}$$

$$R^2 = 0.992$$

Appendix 4

This Appendix is for Chapter 5

Exploring the use of IR and VCD spectroscopy for the study of reaction mechanisms involving stereogenic centres.

A4.1. Examples of simulated ECD and VCD signals for hypothetical S_E2 racemisation of generic molecules in deuterated media, assuming values for the ratio k_2/k_1 close to unity

Simulations in **Figure S4.1, left** show that, for values of the ratio of rate constants k_2 and k_1 near unity, the resulting temporary enantiomeric excess of the species B (**Scheme 5.5**) is expected to be small and, therefore hardly experimentally detectable by ECD. On the other hand the temporary enantiomeric excess of the species B during racemisation should be clearly detectable by means of VCD spectroscopy **Figure S4.1, right**, even in an hypothetical limit case of $k_2/k_1=1$.

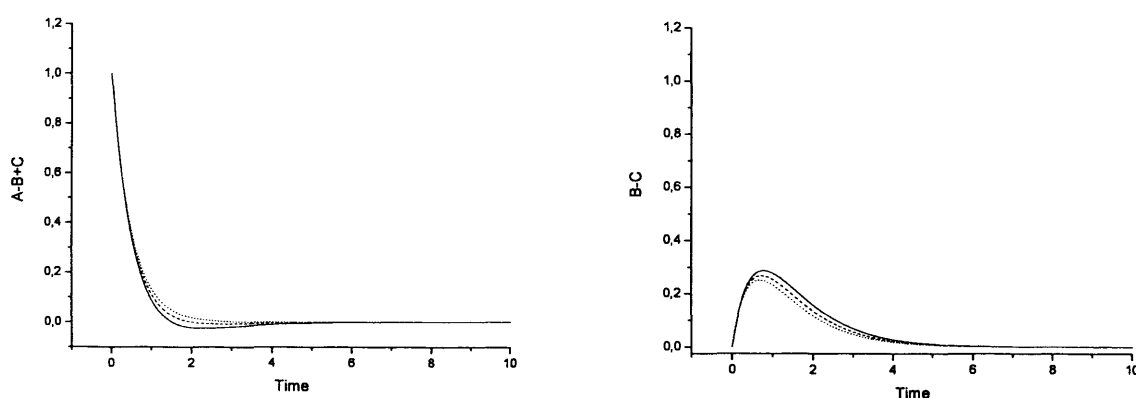


Figure S4.1: expected ECD (**left**) and VCD (**right**) signals plotted as a function of time in a simulated S_E2 racemisation in D_2O as a function of time for different values of the ratio k_2/k_1 . Dotted line $k_2/k_1=1$, dashed line $k_2/k_1=0.9$, Solid line $k_2/k_1=0.8$. The time scale of the x axis is in arbitrary units.

A4.2. Optimised geometries of conformers of compounds 5.1, 5.2, 5.3, for the construction of the VCD spectra in Figures 5.1, 5.2 and 5.3 (top spectra). Input geometries obtained from conformational searches carried out by means of Force Field methods.

COMPOUND 5.1

5.1_1

Free Energy/Hartrees= -1021.661444

Enthalpy/Hartrees =-1021.599179

Center Number	Atomic Number	Coordinates (Angstroms)		
		X	Y	Z
1	6	-1.585538	-7.285295	-9.373694
2	8	-1.626486	-6.319279	0.429107
3	6	-2.795197	-6.474302	-9.607403
4	6	-4.019161	-7.053949	10.262198
5	6	-3.051479	-5.318079	-8.655677
6	8	-4.018555	-5.313386	-7.909343
7	7	-2.098157	-4.336301	-8.735457
8	6	-1.992599	-3.159554	-7.993834
9	6	-2.887783	-2.808477	-6.974081
10	6	-2.700284	-1.618452	-6.283231
11	6	-1.63696	-0.754432	-6.579257
12	6	-1.507744	0.452105	-5.82169
13	7	-1.447128	1.418284	-5.176582
14	6	-0.742733	-1.113325	-7.608551
15	6	0.421247	-0.218641	-7.96618
16	9	1.262392	-0.060009	-6.924903
17	9	1.146038	-0.72353	-8.987477
18	9	0.009128	1.007639	-8.341596
19	6	-0.924956	-2.30002	-8.300348
20	1	-1.582202	-8.323986	-9.70048
21	1	-0.916415	-7.044386	-8.548231
22	1	-3.744643	-7.911387	10.880677
23	1	-4.734289	-7.368468	-9.498525
24	1	-4.504542	-6.305743	10.896231
25	1	-1.404819	-4.501083	-9.459119
26	1	-3.715368	-3.463978	-6.737536
27	1	-3.391986	-1.345193	-5.493124
28	1	-0.22848	-2.562475	-9.08997

5.1_2

Free Energy/Hartrees= -1021.661119

Enthalpy/Hartrees = -1021.598588

Center Number	Atomic Number	Coordinates (Angstroms)		
		X	Y	Z
1	6	-3.783219	-6.593479	-9.94846
2	8	-3.58621	-6.899717	-8.563931
3	6	-2.429828	-6.59692	-9.36239
4	6	-1.462036	-7.719487	-9.619029
5	6	-1.797036	-5.247921	-9.065432
6	8	-0.79899	-4.871278	-9.65968
7	7	-2.466029	-4.543063	-8.097868
8	6	-2.196887	-3.269654	-7.596449
9	6	-3.017225	-2.786055	-6.56721
10	6	-2.801779	-1.527064	-6.032098
11	6	-1.762261	-0.713661	-6.507025
12	6	-1.590746	0.577365	-5.914933
13	7	-1.501046	1.61489	-5.396452
14	6	-0.940204	-1.20409	-7.540868
15	6	0.189985	-0.355857	-8.080824
16	9	0.870223	-0.9826	-9.058223
17	9	-0.268368	0.804437	-8.59484
18	9	1.077152	-0.043168	-7.114127
19	6	-1.152371	-2.466239	-8.080876
20	1	-4.085881	-7.436573	10.567533
21	1	-4.290228	-5.650136	10.148918
22	1	-0.789944	-7.448467	10.436573
23	1	-0.855214	-7.912735	-8.729198
24	1	-2.003412	-8.631966	-9.878671
25	1	-3.239311	-5.055626	-7.684898
26	1	-3.827475	-3.400251	-6.183079
27	1	-3.439298	-1.158163	-5.235638
28	1	-0.517261	-2.839921	-8.872178

COMPOUND 5.2

5.2_1

Free Energy/Hartrees= -1482.443031

Enthalpy/Hartrees = -1482.375451

Center Number	Atomic Number	Coordinates (Angstroms)		
		X	Y	Z
1	6	-19.901754	-7.00144	11.273864
2	17	-19.427017	-8.736452	11.169515
3	6	-21.341591	-6.846696	11.787267
4	8	-21.473586	-7.422184	-3.080248
5	6	-22.381341	-7.416901	10.822021
6	6	-21.57002	-5.325848	11.921147
7	8	-21.481291	-4.601458	10.939782
8	7	-21.860177	-4.912091	13.189602
9	6	-22.122761	-3.618246	13.644333
10	6	-22.145381	-2.494658	12.807245
11	6	-22.416069	-1.245653	13.350872
12	6	-22.667597	-1.077235	14.719271
13	6	-22.93669	0.240977	-15.20575
14	7	-23.149321	1.331461	15.550544
15	6	-22.644333	-2.212895	15.554669
16	6	-22.907503	-2.085369	17.037186
17	9	-22.002693	-1.284919	17.634179
18	9	-22.85106	-3.28155	-17.66896
19	9	-24.127188	-1.568457	-17.28239
20	6	-22.375483	-3.461338	15.016875
21	1	-19.798612	-6.567715	10.279603
22	1	-19.195857	-6.531836	-11.96131
23	1	-21.161119	-8.33693	13.043531
24	1	-22.335872	-6.897606	-9.861785
25	1	-23.382059	-7.293734	11.244411
26	1	-22.20039	-8.482928	-10.65868
27	1	-21.874053	-5.661364	-13.87364
28	1	-21.952071	-2.60872	11.749061
29	1	-22.434335	-0.374456	-12.70432
30	1	-22.360675	-4.326462	15.671663

5.2_2

Free Energy/Hartrees= -1482.442664

Enthalpy/Hartrees = -1482.375691

Center Number	Atomic Number	Coordinates (Angstroms)		
		X	Y	Z
1	6	-19.948334	-7.251858	-10.94066
2	17	-18.520207	-7.034447	12.023108
3	6	-21.248537	-6.898914	11.660178
4	8	-21.370536	-7.586455	12.897081
5	6	-22.435304	-7.315936	-10.78811
6	6	-21.32002	-5.362548	11.855454
7	8	-21.041647	-4.598633	10.943009
8	7	-21.771288	-4.994835	13.091443
9	6	-22.013202	-3.713273	13.588303
10	6	-21.762453	-2.544205	-2.857437
11	6	-22.030968	-1.309802	13.434305
12	6	-22.548792	-1.200407	14.732162
13	6	-22.799885	0.106001	15.258271
14	7	-22.986092	1.189479	15.638668
15	6	-22.799152	-2.381361	15.460479
16	6	-23.361163	-2.319535	16.861771
17	9	-23.53103	-3.551599	17.388226
18	9	-24.562243	-1.709466	16.887424
19	9	-22.547058	-1.642339	17.694708
20	6	-22.532151	-3.615414	14.889419
21	1	-19.952025	-8.299495	10.636224
22	1	-19.805384	-6.596393	10.082052
23	1	-20.482127	-7.676895	13.277594
24	1	-22.41744	-6.784553	-9.833642
25	1	-23.372635	-7.082251	11.300633
26	1	-22.401784	-8.394349	-10.61137
27	1	-21.953512	-5.782548	13.705128
28	1	-21.363867	-2.612678	11.853972
29	1	-21.836184	-0.403351	12.870585
30	1	-22.732079	-4.515538	15.461483

5.2_3

Free Energy/Hartrees= -1482.442126

Enthalpy/Hartrees = -1482.374841

Center Number	Atomic Number	Coordinates (Angstroms)		
		X	Y	Z
1	6	-21.7951	-8.173519	12.721122
2	17	-21.849923	-9.564811	11.576986
3	6	-21.29562	-6.898517	12.024348
4	8	-22.149035	-6.55817	10.939045
5	6	-19.840017	-7.00243	11.568651
6	6	-21.406748	-5.780405	3.082927
7	8	-20.776794	-5.857908	14.127732
8	7	-22.246934	-4.761099	12.735343
9	6	-22.56828	-3.608666	13.454974
10	6	-23.486369	-2.718093	12.880591
11	6	-23.846851	-1.557785	-13.54529
12	6	-23.301959	-1.25131	14.801017
13	6	-23.715621	-0.039074	15.438554
14	7	-24.089273	0.957672	15.907711
15	6	-22.378068	-2.147868	15.372912
16	6	-21.76915	-1.852203	16.725797
17	9	-20.899517	-2.805456	17.108118
18	9	-22.71583	-1.768227	17.683289
19	9	-21.100268	-0.681077	16.719675
20	6	-22.013981	-3.313364	14.710291
21	1	-21.136207	-8.445997	13.545066
22	1	-22.814393	-8.038246	13.087337
23	1	-22.232824	-7.329262	10.360816
24	1	-19.182192	-7.158357	12.426974
25	1	-19.546674	-6.079945	11.060736
26	1	-19.72123	-7.83736	10.872567
27	1	-22.690086	-4.884749	11.831164
28	1	-23.920695	-2.936393	11.908517
29	1	-24.558503	-0.872841	13.096664
30	1	-21.305558	-3.998642	15.154486

5.2_4

Free Energy/Hartrees= -1482.442126

Enthalpy/Hartrees = -1482.374841

Center Number	Atomic Number	Coordinates (Angstroms)		
		X	Y	Z
1	6	-21.232939	-8.363887	12.568013
2	17	-22.925799	-8.757545	13.056355
3	6	-21.144504	-6.972003	11.944732
4	8	-22.090174	-6.802909	-10.89787
5	6	-19.752604	-6.77945	11.338308
6	6	-21.32971	-5.905862	13.054843
7	8	-20.735083	-5.996914	14.118253
8	7	-22.150129	-4.876872	-12.68559
9	6	-22.496418	-3.730029	13.402204
10	6	-23.347099	-2.804236	12.781861
11	6	-23.727848	-1.649115	-13.44432
12	6	-23.271299	-1.383654	-14.74387
13	6	-23.700802	-0.174015	15.375799
14	7	-24.083125	0.822983	15.837418
15	6	-22.415559	-2.316343	15.362476
16	6	-21.903688	-2.06586	16.763802
17	9	-21.087432	-3.048346	-17.18724
18	9	-22.917408	-1.979118	17.649629
19	9	-21.209148	-0.911691	16.835553
20	6	-22.031697	-3.476658	14.702273
21	1	-20.932012	-9.125394	-11.84756
22	1	-20.618453	-8.412773	13.466569
23	1	-22.884342	-7.310909	-11.12916
24	1	-18.982833	-6.852373	-12.11019
25	1	-19.685625	-5.793288	10.870425
26	1	-19.577402	-7.53601	10.568718
27	1	-22.542023	-4.987701	11.757019
28	1	-23.712097	-2.989835	11.775058
29	1	-24.38634	-0.936085	-12.95971
30	1	-21.376007	-4.190406	-15.18157

5.2_3

Free Energy/Hartrees= -1482.441934

Enthalpy/Hartrees = -1482.375004

Center Number	Atomic Number	Coordinates (Angstroms)		
		X	Y	Z
1	6	0.132654	0.152704	0.000676
2	17	1.912053	0.433682	-0.119812
3	6	-0.639039	1.470955	-0.00686
4	8	-0.267976	2.291875	-1.105703
5	6	-2.135047	1.177151	-0.140757
6	6	-0.416682	2.19724	1.344401
7	8	-0.500302	1.59373	2.403372
8	7	-0.189655	3.537984	1.207764
9	6	-0.00446	4.503125	2.198472
10	6	0.187144	5.830579	1.790205
11	6	0.378484	6.831547	2.728117
12	6	0.383876	6.53807	4.099823
13	6	0.587081	7.614974	5.019612
14	7	0.756588	8.529774	5.717958
15	6	0.189993	5.202824	4.505054
16	6	0.189128	4.846364	5.975243
17	9	1.365278	5.157641	6.55785
18	9	-0.777187	5.510514	6.642408
19	9	-0.019609	3.53236	6.176789
20	6	-0.00131	4.195427	3.56804
21	1	-0.14474	-0.457639	-0.860027
22	1	-0.047174	-0.382616	0.932625
23	1	0.674854	2.143411	-1.282848
24	1	-2.487909	0.58362	0.705923
25	1	-2.696204	2.115367	-0.16781
26	1	-2.323244	0.63865	-1.073465
27	1	-0.16269	3.84508	0.24088
28	1	0.185885	6.080369	0.732414
29	1	0.526539	7.857011	2.406626
30	1	-0.148904	3.172046	3.884216

COMPOUND 5.3

5.3_1

Free Energy/Hartrees= -1098.081317

Enthalpy/Hartrees = -1098.012352

Center Number	Atomic Number	Coordinates (Amstrong)		
		X	Y	Z
1	6	3.020728	2.515542	-0.582332
2	8	1.79149	2.851217	0.050167
3	6	3.111632	1.001736	-0.797299
4	8	1.914043	0.544355	-1.417492
5	6	4.286293	0.638525	-1.701311
6	6	3.306453	0.307405	0.572077
7	8	4.062149	0.76379	1.421379
8	7	2.586123	-0.848354	0.697365
9	6	2.562715	-1.75909	1.753548
10	6	3.344137	-1.619131	2.908803
11	6	3.258784	-2.577829	3.909878
12	6	2.408825	-3.686611	3.797087
13	6	2.373574	-4.630734	4.871217
14	7	2.382335	-5.367425	5.771525
15	6	1.627261	-3.821449	2.631276
16	6	0.694577	-4.997942	2.459494
17	9	-0.244745	-5.031521	3.4252
18	9	0.045242	-4.953888	1.276536
19	9	1.359396	-6.168978	2.502644
20	6	1.708801	-2.867401	1.629661
21	1	3.009335	3.00627	-1.56005
22	1	3.884632	2.867108	-0.010832
23	1	1.906345	2.792386	1.006335
24	1	1.205134	1.125387	-1.094246
25	1	5.232369	0.93453	-1.240118
26	1	4.309274	-0.439379	-1.884781
27	1	4.17711	1.146171	-2.663852
28	1	1.97857	-1.025194	-0.097384
29	1	4.004009	-0.767728	3.009653
30	1	3.863379	-2.471181	4.8046
31	1	1.101432	-2.985187	0.738251

5.3_2

Free Energy/Hartrees= -1098.080964

Enthalpy/Hartrees= -1098.011856

Center Number	Atomic Number	Coordinates (Angstroms)		
		X	Y	Z
1	6	2.401792	1.75417	-0.208668
2	8	3.164429	2.950295	-0.101831
3	6	3.060128	0.631177	0.598592
4	8	3.343891	1.103658	1.912349
5	6	2.141843	-0.581902	0.714468
6	6	4.366668	0.20131	-0.110834
7	8	4.425019	0.079099	-1.327851
8	7	5.395375	-0.043487	0.757246
9	6	6.688677	-0.491735	0.490033
10	6	7.564786	-0.647907	1.573767
11	6	8.861604	-1.088911	1.368811
12	6	9.323045	-1.387532	0.078055
13	6	10.673624	-1.835787	-0.069658
14	7	11.778495	-2.195203	-0.127965
15	6	8.438566	-1.231719	-1.007356
16	6	8.897539	-1.542149	-2.414886
17	9	7.920277	-1.345206	-3.319441
18	9	9.938096	-0.763354	-2.776797
19	9	9.296991	-2.825005	-2.532331
20	6	7.137067	-0.789776	-0.806583
21	1	1.423021	1.970841	0.229474
22	1	2.272218	1.442984	-1.249283
23	1	3.842845	2.949441	-0.78798
24	1	3.533162	2.052585	1.82069
25	1	1.936979	-1.004658	-0.272808
26	1	2.603749	-1.354413	1.335748
27	1	1.200028	-0.28426	1.184133
28	1	5.156541	0.166936	1.721866
29	1	7.227826	-0.42329	2.582342
30	1	9.53513	-1.207376	2.210968
31	1	6.461789	-0.670826	-1.642569

5.3_3

Free Energy/Hartrees= -1098.080928

Enthalpy/Hartrees= -1098.011913

Center Number	Atomic Number	Coordinates (Angstroms)		
		X	Y	Z
1	6	2.196295	0.516121	-0.093605
2	8	3.420247	1.029029	0.418945
3	6	1.12472	1.610259	-0.099698
4	8	1.650284	2.776681	-0.726467
5	6	-0.115507	1.171219	-0.872572
6	6	0.716521	1.923779	1.359757
7	8	0.569358	1.036091	2.190232
8	7	0.515932	3.258002	1.587187
9	6	0.082942	3.901344	2.746338
10	6	-0.039761	5.297884	2.712327
11	6	-0.469188	5.99142	3.831529
12	6	-0.788601	5.313429	5.017411
13	6	-1.226537	6.084953	6.139788
14	7	-1.576516	6.763632	7.017418
15	6	-0.663885	3.910424	5.047059
16	6	-0.998157	3.143437	6.307273
17	9	-2.284405	3.327152	6.669636
18	9	-0.812756	1.818695	6.157125
19	9	-0.229023	3.538645	7.342694
20	6	-0.23394	3.210494	3.926886
21	1	2.394435	0.215957	-1.126893
22	1	1.845749	-0.350348	0.474567
23	1	3.419702	0.934043	1.379206
24	1	2.600622	2.784777	-0.522703
25	1	-0.579262	0.303276	-0.396063
26	1	-0.849049	1.981479	-0.910829
27	1	0.164537	0.915392	-1.898373
28	1	0.74503	3.835179	0.783339
29	1	0.200694	5.842828	1.803243
30	1	-0.562582	7.071764	3.799228
31	1	-0.140298	2.133664	3.954015

5.3_4

Free Energy/Hartrees= -1098.080225

Enthalpy/Hartrees= -1098.080225

Center Number	Atomic Number	Coordinates (Angstroms)		
		X	Y	Z
1	6	2.835559	2.512236	-0.445694
2	8	1.420343	2.400943	-0.323976
3	6	3.366141	1.081585	-0.54137
4	8	2.588583	0.350015	-1.483226
5	6	4.820918	1.063262	-1.003289
6	6	3.298278	0.427363	0.862012
7	8	3.75836	0.988735	1.845926
8	7	2.737441	-0.819882	0.851225
9	6	2.556067	-1.7076	1.909673
10	6	2.928686	-1.419542	3.230131
11	6	2.70528	-2.36405	4.223185
12	6	2.114767	-3.603876	3.941643
13	6	1.913386	-4.523746	5.01831
14	7	1.770901	-5.234254	5.928508
15	6	1.744683	-3.887377	2.61084
16	6	1.101804	-5.206812	2.25296
17	9	1.891537	-6.249754	2.575762
18	9	-0.071871	-5.377177	2.89398
19	9	0.846515	-5.29808	0.929905
20	6	1.965199	-2.948005	1.616484
21	1	3.105754	3.054356	-1.36186
22	1	3.280112	3.004716	0.425692
23	1	1.02054	3.276627	-0.312074
24	1	1.70327	0.750745	-1.472504
25	1	5.455565	1.595998	-0.290596
26	1	5.177971	0.032783	-1.08467
27	1	4.900122	1.531596	-1.988095
28	1	2.416856	-1.10348	-0.069696
29	1	3.384849	-0.466245	3.46196
30	1	2.992362	-2.141919	5.245801
31	1	1.674721	-3.180159	0.597152

5.3_5

Free Energy/Hartrees= -1098.079871

Enthalpy/Hartrees= -1098.010789

Center Number	Atomic Number	Coordinates (Angstroms)		
		X	Y	Z
1	6	2.300103	0.654852	-0.096183
2	8	3.4292	1.432825	0.291129
3	6	1.111959	1.616396	-0.119807
4	8	1.477504	2.804996	-0.814203
5	6	-0.086922	0.994651	-0.831128
6	6	0.693439	1.931974	1.33872
7	8	0.509922	1.038695	2.152444
8	7	0.50582	3.267126	1.570708
9	6	0.077472	3.906381	2.732068
10	6	-0.049325	5.30285	2.702715
11	6	-0.472054	5.992794	3.826571
12	6	-0.781441	5.311489	5.013227
13	6	-1.213581	6.079671	6.139975
14	7	-1.559175	6.756097	7.021211
15	6	-0.652518	3.908551	5.038471
16	6	-0.976488	3.138212	6.298944
17	9	-2.26037	3.320541	6.672326
18	9	-0.792249	1.813913	6.145003
19	9	-0.200088	3.531225	7.330214
20	6	-0.22839	3.212296	3.914038
21	1	2.441805	0.2378	-1.10235
22	1	2.098287	-0.150556	0.617962
23	1	4.221306	0.885686	0.293559
24	1	2.435748	2.907277	-0.689081
25	1	-0.41256	0.090013	-0.311532
26	1	-0.920614	1.702073	-0.853531
27	1	0.182617	0.750258	-1.862163
28	1	0.717763	3.843348	0.761907
29	1	0.183917	5.850477	1.793373
30	1	-0.568082	7.073027	3.797498
31	1	-0.130706	2.135662	3.937015

5.3_6

Free Energy/Hartrees= -1098.079859

Enthalpy/Hartrees= -1098.010357

Center Number	Atomic Number	Coordinates (Angstroms)		
		X	Y	Z
1	6	2.080808	0.663791	-0.814224
2	8	1.301	1.823909	-1.082846
3	6	3.219141	1.129144	0.107558
4	8	3.875815	2.236846	-0.50175
5	6	2.705248	1.506648	1.498883
6	6	4.220224	-0.029404	0.22955
7	8	3.874226	-1.105277	0.698636
8	7	5.474148	0.26889	-0.227761
9	6	6.611012	-0.537776	-0.246093
10	6	6.628531	-1.859737	0.220207
11	6	7.810244	-2.586932	0.164357
12	6	8.992148	-2.033998	-0.34762
13	6	10.170041	-2.845261	-0.37156
14	7	11.098762	-3.545956	-0.367701
15	6	8.966656	-0.703902	-0.815252
16	6	10.21348	-0.058842	-1.373766
17	9	10.687	-0.732327	-2.440852
18	9	9.985171	1.209858	-1.77584
19	9	11.200768	-0.01125	-0.457669
20	6	7.790078	0.025845	-0.761712
21	1	1.496116	-0.116162	-0.314445
22	1	2.504458	0.257153	-1.742832
23	1	0.664121	1.631931	-1.778826
24	1	3.182496	2.785968	-0.898165
25	1	2.3045	0.627289	2.009273
26	1	3.521856	1.922131	2.095443
27	1	1.917665	2.259491	1.408593
28	1	5.555901	1.210686	-0.598092
29	1	5.723901	-2.299784	0.618248
30	1	7.825051	-3.610156	0.525245
31	1	7.785935	1.048681	-1.123686

5.3_7

Free Energy/Hartrees= -1098.079465

Enthalpy/Hartrees= -1098.010427

Center Number	Atomic Number	Coordinates (Angstroms)		
		X	Y	Z
1	6	2.467253	2.399004	-0.13379
2	8	2.19919	2.94216	-1.421987
3	6	3.185576	1.063336	-0.384463
4	8	2.399923	0.285318	-1.282298
5	6	4.594837	1.272391	-0.94393
6	6	3.273742	0.324376	0.95919
7	8	3.886669	0.811277	1.899644
8	7	2.615584	-0.874377	0.978314
9	6	2.508637	-1.794581	2.020034
10	6	3.109491	-1.6165	3.274084
11	6	2.950811	-2.591031	4.250648
12	6	2.202678	-3.753121	4.017261
13	6	2.08514	-4.711836	5.072314
14	7	2.021072	-5.45887	5.961894
15	6	1.600451	-3.924833	2.753811
16	6	0.785485	-5.160025	2.449329
17	9	1.528333	-6.280755	2.543324
18	9	-0.252145	-5.292981	3.298767
19	9	0.273007	-5.12807	1.20032
20	6	1.756566	-2.955831	1.775834
21	1	3.107784	3.057636	0.462776
22	1	1.531702	2.214741	0.412018
23	1	1.607035	3.696647	-1.33861
24	1	2.0501	0.898886	-1.946236
25	1	5.227808	1.771034	-0.205663
26	1	5.039686	0.306587	-1.19849
27	1	4.545106	1.885148	-1.847919
28	1	2.148819	-1.093376	0.103679
29	1	3.689693	-0.72439	3.468933
30	1	3.415885	-2.454676	5.22151
31	1	1.28888	-3.102389	0.807801

5.3_8

Free Energy/Hartrees= -1098.079448

Enthalpy/Hartrees= -1098.006954

Center Number	Atomic Number	Coordinates (Angstroms)		
		X	Y	Z
1	6	2.132908	0.588399	-0.918681
2	8	1.337001	1.659783	-1.407665
3	6	3.220388	1.130934	0.035984
4	8	3.862318	2.230243	-0.600784
5	6	2.64477	1.558461	1.387075
6	6	4.244003	0.008122	0.253132
7	8	3.922979	-1.023008	0.829414
8	7	5.479779	0.274421	-0.26766
9	6	6.624833	-0.521248	-0.249938
10	6	6.673136	-1.791899	0.34008
11	6	7.86062	-2.511365	0.313504
12	6	9.017807	-2.000575	-0.290349
13	6	10.203937	-2.800022	-0.275999
14	7	11.140588	-3.488883	-0.235757
15	6	8.960829	-0.722641	-0.88375
16	6	10.180055	-0.125705	-1.547071
17	9	10.632017	-0.90466	-2.54936
18	9	9.919624	1.089118	-2.075956
19	9	11.193104	0.032792	-0.672321
20	6	7.778561	-0.000496	-0.85923
21	1	1.536554	-0.180416	-0.417433
22	1	2.60773	0.143416	-1.798317
23	1	0.62336	1.843474	-0.786603
24	1	3.180095	2.682908	-1.121869
25	1	2.23808	0.697571	1.923639
26	1	3.426476	2.01817	1.997544
27	1	1.855949	2.304555	1.243364
28	1	5.540759	1.184879	-0.713257
29	1	5.787728	-2.199006	0.809898
30	1	7.899724	-3.494664	0.770684
31	1	7.749786	0.981741	-1.319319

5.3_9

Free Energy/Hartrees= -1098.079269

Enthalpy/Hartrees= -1098.009779

Center Number	Atomic Number	Coordinates (Angstroms)		
		X	Y	Z
1	6	2.845565	1.196277	-1.399035
2	8	3.508524	2.369072	-1.852743
3	6	2.33153	1.405203	0.043577
4	8	3.398305	1.940452	0.820153
5	6	1.115391	2.330782	0.097337
6	6	1.946538	0.026885	0.598747
7	8	1.011969	-0.598939	0.117111
8	7	2.747157	-0.40243	1.621149
9	6	2.688713	-1.595309	2.340395
10	6	3.642294	-1.795734	3.34903
11	6	3.635961	-2.959742	4.099099
12	6	2.678306	-3.95821	3.866799
13	6	2.724608	-5.139016	4.673105
14	7	2.812524	-6.075016	5.358394
15	6	1.720984	-3.751988	2.85379
16	6	0.673228	-4.805889	2.572014
17	9	-0.16698	-4.434212	1.588356
18	9	1.237199	-5.972263	2.194821
19	9	-0.077858	-5.059147	3.663496
20	6	1.723794	-2.586331	2.098296
21	1	2.022503	0.900339	-2.056967
22	1	3.600534	0.404346	-1.407082
23	1	2.864992	2.980241	-2.228312
24	1	3.906558	2.516015	0.226395
25	1	0.263511	1.879236	-0.417192
26	1	0.838146	2.523529	1.137053
27	1	1.352742	3.294527	-0.365677
28	1	3.472621	0.263395	1.868876
29	1	4.392297	-1.034427	3.546558
30	1	4.376476	-3.109165	4.877715
31	1	0.987468	-2.432784	1.321542

5.3_10

Free Energy/Hartrees= -1098.079157

Enthalpy/Hartrees= -1098.010288

Center Number	Atomic Number	Coordinates (Angstroms)		
		X	Y	Z
1	6	2.376899	2.377014	-0.035265
2	8	1.867115	2.999799	-1.206851
3	6	3.105471	1.065763	-0.40833
4	8	2.258606	0.320723	-1.276699
5	6	4.458018	1.323061	-1.073774
6	6	3.316285	0.273957	0.889767
7	8	4.063155	0.696621	1.762693
8	7	2.585998	-0.879675	0.960629
9	6	2.525514	-1.81276	1.995062
10	6	3.257509	-1.695868	3.18485
11	6	3.13214	-2.675411	4.161268
12	6	2.290111	-3.782736	3.989994
13	6	2.212458	-4.749373	5.041547
14	7	2.185749	-5.505129	5.925621
15	6	1.557789	-3.893885	2.790085
16	6	0.635977	-5.067742	2.555471
17	9	-0.337198	-5.128907	3.485798
18	9	0.028576	-4.996157	1.351658
19	9	1.30285	-6.238165	2.592954
20	6	1.679787	-2.919453	1.812624
21	1	3.043867	3.034698	0.531019
22	1	1.504741	2.147365	0.584317
23	1	2.547193	3.558384	-1.599323
24	1	1.781019	0.969693	-1.81786
25	1	5.14366	1.813901	-0.378573
26	1	4.900751	0.37787	-1.39871
27	1	4.327806	1.950145	-1.962191
28	1	2.022573	-1.050403	0.133187
29	1	3.910831	-0.845989	3.330919
30	1	3.698215	-2.586414	5.082731
31	1	1.110236	-3.018229	0.894382

5.3_11

Free Energy/Hartrees= -1098.079131

Enthalpy/Hartrees= -1098.009853

Center Number	Atomic Number	Coordinates (Angstroms)		
		X	Y	Z
1	6	2.669894	1.278372	-1.38791
2	8	3.22312	2.528059	-1.786192
3	6	2.297407	1.439466	0.094579
4	8	3.439672	1.913526	0.802617
5	6	1.113997	2.391247	0.282689
6	6	1.926762	0.049114	0.632298
7	8	0.979944	-0.567847	0.164486
8	7	2.743507	-0.393779	1.636558
9	6	2.687555	-1.590165	2.349511
10	6	3.6568	-1.804156	3.340445
11	6	3.654272	-2.972318	4.083988
12	6	2.685248	-3.962217	3.862419
13	6	2.736514	-5.148129	4.660864
14	7	2.829303	-6.089048	5.338764
15	6	1.712299	-3.742618	2.867223
16	6	0.652409	-4.78725	2.597012
17	9	1.201964	-5.956299	2.206405
18	9	-0.083963	-5.039839	3.698645
19	9	-0.199782	-4.405398	1.627725
20	6	1.710854	-2.572487	2.118668
21	1	1.776461	1.022266	-1.967709
22	1	3.411206	0.474428	-1.494741
23	1	3.609216	2.446209	-2.664335
24	1	3.867103	2.568447	0.229983
25	1	0.210625	1.968795	-0.164105
26	1	0.937963	2.557917	1.348801
27	1	1.335022	3.351091	-0.191602
28	1	3.486044	0.258275	1.868986
29	1	4.415557	-1.049483	3.529894
30	1	4.406647	-3.131661	4.849162
31	1	0.962182	-2.408517	1.355972

5.3_12

Free Energy/Hartrees= -1098.078693

Enthalpy/Hartrees= -1098.009740

Center Number	Atomic Number	Coordinates (Angstroms)		
		X	Y	Z
1	6	1.960512	0.787731	0.124131
2	8	1.72664	1.097465	1.473505
3	6	3.227334	1.459234	-0.458452
4	8	3.310888	1.14059	-1.850073
5	6	3.224743	2.970117	-0.234551
6	6	4.458157	0.845814	0.224504
7	8	4.507793	0.755205	1.449682
8	7	5.440371	0.438612	-0.627567
9	6	6.670605	-0.152517	-0.330891
10	6	7.119838	-0.388765	0.975108
11	6	8.361057	-0.980009	1.171969
12	6	9.180073	-1.347853	0.095844
13	6	10.4454	-1.953092	0.377566
14	7	11.46294	-2.440836	0.66022
15	6	8.72135	-1.105842	-1.215192
16	6	9.564697	-1.485155	-2.41049
17	9	10.753986	-0.852145	-2.400345
18	9	9.812593	-2.808957	-2.442338
19	9	8.956166	-1.167261	-3.573245
20	6	7.48347	-0.516443	-1.416483
21	1	2.034101	-0.29723	-0.047667
22	1	1.097726	1.154055	-0.444443
23	1	2.539769	0.877635	1.956999
24	1	2.774985	1.767495	-2.349855
25	1	3.181555	3.19906	0.831802
26	1	4.119756	3.429605	-0.665287
27	1	2.336625	3.410711	-0.703395
28	1	5.19569	0.551903	-1.60621
29	1	6.498042	-0.112581	1.815964
30	1	8.710426	-1.164557	2.18252
31	1	7.142714	-0.337685	-2.43103

5.3_13

Free Energy/Hartrees= -1098.078539

Enthalpy/Hartrees= -1098.009759

Center Number	Atomic Number	Coordinates (Angstroms)		
		X	Y	Z
1	6	2.037257	0.952427	0.267707
2	8	1.926276	1.655868	1.47778
3	6	3.233509	1.399945	-0.606091
4	8	3.188207	0.678341	-1.839961
5	6	3.231839	2.908553	-0.84478
6	6	4.532103	1.000306	0.109231
7	8	4.698574	1.278058	1.295294
8	7	5.435453	0.34477	-0.672349
9	6	6.699629	-0.143306	-0.334234
10	6	7.27463	0.010578	0.934271
11	6	8.5411	-0.506199	1.174966
12	6	9.26275	-1.179223	0.179809
13	6	10.561805	-1.683833	0.503273
14	7	11.611775	-2.074084	0.817038
15	6	8.677623	-1.329126	-1.094178
16	6	9.413403	-2.047415	-2.201598
17	9	9.67921	-3.326472	-1.87215
18	9	8.695899	-2.07312	-3.345263
19	9	10.587913	-1.451372	-2.484799
20	6	7.413933	-0.815954	-1.338702
21	1	2.110646	-0.134978	0.423366
22	1	1.119572	1.143235	-0.300867
23	1	2.784001	1.579634	1.926816
24	1	2.601025	1.137124	-2.452079
25	1	3.293095	3.445295	0.103488
26	1	4.072584	3.203185	-1.480432
27	1	2.29486	3.203733	-1.332159
28	1	5.096979	0.164464	-1.612257
29	1	6.729261	0.526281	1.71316
30	1	8.988142	-0.388685	2.156626
31	1	6.975447	-0.940029	-2.323425

5.3_14

Free Energy/Hartrees= -1098.077014

Enthalpy/Hartrees= -1098.008420

Center Number	Atomic Number	Coordinates (Angstroms)		
		X	Y	Z
1	6	1.967663	1.122815	0.32643
2	8	1.976422	1.980837	1.432898
3	6	3.147488	1.338694	-0.645641
4	8	2.983329	0.496861	-1.790021
5	6	3.2098	2.776788	-1.150378
6	6	4.467068	1.000917	0.077888
7	8	4.669818	1.353983	1.238386
8	7	5.360267	0.316533	-0.693048
9	6	6.655516	-0.104842	-0.382324
10	6	7.260941	0.116155	0.8618
11	6	8.554023	-0.340956	1.08046
12	6	9.272264	-1.019837	0.086789
13	6	10.598752	-1.463609	0.387414
14	7	11.671112	-1.804209	0.682594
15	6	8.656709	-1.236334	-1.162981
16	6	9.38749	-1.964492	-2.267527
17	9	10.532532	-1.339261	-2.60158
18	9	9.705347	-3.222691	-1.904677
19	9	8.64042	-2.051965	-3.388941
20	6	7.366586	-0.78214	-1.385775
21	1	1.96086	0.060849	0.637788
22	1	1.043149	1.314369	-0.229412
23	1	2.85546	1.900254	1.840662
24	1	2.513289	-0.30703	-1.529806
25	1	3.356281	3.466588	-0.317102
26	1	4.027192	2.89797	-1.867237
27	1	2.268424	3.020647	-1.650385
28	1	4.998617	0.089377	-1.614454
29	1	6.718697	0.63828	1.638637
30	1	9.024847	-0.171231	2.043168
31	1	6.906736	-0.954822	-2.353326

A4.3.Optimised geometries of conformers of compounds 5.1, 5.2, 5.3, for the construction of the VCD spectra in Figures 5.1, 5.2 and 5.3 (bottom spectra). Input geometries obtained from manual conformational samplings of conformers.

COMPOUND 5.1

5.1`-1

Free Energy/Hartrees= -1021.660890

Enthalpy/Hartrees= -1021.596001

Center Number	Atomic Number	Coordinates (Angstroms)		
		X	Y	Z
1	6	1.230163	2.104071	0.124188
2	6	2.258879	1.153942	0.065193
3	6	1.913391	-0.209758	-0.030145
4	6	0.579724	-0.584738	-0.061836
5	6	-0.44313	0.375876	-0.000149
6	6	-0.107761	1.733622	0.09261
7	6	3.613314	1.612529	0.105524
8	6	2.985064	-1.272911	-0.095747
9	7	4.695689	2.037267	0.142994
10	9	3.794448	-1.097665	-1.158324
11	9	3.759749	-1.264057	1.007176
12	9	2.457591	-2.511465	-0.198883
13	7	-1.75845	-0.087728	-0.034299
14	6	-2.922935	0.635387	-0.014352
15	6	-4.16637	-0.237124	-0.025386
16	8	-3.00433	1.853932	0.016431
17	6	-4.393228	-1.105941	1.144863
18	6	-5.308735	0.280823	-0.85592
19	8	-3.901868	-1.648151	-0.085357
20	1	1.491755	3.154692	0.196003
21	1	0.328558	-1.637787	-0.136849
22	1	-0.891281	2.478417	0.135257
23	1	-1.90318	-1.089691	-0.115593
24	1	-5.414945	-1.386801	1.395648
25	1	-3.683014	-1.108057	1.971118
26	1	-5.578223	1.287404	-0.527723
27	1	-6.174123	-0.378591	-0.759093
28	1	-5.022994	0.331425	-1.910995

COMPOUND 5.2

5.2'-1

Free Energy/Hartrees= -1482.432993

Enthalpy/Hartrees= -1482.362933

Center Number	Atomic Number	Coordinates (Angstroms)		
		X	Y	Z
1	6	2.05287	2.08113	-0.270711
2	6	3.014405	1.063581	-0.211411
3	6	2.585176	-0.258019	0.024591
4	6	1.235657	-0.526284	0.190125
5	6	0.281453	0.500676	0.126577
6	6	0.699158	1.817074	-0.104995
7	6	4.389845	1.413228	-0.393571
8	6	3.580517	-1.393714	0.095441
9	7	5.492448	1.749366	-0.548625
10	9	4.257426	-1.529635	-1.060729
11	9	4.484575	-1.200584	1.074045
12	9	2.973252	-2.574609	0.342013
13	7	-1.06057	0.133059	0.297629
14	6	-2.172113	0.928773	0.302786
15	6	-3.537875	0.206282	0.450301
16	8	-2.149705	2.144861	0.161758
17	6	-3.864428	-0.345586	-0.956526
18	6	-3.530999	-0.880735	1.524066
19	8	-4.476835	1.176941	0.828628
20	17	-5.417889	-1.235059	-1.016231
21	1	2.379068	3.100199	-0.450332
22	1	0.923017	-1.549895	0.37055
23	1	-0.028922	2.615425	-0.150039
24	1	-1.219142	-0.846678	0.486845
25	1	-3.947681	0.485091	-1.660424
26	1	-3.093592	-1.037109	-1.306901
27	1	-3.13792	-0.485321	2.464092
28	1	-2.958389	-1.7678	1.229655
29	1	-4.560459	-1.203515	1.690966
30	1	-4.101962	2.039245	0.577395

5.2`-2

Free Energy/Hartrees= -1482.432329

Enthalpy/Hartrees= -1482.362272

Center Number	Atomic Number	Coordinates (Angstroms)		
		X	Y	Z
1	6	2.166329	2.308763	-0.09712
2	6	3.03741	1.216723	0.027033
3	6	2.495499	-0.083034	0.02273
4	6	1.126143	-0.283492	-0.101249
5	6	0.266616	0.818041	-0.222385
6	6	0.800476	2.11362	-0.219588
7	6	4.438263	1.480704	0.152398
8	6	3.402352	-1.287531	0.15665
9	7	5.563855	1.756255	0.251669
10	9	4.311169	-1.331636	-0.837804
11	9	4.080451	-1.261894	1.321809
12	9	2.713475	-2.44283	0.120598
13	7	-1.124125	0.69101	-0.344441
14	6	-1.882646	-0.445835	-0.392878
15	6	-3.420312	-0.247847	-0.472327
16	8	-1.427528	-1.580825	-0.341069
17	6	-3.871733	0.056683	0.974403
18	6	-3.835921	0.839098	-1.462725
19	8	-3.967928	-1.461266	-0.913144
20	17	-5.635475	0.337791	1.112481
21	1	2.57403	3.313958	-0.095869
22	1	0.719669	-1.284814	-0.108099
23	1	0.14502	2.976001	-0.313032
24	1	-1.626281	1.559894	-0.460322
25	1	-3.635896	-0.796707	1.613549
26	1	-3.38022	0.949012	1.37118
27	1	-3.356032	0.676105	-2.431074
28	1	-3.610861	1.850413	-1.105162
29	1	-4.917171	0.780807	-1.601405
30	1	-3.304344	-2.149366	-0.729925

COMPOUND 5.3

5.3'-1

Free Energy/Hartrees= -1098.075476

Enthalpy/Hartrees= -1098.006444

Center Number	Atomic Number	Coordinates (Angstroms)		
		X	Y	Z
1	6	-1.480093	2.07504	0.115102
2	6	-2.564969	1.190482	0.047865
3	6	-2.304888	-0.193961	-0.01223
4	6	-0.997271	-0.65249	-0.002992
5	6	0.082357	0.24276	0.065506
6	6	-0.167864	1.620166	0.12448
7	6	-3.888531	1.733591	0.043849
8	6	-3.439942	-1.188833	-0.087079
9	7	-4.94278	2.225246	0.044155
10	9	-4.246351	-1.103361	0.989133
11	9	-4.20241	-0.989791	-1.179649
12	9	-2.988855	-2.460108	-0.144096
13	7	1.36543	-0.309004	0.077408
14	6	2.571016	0.325495	0.09937
15	6	3.789338	-0.608762	0.118743
16	8	2.723655	1.545531	0.109031
17	6	4.779645	-0.142699	-0.975573
18	6	4.423828	-0.582553	1.507899
19	8	3.325602	-1.919161	-0.216867
20	8	5.366615	1.10512	-0.7116
21	1	-1.676073	3.141249	0.160755
22	1	-0.811932	-1.720574	-0.050458
23	1	0.659258	2.315386	0.174745
24	1	1.444136	-1.31957	0.022455
25	1	4.257963	-0.161012	-1.944933
26	1	5.592226	-0.877041	-1.024609
27	1	5.307858	-1.231425	1.521957
28	1	3.715545	-0.928581	2.267031
29	1	4.752985	0.427536	1.758068
30	1	3.955556	-2.570663	0.112699
31	1	4.63974	1.729019	-0.551284

5.3`-2

Free Energy/Hartrees= -1098.075348

Enthalpy/Hartrees= -1098.006416

Center Number	Atomic number	Coordinates (Angstroms)		
		X	Y	Z
1	6	1.924274	2.297364	0.01488
2	6	2.766141	1.175969	-0.028309
3	6	2.183036	-0.106325	-0.004823
4	6	0.804103	-0.260132	0.058519
5	6	-0.027397	0.870622	0.099342
6	6	0.548829	2.149072	0.077985
7	6	4.178527	1.393522	-0.095028
8	6	3.0563	-1.340365	-0.053829
9	7	5.315891	1.63222	-0.148596
10	9	3.788917	-1.3795	-1.186405
11	9	3.919114	-1.376894	0.982485
12	9	2.332599	-2.474397	-0.00921
13	7	-1.417677	0.785433	0.16161
14	6	-2.210089	-0.328716	0.200614
15	6	-3.713121	-0.02364	0.255875
16	8	-1.811444	-1.485354	0.174987
17	6	-4.336965	-0.523455	-1.066897
18	6	-4.323495	-0.709002	1.479524
19	8	-3.901672	1.385635	0.330168
20	8	-5.649635	0.002056	-1.213079
21	1	2.364091	3.288919	-0.001594
22	1	0.361326	-1.246255	0.076403
23	1	-0.084915	3.031326	0.111317
24	1	-1.943944	1.653416	0.184055
25	1	-3.76279	-0.13312	-1.912586
26	1	-4.317532	-1.616981	-1.107207
27	1	-5.408378	-0.559662	1.494276
28	1	-3.917673	-0.270657	2.395075
29	1	-4.102705	-1.779307	1.472697
30	1	-4.759296	1.569284	-0.08543
31	1	-6.280215	-0.571595	-0.763658

A4.4. Optimised geometries for conformers of compound 5.5 for the construction of the VCD spectra in Figures 5.8 and 5.9. Input geometries obtained from conformational searches carried out by means of Force Field methods.

COMPOUND (R)-5.5

(R)-5.5_1

Free Energy/Hartrees= -646.728405

Enthalpy/Hartrees= -646.675879

Center Number	Atomic Number	Coordinates (Angstroms)		
		X	Y	Z
1	7	-0.01552	0.000483	.009803
	6	1.347867	0.070649	0.026528
3	8	2.060468	1.053148	0.032699
4	7	1.790945	-1.266894	0.047001
5	6	0.764236	-2.178362	0.063652
6	8	0.852447	-3.38836	0.07223
7	6	-0.52849	-1.35251	0.061598
8	1	-1.04315	-1.532169	1.016272
9	6	-1.46088	-1.742614	1.097177
10	6	-2.74823	-0.954998	1.085499
11	6	-3.8149	-1.341651	0.262844
12	6	-4.99249	-0.596687	0.222168
13	6	-5.12346	0.550676	1.006234
14	6	-4.07117	0.94377	1.832314
15	6	-2.89337	0.195582	1.870376
16	1	-0.57903	0.831729	0.074044
17	1	2.771394	-1.508101	0.04476
18	1	-0.9275	-1.587689	2.041501
19	1	-1.65971	-2.815758	1.004847
20	1	-3.72611	-2.240743	0.3438
21	1	-5.81101	-0.915915	0.417257
22	1	-6.04218	1.12971	0.977766
23	1	-4.16683	1.830686	2.452771
24	1	-2.08106	0.502154	2.525675

(R)-5.5_2

Free Energy/Hartrees= -646.725981

Enthalpy/Hartrees= -646.673559

Center Number	Atomic Number	Coordinates (Angstroms)		
		X	Y	Z
1	7	0.245874	1.398413	0.712634
2	6	0.835146	1.823033	0.444391
3	8	0.9712	2.955846	-.857229
4	7	1.288686	0.652605	1.082986
5	6	0.973262	-0.49368	0.400131
6	8	1.232051	-1.636565	0.717046
7	6	0.222968	-0.041702	0.860206
8	1	0.81874	-0.35988	1.727266
9	6	-1.17766	-0.678133	0.97849
10	6	-2.1279	-0.33976	0.144336
11	6	-3.00119	0.749805	0.041116
12	6	-3.87035	1.073902	-1.08241
13	6	-3.88135	0.306354	2.246759
14	6	-3.02135	-0.786301	2.359531
15	6	-2.15339	-1.10766	-1.31641
16	1	-0.22928	2.054379	1.310806
17	1	1.773237	0.677027	1.968318
18	1	-1.02108	-1.760997	1.034576
19	1	-1.60567	-0.368825	1.939508
20	1	-3.01061	1.347236	0.868284
21	1	-4.54023	1.923452	-0.98199
22	1	-4.55929	0.555027	3.058442
23	1	-3.02864	-1.39478	3.259808
24	1	-1.48857	-1.962597	1.411177

(R)-5.5_3

Free Energy/Hartrees= -646.724199

Enthalpy/Hartrees= -646.670972

Center Number	Atomic Number	Coordinates (Angstroms)		
		X	Y	Z
1	7	0.910842	2.042778	0.544918
2	6	2.092898	1.642319	0.013889
3	8	3.154209	2.230485	0.045974
4	7	1.83539	0.371863	0.555085
5	6	0.526381	-0.028656	0.4129
6	8	0.047734	-1.079174	0.781475
7	6	-0.18847	1.123078	-0.312909
8	1	-0.9276	1.548966	0.380202
9	6	-0.90034	0.693184	-0.615164
10	6	-2.25605	0.061376	-0.403844
11	6	-2.41843	-1.327645	-0.378001
12	6	-3.67706	-1.893268	-0.177689
13	6	-4.79423	-1.077515	0.999186
14	6	-4.64559	0.30936	1.025009
15	6	-3.38592	0.870905	-0.229153
16	1	0.803282	2.992139	0.865325
17	1	2.553919	-0.182137	0.998075
18	1	-1.01735	1.599112	2.222188
19	1	-0.24026	0.024179	2.177637
20	1	-1.55178	-1.971025	1.499127
21	1	-3.78335	-2.974379	1.158009
22	1	-5.77461	-1.519098	0.843483
23	1	-5.51037	0.954217	-0.89415
24	1	-3.28198	1.954235	1.261731

COMPOUND (S)-5.5

(S)-5.5_1

Free Energy/Hartrees= -646.728399

Enthalpy/Hartrees= -646.675913

Center Number	Atomic Number	Coordinates (Angstroms)		
		X	Y	Z
1	7	-0.186433	0.720707	-0.421281
2	6	0.660352	1.789774	-0.494036
3	8	0.464742	2.885399	-0.978278
4	7	1.849895	1.368231	0.132861
5	6	1.803552	0.065891	0.564821
6	8	2.67365	-0.55058	1.143551
7	6	0.416232	-0.456386	0.170318
8	1	0.558069	-1.248692	-0.57866
9	6	-0.351652	-1.029083	1.373136
10	6	-1.705529	-1.567775	0.979819
11	6	-2.859203	-0.786622	1.120953
12	6	-4.105031	-1.2714	0.719094
13	6	-4.215142	-2.548072	0.169338
14	6	-3.073266	-3.33845	0.028599
15	6	-1.830843	-2.851216	0.43105
16	1	-1.076301	0.731648	-0.894124
17	1	2.643347	1.982089	0.247212
18	1	0.270944	-1.818033	1.808583
19	1	-0.458423	-0.241364	2.126884
20	1	-2.782871	0.206327	1.558561
21	1	-4.989323	-0.651778	0.840943
22	1	-5.184338	-2.928173	-0.140997
23	1	-3.151183	-4.338642	-0.388882
24	1	-0.947945	-3.478797	0.327037

(S)-5.5_2

Free Energy/Hartrees= -646.725640

Enthalpy/Hartrees= -646.673522

Center Number	Atomic Number	Coordinates (Angstroms)		
		X	Y	Z
1	7	0.208706	0.782557	-0.969116
2	6	0.188693	1.623741	0.107303
3	8	-0.299279	2.730896	0.198141
4	7	0.885782	0.944017	1.124651
5	6	1.303065	-0.307661	0.752087
6	8	1.916609	-1.111544	1.423592
7	6	0.837675	-0.49342	-0.69887
8	1	1.736054	-0.630035	-1.316867
9	6	-0.06382	-1.733002	-0.878757
10	6	-1.346366	-1.710172	-0.083441
11	6	-1.381097	-2.191301	1.232436
12	6	-2.562968	-2.15837	1.971782
13	6	-3.731214	-1.646356	1.406642
14	6	-3.710886	-1.170785	0.095793
15	6	-2.527356	-1.205486	-0.641009
16	1	-0.307898	1.013184	-1.80215
17	1	1.02877	1.346494	2.039401
18	1	-0.286205	-1.832377	-1.947998
19	1	0.544466	-2.600317	-0.599411
20	1	-0.475162	-2.593709	1.678691
21	1	-2.571174	-2.538445	2.989734
22	1	-4.652567	-1.623076	1.981825
23	1	-4.616739	-0.775676	-0.355763
24	1	-2.526389	-0.845456	-1.667797

(S)-5.5_3

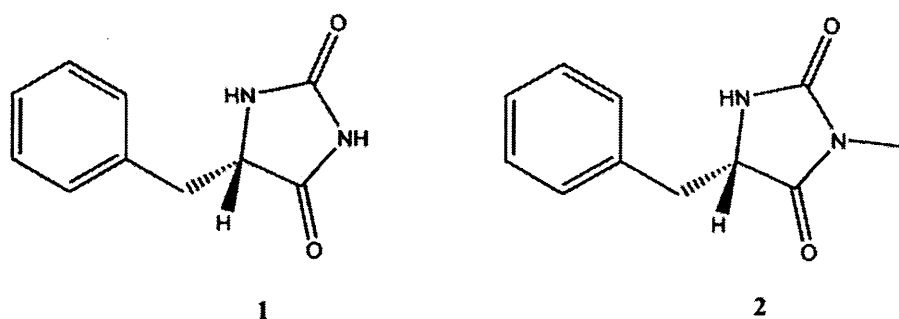
Free Energy/Hartrees= -646.724415

Enthalpy/Hartrees= -646.671048

Center Number	Atomic Number	Coordinates (Angstroms)		
		X	Y	Z
1	7	0.146492	1.875926	0.171428
2	6	1.495877	1.980445	-0.020115
3	8	2.191212	2.975065	0.006105
4	7	1.938958	0.668059	-0.255111
5	6	0.921881	-0.258826	-0.270831
6	8	1.03341	-1.451894	-0.452055
7	6	-0.370024	0.531034	-0.004427
8	1	-1.000126	0.45684	-0.9017
9	6	-1.165336	0.027741	1.221019
10	6	-1.990292	-1.210793	0.963354
11	6	-3.245165	-1.102411	0.350221
12	6	-4.020392	-2.233724	0.099768
13	6	-3.551409	-3.495241	0.467254
14	6	-2.305668	-3.614452	1.083069
15	6	-1.531953	-2.480784	1.328337
16	1	-0.420884	2.705787	0.239157
17	1	2.912644	0.445725	-0.402894
18	1	-0.470955	-0.131319	2.05307
19	1	-1.830448	0.846831	1.521143
20	1	-3.625804	-0.120692	0.073161
21	1	-4.992568	-2.128919	-0.374277
22	1	-4.154169	-4.378855	0.276791
23	1	-1.931862	-4.593066	1.371229
24	1	-0.556318	-2.585378	1.794404

Global analysis of racemisation of benzyl hydantoins

```
foldername = "C:\\Users\\User\\Desktop\\math\\"  
C:\\Users\\User\\Desktop\\math\  
datapoints60c1 = 22;  
datapoints60c2 = 13;  
Import[foldername <> "structures as defined in mathematica.gif"]
```



Constants and pKas

K_w for D₂O at 60 °C from "Handbook of Chemistry and Physics", 74th edition, 1993-1994, CRC Press, David R. Lide Editor-in-Chief, p.8-48

$$K_w60C = 10^{-13.918}$$

$$1.20781 \times 10^{-14}$$

pKas for phosphate from Fukada, H.; Takahashi, K., Proteins-Structure Function and Genetics 1998, 33 (2), 159-166".

$$pK_{aHphosphate25C} = 6.81$$

$$6.81$$

$$pK_{aHphosphate60C} = 6.76$$

$$6.76$$

$$pK_{aDphosphate60C} = pK_{aD}[pK_a] /. \{pK_a \rightarrow pK_{aHphosphate60C}\}$$

$$pK_{aD}[6.76]$$

The pK_a for the hydantoin is a pK_a^{**}, i.e. it has been determined using a standard electrode, but in D₂O and at 25 °C whereas the actual sigmoidal was determined at 60 °C.

$$pK_{ahyd1} = 8.65$$

$$8.65$$

Setting the pKa of hydantoin 2 to 20 "switches off" deprotonation for all practical purposes. Alternatively, we could use only the contribution to the rate constants of the protonated hydantoin.

$$\text{pKa}_{\text{hyd}2} = 20$$

20

Equations

Traditional conversion from pKaH to pKaD from reference: R. P. Bell, "The proton in Chemistry", Cornell University press, Ithaca, N. Y., 1959, p.189 as cited by Glasoe, P. K.; Ebersson, L., Journal of Physical Chemistry 1964, 68 (6), 1560-&

$$\text{pKaD}[\text{pKa}_] := \text{pKa} + 0.5$$

$$\text{pKaD}_{\text{phosphate}25\text{C}} = \text{pKaD}[\text{pKa}] /. \{\text{pKa} \rightarrow \text{pKaH}_{\text{phosphate}25\text{C}}\}$$

7.31

$$\text{fracacid}_{\text{hyd}}[\text{pH}_, \text{pKa}_{\text{hyd}}_] := 1 / (1 + 10^{(\text{pH} - \text{pKa}_{\text{hyd}})})$$

$$\text{fracbase}_{\text{hyd}}[\text{pH}_, \text{pKa}_{\text{hyd}}_] := 10^{(\text{pH} - \text{pKa}_{\text{hyd}})} / (1 + 10^{(\text{pH} - \text{pKa}_{\text{hyd}})})$$

The following lines assume cancellation of the correction factor from pH* -> pD and the correction factor from pKaH -> pKaD at 25 °C. Assuming sufficient buffering capacity, the ratio H2phos : H1phos should remain more or less constant with increasing temperature. This ratio can then be used to calculate pD at different temperatures. Use the pKa for the phosphate buffer at 25 °C as that is where the pH* was measured.

$$\text{H2phos}[\text{pH}_, \text{pKa}_{\text{phosphate}}_, \text{phostot}_] := (1 / (1 + 10^{(\text{pH} - \text{pKa}_{\text{phosphate}})})) \text{phostot}$$

$$\text{H1phos}[\text{pH}_, \text{pKa}_{\text{phosphate}}_, \text{phostot}_] := (10^{(\text{pH} - \text{pKa}_{\text{phosphate}})} / (1 + 10^{(\text{pH} - \text{pKa}_{\text{phosphate}})})) \text{phostot}$$

The pD needs to be calculated at 60 °C in D2O. Using "pH" in the following equation is probably a bit bad, it would be better to refer to it as pH25*. Correct this later on

$$\text{pD60C}[\text{pH}_, \text{pKa}_{\text{phosphate}}_, \text{phostot}_] := \text{pKaD}_{\text{phosphate}60\text{C}} + (\text{Log}[\text{H1phos}[\text{pH}, \text{pKa}_{\text{phosphate}}, \text{phostot}] / \text{H2phos}[\text{pH}, \text{pKa}_{\text{phosphate}}, \text{phostot}]] / \text{Log}[10])$$

[OH⁻] is calculated from the pD using the appropriate Kw

$$\text{OH60C}[\text{pH}_, \text{phostot}_] := \text{Kw60C} / (10^{(-1 \text{pD60C}[\text{pH}, \text{pKaH}_{\text{phosphate}25\text{C}}, \text{phostot}])})$$

Rate equations for racemisation of protonated and deprotonated hydantoin are defined

$$\begin{aligned} &\text{kobspartacid}_{\text{hyd}}[\text{pH}_, \text{pKa}_{\text{phosphate}}_, \text{phostot}_, \\ &\quad \text{Kw}_, \text{kOH}_{\text{hyd}}_, \text{kOHH}_{\text{hyd}}_, \text{kH2phosH}_{\text{hyd}}_, \text{kH1phosH}_{\text{hyd}}_] := \\ &\text{kOH}_{\text{hyd}} + \text{kOHH}_{\text{hyd}} \text{OH60C}[\text{pH}, \text{phostot}] + \text{kH2phosH}_{\text{hyd}} \text{H2phos}[\text{pH}, \text{pKa}_{\text{phosphate}}, \text{phostot}] + \\ &\quad \text{kH1phosH}_{\text{hyd}} \text{H1phos}[\text{pH}, \text{pKa}_{\text{phosphate}}, \text{phostot}] \end{aligned}$$

$$\begin{aligned} &\text{kobspartbase}_{\text{hyd}}[\text{pH}_, \text{pKa}_{\text{phosphate}}_, \text{phostot}_, \\ &\quad \text{Kw}_, \text{kOB}_{\text{hyd}}_, \text{kOHB}_{\text{hyd}}_, \text{kH2phosB}_{\text{hyd}}_, \text{kH1phosB}_{\text{hyd}}_] := \\ &\text{kOB}_{\text{hyd}} + \text{kOHB}_{\text{hyd}} \text{OH60C}[\text{pH}, \text{phostot}] + \text{kH2phosB}_{\text{hyd}} \text{H2phos}[\text{pH}, \text{pKa}_{\text{phosphate}}, \text{phostot}] + \\ &\quad \text{kH1phosB}_{\text{hyd}} \text{H1phos}[\text{pH}, \text{pKa}_{\text{phosphate}}, \text{phostot}] \end{aligned}$$

The observed rate constant is given as the sum of the contributions of protonated and deprotonated fractions.

$$\begin{aligned} &\text{kobs}[\text{pH}_, \text{pKa}_{\text{hyd}}_, \text{pKa}_{\text{phosphate}}_, \text{phostot}_, \text{Kw}_, \text{kOH}_{\text{hyd}}_, \text{kOB}_{\text{hyd}}_, \text{kOHH}_{\text{hyd}}_, \\ &\quad \text{kOHB}_{\text{hyd}}_, \text{kH2phosH}_{\text{hyd}}_, \text{kH2phosB}_{\text{hyd}}_, \text{kH1phosH}_{\text{hyd}}_, \text{kH1phosB}_{\text{hyd}}_] := \\ &\text{kobspartacid}_{\text{hyd}}[\text{pH}, \text{pKa}_{\text{phosphate}}, \text{phostot}, \text{Kw}, \text{kOH}_{\text{hyd}}, \text{kOHH}_{\text{hyd}}, \text{kH2phosH}_{\text{hyd}}, \\ &\quad \text{kH1phosH}_{\text{hyd}}] * \text{fracacid}_{\text{hyd}}[\text{pH}, \text{pKa}_{\text{hyd}}] + \text{kobspartbase}_{\text{hyd}}[\text{pH}, \text{pKa}_{\text{phosphate}}, \\ &\quad \text{phostot}, \text{Kw}, \text{kOB}_{\text{hyd}}, \text{kOHB}_{\text{hyd}}, \text{kH2phosB}_{\text{hyd}}, \text{kH1phosB}_{\text{hyd}}] * \text{fracbase}_{\text{hyd}}[\text{pH}, \text{pKa}_{\text{hyd}}] \end{aligned}$$

Experimental Data

■ Import data

Note, the pH values in this table are actually pH ** as defined above. The table holding the kinetic data is of the form pH **, [phosphate] total, kobs, errors

```
kineticdata60c1all = Import[foldername <> "kinetic_data\\kineticdata60C1.csv"];
```

```
MatrixForm[kineticdata60c1all]
```

6	0.25	55.46	0.33
6	0.5	95.2	1
7.2	0.045	42.9	0.45
7.2	0.09	58.97	1.16
7.2	0.18	116.78	1.4
7.2	0.27	168.28	1.75
7.2	0.5	288.4	1.1
8	0.1	137.1	1.3
8	0.2	193.5	1.4
8	0.3	268	1.7
8	0.35	305.4	0.3
9	0.05	245.1	1.2
9	0.1	259.6	0.7
9	0.2	312.7	1.5
9	0.3	355.7	2
10	0.05	304.9	1.5
10	0.1	344.6	1.5
10	0.2	365.3	1.3
10	0.3	420.7	3.4
11	0.1	362	2
11	0.2	375	5
11	0.3	404	5

```
kineticdata60c2all = Import[foldername <> "kinetic_data\\kineticdata60C2.csv"];
```

```
MatrixForm[kineticdata60c2all]
```

6	0.3	34.88	0.16
6	0.5	52.3	0.26
6	0.7	64.86	0.2
7.2	0.045	31.2	0.1
7.2	0.09	45.1	0.1
7.2	0.27	110.5	0.4
7.2	0.5	186.1	0.5
8	0.1	126.6	0.4
8	0.2	159.8	0.7
8	0.35	228.8	0.9
9	0.05	590	2
9	0.1	607	4
9	0.2	712	2

■ Separate data into kobs and errors. Set weighting factors to inverse errors.

```
kineticdata60c1 := Drop[kineticdata60c1all, None, {4}]
```

```
kineticdata60c2 := Drop[kineticdata60c2all, None, {4}]
```

```
errors60c1 := Drop[kineticdata60c1all, None, 3]
```

```

errors60c2 := Drop[kineticdata60c2all, None, 3]

weights60c1 := Flatten[1 / errors60c1]

weights60c2 := Flatten[1 / errors60c2]

```

Fit

■ Fit for compound 1

```

fit1 = NonlinearModelFit[kineticdata60c1,
  kobs[pH, pKahyd1, pKaHphosphate25C, phostot, Kw60C, kOHhyd, kOBhyd, kOHHhyd,
  kOHBhyd, kH2phosHhyd, kH2phosBhyd, kH1phosHhyd, kH1phosBhyd], {{kOHhyd, 0.1},
  {kOBhyd, 0.1}, {kOHHhyd, 1}, {kOHBhyd, 1}, {kH2phosHhyd, 1}, {kH2phosBhyd, 1},
  {kH1phosHhyd, 1}, {kH1phosBhyd, 1}}, {pH, phostot}, Weights -> weights60c1]

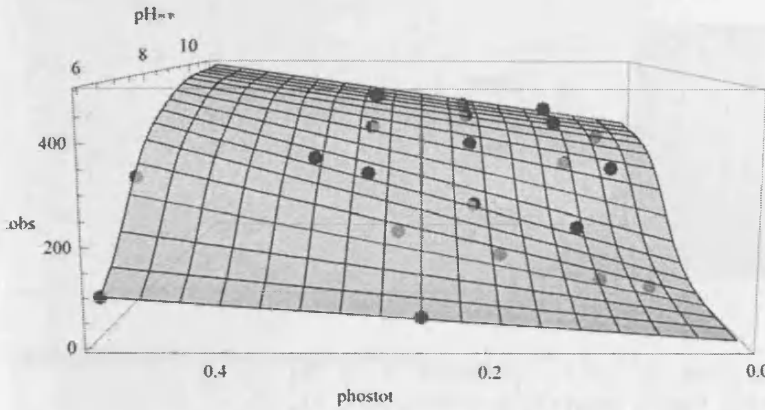
```

$$\text{FittedModel} \left[\frac{10^{-8.65+\text{pH}} \left(154.232 + \langle 22 \rangle \langle 2 \rangle^{\langle 1 \rangle} + \langle 1 \rangle + \frac{\langle 19 \rangle \langle 1 \rangle \text{phostot}}{1+10^{\langle 1 \rangle}} \right)}{1 + 10^{-8.65+\text{pH}}} + \frac{7.94332 + \langle 1 \rangle \langle 1 \rangle \langle 1 \rangle + \frac{\langle 1 \rangle}{\langle 1 \rangle}}{1 + 10^{-8.65+\text{pH}}} \right]$$

```
fit1["ParameterTable"]
```

	Estimate	Standard Error	t Statistic	P-Value
kOHhyd	7.94332	5.03612	1.57727	0.137056
kOBhyd	154.232	8.36229	18.4438	3.21487×10^{-11}
kOHHhyd	1.01432×10^7	0.000127153	7.97719×10^{10}	5.22547×10^{-146}
kOHBhyd	2256.21	3291.02	0.685566	0.504182
kH2phosHhyd	77.7003	21.1959	3.66581	0.00254387
kH2phosBhyd	27386.4	0.319698	85663.2	1.92709×10^{-62}
kH1phosHhyd	395.854	22.1177	17.8976	4.81908×10^{-11}
kH1phosBhyd	354.473	49.0546	7.22609	4.38346×10^{-6}

```
Show[Plot3D[fit1[pH, phostot], {pH, 6, 11.1}, {phostot, 0, 0.5},
  AxesLabel -> {"pH**", phostot, kobs}, PlotStyle -> Opacity[0.7],
  ViewPoint -> {-2, 0, 0.3}, LabelStyle -> Directive[Blue]],
ListPointPlot3D[{kineticdata60c1}, PlotStyle -> PointSize[Large]]]
```



```
Export[foldername <> "kinetic_data\global_fit1.jpg",
Show[Plot3D[fit1[pH, phostot], {pH, 6, 11.1}, {phostot, 0, 0.5},
  AxesLabel -> {"pH**", phostot, kobs}, PlotStyle -> Opacity[0.7],
  ViewPoint -> {-2, 0, 0.3}, LabelStyle -> Directive[Blue]],
ListPointPlot3D[{kineticdata60c1}, PlotStyle -> PointSize[Large]]],
"JPEG", ImageResolution -> 300]
C:\Users\User\Desktop\math\kinetic_data\global_fit1.jpg
```

■ Fit for compound 2

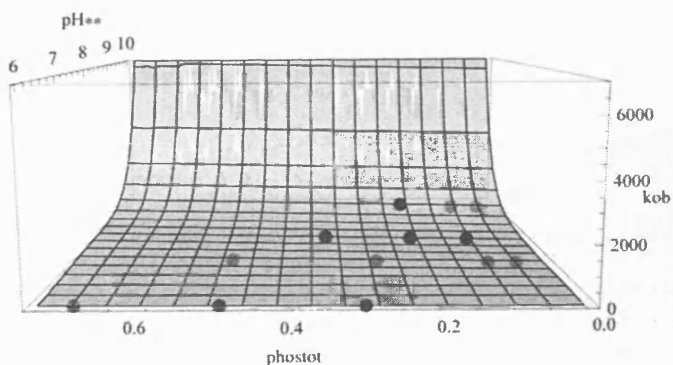
```
fit2 = NonlinearModelFit[kineticdata60c2, kobs[pH, pKahyd2, pKaHphosphate25C, phostot,
  Kw60C, kOHhyd, 0, kOHHhyd, 0, kH2phosHhyd, 0, kH1phosHhyd, 0], {{kOHhyd, 0.1},
  {kOBhyd, 0}, {kOHHhyd, 1}, {kOHBhyd, 0}, {kH2phosHhyd, 1}, {kH2phosBhyd, 0},
  {kH1phosHhyd, 1}, {kH1phosBhyd, 0}}, {pH, phostot}, Weights -> weights60c2]
```

$$\text{FittedModel} \left[\frac{7.20528 + \frac{487.385}{1 + 10^{-6.81}}}{1 + 10^{-20 + \text{pH}}} \right]$$

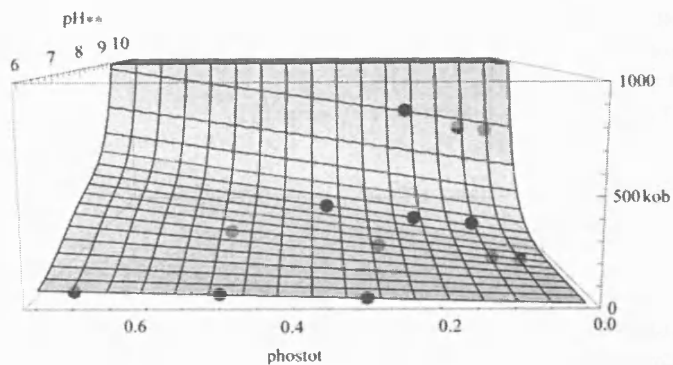
```
fit2["ParameterTable"]
```

	Estimate	Standard Error	t Statistic	P-Value
kOHhyd	7.20528	4.6875	1.53713	0.184868
kOBhyd	-2.27374×10^{-13}	1.07813×10^{-7}	-2.10897×10^{-6}	0.999998
kOHHhyd	1.70337×10^7	507 800.	33.5441	4.42689×10^{-7}
kOHBhyd	0.	0.	ComplexInfinity	$0. \times 10^{-308}$
kH2phosHhyd	21.3134	13.6644	1.55978	0.179559
kH2phosBhyd	0.	0.	ComplexInfinity	$0. \times 10^{-308}$
kH1phosHhyd	487.385	33.4313	14.5787	0.0000274194
kH1phosBhyd	0.	0.	ComplexInfinity	$0. \times 10^{-308}$

```
Show[Plot3D[fit2[pH, phostot], {pH, 6, 10.1}, {phostot, 0, 0.75},
  AxesLabel -> {"pH**", phostot, kobs}, PlotStyle -> Opacity[0.7],
  ViewPoint -> {-2, 0, 0.3}, LabelStyle -> Directive[Blue], PlotRange -> {0, 7000}],
ListPointPlot3D[{kineticdata60c2}, PlotStyle -> PointSize[Large]]]
```

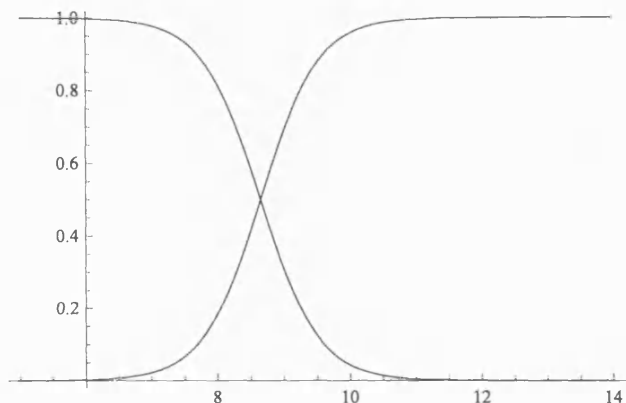


```
Show[Plot3D[fit2[pH, phostot], {pH, 6, 10.5}, {phostot, 0, 0.75},
  AxesLabel -> {"pH**", phostot, kobs}, PlotStyle -> Opacity[0.7],
  ViewPoint -> {-2, 0, 0.3}, LabelStyle -> Directive[Blue], PlotRange -> {0, 1000}],
ListPointPlot3D[{kineticdata60c2}, PlotStyle -> PointSize[Large]]]
```

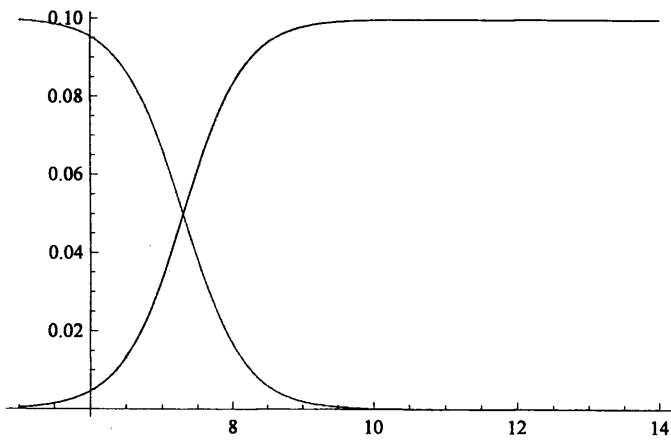


some checks

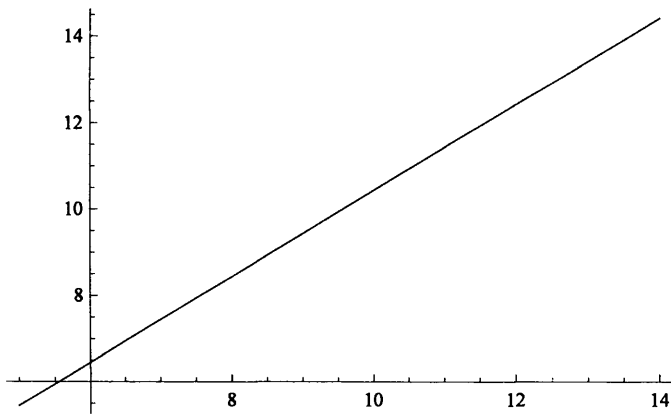
```
Show[Plot[fracacidhyd[pH, pKahyd /. {pKahyd -> pKahyd1}], {pH, 5, 14}],
Plot[fracbasehyd[pH, pKahyd /. {pKahyd -> pKahyd1}], {pH, 5, 14}]]
```



```
Show[Plot[H2phos[pH, pKaDphosphate25C, 0.1], {pH, 5, 14}, PlotStyle -> Green],
Plot[H1phos[pH, pKaDphosphate25C, 0.1], {pH, 5, 14}]]
```



```
Plot[pD60C[pH, pKaHphosphate25C, 0.1], {pH, 5, 14}]
```



```
pD60C[8, pKaHphosphate25C, 0.1]
```

8.45

```
OH60C[8, 0.1]
```

3.40408×10^{-6}

```
N[Log[10]]
```

2.30259

```
fit2["FitResiduals"]
```

{1.94933, 2.60564, -1.59806, -1.05656, -3.01797, -1.06365,
-6.53313, 15.4989, 2.78706, 2.91936, -21.2655, -28.4853, 28.0752}

```
fit2["BestFit"]
```

$$\frac{7.20528 + 3.74376 \cdot 10^{-6.81 \cdot \text{pH}} + \frac{21.3134 \text{ phostot}}{1 + 10^{-6.81 \cdot \text{pH}}} + \frac{487.385 \cdot 10^{-6.81 \cdot \text{pH}} \text{ phostot}}{1 + 10^{-6.81 \cdot \text{pH}}}}{1 + 10^{-20 \cdot \text{pH}}}$$

```
fit2["BestFitParameters"]
```

{kOHhyd -> 7.20528, kOBhyd -> -2.27374×10^{-13} , kOHHhyd -> 1.70337×10^7 , kOHBhyd -> 0.,
kH2phosHhyd -> 21.3134, kH2phosBhyd -> 0., kH1phosHhyd -> 487.385, kH1phosBhyd -> 0.}

```
aha = fit2["BestFitParameters"]
```

```
{k0Hhyd → 7.20528, k0Bhyd → -2.27374 × 10-13, kOHHhyd → 1.70337 × 107, kOHBhyd → 0.,
kH2phosHhyd → 21.3134, kH2phosBhyd → 0., kH1phosHhyd → 487.385, kH1phosBhyd → 0.}
```

This construction extracts the optimised values from the list

```
kH2phosHhyd2test = kH2phosHhyd /. aha
```

```
21.3134
```

■ ReFit for compound 1 using parameters as for 2

Refit the data for 1 using the optimised variables for 2 for the protonated hydantoin.

```
fit1a = NonlinearModelFit[kineticdata60c1,
kobs[pH, pKahyd1, pKaHphosphate25C, phostot, Kw60C, k0Hhyd /. aha, k0Bhyd, kOHHhyd /. aha,
kOHBhyd, kH2phosHhyd /. aha, kH2phosBhyd, kH1phosHhyd /. aha, kH1phosBhyd],
{{k0Bhyd, 0.1}, {kOHBhyd, 1}, {kH2phosBhyd, 1}, {kH1phosBhyd, 1}},
{pH, phostot}, Weights -> weights60c1]
```

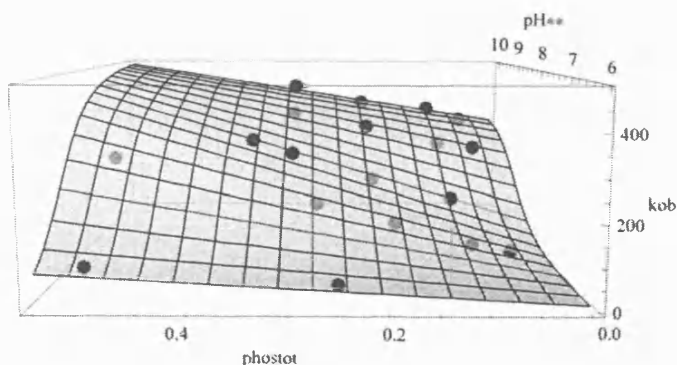
```
FittedModel[
```

$$\frac{10^{-8.65+\text{pH}} \left(50.6357 + \langle\langle 22 \rangle\rangle \langle\langle 2 \rangle\rangle \langle\langle 1 \rangle\rangle + \langle\langle 1 \rangle\rangle + \frac{\langle\langle 19 \rangle\rangle \langle\langle 1 \rangle\rangle \text{phostot}}{1 + 10^{\langle\langle 1 \rangle\rangle}} \right)}{1 + 10^{-8.65+\text{pH}}} + \frac{7.20528 + \langle\langle 2 \rangle\rangle + \frac{\langle\langle 1 \rangle\rangle}{1 \langle\langle 1 \rangle\rangle \langle\langle 1 \rangle\rangle}}{1 + 10^{-8.65+\text{pH}}}$$

```
fit1a["ParameterTable"]
```

	Estimate	Standard Error	t Statistic	P-Value
k0Bhyd	50.6357	10.1322	4.9975	0.0000933456
kOHBhyd	2837.46	4063.38	0.6983	0.493913
kH2phosBhyd	22542.6	1241.8	18.1531	5.09444 × 10 ⁻¹³
kH1phosBhyd	336.973	60.1057	5.60634	0.0000254873

```
Show[Plot3D[fit1a[pH, phostot], {pH, 6, 10.1}, {phostot, 0, 0.55},
AxesLabel -> {"pH**", phostot, kobs}, PlotStyle -> Opacity[0.7],
ViewPoint -> {-2, 0, 0.3}, LabelStyle -> Directive[Blue]],
ListPointPlot3D[{kineticdata60c1}, PlotStyle -> PointSize[Large]]]
```




```
Export[foldername <> "kinetic_data\global_fit1a.jpg",
Show[Plot3D[fit1a[pH, phostot], {pH, 6, 10.1}, {phostot, 0, 0.5},
  AxesLabel -> {"pH**", phostot, kobs}, PlotStyle -> Opacity[0.7],
  ViewPoint -> {-2, 0, 0.3}, LabelStyle -> Directive[Blue]],
ListPointPlot3D[{kineticdata60c1}, PlotStyle -> PointSize[Large]],
"JPEG", ImageResolution -> 300]
C:\Users\User\Desktop\math\kinetic_data\global_fit1a.jpg
```

Output fit data for construction of 2 D graphs

■ fit 1

```
outdata60c1 = ArrayPad[kineticdata60c1all, {{0, 0}, {0, 1}}];
Do[outdata60c1[[q, 5]] = fit1[pH, phostot] /. {pH -> kineticdata60c1all[[q, 1]],
  phostot -> kineticdata60c1all[[q, 2]]}, {q, datapoints60c1}]
MatrixForm[outdata60c1, TableHeadings -> {None, {pH, total phosphate, kexp, error, kfit}}]
```

pH	phosphate total	kexp	error	kfit
6	0.25	55.46	0.33	51.9083
6	0.5	95.2	1	95.202
7.2	0.045	42.9	0.45	44.0536
7.2	0.09	58.97	1.16	69.8662
7.2	0.18	116.78	1.4	121.492
7.2	0.27	168.28	1.75	173.117
7.2	0.5	288.4	1.1	305.048
8	0.1	137.1	1.3	130.158
8	0.2	193.5	1.4	197.399
8	0.3	268	1.7	264.64
8	0.35	305.4	0.3	298.261
9	0.05	245.1	1.2	240.052
9	0.1	259.6	0.7	264.376
9	0.2	312.7	1.5	313.025
9	0.3	355.7	2	361.674
10	0.05	304.9	1.5	314.996
10	0.1	344.6	1.5	333.643
10	0.2	365.3	1.3	370.936
10	0.3	420.7	3.4	408.228
11	0.1	362	2	350.413
11	0.2	375	5	386.053
11	0.3	404	5	421.692

```
Export[foldername <> "kinetic_data\global_fit1.xls", outdata60c1]
C:\Users\User\Desktop\math\kinetic_data\global_fit1.xls
```

■ fit 2

```
outdata60c2 = ArrayPad[kineticdata60c2all, {{0, 0}, {0, 1}}];
Do[outdata60c2[[q, 5]] = fit2[pH, phostot] /. {pH -> kineticdata60c2all[[q, 1]],
  phostot -> kineticdata60c2all[[q, 2]]}, {q, datapoints60c2}]
```

```
MatrixForm[outdata60c2, TableHeadings → {None, {pH, total phosphate, kexp, error, kfit}}]
```

pH	phosphate total	kexp	error	kfit
6	0.3	34.88	0.16	32.9307
6	0.5	52.3	0.26	49.6944
6	0.7	64.86	0.2	66.4581
7.2	0.045	31.2	0.1	32.2566
7.2	0.09	45.1	0.1	48.118
7.2	0.27	110.5	0.4	111.564
7.2	0.5	186.1	0.5	192.633
8	0.1	126.6	0.4	111.101
8	0.2	159.8	0.7	157.013
8	0.35	228.8	0.9	225.881
9	0.05	590	2	611.266
9	0.1	607	4	635.485
9	0.2	712	2	683.925

```
fit2[5.5, 0]
```

```
7.38865
```

```
fit2[8, 0]
```

```
65.1893
```

```
fit2[9, 0]
```

```
587.046
```

```
fit2[6, 0]
```

```
7.78512
```

```
fit2[7.2, 0]
```

```
16.395136475400996`
```

```
fit2[5.5, 0]
```

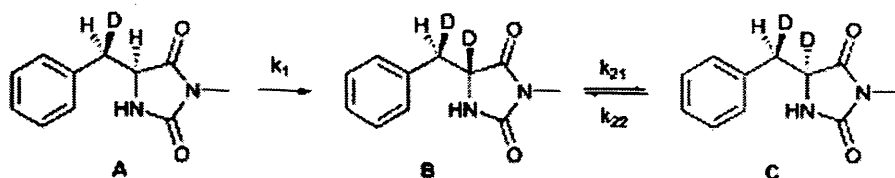
```
Export[foldername <> "kinetic_data\\global_fit2.xls", outdata60c2]
```

```
C:\Users\User\Desktop\math\kinetic_data\global_fit2.xls
```

Analysis of H / D exchange of labelled hydantoin

2.2 a following an hypothetical SE2 mechanism

```
foldername = "C:\\Users\\User\\Desktop\\math\\"
Import[foldername <> "Scheme.gif"]
C:\\Users\\User\\Desktop\\math\\
```



2.2 a

Import data

```
filename = "D:\\Lavinia\\CARDIFF\\results_projects\\Racemization_equations\\"
D:\\Lavinia\\CARDIFF\\results_projects\\Racemization_equations\\
dataAll = Import[filename <> "dataSN7025bALL.csv"];
```

```
MatrixForm[dataAll]
```

1	0	0.201
1	0.01314	0.197
1	0.02646	0.18
1	0.0843	0.147
1	0.09882	0.153
1	0.11136	0.142
1	0.17046	0.105
1	0.18216	0.107
1	0.2013	0.099
1	0.26034	0.087
1	0.27366	0.081
1	0.28524	0.068
1	0.34344	0.065
1	0.36252	0.059
1	0.37482	0.058
1	0.43434	0.042
1	0.6051	0.03
1	0.63492	0.03
1	0.6912	0.021
1	0.77772	0.025

1	0.8643	0.016
1	0.95184	0.013
1	1.21158	0
1	1.47252	0
1	1.81692	0
1	2.4222	0
2	0	0
2	0.01314	0.0106
2	0.02646	0.0177
2	0.0843	0.0319
2	0.09882	0.0335
2	0.11136	0.0365
2	0.17046	0.0447
2	0.18216	0.0495
2	0.2013	0.0475
2	0.26034	0.064
2	0.27366	0.0623
2	0.28524	0.0436
2	0.34344	0.0705
2	0.36252	0.0711
2	0.37482	0.0702
2	0.43434	0.0785
2	0.6051	0.0957
2	0.63492	0.0903
2	0.6912	0.0954
2	0.77772	0.0963
2	0.8643	0.0904
2	0.95184	0.0967
2	1.21158	0.0948
2	1.47252	0.0971
2	1.81692	0.0926
2	2.4222	0.0947
3	0	0.2027
3	0.01314	0.1918
3	0.02646	0.1841
3	0.0843	0.173
3	0.09882	0.1557
3	0.11136	0.1476
3	0.17046	0.1456
3	0.18216	0.1493
3	0.2013	0.1328
3	0.26034	0.1325
3	0.27366	0.1217
3	0.28524	0.1223
3	0.34344	0.1215
3	0.36252	0.1101
3	0.37482	0.1166
3	0.43434	0.1143
3	0.6051	0.1065

```

3 0.63492 0.106
3 0.6912 0.1096
3 0.77772 0.1104
3 0.8643 0.0994
3 0.95184 0.0953
3 1.21158 0.0957
3 1.47252 0.098
3 1.81692 0.0955
3 2.4222 0.0919

```

```

data1 = Import[filename <> "dataSN7025b_A.csv"];
data2 = Import[filename <> "dataSN7025b_B.csv"];
data3 = Import[filename <> "dataSN7025b_A+C.csv"];

```

Define equations (S represents A+C)

```

Ain = .2018
0.2018

A[k1_, t_] := Ain e-k1 t

B[k1_, k21_, k22_, t_] := Ain ((k1 - k22) / (k21 + k22 - k1)) e-k1 t -
(k1 k21 / ((k21 + k22) (k21 + k22 - k1))) e-(k21+k22) t + k22 / (k21 + k22)

S[k1_, k21_, k22_, t_] = Ain (1 - ((k1 - k22) / (k21 + k22 - k1)) e-k1 t +
(k1 k21 / ((k21 + k22) (k21 + k22 - k1))) e-(k21+k22) t - k22 / (k21 + k22))

0.2018 (1 -  $\frac{k22}{k21 + k22} - \frac{e^{-k1 t} (k1 - k22)}{-k1 + k21 + k22} + \frac{e^{-(k21+k22) t} k1 k21}{(k21 + k22) (-k1 + k21 + k22)})$ 

```

Fitting

```

model[selector_, k1_, k21_, k22_, t_] :=
Chop[KroneckerDelta[1, selector] A[k1, t] + KroneckerDelta[2, selector]
B[k1, k21, k22, t] + KroneckerDelta[3, selector] S[k1, k21, k22, t]]

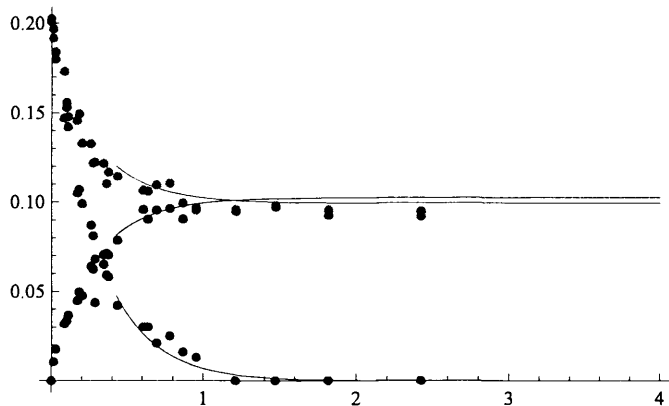
fit1 = FindFit[dataAll, model[selector, k1, k21, k22, t],
{{k1, 5.}, {k21, 6}, {k22, 6.}}, {selector, t}]
{k1 → 3.38261, k21 → 13.3473, k22 → 13.7693}

fit1["ParameterConfidenceIntervalTable"]
{k1 → 3.38261, k21 → 13.3473, k22 → 13.7693}[ParameterConfidenceIntervalTable]

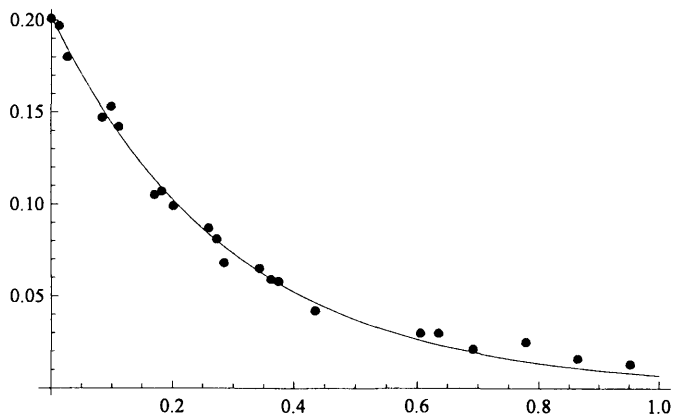
```

Graphs

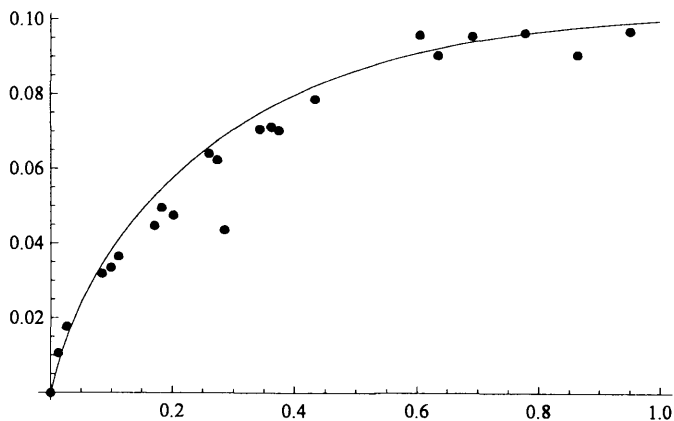
```
Show[ListPlot[data1, PlotStyle -> Directive[Blue, PointSize[0.015]]],
ListPlot[data2, PlotStyle -> Directive[Black, PointSize[0.015]]],
ListPlot[data3, PlotStyle -> Directive[Red, PointSize[0.015]]],
Plot[A[k1, t] /. fit1, {t, 0, 4}, PlotStyle -> {Blue, Thickness[0.001]}],
Plot[B[k1, k21, k22, t] /. fit1, {t, 0, 4}, PlotStyle ->
{Black, Thickness[0.001]}],
Plot[S[k1, k21, k22, t] /. fit1, {t, 0, 4}, PlotStyle -> {Red, Thickness[0.001]}]]
```



```
Show[Plot[A[k1, t] /. fit1, {t, 0, 1}, PlotStyle -> {Blue, Thickness[0.001]}],
ListPlot[data1, PlotStyle -> Directive[Blue, PointSize[0.015]]]]
```



```
Show[Plot[B[k1, k21, k22, t] /. fit1, {t, 0, 1}, PlotStyle -> {Black, Thickness[0.001]}],
ListPlot[data2, PlotStyle -> Directive[Black, PointSize[0.015]]]]
```



```
Show[Plot[S[k1, k21, k22, t] /. fit1, {t, -0.06, 1.}, PlotStyle -> {Red, Thickness[0.001]}],  
ListPlot[data3, PlotStyle -> Directive[Red, PointSize[0.015]]]
```

